EFFICIENT AND ECONOMICAL ELECTROCHEMOTHERAPY TREATMENTS FOR TRIPLE NEGATIVE BREAST CANCER: AN *IN VITRO* MODEL STUDY

by

Lakshya Mittal

A Dissertation

Submitted to the Faculty of Purdue University

In Partial Fulfillment of the Requirements for the degree of

Doctor of Philosophy

School of Engineering Technology

West Lafayette, Indiana

December 2020

THE PURDUE UNIVERSITY GRADUATE SCHOOL

STATEMENT OF COMMITTEE APPROVAL

Dr. Raji Sundararajan, Chair

School of Engineering Technology

Dr. Ignacio G. Camarillo

Department of Biological Sciences

Dr. Allen L. Garner

School of Nuclear Engineering

Dr. Ken Burbank

School of Engineering Technology

Approved by:

Dr. Kathryne Newton

To my family and teachers

ACKNOWLEDGMENTS

Now, when I look back at my Ph.D. journey, I cannot thank enough many people who supported me along the way. Due to the limitation on the length, I cannot mention everyone here, but I would like to especially thank those who played the most significant part.

I am forever indebted to my advisor and mentor Dr. Raji Sundararajan for recruiting me into her group and giving me the opportunity to work on this research. The successful completion of the research would not have been possible without her valuable guidance, support, nurturement, and inspiration. Her guidance has inculcated me with the confidence to think and work independently to pursue my own research questions, while collaborating effectively with other labs and core facilities, and to mentor new students. Moreover, her suggestions to improve my technical writing has made me a better writer. I am inspired by her desire and hard work to bring awareness of alternate treatments to relieve suffering of many patients.

I express my deepest appreciation to my committee members, Dr. Ignacio G. Camarillo, Dr. Allen L. Garner, and Dr. Ken Burbank, whose useful feedback and advice throughout my Ph.D. has added so much to my research experience and to the content of my publications.

This work would not have been possible without the generous support from Dr. Camarillo, who allowed me to work in his lab and shared his valuable guidance to complete the research. Discussions with him on various topics have always been so encouraging and motivating. Outside the lab, I will always remember LSAMP meetings and thanksgiving lunches at his home with his wife and children. Thank you for everything.

I am also grateful to Dr. Garner for presenting our research at various conferences and helping me in manuscript preparation, while giving suggestions to improve the written communication. His hard work and extraordinary capability of juggling multiple responsibilities at once is something I wish to emulate.

I cannot begin to express my thanks to Dr. Burbank, who has been instrumental behind this research, due to his extraordinary efforts to make our department a nice place to work. Thank you for agreeing to be on my committee and providing your insight on this research. I will forever be grateful to him for entrusting me with TA responsibilities, which gave me countless opportunities to interact with and mentor undergraduate students.

Prof. Richardson for being patient and guiding me as his TA for over three semesters. It would be a great mistake, if I do not mention the office and technical staff (Shawn Davis, Niedra McLeland, Debbie Hulsey, Amanda Wilson, and Nicky Federer), who work behind curtains to make our work smooth. Many thanks to Prof. Clark Cory for printing posters at short notices.

I am also grateful to my M.S. thesis advisor Dr. R. Sarathi of IIT Madras, who gave me the first research opportunity of my life in 2013. Special thanks to Dr. Uma K. Aryal for offering his expertise in proteomics studies, adding immense value to my publications, Dr. Gowri Sree Varadarajan for collaboration and hosting me to her lab in summer 2018, and Dr. Hemalatha Srinivasan for collaboration and hosting me to her lab in summer 2018.

I gratefully acknowledge Vishak for his mentorship, teaching experimental techniques, and troubleshooting protocols to get my research going. I learned a great deal from him. I acknowledge the joy of mentoring Jeya Shree and Alexis, and their great assistance in my experiments. I would never forget the company, encouragement, and co-operation I received from my lab mates: Mochen, Rodrigo, Ivy, Pragatheiswar, Vishveswaran, and Tejasvi.

I am indebted to the funding support from PPI Dean's RA award, SOET TA awards, Purdue Graduate School Bilsland Dissertation fellowship, and IEEE Dielectrics and Electrical Insulation Society (DEIS) Graduate fellowship. I am also thankful to Indo-US Science & Technology Forum for the RISE fellowship.

In the last, I would like to thank my family for their continuous and unparalleled love, sacrifice, help and support. Thank you for encouraging me to pursue my dreams. I am grateful to my younger brother Somya, who has been wonderfully able to fulfill my share of the responsibilities towards the family. Realization that my family was there for me allowed me to remain motivated and keep going throughout my time in grad school. Also, I would acknowledge my cousins (Aakriti, Ankit, Meghna, and Anvesha), whose presence in the U.S. constantly reminded me the close by existence of the family.

Living in a new country far away from home is never easy. I would be unfair, if I forget to mention the people (Sakshi, Karna, Rohan, Madhav, Vedant, Sagar, Harpreet, Craig, and Mary), who made me feel like a home away from home at Purdue. A special shout out to my old friends Prateek, Gaurav, Nikhil, Shadab, and Akash, who kept me motivated through their little chit-chats.

I acknowledge that the previous versions of various sections in this dissertation have been originally published in (Mittal, Aryal, Camarillo, Ferreira, & Sundararajan, 2019; Mittal, Aryal, Camarillo, Raman, & Sundararajan, 2020; Mittal, Camarillo, et al., 2020; Mittal, Raman, Camarillo, Garner, & Sundararajan, 2019; Mittal, Raman, Camarillo, & Sundararajan, 2017; Mittal, S., et al., 2020).

TABLE OF CONTENTS

LIST OF TABLES

LIST OF FIGURES

GLOSSARY AND LIST OF ABBREVIATIONS

ABBREVIATION	TERM
2DE	2-dimensional gel electrophoresis
4-OHT	4-Hydroxytamoxifen
5-FU	5-fluorouracil
7-AAD	7-Aminoactinomycin D
AA	Amino acid
ABCA8	ATP binding cassette subfamily A member 8
ABCB1	ATP-binding cassette sub-family B member 1
ABC transporters	ATP-binding cassette transporters
AC	Anthracycline (doxorubicin) plus cyclophosphamide
ACAT1	Acetyl CoA acetyltransferase
Acetyl CoA	Acetyl coenzyme A
ACTA2	Actin alpha 2
ACN	Acetonitrile
ADP	Adenosine diphosphate
αKG	α-ketoglutarate
Akt/AKT	Protein kinase B
ALCAM	Activated leukocyte cell adhesion molecule
ALDHA1	Aldehyde dehydrogenase 1 family, member A1
ALDOA	Fructose-bisphosphate aldolase A
ALDOB	Fructose-bisphosphate aldolase B
ALDOC	Fructose-bisphosphate aldolase C
ALK	Anaplastic lymphoma kinase

ANOVA	Analysis of variance
AP1	Activating protein-1
APC	Adenomatous polyposis coli (protein)
AR	Androgen receptor
ASR	Age-standardized incidence rate
ATP	Adenosine triphosphate
AURKA	Aurora kinase A
AURKB	Aurora kinase B
BCA	Bicinchoninic acid
BCL2	B-cell lymphoma 2
Bcl-xL	B-cell lymphoma-extra large
BMI	Body mass index
BRCA1	Breast cancer type 1 susceptibility protein
BRCA2	Breast cancer type 2 susceptibility protein
BCIRG	Breast Cancer International Research Group
BL1	Basal-like 1
BL2	Basal-like 2
CAF	Cancer-associated fibroblasts
CARE	Contraceptive and reproductive experiences
CBCS	Carolina breast cancer study
CBF1	Centromere-binding protein 1
cDNA	Complementary DNA
cFLIP	Cellular FLICE-inhibitory protein
CHEK1	Checkpoint kinase 1
CI	Confidence interval

CIMBA	Consortium of Investigators of Modifiers of BRCA1/2
CK	Cytokeratin
CKAP4	Cytoskeleton associated protein 4
CMF	Cyclophosphamide, methotrexate, 5-fluorouracil
c-Myc	Cellular myelocytomatosis
COX	Cyclooxygenase
CR	Complete response
c-Rel	Proto-oncogene REL
CSC	Cancer stem cell
CSL	CBF1, suppressor of hairless, lag-1
CsP	Cisplatin
CNA	Copy number alterations
CSNK1G	Casein kinase I gamma 3
Ctrl	Control
Cur	Curcumin
CWR	Chest wall recurrence
CXCR4	C-X-C chemokine receptor type 4
Cys	Cysteine
DAnTE	Data Analysis and Extension Tool
DCIS	Ductal carcinoma *in situ*
DFS	Disease-free survival
DHCR24	24-Dehydrocholesterol reductase
DLD	Dihydrolipoamide dehydrogenase
DLST	Dihydrolipoamide s-succinyltransferase
DMEM	Dulbecco's modified essential medium

DMSO	Dimethyl sulfoxide
DSB	Double-strand breaks
DTT	Dithiothreitol
DNA	Deoxyribonucleic acid
DPPH	2,2-diphenyl-1-picryl-hydrazyl
ECM	Extracellular matrix
ECT	Electrochemotherapy
EDTA	Ethylenediaminetetraacetic acid
EDS	Energy-dispersive X-ray spectroscopy
EGF	Epidermal growth factor
EGFR	Epidermal growth factor receptor
ELISA	Enzyme-linked immunosorbent assay
ELK1	ETS domain-containing protein Elk-1
EMT	Epithelial-mesenchymal transition
ENG	Endoglin
ENO	Enolase
EP	Electrical pulse
ER	Estrogen receptor
ERK	Extracellular-signal-regulated kinase
ESMO	European Society for Medical Oncology
ETC	Electron transport chain
ETS1	ETS proto-oncogene 1
FA	Fatty acid
FAC	5-fluorouracil, doxorubicin, and cyclophosphamide
FADH2	Flavin adenine dinucleotide

FAK	Focal adhesion kinase
FANCA	Fanconi anaemia, complementation group A
FANCG	FA Complementation Group G
FASN	Fatty acid synthase
FBS	Fetal bovine serum
FDA	Food and Drug Administration
FDR	False discovery rate
FEC	5'-fluorouracil, epirubicin, and cyclophosphamide
FEC-T	5'-fluorouracil, epirubicin, cyclophosphamide, and docetaxel
FEC-P	5'-fluorouracil, epirubicin, and cyclophosphamide-paclitaxel
FGF	Fibroblast growth factor
FNCLCC	Fédération Nationale des Centres de Lutte Contre le Cancer
FTIR	Fourier-transform infrared
GAPDH	Glyceraldehyde 3-phosphate dehydrogenase
GLOBOCAN	Global Cancer Incidence, Mortality, and Prevention
GLS	Glutaminase
GLUT	Glucose transporter
GLUT1/SLC2A1	Glucose transporter 1
GANAB	Glucosidase II Alpha Subunit
GO	Gene ontology
GSK-3β	Glycogen synthase kinase-3β
hCTR1/SLC31A1	High affinity copper transporter 1
HER2/neu/erbb2	Human epidermal growth factor receptor 2
HF	High field
HGF	Hepatocyte growth factor

HIF	Hypoxia-inducible factor
HSD	Honest significance difference
Hh	Hedgehog
HK	Hexokinase
HOX	Homeobox
HOXA10	Homeobox protein A10
HOXA5	Homeobox protein A5
HPLC-ESI-MS/MS	High performance liquid chromatography-electrospray ionization-tandem mass spectrometry
HR	Hazard ratio
HRAS	Harvey rat sarcoma viral oncogene homolog
HSP	Heat shock protein
HV	High voltage
IAP	Intestinal alkaline phosphatase
IHC	Immunohistochemistry
IDC	Invasive ductal carcinoma
IRE	Irreversible electroporation
IGF-1R	Insulin-like growth factor-1 receptor
IHC	Immunohistochemistry
IL	Interleukin
ILC	Invasive lobular carcinomas
IκB	NF-κB inhibitor
IM	Immunomodulatory
INSPECT	International Network for Sharing Practice on Electrochemotherapy
i.t.	Intratumorally

i.v.	Intravenously
JAK	Janus kinase
KDR	Kinase Insert Domain Receptor
KEGG	Kyoto encyclopedia of genes and genomes
LAR	Luminal androgen receptor
LCIS	Lobular neoplasia/lobular carcinoma *in situ*
LDH	Lactate dehydrogenase
LFQ	Label-free quantitation
LOX	Lipoxygenase
LPFS	Local progression free survival
Lum	Luminescence
LV	Low voltage
M	Mesenchymal
MAPK	Mitogen-activated protein kinase
MCP	Methyl-accepting chemotaxis proteins
MCT	Monocarboxylate transporter
MDC1	Mediator of DNA damage checkpoint protein 1
MDH	Malate dehydrogenase
MEK	Mitogen-activated protein kinase
MEOX	Mesenchyme Homeobox
miRNA	microRNA
MMP	Matrix metalloprotease
MS	Mass spectroscopy
MS/MS	Tandem mass spectrometry
MSL	Mesenchymal stem–like

mtDNA	Mitochondrial DNA
mTOR	Mammalian target of rapamycin
MTT	3-(4,5-dimethylthiazol-2-yl)-2,5-diphenyltetrazolium bromide
NADH	Nicotinamide adenine dinucleotide, reduced
NADPH	Nicotinamide adenine dinucleotide phosphate, reduced
NCI	National Cancer Institute
NF-κB	Nuclear factor κB
NGF	Nerve Growth Factor
NGFR	Neuronal growth factor receptor
NICD	Notch receptor intracellular domain
NIH	National Institutes of Health
NK cells	Natural killer cells
NR	Not reported
Nrf2	Nuclear factor erythroid 2–related factor 2
OC	Oral contraceptive
OD	Optical density
OGDH	Oxoglutarate dehydrogenase
OR	Objective response
OS	Overall survival
OXPHOS	Oxidative phosphorylation
P4HB	Protein disulfide-isomerase
p50/p105	NFKB1 - Nuclear factor NF-kappa-B p105 subunit
p52/p100/NFKB2	NFKB2 - Nuclear factor NF-kappa-B p100 subunit
p53	Tumor protein 53
p65/RELA	Nuclear factor NF-kappa-B p65 subunit

PARP	Poly-ADP ribose polymerase
PBS	Phosphate buffered saline
pCR	Pathological complete response
PCR	Polymerase chain reaction
PDC	Pyruvate dehydrogenase complex
PDGF	Platelet-derived growth factor
PDH	Pyruvate dehydrogenase
PDIA3	Protein disulfide-isomerase A3
PDX	Patient-derived xenograft
PFK	Phosphofructokinase
PGAM	Phosphoglycerate mutase
PGK	Phosphoglycerate kinase
PHDGH	3-phosphoglycerate dehydrogenase
PI	Propidium iodide
PI3K	Phosphatidylinositol-3-kinase
PIK3CA	Phosphatidylinositol 3-kinase, catalytic, alpha
PKA	Protein kinase A
PKA	Protein kinase B
PKM	Pyruvate kinase muscle isozyme
PPP	Pentose phosphate pathway
PPAR	Peroxisome proliferator-activated receptor
PR	Progesterone receptor
PR	partial response
PRN1	Pirin1
PTEN	Phosphatase and tensin homolog

PUMA	p53 upregulated modulator of apoptosis
PVDF	Polyvinyl difluoride
QE	Q-Exactive
qPCR	Realtime quantitative polymerase chain reaction
RB1	Retinoblastoma protein
RIP1	Receptor-interacting protein 1
RIPA	Radioimunnoprecipitation assay
RLU	Relative light units
RNA	Ribonucleic acid
ROS	Reactive oxygen species
RPM	Revolutions per minute
RTK	Receptor tyrosine kinases
SCID	Severe combined immunodeficient
SDS-PAGE	Sodium dodecyl sulfate-polyacrylamide gel electrophoresis
SF	Serum free
SLC1A5/ASCT2	Solute carrier family 1 member 5
SLC22	Organic solute carrier 22
SNAI2	Snail Family Transcriptional Repressor 1
SPDEF	SAM pointed domain-containing Ets transcription factor
STAT	Signal transducer and activator of transcription
TAC	Docetaxel, doxorubicin, and cyclophosphamide
TCA	Tricarboxylic acid
TCF/LEF	T-cell factor/lymphoid enhancer factor
TGF	Transforming growth factor
THY1	Thy-1 Cell Surface Antigen

TIC	Tumor-initiating cells
TNBC	Triple negative breast cancer
TNF	Tumor necrosis factor
TNFR1	Tumor necrosis factor receptor 1
TPI1	Triosephosphate isomerase 1
TTK	TTK protein kinase
TurNP	Turmeric silver nanoparticles
TWIST1	Twist family BHLH transcription factor 1
UPR	Unfolded protein response
USP6NL	USP6 N-terminal like
UV–vis	Ultraviolet–visible
VCAM1	Vascular cell adhesion molecule 1
VEGF	Vascular endothelial growth factor
Veh	Vehicle - DMSO
WHO	World Health Organization
Wnt	Wingless
ZEB1	Zinc finger e-box binding homeobox 1
ZEB2	Zinc finger e-box binding homeobox 2
ZNRF3	Zinc and ring finger 3

ABSTRACT

With 2.1 million new cases, breast cancer is the most common cancer in women. Triple negative breast cancer (TNBC), which is 15-20% of these breast cancer cases is clinically negative for expression of estrogen and progesterone receptors (ER/PR) and human epidermal growth factor receptor 2 (HER2) receptors. It is characterized by its unique molecular profile, aggressive behavior, distinct patterns of metastasis, and lack of targeted therapies. TNBCs utilize glycolysis for growth, proliferation, invasiveness, chemotherapeutic resistance and hence has poor therapeutic response. There is an urgent need for novel/alternate therapeutic strategies beyond current standard of treatment for this subset of high-risk patients. Electrical pulse-based chemotherapy, known as electrochemotherapy (ECT) could be a viable option for TNBC therapy. ECT involves the local application of precisely controlled electrical pulses to reversibly permeabilize the cell membrane for enhanced uptake. ECT can increase the cytotoxicity of the chemotherapeutics up-to 1000 times, facilitating a potent local cytotoxic effect.

The high cost and severe side-effects of conventional chemotherapeutics motivate the application of effective natural compounds. Combining electrical pulses with natural compounds will enhance the treatment efficacy. This dissertation focuses on curcumin, the yellow pigment of natural herb turmeric, that has been used for over 5000 years for its excellent anticancer properties. Previous studies have demonstrated the effectiveness of curcumin for treating multiple cancers, including TNBC, with limited side effects. The potency of curcumin can be enhanced further by combining it with ECT to provide an attractive and cost-effective alternative for TNBC treatment.

Towards this we studied the effect of ECT with curcumin on MDA-MB-231 cell line, a human adenocarcinoma epithelial TNBC cell line. We performed various assays, including cell viability, colony forming, cell cycle, apoptosis, H_2O_2 reactive oxygen species (ROS), immunoblotting, real time quantitative PCR (qPCR), and cellular metabolites detection to study the impact of ECT with curcumin on MDA-MB-231 cells. In addition, to better understand the underlying mechanisms, we used high throughput, label-free quantitative proteomics. While several studies have attempted to define the mechanism of action of curcumin on cancer cells, little is known on the action mechanism of the curcumin delivered with electrical pulses. This work unravels the molecular mechanism behind the enhanced effects observed under the ECT-based curcumin therapy in TNBC cells, employing a high-throughput, quantitative, label-free mass

spectroscopy-based proteomics approach. The proteomics approach provides information on the thousands of cellular proteins involved in the cellular process, allowing a comprehensive understanding of the electro-curcumin-therapy mechanism. Similar studies were also performed for ECT with cisplatin to compare the efficacy of the electro-curcumin-therapy to the standard stand-alone cisplatin-based therapy.

Our results revealed a switch in the metabolism from glycolysis to mitochondrial metabolic pathways. This metabolic switch caused an excessive production of H_2O_2 ROS to inflict apoptotic cell death in MDA-MB-231 cells, demonstrating the potency of this ECT based curcumin therapy. These results encourage further studies to extend the application of ECT for clinical practice.

CHAPTER 1. INTRODUCTION

1.1 Breast cancer

Breast cancer is the several types of uncontrolled tumor growth, arising from breast tissue. The most common breast cancer is adenocarcinoma of the epithelial cells lining the ducts. Cancer results from the various gradual accumulation of genetic abnormalities, such as point mutations and chromosomal amplifications and mutations, including translocation, duplication, deletion, and inversion. While the majority of the breast cancers are sporadic in nature usually resulting from somatic mutations, only 10% of the breast cancers are associated with germ-line mutations (DeVita, Lawrence, & Rosenberg, 2015). Breast cancer is more common in female mice, dogs, and humans. Figure 1.1 shows a microscopic view of invasive ductal carcinoma subtype of breast cancer.

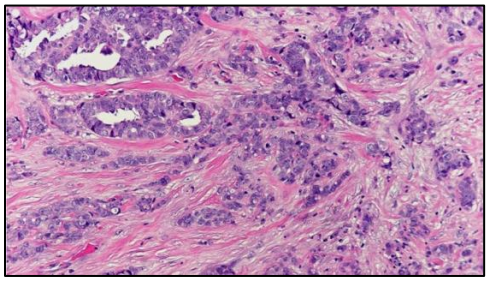

Figure 1.1: A microscopic view of the breast cancer - invasive ductal carcinoma (IDC) subtype. IDC is the most common breast cancer subtype.

1.1.1 Breast cancer statistics

Breast cancer is the most common cancer in women (Bray et al., 2018). According to the Global Cancer Incidence, Mortality, and Prevention (GLOBOCAN), worldwide, breast cancer is the second most common cancer with over 2 million new cases (11.6% of all cancers) and fifth leading cause of cancer-related mortality with 626,679 deaths (6.6% of all cancers) (Bray et al., 2018). In the United States, breast cancer is the leading cause of cancer-related incidence and mortality in women, with 271,270 new cases and 42,260 mortality each year (Siegel, Miller, & Jemal, 2019).

The breast cancer incidence rates are highest in developed countries in Western Europe and the U.S., and the lowest in Asia and Africa (European Society for Medical Oncology (ESMO), 2018). According to GLOBOCAN, breast cancer age-standardized incidence rate (ASR) is 468,

352, 344, 337, 334, 319, 311 in Australia, U.S., Norway, France, Canada, UK, and Switzerland, respectively (Ferlay et al., 2018) (Figure 1.2). On the other hand, the ASR is 163, 136, 112, 91.4, 89, 88.7, 87.8, Philippines, Indonesia, UAE, Uzbekistan, India, Saudi Arabia, and Bhutan in Asia and 131, 104, 92, 77, 72, 57 in Algeria, Nigeria, Central African Republic, Republic of Congo, Niger, The Republic of the Gambia, respectively. However, the survival rates remain high at 80% in high-income countries (USA, Canada, Sweden, Finland, Japan, and Australia), compared to 60% in middle-income countries (Brazil (ASR: 217.2) and Slovakia (ASR: 298)) and less than 40% in low-income countries (Algeria) (Coleman et al., 2008).

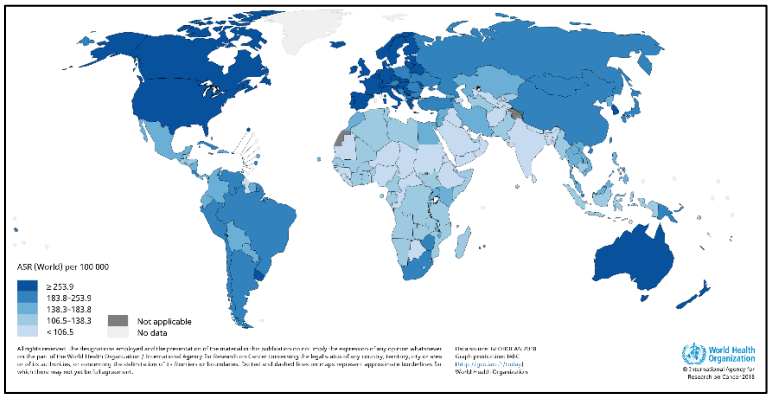

Figure 1.2: Worldwide breast cancer age-standardized incidence rate (ASR) in women of all ages in 2018 (Ferlay et al., 2018).

The higher breast cancer incidence is usually attributed to the lifestyle factors, such as high-calorie and high-sugar diets, lack of physical activities/exercise leading to obesity, high rate of smoking, and alcohol consumption (Dieterich, Stubert, Reimer, Erickson, & Berling, 2014). Particularly, high-fat diets and high rate of obesity are considered key major preventable risk factors of breast cancers in western countries (Shapira, 2017). According to the World Health Organization (WHO), low breast cancer survival in less developed countries could be attributed to the lack of early screening and detection, resulting in a high-proportion of late-stage disease and the lack of sufficient diagnosis and treatments (World Health Organization, n.d.). While in developing countries, 40-90% of patients are diagnosed with advanced disease, in developed countries only 10-15% cases are diagnosed with advanced disease (European Society for Medical Oncology (ESMO), 2018).

Additionally, breast cancer incidence, subtype, and mortality are also influenced by the age at first menstruation, pregnancy and menopause, parity, breastfeeding and its duration, race,

genetics and family history, and environmental exposure to carcinogens from pollution and passive smoking (Ataollahi, Sharifi, Paknahad, & Paknahad, 2015; Chakravarthi & Varambally, 2013; C. Chen et al., 2014; Skol, Sasaki, & Onel, 2016; Surakasula, Nagarjunapu, & Raghavaiah, 2014; Zhou et al., 2015).

A longer exposure to estrogen due to lower age at menstruation (<12) and higher age at menopause (>55) increases the breast cancer risk in women (Surakasula et al., 2014). Breast feeding reduces the risk of estrogen receptor (ER) negative breast cancer, but has no association with ER-positive breast cancer (Fortner et al., 2019). The parity reduces the risk of ER-positive breast cancer, but has no association with ER-negative breast cancer (Fortner et al., 2019). Race also influences the subtype of breast cancer, as more African-American women are diagnosed with triple negative breast cancer (TNBC) compared to White or Hispanic women, while Hispanic women are more likely to develop luminal subtype of breast cancer (Kurian, Fish, Shema, & Clarke, 2010). The link between active smoking and breast cancer incidence is controversial due to mixed findings, possibly due to the confounding by other factors, such as alcohol consumption, body mass index (BMI) and family history (Nyante et al., 2014; Prescott, Ma, Bernstein, & Ursin, 2007). On the other hand, several studies have established the role of second-hand smoking in increased breast cancer risk.

Although, the number of breast cancer could be prevented by modifying lifestyle factors, the breast cancer incidences due to genetics (~10% (Tung et al., 2016)), race and hormonal changes are difficult to prevent. Further, as per the GLOBOCAN's estimation, the number of breast cancer incidence and mortality are only expected to rise (incidence: three million and mortality: ~one million mortality in 2040) (Bray et al., 2018). Therefore, it is of practical interest to identify novel therapeutic strategies beyond conventional therapies to improve patient survival.

1.1.2 Breast cancer risk factors

The major breast cancer risk factos are as follows:

1. Gender - higher risk in females (lifetime risk of 1:8 compared to 1:1000 in men).
2. Aging (risk of 1:217 at age 40 vs risk of 1:10 at age of 80).
3. Obesity - high body mass index (BMI) in postmenopausal women.
4. Race - higher risk among black compared to white population.
5. Longer exposure to estrogen - early menarche (age <12) and late menopause (>55).
6. Reproductive history - late first full birth (age >35) and nulliparity.
7. Height - higher risk in taller women, likely to be linked with hormonal stimulation.

8. Lifestyle factors - high-calorie and high-sugar diets, lack of physical activities/exercise leading to obesity, high rate of smoking and alcohol consumption.
9. Exposure history - exposure radiation, smoking, alcohol.
10. Family history - positive maternal history increases risk from 1:8 to 3:8.
11. BRAC1/BRCA2 mutations - 85% chance of developing breast cancer.

1.1.3 Normal breast anatomy and histology

The tissue overlying the chest pectoral muscles in humans is called breast. Human breast consists of the mammary gland, which is a modified apocrine sweat gland that produces and delivers milk through a tree-like branched network of ducts. The mammary gland originated around 160 million years ago, when mammals were considered to evolve on the earth (Haagensen, 1986).

The breast is a very dynamic organ due to constant changes in hormones in female's lifetime - from birth to puberty to pregnancy to motherhood to menopause. The normal physiology, abnormal growth and changes in breast are affected by these hormonal variations. The two main hormones are estrogen and progesterone. The ductal proliferation is controlled by estrogen and lobular proliferation and growth is controlled by progesterone (Camarillo et al., 2014).

Figure 1.3 shows the anatomy and histology of the normal breast (Wong, Chaudhry, & Rossi, 2016). The breast anatomy shown in Figure 1.3(a) shows various muscles, tissues, and skin of breast. The breast consists of three types of tissues: fat, glandular (produces milk) and normal breast tissues. The milk producing structure of breast is divided into 15-20 lobes, and each lobe is composed of 20-40 lobules (Pandya & Moore, 2011). Lobes drain into lactiferous duct that enlarges to form lactiferous sinus beneath areola, just before the nipple (Figure 1.3(a)). Figure 1.3(b) shows a terminal ductual lobular unit. Each terminal duct lobular unit is composed of branched tubuloalveolar glands organized into lobes. Figure 1.3(c) shows the ductal structure. Ductal structures are primarily composed of two types of epithelial cells:

1. Luminal epithelial cells: Form inner layer, which produces and transport milk during lactation.
2. Myoepithelial cells: Form outer basal layer, which provides structural support and aid in milk ejection during lactation.

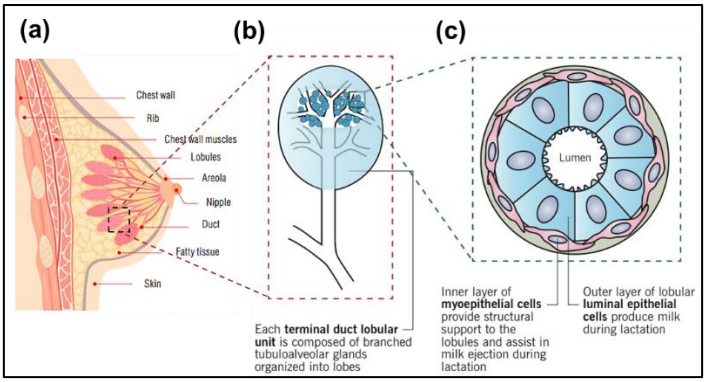

Figure 1.3: Schematic representation of (a) breast anatomy, (b) terminal ductual lobular unit, (c) ductal structure and cells. Adapted with permission from (Wong et al., 2016).

1.1.4 Types of breast cancers

A. Non-invasive breast cancer (in situ)

i. Ductal carcinoma in situ (DCIS)

When cancer cells are confined to the breast milk ducts, but have not spread into the surrounding healthy breast tissues, this non-invasive form of breast cancer is called ductal carcinoma in situ (DCIS) (as shown in Figure 1.4(c)). The DCIS is 100% curable.

ii. Lobular neoplasia/lobular carcinoma in situ (LCIS)

When the changes are observed in the cells lining lobules (milk-producing glands) and are marked with a high-risk of breast cancer development in future, it is called lobular neoplasia (formerly known as lobular carcinoma in situ (LCIS)) (Figure 1.4(f)). Frequently, lobular neoplasia does not transform into breast cancer, however it requires regular check-ups.

B. Invasive breast cancer

i. Invasive ductal carcinoma (IDC)

When breast cancer cells spread beyond the ducts and invade surrounding breast cancer tissues, they are called invasive ductal carcinomas (IDC) (as shown in Figure 1.4(d)). The IDC

contributes to the 80% of all breast cancers to be the most common breast cancer (G. N. Sharma, Dave, Sanadya, Sharma, & Sharma, 2010).

ii. Invasive lobular carcinomas (ILC)

When breast cancer cells spread beyond the lobules and invade surrounding breast cancer tissues, they are called invasive lobular carcinomas (ILC) (Figure 1.4(g)). The ILC represents 10%-15% of all breast cancers (G. N. Sharma et al., 2010).

The histological analysis is conduct for further classification of invasive breast cancers into tubular, mucinous, medullary, and papillary breast cancers (a rare subtype, representing 1-2% of all breast cancer).

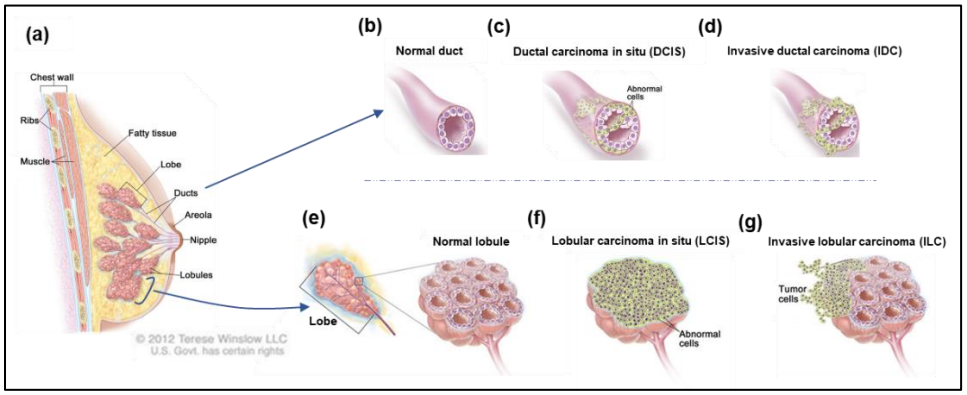

Figure 1.4: Schematic representation of (a) breast anatomy, (b) a normal duct (c) ductal carcinoma in situ (DCIS), (d) invasive ductal carcinoma (IDC). (e) a lobe and normal lobule (f) lobular carcinoma in situ (LCIS), (g) invasive lobular carcinoma (ILC). Adapted with permission from Terese Winslow LLC.

1.1.5 Molecular subtypes of breast cancer

Breast ductal structures are primarily composed of two types of epithelial cells - inner luminal epithelial cells and an outer layer of myoepithelial basal cells. As shown in Figure 1.5, normal breast stem cells or progenitor cells transform into breast cancer cells. The cancer cells are similar in phenotype to the normal basal and luminal cells of the ductal structure.

Accumulating evidences from the histopathology, molecular gene signatures, copy number alterations (CNAs), and gene mutation studies have confirmed that the breast cancer is an extremely heterogeneous disease. The differences in these signatures result in distinct tumor

behaviors, leading to different treatment responses. This highlights the importance of screening of these signatures and designing appropriate therapies.

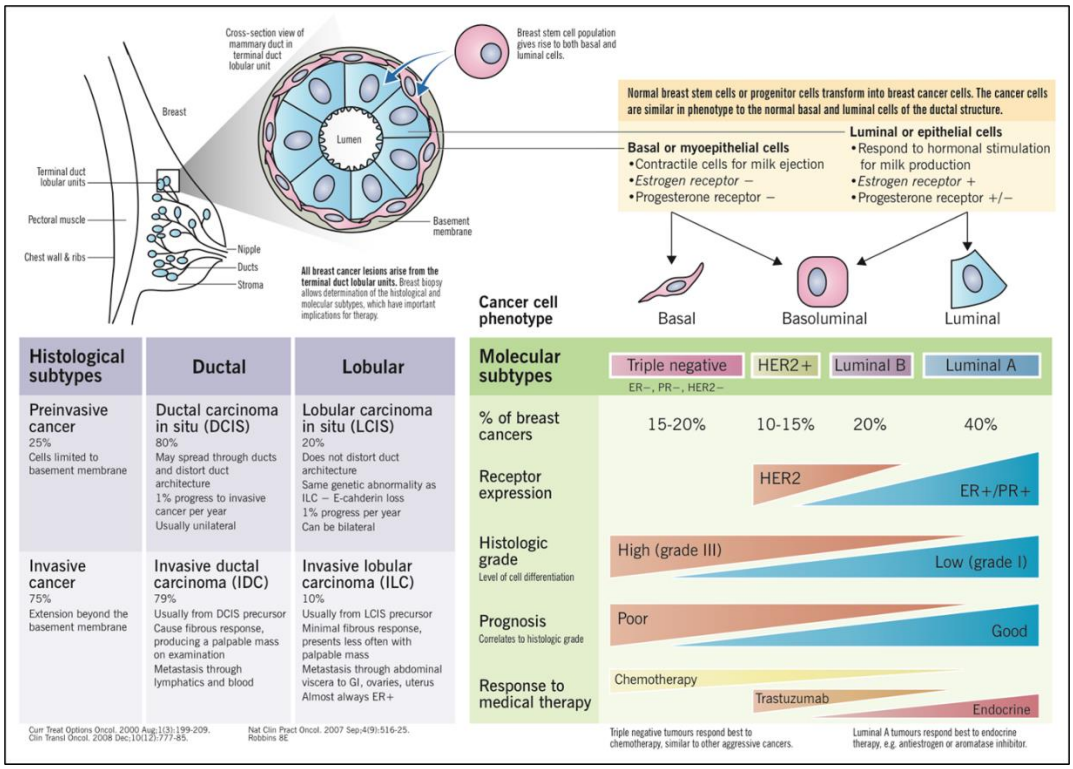

Figure 1.5: Breast cancer pathogenesis and histological vs. molecular subtypes. Reproduced with permission from (Wong et al., 2016).

Traditionally, immunohistochemistry (IHC) markers, including estrogen receptor (ER), progesteron receptor (PR), and human epidermal growth factor receptor 2 (HER2), along with patient clinical information, such as tumor size, grade, and nodal status are used for breast cancer management and prognosis (Dai et al., 2015). With the advent of high-throughput gene expression screening assays and through the pioneering studies of Sørlie and Perou in the early 2000s, molecular gene signature screening was integrated with the tradition approach of the histopathological features-based subtype classification, resulting into a new intrinsic molecular subtype classification (Dai et al., 2015; Perou et al., 2000; Sørlie et al., 2001).

The Sørlie and Perou used the cDNA arrays to study the expression of 9000 genes in breast carcinoma samples collected pre- and post- chemotherapy. Out of these 9000 genes, a total of 550 genes with similar expression between the two samples from a patient, but differential expression

between two patients were identified and called “intrinsic genes”, as they represented the phenotype of the individual tumors. The hierarchical clustering analysis based on the gene expression patterns revealed two main clusters (mostly according to ER status) and five sub clusters called intrinsic subtypes (Russnes, Lingjærde, Børresen-Dale, & Caldas, 2017). Other studies also corroborated these findings (Russnes et al., 2017). Five subtypes emerged from these studies are (Table 1.1):

1. Luminal-A: Enriched for the genes typically expressed by the luminal breast epithelial cells.
2. Luminal-B: Enriched for the genes typically expressed by the luminal breast epithelial cells and also shows elevated expression of the mitosis and cell proliferation related genes (as shown by the positivity of the Ki67 proliferative marker).
3. HER2 (ERBB2) overexpressing: ER-negative and often show elevated expression of ERBB2/HER2-related genes - therefore the name HER2 over-expression.
4. Basal-like: Usually have ER^-, PR^-, and $HER2^-$ (triple negative breast cancer), with expression of genes, such as basal cytokeratin, typically expressed in myoepithelial/basal epithelial cells - therefore the name basal-like.
5. Normal-like: IHC profile of the normal-like subtype is very similar to the luminal A, but the gene expression is like that of the normal breast tissues - so, the name normal-like.

Table 1.1 shows the intrinsic subtypes correlate extremely well with the IHC-defined subtypes, with the exception of the fifth subtype (normal-like) (Dai et al., 2015). The U.S. FDA approved test Prosigna is now widely used to diagnose the intrinsic breast tumor subtypes. The test relies on the modified definition of the original intrinsic subtype, the PAM50, and classifies each tumor to luminal A, luminal B, HER2-enriched, or basal-like subtype (Russnes et al., 2017).

Table 1.1: Breast tumor classification into intrinsic molecular subtypes based on the gene expression profiling. Source: (Dai et al., 2015).

Intrinsic Subtype	Immunohistochemistry Status	Grade	Outcome	Prevalence
Luminal A	[ER^+ | PR^+], $HER2^-$, $Ki67^-$	I | II	Good	23.7%
Luminal B	[ER^+ | PR^+], $HER2^-$, $Ki67^+$	II | III	Intermediate	38.8%
	[ER^+ | PR^+], $HER2^+$, $Ki67^+$		Poor	14%
HER2 over-expressing	[ER^- | PR^-], $HER2^+$	II | III	Poor	11.2%
Basal	[ER^- | PR^-], $HER2^-$, basal $marker^+$	III	Poor	12.3%
Normal-like	[ER^+ | PR^+], $HER2^-$, $Ki67^-$	I | II | III	Intermediate	7.8%

Even though the five subtypes are separated by their clinical and biological features, each of these subtypes also show a substantial variability within themselves. The basal-like subtypes share few similarities with the other groups but also express the most diversity within the group.

1.2 Triple negative breast cancer (TNBC)

Triple negative breast cancer (TNBC) is an aggressive subtype of breast cancer, which accounts for up to 15-20% of total breast cancer cases (Brouckaert, Wildiers, Floris, & Neven, 2012). TNBC, which was first officially characterized as a distinct type of breast cancer in the literature in 2005, lacks the clinical expression of three dominant receptors (<1% tumor cells express) - the ER, PR and HER2, commonly used for breast cancer subtyping (Brenton, Carey, Ahmed, & Caldas, 2005). "In absence of these receptors, TNBC is characterized by a critical lack of targeted therapies, as patients do not benefit from endocrine based therapies (Dent et al., 2007)"(Mittal, Camarillo, et al., 2020).

Compared to other breast cancers, TNBC patients show poor prognosis, increased distance recurrence and higher probability of metastasis in nervous system and visceral, including lung, liver, and brain metastasis (Rakha & Chan, 2011). In a study on 1,601 breast cancer patients with a median follow-up of 18.1 months, 180 (11.2%) TNBC patients showed increased likelihood of the distance recurrance "[hazard ratio = 2.6; 95% confidence interval = 2.0-3.5; $P < 0.0001$] and

death [hazard ratio = 3.2; 95% confidence interval = 2.3-4.5; P < 0.001)] within 5-years but not thereafter" (Dent et al., 2007).

1.2.1 Mammographic features of Triple negative breast cancer

The most common mammographic presentations of TNBC include mass "without associated calcification (49%-100% cases), hyperdense mass (89.3%) with oval (68.9%) or lobular (28.6%) shape and indistinct (42.9%) or circumscribed (32.1%) margins" (Schmadeka, Harmon, & Singh, 2014).

1.2.2 Histological features of Triple negative breast cancer

Histologically, most TNBC tumors are associated with high grade invasive ductal carcinoma at diagnosis. Additional TNBC histological features include, high histological grade, poor differentiation, central necrotic zones, pushing borders of invasion, cellular fibrous proliferation, and thick-walled vessels (Schmadeka et al., 2014). However, regional and racial profile often affect the clinical presentation and histological features of TNBC (Schmadeka et al., 2014). TNBCs share multiple histological features with basal-like breast cancers, however not all TNCs are basal-like or vice versa. Over 71 % of TNBCs are basal-like breast cancers, and 77% of basal-like are TNBC (Bertucci et al., 2008) (Figure 1.6). The basal-like breast cancers express common basal epithelial markers, such as "cytokeratin (CK) 5/6, CK14, CK17, laminin, epidermal growth factor receptor (EGFR), fatty acid binding protein, p16, and p53" (Schmadeka et al., 2014).

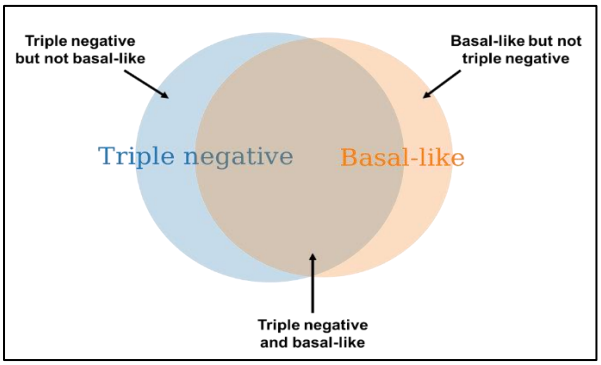

Figure 1.6: The distribution of triple negative and basal-like breast cancers. Over 71 % of TNBCs are basal-like breast cancers, and 77% of basal-like are TNBC (Bertucci et al., 2008).

1.2.3 Triple negative breast cancer statistics

TNBC contributes to 15-20% of total breast cancer cases (Brouckaert et al., 2012). TNBC is more frequent in younger as well as African-American and West African women, and women of low-socioeconomic status (Schmadeka et al., 2014). The rate of TNBC incidence in African women was two times higher as compared to non-Hispanic white women and three times higher as compared to Asian/Pacific Islander women (American Cancer Society, 2018). African ancestry is shown to correlate well with younger age of cancer diagnosis (48 for Ghanaian women, compared to 60.8 and 62.4 in for African Americans and white Americans, respectively), and increased frequency of TNBC (82.2% for Ghanaian women, compared to 26.4% and 16% for African Americans and white Americans, respectively) (Stark et al., 2010).

1.2.4 Triple negative breast cancer risk factors

A. Age

The TNBC incidence is higher in women aged less than 40, and they exhibit higher occurrence of ER-negative tumors (33.8%), compared to in women above 40 (21.9%) (Suba, 2014). Similarly, African-American premenopausal women showed higher TNBC prevalence compared to their postmenopausal counterparts in the 496 samples from Carolina breast cancer study (CBCS) (39% vs 14%) (Carey et al., 2006). It has been suggested that the higher proportion of TNBC incidence in younger women could be attributed to a lower fraction of ER-positive breast cancers due to preserved estrogen surveillance in young women (Suba, 2013, 2014).

B. Obesity

Factors including obesity and overweight are inconsistently associated with the increased risk for TNBC and other ER-negative breast cancers as well as probability of recurrence to the viscera and soft tissue, particularly in premenopausal women (Rose & Vona-Davis, 2009; Trivers et al., 2009; Vona-Davis et al., 2008; Yee, Mortimer, Natarajan, Dietze, & Seewaldt, 2020). In the U.S., 40.4 % of women were identified as obese in 2014, among these African-American women are more likely to be obese than white women and Hispanic women (Dietze, Chavez, & Seewaldt, 2018; Flegal, Kruszon-Moran, Carroll, Fryar, & Ogden, 2016). A 2009 report of 20-54

year old 476 Atlanta women (116 black and 360 white) between 1990 and 1992 reported that the TNBC women were more prone to be obese [odd ratio = 1.89; 95% confidence interval = 1.22, 2.92] (Trivers et al., 2009). Another study including both American-African and white women conducted by Millikan et al. using the CBCS sample also indicated that weight gain since childhood and higher upper body adiposity (waist-to-hip ratio) correlated with higher probability of TNBC (Millikan et al., 2008).

However, some conflicting reports indicate that the BMI and obesity are not consistently associated with increased TNBC risk as inverse association of high BMI with ER^-/PR^- breast cancer. A case-controlled Women's Contraceptive and Reproductive Experiences (CARE) study in non-Hispanic white and African-American women indicated an inverse association of high BMI at age 18 with pre-menopausal ER^-/PR^- breast cancer (Berstad et al., 2010). Another study by the Premenopausal Breast Cancer Collaborative group found no consistent relationship between BMI at 25-54 age and TNBC. Such conflicting outcomes could be attributed to the inability of BMI to reflect metabolic health as it remains an indirect measure of obesity (Yee et al., 2020). Since muscle weighs more than fat, healthy muscular people can be misclassified as obese, when BMI is used. Therefore, the link between parameters of metabolic health, such as insulin and Hemoglobin A1C and TNBC is being investigated.

i. Mechanisms of obesity related TNBC tumorigenesis

Various mechanisms by which obesity may contribute to TNBC tumorigenesis, progression, and metastasis are proposed. Sabol et al. demonstrated that obesity alters adipose stem cells to acquire tumorigenic characteristics and secrete elevated levels of leptin to upregulate the expression of SNAI2, interleukin 6 (IL6), serpine1, PTGS2, and TWIST1 genes in TNBC, which represent epithelial-mesenchymal transition (EMT) and cancer stem cell (CSC) pathways (Sabol et al., 2019). Insulin signaling can activate PI3K/AKT/mTOR to promote glycolysis and the downstream NF-κB mediated inflammatory cytokines, such as IL1, IL2, IL6, IL8, IL12 and TNFα (Yee et al., 2020). Activation of these pathways through insulin signaling can promote proliferation, apoptosis resistance, and invasion in TNBC.

C. Reproductive factors and use of oral contraceptive

A study investigating the effect of reproductive factors and use of oral contraceptive (OC) on the breast cancer incidence revealed a 2.9-fold elevated risk of TNBC among women aged 45-64, with history of OC usage before age 18 (H. Ma et al., 2010). Also, the longer duration of breast feeding decreased the risk of TNBC, which was also shown in another study by Ma et al. in 2014 (H. Ma et al., 2017). The risk of TNBC was 31% lower in parous women who breast fed for minimum 1 year compared to parous women without breastfeeding "[odds ratio = 0.69; 95% confidence interval = 0.50-0.96]" (H. Ma et al., 2017). Interestingly, race and age also altered the TNBC risk, as the risk of TNBC was 82% lower in parous African-American women, who breast fed for at least 6 month compared to parous women who did not breastfeed.

D. Genetic mutations

i. Germline mutations in BRCA1 and BRCA2

Germline mutations in breast cancer genes BRCA1 or BRCA2 are also commonly associated with the increased breast cancer risk, including TNBC (Garrido-Castro, Lin, & Polyak, 2019). The BRCA1 (located on chromosome 17q21) and BRCA2 (located on chromosome 13q12–q13) are involved in double-strand breaks (DSB) repair and play an important role in maintaining genomic stability (Duncan, Reeves, & Cooke, 1998; Gudmundsdottir & Ashworth, 2006). A Consortium of Investigators of Modifiers of BRCA1/2 (CIMBA) utilized "4,325 BRCA1 and 2,568 BRCA2 mutation carriers to analyze the pathology of invasive breast, ovarian, and contralateral breast cancers" (Mavaddat et al., 2012). They reported that "the portion of triple-negative tumors decreased with age at diagnosis in BRCA1 carriers but increased with age at diagnosis of BRCA2 carriers". The 69% of total breast cancers in women harboring BRCA1 mutations are TNBC and up to 20% of women with TNBC harbor BRCA1 mutations (Greenup et al., 2013). The germline mutation in BRCA1 gene predisposes for the basal-like breast cancers, and thus majority of the basal-like TNBCs are linked with the BRCA mutation (Sørlie et al., 2003; Yao et al., 2017). Figure 1.7 shows the origin of basal-like and non-basal-like TNBC (Yao et al., 2017).

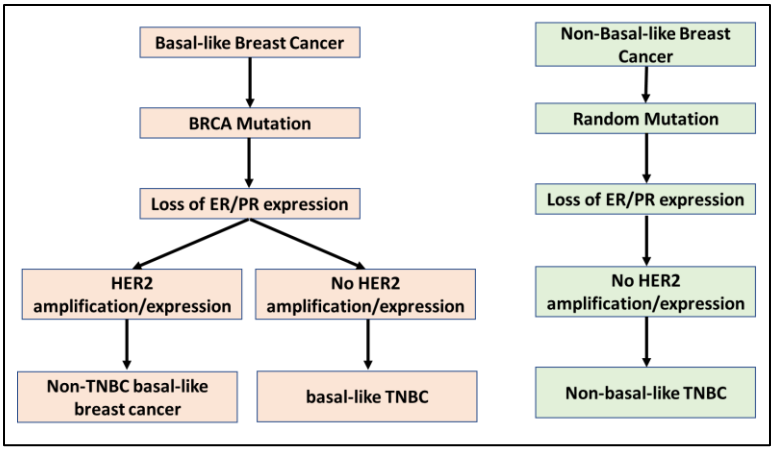

Figure 1.7: Origin of basal-like and non-basal-like TNBC. Non-TNBC basal-like breast cancer and basal-like TNBC originate from basal-like breast cancers upon BRCA mutation and loss of ER/PR expression and depending upon the expression status of HER2. "Non-basal-like triple negative breast cancer may originate from non-basal-like breast cancer without BRCA mutation" (Yao et al., 2017).

ii. Somatic mutations

The most frequently somatically mutated or lost genes in TNBC are tumor suppressors p53, retinoblastoma protein (Rb), and phosphatase and tensin homolog (PTEN) (Engebraaten, Vollan, & Børresen-Dale, 2013). Approximately, 53.8 to 85.7% of the TNBCs harbor somatic mutations in p53, and nearly all basal-like tumors accompany loss of p53 function as revealed by the pathway analysis (Yao et al., 2017). The basal-like tumors carry nonsense and frame-shift type mutations, compared to more frequently found missense mutations in luminal tumors (Yao et al., 2017). "The combined loss of activity of p53, Rb, and BRCA pathways is responsible for the high level of genomic instability observed in basal-like tumors" (Yao et al., 2017), including heavy chromosomal changes, translocations, and losses (Perou, 2010).

1.2.5 Triple negative breast cancer subtypes and molecular heterogeneity

"Triple-negative breast cancer (TNBC) is a highly diverse group of cancers, and subtyping is necessary to better identify molecular-based therapies" (Lehmann et al., 2011). In a seminal work, Lehmann et al. analyzed 21 breast cancer datasets for the gene expression and identified 587 TNBC cases (Lehmann et al., 2011). They studied the expression profile of 13,060 unique genes and ontologies to identify six different TNBC subtypes, "including 2 basal-like (BL1 and BL2),

an immunomodulatory (IM), a mesenchymal (M), a mesenchymal stem–like (MSL), and a luminal androgen receptor (LAR) subtype" (Lehmann et al., 2011), as described below (Figure 1.8):

A. Basal-like 1 (BL1) subtype

The BL1 subtype is characterized by the increased expression of genes associated with cell proliferation (e.g. AURKA, AURKB, MYC, and TTK etc.) and DNA damage response (e.g. CHEK1, FANCA, FANCG, and MDC1 etc.) pathways. The expression of the proliferation marker Ki67 is also upregulated in BL1 subtype.

B. Basal-like 2 (BL2) subtype

The BL2 subtype show unique gene expression signature with overexpression genes involving growth factor signaling (e.g. EGF, MET, Wnt/β-catenin, NGF, and IGF1R pathways), glycolysis and gluconeogenesis.

The TNBC patients with basal-like (BL1 and BL2) subtype respond better to antimitotic agents-based therapy, such as taxanes (paclitaxel and docetaxel), compared to M and LAR subtypes as indicated by the significantly higher pathological complete response (pCR) (63% vs 31% for M and 14% for LAR).

C. Immunomodulatory (IM) subtype

The IM subtype is characterized by the enrichment for gene ontologies in immune cell processes, including B cell receptor, T cell receptor, NK cell and DC signaling pathways. As well as genes for cytokine signaling (cytokine, IL-7 and IL-12 pathways), and other immune signaling pathways (NF-κB, TNF, and JAK/STAT signaling), which are immune cell specific are also overexpressed in IM subtype.

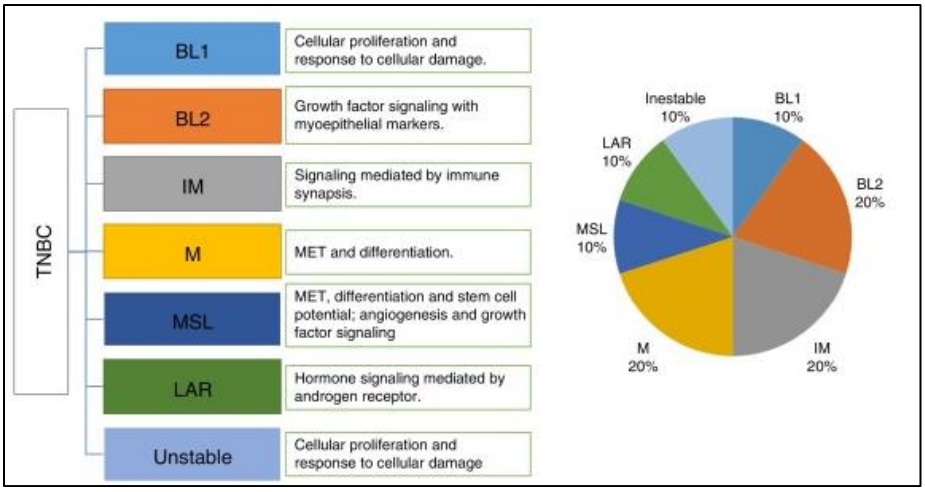

Figure 1.8: Triple negative breast cancer classification by Lehman et al., gene ontology and proportion. TNBC subtypes include "2 basal-like (BL1 and BL2), an immunomodulatory (IM), a mesenchymal (M), a mesenchymal stem–like (MSL), and a luminal androgen receptor (LAR) subtype" (Lehmann et al., 2011). Reproduced under Creative Commons Attribution-Non Commercial-No Derivatives License (CC BY NC ND) from (Uscanga-Perales, Santuario-Facio, & Ortiz-López, 2016).

D. Mesenchymal (M) and mesenchymal stem–like (MSL) subtypes

The M and MSL subtypes show enrichment for genes in "cell motility (Rho pathway), cellular differentiation, and growth pathways (ALK pathway, TGF-β signaling, and Wnt/β-catenin pathway)"(Varghese et al., 2018). Both subtypes are characterized by the enrichment in EMT genes (e.g. MMP2, ACTA2, TWIST1, ZEB1, ZEB2, and reduced E-cadherin level etc.), and frequently have elevated abnormalities in the PI3K/AKT/mTOR pathway. "However, unique to the MSL are genes representing components and processes linked to growth factor signaling pathways that include inositol phosphate metabolism, EGFR, PDGF, calcium signaling, G-protein coupled receptor, and ERK1/2 signaling as well as ABC transporter and adipocytokine signaling" (Lehmann et al., 2011). Compared to M subtype, MSL has low levels of proliferation genes, but greater enrichment in genes linked with stem cells (e.g. ALDHA1, BCL2, ABCA8, ABCB1, and THY1 etc.), HOX genes (e.g. HOXA5, HOXA10, MEOX1, and MEOX2 etc.), and mesenchymal stem cell–specific markers (ENG, NGFR, THY1, KDR, and VCAM1). The signaling pathways expressed differentially for M and MSL subtypes share morphological similarity with a class of rare, malignant form of chemoresistant breast cancer with mesenchymal/sarcomatoid or squamous features and termed as metaplastic breast cancer (Gibson, Qian, Ku, & Lai, 2005). The MSL

subtype tumors also show low expression of claudins 3, 4, and 7, correlating with claudin-low breast cancer subtype.

Lehmann et al. also used GSE-10890 and ETABM-157 GE data sets to identify 30 nonoverlapping TNBC cell lines and classified them into the six TNBC subtypes using their gene expression profile (Lehmann et al., 2011). *The MDA-MB-231 cell line, a representative model of the aggressive TNBC utilized in this dissertation, was classified into MSL subtype*.

E. Luminal androgen receptor (LAR) subtype

The LAR subtype shows the most unique gene expression profile among six TNBC subtypes. Despite being ER-negative, the tumors in LAR subtypes show gene enrichment of "hormonally regulated pathways, including steroid synthesis, porphyrin metabolism, and androgen/estrogen metabolism" (Gerratana, Fanotto, Pelizzari, Agostinetto, & Puglisi, 2016). The androgen receptor (AR) expression is 9-fold higher in LAR subtype compared to other subtypes, with expression of downstream AR targets and coactivators (e.g. ALCAM, DHCR24, FASN, and SPDEF etc.). Consequently, the androgen signaling is responsible for the unique gene expression profile of the LAR subtype, offering an exciting therapeutic opportunity in this TNBC subtype, by blocking androgen signaling. LAR subtype contribute to 11% of the total TNBC population, with poor 10% pCR for sequential taxane and anthracycline-based cytotoxic neoadjuvant chemotherapy, compared to 52% for those with BL1 TNBC (Masuda et al., 2013). However, in clinical studies in AR-positive TNBC, anti-androgen agents bicalutamide and enzalutamide showed a clinical benefit rate of 19% and 29%, respectively at 24 weeks.

In summary, the gene expression studies of TNBC tumors have revealed the heterogeneity and various TNBC subtypes of clinical importance. These studies have revealed features and biomarkers, which could be exploited to design molecular therapies for TNBC and better patient prognosis.

1.2.6 Overview of major signaling pathways in triple negative breast cancer

The oncogenesis, proliferation, survival, migration, invasion, metastasis, inflammation and development of drug-resistance in TNBCs is fueled by aberrant activation of various signaling

pathways, including PI3K/Akt/mTOR, Ras/MAPK, Notch, NF-κB, and Wnt/β-catenin. This section presents an overview of the role these pathways play in TNBC.

A. PI3K/Akt/mTOR signaling keep only a few lnes, rest use in discussion-for all the pathways

The phosphoinositide 3 (PI3)-kinase (PI3K)/Akt and the mammalian (or mechanistic) target of rapamycin (mTOR) are two signaling pathways, which are intertwined in certain sense that they are often regarded as a single pathway (Porta, Paglino, & Mosca, 2014). The tumor environment is characterized by intrinsic stress due to low supply of nutrients, oxygen, and low pH. The PI3K/Akt plays a key role in cell survival during these stressful conditions. The mTOR is a serine/threonine kinase expressed ubiquitously in mammalian cells, which plays a key role in integrating the signaling initiated by various stimuli, including growth factors and nutrient intake to the downstream cellular signaling and protein synthesis essential for growth, cell cycle progression, and metabolism (Porta et al., 2014).

Genetic alterations caused by the somatic mutations and/or gains and losses of function in key genes affect the PI3K/Akt/mTOR pathway, disturbing the cell growth control in various cancers, including breast cancers (Porta et al., 2014). The activation of PI3K/Akt/mTOR promotes cell growth, survival, tumor proliferation, and endocrine resistance in breast cancers (Paplomata & O'Regan, 2014).

"PI3K is the most commonly mutated pathway in TNBC" (Conway, Iglesias, Hired, Rutledge, & Kirmani, 2019). The overexpression of an upstream PI3K regulator epidermal growth factor receptor (EGFR), gain of function mutations in PI3K catalytic subunit α (PIK3CA), and loss of function mutations in key downstream molecules PTEN and proline-rich inositol phosphate primarily cause the aberrant activation of the PI3K/Akt signaling (Cossu-Rocca et al., 2015; Davis et al., 2014; Ooms et al., 2015). The PI3K/Akt/mTOR inhibition using NVP-BEZ235 dual PI3K/Akt/mTOR inhibitor re-sensitized the cisplatin resistant MDA-MB-231 and HCC38 TNBC cells to cisplatin, and also showed synergistic effects with carboplatin in TNBCs (Gohr, Hamacher, Engelke, & Kassack, 2017; Montero et al., 2014). These studies highlight that targeting PI3K/Akt/mTOR signaling in TNBC could be an exciting avenue.

B. Ras/MAPK signaling pathway

Through retrovirus research, the first human proto-oncogene Harvey rat sarcoma viral oncogene homolog (HRAS) was discovered in 1982, which stimulated an intensive research on targeting RAS/MAPK pathway for cancer treatment (A. D. Cox & Der, 2010). The external stimuli, including receptor-specific ligands activate receptor tyrosine kinases (RTKs), such as EGFR and HER2 to indirectly activate Ras family members (H-Ras, K-Ras, N-Ras, and M-Ras) (Giltnane & Balko, 2014). The activation of Ras results into a kinase signaling cascade through Raf, MEK , and ERK1/2 (known as MAPK1/3) to the nucleus to activate the key downstream transcription factors, including ELK1, ETS1/2, NF-κB, and MYC to trigger the transcription of genes responsible for cancer cell cycle progression, survival, proliferation, and invasion (Giltnane & Balko, 2014; Schäfer, Tchernitsa, & Sers, 2006). The mutations in Ras and Raf are common in various cancers, and small molecule inhibitors for Raf and MEK are highly effective against BRAF-mutant advanced melanomas (Giltnane & Balko, 2014; Jang & Atkins, 2014). However, the frequency of mutation in Ras and Raf family remains low for breast cancer and the Ras/MAPK pathway can activated by the overexpression of RTKs, such as EGFR and HER2 (Giltnane & Balko, 2014). The high levels of ERK1/2 phosphorylation are more frequent in metastatic sites compared to primary tumors and in basal-like breast cancers/TNBCs compared to other breast cancer subtypes (Adeyinka et al., 2002; Sivaraman, Wang, Nuovo, & Malbon, 1997). Moreover, compared to other subtypes, the aberrant activation of the Ras/MAPK pathway is more frequent in basal-like breast cancers and TNBCs, and forms a major component of their oncogenic activity (Balko et al., 2012; Giltnane & Balko, 2014). Despite these reports, the role of Ras/MAPK pathway remains controversial due to conflicting evidences and the lack of proper understanding in TNBCs (Giltnane & Balko, 2014).

Since TNBCs are characterized by the highest number of CNA, alternative mechanisms of Ras/MAPK pathway activation through these CNA resulting in the amplification or gain of function of KRAS and BRAF have also been proposed for basal-like breast cancers and TNBCs (Craig et al., 2013). In addition, analogous to the loss of negative regulation of PI3K/Akt signaling pathway upon PTEN mutation, the loss of negative regulation of Ras upon neurofibromin (NF1) mutation could result in aberrant activation of Ras/MAPK pathway in TNBCs (Sabova, Kretova, & Luciakova, 2013). The microRNAs (miRNAs), which specifically target KRAS are deregulated in basal-like breast cancers and TNBCs, and may serve as an additional mechanism of the aberrant

activation of the Ras/MAPK pathway in these breast cancers (Kopp, Wagner, & Roidl, 2014; Shah & Calin, 2011).

The Ras/MAPK inhibition using MEK inhibitors decreased the proliferation of basal-like breast cancer and TNBC cell lines, compared to luminal-like or ER-positive breast cancer cells (Hoeflich et al., 2009; Jing et al., 2012; Mirzoeva et al., 2009). Moreover, a good *in vivo* response for MEK inhibitors in combination with chemotherapy was observed in xenografts and patient derived (PDX) tumor models of basal-like breast cancer, giving hopes against TNBC (Balko et al., 2012; Hoeflich et al., 2009).

C. Notch signaling

The Notch signaling pathway is a highly conserved pathway in most animals, from sea urchins to humans, and plays a key role in controlling the differentiation of breast epithelial cells during normal development (Kontomanolis et al., 2018). The Notch signaling is dysregulated in various cancers, including TNBCs, which contributes to oncogenesis, renewal of stem cells, angiogenesis, and chemoresistance (Krishna et al., 2019). The overexpression of notch receptor Notch-1 and its ligand Jagged-1 is correlated with the low overall survival in breast cancer patients (Reedijk et al., 2005). The Notch signaling is usually triggered when transmembrane Notch ligands (named Delta-like and Jagged-like in humans) bind to Notch receptors of neighboring cells, leading to the cleavage and release of the notch receptor intracellular domain NICD (Kopan, 2012). The NICD then translocates to nucleus to activate the "transcriptional complexes containing the DNA-binding protein CBF1/RBPjk/Su(H)/Lag1 (CSL)" (McManus, Weiss, & Hughes, 2014) to regulate the expression of genes implicated in cell proliferation, cell fate, differentiation, and chemo-resistance.

The Notch pathway plays an important role in cancer stem cells maintenance and expansion and in TNBCs the "Notch receptors are associated with the regulation of tumor-initiating cells (TICs) behavior" (Giuli, Giuliani, Screpanti, Bellavia, & Checquolo, 2019). The Notch-1 receptor expression is particularly upregulated in BL1 and MSL TNBC subtypes. The inhibition of Notch-1 potentiated the anticancer effects of paclitaxel in MDA-MB-231 TNBC cells. The knockdown of Notch-1 significantly reduced the TNBC tumor formation and depleted the stem-like cell subpopulation, and Notch-3 inhibition also impaired the invasive potential of MDA-MB-231 TNBC cells (reviewed in Giuli, Giuliani, Screpanti, Bellavia, & Checquolo, 2019). The silencing

of Notch-4 reduced the tumorigenesis and tumor volume in MDA-MB-231 TNBC cells xenograft SCID mice model (Nagamatsu et al., 2014). These observations highlight that the Notch signaling could be a possible therapeutic lead in TNBCs.

D. NF-κB signaling

The nuclear factor-kappaB (NF-κB) is a family of five proinflammatory transcription factors: p65 (RelA), RelB, c-Rel, p50/p105 (NF-κB1), and p52/p100 (NF-κB2). A dimer composed of two RelA-family subunits, most commonly p50/RelA is sequestered to the perinuclear cytoplasm by IκB proteins. The tumor necrosis factor alpha (TNFα), a multifunctional cytokine binds to its receptor tumor necrosis factor receptor 1 (TNFR1) to trigger canonical NF-κB signaling. Upon trimerization of TNFR1, complex I is recruited, eventually leading to the nuclear translocation of p50/RelA to work as a transcription factor to regulate several pro-survival genes (Khoshnan et al., 2000; O Micheau, Lens, Gaide, Alevizopoulos, & Tschopp, 2001; Olivier Micheau & Tschopp, 2003; Wirth & Baltimore, 1988).

Upon inhibition of complex I or downstream canonical pathway, TNFR1 instead recruits complex II, which activates caspase-8 leading to apoptosis (Olivier Micheau & Tschopp, 2003). RIP1, a key kinase of complex I is also cleaved by caspase-8, thereby inhibiting the pro-survival canonical signaling (Y. Lin, Devin, Rodriguez, & Liu, 1999).

On the other hand, the complex I mediated canonical signaling pathway elevates the expression of cFLIP, a complex II inhibitor. Therefore, upon TNFR1 activation, the cell outcome is determined by the activation of complex I or complex II

The constitutive activation of NF-κB signaling is implicated in promoting "hormone-independent, invasive, high-grade, and late-stage tumor phenotype" (W. Wang, Nag, & Zhang, 2015). NF- κB signaling is constitutively active in MDA-MB-231 TNBC cells. The direct inhibition of NF-κB signaling or knockout of TNF-α to prevent positive mechanism induces apoptosis in both ER-positive and negative breast cancer cells and in other cancer cell lines (Ciucci et al., 2006; Horie et al., 2006; N. M. Patel et al., 2000; Pileczki, Braicu, Gherman, & Berindan-Neagoe, 2012). Considering this, the interest has been growing in finding novel NF-κB inhibitors to target TNBCs.

E. Wnt/β-catenin signaling

The Wnt/β-catenin signaling is a highly conserved pathway through evolution, which is dysregulated in various cancers, including TNBCs, and contributes to proliferation and survival (Zeng, Apte, Cieply, Singh, & Monga, 2007), and EMT (Sánchez-Tilló et al., 2011). "In the absence of Wnt-signal (Off-state), β-catenin, an integral E-cadherin cell-cell adhesion adaptor protein and transcriptional co-regulator, is targeted by coordinated phosphorylation by CK1 and the APC/Axin/GSK-3β-complex leading to its ubiquitination and proteasomal degradation through the β-TrCP/Skp pathway" (Cadigan, 2003). In on-state, "Wnt proteins, by binding to frizzled receptors and the LRP co-receptor, act to suppress the activity of glycogen synthase kinase-3β (GSK-3β)" (Pai et al., 2017). The ZNRF3 facilitates degradation of Wnt receptor working as tumor suppressor. This leads to the cytoplasmic accumulation of β-catenin, which eventually translocates to the nucleus and associates with TCF/LEF-family transcription factors to regulate the expression of genes implicated in proliferation, EMT, and migration, such as Cyclin D1 and c-myc (Pai et al., 2017).

The knockdown of β-catenin significantly reduced the tumor size and growth rate in a TNBC xenograft mice model, highlighting the importance of Wnt signaling in TNBC (Xu, Prosperi, Choudhury, Olopade, & Goss, 2015). Moreover, a cohort study on patient samples revealed the overexpression of elevated Wnt/β-catenin signaling, which correlated with higher tumor grade, increased lung and brain metastasis, and poorer prognosis (Dey et al., 2013).

1.2.7 Overview of metabolism in triple negative breast cancer

In presence of the oxygen, normal cells utilize glycolysis, followed by the citric acid (TCA) cycle and oxidative phosphorylation (OXPHOS) (Figure 1.9) (Weinberg, 2014, p. 54).

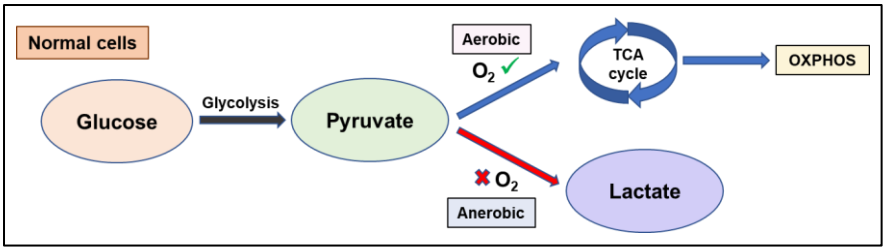

Figure 1.9: A schematic representation of glucose metabolism in normal cells. In presence of the oxygen (aerobic), normal cells utilize glycolysis, followed by the citric acid (TCA) cycle and oxidative phosphorylation (OXPHOS). In hypoxic or anerobic (low oxygen) conditions, the normal cells utilize glycolysis to generate ATP, and shift away from mitochondrial metabolism (i.e. TCA cycle and OXPHOS) in a phenomenon called "anerobic glycolysis".

In normal cells, the glucose transporter 1 (GLUT1) facilitates the energy-independent and concentration gradient-based transport of glucose across plasma membrane. One glucose molecule is broken down into two pyruvate molecules and two net molecules of ATP through a series of reactions in the glycolysis pathway. The pyruvate is transported to the mitochondria, where it is oxidized by the pyruvate dehydrogenase (PDH) into acetyl coenzyme A (acetyl CoA) for processing in the TCA cycle. TCA cycle generates six nicotinamide adenine dinucleotide (NADH), two FADH2, and two ATP from two acetyl CoA molecules. The high energy carriers NADH and flavin adenine dinucleotide (FADH2) are utilized in the OXPHOS to produce remaining ATP. Altogether mitochondrion can generate as much as 36 ATP molecules per glucose molecule. However, in hypoxic or anerobic (low oxygen) conditions, the normal cells utilize glycolysis to generate ATP, and shift away from mitochondrial metabolism (i.e. TCA cycle and OXPHOS) in a phenomenon called "anerobic glycolysis" (Figure 1.9). The pyruvate kinase M2 (PKM2) diverts pyruvate generated from the glycolysis to lactate dehydrogenase (LDH) and produces lactate, which is then secreted from cells. Since the participation of mitochondrial metabolism is limited and only glycolysis is used, this process is ATP inefficient as only two ATPs per glucose molecule are generated.

The cancer cells harbor different energy metabolism compared to normal cells, a trait first reported in 1924 by the Nobel laureate Otto Warburg. Cancer cells exclusively utilize the glycolysis pathway to convert glucose to lactate, but not TCA cycle and OXPHOS, irrespective of the oxygen availability (Figure 1.10) (Weinberg, 2014, p. 54). Warburg discovered this peculiar tendency of cancer cells to limit themselves to convert glucose to lactate, even in the exposure of

oxygen, and termed this process as "aerobic glycolysis" (later called the "Warburg effect", in honor of Otto Warburg).

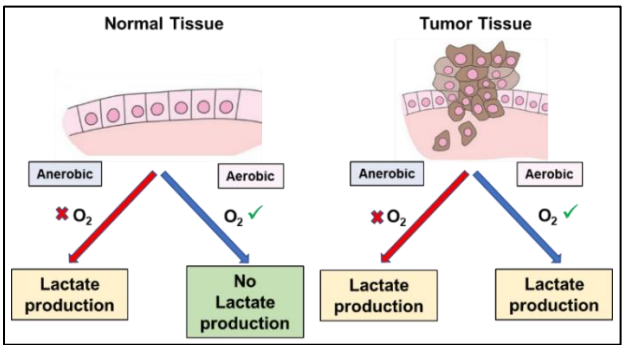

Figure 1.10: A schematic representation of Warburg effect in cancer cells. While normal cells only convert glucose to lactate in anerobic condition, cancer cells convert glucose to lactate, irrespective of the presence of the oxygen. This unusual phenomenon in cancer cells is called "aerobic glycolysis" or Warburg effect.

This metabolic shift in cancer cells could be in parts due to the hypoxia caused by the inadequate supply of oxygen to cancer cells within the tumors, forcing cells to follow this inefficient ATP production pathway - similar to normal cells going through anerobic glycolysis under hypoxia. However, this fails to explain the metabolic shift observed even in the abundance of oxygen, as seemingly counter intuitive, cancer cells still do not prefer to generate larger amount of ATP using efficient TCA cycle and OXPHOS mitochondrial pathways (Figure 1.10). Alternate explanation for this behavior develops from the possibility that glycolysis also plays other important role in cancer cell proliferation and growth, which is independent of the ATP production. The intermediates (nucleosides and amino acids) produced during the glycolysis, serve as precursors for biosynthetic reactions responsible for cell proliferation and growth. For example, a glycolysis intermediate glucose-6-phosphate can generate nucleic acids through pentose phosphate pathway (PPP) to produce NADPH and ribose-5-phosphate, a nucleotide precursor to fuel the cell proliferation and growth. This state of cancer cells is similar to the metabolic state of the rapidly dividing normal cells (Weinberg, 2014, p. 54).

A. Metabolic vulnerabilities in triple negative breast cancer

"Recent reports suggest that TNBC harbor alterations in their metabolism, which correlate with the increased growth, proliferation, invasiveness, chemotherapeutic resistance and poor therapeutic response (S. Kim, Kim, Jung, & Koo, 2013; Lanning et al., 2017; Liangliang Shen et al., 2015)" (Mittal, Aryal, et al., 2019). TNBCs show "higher rates of glycolysis compared to ER-positive tumors, with concomitant lactate production (McCleland et al., 2012). Compared to ER-positive, TNBCs also have increased glycolytic intermediates, including glucose-6-phosophate, which is utilized in the pentose phosphate pathway to synthesize nucleic acid (Jóźwiak, Forma, Bryś, & Krześlak, 2014; Kanaan et al., 2014)" (Mittal, Aryal, et al., 2020). These distinct metabolic signatures of the TNBC tumors, as shown in Figure 1.11 highlight their vulnerabilities, providing an exciting avenue to specifically target TNBC by therapeutic metabolic manipulation.

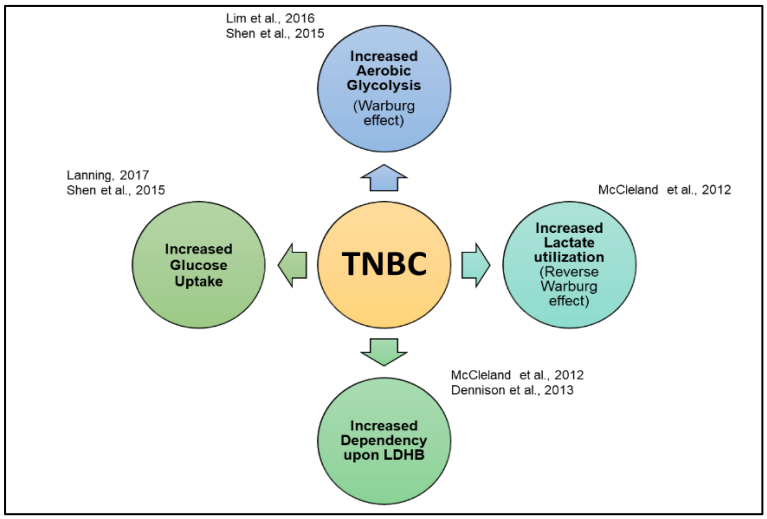

Figure 1.11: The distinct metabolism in the TNBC tumors. TNBCs harbor increased glucose uptake, increased aerobic glycolysis, increased lactate utilization and reverse Warburg effect, and the increased dependency upon lactate dehydrogenase B (LDHB) (Dennison et al., 2013; Lanning et al., 2017; Lim et al., 2016; McCleland et al., 2012; Liangliang Shen et al., 2015). Therefore, the inhibition of glycolysis and LDHB sensitizes TNBCs to therapy.

i. Increased glucose uptake in triple negative breast cancer

The glucose uptake and the expression of its transporter GLUT1 are upregulated in TNBCs, and they promote cell proliferation and invasion (Oh, Kim, Nam, & Shin, 2017). Grover-McKay et al. showed that the GLUT1 expression was correlated with the invasive ability of breast cancer cells and demonstrated a significantly increased expression of GLUT1 in highly invasive MDA-MB-231 TNBC cells (Grover-McKay, Walsh, Seftor, Thomas, & Hendrix, 1998). In a study comparing the GLUT1 expression in patients with basal-like breast cancers (authors defined as "negative to ER, PR, and HER2 plus the expression CK5/6 and/or EGFR") to non-basal-like breast cancers, the GLUT1 was expressed in 42 (76.4%) of 55 basal-like breast cancers (Hussein et al., 2011). Moreover, these authors reported that "GLUT1 expression was significantly associated with high histologic grade, ER-negativity, PR-negativity, CK5/6-positivity, EGFR expression, and high p53 expression ($P < .001$)" (Hussein et al., 2011). Basal-like TNBC frequently overexpress "USP6NL, a GTPase-activating protein involved in signal transduction regulation" (X. Sun et al., 2020). The knockdown of USP6NL downregulates the EGFR/Akt signaling and accelerates GLUT1 degradation to specifically target aggressive basal-like TNBC tumors (Avanzato et al., 2018).

Metformin, a widely used anti-diabetic agent and mitochondrial complex I inhibitor significantly downregulated a number of GLUT-family transport proteins (GLUT1, GLUT10, GLUT12, GLUT14, and glucose-6-phosphate transporter) to target TNBC cell proliferation, colony growth, cell cycle arrest, and population of stem cells (Alimova et al., 2009; Shi et al., 2017; Wahdan-Alaswad, Edgerton, Salem, & Thor, 2018).

ii. Increased aerobic glycolysis (Warburg effect) in triple negative breast cancer

Upon transportation into the cells, glucose is utilized in the aerobic glycolysis pathway in a series of ten reactions to produce pyruvate, as shown in Figure 1.12. TNBC cells display increased glycolysis and lactate production compared to other breast cancer cells, as revealed by the analysis of extracellular acidification rate and oxygen consumption rate to investigate the relative contribution of glycolysis and mitochondrial metabolism in a panel of breast cancer cells (Lim et al., 2016).

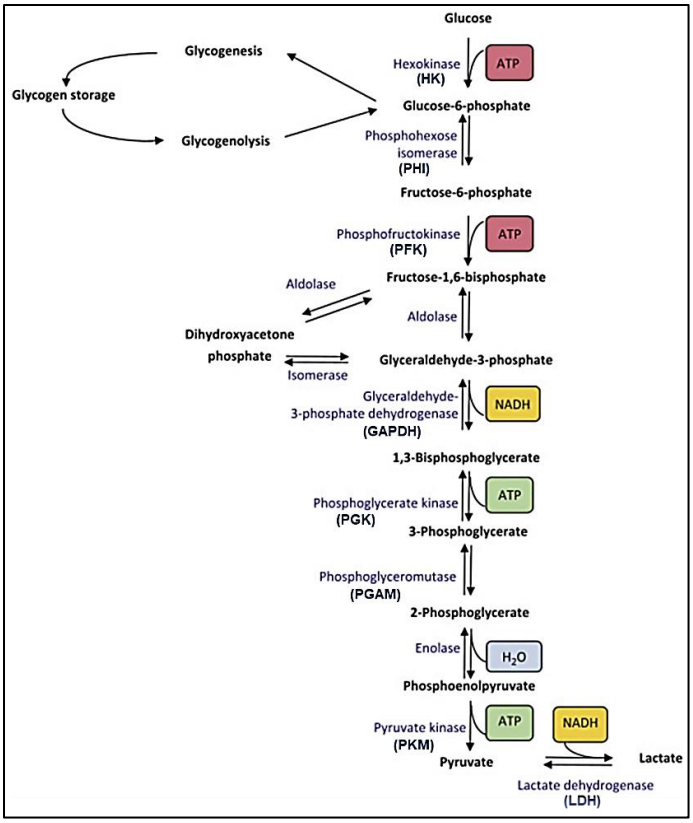

Figure 1.12: The glycolysis pathway. Adapted with permission from (Werner, Doenst, & Schwarzer, 2016).

Several key glycolytic enzymes are preferentially upregulated in TNBC compared to other breast cancer subtypes. The Hexokinase (HK) family enzymes (HK1 and HK2) play an important role in the first step of glycolysis by catalyzing the phosphorylation of glucose. The EGFR signaling upregulates HK2 activity and elevate aerobic glycolysis in TNBC cells, resulting in build-up of intermediates to stimulate tumor growth and immune escape (Lim et al., 2016). In 54 breast cancer mastectomy samples, the levels of HK and phosphofructokinase (PFK) were higher, compared to other breast cancer samples and correlated with the invasiveness and aggressiveness. PFK is the most important regulator in mammalian glycolysis, which "catalyzes the conversion of fructose 6-phosphate and ATP to fructose 1,6-bisphosphate and ADP" (Krüger et al., 2013).

Aldolase family members (ALDOA, ALDOB, and ALDOC) are the fourth enzyme in the glycolysis (Chang, Yang, Tien, Yang, & Hsiao, 2018). The ALDOA has a major function in glycolysis, as it maintain the glucose homeostasis (Chang et al., 2018) and its inhibition disrupts

the “feed-forward loop of glycolysis to inhibit the proliferation of cancer cells (Grandjean et al., 2016)” (Mittal, Aryal, et al., 2019). The ALDOC is also involved in fructolysis and is overexpressed in multiple cancers (Chang et al., 2018). The knockdown of ALDOA or the combination of ALDOA, ALDOB, and ALDOC inhibited glycolysis in MDA-MB-231 TNBC cells (Grandjean et al., 2016).

The Glyceraldehyde 3-phosphate dehydrogenase (GAPDH) enzyme that catalyzes the sixth step of glycolysis, converting glyceraldehyde 3-phosphate to 1,3-bisphosphate, and may play a key role in TNBC progression via cell cycle pathway (Peng, Ma, Xia, & Zheng, 2017). The seventh enzymes in the glycolysis are phosphoglycerate kinase (PGK) family enzymes (PGK1 and PGK2), which catalyze the conversion of 1,3-Biphosphoglycerate to 3-Phosphoglycerate and ATP. Increased PGK1 expression is correlated with higher breast tumor grade in patients and “is a prognostic biomarker of chemoresistance to paclitaxel treatment in breast cancer” (S. Sun et al., 2015). Grandjean et al., reported that the combined knockdown of PGK1 and PGK2 inhibited glycolysis in MDA-MB-231 TNBC cells (Grandjean et al., 2016).

The eighth enzymes in the glycolysis are phosphoglycerate mutase (PGAM) family enzymes (PGAM1, PGAM2, and PGAM3), which catalyze the conversion of 3-phosphoglycerate to 2-phosphoglycerate. PGAM1 can modulate the cytoskeleton to regulate breast cancer cell mobility and migration (Gandhi & Das, 2019). PGAM1 promotes homologous recombination repair of DSBs induced by DNA-damaging agents in a metabolic-dependent manner, and PGAM1 inhibition sensitizes BRCA1/2-proficient MDA-MB-231 TNBC tumors toward the PARP inhibitor olaparib (Qu et al., 2017).

The ninth and penultimate enzymes in the glycolysis pathway are enolase family enzymes (ENO1 and ENO2), which catalyze the conversion of 2-phosphoglycerate to phosphoenolpyruvate. “The ENO1 is a potential biomarker of TNBC, and its function in glycolysis consistent with the distinct TNBC metabolism compared to other breast cancer subtypes (Miah et al., 2017; Vergara et al., 2013)” (Mittal, Aryal, et al., 2019). A study integrating transcriptomic and genomic data of TNBC revealed that ENO2 is overexpressed in the TNBC glycolytic subtypes, along with other key glycolytic enzymes, such as GAPDH, triosephosphate isomerase 1 (TPI1), and lactate dehydrogenase B (LDHB) (Gong et al., 2019).

The final step in the glycolysis pathway involve pyruvate kinase muscle (PKM) family enzymes (PKM1 and PKM2), which work as rate-limiting enzymes in the conversion of

phosphoenolpyruvate to pyruvate. The PKM1 and PKM2 are overexpressed in TNBC cells and tissues, and the knockdown of PKM impaired TNBC cell proliferation, migration, and induced cell cycle arrest, which was accompanied by the suppression of NF-κB pathway (C. Ma et al., 2019).

In aerobic glycolysis, PKM2 diverts pyruvate generated from the glycolysis to lactate dehydrogenase (LDH) (Weinberg, 2014, p. 54). The LDH subunits LDHA and LDHB catalyze the interconversion of pyruvate to lactate, which is then secreted from cells. The LDHA levels correlate with the TNBC malignancy its inhibition prevents brain metastasis (Dong et al., 2017). The TPI1 and LDHB are highly expressed in basal-like immune-suppressed subtype of TNBC tumors (Jézéquel et al., 2019).

TNBCs are now known to have a fundamentally altered metabolic profile, which provides opportunities of potential therapeutic avenues against TNBC.

iii. Reverse Warburg effect in triple negative breast cancer

In 2009, Pavlides et al. first hypothesized the "reverse Warburg effect", in which cancer cells secrete reactive oxygen species (ROS) to induce oxidative stress on neighboring cancer-associated fibroblasts (CAF) and trigger aerobic glycolysis in CAF to produce high energy metabolites - pyruvate and lactate, which are then transported to cancer cells (called lactate shuttle) via monocarboxylate transporter (MCT) and utilized to fuel oxidative metabolism and produce ATP (Pavlides et al., 2009). A schematic diagram of reverse Warburg effect is shown in Figure 1.13.

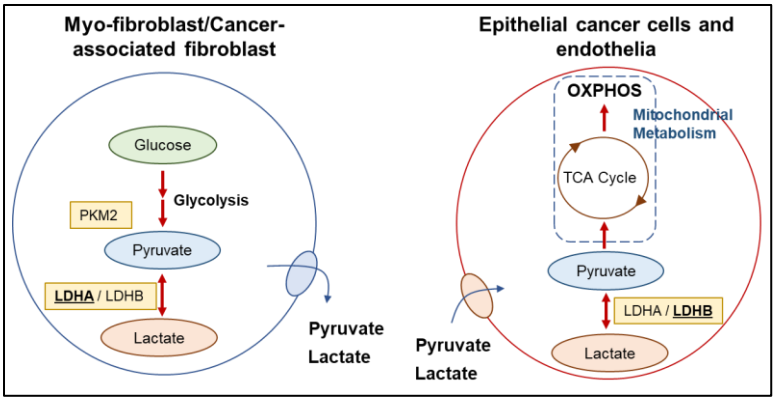

Figure 1.13: The reverse Warburg effect. LDHA favorably converts pyruvate to lactate (in normal fibroblasts), and LDHB favors conversion of lactate to pyruvate (in cancer cells) (Pavlides et al., 2009).

The net charge on LDHA is -6 and it has high affinity for pyruvate, and with the net charge of +1 LDHB shows higher affinity for lactate (Urbańska & Orzechowski, 2019; Valvona, Fillmore, Nunn, & Pilkington, 2016; Ždralević et al., 2018). Considering these affinities, while LDHA favorably converts pyruvate to lactate, LDHB favors conversion of lactate to pyruvate (Urbańska & Orzechowski, 2019). Therefore, LDHB must play a key role in the reverse Warburg effect, as cancer cells preferentially rely upon LDHB to convert the secreted lactate to pyruvate.

TNBCs harbor a comprehensive shift in the metabolism to reverse Warburg effect as indicated by the increased dependency on LDHB (McCleland et al., 2012). "While LDHA is upregulated in variety of cancers, LDHB is specifically upregulated in basal-like/TNBC and is an essential gene in TNBC" (Mittal, Camarillo, et al., 2020), as its knockdown causes a significant loss in cell proliferation and arrests growth in mouse tumors (Dennison et al., 2013; McCleland et al., 2012). "Patients with elevated LDHB levels in breast tumors show a poor clinical outcome (McCleland et al., 2012)" (Mittal, Camarillo, et al., 2020). On the other hand, a stable, long-term knockdown of LDHA in MDA-MB-231 TNBC cells did not change the glycolytic profile (production of lactic acid and ATP) (Mack, Mazzio, Bauer, Flores-Rozas, & Soliman, 2017).

B. Mitochondrial metabolism in triple negative breast cancer

Until recently, it was widely accepted that the TNBC cells going aerobic glycolysis (Warburg effect) experience a shift from mitochondrial metabolism (TCA cycle and OXPHOS) to

glycolysis, with disrupted mitochondrial function (Pelicano et al., 2014). However, recent evidences suggest that both the increased and decreased OXPHOS activities are observed in TNBCs, which reflect the mitochondrial heterogeneity among TNBCs. For example, TNBC cells going through reverse Warburg effect experience increased OXPHOS activity.

TNBC frequently harbor defects in the mitochondrial DNA (mtDNA) compared to other breast cancer subtypes, resulting in lesser mtDNA content coding for OXPHOS subunits, and impaired mitochondrial functions (Guha et al., 2018). On the contrary, TNBCs with RB1 deficiency show higher OXPHOS activity due to the prototypic oncogenic property of RB1 (X. Sun et al., 2020). Other hypothesis suggests that TNBCs simultaneously upregulate glycolysis and OXPHOS (X. Sun et al., 2020). Recent study suggests that despite being highly glycolytic, TNBC cells have tightly coupled mitochondria with considerable mitochondrial respiratory reserve capacity, which mediates the survival of the MDA-MB-231 TNBC cell subpopulation under metabolic stress (Reda et al., 2019). Other studies also report a shift in tumor metabolism to glycolysis-driven or mitochondrial-driven ATP production, based on the tumor stage, cancer type, tumor microenvironment, and nutrient accessibility (Raman, 2019). The mitochondria metabolism plays a key role in early relapse and metastatic of TNBC and should be targeted together with the glycolysis in these tumors to enhance the treatment response.

1.3 Breast cancer treatments

The standard breast cancer treatment involves surgery, radiotherapy and chemotherapy. Figure 1.14 shows a timeline of the evolution of breast cancer and its treatments from 3500 B.C. to 2016.

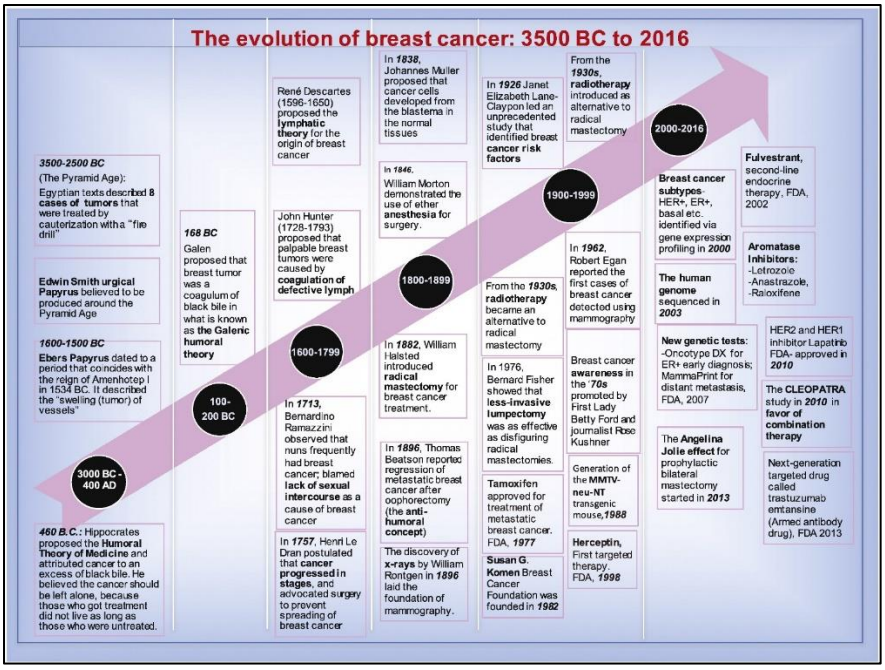

Figure 1.14: The evolution of breast cancer treatment from 3500 B.C. to 2016. Reproduced under Creative Commons Attribution-Non Commercial-No Derivatives License (CC BY NC ND) from (Lukong, 2017).

1.3.1 Surgery of breast cancer treatment

A. Historical perspective of breast cancer surgery

Breast cancer is an ancient disease. The first known description of breast cancer dates back to 3,000-2,500 B.C. in Edwin Smith Surgical papyrus (Mukherjee, 2010, p. 40). Indian literatures dates back to 2000 B.C. with discussion of surgical removal of tumorous growth (Reiter, 2010, p. 204). Greeks practiced surgeries for breast cancer treatment and Hippocrates (460 - 377 B.C.) considered it to be the best of all available treatments (Ray & Baum, 1985, p. 1). Early in the first century A.D., the accounts of a possible primitive form of mastectomy are found in the texts of Aulus Cornelius Celsus (25 B.C. - 50 A.D.) in the ancient Rome (Ray & Baum, 1985, p. 1; Yan, 2013).

The Renaissance brought a phase of rapid innovation in science, engineering, navigation, and medicine disciplines. William Fabry (1560 – 1634), the father of German surgery, designed an apparatus to fix and compress the breast base during mastectomy (Freeman, Gopman, & Salzberg, 2018).

In 1757 Henri LeDran, a French surgeon, propagated the theory that initially breast cancer is a local disease, which eventually spreads via the lymphatic system (Akram & Siddiqui, 2012; Freeman et al., 2018). This theory encouraged other surgeons to adopt early curative surgeries as they could help cure the disease (Akram & Siddiqui, 2012). Jean Petit (born 1674), a colleague of LeDran suggested the removal of breast, pectoral muscle, and axillary lymph node (Freeman et al., 2018). However, this procedure was performed without anesthesia resulting in unbearable pain and further lack of the reconstruction techniques meant the disfigurement of the chest wall. This resulted in the fall of the mastectomy by the late 18th century, despite the increased prevalence of mastectomy in the early 1700s (Freeman et al., 2018).

The invention of anesthesia in 19th century revolutionized the field of surgery. The world's first surgery (mastectomy) under general anesthesia was successfully performed by A Japanese surgeon Seishu Hanaoka in 1804 (Izuo, 2004). This preceded the C W Long's trial of ether anesthesia in 1842 by 38 years in the Western World (Izuo, 2004).

i. Halsted radical mastectomy

William S. Halsted, one of the co-founders and the first professor of surgery at the Johns Hopkins School of Medicine published a seminal paper on the radical mastectomy for breast cancer in 1894 (Halsted, 1894). "This operation involved an extensive resection of the skin and breast tissue, underlying pectoralis major and minor muscles with Level I to III axillary lymph nodes" (Akram & Siddiqui, 2012). This procedure emerged as "Halsted radical mastectomy" (Akram & Siddiqui, 2012; Freeman et al., 2018) (Figure 1.15). The Halsted radical mastectomy brought down the recurrence rates from 51-82% to 6% (Halsted, 1907).

Between 1889 to 1931, Halsted or his disciples performed radical mastectomy on 900 patients but the results were quite disappointing, as 6% died soon after the surgery, local recurrence rate was 30% and 10-year survival rate was mere 12% (Ray & Baum, 1985, p. 2). Between the early 1930s and 1950s, improvements in the outcome of breast cancer treatment were observed, and 10-year survival improved to about 50% by the 1950s (Ray & Baum, 1985, p. 3). However, Ray & Baum argued that these improvements were largely artifacts resulting from a better selection of patients facilitated by the staging systems developed in 1940s (Ray & Baum, 1985, p. 3).

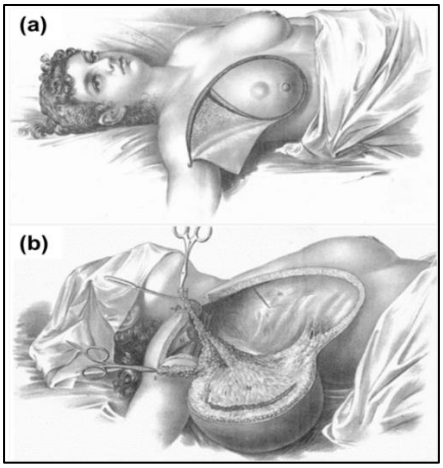

Figure 1.15: The visuals of "Halsted radical mastectomy" by William S. Halsted of Johns Hopkins University - called "Halsted radical mastectomy". (a) Skin incision and triangular flap of fat. (b) Mastectomy sample before final amputation. Reproduced with permission from (Halsted, 1894).

ii. Modified radical mastectomy

The radical mastectomy caused deformity and other frequent problems, including infections, swelling (lymphedema) of the arm and the sensory defects of the chest and arm (Akram & Siddiqui, 2012). Due to the lack of recurrences in pectoralis muscles, J. B. Murphy and other surgeons argued against the radical mastectomy and discontinued the resection of the pectoralis muscles by 1912 (Akram & Siddiqui, 2012). This was an early foundation stone towards a modified radical mastectomy (Bartlett, 2011, p. 9).

D. H. Patey from London further propagated these thoughts and coined the word "modified radical mastectomy", which prompted the elimination of the breast tissues, axillary nodes, and pectoralis minor muscles but saved pectoralis major muscles (Bartlett, 2011, p. 9). Further, Auchincloss and Madden perfected this procedure and saved both pectoralis major and minor muscles (Bartlett, 2011, p. 9). The present day modified radical mastectomy is shown in Figure 1.16(a) (National Cancer Institute, n.d.).

The results of the modified procedures were comparable to the classical radical procedure, resulting into a wide adoption of this procedure as a standard care in North America in 1970s (Bartlett, 2011, p. 9). Yet, a report from the 1976 national survey of American College of Surgeons revealed that the radical mastectomy was employed for 20% cases out of 6793 cases reviewed

(Rosner, Bedwani, Vana, Baker, & Murphy, 1980). However, another successive the U.S. national survey in 1982 indicated only 3.4% cases of radical mastectomy (Wilson et al., 1984).

The addition of the radiotherapy as an adjuvant therapy helped in the shift from the classical radical mastectomy procedure to the modified radical mastectomy, total ("simple") mastectomy (removal of the breast tissue, nipple, areola (The American Cancer Society medical and editorial content team, 2019b)) and eventually to the lumpectomy (breast-conserving surgery (The American Cancer Society medical and editorial content team, 2019a)).

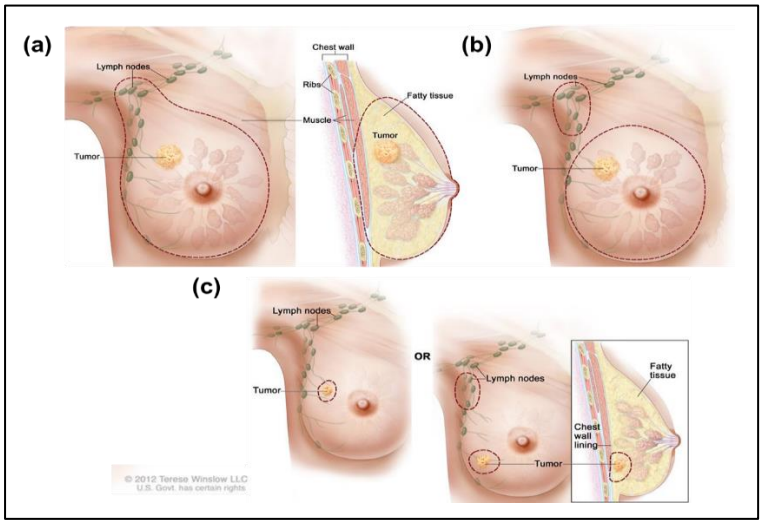

Figure 1.16: (a) The modified radical mastectomy: "Surgery for breast cancer in which the breast, most or all of the lymph nodes under the arm, and the lining over the chest muscles are removed. Sometimes the surgeon also removes part of the chest wall muscles". (b) The simple mastectomy (also called total mastectomy): "Surgery to remove the whole breast. Some of the lymph nodes under the arm may also be removed. Also called total mastectomy". (c) The lumpectomy (also called breast-conserving surgery, breast-sparing surgery, partial mastectomy, tylectomy, quadrantectomy, or segmental mastectomy): "An operation to remove the cancer and some normal tissue around it, but not the breast itself. Some lymph nodes under the arm may be removed for biopsy. Part of the chest wall lining may also be removed if the cancer is near it. Also called breast-conserving surgery, breast-sparing surgery, partial mastectomy, quadrantectomy, and segmental mastectomy". All definitions are reproduced from (National Cancer Institute, n.d.). Figures adapted with permission from Terese Winslow LLC.

iii. Simple mastectomy

In the 1940s, McWhirter emerged as one of the leading advocates of the use of radiation therapy as adjuvant therapy to surgery. Robert McWhirter conducted a simple mastectomy then radiotherapy on internal mammary, axillary, and supraclavicular lymph nodes in 759 patients in

1948 (McWhirter, 1948). This study reported a five-year survival of 62%, similar to that of the radical mastectomy, which promoted the idea that radiotherapy-based simple mastectomy was equally good in treating nodal disease. Baclesse also reported that the majority of breast cancers were responsive to radiotherapy and the tumor size was a key factor in determining the prospects of local control (Baclesse, 1949). The present day simple mastectomy is shown in Figure 1.16(b) (National Cancer Institute, n.d.).

In the 1950s, several researchers, including Wallace Park and Lees , McKinnon, and Hardin Jones suggested that the survival rates of patients with localized breast cancer after minimal surgical interference would be equivalent to that of the radical mastectomy (H. Atkins, Hayward, Klugman, & Wayte, 1972; Jones, 1956; Mckinnon, 1954).

iv. Breast-conserving surgery (lumpectomy)

Reports from the1950s triggered a shift to breast conservation and the addition of adjuvant radiation therapy. Bernard Fisher, a Pittsburgh native proposed that the breast cancer is a systemic disease and it is likely to spread throughout the body before diagnosis, therefore radical mastectomies were superfluous in improving the survival (Cavallo, 2013). The lumpectomy, which removes the tumor and surrounding tissues would probably result in similar survival, but without deformity caused by the radical mastectomy (Cavallo, 2013).

A relatively large number of randomized clinical trials were conducted comparing mastectomy and lumpectomy, and they showed comparable survival (Harris, 2014). In 1972, Atkins et al. conducted the first randomized controlled trial for comparing the radical mastectomy to extended lumpectomy with radiotherapy in 370 patients aged over 50 during a period of 10 years at London's Guy's Hospital (H. Atkins et al., 1972).

Fisher et al. conducted a series of randomized clinical trials and published several follow up reports comparing radical mastectomy to the simple mastectomy as well as to the lumpectomy with radiation (Fisher, Anderson, et al., 2002; Fisher, Bauer, et al., 1985; Fisher, Jeong, et al., 2002; Fisher, Redmond, et al., 1985; Fisher et al., 1989). These studies established a strong justification of the less radical surgical approaches for breast cancer treatment with a focus on breast conservation.

The groundbreaking research by Fisher and others eventually managed to end the Halsted radical mastectomy, a procedure which remained in mainstream for more than 75 years. The present day lumpectomy is shown in Figure 1.16(c) (National Cancer Institute, n.d.).

B. Present day approach of breast cancer surgery

"Nowadays surgical management of patients with operable breast cancer addresses both the primary tumor and regional lymphatics" (Akram & Siddiqui, 2012).

A lumpectomy or mastectomy is performed to manage primary tumor while addressing the nodal regions using lymph node dissection or sentinel lymph node biopsy (Akram & Siddiqui, 2012). First, lymph nodes are checked for cancer using imaging test and then sentinel lymph node biopsy is performed to examine the sentinel lymph node for cancer (European Society for Medical Oncology (ESMO), 2018). If the sentinel lymph node tests negative for cancer, no more lymph nodes are removed. However, more nodes are removed (called axillary dissection), if the sentinel lymph node tests positive for cancer.

Neoadjuvant chemotherapy is used for locally advanced breast cancer to reduce the size, subsequently breast conservation therapy or modified radical mastectomy is performed (Akram & Siddiqui, 2012). Breast reconstruction is performed on patients after mastectomy, except for the inflammatory breast cancer cases.

C. Advantages and disadvantages of surgery

i. Advantages

1. Able to remove all cancer cells in small area.
2. Enables pathological examination of tumor tissues.
3. The removal of tumor tissue induces a mass effect and may reduce symptoms immediately.
4. Can be easily coupled with chemotherapy or radiation therapies.
5. Procedure is convenient for patients, as they are asleep during the surgery.

ii. Disadvantages

1. Elimination of lymph nodes in breast cancer patients commonly results in lymphoedema in the arm and breast area.
2. Poor quality of life due to the deformity, which require additional tissue reconstruction procedures.

3. Surgery can only treat a local tumor and it is not feasible for large tumors and advanced or metastatic cases.
4. Inability in discerning between cancer cells and healthy cells through naked eyes during the procedure.
5. Residual cancer cells can cause the relapse and additional treatments are required.
6. Damage to nearby healthy tissue as wide excision margins are required.
7. Can result into complications, such as infection.

1.3.2 Radiotherapy of breast cancer treatment

Following the discovery of X-rays by Wilhelm Conrad Roentgen in 1895 (Gianfaldoni et al., 2017), radiotherapy began making its headway into the breast cancer therapy in the early 20th century.

Radiotherapy utilizes ionizing radiation to break the DNA of cancer cells, resulting in cell death. Radiotherapy is performed following breast-conserving surgery and mastectomy. Patients with locally-advanced and inoperable breast cancers after systemic treatment may be given radiotherapy. Radiotherapy may also be performed in some patients with metastatic breast cancer for treating the symptoms of primary tumor or metastasis and improve life quality (European Society for Medical Oncology (ESMO), 2018).

A. Advantages and disadvantages of radiotherapy

i. Advantages

1. Unlike chemotherapy, radiotherapy can be targeted to the tumor tissues.
2. Can be easily combined with surgery or chemotherapy.
3. Opportunity of organ preservation.
4. Death of tumor cells at the tumor periphery is possible, which would not be visible through naked eyes during surgery.

ii. Disadvantages

1. Serious side effects, such as skin reaction, rib fracture, arm edema, pulmonary fibrosis, rarely, a second breast malignancy.
2. Damage to surrounding healthy tissue.
3. Not possible on every location. Radiation therapy is considered based on the tumor location, as radiation beam can adversely affect the surrounding vital organs.
4. Unable to induce mass effects as observed by surgical removal of tumor mass.
5. Poor cancer cell death in areas with limited oxygen supply.
6. Poor wound healing and recovery.

1.3.3 Chemotherapy of breast cancer treatment

A. Historical perspective of breast cancer chemotherapy

The birth of chemotherapy has played a vital role in the advancement of the breast cancer techniques less morbid than those founded by Halsted. During World War II, two Yale pharmacologists Goodman and Gilman studied the anticancer effects of nitrogen mustard in the world's first chemotherapy patient (named JD) on August 27, 1942, suffering with a relapse of lymphosarcoma (Christakis, 2011; Gilman & Philips, 1946). In parallel, Sidney Farber, a pathologist at Harvard and later known as the father of modern chemotherapy, also demonstrated temporary remissions in children with acute leukemia using antifolates (Farber & Diamond, 1948). These discoveries founded the medical oncology field and eventually paved a way to the first successful cancer treatment drug (Christakis, 2011; Goodman et al., 1984).

"In breast cancer initially single-agent chemotherapy was used in hormone-resistant metastatic setting. The chemotherapeutic agents were cyclophosphamide, phenylalanine mustard, vincristine, vinblastine, methotrexate and 5-fluorouracil (5-FU). Response rates had ranged from 0-38%" (Akram & Siddiqui, 2012).

Eventually, the first effective breast cancer chemotherapy regime was developed combining cyclophosphamide (an alkylating agent), methotrexate (an antimetabolite), and 5-FU (an antimetabolite), popularly called CMF (Bonadonna et al., 1976; Verrill, 2009). The simplicity in administration and the lack of the severe cytotoxicity made CMF the most common combinational regimen drugs in clinics and it was considered a gold standard in the 1970s (Akram & Siddiqui, 2012).

Other chemotherapy agents were also explored for breast cancer therapy. Anthracycline (doxorubicin) was first used for the metastatic breast cancer in 1969 (Bonadonna, Monfardini, De Lena, & Fossati-Bellani, 1969). However, it became a 'gold standard' after the trial combining doxorubicin and cyclophosphamide (AC) in the 1990s (Fisher et al., 1990). "Over the ensuing 30 years, CMF and AC became references for the development of newer, more effective chemotherapy regimens" (Verrill, 2009).

Various investigators replaced methotrexate with an anthracycline (doxorubicin or epirubicin) in CMF to form FAC (5-FU, doxorubicin, and cyclophosphamide) or FEC (5-FU, epirubicin, and cyclophosphamide) to improve the efficacy of CMF. Few investigators added an

anthracycline to the CMF regime, which is called the block-sequential design. In a clinical trial, four epirubicin cycles followed by four CMF cycles enhanced the effectiveness, compared to the six CMF only cycles (Poole et al., 2006).

The discovery of taxanes in 1970s was a major milestone in the natural product-based anticancer drug discovery and development (Murugan et al., 2015; Wani, Taylor, Wall, Coggon, & McPhail, 1971). Taxanes (paclitaxel and docetaxel) showed effectiveness against metastatic breast cancer (Wani et al., 1971), and were rapidly included in various adjuvant chemotherapy trials across the world (Verrill, 2009). In the U.S., a block-sequential design with AC followed by paclitaxel showed better efficacy than AC alone (Henderson et al., 2003). This regime was further fast-tracked (administrated every two weeks instead of three weeks), increasing the efficacy. The "Breast Cancer International Research Group" (BCIRG)-001 trial substituted 5-FU with docetaxel in FAC to make the TAC (docetaxel, doxorubicin, and cyclophosphamide) regime, and demonstrated a better DFS and overall survival for TAC compared with FAC in node positive breast cancer patients (Martin et al., 2005). The "Fédération Nationale des Centres de Lutte Contre le Cancer" (FNCLCC) PACS 01 trial, "modified FEC into a block-sequential regimen in which three cycles of FEC were followed by three cycles of docetaxel (FEC-T). Since then, FEC-T has become a commonly used regimen following surgery for axillary lymph node-positive breast cancer" (Verrill, 2009).

B. Present day approach of breast cancer chemotherapy

The discovery of taxanes and the clear establishment of their benefits through several clinical trials changed the course of breast cancer chemotherapy. Currently, breast cancer chemotherapy is employed in neoadjuvant, adjuvant and in metastatic settings (Akram & Siddiqui, 2012). However, there exists no universal gold standard procedure for early breast cancer as the large number and variety of trials with differing drug combinations and outcomes has led to endless combinations for treatment.

There is a general understanding that No chemotherapy < CMF < Anthracycline < Taxanes, as also suggested by the worldwide Oxford overview after meta-analysis of trial results (Verrill, 2009). Chemotherapy is usually administered through intravenous infusions every 1-3 weeks (European Society for Medical Oncology (ESMO), 2018). After completing intravenous therapy, few patients may also be recommended additional oral chemotherapy.

C. Advantages and disadvantages of chemotherapy

i. Advantages

1. Chemotherapy drugs can distribute throughout the body to attack widespread cancer cells, whereas surgery and radiation can treat only local tumors.
2. Can be easily combined with radiation and surgery.
3. Multiple drugs could be combined to increase the efficacy.
4. New chemotherapy drugs are very specific in action.
5. Organ preservation.

ii. Disadvantages

1. Repeated administration of chemotherapy drugs results in drug resistance.
2. High susceptibility of infections due to the reductions in levels of neutrophils.
3. Blisters and ulcerations due to the accidental leakage of chemotherapy drug from the vein into the surrounding tissues.
4. Severe side effects, resulting in poor quality of life of patients. Table 1.2 lists side effects of various commonly used chemotherapy drugs.

1.3.4 Triple negative breast cancer clinical outcomes and treatment options

A. Clinical outcomes

"Compared to other breast cancer subtypes, TNBCs have an aggressive clinical course and poor prognosis with a short five-year survival, increased three-year recurrence rates (Dent et al., 2007; Lanning et al., 2017). There is a significantly increased likelihood of distant recurrence in TNBC compared to other breast cancers (Dent et al., 2007)" (Mittal, Aryal, et al., 2019). The poor prognosis of TNBCs is usually attributed to the late stage diagnosis and lymph node positivity (Urru et al., 2018). The most common sites for TNBC metastasis are brain and lungs, with lower occurrence of bone metastasis (Pogoda, Niwińska, Murawska, & Pieńkowski, 2013). An evaluation of 15,204 women with stage I-III breast cancer, presented at National Comprehensive Cancer Network centers between 2000-2006 showed reduced overall survival (OS) for TNBC patients, compared to hormone receptor-positive or HER2-negative cancers "[hazard ratio = 2.72; 95% confidence interval = 2.39-3.10, p <0.0001]" (N. U. Lin et al., 2012). Moreover, TNBC patients showed a greater risk of brain and lung metastases, with a considerably higher risk of

death within the first two years of diagnosis "[overall survival for 0-2 y = 6.10; 95% confidence interval = 4.81-7.74]", with decreased risk over time (N. U. Lin et al., 2012).

B. Treatment options

Intriguingly, increasing evidence suggests that compared to other breast cancer phenotypes, TNBCs exhibit significantly higher sensitivity to chemotherapy (Khosravi-Shahi, Cabezón-Gutiérrez, & Custodio-Cabello, 2017; Poggio et al., 2018). The standard treatment involves neoadjuvant chemotherapy followed by surgery (Figure 1.17). In post recurrence cases, surgery is performed followed by chemotherapy.

The TNBC achieved higher clinical response (85%) to anthracycline-based (doxorubicin plus cyclophosphamide, AC) neoadjuvant chemotherapy, compared to the luminal subtype (47%, $p < 0.0001$) (Carey et al., 2007). "Despite initial chemosensitivity, patients with the basal-like and $HER2^+$/ER subtypes had worse distant disease free survival ($p = 0.04$) and overall survival ($p = 0.02$) than those with the luminal subtypes" (Carey et al., 2007). The poor overall survival of TNBC patients is attributed to the limited treatment options post-recurrence. The median survival of TNBC patients from the time of developing metastases rarely exceed one year (Guarneri, Dieci, & Conte, 2013).

The optimal neoadjuvant chemotherapy regimen for TNBC has not been clearly defined (McAndrew & DeMichele, 2018). The neoadjuvant chemotherapy for TNBC including the combination of anthracycline (epirubicin and doxorubicin) and taxane (such as paclitaxel and docetaxel) is often recommended (McAndrew & DeMichele, 2018). The anthracycline and taxanes-based regimen can marginally improve three-year disease-free survival (DFS) to 73.5 from 68% in TNBCs "[hazard ratio = 0.50; 95% confidence interval = 0.29-1.00, p = 0.051]" (Hugh et al., 2009). A pathological complete response (pCR) of 30-40% is observed for anthracycline and taxanes-based neoadjuvant chemotherapy (Figure 1.17) (Poggio et al., 2018). Anthracyclines inhibit DNA and RNA synthesis in rapidly dividing and proliferating cells "by intercalating between base pairs of the DNA/RNA strand"(Yao et al., 2017). Similarly, taxanes disrupt the microtubule to inhibit the cell division and proliferation. However, anthracyclines and taxanes induces various severe side effects, including cutaneous toxicity and cardiotoxicity, which drive morbidity and mortality (Ho & Mackey, 2014; Rayner & Cutts, 2014).

A treatment option with lower toxicity is CMF (cyclophosphamide, methotrexate, and 5-FU); however, it requires a longer treatment duration. CMF treatment significantly reduces the cumulative relapse rate compared to no chemotherapy and increases the time to relapse in TNBC patients (Colleoni et al., 2010). A modification of CMF and commonly used sequential regimen for medium-to-high risk TNBCs is FEC-P, which includes FEC (5-FU, epirubicin, and cyclophosphamide) followed by paclitaxel/docetaxel, significantly improves the DFS compared to FEC alone (Martín et al., 2008).

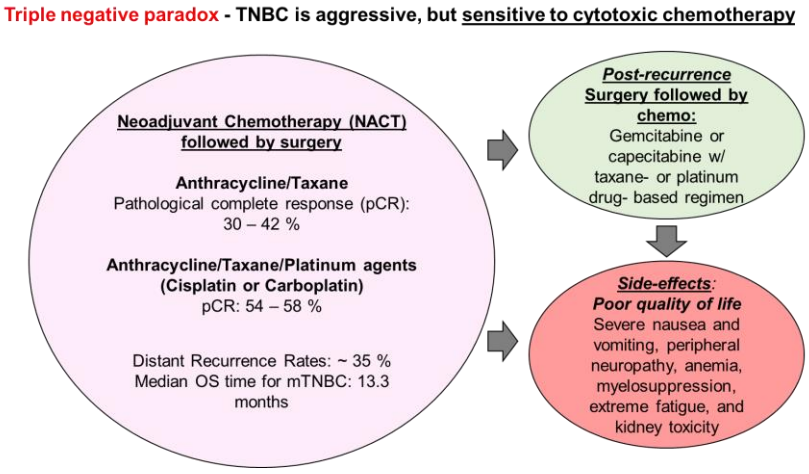

Figure 1.17: Current triple negative breast cancer treatment regimens and their response rates and severe side-effects.

The platinum salts (cisplatin and carboplatin) based single agent or neoadjuvant therapy may also be particularly effective for sporadic and BRCA1-deficient metastatic TNBC (Isakoff, 2010; Isakoff et al., 2015; Khosravi-Shahi et al., 2017; Poggio et al., 2018). Several clinical trials have demonstrated an improved overall response rate of 23-35% (Khosravi-Shahi et al., 2017) as the single agent and significantly increased pathological complete response from 37% to 52% in neoadjuvant setting (Poggio et al., 2018) for cisplatin and carboplatin in TNBC, renewing the interest towards platinum salts. The addition of platinum agent carboplatin to anthracycline and taxanes-based neoadjuvant regimen increased the pCR to 54-58% (Poggio et al., 2018) (Figure 1.17). However, the use of platinum-based therapies comes at the cost of increased toxicity, and increased anti-drug resistance.

The PARP inhibitors (veliparib and Olaparib) are also currently being investigated in clinical research for TNBC treatment, as they present high lethality to BRCA-mutated TNBC tumors (Han et al., 2018).

In summary, while TNBCs respond better to neoadjuvant chemotherapy compared to other subtypes, on the contrary, response rate remains poor to adjuvant chemotherapy post-relapse. Compared to other breast cancer subtypes, TNBCs are characterized by higher three-year relapse rate, poor chemo-sensitivity in adjuvant setting with severe side effects (Figure 1.17), and worst median survival time (< six months) in metastatic setting, underlining a critical need to develop novel targeted therapies by exploiting the TNBC-specific pathways and vulnerabilities.

Table 1.2: Side effects of various commonly used chemotherapy drugs. Source: (European Society for Medical Oncology (ESMO), 2018).

Drug	Possible side effects
Capecitabine	Abdominal pain, anorexia, asthenia, diarrhea, fatigue, hand-foot syndrome, nausea, stomatitis, vomiting, etc.
Carboplatin	Anemia, constipation, fatigue, hepatic (liver) toxicity, increased risk of infection, nausea, neutropenia, renal (kidney) toxicity, thrombocytopenia, vomiting, etc.
Cisplatin	Anemia, anorexia, changes in kidney function, decreased fertility, diarrhea, fatigue, increased risk of infection, increased risk of thrombosis, nausea/vomiting, neutropenia, peripheral neuropathy, taste changes, thrombocytopenia, tinnitus/changes in hearing, etc.
Cyclophosphamide	Alopecia, fever, nausea, neutropenia, renal and urinary tract toxicity, vomiting, etc.
Docetaxel	Alopecia, anemia, anorexia, asthenia, diarrhea, extravasation-related tissue damage, increased infections, nail disorders, nausea, neutropenia, edema, peripheral neuropathy, skin reaction, stomatitis, thrombocytopenia, vomiting, etc.
Doxorubicin	Abnormal hepatic, enzymes, alopecia, anemia, anorexia, asthenia, cardiac effects, chills, diarrhea, extravasation-related, tissue damage, fever, hand-foot syndrome, increased infections, increased weight, leukopenia, mucositis, nausea, neutropenia, stomatitis, thrombocytopenia, vomiting, etc.
Gemcitabine	Alopecia, anemia, dyspnea, flu-like symptoms, increased hepatic enzymes, leukopenia, nausea, edema, rash, renal effects, thrombocytopenia, vomiting, etc.
Methotrexate	Abdominal pain, allergic reactions, anorexia, fever, increased infections, leukopenia, nausea, renal effects, stomatitis, thrombocytopenia, vomiting, etc.
Paclitaxel	Alopecia, anemia, arthralgia, bleeding, diarrhea, hypersensitivity reactions, increased infections, leukopenia, low blood pressure, mucositis, myalgia, nail disorders, nausea, neutropenia, peripheral neuropathy, thrombocytopenia, vomiting, etc.
5-fluorouracil (5-FU)	Agranulocytosis, alopecia, anaemia, anorexia, bronchospasm, cardiac effects, decreased bone marrow function, delayed wound healing, diarrhoea, excess uric acid, fatigue, hand-foot syndrome, increased infections, leukopenia, mucositis, nausea, neutropenia, nose bleeds, pancytopenia, thrombocytopenia, vomiting, weakness, etc.

1.4 Curcumin

Due to the various serious long and short term side effects of commonly administered chemotherapy drugs, it is of practical interest to use natural compounds, such as curcumin.

1.4.1 Rationale for using natural compound curcumin

The use of natural products for medicine is deeply rooted in the history of various cultures across the globe. Today, approximately 80% of the world's population rely on natural products for some part of primary healthcare (Ekor, 2014). Over last three decades, the use of natural products in medication has caught much needed attention of scientists, resultingly over 47% of new anticancer drugs were developed from natural products during this time (Newman, 2012). These compounds include taxanes, vinca alkaloids, epipodophyllotoxins, and camptothecins, which are currently used against a variety of cancers, such as breast, colon, ovarian, prostate, stomach, small cell lung, head and neck cancers, neuroblastomas, leukemia, and lymphomas. However, due to the high cost and toxicity of commonly administered breast cancer chemotherapy drugs, it is of practical interest to use natural compounds in cancer therapies, which are not only cost effective, but also have less side effects compared to conventional therapeutics.

Turmeric, a dried rhizome of the plant *curcuma longa* of the *zingiberaceae* family, is a golden spice regularly used in the Indian subcontinent, China, and other Asian countries as a dietary supplement, food preservative, coloring agent, and medicine for over 4000 years (Aggarwal, Sundaram, Malani, & Ichikawa, 2007). In Ayurveda (science of life), turmeric is recommended for various diseases and conditions, such as skin, pulmonary, and gastrointestinal systems, aches, pains, wounds, sprains, and liver disorders (Aggarwal et al., 2007). Turmeric contains various phytochemicals, including but not limited to phenols, alkaloids, flavonoids, saponin, steroids, tannins, terpenoids, and triterpenes (Oghenejobo & Bethel, 2017; S. Prasad & Aggarwal, 2011). These phytochemicals show "antioxidant, antibacterial, antiviral, anti-cancerous, anti-inflammatory properties (Aggarwal, Yuan, Li, & Gupta, 2013; Nair, Amalraj, Jacob, Kunnumakkara, & Gopi, 2019)" (Mittal, Camarillo, et al., 2020).

Curcumin, a polyphenol constitutes to 2–5% of dried turmeric rhizome. "Majority of the bioactivities of turmeric are attributed to curcumin, the most extensively studied compound of

turmeric. However, recent evidences suggest that other compounds of turmeric can also show a potent bioactivity (Aggarwal et al., 2013)" (Mittal, Camarillo, et al., 2020).

1.4.2 History of curcumin and curcuminoids

Two German scientists Vogel and Pelletier first isolated curcumin from turmeric as yellow-coloring matter in 1815 and named it curcumin (Vogel & Pelletier, 1815). Vogel Jr. prepared pure curcumin in 1842 but did not offer details on its formula. In 1910, Lampe et al., determined curcumin's structure as diferuloylmethane: 1,6-heptadiene-3,5-dione-1,7-bis (4-hydroxy-3-methoxyphenyl)-(1E, 6E) (Lampe, Milobedzka, & Kostaneski, 1910). Subsequently, Lampe and Milobedzka synthesized curcumin in 1913 (Lampe & Milobedzka, 1913). In 1953, Srinivasan performed chromatography studies to separate and quantify the curcumin into three main constituents and a few minor fractions (K. R. Srinivasan, 1953). Three main curcuminoids are found in turmeric, diferuloylmethane (curcumin), desmethoxycurcumin and bis-desmethoxycurcumin (Pimple & Badole, 2014). Most preparations of curcumin also contain other curcuminoids, such as 18% demethoxycurcumin, and 5% bisdemethoxycurcumin with 77% diferuloylmethane (Aggarwal et al., 2007). Curcuminoids have also been isolated from other plants *curcuma aromatica* (wild turmeric), *curcuma zedoaria* (white turmeric, zedoary root), *curcuma phaeocaulis* (ezhu, zedoary rhizome), *curcuma mangga* (mango ginger), *etlingera elatior* (torch ginger), *zingiber cassumunar* (cassumunar ginger), and *curcuma xanthorrhiza* (temulawak) (Aggarwal et al., 2007).

1.4.3 Biological activities of curcumin

The first study on curcumin's biological activity as an antibacterial agent was reported in 1949 in Nature "against strains of staphylococcus aureus, salmonella paratyphi, trichophyton gypseum, and mycobacterium tuberculosis (Schraufstatter & Bernt, 1949)" (S. C. Gupta, Patchva, Koh, & Aggarwal, 2012). Curcumin's first clinical trial by Oppenheimer on human biliary diseases was published in 1937 in Lancet (Oppenheimer, 1937). Despite these early findings, the research on curcumin remained sluggish over the following two decades, and only five paper were published (S. C. Gupta et al., 2012). In 1970s, various attributes of curcumin, including hypocholesterolemic (Patil & Srinivasan, 1971), anti-diabetic (M. Srinivasan, 1972), anti-

inflammatory (Srimal & Dhawan, 1973), and anti-oxidant (O. P. Sharma, 1976) were discovered, which resulted into an increased interest in studying curcumin for various diseases. Resultingly, in 1980s, the anticancer activity of both the turmeric extract and curcumin was demonstrated by Kuttan et al., in both *in vitro* and *in vivo* models (Kuttan, Bhanumathy, Nirmala, & George, 1985). Subsequently, in 1995, Bharat B. Aggarwal and colleague's pioneer work demonstrated the anti-inflammatory activity of curcumin by the suppression of NF-κB, and delineated the action mechanisms of curcumin (S. Singh & Aggarwal, 1995). The curcumin was found to be safe and effective in multiple human clinical trials, resulting into its endorsement by U.S. FDA as a "generally regarded as safe" compound (S. C. Gupta et al., 2012).

The research on curcumin has increased significantly over the years, as demonstrated by more than 15,000 published articles with keyword curcumin as of June 2020, on the PubMed database by the National Institutes of Health (Pubmed.gov, 2020). Curcumin is shown to be effective in multiple cancers, including breast, cervical, colorectal, bladder, lung, skin, stomach, oral cancers etc. (Aggarwal et al., 2007). Curcumin does not have the harsh side effects and has been found to suppress the initiation, progression, and metastasis of a variety of tumors by modulating multiple factors (A. Goel, Kunnumakkara, & Aggarwal, 2008).

"Curcumin inhibits cell cycle progression and induces apoptosis in multiple breast cancer cells, including TNBC, by downregulating NF-κB, Wnt/ß-catenin and their downstream targets, while increasing Bax to Bcl-2 ratio (Y. H. Bae et al., 2013; Chiu & Su, 2009; C. P. Prasad, Rath, Mathur, Bhatnagar, & Ralhan, 2009). Curcumin can also result in the downregulation of mutant p53 levels to induce apoptosis and cell cycle arrest in TNBC cells (Y. H. Bae et al., 2013; Chiu & Su, 2009). Therefore, curcumin can induce multiple signaling pathways to target TNBC, which motivates the current dissertation to investigate the effect of curcumin on TNBC cells" (Mittal, Raman, et al., 2019).

1.5 Electrochemotherapy

The death of a woman every minute, with more than 500,000 women since 2015, indicates that the current standard of treatment is not adequate, especially for TNBC with its lack of three dominant receptors (ER, PR and HER2). There are advanced, recurrent, and metastatic cancers, which are refractory to multiple standard modalities, such as surgery, chemotherapy, and radiation. These highlight a critical need of alternate treatment to address these issues. Towards this a novel,

efficient, effective, and economical alternate electroporation-based electrochemotherapy (ECT) treatment is explored in this dissertation. "Typically, bleomycin, and occasionally cisplatin is used in ECT" (Mittal, Camarillo, et al., 2020). We intend to use curcumin with ECT as the chemotherapy drug and study their efficacy. In addition, proteomics studies were conducted to gain insights into the mechanisms of ECT with curcumin.

1.5.1 Overview of electroporation

When cells or tissues are subjected to short duration (microsecond to millisecond), high voltage electrical pulses, the transmembrane voltage (V_m) increases. "When the V_m increases beyond the threshold (>0.5V), across its 5nm thickness, there is a several-fold enhancement of electric field (100MV/cm), leading to the pore formation (Kotnik, Kramar, Pucihar, Miklavcic, & Tarek, 2012; Zimmermann, Pilwat, & Riemann, 1974)" (Mittal, Camarillo, Aryal, & Sundararajan, 2019). This phenomenon is called electroporation and based on the electrical pulse parameters (intensity, pulse duration, and number of pulses), the pores can either reseal (reversible electroporation) or remain open permanently (irreversible electroporation).

"The pore formation is a two-step process (Neu & Krassowska, 1999) (Figure 1.18). First, small and non-conducting hydrophobic pores form in the cell membrane. Second, these hydrophobic pores expand in size and lipid molecules invert on the edges to create conducting hydrophic pores" (Mittal, Camarillo, et al., 2019).

The energy of pore formation $E(r)$ for hydrophobic and hydrophilic pores is given by:

$$E(r) = 2\pi hr\sigma_0(\infty)\,[I_1(r/r_0)/I_0(r/r_0)]) - \pi a_p V_m^2 r^2, \quad (1.1)$$

and

$$E(r) = 2\pi\gamma r - \int_0^r 2\pi\Gamma(r^*)r^* dr^* + (C/r)^4 - \pi a_p V_m^2 r^2, \quad (1.2)$$

where r is pore radius, V_m is transmembrane potential, as shown in equation (1.1) for hydrophobic and equation (1.2) for hydrophilic pores, respectively, "h is the cell membrane thickness, $\sigma_0(\infty)$ is a constant (5×10^{-2}N/m), r_0 is the characteristic length, I_0 and I_1 are 0th and 1st order modified Bessel functions, respectively, γ is the strain energy per unit length of the bilayer pore edge or perimeter, Γ is the surface energy per unit area of the intact bilayer, C is a constant (9.67×10^{-15}J$^{1/4}$m), and $a_p = (\varepsilon_w - \varepsilon_m)/(2h)$, where ε_w is the permittivity of water and ε_m is the permittivity of the cell membrane,

as: $a_p = (\varepsilon_w - \varepsilon_m)/(2h)$ (Joshi, Hu, Aly, Schoenbach, & Hjalmarson, 2001)" (Mittal, Camarillo, et al., 2019).

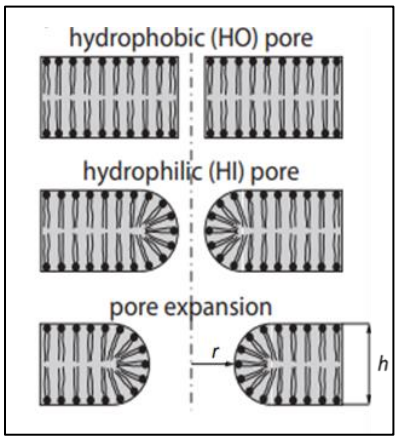

Figure 1.18: Types of pore formed in the lipid membrane. Adapted with permission from (Rems, 2017).

Depending upon the external electric field strength, four electroporation outcomes are possible (Kranjc & Miklavčič, 2016). If E_{ext} is the external electric field, E_{rev} is the reversible threshold, E_{irrev} is the irreversible threshold, and E_{therm} is the thermal damage threshold:

1. $E_{ext} < E_{rev}$: No electroporation
2. $E_{rev} < E_{ext} < E_{irrev}$: Temporary membrane permeabilization and cells viability remains intacts following pulse application - Reversible electroporation.
3. $E_{irrev} < E_{ext} < E_{therm}$: Permanent membrane permeabilization causing extensive outflow of intracellular contents to induce cells death - Irreversible electroporation (IRE).
4. $E_{ext} > E_{therm}$: Causes high electrical current resulting into temperature rise and damage to cells.

In addition to the electrical field strength, the duration of electric field exposure (t_{exp}), given by:

$$t_{exp} = t_p \times N_p, \qquad (1.3)$$

where, t_p is the duration of a single electric pulse and N_p is the number of pulses applied, also determines electroporation outcome. Based on this, different thresholds for reversible and irreversible electroporation are shown in Figure 1.19.

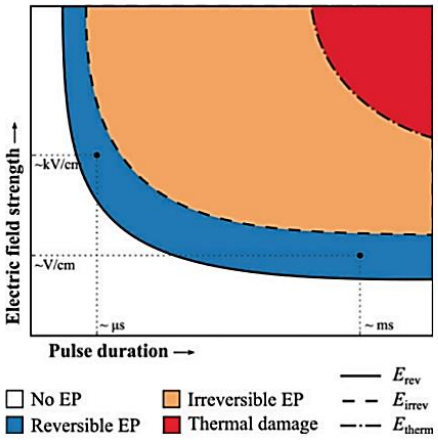

Figure 1.19: "Reversible electroporation, irreversible electroporation, and thermal damage as functions of electric field strength and pulse duration. Two points with different combinations of pulse parameters but with the same outcome, i.e., reversible electroporation, are depicted" (Kranjc & Miklavčič, 2016). Reproduced with permission from (Kranjc & Miklavčič, 2016).

Different electroporation applications require different settings of pulse parameters such as amplitude, t_p, and N_p, depending upon the sensitivity of the cells or tissue to the electrical pulses. Thus, there exists a difference in threshold values of electrical pulse parameters in the literature. The thresholds for *in vitro* electroporation are different with respect to different cells. The threshold for reversible electroporation is reported to be 400-600V/cm for various cell lines exposed to 8 electric pulses 100µs (Maja Čemažar et al., 1998). On the other hand, electric field strength for IRE is reported to be between 1000-2000 V/cm depending on t_{exp} (C. Jiang, Davalos, & Bischof, 2015).

1.5.2 Overview of electrochemotherapy

During reversible electroporation, the transient permeabilization of the cell membrane can be used to increase the uptake of external molecules up to 1000 times (Probst, Fuhrmann, Beyer, & Wiggermann, 2018). "When electroporation is applied towards the uptake of chemotherapeutics, this non-surgical procedure is called electrochemotherapy (ECT)" (Mittal, Camarillo, Aryal, & Sundararajan, 2019. Figure 1.20 shows the ECT process.

ECT is now increasingly used to improve cellular uptake of chemotherapeutic drugs that are poorly permeant, but cytotoxic at the intracellular targets. Cytotoxicity of these drugs can be improved by several fold (Mir & Orlowski, 1999; Rols et al., 2000; Rols, Tamzali, & Teissié, 2002;

G Sersa, Stabuc, Cemazar, Miklavcic, & Rudolf, 2000a). "Increased cytotoxicity of cisplatin and bleomycin by ECT has also been demonstrated in several studies on rodent and human cell lines (Rols et al., 2000) and animal models (G Sersa et al., 2000a)" (Mittal, Aryal, et al., 2019).

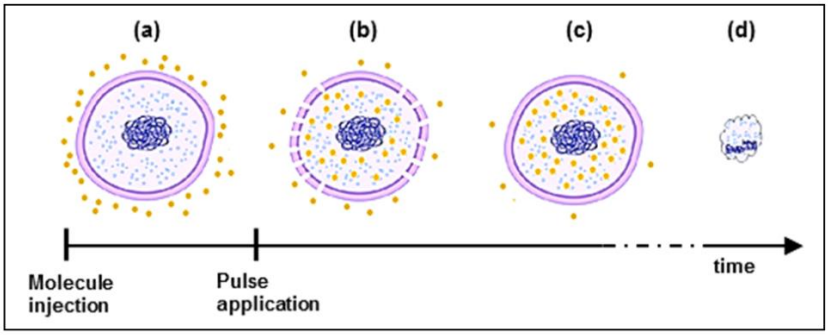

Figure 1.20: The electrochemotherapy (ECT) process: (a) molecules surround the cell after injection; (b) electrical pulses cause pore formation, molecules overcome the membrane; (c) cell membrane reseals, molecules are entrapped; (d) cellular response to the molecules.

ECT is used to treat "melanomas, carcinomas, sarcomas, and many other types of cancers" (Mittal, Aryal, et al., 2019), as it is applicable to all histology of cancers (Campana et al., 2017, 2016a; "Endoscopic Assisted Electrochemotherapy in Addition to Neoadjuvant Treatment of Locally Advanced Rectal Cancer - Full Text View - ClinicalTrials.gov," n.d.; Matthiessen et al., 2011). ECT with cisplatin resulted in 77% long lasting complete responses, compared to 19% obtained with cisplatin alone, "at the drug doses that by themselves have no anti-tumor activity and produce no side effects (Marty et al., 2006; G Sersa et al., 2000a)". "ECT is also shown to sensitize the cisplatin resistant solid tumors to the cisplatin treatment (M Čemažar et al., 2001)" (Mittal, Aryal, et al., 2020). Therefore, ECT is increasingly viewed as an "alternate modality to treat advanced, inoperable, radiation and chemo-resistant tumors (Marty et al., 2006)" (Mittal, Raman, et al., 2019).

"Typically, bleomycin and, occasionally cisplatin is used for ECT" (Mittal, Camarillo, et al., 2020). Due to the severe side effects of these drugs, we intend to use curcumin as the chemo drug and study its efficacy against TNBC cells. In addition, proteomics studies were conducted to gain insights into the mechanisms of ECT with curcumin against TNBC. Proteomics studies of ECT were performed with turmeric silver nanoparticles, and also with commonly used chemotherapy drug cisplatin against TNBC for comparison.

1.6 Mass spectroscopy (MS)-based proteomics

The term proteome stands for the total set of proteins encoded by the genome (Uniprot.org, n.d.). Proteomics is an interdisciplinary high-throughput technique that can screen multiple protein properties, such as protein expression levels, post-translational modification, and interaction with other molecules to acquire a complete picture of the cellular process at the protein level after the treatment (Palzkill, 2002).

Recent advances in tandem mass spectroscopy techniques have enabled us to generate database of protein expression profiles for various cells and tissues (Rasmussen, Orntoft, Wolf, & Celis, 1996). Moreover, rapid progress has been made in the identifying upregulated or downregulated protein expression or protein modification in cells and clinical samples, which provides an opportunity to study mechanisms and identify possible therapeutic targets (Y. Huang & Zhu, 2017).

1.6.1 Rationale for using proteomics

The effects of ECT with curcumin could be "driven by multiple signaling pathways that involve a collection of genes, which encode proteins with different functions ranging from cell surface receptors to transcription factors" (Mittal, Aryal, et al., 2019). Therefore, a technique, which can screen thousands of proteins could be effective to gain insights into the mechanisms of ECT with curcumin.

Considering this, in this dissertation, mass spectroscopy (MS)-based proteomics is used to study the mechanisms of enhanced effects of ECT with curcumin, turmeric silver nanoparticles and cisplatin in TNBC cells.

1.7 Statement of problem

The lack of three main receptors (ER, PR, and HER2) make TNBCs difficult to treat using standard therapies. Will the ECT with curcumin, which does not depend upon the receptors to target cancer cells be effective against TNBC, by influencing multiple signaling pathways?

1.8 Research questions

This research study answers the following research questions:

- Is the ECT with curcumin effective in targeting TNBC cells?
- What are the optimal electrical pulse parameters and the curcumin dosage to obtain synergistic effects against TNBC cells?
- Can ECT, which utilizes an electro-physical phenomenon, manipulate multiple signaling pathways in TNBC cells, when coupled with the curcumin?
- What is the efficacy of ECT with turmeric silver nanoparticles against TNBC?
- What is the efficacy of ECT with curcumin compared to the standard FDA approved cisplatin-based therapy?

1.9 Scope

This research aims to develop an effective and alternate therapy for TNBC, utilizing the synergy of electrical pulses and curcumin. First, the optimal electrical pulse parameters and curcumin concentration were identified for the maximum cell death in TNBC cells, while minimizing the cell death in non-cancerous cells, using the cell viability assays. Further, the molecular mechanisms of the enhanced effects of ECT with curcumin, employing mass spectroscopy-based label-free quantitative proteomics studies. The proteomics approach provides information of the of thousands of proteins involved in the cellular process, allowing a comprehensive understanding of the mechanisms.

Similar studies were also performed for ECT with cisplatin to compare the efficacy of the ECT with curcumin to the standard stand-alone cisplatin-based therapy used in clinics for TNBC (Tian et al., 2015). The results obtained from this research indicate that ECT with curcumin target MDA-MB-231 TNBC cells, by influencing multiple pathways and causing metabolic shift from glycolysis to oxidative phosphorylation, generating a significant oxidative stress in TNBC cells to induce apoptosis.

1.10 Purpose

With the rise of the breast cancer cases and the high recurrence and mortality rates for the TNBC patients, it is important to develop effective and alternate therapies against TNBC. The

absence of the three main receptors and thus the lack of targeted therapies for TNBC, create a gap in the TNBC treatment. This research aims to examine the efficacy of ECT with curcumin as an effective and alternate therapy for TNBC. This therapy utilizes the principles of the ECT, which is demonstrated to be safe, effective, affordable, quick (it takes only a few minutes per nodule), and outpatient-based physical therapy, and is applicable to all histology and stages of cancer (Marty et al., 2006). Therefore, if successful, this ECT-based curcumin therapy has the potential to be extended to other cancers in future. Compared to conventional chemotherapeutics, which cost $45,000 to $50,000 per dose, the cost of curcumin is 22 times less, with reduced side effects compared to the conventional chemotherapeutics (Gazella, 2009). This therapy can be useful in the U.S. to reduce the economic burden of TNBC. Furthermore, it will be helpful for women in low- and medium- income countries, where the treatment options are limited due to availability and unaffordability. This research addresses the global challenge of engineering better medicines (R. Atkins, 2008).

CHAPTER 2. LITERATURE REVIEW

2.1 Triple negative breast cancer and cisplatin

"Recent studies have indicated that triple-negative breast cancers possess an altered metabolic state with higher rates of glycolysis" (Raman et al., 2018), which is correlated with increased chemotherapeutic resistance (Lanning et al., 2017; Wahdan-Alaswad et al., 2013; Zielinski et al., 2015). Therefore, interest has been growing in advancing novel therapeutic strategies for this subset of high-risk patients. Increasing evidence suggests that platinum salt (cisplatin and carboplatin) based single agent or neoadjuvant therapy may be particularly effective for sporadic and BRCA1-deficient metastatic TNBC (A. K. Goel, Nandy, & Sharma, 2010; Isakoff, 2010; Khosravi-Shahi et al., 2017; Poggio et al., 2018). Studies have demonstrated an improved overall response rate of 23-35% (Khosravi-Shahi et al., 2017) as the single agent and significantly increased pathological complete response from 37% to 52% in neoadjuvant setting (Poggio et al., 2018) for cisplatin and carboplatin in TNBC, renewing the interest towards platinum salts. In general, depending upon the cancer type, the cisplatin is 8-45 times more effective than carboplatin (Dasari & Bernard Tchounwou, 2014). Resultingly, usually a four times higher carboplatin dosage is required than that of cisplatin in clinics (Dasari & Bernard Tchounwou, 2014).

Cisplatin (Cis-diamminedichloroplatinum) contains two ammine ligands and two chloro-ligands oriented in a cis planar configuration around the central platinum ion, as shown in Figure 2.1. Cisplatin was the first FDA approved platinum drug in 1978. Towards the end of 1970s, cisplatin was routinely added into the treatment regimens for germ cell cancers, including testicular and ovarian cancers. Now, cisplatin is widely used in therapeutic regimen against variety of cancers, including breast, ovarian, testicular, cervical, prostate, head and neck, bladder, lung and refractory non-Hodgkin's lymphomas (Dasari & Bernard Tchounwou, 2014; Dhar, Kolishetti, Lippard, & Farokhzad, 2011; Tsimberidou, Braiteh, Stewart, & Kurzrock, 2009).

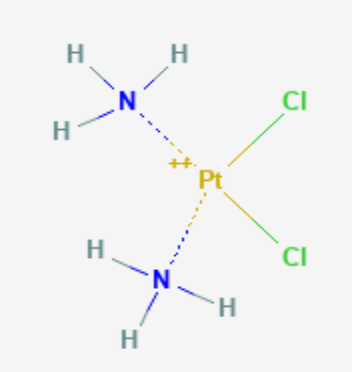

Figure 2.1: The chemical structure of cisplatin (National Center for Biotechnology Information. PubChem Database, 2004a).

2.1.1 Pharmacokinetics of cisplatin

Upon intravenous administration, cisplatin distributes widely to various tissues, with largest amount in kidneys, liver, and prostate (The Global Library of Women's Medicine, n.d.). Cisplatin does not easily overcome the blood-brain barrier. In aqueous environment, such as body, the water molecules replace cisplatin's chloro-ligands to produce aquated complexes (Farris, Dedrick, & King, 1988). Both the parent and aquated forms of the cisplatin react at different rates to form metabolites.

Cisplatin irreversibly binds to nucleophiles of low molecular weight and nucleophilic sites of macromolecules, such as proteins in the blood plasma and tissues to produce mobile and fixed metabolites, respectively (Farris et al., 1988; Urien & Lokiec, 2004). The formation of the both metabolites is tissue specific. The mobile metabolites of cisplatin and its unbound form is largely thought to be active (Urien & Lokiec, 2004). The fixed metabolites are confined to the compartments of their origin and are cleared through catabolism to generate mobile metabolites (Farris et al., 1988). A schematic of biotransformation and elimination of cisplatin is shown in Figure 2.2.

Cisplatin is mainly eliminated through urinary excretion in form of parent drug and mobile metabolite. The half-life of cisplatin's initial elimination phase is 25-79 min and the erminal phase is 58-78 hours in patients with regular renal function, and its terminal half-life of is up to 10 days (The Global Library of Women's Medicine, n.d.). Usually eliminated from tissues within days to a week, cisplatin can remain in some body tissues, such as cochleae (a part of inner ear that enables hearing), for months-to-years (Breglio et al., 2017).

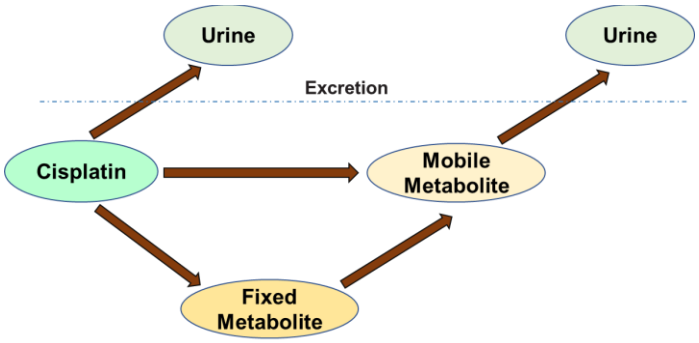

Figure 2.2: Schematic of biotransformation and elimination of cisplatin. Modified from (King, Dedrick, & Farris, 1986).

2.1.2 Mechanisms of action of cisplatin

"Cisplatin's mechanisms of cellular uptake and efflux are not completely clear" (Mittal, Aryal, et al., 2019). Evidence suggests that the net zero charge on cisplatin causes the majority of its uptake to occur through passive diffusion and facilitated transport through organic cation transporters, such as high affinity copper transporter 1 (hCTR1/SLC31A1) or SLC22 family members (Martinho, Santos, Florindo, & Silva, 2019; Raudenska, Balvan, Fojtu, Gumulec, & Masarik, 2019). Figure 2.3 shows the mechanisms of action of cisplatin.

Cisplatin is relatively inactive and does not directly interact with biological molecules (Berners-Price & Appleton, 2000). However, upon entering the cell cytoplasm, cisplatin goes through a necessary activation step by hydrolysis, where cisplatin's chloro-ligands are replaced by water molecules (Berners-Price & Appleton, 2000). Due to the high lability of water molecules, cisplatin can actively react with S- and N-donor ligands in the cell (Legin et al., 2014). The majority of the cytoplasmic cisplatin accumulates in acidic organelles (e.g. lysosomes), with only 1-10% entering the nucleus (Legin et al., 2014).

"Cisplatin interacts with various cellular components, including DNA to form platinum-DNA adducts by covalently binding to N7 positions of the purine bases (Dasari & Bernard Tchounwou, 2014)" (Mittal, Aryal, et al., 2019). Cisplatin's cytotoxicity is therefore attributed to these cisplatin-DNA adducts, which inhibit DNA replication during cell division and activate several pathways to induce apoptosis (Siddik, 2003).

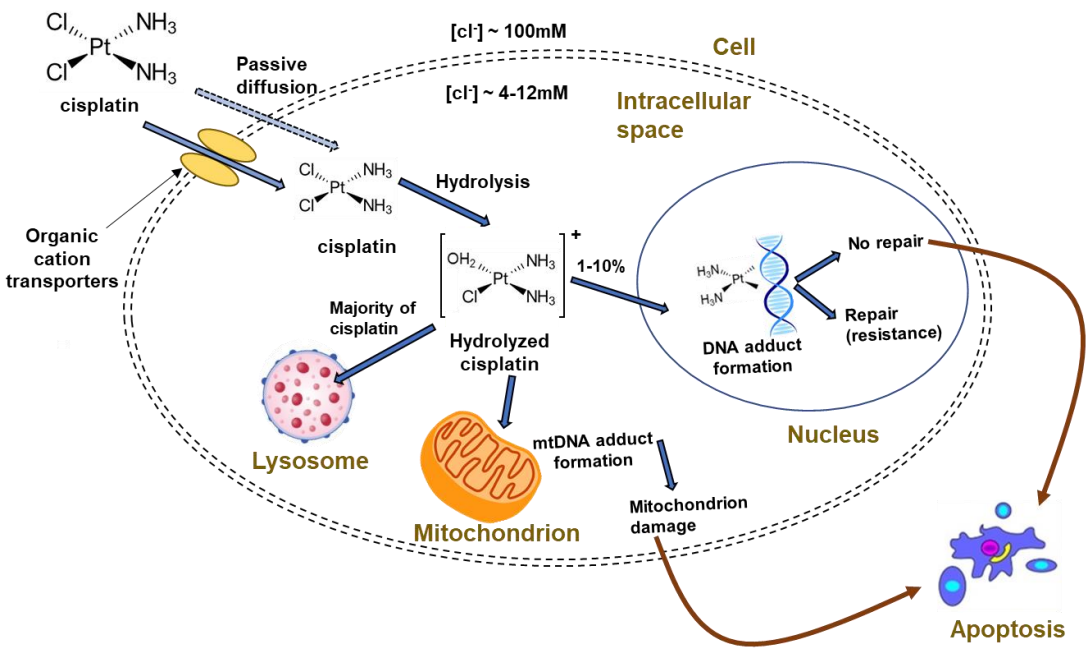

Figure 2.3: The cisplatin's mechanism of action. Idea adopted from (Browning et al., 2017).

In breast cancer cells, cisplatin induced caspase and cathepsin mediated apoptotic cell death (Lauritzen et al., 2010; Sigurethsson, Olesen, Dybboe, Lauritzen, & Pedersen, 2015). In these studies, cisplatin promoted cytochrome c release with caspase-9, caspase-7, and PARP-1 cleavage and no cleavage of caspase-8, suggesting the activation of intrinsic apoptosis pathway. Cisplatin upregulated the expression of proapoptotic proteins (PUMA and Noxa), while downregulating antiapoptotic proteins (Bcl-2 and Bcl-xL) expression (Sigurethsson et al., 2015).

Since the nuclear DNA damage alone is not sufficient to explain the high effectiveness of cisplatin, additional mechanisms of cisplatin's action, including the alternation in cellular metabolism are reported recently (Marullo et al., 2013; Raudenska et al., 2019). Cisplatin can also form adducts in mtDNA in a larger number than DNA adducts. Due to the inability of mitochondria to perform nucleotide excision repair, as observed in the nucleus to remove cisplatin induced DNA adducts, these mtDNA adducts induce a serious damage to mitochondria, which is an important mediator of energy supply and apoptosis (Raudenska et al., 2019). Cisplatin also downregulated glycolysis metabolism and lactate production, with increase in ROS generation to induce cell death (Marullo et al., 2013; Yu et al., 2018). Cisplatin also exerted the anti-cancer effects in MDA-MB-231 TNBC cells by downregulating glucose transporter 1 and 4, and lactate dehydrogenase B (LDHB) to inhibit glycolysis and lactate metabolism (S. Wang et al., 2016).

These studies highlight that inhibition of glycolysis could be an important anticancer mechanism of cisplatin.

2.1.3 Side effects of cisplatin

The use of platinum-based therapies comes at the cost of increased toxicity and increased anti-drug resistance (Smith et al., 2007). Cisplatin induces various side effects (European Society for Medical Oncology (ESMO), 2018; Staff, Grisold, Grisold, & Windebank, 2017):

1. Neurotoxicity ("high-frequency hearing loss, tinnitus, and peripheral neuropathy" (Mittal, Aryal, et al., 2019)).
2. Nephrotoxicity.
3. Ototoxicity.
4. Anemia.
5. Neutropenia.
6. Thrombocytopenia.
7. Anorexia.
8. High risk of thrombosis.
9. High risk of infection.
10. Fatigue.
11. Diarrhea.
12. Nausea/vomiting.
13. Decreased fertility.

"Improving cisplatin's effectiveness at low concentration is important for reducing cisplatin related toxic side effects, and for developing chemotherapy as a front-line cancer therapy. Cisplatin is also a poorly permeant molecule and one of the ways to address this problem is to improve drug permeabilization to the cells" (Mittal, Aryal, et al., 2019). Therefore, electrochemotherapy (ECT), which involves the electrical pulses (EPs) application can be effective against TNBC, without causing severe toxicity and drug-resistance because ECT does not depend upon the receptors to target cancer cells (Probst et al., 2018).

Although smaller dosage of cisplatin is used with ECT, its toxicity cannot be ignored. Therefore, there is a critical need to study the alternate and less toxic natural compounds for ECT applications.

2.2 Curcumin

Curcumin ((1E,6E)-1,7-bis (4-hydroxy- 3-methoxyphenyl) -1,6- heptadiene-3,5-dione) is a beta-diketone, a methane where two of the hydrogens are substituted by feruloyl groups, as shown in Figure 2.4. Curcumin is one of the most potentially advantageous natural compounds. Curcumin does not have the harsh side effects of many commonly administered chemo drugs (A. Goel et al., 2008).

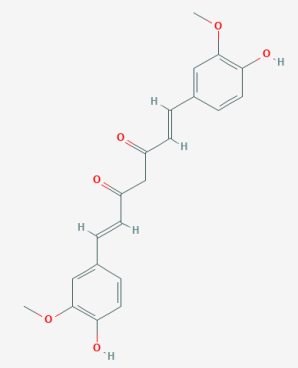

Figure 2.4: The chemical structure of curcumin (National Center for Biotechnology Information. PubChem Database, 2004b).

2.2.1 Pharmacokinetics of curcumin

Curcumin is rapidly and efficiently transformed into metabolites, which reduces the bioavailability of parent compound curcumin upon entering the body (R. A. Sharma, Steward, & Gescher, 2007). In circulation, curcumin undergoes conjugation, including glucuronidation and sulfation in tissues, mostly in the liver (Toden & Goel, 2017). These conjugates are now known to exert anti-cancer and anti-inflammatory effects. Orally administered curcumin in parent from is detected in colorectal tissues, sufficient for exerting bioactivities, and also in additional tissues outside the gastrointestinal tract, such as liver tissue, but in negligible amount (R. A. Sharma et al., 2007). Administering curcumin through the intravenous and intraperitoneal routes results in a large amount of curcumin and its metabolites in bile (R. A. Sharma et al., 2007).

The majority of orally administered curcumin is excreted through fecal route (75%), with a negligible presence in urine (R. A. Sharma et al., 2007). The urinary excretion of curcumin mainly includes glucuronide and sulfate conjugates (Ravindranath & Chandrasekhara, 1980). The half-life of curcumin is 32.7 ± 12.92 for oral and 8.64 ± 2.31 for intravenous route in

streptozotocin-diabetic rats (Gutierres et al., 2015). In humans, the half-life of curcumin is estimated to be 6-7 hours following oral administration (Jäger et al., 2014).

2.2.2 Molecular mechanisms of curcumin in triple negative breast cancers

"Curcumin can suppress initiation, progression, and metastasis of a variety of tumors by modulating multiple receptors, growth factors, inflammatory cytokines, kinases, enzymes, and transcription factors (Aggarwal et al., 2007; Banik, Parasuraman, Adhikary, & Othman, 2017)" (Mittal, Raman, et al., 2019).

As shown in Figure 2.5, curcumin targets several genes and proteins to modulate multiple pathways (Wnt/β-catenin, Notch, NF-κB, PI3K/Akt/mTOR, MAPK and Hh pathways) to exert its anticancer action (Kunnumakkara et al., 2017; Varghese et al., 2018)" (Figure 2.5) (Mittal, Aryal, et al., 2020). Curcumin modules "several molecular targets that include transcription factors (NF-κB, AP1, HIF1, Nrf2, STATs, PPAR-γ etc.), growth factors (VEGF, FGF, HGF, PDGF etc.), inflammatory cytokines (interleukins, TNF-α, MCP etc.), kinases (PKA, PKB, MAPK, FAK, ERK etc.), receptors (FasR, ER-α, HER2, CXCR4 etc.), enzymes (ATPase, COX2, LOX-5, telomerase, MMPs etc.), and other effector molecules such as Bcl2, Bcl-xL, cyclin D1, IAPs, and p53" (Varghese et al., 2018). Through these curcumin inhibits cell proliferation, survival, invasion, metastasis, and angiogenesis, and promote apoptotic cell death by caspase activation in multiple cancers, including TNBCs (Aggarwal et al., 2007; Varghese et al., 2018).

Several researchers have attempted to define the molecular mechanism of curcumin's actions in TNBC, and have reported that it can modulate NF-κB, Wnt/β-catenin, and MAPK signaling pathways (Chiu & Su, 2009; C. P. Prasad et al., 2009; X.-D. Sun, Liu, & Huang, 2012; Varghese et al., 2018).

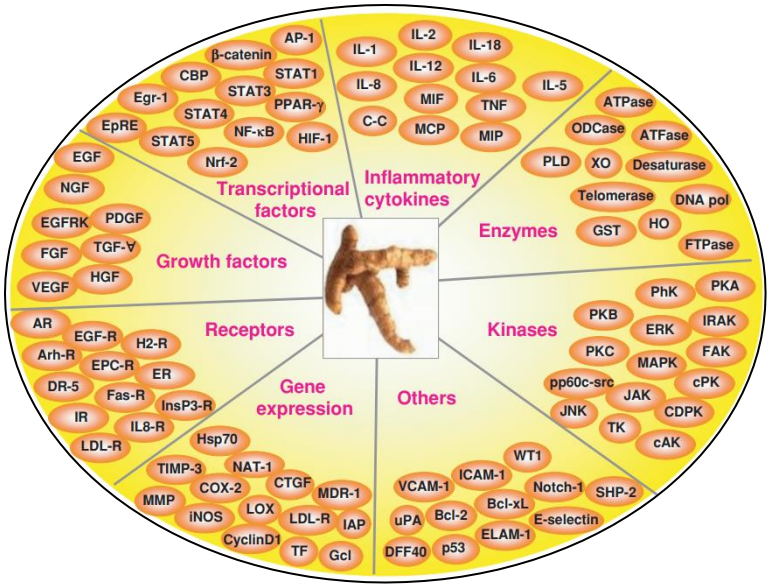

Figure 2.5: Molecular targets of curcumin. Reproduced with permission from (Aggarwal et al., 2007).

A. Curcumin targets NF-κB signaling in triple negative breast cancers

TNBC harbor unusual activation of NF-κB, which contributes to its aggressiveness and its capability to continue hormone-independent growth (Chiu & Su, 2009; Poma, Labbozzetta, D'Alessandro, & Notarbartolo, 2017).

Curcumin downregulated the nuclear and cytoplasmic p65 expression, and nucleus translocation of phospho-p65 and RelB to suppress NF-κB signaling in MDA-MB-231 and MDA-MB-435 TNBC cells (Coker-Gurkan et al., 2018; Q. Liu, Loo, Sze, & Tong, 2009). In these studies and others, curcumin induced cell cycle arrest and decreased expression of cell migration, invasion and proliferation proteins, such as cyclinD1 and MMP-1, and activated both intrinsic and extrinsic apoptosis pathways by regulating Bax/Bcl-2 ratio, caspase -2, -8, -7 and -9 proteins to inhibit the invasion and metastasis in TNBC cells (Banik et al., 2017; Chiu & Su, 2009; Coker-Gurkan et al., 2018; Fan et al., 2016; Q. Liu et al., 2009; Poma et al., 2017).

Curcumin's effectiveness for suppressing NF-κB signaling to target metastasis and angiogenesis is also demonstrated in TNBC animal models (Ferreira et al., 2015; Shanmugam et al., 2015).

B. Curcumin targets Wnt/β-catenin, MAPK signaling, and cell adhesion in triple negative breast cancers

Curcumin can also inhibit Wnt/β-catenin signaling and target its downstream components c-Myc and cyclin D1 to impede cell proliferation and induce apoptosis in breast cancer cells, including TNBC (C. P. Prasad et al., 2009). "Curcumin modulated EGFR-MAPK signaling to significantly reduce cell proliferation and induced apoptosis" (Mittal, Aryal, et al., 2020) by downregulating phosphorylated ERK1/2 and EGFR (X.-D. Sun et al., 2012). Moreover, curcumin can suppress Notch1 due to, at least in part, a reduction in the mutant p53 level, which may induce apoptotic response in TNBC cells in vitro (Y. H. Bae et al., 2013).

"Curcumin also altered the expression of cell adhesion molecules to reduce migration and invasion of MDA-MB-231 cells by downregulating β-catenin, slug, AXL, and vimentin expression, while upregulating E-cadherin and N-cadherin (Gallardo & Calaf, 2016; Palange et al., 2012)" (Mittal, Aryal, et al., 2020).

C. Curcumin targets metabolism

Curcumin can target cancer metabolism. "Curcumin downregulated key glycolytic pathway enzymes with significant decreases in glucose uptake and lactate production in colorectal tumor cells (K. Wang et al., 2015) and in esophageal cancer cells (F.-J. Zhang, Zhang, Liu, & Huang, 2015)" (Mittal, Aryal, et al., 2020). The effect of curcumin on glycolysis downregulation due to decreased pyruvate kinase M2 (PKM2) expression through mTOR-HIF1α inhibition is also demonstrated on breast cancer cells (Siddiqui et al., 2018).

Using a 2DE-based proteomic approach, a group demonstrated that curcumin downregulated ALDOA and TPI1 glycolysis proteins among the 5 down-regulated proteins in MCF-7 breast cancer cells (Fang, Chen, Guo, Pan, & Yu, 2011). The inflammatory cytokine tumor necrosis factor alpha (TNF- α) promotes glycolysis and inhibits mitochondrial biogenesis in malignant breast cancer cells (Banik et al., 2017). Curcumin reversed this TNF- α induced elevated aerobic glycolysis in breast cancer cells (Vaughan et al., 2013).

Curcumin targeted the SLUG/Hexokinase-2 (HK2) nexus in TNBC cells to mediate 4-hydroxytamoxifen (4-OHT) resistance (Geng et al., 2016). Curcumin inhibited the SLUG expression and its binding to the HK2 promoter, which suppressed the elevated levels of glycolytic rate limiting enzyme HK2 to sensitize MDA-MB-231 cells to 4-OHT.

These observations suggest that "curcumin can be a strong drug candidate to target the metabolic vulnerabilities present in TNBC" (Mittal, Aryal, et al., 2020).

2.2.3 Binding proteins partners of curcumin to regulate various signaling pathways

Several binding protein partners of curcumin have been discovered (Kujundžić et al., 2019). The *in situ* proteomic profiling of HCT116 colorectal carcinoma cells revealed 197 covalent binding partners of curcumin, which included multiple cancer-associated glycolytic enzymes, such as LDHA, LDHB, ENO1, ALDOA, GAPDH, TPI1, PGK1, PKM, and also pyruvate metabolism enzymes MDH1 and MDH2 (Jigang Wang et al., 2016). Additionally, eight binding partners were from protein processing in endoplasmic reticulum pathway, including CKAP4, GANAB, HSP90AB1, HSPA5, HSPA8, P4HB, PDIA3, and PRN1. The protein processing in endoplasmic reticulum pathway regulation is also shown to be linked with endoplasmic reticulum stress and apoptosis (Luyan Shen et al., 2016).

In HEI-193 human schwannoma cells, approximately 60 binding partner proteins of curcumin were discovered (Angelo et al., 2013). These included β-actin, 3-phosphoglycerate dehydrogenase (PHDGH) as well as heat shock proteins, such as HSP70 and HSP90, which function as chaperones to play important role in protein folding and are produced in response to stress (Mayer & Bukau, 2005; Vabulas, Raychaudhuri, Hayer-Hartl, & Hartl, 2010). A proteome-wide screening in HeLa human cervix adenocarcinoma cells identified curcumin covalently bound to cysteine (Cys) residues of 42 proteins (Abegg et al., 2015). Abegg and colleagues demonstrated that the covalently bound curcumin modified proteins involved in various cellular signaling and metabolic pathways, such as Akt and MAPK signaling pathways. Among these, curcumin bound to Cys51 and inhibited the catalytic activity of enzyme casein kinase I gamma 3 (CSNK1G), which participates in Akt signaling (Abegg et al., 2015).

Considering these, the binding of curcumin to cysteine residues of protein targets could be a potential mediator of curcumin's effect on various cellular and metabolic signaling pathways in cancers. However, how such bindings could influence the activity of these target proteins is not quite clear (Kujundžić et al., 2019).

2.3 Turmeric silver nanoparticles

"The majority of the bioactivities of turmeric are attributed to curcumin, and it remains the most extensively studied compound of turmeric. However, recent evidences suggest that other compounds of the mother herb turmeric can also show a potent bioactivity (Aggarwal et al., 2013)" (Mittal, Camarillo, et al., 2020). Turmeric is richly loaded with proteins and various phytochemicals, including but not limited to alkaloids, flavonoids, phenols, saponin, steroids, tannins, terpenoids, and triterpenes (Oghenejobo & Bethel, 2017; S. Prasad & Aggarwal, 2011). To enhance the efficacy of turmeric, various researchers have previously synthesized silver nanoparticles using an aqueous turmeric extract exploiting the green biosynthesis technique (Alsammarraie, Wang, Zhou, Mustapha, & Lin, 2018; Nayak, Goveas, & Vaman Rao, 2017; Shameli, Ahmad, Jazayeri, et al., 2012; Shameli, Ahmad, Zamanian, et al., 2012).

The green biosynthesis technique using plant extract provides a simple, environment friendly, efficient, and cost effective avenue for metal nanoparticles preparation (Singh et al., 2018). The mechanism of silver nanoparticles biosynthesis using green biosynthesis technique is shown in Figure 2.6. The plant extracts contain various phytochemicals (such as flavonoids, alkaloids, phenols, and anthracenes), carbohydrate and proteins, which can actively reduce metal ions to generate metal nanoparticles (Singh et al., 2018).

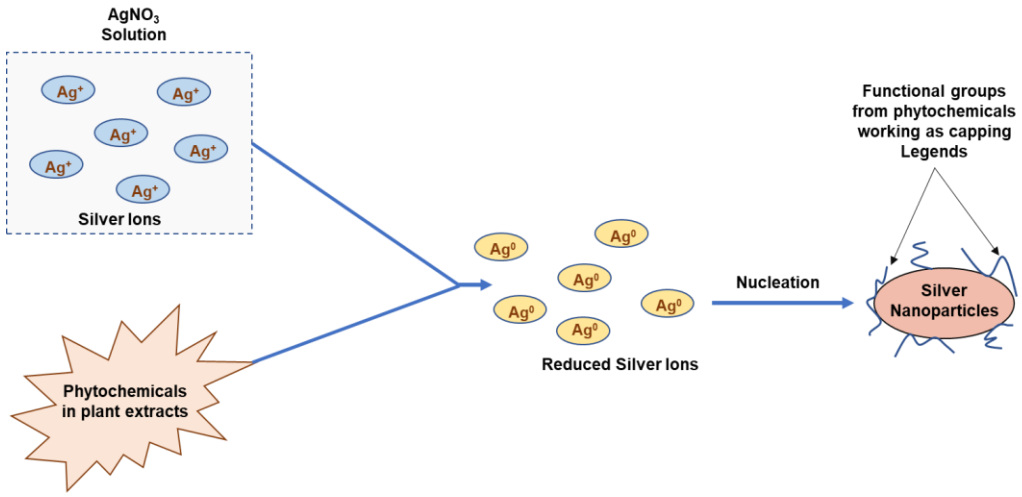

Figure 2.6: Mechanism of silver nanoparticles biosynthesis using green biosynthesis technique. The aqueous AgNO3 solution contains silver ions. The phytochemicals present in plant extracts reduce these silver ions to generate metal nanoparticles. Various functional groups present in these compounds, such as C–O–C, C–O, C=C, and C=O function as capping agents. Idea from (J. Singh et al., 2018).

Various functional groups present in these compounds, such as C–O–C, C–O, C=C, and C=O function as capping agents (Mude, Ingle, Gade, & Rai, 2009) to control nanoparticle growth, stability and agglomeration of metal nanoparticles during biosynthesis (Ajitha, Kumar Reddy, Reddy, Jeon, & Ahn, 2016).

Shameli and colleagues prepared turmeric silver nanoparticles from aqueous silver nitrate and characterized them. They demonstrated the antibacterial activities of turmeric silver nanoparticles against Gram-positive (Staphylococcus aureus) and Gram-negative (Salmonella typhimurium SL1344) strains of bacteria (Shameli, Ahmad, Jazayeri, et al., 2012; Shameli et al., 2014; Shameli, Ahmad, Zamanian, et al., 2012).

Nayak et al. also synthesized and characterized turmeric silver nanoparticles and showed their catalytic through methylene blue reduction (Nayak et al., 2017). They also successfully demonstrated the antibacterial activities of turmeric nanoparticle impregnated cotton bandage gauze against Gram-positive (Bacillus subtilis) and Gram-negative (Pseudomonas aeruginosa) bacteria.

Similarly, Alsammarrai et al. synthesized turmeric silver nanoparticles from aqueous turmeric extract and characterized them (Alsammarraie et al., 2018). The nanoparticles showed excellent antibacterial properties against Escherichia coli O157:H7 and Listeria monocytogenes food-borne pathogens. The scanning electron microscopy and transmission electron microsopy studies revealed a shrinkage and damage to bacterial cell wall and leakage of intracellular contents upon treatment with turmeric nanoparticles.

Previous research revealed that the turmeric silver nanoparticles show excellent antibacterial activity against various bacterial strains. However, there is no study on the anti-cancer properties of turmeric silver nanoparticles.

2.4 Electrochemotherapy

Electrochemotherapy is an efficient modality to treat local tumors, and it has shown promising success in the clinics for the treatment of various types of cancers, including melanomas, sarcomas, carcinomas and many other types of cancers, and it is applicable to all histology of cancers (Marty et al., 2006). Among the several clinically approved drugs tested with ECT, bleomycin and cisplatin are the most suitable drugs to use with electrochemotherapy in clinics (Jaroszeski et al., 2000; Kunte et al., 2017; Marty et al., 2006; G Sersa, Cemazar, & Miklavcic,

1995). "Typically, bleomycin, and occasionally, cisplatin, is used in ECT (Marty et al., 2006)" (Mittal, Camarillo, et al., 2020). When used intratumorally, cisplatin-based ECT offers a better tolerated alternative to bleomycin-based ECT (De Giorgi et al., 2020).

Several clinical "studies have demonstrated the clinical efficacy of ECT with cisplatin in treating advanced subcutaneous and cutaneous tumor nodules" (Mittal, Aryal, et al., 2020), including malignant melanoma, squamous cell carcinoma, basal cell carcinoma, keratoacanthoma, and breast cancer and its metastases (Cadossi, Ronchetti, & Cadossi, 2014; De Giorgi et al., 2020; Marty et al., 2006; Rebersek, Cufer, Cemazar, Kranjc, & Sersa, 2004; G Sersa et al., 1998; G Sersa, Stabuc, Cemazar, Miklavcic, & Rudolf, 2000b; G Sersa et al., 2000a; Gregor Sersa, Cemazar, & Rudolf, 2003). A long lasting complete response of 77% was observed for ECT with cisplatin in malignant melanoma patients, compared to19% in the patients treated with cisplatin alone (Marty et al., 2006; G Sersa et al., 2000a). "Recently, Kis et al. successfully performed (bleomycin-based) ECT for challenging eyelid-periocular BCC conditions to obtain CR in advanced primary and recurrent cases of eyelid BCCs (Kis et al., 2019)" (Mittal, Camarillo, et al., 2020). Typical electrical pulse parameters in ECT application for breast cancer are as follows (Table 2.1):

- Electrical field strength: 910-1400V/cm.
- Pulse duration: 100μs.
- Number of pulses: 8 pulses or 96 pulses (8 pulses per12 different pairs of needles).
- Frequency: 1Hz or 5kHz.

The choice of electrical pulse parameters used in ECT depends upon the electrodes (plate electrodes or needle electrodes - needle row type or seven-needles, hexagonal array type) used for pulse application. In clinical settings, ECT produced less toxicity to normal tissues compared to cancerous tissues, and larger normal vessels surrounding tumor were not damaged (Edhemovic et al., 2011; Matthiessen et al., 2012). ECT also caused less damage to "healthy tissues located at tumor margins, which ensures a good wound healing and an exceptional aesthetic and functional recovery after treatment (Campana et al., 2019; Gehl, 2005; Kis et al., 2012; Marty et al., 2006)" (Mittal, Aryal, et al., 2020). In malignant melanoma treated with ECT with bleomycin, only needle marks were observed in much less effected normal tissues, compared to the surrounding tumor tissue (Gehl, 2005). In a study of ECT in liver metastases the functionality of larger normal vessels was preserved while the tumor tissue was necrotic (Gasljevic et al., 2017). Furthermore, the effect of ECT on tumor blood vessels was more prominent compared to normal blood vessels (Markelc,

Sersa, & Cemazar, 2013). "In the clinical trial comparing calcium electroporation to ECT using bleomycin, the effect on the surrounding normal tissue was not directly investigated, but no damage on normal structures was reported (Falk, Matthiessen, Wooler, & Gehl, 2018)"(Frandsen & Gehl, 2018).

"Considering these excellent results, its safety, and affordability, ECT is now recommended for primary skin cancer and cutaneous metastases by several national and international guidelines" (Gehl et al., 2018; "Overview | Electrochemotherapy for primary basal cell carcinoma and primary squamous cell carcinoma | Guidance | NICE," 2014) - (Mittal, Camarillo, et al., 2020).

2.5 Electrochemotherapy for breast cancers in clinics

In clinic, Campana and colleagues used ECT to treat chest wall recurrence (CWR) of breast cancer after mastectomy in 51 patients of median age 70 year (range 38-88), who faced tumor progression despite re-irradiation and were refractive to several systemic treatments, as shown in Figure 2.7 (Campana, Falci, Basso, Sieni, & Dughiero, 2014; Campana et al., 2009, 2012). In this study, a median of two ECT courses (range1-5) were performed to obtain a complete 2-month objective response (OR) in 43.2% of patients (22/51) and a partial response (PR) in 47.5% of patients (24/51) (Campana, Falci, et al., 2014). The 3-year local control rate was 71%. The ECT parameters were as follows:

- Electrical pulse parameters: 910-1000V/cm, 100µs, 8 pulses at 5kHz frequency.
- Electroporator: Cliniporator™ device, Igea, Modena, Italy.
- Electrodes: Seven-needles hexagonal array needle electrodes.
- Drug: Bleomycin.
- Drug route and dosage: Intravenously (i.v.) (15,000IU/m^2 of body surface area) or intratumorally (i.t.) with dosage depending upon the nodule size (1000IU/cm^3 for < 0.5cm^3, 500IU/cm^3 for 0.5-1cm^3, 500IU/cm^3 for > 0.5cm^3).
- Number of patients: 51 patients.
- Number of tumor nodules/lesions: 212.

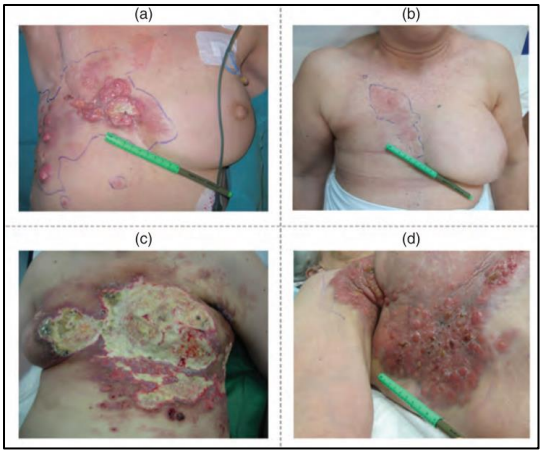

Figure 2.7: "Different clinical presentations of chest wall recurrence (CWR) from breast cancer: (a) Multiple palpable nodules disseminated from the mastectomy scar to the lateral portion of the chest wall, the skin of the ipsilateral axilla and the abdominal wall. (b) In this case, the chest wall skin presents inflammatory changes without a discernible mass. (c) In more advanced patients, the chest wall may be diffusely involved with widespread ulceration. (d) Alternatively, diffuse soft tissues infiltration with woody induration beyond the limits of standard surgical or radiation boundaries may be present". (Campana, Falci, et al., 2014). Reproduced with permission from (Campana, Falci, et al., 2014).

Whelan et al. performed three sessions of ECT over 47-months to treat a patient with extensive CWR of inflammatory breast cancer, which was refractive to multimodal therapies (Whelan et al., 2006). The bleeding tumor was completely eliminated following the third ECT application, dramatically improving the quality of life. ECT delayed the tumor recurrence to 30 months, which responded well to ECT. The ECT parameters were as follows:

- Electrical pulse parameters: 1400V/cm, 100µs. Other information not reported (NR).
- Electroporator: NR.
- Electrodes: Linear array needle electrodes.
- Drug: Bleomycin.
- Drug route and dosage: i.v. (20,000IU) and i.t. (5,000IU).
- Number of patients: 1 patient.
- Number of tumor nodules/lesions: 1

In a multiple cancer study, Larkin et al. performed ECT on 17 breast cancer patients with tumors refractory to surgery, chemotherapy, and radiotherapy (Larkin et al., 2007). Among 100 tumor nodules (including 67 of breast cancer CWR) treated with ECT, 63 (63%) showed a complete response (CR) and 20 (20%) showed a PR. In the breast cancer CWR cases, 45 (67%)

showed a CR and 14 (21%) showed a PR (Figure 2.8). The response rate was better in tumor sized < 3cm. The ECT parameters were as follows:

- Electrical pulse parameters: 1400V/cm, 100µs, 8 or 96 pulses at 1 or 5000Hz frequency.
- Electroporator: Cliniporator™ device, Igea, Modena, Italy.
- Electrodes: Plate electrodes or parallel needle electrodes.
- Drug: Bleomycin.
- Drug route and dosage: i.v. (15,000IU/m^2 body surface area) or i.t. for tumors < 3cm diameter (dosage: NR).
- Number of patients: 17 breast cancer patients.
- Number of tumor nodules/lesions: 100 nodules.

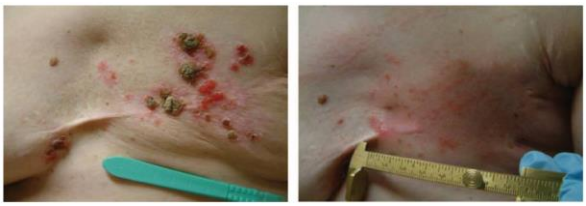

Figure 2.8: A 52-year old patient with breast cancer CWR, four years after mastectomy and axillary node clearance and adjuvant radiation therapy. The tumors did not respond to systemic chemotherapy. Following 2 month of the ECT treatment, a complete response was observed. At 14-month follow-up, no recurrence was observed at the treatment site. Reproduced with permission from (Larkin et al., 2007).

Rebersek et al. used ECT with cisplatin to treat six metastatic breast cancer patients (five female and one male) with CWR, who did not respond well to standard treatments (Rebersek et al., 2004). All 12 lesions treated with ECT showed OR, among these 4 lesions (33%) showed CR (median response duration – 10 weeks), and 8 (67%) showed PR (median response duration - 5 weeks), with more than 50% decrease in the lesion. The efficacy of the ECT was lesion size dependent, as all the smaller sized lesions (72mm^3) showed CR, while larger sized tumors showed PR (192mm^3). On the contrary, all the untreated lesions showed progression, and for 6 lesions treated with cisplatin alone, no CR was observed, even with pre-treatment volume of 73 mm^3, and 5 lesions showed PR (average duration - 5 weeks). After ECT no systemic side effects (early or late) were recorded, and only a minimal local scarring and depigmentation of the skin was observed as late side effects (as shown in Figure 2.9, and later reported by the same group in a review article: (Gregor Sersa, Cufer, Paulin, Cemazar, & Snoj, 2012)). The ECT parameters were as follows:

- Electrical pulse parameters: 910V (=1300V/cm for 7mm electrodes), 100µs, 8 pulses (4+4 pulses - perpendicular to each other) at 1Hz frequency.
- Electroporator: GHT 1287 (Jouan, France).
- Electrodes: Superficial plate electrodes (thickness: 1mm, width: 7mm, length: 14mm, inner distance between electrodes: 7mm).
- Drug: Cisplatin.
- Drug route and dosage: i.t. (1mg/100mm^3).
- Number of patients: 6 patients (female: 5, male: 1).
- Number of tumor nodules/lesions: 26 lesions (ECT: 12, cisplatin i.t. only: 6, control: 8).

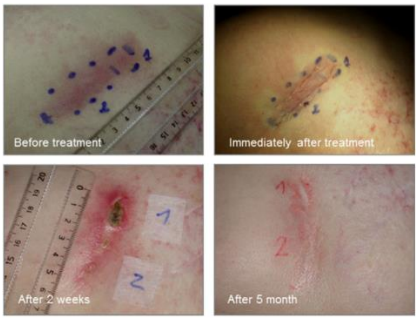

Figure 2.9: The ECT with cisplatin treatment of two tumor nodules of a breast cancer patient with CWR. The cisplatin was injected (i.t.) and whole tumor area was covered in a sequence of multiple electroporation. A scab appeared 2 weeks post-ECT, which eventually fell off. A good aesthetic recovery was observed after 5 months, and the CR lasted for 2 years. Subsequent disease in visceral organs was treated using systemic chemotherapy. Reproduced with permission from (Gregor Sersa et al., 2012).

In a two year long prospective non-randomized clinical study over four centers under the European Standard Operating Procedures for ECT (ESOPE) project, the breast cancer CWR was the second most treated tumor (14 patients of 41 total patients), after melanoma (Marty et al., 2006). Other patients included were of colon cancer, squamous cell carcinoma of the skin, squamous cell carcinoma of cervix, and Kaposi and leiomyosarcoma. Out of total 58 breast cancer nodules treated with ECT, 52 (~90%) showed CR and 6 (5%) showed PR. Irrespective of the tumor size, no difference in the tumor response was observed for ECT. However, a systemic i.v. administration of bleomycin resulted into a better antitumor response with ECT for bigger nodules (>0.5cm^3), compared to local i.t. route of bleomycin and cisplatin. Additionally, ECT treatment toxicology studies performed on 61 patients revealed limited side effects, such as acceptable level of pain limited to the local site of ECT, low level of muscle contraction, and the whole procedure

was viewed favorably (not too stressful and painful) by 57 patients (93%). The ECT parameters were as follows:

- Electrical pulse parameters: 1000 or 1300V/cm, 100µs, 8 or 96 pulses at 1 or 5000Hz frequency. Depended upon the electrodes type (Type I electrodes: 1300V/cm, 100µs, 8 pulses at 1 or 5000Hz; Type II: 1000V/cm, 100µs, 8 pulses at 1 or 5000Hz; Type III: 1000V/cm, 100µs, 96 pulses (8 pulses/pair of needles) at 5000Hz).
- Electroporator: Cliniporator™ device, Igea, Modena, Italy.
- Electrodes: Plate electrodes (superficial nodules - Type I electrodes) or needle electrodes (deep seated nodules- maximum depth 3cm). They used two types of needle electrodes: (1) needle row type (small nodules - Type II electrodes) and (2) Seven-needles, hexagonal array type (large nodules- Type III electrodes). Needle electrodes were also used for larger and thick superficial nodules.
- Drug: Bleomycin or cisplatin.
- Drug route and dosage: Bleomycin - i.v. (15,000IU/cm^3) or i.t. (1000IU/cm^3 for < 0.5 cm^3, 500IU/cm^3 for 0.5-1cm^3, 250IU/cm^3 for >1cm^3). Cisplatin - i.t. (2mg/cm^3 for < 0.5 cm^3, 1mg/cm^3 for 0.5-1cm^3, 0.5mg/cm^3 for >1cm^3).
- Number of patients: 14 patients.
- Number of tumor nodules/lesions: 59 nodules.

Cabula et al. reported a large multicenter retrospective cohort study of ECT on 125 patients with breast cancer skin metastases (as shown in Figure 2.10) (Cabula et al., 2015). A 90% of response rate was obtained at 2-months with CR of 58.4%. The 1-year local progression free survival (LPFS) was 86.2% overall and was 96% for the patients with CR. The predictors for the CR following ECT included – smaller size of tumor (< 3cm diameter), no visceral metastases, ER-positivity, and lower Ki-67 expression. No treatment toxicity was observed during the ECT procedure. The ECT parameters were as follows:

- Electrical pulse parameters: NR.
- Electroporator: NR.
- Electrodes: Seven-needles hexagonal array type (207 tumors), needle row type (10 tumors), and plate electrodes (13 tumors).
- Drug: Bleomycin.
- Drug route and dosage: i.v. in 100 patients (15,000IU/cm^3) or i.t. in 25 patients (1000IU/cm^3 for < 0.5 cm^3, 500IU/cm^3 for 0.5-1cm^3, 250IU/cm^3 for >1cm^3).
- Number of patients: 125 patients.
- Number of tumor nodules/lesions: 239 tumors.

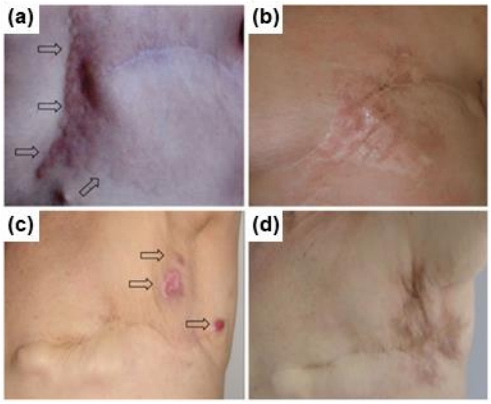

Figure 2.10: The ECT on breast cancer skin metastasis in two patients. (a,c) At baseline, (b,d) After 1-year of follow up. Reproduced with permission from (Cabula et al., 2015).

Campana et al. reported a retrospective analysis of ECT on 55 patients with breast cancer superficial metastasis, and compared two groups of patients based on age (< 70 years, n = 27 or ≥ 70 years, n = 28) (Campana, Galuppo, et al., 2014). In a median follow up of 32 months (range 6-53), an overall CR of 40% was obtained. The CR was 57% for the elderly group, significantly higher than 26% for the younger patients. On the contrary, the 2-year LPFS was higher in the younger group (93% vs 67 in elderly group), indicating a better local tumor control in younger patients. The ECT associated complication included, post-ECT pain and ulceration. The ECT parameters were as follows:

- Electrical pulse parameters: 400-730V, 100µs, 8 pulses. Other information NR.
- Electroporator: Cliniporator™ device, Igea, Modena, Italy.
- Electrodes: Needle electrodes (type is NR).
- Drug: Bleomycin.
- Drug route and dosage: i.v. (15,000IU/m^2 of body surface area) or i.t. (1000IU/cm^3 for < 0.5 cm^3, 500IU/cm^3 for 0.5-1cm^3, 250IU/cm^3 for >1cm^3).
- Number of patients: 55 patients.
- Number of tumor nodules/lesions: 212 lesions.

The ECT was used to treat 12 elderly patients, with breast cancer metastases (regional or distant skin or subcutaneous), with or without visceral disease by Benevento et al. (Benevento, Santoriello, Perna, & Canonico, 2012). An excellent OR of 92% was observed, with 75% of CR and 17% of PR. Other than sharp pain at 48h in one patient and ulceration caused by tumor

necrosis in one patient, no serious complication was recorded. The ECT parameters were as follows:

- Electrical pulse parameters: NR.
- Electroporator: Cliniporator™ device, Igea, Modena, Italy.
- Electrodes: 2-3cm long needle electrodes (type is NR).
- Drug: Bleomycin.
- Drug route and dosage: i.v. (15,000IU/m^2 of body surface area).
- Number of patients: 12 patients (female: 11, male: 1).
- Number of tumor nodules/lesions: 142 lesions.

Wichtowski et al. also used ECT to treat breast cancer skin metastasis in 7 patients. An OR of 86% was obtained, with 43% of CR and 43% of PR (Witkiewicz, 2016). Only 14% of the tumor nodules showed progressive disease in a follow up of average 12 weeks. The ECT parameters were as follows:

- Electrical pulse parameters: 1000V/cm, 5000Hz. Other information NR.
- Electroporator: Cliniporator™ device, Igea, Modena, Italy.
- Electrodes: 6 needles disposable electrodes.
- Drug: Bleomycin.
- Drug route and dosage: i.v. (15,000IU/m^2 of body surface area).
- Number of patients: 7 patients.
- Number of tumor nodules/lesions: 35 lesions.

Campana and colleagues across 10 Italian clinics treated 376 patients between October 2008 to March 2013, with various tumor types – "carcinomas (breast, basal cell, and squamous cell), melanomas, sarcomas (Kaposi, and soft tissue), and other (Campana et al., 2016b)" (Mittal, Camarillo, et al., 2020). These patients were previously treated with combination of modalities - surgery, chemotherapy, radiotherapy, and immunotherapy. There were 31 breast carcinoma patients, among those 16 (51.6%) patients had visceral metastases. The ECT treatment showed an excellent OR of 89.5%, with CR of 36.8% in breast carcinoma patients, with side effects mainly limited to skin. Only 51.6% of breast carcinoma patients reported skin toxicity (grade 2-4) and bigger tumor size (> 2cm) were particularly associated with higher skin toxicity incidences. The ECT parameters were as follows:

- Electrical pulse parameters: NR.
- Electroporator: Cliniporator™ device, Igea, Modena, Italy.

- Electrodes: Tumor size < 0.8cm - plate electrodes (superficial tumors) or needle linear array (deep seated tumors). Tumor size ≥ 0.8cm - Seven-needles hexagonal array type.
- Drug: Bleomycin or cisplatin (in 2 out of 376 total patients).
- Drug route and dosage: Bleomycin - i.v. or i.t. (depending upon the tumor number and size) and cisplatin - i.t. (NR).
- Number of patients: 31 patients.
- Number of tumor nodules/lesions: NR.

Matthiessen et al. reported a large cohort of breast cancer patients treated with ECT from International Network for Sharing Practice on Electrochemotherapy (INSPECT) database from 10 clinics across Europe (Matthiessen et al., 2018). A total of 119 patients with breast cancer cutaneous metastases were treated with ECT. The median diameter of cutaneous metastases was 25mm, with chest being the most common site (89%). The evaluation of response in 90 patients at 2-months following ECT resulted into a CR in 45 patients (50%) (an example shown in Figure 2.11), PR in 19 (21%), stable disease in 16 (18%), and disease progression in 7 (8%). Common side effects were - low-grade pain, ulceration, and long-lasting hyperpigmentation, however no serious complication was recorded. Based on these data, authors recommended the use of ECT for cutaneous metastases, which are refractory to surgery and chemotherapy.

- Electrical pulse parameters: 1000 or 1300V/cm, 100µs, 8 pulses at 1 or 5000Hz frequency. Depended upon the electrodes type (Type I electrodes: 1300V/cm, 100µs, 8 pulses at 1 or 5000Hz; Type II: 1000V/cm, 100µs, 8 pulses at 1 or 5000Hz; Type III: 1000V/cm, 100µs, 8 pulses at 5000Hz).
- Electroporator: Cliniporator™ device, Igea, Modena, Italy.
- Electrodes: Plate electrodes (2 plates with 6mm gap - Type I electrodes) or needle electrodes (deep seated nodules- maximum depth 3cm). Needle electrodes were of two types: (1) needle row type (4mm gap between rows - Type II electrodes) and (2) hexagonal array type (7.9mm between needles- Type III electrodes).
- Drug: Bleomycin.
- Drug route and dosage: i.v. (15,000IU/m^2 of body surface area) or i.t. (1000IU/cm^3).
- Number of patients: 119 patients.
- Number of tumor nodules/lesions: NR.

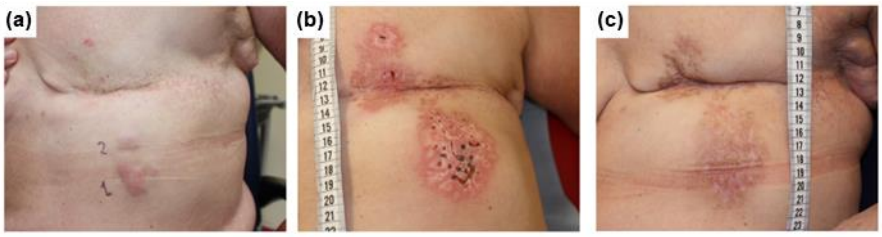

Figure 2.11: The result of ECT on a patient with breast cancer cutaneous metastasis on the chest wall and abdomen. (a) Pre-treatment, (b) 23 days following treatment, (c) 135 days following treatment. The patient displayed CR, but eventually established bone metastases following last follow-up and began new systemic treatment. Reproduced with permission from (Matthiessen et al., 2018).

In summary, the results from these clinical studies indicate that ECT is effective in treating advanced, recurrent, and metastatic breast cancers, which are refractory to multiple modalities, such as surgery, chemotherapy, and radiation. ECT is more effective in smaller breast tumor nodules, highlighting a need of early ECT application for better response. No serious side effects were observed in patients, except local, low-grade pain, ulceration, and long-lasting hyperpigmentation. Table 2.1 summarizes the breast cancer clinical studies discussed above.

Table 2.1: A summary of the clinical studies of ECT for advanced, recurrent, and metastatic breast cancers. Abbreviations - PR: partial response (when following treatment tumor size decreases), CR: complete response (when following treatment when all cancer signs disappear), OR: objective response (A measurable response - when tumors display either PR or CR).

S.N.	Reference	Disease	Patients	Nodules/ Lesions	Drug route	ECT parameter	Electrode	Response to treatment (%)		
								PR	CR	OR
1	Campana et al. (2014)	Breast cancer chest wall recurrence (CWR)	51	43.2	Bleomycin (i.v. or i.t.)	910-1000V/cm, 100µs, 8 pulses at 5000Hz	Seven-needles hexagonal array needle electrodes.	47.5	-	43.2
2	Whelan et al. (2006)	Breast cancer CWR	1	-	Bleomycin (i.v. or i.t.)	1400V/cm, 100µs. Other information NR.	Linear array needle electrodes	-	-	-
3	Larkin et al. (2007)	Breast cancers, including CWR	17	83	Bleomycin (i.v. or i.t.)	1400V/cm, 100µs, 8 or 96 pulses at 1 or 5000Hz	Plate electrodes or parallel needle electrodes	20	63	83
4	Rebersek, et al. (2004)	Breast cancer CWR	6	100	Cisplatin - i.t.	910V (=1300V/cm for 7mm electrodes), 100µs, 8 pulses at 1Hz	Superficial plate electrodes	67	33	100

Table 2.1 continued

5	*Marty et al. (2006) - ESOPE*	*Breast cancer CWR*	*14*	*100*	*Bleomycin (i.v. or i.t.) or cisplatin (i.t.)*	*1000 or 1300V/cm, 100µs, 8 or 96 pulses at 1 or 5000Hz*	*Plate electrodes or needle electrodes (needle row type or Seven-needles, hexagonal array type)*	*10*	*90*	*100*
6	Cabula et al. (2015)	Breast cancer skin metastases	125	90.2	Bleomycin (i.v. or i.t.)	NR	Plate electrodes or needle electrodes (needle row type or Seven-needles, hexagonal array type)	31.8	58.4	90.2
7	Witkiewicz, et al. (2016)	Breast cancer skin metastasis	7	86	Bleomycin - i.v.	1000V/cm, 5000Hz. Other information NR.	6 needles disposable electrodes	43	43	86
8	Campana et al. (2014)	Breast cancer superficial metastasis	55	87.3	Bleomycin (i.v. or i.t.)	400-730V, 100µs, 8 pulses. Other information NR.	Needle electrodes (type is NR)	47.3	40	87.3
9	Benevento et al. (2012)	Breast cancer metastases	12	92	Bleomycin - i.v.	NR	2-3cm long needle electrodes (type is NR)	17	75	92
10	Campana et al. (2016)	Breast carcinoma	31	89.5	Bleomycin (i.v. or i.t.)	NR	Plate electrodes or needle electrodes (needle row type or Seven-needles, hexagonal array type)	-	36.8	89.5
11	Matthiessen et al. (2018)	Breast cancer cutaneous metastases	119	64	Bleomycin (i.v. or i.t.)	1000 or 1300V/cm, 100µs, 8 pulses at 1 or 5000Hz	Plate electrodes or needle electrodes (needle row type or Seven-needles, hexagonal array type)	19	45	64

2.6 Mechanisms of ECT

At present the mechanistic understanding of the effects induced by ECT is based on the three pillars to induce an overall antitumor effectiveness in patients:

- Increased drug concentration.
- Vascular effects.
- Elicit local immune response.

The amount of individual contribution of each of three mechanisms has not been studied yet, however it may vary according to the tumor type. While the vascular disruption by ECT may have a greater influence on better vascularized tumors, more immunogenic tumors may have a greater contribution of immune response (Gregor Sersa, Bosnjak, Cemazar, & Heller, 2016).

The increased drug uptake in tumors and tumor cells leads to a slow, mitotic or apoptotic cell death of tumor cells due to the DNA damaging effect produced by drugs, such as bleomycin or cisplatin. The cytotoxicity of ECT with cisplatin is proportional to the higher uptake of cisplatin, as 2-3 times higher cisplatin-DNA binding occured for ECT with cisplatin in tumors (M. Čemažar et al., 1999; Serša, Čemažar, & Miklavcic, 1995). Further, the ECT with cisplatin enhanced cytotoxicity and induced apoptosis in primary cells derived from pancreatic ductal adenocarcinoma pulmonary metastases (Michel et al., 2018). Another study investigating the histopathology and mechanism of cell death after ECT in patients with cutaneous melanoma metastases reported early morphological changes in tumor cell 10 min after ECT (Bigi et al., 2016). As demonstrated by histological and caspase-3 staining, the cell damage continued until 10 days after the treatment and it was highest at 3 days, with apoptosis as the prominent mechanism of the cell death after ECT.

2.7 Advantages and disadvantages of ECT

2.7.1 Advantages of ECT

ECT has the following advantages:

1. In clinics, ECT is simple, repeatable, highly effective and safe in various subsets of patients with advanced, recurring, radio- and chemo-resistant tumors.
2. ECT improves the quality of life of patients.

3. No serious side effects are observed in patients, except local, low-grade pain, ulceration, and long-lasting hyperpigmentation.
4. ECT is short and can be performed on out-patient basis, as side-effects are minimal and patients do not require special post-treatment attention.
5. ECT can be performed on any part of the body.
6. ECT is easy to perform and requires minimal personnel (one physician, one nurse and one technician to handle electroporator), and no specific skills (one-day training is sufficient).
7. The ECT is cost effective. The technology and equipment required are relatively inexpensive, making it budget friendly for small hospitals and developing countries.
8. Multi target approach is feasible as ECT utilizes the synergy of chemotherapy drugs and electrical pulses. ECT could be a valuable tool to deal with tumor heterogeneity.
9. ECT does not induce thermal effects.
10. ECT induces apoptotic cell death, which allows aesthetic recovery of the tissues post-ECT.

2.7.2 Disadvantages of ECT

ECT has the following disadvantages:

1. Pain could be limiting factor in some patients. However, pain could be avoided by lifting the tumor tissues at the time of ECT (Gregor Sersa et al., 2003).
2. Muscle contraction during electrical pulse application could cause unpleasant sensation in some patients. However, the total number of muscle contractions could be reduced by increasing the frequency of pulses, above the frequency of tetanic contraction (Miklavčič et al., 2005).
3. ECT is not suitable for patients with cardiac pacemakers.
4. The efficacy of ECT is dependent upon drug distribution and coverage of electrical pulses.
5. Large area coverage is required by electrodes for better outcomes. ECT is often cumbersome in large and multiple nodules, as it cannot be performed in one session. However, these problems can be solved by better electrode design.
6. ECT utilizes drugs, such as bleomycin and cisplatin. Although smaller dosage of these drugs is used with ECT, their toxicity cannot be ignored. Therefore, there is a critical need to study the alternate and less toxic natural compounds for ECT applications.

2.8 Electrochemotherapy and Curcumin

Despite the several efforts focused on to discover the action mechanism of curcumin, a holistic understanding of the multiple effects induced by curcumin is still absent. Moreover, the limited bioavailability and the poor tissue absorption of the curcumin remains to be an impedance to its success in the human cancer subjects (W.-Y. Lin et al., 2014). Several formulations such as curcumin-derivative nano-micelles, and curcumin-loaded nanoparticles are being explored to increase the limited bioavailability and absorption of curcumin (Pignanelli et al., 2017). “However, the potential of these formulations is yet to be established” (Mittal et al., 2017).

Lu et al. showed a significant increased uptake of curcumin in human pancreatic cancer cells (PANC-1) cells upon electrical pulse application (C.-H. Lu, Lin, Hsieh, Chen, & Chao, 2018).

Towards this, electrical pulse application can be effective to increase the delivery of curcumin in TNBC cells by opening pores in the cell membrane, since an enhanced cytotoxicity (up to 1000 times) can be obtained at lower concentration of curcumin (Marty et al., 2006). Our group has previously shown higher efficacy of ECT with curcumin on hormone receptor-positive MCF-7 breast cancer cells (Camarillo et al., 2014). However, the research on evaluating the efficacy and molecular mechanisms of ECT with curcumin for TNBC is inadequate.

2.9 Electrochemotherapy and mass spectroscopy (MS)-based proteomics

Conventional bioassay-driven fractionation and target-identification have been successful in identifying treatment targets in cancer, however, these methods are both slow and expensive (Kingston, 2011). Therefore, the use of conventional low-throughput techniques, such as "Western-blots, Polymerized Chain Reaction (PCR), and Enzyme-linked Immunosorbent Assay (ELISA) to identify the effects of treatments on specific signaling pathways does not provide information on off-target side effects that only come to light during clinical trials (Beutler, 2009)"(Raman et al., 2018).

Despite the number of pathways and processes involved in cancer is large, their count is finite (Patterson & Aebersold, 2003). This makes it theoretically possible to visualize all the possible pathway involved in cancer development and treatment, if enough observations are recorded on all the elements that create the system (Patterson & Aebersold, 2003).

Since most treatments target proteins; a high-throughput mass spectroscopy (MS)-based proteomics technique, that can screen multiple protein properties, such as protein expression levels, post-translational modification, and interaction with other molecules is capable to acquire a complete picture of the cellular process at the protein level after the treatment (Palzkill, 2002).

Towards this, proteomics technique can be effectively utilized to gain insights into the molecular mechanisms of ECT with curcumin in TNBCs. However, there is an absence of published literature utilizing MS-based proteomics to study the molecular mechanisms of ECT, and our group remains the first one to undertake such studies.

2.10 Conclusions from literature survey

The conclusions from the literature survey are:

1. TNBCs are difficult to treat as no targeted therapy exists.
2. The existing FDA approved chemotherapy regimens for TNBC are costly, cytotoxic, and show poor response in advanced cases.
3. TNBCs harbor molecular and metabolic vulnerabilities, which could be utilized to target them effectively and develop alternate therapies.
4. Curcumin is a safe natural compound, which is effective against multiple cancers, including TNBCs. Curcumin utilizes the molecular and metabolic vulnerabilities of TNBCs to target them.
5. Non-curcuminoid compounds of the parent herb turmeric also show a potent bioactivity.
6. The silver nanoparticles increase the efficacy of turmeric and show a potent antibacterial activity. However, no study investigates the anticancer activity of turmeric silver nanoparticles.
7. ECT is a safe, effective, affordable, rapid (it takes only a few minutes per nodule), and outpatient-based physical modality to treat various advanced, chemo- and radio- resistant tumors, and it is applicable to all histology of the cancer.
8. ECT is clinically proven, as it has shown promising success in clinics for the treatment of various types of cancers, including breast cancers.
9. ECT with curcumin is effective against hormone receptor-positive breast cancers. However, the research on evaluating the efficacy of ECT with curcumin in TNBCs is inadequate.
10. MS-based proteomics is a state of the art, high-throughput technique to study the mechanisms. However, there is no existing literature studying the molecular mechanisms of ECT using MS-based proteomics; especially for ECT with curcumin in TNBCs.

These gaps motivated the present dissertation to examine the efficacy of ECT with curcumin as an effective and alternate therapy for TNBC.

The objectives of this dissertation are:

1. To optimize the ECT electrical pulse parameters and curcumin dosage for maximum cell death in MDA-MB-231 TNBC cells, while minimizing cell death in MCF10A non-cancerous epithelial cells, using cell viability assays.
2. To study the anticancer effects of turmeric nanoparticles against the above TNBC cells.
3. To perform the state-of-the-art, high throughput, mass spectroscopy-based, label-free quantitative proteomics studies to gain insights into the molecular mechanisms of the enhanced effects of ECT with curcumin and ECT with turmeric nanoparticles.
4. To conduct additional similar studies using cisplatin, the most commonly administered chemotherapeutic for TNBC patients and to compare the efficacy of the ECT with curcumin.

CHAPTER 3. METHODS

3.1 Cell Lines

The following two cell lines were used in this dissertation:

- MDA-MB-231
- MCF10A

3.1.1 MDA-MB-231 cells

The MDA-MB-231 is a human adenocarcinoma epithelial TNBC cell line. MDA-MB-231 cell line was first isolated and established as continuous culture at M. D. Anderson Hospital and Tumor Institute from a 51-year-old Caucasian female with metastatic mammary adenocarcinoma (Cailleau, Olive, & Cruciger, 1978). The cells were isolated from metastatic site from a pleural effusion. MDA-MB-231 cell line is one of the most commonly used cell lines in breast cancer research.

The morphology of MDA-MB-231 cells in 2D culture is shown in Figure 3.1(a), which shows spindle-like morphology of these cells. The MDA-MB-231 cells form stellate-like morphology in 3D culture (Lehmann et al., 2011).

"MDA-MB-231 cells were cultured as monolayer in DMEM (Gibco™, USA) with 10% FBS and 1% Penicillin-Streptomycin. The cells were incubated at 70%–80% humidity, 5% CO_2, and 37℃. Cells were trypsinized, centrifuged for 5 min at 1000 rpm at 4 ℃ and were resuspended in fresh-media for treatment" (Mittal, Aryal, et al., 2020). The cells were counted using hemocytometer or Nexcelom Bioscience Cellometer.

Properties of MDA-MB-231 cells are as below (Chavez, Garimella, & Lipkowitz, 2011; H. Liu, Zang, Fenner, Possinger, & Elstner, 2003):

1. Negative for ER, PR and HER2 receptors.
2. Poorly differentiated (less resemblance to the normal cells but more to cancer cells).
3. Highly aggressive (fast growth or spread)
4. Invasive cell line. The invasion is facilitated by proteolytic degradation of the extracellular matrix.

5. Express epidermal growth factor (EGF) and transforming growth factor alpha (TGF alpha) receptors.
6. MDA-MB-231 is aneuploid female (modal chromosome number = 64, range = 52 to 68), with count of chromosome in near-triploid range. The N8 and N15 normal chromosomes are lacking.

Since most TNBCs are basal-like (Lehmann et al., 2011), initially, MDA-MB-231 cell line was classified as "basal" breast cancer cell line, due to the lack of ER, PR and HER2 receptors (Cruz, 2017). The present molecular subclassification of MDA-MB-231 cell line is done based on the following markers (Holliday & Speirs, 2011):

1. Downregulated markers:
    - Claudin-3, claudin-4, Ki-67 proliferative markers.
2. Enriched markers:
    - EMT and stem cell markers.

Based on the gene expression, Lehmann et al, classified MDA-MB-231 into mesenchymal stem-like subtype of TNBC (Lehmann et al., 2011).

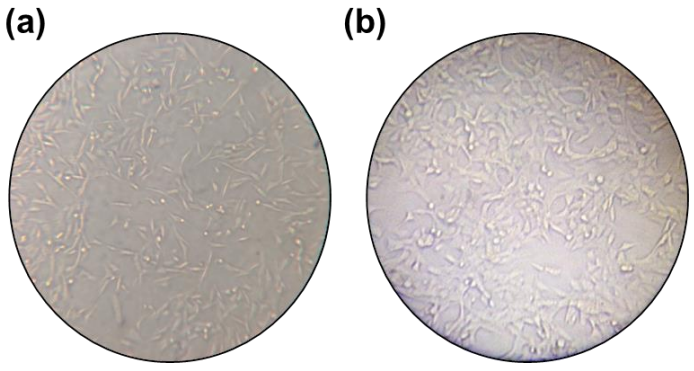

Figure 3.1: The morphology of cells: (a) MDA-MB-231, (b) MCF10A cells. The MDA-MB-231 cells show spindle-like morphology and MCF10A cells show cuboidal epithelial morphology.

3.1.2 MCF10A cells

The MCF10A is a non-tumorigenic, non-transformed human mammary epithelial cell line. MCF10A cell line was first isolated and established as continuous culture at Michigan Cancer Foundation (MCF) from a 36-year-old Caucasian female with extensive fibrocystic disease (Soule et al., 1990). The woman was free of disease, with no family history of malignancy. The MCF10A cells injections do not develop tumors at the injection or remote sites in animals after 6 months (Soule et al., 1990).

The morphology of MCF10A cells in 2D culture is shown in Figure 3.1(b), which shows cuboidal epithelial morphology of these cells, compared to MDA-MB-231 cells, which show spindle-like morphology. In collagen MCF10A demonstrate 3D growth, and form domes upon confluency.

"The MCF10A cells were cultured in a 1:1 ratio of DMEM:Ham's F12 supplemented with 5% horse serum (HS; Atlanta Biologicals), 20ng/ml human epidermal growth factor (SigmaAldrich, USA), 0.5mg/ml hydrocortisone (Sigma-Aldrich), 100ng/ml cholera toxin (Sigma-Aldrich), 10μg/ml bovine insulin (Sigma-Aldrich), 100IU/ml penicillin and 100μg/ml streptomycin and were incubated at 70%–80% humidity, 5% CO_2, and 37°C. Cells were trypsinized, centrifuged for 5 min at 1000 rpm at 4°C and were resuspended in fresh-media for treatment" (Mittal, Aryal, et al., 2020). The cells were counted using hemocytometer or Nexcelom Bioscience Cellometer.

Properties of MCF10A cells are as below:

1. Non-tumorigenic and non-transformed (lack of any obvious malignancy).
2. Do not express ER (Soule et al., 1990).
3. Responsive to insulin, cholera enterotoxin, glucocorticoids, and EGF.

MCF10A cell line could be classified as a basal-like epithelial cells with luminal features or a luminal-type going through EMT (Sarrio et al., 2008).

3.2 Drugs

3.2.1 Curcumin

"Curcumin (Diferuloylmethane, [$C_{21}H_{20}O_6$]; Sigma-Aldrich, USA) was dissolved in dimethyl sulfoxide (DMSO, Thermo Fisher) to prepare a stock solution. The required volume of the curcumin stock solution was added into cells to prepare 10-50μM final curcumin concentration for treatment" (Mittal, Aryal, et al., 2020). The concentration of stock solution was 20mM and it was stored at -20℃.

3.2.2 Cisplatin

"Cisplatin (Cis-diamminedichloroplatinum, [$Pt(NH_3)_2Cl_2$]; Sigma-Aldrich) stock solution was prepared by dissolving it in sterile double-distilled water. The required volume from cisplatin stock was added into cells to make 100μM Cisplatin treatment concentration" (Mittal, Aryal, et al., 2019).

3.2.3 Turmeric nanoparticles (TurNP)

A. TurNP preparation and characterization

i. Turmeric extract preparation

"TurNP synthesis was carried out with some modification (Nayak et al., 2017; Shameli, Ahmad, Zamanian, et al., 2012) First, an aqueous extract from the dried Turmeric tuber (Curcuma longa) was prepared. 2g of the manually ground fine powder from Turmeric tuber was added to 20mL of sterile distilled water (10% w/v), and was incubated overnight at 40℃ and 100rpm (Scigenics biotech pvt. Ltd). The solution was boiled for 1min in the microwave and for 10min at 1000rpm at 25℃. The supernatant was filtered through Whatmann No:1 filter paper, and was concentrated to a final volume of 5mL (Akther & Hemalatha, 2019; Akther, Khan, & Srinivasan, 2018)" (Mittal, Camarillo, et al., 2020).

ii. Biosynthesis and physio-chemical characterization of turmeric nanoparticles

"For TurNP synthesis, 5mL of filtered turmeric extract was added to 45mL of 1mM $AgNO_3$ solution, and incubated for 3 days in dark at 100 RPM at 40℃. 1mM $AgNo_3$ solution was used as control. The TurNP synthesis was observed by UV–vis spectroscopy between 300nm to 650nm. The TurNP synthesis was confirmed by a peak at 440nm in UV–vis spectrum, and visually by the change in color from yellow to brown (not in $AgNO_3$ control). After confirmation, the extract was centrifuged at 15,000rpm for 20min at 4℃, the pellet was resuspended in sterile water for washing and drying to obtain TurNP used in the study. The pellet was resuspended in sterile water for washing and drying. The dried TurNP were then characterized by using UV-Visible (UV-Vis) spectroscopy, Fourier-transform infrared (FTIR) spectroscopy, Energy-dispersive X-ray spectroscopy (EDS), Scanning electron microscopy (SEM), and Zeta potential" (Mittal, Camarillo, et al., 2020).

B. TurNP treatment

"A stock solution of 1mg/mL was prepared by suspending the TurNP into sterile double-distilled water with 10% DMSO, and sonicated for 2min at 5% intensity for homogenization. The required volume from the stock solution was directly added into the cell culture media with cells to obtain the desired final treatment concentration (5, 10, 15, and 25µg/mL) of TurNP" (Mittal, Camarillo, et al., 2020).

3.3 Electrical pulse application (electroporation)

"BTX ECM 830 electroporator (Genetronics Inc. San Diego, CA, USA) was used to generate 8 square wave unipolar pulses of 1Hz frequency" (Mittal et al., 2017). Electrical pulses of desired electrical field strengths (200V/cm-5000V/cm) and pulse durations (10µs-5ms) were generated (Figure 3.2(a)). The electrical specifications of the BTX ECM 830 are listed in Table 3.1.

Table 3.1: The electrical specifications of the BTX ECM 830 square wave electroporator.

Parameters	Low voltage (LV) mode	High voltage (HV) mode
Voltage	5-500V (resolution:1V)	505-3000V (resolution:5V)
Pulse length	10µs-999µs (resolution:1µs) 1ms-999ms (resolution:1ms) 1s-10s (resolution:0.1s)	10µs-600µs (resolution:1µs)
Pulse interval	100ms-999ms (resolution:1ms) 1s-10s (resolution: 0.1s)	
Multiple pulsing	1-99 pulses	
Current limit	500 A (at 100 µs)	

A. Suspension cell electroporation studies

Cells were suspended at 1×10^6 cells/mL and were transferred to the BTX electroporation cuvettes (4mm gap). The electrical pulses of appropriate pulse parameter were generated using BTX ECM 830 electroporator, and were applied to the cells suspended in cuvettes (Figure 3.2(b)).

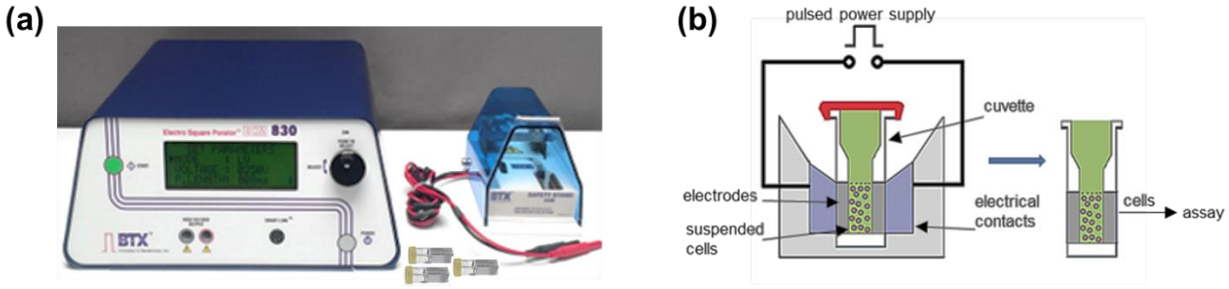

Figure 3.2: (a) BTX ECM 830 electroporator (left) and electroporation cuvettes and cuvette holder (right) (Genetronics Inc. San Diego, CA, USA), (b) The experimental setup of *in vitro* suspension cell electroporation.

B. Adherent cell electroporation studies

"We used NEPA21 electrodes (NepaGene, Japan) to apply electrical pulses to adherent cells incubated in a 24-well plate (1.5×10^5 cells/well) with a gap of 1cm, yielding an applied electric field of 200V/cm" (Mittal, Raman, et al., 2019) (Figure 3.3).

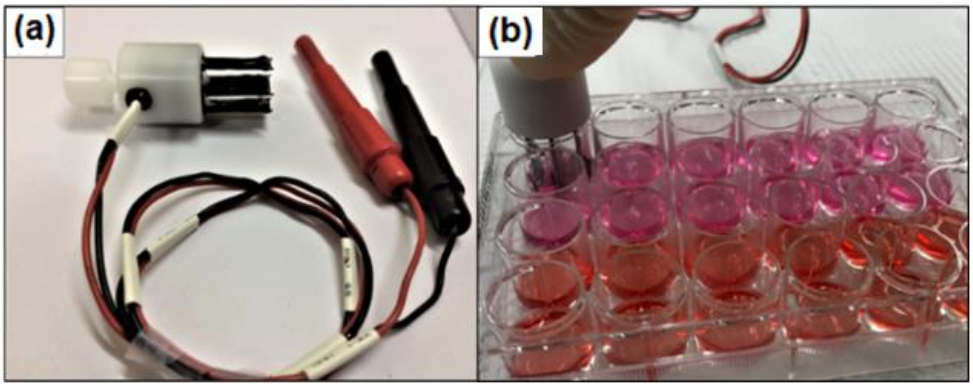

Figure 3.3: The experimental setup of *in vitro* adherent cell electroporation. (a) NEPA21 electrode used to apply electrical pulses from BTX ECM 830 electroporator. (b) Adherent cell electroporation in a 24-well culture plate.

3.4 Hemocytometer based Cell Counting

The cultured cells were trypsinized, centrifuged, and the cell pellets were resuspended in fresh media. A sample from cell suspension was transferred to an Eppendorf tube and were diluted (1:10 or 1:20; i.e. dilution of 10 or 20) with fresh media for counting the cells using Neubauer hemocytometer. 10µL of diluted cells were transferred to the chambers of hemocytometer in duplicate. Total cells in outer four squares A, B, C, and D of hemocytometer (as shown in Figure 3.4) were counted under a light microscope and the concentration of cells in the original cell suspension was estimated using equation (3.1).

$$Concentration = \frac{sum\ of\ cells\ in\ squares\ A,B,C,D}{4} \times Dilution \times 10^4\ Cells/mL, \qquad (3.1)$$

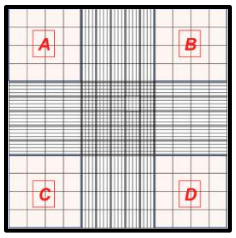

Figure 3.4: The squares and grid lines of a Neubauer hemocytometer. Total cells in outer four squares A, B, C, and D of hemocytometer were counted and averaged by four to calculate the cell concentration.

3.5 Assays

3.5.1 Viability Assays:

A. Trypan Blue viability assay

"Nexcelom Bioscience Cellometer was used for this assay. 20µL of treated sample was added into 20µL of trypan blue. 20µL of this mixture was used to determine cell viability at 0 and 2h following the treatment" (Mittal et al., 2017).

B. MTT viability assay

"Thiazolyl Blue Tetrazolium Bromide (MTT, Sigma) was used to assess the viability following 24, 48 and 72h of the treatment. After electroporation, cells were transferred into three different 96-well plates, which were cultured for 24, 48, and 72h respectively. Then MTT reagent 2mg/mL was added, and incubation was continued for an additional 24h. The 80µL DMSO was used to terminate the reaction. Absorbance values were quantified at 570nm and 630nm using SpectraMax M5 multi-detection microplate reader system (Molecular Devices, Sunnyvale, CA, USA). The optical density (OD) values for blank media and 630nm were subtracted from OD value for 570nm to calculate the experimental OD value. The cells in DMEM, without curcumin and electroporation treatment served as the control group. All experimental OD values were normalized with respect to the control OD value at 24h, using equation (3.2)" (Mittal et al., 2017).

$$Cell\ Viability\ (\%) = \frac{\text{Experimental OD value}}{\text{Control OD value at 24 h}} \times 100, \qquad (3.2)$$

C. MT Realtime viability assay

i. Drug dosage curve studies

"Cells were seeded in 96-well plates (10×10^3 cells/well) and allowed to attach for 24h. The spent media was replaced with media containing drug at appropriate concentrations for treatment. The control was not treated. The cells were incubated for required time with RealTime-Glo MT reagent (Promega, USA) to assess the viability at different time points, as per the manufacturer's protocol. Luminescence (Lum) was measured for 1s integration time using a SpectraMaxM5 multiplate reader (Molecular Devices, USA) or Synergy LX Multi-Mode Reader (BioTek Instruments, USA). Experimental Lum was normalized with control Lum to determine viability at a time point using equation (3.3)" (Mittal, Raman, et al., 2019):

$$Cell\ Viability\ (\%) = \frac{\text{Experimental Lum value}}{\text{Control Lum value}} \times 100, \qquad (3.3)$$

ii. Suspension cell electroporation studies

"Following treatment, cells were transferred to 96-well plates (MDA-MB-231: 20,000 cells and MCF 10A: 10,000 cells (as suggested by manufacturer's protocol)) with fresh-media" (Mittal, Camarillo, et al., 2020). The cells were incubated for required treatment time with RealTime-Glo MT Cell Viability reagent as per manufacturer's protocol. The Lum was recorded for 1s integration time and the cell viability was quantified using equation (3.3).

iii. Adherent cell electroporation studies

Prior to EP application, cells were seeded in 24 well plates (1.5×10^5 cells/well) and allowed to attach for 24h. "To assess viability after EP application, we treated the cells in media containing 50μm curcumin with or without EPs. Vehicle and EP only treatments had media containing DMSO. The above cells were incubated with RealTime-Glo MT reagent for required time to assess the viability, as per the manufacturer's protocol. The Lum was recorded for 1s integration time and the cell viability was quantified using equation (3.3)" (Mittal, Raman, et al., 2019).

D. Flowcytometric viability assay

After treatment, cells were incubated in 6-well plates (600,000cells/well). "Following 4h of treatment, all cells were detached using trypsin, centrifuged, and were resuspended in fresh media, after the removal of supernatant. Suspended cells (20µL) were stained with 380 µL Muse™ Count & Viability Reagent (EMD Millipore, USA). For apoptosis, suspended cells (100 µL) were stained with 100µL Muse Annexin V Dead Cell Assay kit (EMD Millipore). Following staining, samples were incubated in dark and were run on Muse Cell Analyzer (EMD Millipore) as per the instrument's protocol" (Mittal, Aryal, et al., 2019).

3.5.2 Clonogenic assay

"Following treatment, cells were incubated with fresh media in 6 well plates (2000cells/well) for 9 days. The colonies were stained with crystal violet (Sigma-Aldrich) and were counted using ImageJ Analyze Particles tool. The data was presented as survival fraction, after normalizing plating efficiency of a treatment with the plating efficiency of Control (survival fraction = 1) (Franken, Rodermond, Stap, Haveman, & van Bree, 2006)" (Mittal, Aryal, et al., 2020). The protocol of crystal violet staining was as follows:

After 9 days, spent media was discarded, cells were washed with 1xPBS and incubated with fixing reagent (7:1-methanol and acidic acid) for 20min at room temperature. The colonies were stained with 0.1% crystal violet (Sigma-Aldrich) and incubated for 30min and washed with water.

3.5.3 Flowcytometric assessment of cell cycle profile

"Cells were incubated in 24 well plates (1.5×10^5 cells/well) for 24h, followed by spent media replacement with serum-free media for 24h to synchronize cell cycle. Following synchronization, cells were treated in fresh media containing 50µm curcumin with or without EPs in adherent cell electroporation. Ctrl cells were treated with either serum-free media as a positive control or media containing the vehicle, DMSO. The EP-only controls were treated with media containing DMSO and EPs. After 36h of treatment, media was aspirated, and the cells were washed with PBS. The cells were then incubated in trypsin-EDTA containing 100µg/mL DNase I (Worthington, USA) for 10min, and then collected. The samples were centrifuged at 2,000rpm

for 5min and the supernatant was drained. The cells were washed and resuspended in PBS containing 2.5mM EDTA (1xPBS-EDTA), fixed by adding drop-wise into fresh ice-cold 70% ethanol, and stored at -20˚C until staining. For staining, fixed cells were centrifuged at 2000rpm for 10min and the supernatant was discarded. Cells were then washed with 1xPBS-EDTA, resuspended in Muse Cell Cycle Reagent (EMD Millipore, USA) containing propidium iodide (PI) and RNaseA, and stored at room temperature for 30min. Stained cells were run on a CytoFLEX (Beckman Coulter, USA) flow cytometer. Cells in different cell cycle phases were quantified using FCS Express software" (Mittal, Raman, et al., 2019).

3.5.4 Flowcytometric apoptosis assay

Following EP treatment, cells were incubated with fresh media in 6-well plates (600,000cells/well) for the required treatment time. "Upon completion, all cells were collected using trypsin, centrifuged, and were resuspended in fresh media, after the removal of supernatant. Suspended cells (100µL) were stained with 100µL Muse Annexin V Dead Cell Assay kit (EMD Millipore). Following staining, samples were incubated in dark and were run on Muse Cell Analyzer (EMD Millipore) as per the instrument's protocol" (Mittal, Aryal, et al., 2019).

3.5.5 Western blotting

Spent media as well as cells were collected by scraping, washed thrice with ice cold 1x PBS. "Treated cells were collected in RIPA buffer and sonicated to obtain lysates. Cell lysates were centrifuged at 14000rpm to clear debris and the protein concentration in the lysates was estimated via the bicinchoninic acid (BCA) assay. A total of 15-20µg of protein from each sample was mixed with 5× sample buffer and was boiled to denature proteins. The denatured protein samples were subjected to SDS-polyacrylamide gel electrophoresis, transferred onto a polyvinyl difluoride (PVDF) membrane, and immunoblotted. The PVDF membrane was blocked overnight at 4ºC with 5% w/v nonfat dry milk, before probing for the proteins using appropriate primary antibody" (Mittal, Raman, et al., 2019). Antibodies used were: P53 (rabbit, 9282S; Cell Signaling Technologies), LDHB (rabbit, PA5-43141; Thermo Fisher Scientific), GLS (rabbit, PA5-35365; Thermo Fisher Scientific) and β-tubulin (mouse, E7; Developmental Studies Hybridoma Bank, University of Iowa). "The proteins were detected using the appropriate Alexa Fluor secondary

antibody (anti-rabbit, A-21109 or anti-mouse, A11375; Thermo Fisher Scientific). The blots were imaged at 680 nm for primary antibodies (P53, LDHB, and GLS), and 790 nm for β-tubulin using the Li-Cor Odyssey infrared imaging System and were quantified using ImageJ" (Mittal, Aryal, et al., 2019) or Image Studio.

3.5.6 Realtime quantitative polymerase chain reaction (qPCR)

Following treatment, cells were incubated with fresh media in 6-well plates (600,000cells/well) for the required treatment time. Upon completion, spent media as well as cells were collected by trypsinization, washed thrice with ice-cold 1 × PBS. Total RNA was extracted using RNeasy Mini Kit (QIAGEN, USA) as per manufacturer's protocol. "It was quantified using Synergy LX Multi-Mode Reader. The cDNA was synthesized using iScript cDNA Synthesis Kit and was quantified using Synergy LX Multi-Mode Reader. The equal amount of cDNA was then used with SYBR Green I Master (Roche, USA) and appropriate primers for qPCR reactions in CFX Connect RT-PCR system (Bio-Rad Laboratories, USA) to measure mRNA levels. The parameters were as follow: 10min at 95 ℃, [15 sec at 95 ℃, 10 sec at 60 °C, 30 sec at 72 ℃] × 54 cycles, 10 sec at 95 ℃, 60 sec at 65 °C, 1 sec at 97 °C. The relative mRNA levels were determined using the ΔΔCq technique" (Mittal, Camarillo, et al., 2020). Housekeeping genes - Glyceraldehyde 3-phosphate dehydrogenase (GAPDH) or 18S ribosomal RNA (18s rRNA) were used as internal control. The primer sequences are listed in Table 3.2.

Table 3.2: The primer sequence details for different genes.

Gene	Upstream	Downstream
LDHB	5′-CCT CAG ATC GTC AAG TAC AGT CC-3′	5′-ATC ACG CGG TGT TTG GGT AAT-3′
ENO1	5′-AAA GCT GGT GCC GTT GAG AA-3′	5′-GGT TGT GGT AAA CCT CTG CTC-3′
GLS	5′-TCT ACA GGA TTG CGA ACG TCT-3′	5′-CTT TGT CTA GCA TGA CAC CAT CT-3′
GAPDH	5′-ACA ACT TTG GTA TCG TGG AAG G-3′	5′-GCC ATC ACG CCA CAG TTT C-3′
18s rRNA	5'-CCA GTA AGT GCG GGT CAT AAG-3'	5'-GGC CTC ACT AAA CCA TCC AA-3'

3.5.7 Assessment of hydrogen peroxide (H_2O_2) reactive oxygen species (ROS)

Following treatment, MDA-MB-231 or MCF10A cells were transferred to 96-well plates (20,000 cells/well) with 60µL fresh-media and 20µL of H_2O_2 substrate solution from ROS-Glo H_2O_2 assay kit (Promega) and were cultured for the required treatment time. "ROS-Glo™ detection solution was added to cells and incubated for 20min, and Lum was recorded for 0.5-1s integration using the SpectraMaxM5 spectrophotometer" (Mittal, Aryal, et al., 2020).

3.5.8 Cellular metabolites detection assays

Following treatment, MDA-MB-231 cells were incubated with fresh media in 6-well plates for the required treatment time. Upon completion, "the supernatant as well as cells were collected by scraping. Then they were washed twice with ice-cold 1×PBS, resuspended in 1×PBS and counted using a Cellometer (Nexcelom Bioscience). 35,000 cells were then used as per manufacturer's protocol to detect the metabolites, such as glucose uptake (Glucose Uptake-Glo Assay, Promega), lactate (Lactate-Glo™ Assay, Promega), glutamine, and glutamate (Glutamine/Glutamate-Glo Assay, Promega)" (Mittal, Camarillo, et al., 2020).

3.5.9 Antioxidant activity assay

Antioxidant activity of the samples was measured by free radical method using 2,2-diphenyl-1-picryl-hydrazyl (DPPH). 0.15mL of sample was added to 2mL of DPPH radical solution (1mM DPPH in methanol) and 2.85mL of absolute methanol. Incubate in dark at room temperature for 30min. Discoloration was observed against the control. The color change was read against the control at 517nm. Free radical scavenging was calculated using equation (3.4). Where, A_{blank} is absorbance of blank solution and A_{sample} is absorbance of sample.

$$DPPH\ Radical\ Scavenging\ Ability(\%) = \frac{A_{blank} - A_{sample}}{A_{blank}} \times 100, \qquad (3.4)$$

3.5.10 Qualitative phytochemical screening

A TurNP suspension was prepared by adding 6mg of TurNP into 4.5mL DMSO and 25.5mL distilled water. The phytochemical screening was carried out as follows:

A. Screening for Phenol

TurNP extract (2mL) was added to ferric chloride (2mL). Dark blackish brown formation indicates the presence of phenols.

B. Screening for Tannins

TurNP extract (2mL) was added to few drops of 1% lead acetate. Formation of yellowish precipitate indicates the existence of tannins.

C. Screening for Flavonoid

TurNP extract (2mL) was added to diluted ammonia solution (5mL) and few drops of concentrated H_2SO_4. The color change from yellowish brown to orange indicates the presence of flavonoids.

D. Screening for Saponins

TurNP extract (2mL) was added to distilled water (10mL) and shaken for 15min in a graduated cylinder. Appearance of foam highlights the existence of saponins.

E. Screening for Anthocyanins

TurNP extract (2mL) was added to 2N Hcl and ammonia (2mL). The turning of pink-red to blue-violet highlights the existence of anthocyanins.

F. Screening for Catechin

TurNP extract (2mL) was mixed with few drops of ehrlich reagent and few drops of concentrated HCl. The formation of pink color highlights the presence of catechin.

G. Screening for Alkaloids

TurNP extract (2mL) was added to 2% HCl (1.5mL) and two drops of Mayer's reagent. The appearance of creamy white precipitate highlights the existence of alkaloids.

H. Screening for Steroids

TurNP extract (2mL) was added to chloroform (10mL). An equal volume of concentrated H_2SO_4 was through the sides of the test tube. The turning of upper layer to red and H_2SO_4 layer to yellow with green fluorescence highlights the existence of steroids.

I. Screening for Terpenoids

TurNP extract (2mL) was added to acetic anhydride and concentration of H_2SO_4 (2mL). The appearance of blue-green rings highlights the existence of terpenoids.

J. Screening for Carotenoids

TurNP extract (2mL) was added to chloroform (10mL) in a test tube with vigorous shaking. To the resulting mixture, 85% H_2SO_4 was added. A blue color at the interface indicates the presence of carotenoids.

3.6 Proteomics studies

"Following treatment, MDA-MB-231 cells were incubated in 6 well plates (600,000 cells/well) containing 2mL of fresh-media and were cultured for proteomics experiments. The following methodology was adopted for sample preparation, mass spectroscopy run, and data analysis" (Mittal, Camarillo, et al., 2020).

3.6.1 Sample preparation for mass spectrometry analysis

The proteomics experiments were performed either at 4h or 12h of treatment. Upon completion of treatment time, spent media as well as cells were collected by scraping, washed thrice in ice-cold 1×PBS with centrifugation at 1,000rpm at 4°C, and were re-suspended in 4M urea. "The cells were homogenized in Precellys 24 Bead Mill Homogenizer (Bertin Corp., USA) and were centrifuged at 14,000rpm for 15min at 4°C. Supernatant proteins were incubated overnight at -20°C with pre-chilled (-20°C) acetone (five equivalents (v/v)) for precipitation. Precipitated protein pellets were dissolved in 8M urea and protein concentration was estimated using BCA assay. Protein (50µg) from each sample was reduced with 10mM dithiothreitol (DTT)

at 55℃ for 45min followed by cysteine alkylation with 20mM iodoacetamide at room temperature under dark for 45min and an additional 5mM DTT for 20min at 37℃. Proteins were digested overnight at 37℃ with Trypsin/Lys-C Mix (Promega) enzyme-protein at ratio 1:25 (w/w) and were passed through C18 micro spin columns (The Nest Group Inc., USA). Peptides elution was performed using 0.1% formic acid in 80% acetonitrile (ACN). Eluted peptides were vacuum dried and were re-suspended in 0.1% formic acid in 3% ACN. BCA assay was used to estimate peptide concentration and the concentration was adjusted to 0.5µg/µL" (Mittal, Aryal, et al., 2019).

3.6.2 LC-MS/MS data collection

"LC-MS/MS data were collected using a reverse-phase HPLC-ESI-MS/MS system by coupling an UltiMate 3000 RSLCnano to a Q-Exactive (QE) High Field (HF) Hybrid Quadrupole Orbitrap MS (Thermo Fisher Scientific) and a Nano-spray Flex ion source (Thermo Fisher Scientific). Samples were analyzed using a standard data-dependent acquisition mode. Mobile phase solvent A was a 98% purified water/2% ACN/0.01% FA, and solvent B was 80% ACN/20% purified water/0.1% FA. Peptides (1µg) were loaded onto a trap column (300µm ID × 5mm, 5µm 100Å PepMap C18 medium) at 5µL/min flow rate. After 5min, trap column was switched in-line with Acclaim™ PepMap™ RSLC C18 (75µm x 15cm, 3µm 100Å PepMap C18 medium, Thermo Fisher Scientific) analytical column and peptide were separated using 120min LC gradient method at 35℃. A 5-30% linear gradient of solvent B was run for 80min, followed by 11min of 45% solvent B and 2min of 100% solvent B with an additional 7min of isocratic flow. Solvent A was then applied at 95% for 20min for column equilibration. A Top20 data-dependent MS/MS scan method was used to acquire MS data. Injection time was set to 100 milliseconds, resolution to 120,000 at 200m/z, spray voltage of 2eV and an AGC target of 1×106 for a full MS spectra scan with a range of 400-1650m/z. High-energy C-trap dissociation was used to fragment precursor ions at a normalized collision energy of 27eV. The MS/MS scans were acquired at a resolution of 15,000 at 200m/z. The dynamic exclusion was set at 30s to circumvent repeated scanning of identical peptides" (Mittal, Aryal, et al., 2019).

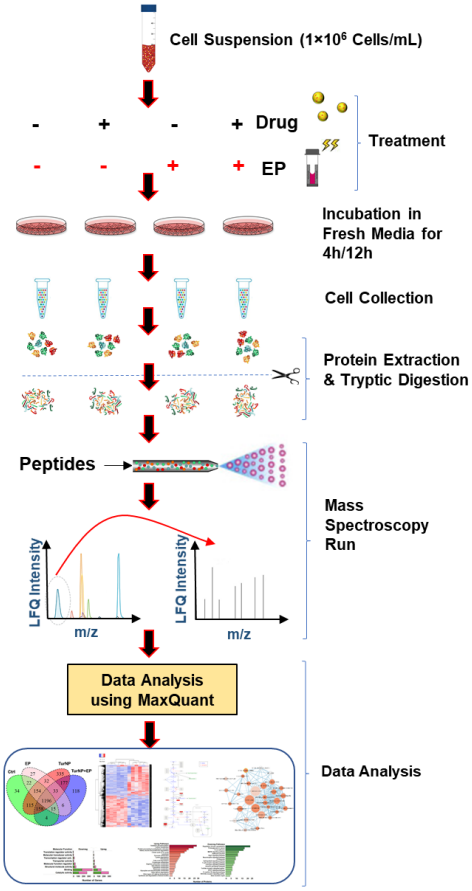

Figure 3.5: The experimental workflow of proteomics studies: "Ctrl and treated cells were incubated for 4h/12h in the fresh media, collected and lysed in urea and analyzed by LC-MS/MS for protein identification and quantification" (Mittal, Camarillo, et al., 2020).

3.6.3 Data Analysis

"MaxQuant (v1.6.1.0) (J. Cox & Mann, 2008; J. Cox et al., 2011) was used to process MS/MS data against the Uniprot Homo sapiens fasta (http://www.uniprot.org) concatenated with a common contaminants and a reverse-decoy database, as previously (Raman et al., 2018). Cleavage enzymes were setup as Trypsin/P and LysC, with toleration of up to 2 missed cleavages. Mass error was set to 10ppm and 20ppm for precursor and fragment ions, respectively. Cysteine alkylation and methionine oxidation was set to fixed and variable modifications, respectively. The 0.01 was estimated false discovery rate threshold for both the peptides and the proteins levels. The peptide quantitation was conducted using 'unique plus razor peptides'. The non-unique peptides assigned to protein/protein group with most other peptides were razor peptides. Following MaxQuant processing, proteins with no MS/MS count and zero LFQ intensity were removed. The

results were transferred to Data Analysis and Extension Tool (DAnTE) for Pearson correlations analysis. Proteins with LFQ≠0 and MS/MS≥2 in at least two replicates for ≥1 of the treatments were retained for further analyses using a MATLAB script. Zero LFQ values were imputed with half of the lowest LFQ value observed across three treatments. LFQ intensities were log2 transformed and average was calculated for three replicates. The fold-change was calculated by subtracting the average log2 values [Δlog2 (LFQ intensity)] between proteins from each comparison group (CsP vs Ctrl; EP+CsP vs Ctrl; EP+CsP vs CsP). Proteins with fold-change of |Δlog2|>0.5, and P<0.05 (Student's unpaired, two-tailed, t test) were significantly regulated" (Mittal, Aryal, et al., 2019).

3.6.4 Enrichment and String Interaction Analysis

"Significantly regulated proteins were compared against the background of total identified proteins to discover the pathway enrichment using KEGG (Kanehisa & Goto, 2000) database in DAVID 6.8 (https://david.ncifcrf.gov/) (D. W. Huang, Sherman, & Lempicki, 2009a, 2009b)" (Mittal, Aryal, et al., 2019). "Proteins from KEGG pathway analysis were uploaded to the Cytoscape 3.6.1 software (Paul Shannon et al., 2003) and matched using the WikiPathway app (beta), with the degree of shading representing the fold change" (Mittal, Camarillo, et al., 2020). GO enrichment analysis for cellular localization, molecular functions, and biological processes of differentially expressed proteins was performed using Genecodis (https://genecodis.genyo.es/) (Carmona-Saez, Chagoyen, Tirado, Carazo, & Pascual-Montano, 2007), against the background of total identified proteins. PANTHER Classification System was also used for Go enrichment analysis against *Homo sapiens* database (http://www.pantherdb.org/) (Mi, Muruganujan, Casagrande, & Thomas, 2013). STRING (https://string-db.org/) (Szklarczyk et al., 2017) was used to visualize the interaction and functional enrichment.

3.7 Statistical Analysis

"The statistical significance was calculated using F-test and Tukey's honest significance difference (HSD) test. To visualize the data from more than one point in time, we used a repeated measure design, where only a single response variable is measured over multiple points in time.

Also, we controlled for the error by including each replicate as a subject into our model. For each treatment type we had three subjects. The model used is (Montgomery, 2012):

$$Y_{ijk} = \mu + G_i + S_{(i)j} + T_k + (G * T)_{ik} + \varepsilon_{ijk,} \qquad (3.5)$$

where, $\sum_{i=1}^{4} G_i = 0$; $\sum_{k=1}^{m} T_k = 0$, $\begin{cases} m = 2 \text{ for Trypan Blue assay} \\ m = 3 \text{ for MTT assay} \end{cases}$; $\sum_{i=1}^{4}\sum_{k=1}^{3} G_i * T_k = 0$;

$S_{(i)j} \approx NID(0, \sigma_s^2)$; $\varepsilon_{ijk} \approx NID(0, \sigma^2)$

Here, Y_{ijk} is the overall response, μ is a constant overall mean, common to all treatments, Gi is the effect of i^{th} level of 'Treatment', $S_{(i)j}$ is the effect of j^{th} level of 'Subject' which is nested under i^{th} level of 'Treatment', T_k is the effect of k^{th} level of time, $G*T_{ik}$ is the effect of interaction between treatment and time, and ε_{ijk} is a random error component, which is assumed to be independently and normally distributed random variable with mean 0 and variance σ^2.

The 'Treatment', 'Time' and 'Treatment*Time' interaction effects are fixed. The 'Subjects' is a random effect as it represents a random sample from a larger population of potential subjects, the mean of $S_{(i)j}$ is zero and the variance is σ_S^2 (Montgomery, 2012). The F-test was performed only on the fixed effects to test the hypothesis of significance. The hypothesis of the interest for an individual fixed effect test is (Montgomery, 2012):

$$\begin{aligned} &H_0: \ \mu_1 = \mu_2 = \mu_3 \ldots = \mu_n \\ &H_1: \ \text{Not all means are equal} \end{aligned} \qquad (3.6)$$

where, *n* = number of independent comparison groups in a fixed effect.

When the p-value from F-test on a fixed effect was <0.05, we rejected the H_0 and concluded that the effect was significant. Post significance, we conducted the Tukey's HSD test on individual fixed effects to compare all possible pairs of means within an effect (Abdi & Williams, 2010). However, when interaction effect was significant, only interaction term was subjected to Tukey's HSD test (Montgomery, 2012). The output of Tukey's HSD test is a letter report. Same letters mean no statistical significance, but different letter mean statistical significance" (Mittal et al., 2017).

"Student's unpaired, two-tailed, t-test was used for testing significance for log2 transformed proteomics data, and few other experimental data" (Mittal, Aryal, et al., 2019).

The statistical analysis was performed in JMP. Experiments were done in triplicate or more and the data was shown as mean ± standard error.

CHAPTER 4. RESULTS AND DISCUSSION

4.1 Curcumin

4.1.1 Curcumin dose curve

We first studied the effect of change in curcumin's concentration on the viability profile of MDA-MB-231, human TNBC cells. "These cells are relatively resistant to commonly used chemotherapeutics (Cisplatin, Paclitaxel, and Doxorubicin) (J. Chen et al., 2011), and are a standard *in vitro* model of highly invasive TNBC" (Mittal, Aryal, et al., 2019).

"The results indicate that curcumin can significantly reduce the viability of MDA-MB-231 cells in a dose and time dependent manner. The Figure 4.1 shows the curcumin dosage curve for MDA-MB-231 cells at 24h and 48h. The viabilities were normalized with control viability at 24h or 48h (100%). The viability for DMSO treated samples (Veh) was 93% and 92% at 24 and 48h, respectively. The DMSO treatment caused only a minimal reduction of 7-8% in viability, compared to control. A 10µM curcumin dosage resulted in 99.8% and 98.2% viability at 24 and 48h, respectively. Applying a curcumin concentration of 30µM resulted in 72% viability at 24h and a reduction to 57% at 48h. Applying 40µM curcumin concentration induced a sharp reduction in viability to 38% and 14% at 24h and 48h, respectively. A curcumin concentration of 50µM resulted in 28% and 15% viability at 24h and 48h, respectively. The viability reduction at 24h was 10% for a 10µM increase in the curcumin concentration from 40µM to 50µM. The cell viabilities were 24.5%, 23.7%, and 20% at 24h, and 16%, 17%, and 14% at 48h for 60µM, 70µM, and 100µM curcumin, respectively. Increasing concentration beyond 50µM caused only a limited viability reduction, as the reduction was 8% for two-fold dosage increase from 50µM to 100µM, indicating nonlinear saturation. This was corroborated by the statistical results" (Mittal, Raman, et al., 2019).

A Repeated Measure ANOVA design was used, where the statistical significance was calculated using F-test, followed by Tukey's test for multiple comparison. "Table 4.1 shows the F-test results, which indicate that all fixed effects are statistically significant ($P<0.05$). The statistical significance of the interaction effect ('Treatment×Time') indicates that the simultaneous influences of 'Treatment' and 'Time' on cell viability were not additive; therefore, only the interaction effect was subjected to Tukey's test" (Mittal, Raman, et al., 2019).

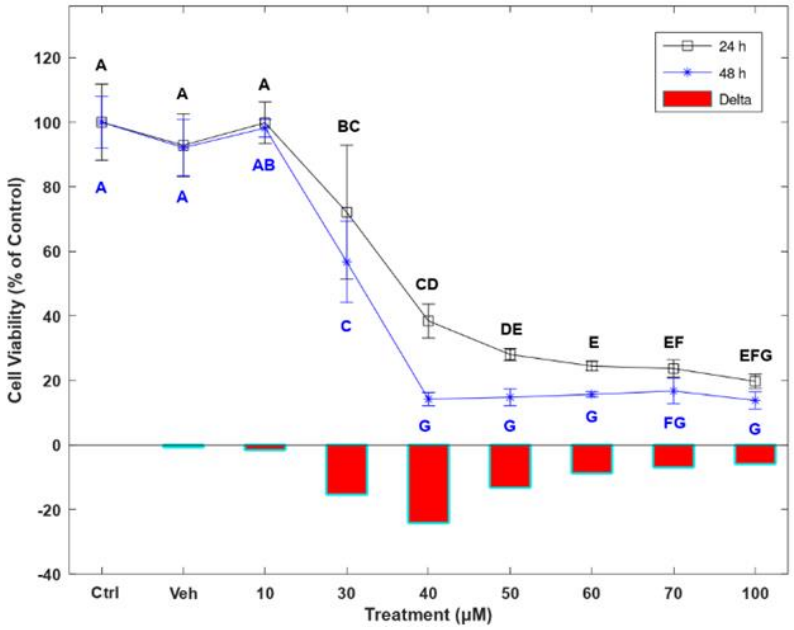

Figure 4.1: Curcumin dose curve for MDA-MB-231 cells at 24h and 48h. Delta shows the differences in viabilities of 24h and 48h. Veh samples contain dimethyl sulfoxide (DMSO) as vehicle. The Promega RealTime MT cell viability assay was utilized to quantify viability. A Repeated Measure ANOVA analysis was performed to obtain significance. Different letters reveal significant difference - $P<0.05$ from Tukey's test. The results include data from experiments done in triplicate, where error bars represent standard error.

Table 4.1: F-test results for three fixed effects of curcumin dose curve at 24h and 48h (* is $P<0.05$).

Source	Mean Square (MS) Numerator	Degree of Freedom (DF) Numerator	F Ratio	Prob > F
Treatment	3.17	8	33.59	<.0001*
Time	1.25	1	93.43	<.0001*
Treatment×Time	0.16	8	11.94	<.0001*

"The Tukey's test letter report in Figure 4.1 indicated no significant difference between Ctrl, Veh, and 10μM curcumin samples at 24h or 48h (share letter 'A'). Treatments with curcumin concentration greater than 10μM were significantly different from control at 24h and 48h, since they do not share any common letter. Treatments at 40μM and 50μM were not significantly different at 24h (share letter 'D') and 48h (share letter 'G'). There was a significant difference between 40μM and curcumin concentrations of 60μM and greater at 24h, since they did not share

any letter. However, there was no significant difference among 50µM, 60µM, 70µM, and 100µM curcumin treatments at 24h (share letter 'E') and 48h (share letter 'G')" (Mittal, Raman, et al., 2019).

These results correlate extremely well with previous studies. Similar to our observations, a limited MDA-MB-231 cell death was observed for smaller curcumin concentrations (below 30µM) in another study by Latifah *et al* (Latifah, Faujan, Sze, Raha, & Hisyam, A.Li, 2006). "They reported a 2% viability reduction from 24h to 48h at 3µg/mL (8.14µM), which correlates extremely well with 1.6% viability reduction we observed from 24h to 48h at 10µM. In our work, 30µM curcumin significantly reduced the viability compared to control at 24h and 48h. Similarly, Huang *et al* reported reduced MDA-MB-231 cell proliferation at curcumin dosages of 30µM and above (T. Huang, Chen, & Fang, 2013). Viability ranged from 13.8% to 16.7% for curcumin dosages from 50µM to 100µM at 48h, indicating that curcumin only does not decrease MDA-MB-231 viability beyond ~86% at 48h" (Mittal, Raman, et al., 2019). Since increasing the dosage above 50µm did not lead to statistically significant changes in cell survival (all denoted with E), we selected 50µM curcumin concentration for further studies, as also used by others (Chiu & Su, 2009).

4.1.2 Impact of conventional microsecond (100us) duration pulses with curcumin on TNBC cells

A. Colony forming ability and apoptosis profile

We studied the effect of curcumin with conventional 100µs EPs used in ECT on MDA-MB-231 cells. "To examine the cytotoxic effects of 50µM curcumin (Cur) and curcumin with 1200V/cm, 100µs, 8pulses EP (EP+Cur) over an extended time period, we performed a clonogenic assay at 9 days after the treatment. Figure 4.2 shows the MDA-MB-231 colony survival curves with different concentration of Cur, with and without EP application. There was a dose dependent decrease in the MDA-MB-231 colonies for Cur treatment, with the lowest survival for 50µM. The survival fractions were 0.97, 0.65, 0.46, and 0.50 for 10, 25, 50, and 100µM of curcumin concentrations, respectively. For EP+Cur treatment, the survival fractions were 0.25, 0.29, 0.23, and 0.18 for 10, 25, 50, and 100µM of curcumin concentrations, respectively. While, with the increase in the survival fraction for 100µM Cur, we observed a saturation in the effect of Cur

treatment beyond 50µM, no such saturation was observed for EP+Cur treatment, as the survival fraction reduced further for 100µM from 50µM in EP+Cur. Compared with Cur, EP+Cur treatment resulted in 2 to 3.9 times significantly lower survival fractions, indicating a greater cytotoxic effects of EP+Cur treatment on MDA-MB-231 cells" (Mittal, Aryal, et al., 2020).

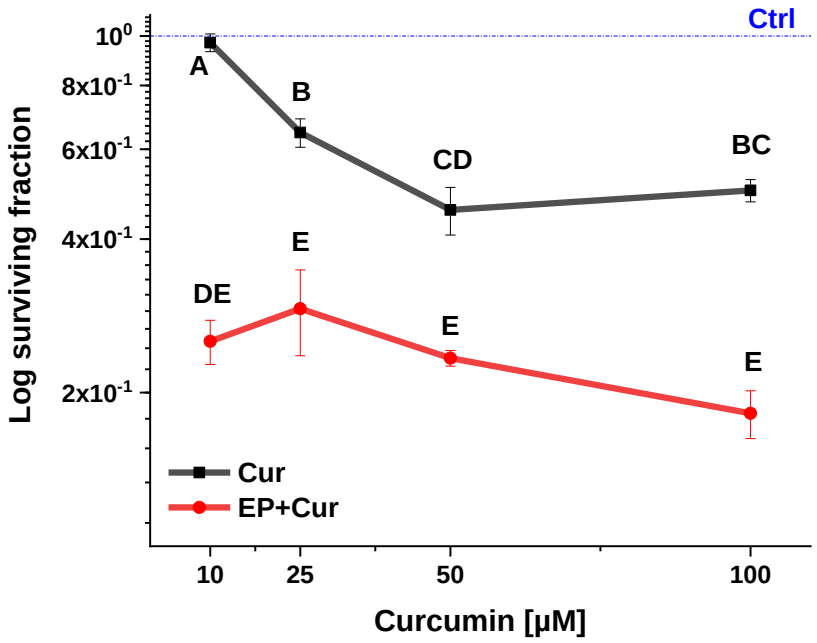

Figure 4.2: Clonogenic survival of MDA-MB-231 cells for various curcumin (Cur) dosages, with (EP+Cur) and without EP (1200V/cm, 100µs, 8 pulses at 1Hz). The plating efficiency for a treatment was normalization with Ctrl plating efficiency to calculate survival fraction (control survival fraction = 1) (Franken et al., 2006). Different letters reveal significant difference - $P<0.05$ from Tukey's test. The results include data from experiments done in triplicate, where error bars represent standard error.

"Further, to understand if the cell death involved the pathway of apoptosis and/or necrosis following ECT with curcumin, we performed flowcytometry after Annexin V/7-Aminoactinomycin D (Annexin-V/7-AAD) staining to quantify, live, early and late apoptosis, and necrotic cells for these treatment conditions. Figure 4.3 shows these results. The live cells were significantly reduced to 8% for Cur and 5% for EP+Cur treatment (letter 'B'), compared to 83% for Control (Letter 'A'). For Cur treatment, 86.6% cells were in the late apoptosis phase, while only 0.87% in early apoptosis phase. The EP+Cur treatment had 94.5% cells in the late apoptosis and 1.7% in early apoptosis. The fraction of cells in the late apoptosis for Cur and EP+Cur was

significantly different (Letter 'A') from Control (Letter 'B'). It was 4.93% for necrosis for Cur and 4.57 for EP+Cur, compared to 1% in Control. There was no significant difference between the cells going through necrosis in all three treatment groups (common letter 'B'). These results indicate that predominant mechanism by which Cur and EP+Cur mediate death in MDA-MB-231 cells is apoptosis, the preferred way, not necrosis" (Mittal, Aryal, et al., 2020).

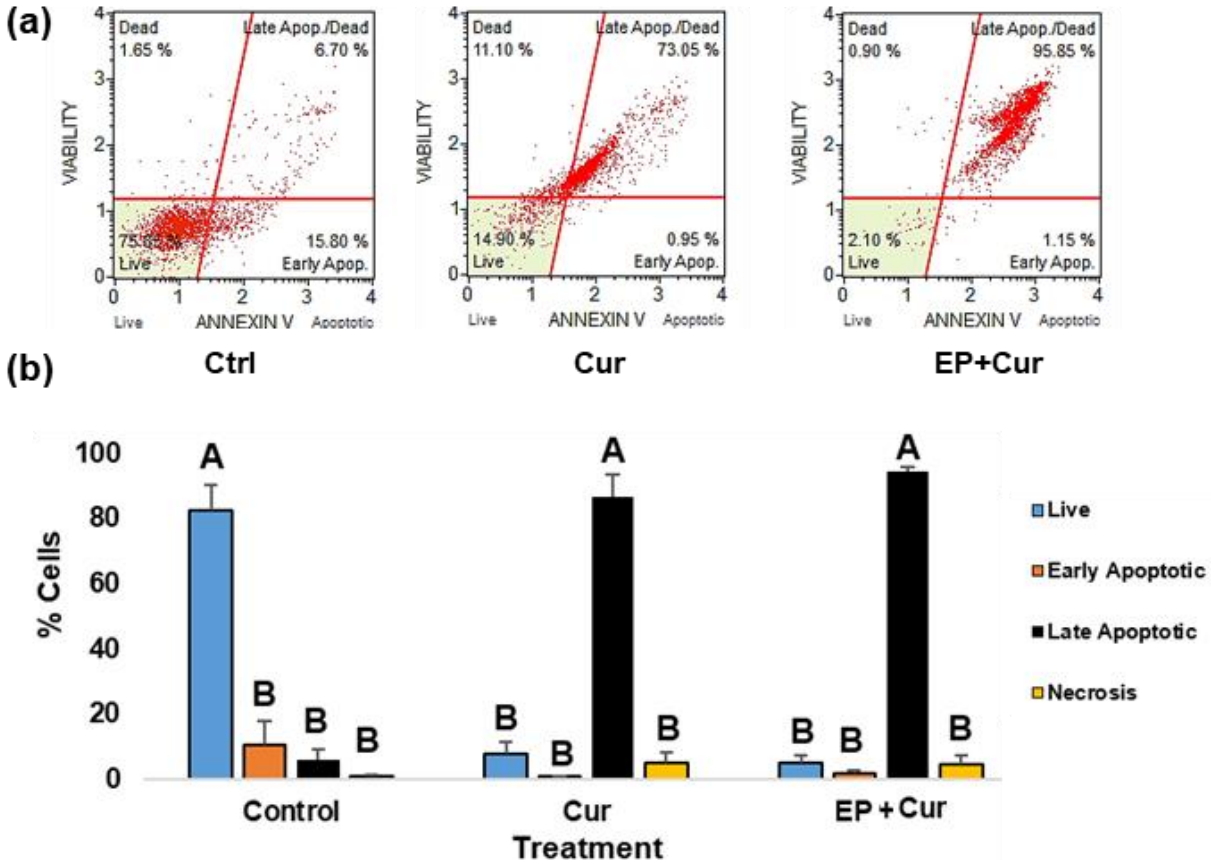

Figure 4.3: Apoptosis profile of MDA-MB-231 cells following 2h of curcumin (Cur) and EP+curcumin (EP+Cur) treatments. Representative dot plots (a) of cells in different phases and their quantification (b). Here Cur concentration of 50µM and EP of 1200V/cm, 100µs, 8 pulses at 1Hz were used. Different letters reveal significant difference - $P<0.05$ from Tukey's test. The results include data from experiments done in triplicate, where error bars represent standard error.

B. Protein expression analysis

To understand the mechanism of ECT with curcumin, a label free quantitative proteomics study was performed, as explained in detail in Chapter 3. "Proteins identified with label-free quantitation (LFQ) as non-zero and with at least 2 MS/MS (spectral) counts were considered for further analysis. There was an unambiguous identification of 1456 proteins/protein families from 13,969 peptides. We used LFQ values to determine relative abundances in each sample. Further, to classify the number of unique and common proteins in each treatment, we used LFQ values and MS/MS counts (LFQ $\neq 0$ and MS/MS ≥ 2). We identified a total of 1326 proteins in Cur. The total was 857 in EP+Cur. There were 727 common proteins in both samples (Figure 4.4(a)). The number of unique proteins was 599 in Cur and 130 in EP+Cur. The greater number of unique proteins in Cur treatment compared to EP+Cur suggest a significant impact of EP+Cur on cellular pathways through the loss of 599 proteins and unique/increased expression of 130 proteins. The expression of total 1456 proteins was visualized using the heatmap, as shown in Figure 4.4(b). The heatmap shows a consistent expression pattern, indicating the consistency of the experiments. The portion of heatmap covered with upregulated proteins (red color) was greater for Cur treatment, while the downregulation portion (green color) was more prominent in EP+Cur treatment, indicating that the protein downregulation was more prominent in EP+Cur compared to Cur" (Mittal, Aryal, et al., 2020).

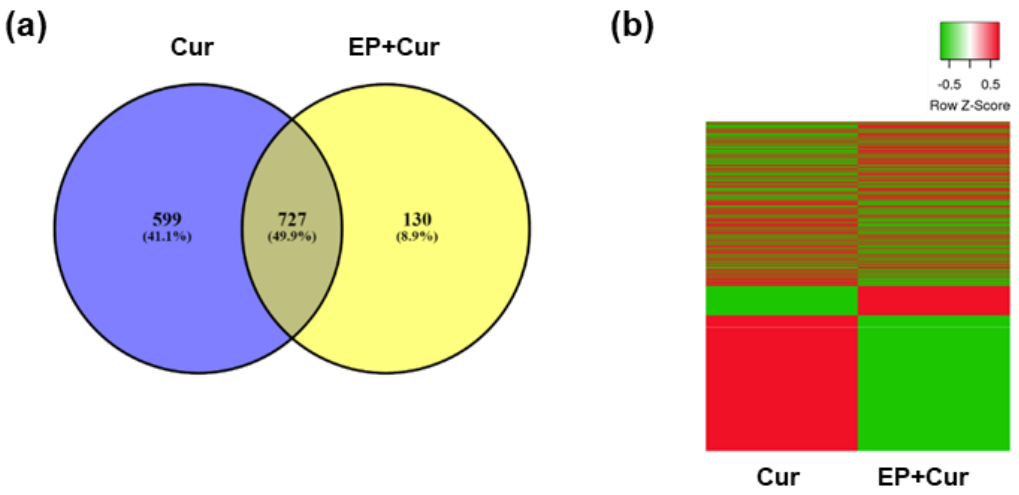

Figure 4.4: (a) Classification of total 1456 proteins in MDA-MB-231 cells at 12h to curcumin only (Cur) and EP+curcumin (EP+Cur) treatments. (b) A heatmap visualizing the LFQ expressions of al proteins across two treatments. This visualization was created using Heatmapper (Babicki et al., 2016). Here Cur concentration of 50µM and EP of 1200V/cm, 100µs, 8 pulses at 1Hz were used.

C. Differentially expressed proteins and associated enrichment

"The LFQ values of the common proteins in these two treatment groups were used to calculate the fold-change. Proteins with absolute log2 fold-change greater than 0.5 ($|\Delta \log 2| > 0.5$) were considered to be differentially regulated. We identified a diverse list of proteins differentially regulated, including kinases, heat shock proteins, transcription factors, structural proteins, and metabolic enzymes. When compared with Cur, 219 proteins were upregulated, and 234 proteins were downregulated in EP+Cur treatment. The proteins uniquely expressed in each treatment group were handled separately.

Table 4.2 shows top 20 upregulated proteins in EP+Cur treatment from Cur treatment. The 3-hydroxyisobutyrate dehydrogenase, mitochondrial (HIBADH), a protein involved in fatty acid (FA) oxidation was the most upregulated protein with an 8.7-fold increase in EP+Cur compared to Cur. Another protein, single-stranded DNA-binding protein (SSBP1), which plays an important role in mtDNA replication, recombination and repair by binding to single-stranded mtDNA was upregulated by 4-fold. The SSBP1 is a suppressor of TNBC metastasis, as its loss may play an early role in the induction of epithelial to mesenchymal transition (H.-L. Jiang et al., 2016), suggesting that EP+Cur treatment may target invasion" (Mittal, Aryal, et al., 2020).

We also studied cellular localization of these 20 proteins and their interaction. These results are shown in Figure 4.5. Out of top 20 upregulated proteins, except NOMO1, 19 were localized in intracellular membrane-bound organelle, mainly in mitochondria and endoplasmic reticulum. Among these 19 proteins, 15 (ACAT1, ACO2, ALDH2, CHCHD3, COX5A, GRPEL1, HIABDH, SLIRP, PHB, SSBP1, SLIRP, TIMM13, UQCRC1, VDAC1, and VDAC2) are mitochondrial and remaining 4 (SSR1, ATP2A2, HLA-C, and SUMF2) are part of endoplasmic reticulum. The interaction analysis results in Figure 4.5 reveal a greater degree of interaction among mitochondrial proteins.

Table 4.2: The top-20 upregulated proteins and their expression in EP+Cur compared to Cur. Here Cur concentration of 50µM and EP of 1200V/cm, 100µs, 8 pulses at 1Hz were used.

S.N.	Uniprot Accession No.	Protein Name	Gene Name	MS/MS Count Cur	MS/MS Count EP+Cur	Fold Change (EP+Cur – Cur)	Regulation
1	P31937	3-hydroxyisobutyrate dehydrogenase	HIBADH	2	18	8.7	Up
2	P43307	Translocon-associated protein subunit alpha	SSR1	6	5	4.3	Up
3	Q546I6	HLA class I histocompatibility antigen, Cw-12 alpha chain	HLA-C	2	6	4.1	Up
4	Q567R6	Single-stranded DNA-binding protein	SSBP1	19	31	4.0	Up
5	P35232	Prohibitin	PHB	44	64	3.7	Up
6	Q8NBJ7	Sulfatase-modifying factor 2	SUMF2	6	5	3.7	Up
7	Q9HAV7	GrpE protein homolog 1, mitochondrial	GRPEL1	5	11	3.7	Up
8	O60220	Mitochondrial import inner membrane translocase subunit Tim8 A	TIMM8A	4	9	3.6	Up
9	Q99798	Aconitate hydratase, mitochondrial	ACO2	3	9	3.6	Up
10	P45880	Voltage-dependent anion-selective channel protein 2	VDAC2	43	37	3.6	Up
11	P05091	Aldehyde dehydrogenase, mitochondrial	ALDH2	8	16	3.5	Up
12	P31930	Cytochrome b-c1 complex subunit 1, mitochondrial	UQCRC1	13	24	3.5	Up
13	Q9NX63	MICOS complex subunit MIC19	CHCHD3	4	7	3.5	Up
14	Q15155	Nodal modulator 1	NOMO1	4	18	3.5	Up
15	P24752	Acetyl-CoA acetyltransferase, mitochondrial	ACAT1	42	57	3.5	Up
16	Q9Y5L4	Mitochondrial import inner membrane translocase subunit Tim13	TIMM13	10	8	3.4	Up
17	P21796	Voltage-dependent anion-selective channel protein 1	VDAC1	49	66	3.4	Up

Table 4.2 continue

18	**Q9GZT3**	**SRA stem-loop-interacting RNA-binding protein, mitochondrial**	**SLIRP**	**7**	**9**	**3.4**	**Up**
19	P20674	Cytochrome c oxidase subunit 5A, mitochondrial	COX5A	10	22	3.3	Up
20	P16615	Sarcoplasmic/endoplasmic reticulum calcium ATPase 2	ATP2A2	4	14	3.3	Up

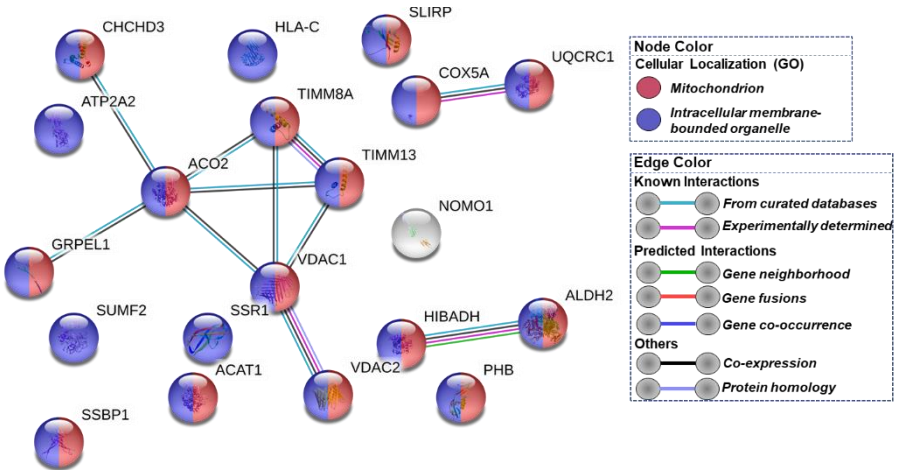

Figure 4.5: The interaction among top-20 upregulated proteins in EP+curcumin (EP+Cur) compared to curcumin (Cur) in MDA-MB-231 cells at 12h of treatment. Here Cur concentration of 50µM and EP of 1200V/cm, 100µs, 8 pulses at 1Hz were used. The top-20 downregulated proteins were uploaded to STRING (Szklarczyk et al., 2017) software to study the interaction and functional enrichment using evidence as meaning of network edge. The edge color in figure legend shows active interaction sources used in analysis, where the highest confidence (0.9) setting for minimum required interaction was used. Localization is represented with node color.

Top 20 downregulated proteins for EP+Cur treatment compared with Cur treatment are shown in Table 4.3. "The phosphoglucomutase-1 (PGM1), a key glycolytic protein was the most downregulated protein with a 32.3-fold decreased in EP+Cur compared to Cur. Another protein small nuclear ribonucleoprotein Sm D1 (SNRPD1), which is reported to be one of the 66 common significantly altered genes in TNBC from normal cells in a cohort study (Mathe et al., 2015) was also downregulated by 19.5-fold" (Mittal, Aryal, et al., 2020).

The results of cellular localization studies of these top 20 downregulated proteins and their interactions are shown in Figure 4.6. Out of these 20 proteins, except TOMM70A, 19 are localized in cytosol, nuclear lumen, and intracellular organelle lumen. Majority of these proteins (14 proteins) are cytosolic (AHNAK2, PGM1, EIF4G1, PSMC5, SNRPD1, EIF4B, EZR, IPO7, VCL, PSMC5, RPL7, DYNC1H1, TXNRD1, and VCL). The interaction analysis results in Figure 4.6 reveal only a minimal interaction among these downregulated proteins.

The analysis of top 20 regulated proteins indicates that the EP+Cur treatment may enhance the activity of proteins in organelles, such as mitochondria and endoplasmic reticulum, which actively participate in inducing apoptotic cell death, while mainly downregulating cytosolic proteins. Moreover, while top upregulated proteins show a higher degree of interaction, minimal interaction is found among top downregulated proteins.

Table 4.3: The top-20 downregulated proteins and their expression in EP+Cur compared to Cur. Here Cur concentration of 50µM and EP of 1200V/cm, 100µs, 8 pulses at 1Hz were used.

S.N.	Uniprot Accession No.	Protein Name	Gene Name	MS/MS Count Cur	MS/MS Count EP+Cur	Fold Change (EP+Cur – Cur)	Regulation
1	P36871	Phosphoglucomutase-1	PGM1	27	2	32.3	Down
2	P62314	Small nuclear ribonucleoprotein Sm D1	SNRPD1	9	2	19.5	Down
3	Q04637	Eukaryotic translation initiation factor 4 gamma 1	EIF4G1	29	2	15.1	Down
4	P11216	Glycogen phosphorylase, brain form	PYGB	46	3	14.4	Down
5	O00410	Importin-5	IPO5	32	3	14.4	Down
6	P23588	Eukaryotic translation initiation factor 4B	EIF4B	12	4	11.7	Down
7	P18206	Vinculin	VCL	50	3	11.3	Down
8	Q14204	Cytoplasmic dynein 1 heavy chain 1	DYNC1H1	117	13	10.1	Down
9	P68431	Histone H3.1	HIST1H3A	12	9	10.0	Down
10	P62195	26S protease regulatory subunit 8	PSMC5	13	2	9.8	Down
11	O95373	Importin-7	IPO7	31	4	8.9	Down
12	P12955	Xaa-Pro dipeptidase	PEPD	17	3	8.9	Down
13	Q8IVF2	Protein AHNAK2	AHNAK2	25	2	8.5	Down
14	O94826	Mitochondrial import receptor subunit TOM70	TOMM70A	4	3	7.8	Down
15	P55060	Exportin-2	CSE1L	56	9	7.3	Down
16	Q16881	Thioredoxin reductase 1, cytoplasmic	TXNRD1	37	5	7.3	Down
17	P15311	Ezrin	EZR	35	6	7.2	Down
18	Q13838	Spliceosome RNA helicase DDX39B	DDX39B	54	10	6.7	Down
19	P18124	60S ribosomal protein L7	RPL7	25	7	6.5	Down
20	Q9BWD1	Acetyl-CoA acetyltransferase, cytosolic	ACAT2	24	3	6.4	Down

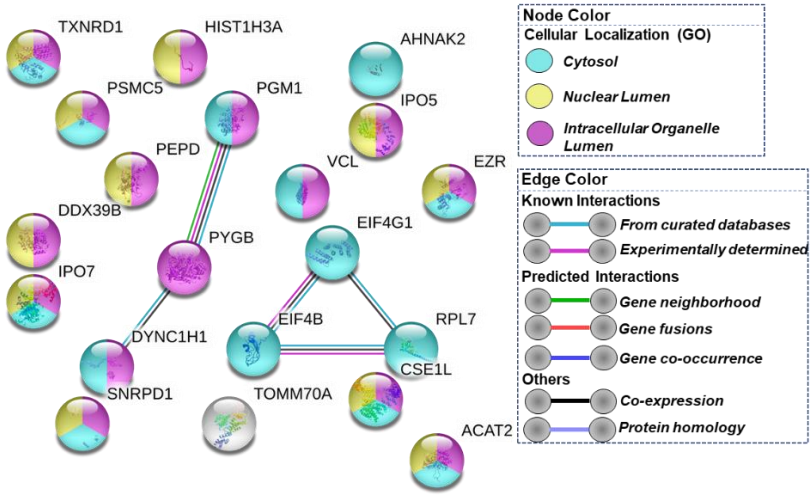

Figure 4.6: The interaction among top-20 downregulated proteins in EP+curcumin (EP+Cur) compared to curcumin (Cur) in MDA-MB-231 cells at 12h of treatment. Here Cur concentration of 50µM and EP of 1200V/cm, 100µs, 8 pulses at 1Hz were used. The top-20 downregulated proteins were uploaded to STRING (Szklarczyk et al., 2017) software to study the interaction and functional enrichment using evidence as meaning of network edge. The edge color in figure legend shows active interaction sources used in analysis, where the highest confidence (0.9) setting for minimum required interaction was used. Localization is represented with node color.

i. Cellular localization analysis of all differentially expressed proteins

"Figure 4.7 shows the gene ontology (GO) enrichment analysis of the cellular localization of the differentially expressed and uniquely identified proteins in EP+Cur. We did not observe enrichment in the cellular localization for the unique proteins in Cur" (Mittal, Aryal, et al., 2020). Among the proteins upregulated for EP+Cur treatment, the largest number of 35 proteins were mitochondrial, followed by 25 membrane proteins (Figure 4.7(a)). Among downregulated proteins, the largest number of 53 proteins were cytoplasmic, followed by 39 cytosolic proteins (Figure 4.7(b)). Similar to upregulated proteins, among the unique EP+Cur proteins also the largest number of 14 proteins were mitochondrial, followed by 13 in the membrane (Figure 4.7(c)). "The upregulation in membrane proteins for EP+Cur highlights that EP application may increase cellular transport, not only through the membrane pore formation, but also via the upregulation of key transport proteins. Additionally, enhanced activity and function of proteins largely localized in organelles (mitochondrion and endoplasmic reticulum) for EP+Cur may activate intrinsic apoptotic pathway of cell death, while downregulating cytosolic proteins" (Mittal, Aryal, et al., 2020).

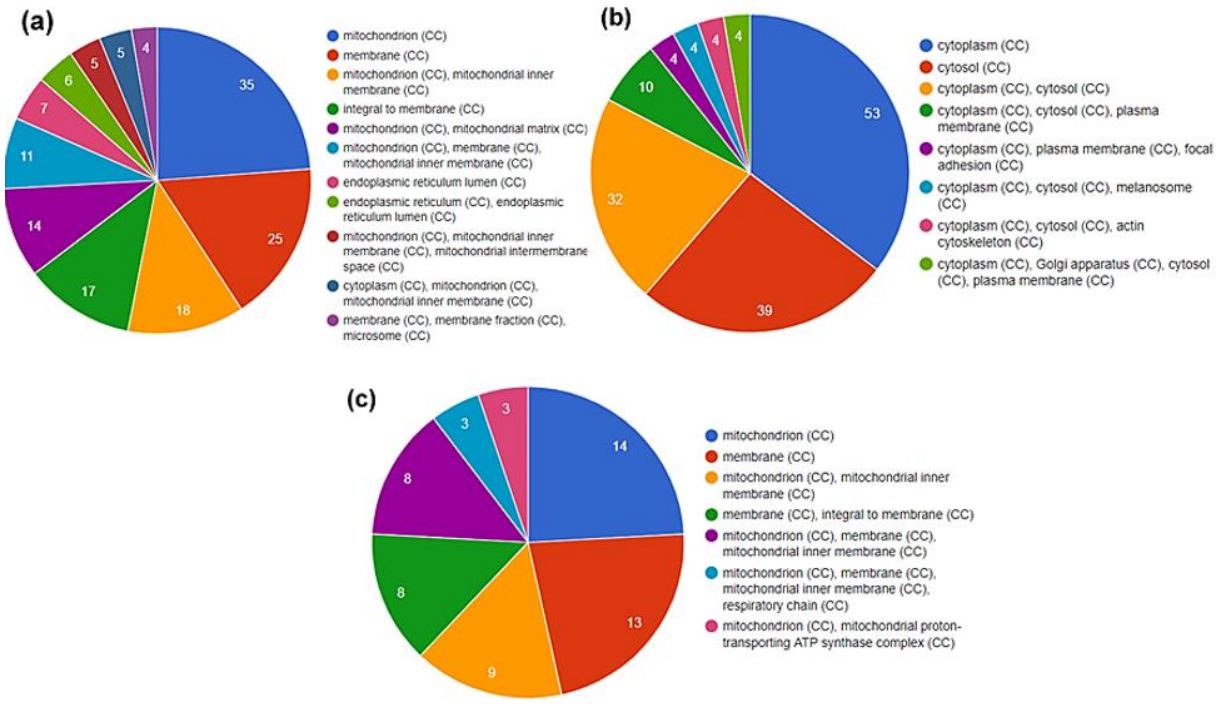

Figure 4.7: Top gene ontology enrichment terms of cellular location for differently expressed proteins in EP+curcumin (EP+Cur) compared to curcumin (Cur) in MDA-MB-231 cells at 12h of treatments: (a) upregulated "(adjusted P value: [0.001, 0.007])", (b) downregulated "(adjusted P value: [0.001, 0.007])", and (c) unique proteins "(adjusted P value: [0.001, 0.005])". There was no enrichment for Cur unique proteins. Here Cur concentration of 50µM and EP of 1200V/cm, 100µs, 8 pulses at 1Hz were used. A web-based tool Genecodis (Carmona-Saez et al., 2007) was used for this analysis.

ii. Pathway Enrichment analysis of differentially expressed proteins

Further, the enrichment in KEGG pathways was studied for differentially regulated proteins and unique proteins in each treatment, as shown in Figure 4.8. "Among the upregulated pathways, protein processing in endoplasmic reticulum showed highest number of proteins with a count of 14, followed by 10 OXPHOS and 8 TCA cycle pathways proteins in EP+Cur (Figure 4.8(a)). Other notable upregulated pathways were aromatic amino acid (AA) (tryptophan) metabolism, peroxisome, calcium signaling pathway, and PI3K-Akt signaling pathway. For downregulated proteins, ribosome showed highest number of proteins with a count of 16, followed by 11 and 8 proteins in focal adhesion and glycolysis, respectively (Figure 4.8(b)). Pathways

which regulate cancer cell apoptosis, proliferation, differentiation and migration were downregulated for EP+Cur, such as glycolysis, PPP, focal adhesion, and hippo signaling pathway.

In the hippo signaling pathway, the Cur + EP downregulated expression of four proteins in 14–3-3 protein family, such as, 14–3-3 beta (YWHAB; ↓2.5×), 14–3-3 epsilon (YWHAE; ↓1.9×), 14–3-3 tau (YWHAQ; ↓1.5×), 14–3-3 zeta (YWHAZ; ↓1.4×). Previous reports suggest that 14–3-3 s integrate and control multiple signaling pathways, playing a major role in regulating apoptosis, cell cycle progression, autophagy, glucose metabolism, and cell motility (Pennington, Chan, Torres, & Andersen, 2018). The YWHAZ promotes chemoresistance and poor patient outcomes (Pennington et al., 2018). The YWHAB is reported to be one of the top five highly expressed and connected target proteins (HSP90AB1, CSNK2B, TK1, YWHAB and VIM) in MDA-MB-231 cells, as their knockout in animal models inhibited colony formation, proliferation, migration, anchorage independence and invasion (Tilli, Carels, Tuszynski, & Pasdar, 2016). We also detected downregulation in HSP90AB1 (↓1.5×) and VIM (↓1.8×), indicating downregulation in three (HSP90AB1, YWHAB and VIM) for Cur + EP treatment, out of five main TNBC targets. Another tumorigenic protein Annexin A1, which promotes cellular invasion and metastasis in MDA-MB-231 TNBC under hypoxia and is associated with worst patient outcome (Okano et al., 2015) was also downregulated (↓1.5 ×) for Cur+ EP treatment.

For unique proteins in Cur, notably enriched pathways were NFkB signaling pathway, toll-like receptor signaling pathway, RNA transport, and Amino sugar (AS) and nucleotide sugar (NS) metabolism (Figure 4.8(c)). Interestingly, OXPHOS pathway was also enriched with 16 proteins for unique EP+Cur proteins (Figure 4.8(d)), indicate a possible switch in metabolic pathway from glycolysis to OXPHOS" (Mittal, Aryal, et al., 2020).

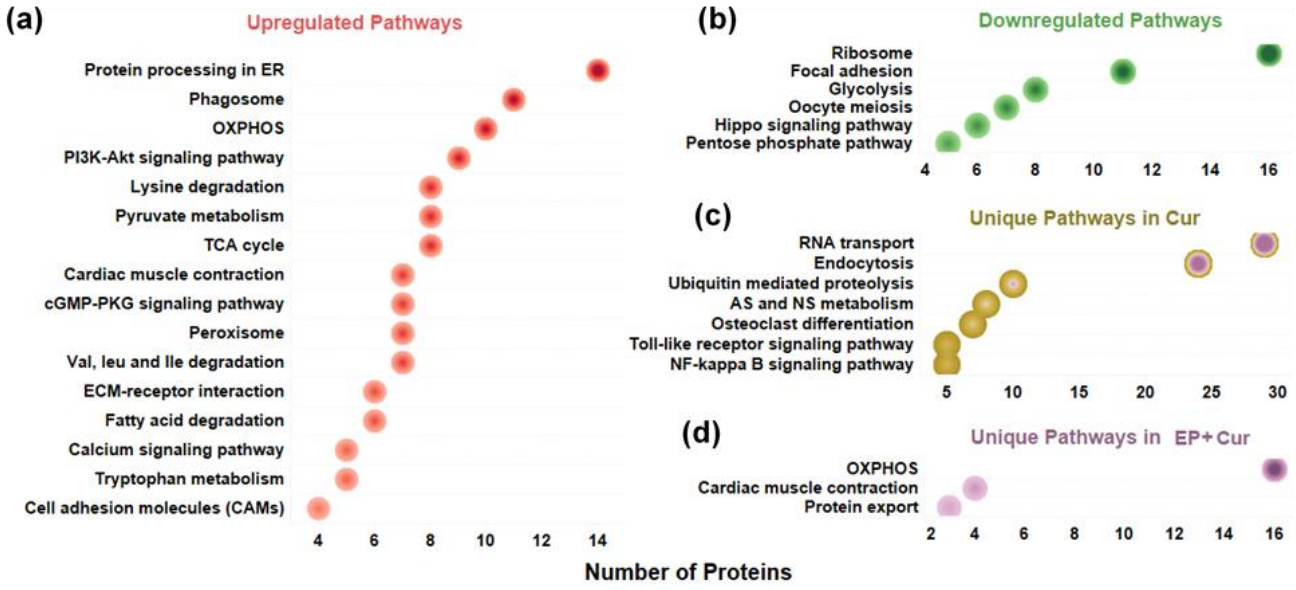

Figure 4.8: The Enriched pathways for (a) upregulated, (b) downregulated for EP+curcumin (EP+Cur) from curcumin (Cur), and unique proteins for (c) Cur and (d) EP+Cur in MDA-MB-231 cells at 12h of treatment. Here Cur concentration of 50µM and EP of 1200V/cm, 100µs, 8 pulses at 1Hz were used. DAVID 6.8 (D. W. Huang, Sherman, & Lempicki, 2008) was used with total 1456background proteins to identify the KEGG pathway enrichment. "Abbreviations: ER-Endoplasmic reticulum, OXPHOS-Oxidative phosphorylation, Isoleucine-Ile, Leu:-Leucin, Lys-Lysine, Pro-Proline" (Mittal, Aryal, et al., 2020).

D. Metabolic switch in TNBC cells upon EP+Cur treatment

i. Downregulation of glycolysis proteins

"TNBCs have elevated uptake and utilization of glucose and are highly reliant on glycolysis with high vulnerability on glycolytic inhibition (Liangliang Shen et al., 2015) (Lim et al., 2016), and disrupted mitochondria function and oxidative phosphorylation (Pelicano et al., 2014) (Guha et al., 2018). We next examined downregulated glycolytic proteins to understand the inhibitory effect produced by EP+Cur on the glycolysis in MDA-MB-231 cells (Figure 4.9(a)). In addition, the proteins in the alternate upregulated metabolic pathways such as TCA cycle and OXPHOS were also visualized (Figure 4.9(b) and Figure 4.9(c)). We observed downregulation in 8 key glycolysis proteins, including PGM1 (↓32.2×), phosphofructokinase (PFKP; ↓5.5×), PGAM1 (↓2.4×) , ALDOA (↓1.5×), phosphoglycerate kinase 1 (PGK1; ↓1.5×), ENO2 (↓4.8×), LDHA (↓2.9×), and LDHB (↓1.5×). STRING analysis revealed strong evidence of interaction among these glycolysis proteins and their cellular cytosolic localization in membrane raft, ficolin-

1-rich-granule lumen, myelin sheath, and tertiary granule lumen (Figure 4.9(a), right panel)" (Mittal, Aryal, et al., 2020).

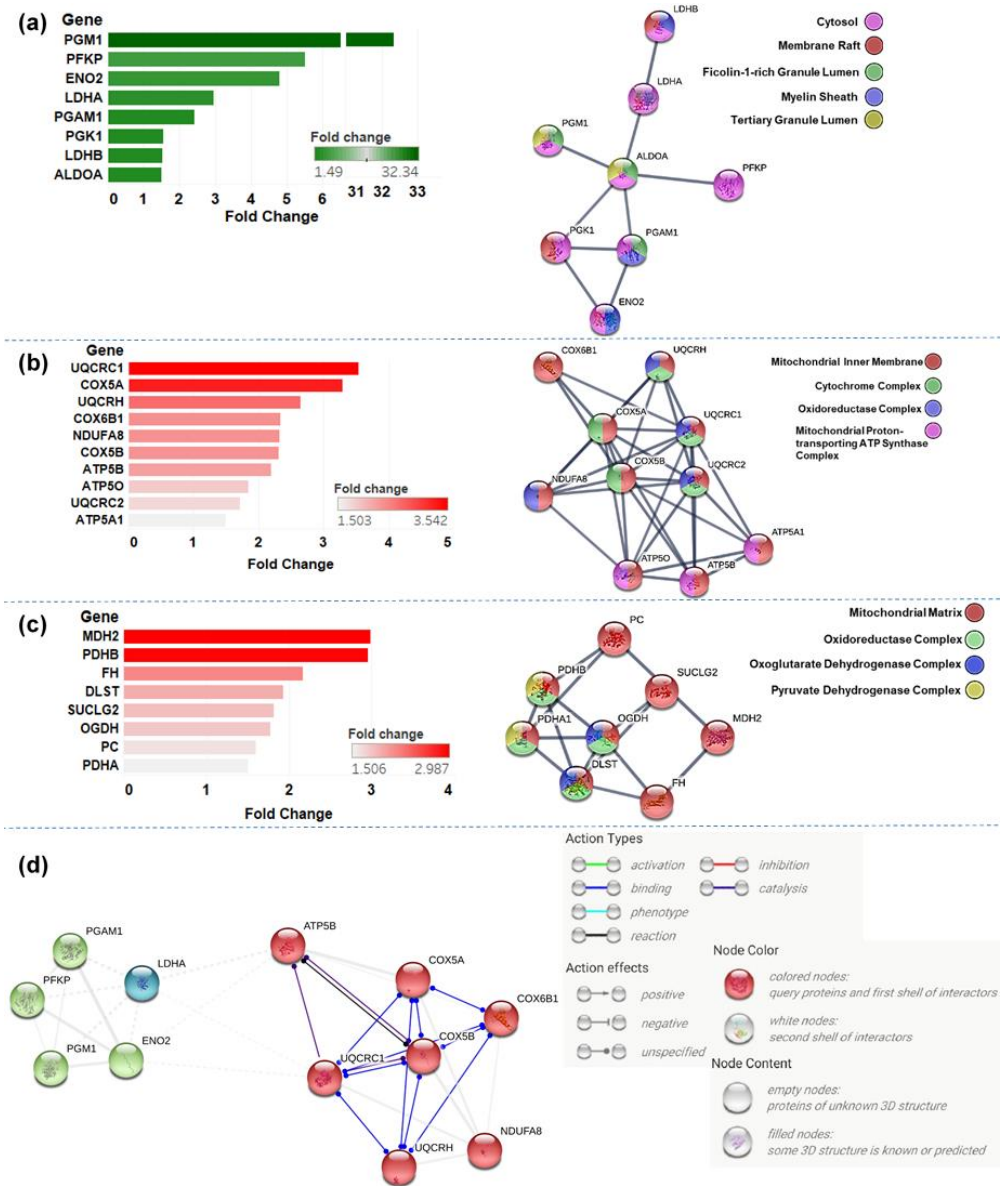

Figure 4.9: (a-c) The levels of up- downregulated proteins in EP+curcumin (EP+Cur) from curcumin (Cur) in MDA-MB-231 cells at 12h of treatment in different pathways (Panel on left) and interaction among them (Panel on right), where colors indicate localization: (a) Glycolysis pathway (downregulated), (b) OXPHOS (upregulated), (c) TCA cycle (upregulated). (d) Interaction among Glycolysis and OXPHOS proteins displaying action types and action effects. Here Cur concentration of 50μM and EP of 1200V/cm, 100μs, 8 pulses at 1Hz were used. Proteins from GO terms "Glycolysis/gluconeogenesis", "Oxidative phosphorylation", and "TCA cycle" from KEGG database were fed to STRING 11.0 (Szklarczyk et al., 2017) to visualize the interactions.

"PGM1 is necessary for sustained cancer cell growth (E. Bae, Kim, Koh, & Kim, 2014). PFKP is known to contribute to metabolic reprogramming to glycolysis pathway and maintains cancer cell proliferation (Jun Wang et al., 2016)" (Mittal, Aryal, et al., 2020). PGAM1 promotes cell migration (D. Zhang et al., 2017). ALDOA has a major function in glycolysis, as it maintain the glucose homeostasis (Chang et al., 2018). ALDOA inhibition disrupts the feed-forward loop of glycolysis by blocking both glycolysis and hypoxia-inducible factor 1 (HIF-1) activity to impede the cancer cell proliferation (Grandjean et al., 2016). PGK1 also forms feed-forward loop of glycolysis in association with HIF-1α (Fu et al., 2018). PGK1 is a promising breast cancer biomarker as its elevated expression is linked with poor prognosis (Fu et al., 2018). The ENO2 and LDHB are overexpressed in the TNBC glycolytic subtypes found using integrative analysis on transcriptomic and genomic data of TNBC (Gong et al., 2019). "Cells expressing LDHA maintain a lower mitochondrial membrane potential and decreased reactive oxygen species production (Newington et al., 2012). LDHA is also an indicator of the breast cancer malignancy and its inhibition is shown to prevent TNBC brain metastasis (Dong et al., 2017)" (Mittal, Aryal, et al., 2020).

Figure 4.10 shows the extent of proteins downregulated in glycolysis by EP+Cur, with considerable reduction in the expression of various glycolytic enzymes.

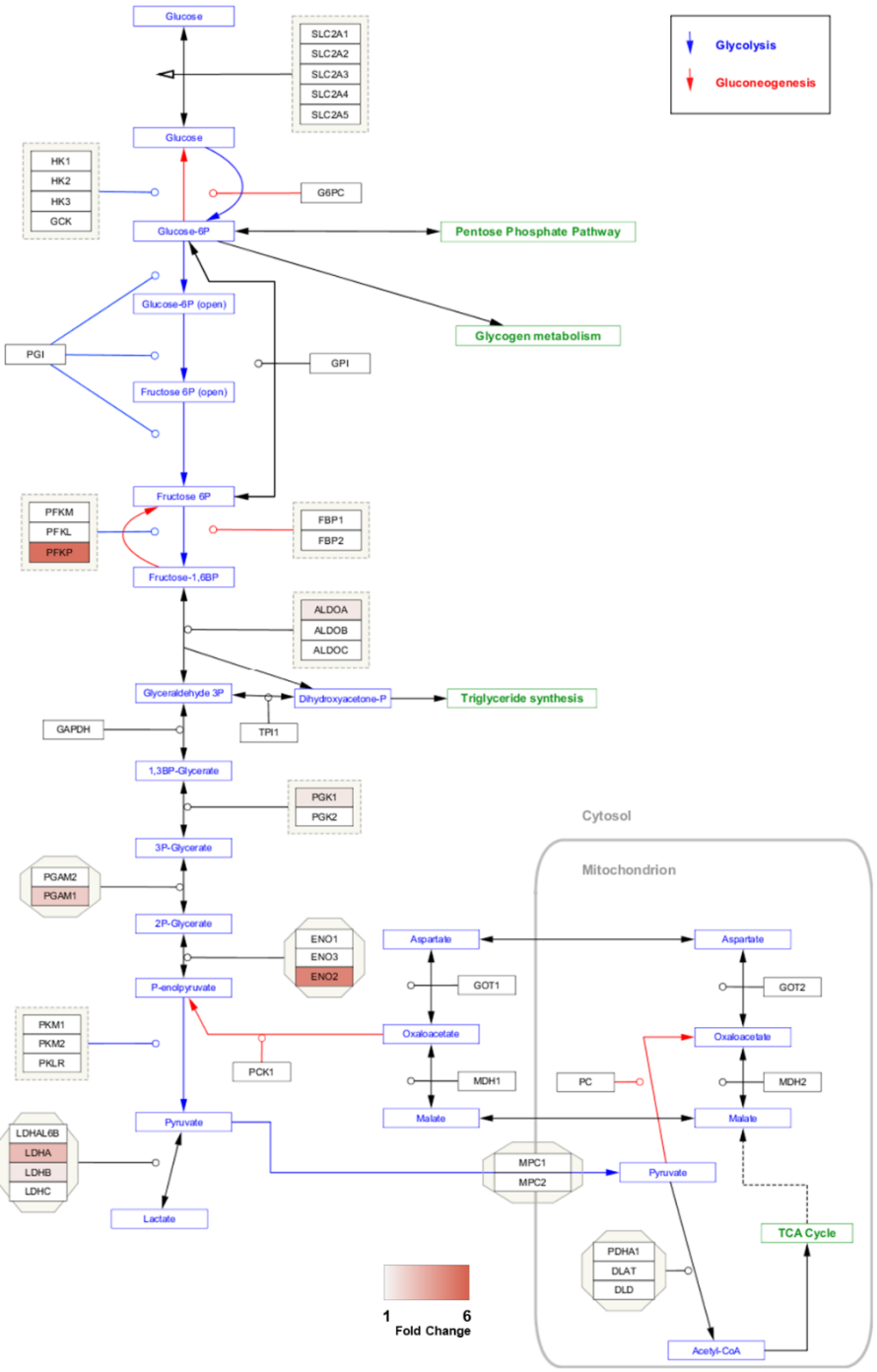

Figure 4.10: Representation of glycolytic proteins downregulated by EP+curcumin (EP+Cur) from Cur in MDA-MB-231 cells at 12h of treatment. Here Cur concentration of 50µM and EP of 1200V/cm, 100µs, 8 pulses at 1Hz were used. “Proteins from GO term Glycolysis/gluconeogenesis from KEGG pathway analysis were uploaded to the Cytoscape 3.6.1 software (P. Shannon et al., 2003) and matched to the glycolysis pathway using the WikiPathway app (beta), with the degree of shading representing the fold change” (Mittal, Aryal, et al., 2020).

a. Clinical expression of LDHB and survival of patients

We further analyzed the clinical expression of LDHB in 833 invasive breast carcinoma patient and normal samples from "The Cancer Genome Atlas" (TCGA) database using UALCAN tool (Chandrashekar et al., 2017). These results are shown in Figure 4.11 for various invasive breast carcinoma subgroups, including TNBC subtypes. Compared to normal tissue samples, LDHB expression was significantly higher in the mesenchymal TNBC subtype, while it was significantly lower in luminal and HER2-positive breast cancer subtypes. Compared to luminal subtype, the LDHB expression was significantly higher in five TNBC subtypes (BL1, BL2, IM, MSL, and M). Similarly, compared to HER2-positive subtype, the LDHB expression was significantly higher in four TNBC subtypes (BL1, BL2, IM, and M). This correlates well with previous observation, where "LDHB is shown to be specifically upregulated in basal-like/TNBC cell lines and tumors compared to luminal subtypes (McCleland et al., 2012)" (Mittal, Aryal, et al., 2019).

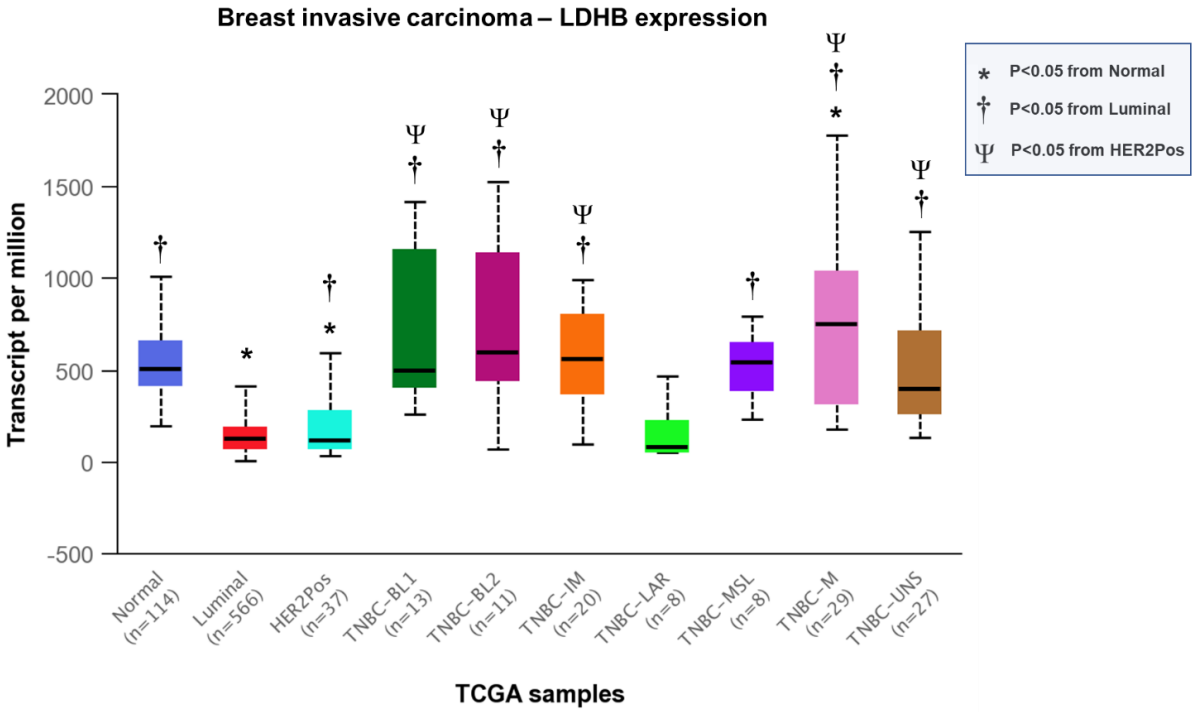

Figure 4.11: Box-whisker plot showing expression levels of LDHB in patients samples from various invasive breast carcinoma subgroups, including TNBC subtypes. The Cancer Genome Atlas (TCGA) database using UALCAN tool was used (Chandrashekar et al., 2017). Abbreviations: "HER2Pos-HER2-positive, BL1-basal-like 1, BL2-basal-like 2, IM-immunomodulatory, LAR-luminal androgen receptor, MSL-mesenchymal stem-like, M-mesenchymal-like, UNS-unspecified".

We also analyzed if the increased expression of LDHB correlated with poor breast cancer patient survival using gene expression data from NCBI GEO database of two microarray platforms (Affymetrix U133A or U133Plus2), using the GENT2 tool (Park, Yoon, Kim, & Kim, 2019). These results are shown in Figure 4.12 in form of Kaplan-Meier overall survival curves. The high LDHB expression in breast cancer patients correlated with a significantly poor survival ($P < 0.01$). Similarly, other researchers have also shown that "the increased expression of LDHB correlates to significantly poor clinical outcomes, and is an essential gene for TNBC proliferation and survival *in vitro* and *in vivo* models (Dennison et al., 2013; McCleland et al., 2012)" (Mittal, Aryal, et al., 2019).

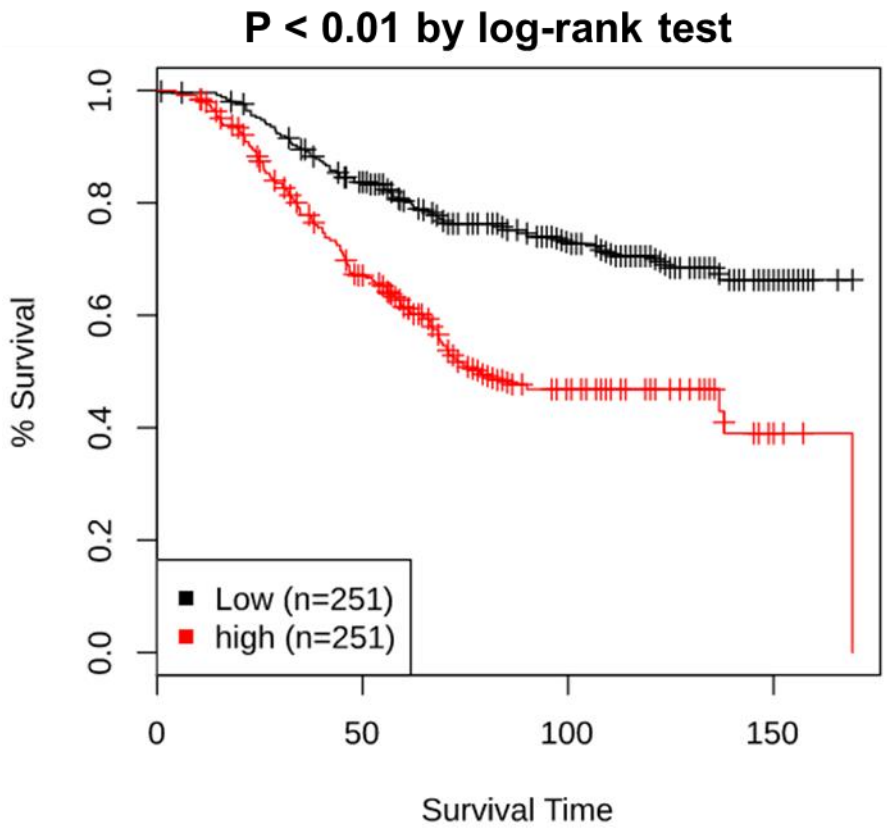

Figure 4.12: Kaplan-Meier survival analysis of patients (overall survival (OS)) with breast cancer, separated by median LDHB expression into low- (black curve) and high- (red curve) expression groups. The log-rank test was used to identify statistical significance between two groups. GENT2 database tool was used (Park et al., 2019).

b. Downregulation of LDHB and reverse Warburg effect

The overexpression of LDHB in TNBC leads to a comprehensive shift in their metabolism (McCleland et al., 2012). A recent novel hypothesis on tumor metabolism, called "reverse Warburg effect" suggest that the hypoxic and glucose-deprived cells rely on LDHB to convert the lactate produced by neighboring cells undertaking aerobic glycolysis (McCleland et al., 2012; Whitaker-Menezes et al., 2011). In these cells to generate energy, the lactate is converted by LDHB to pyruvate (Markert, Goodfriend, Kaplan, & Kaplan, 1963; Porporato, Dhup, Dadhich, Copetti, & Sonveaux, 2011), which supplies the TCA cycle. These observations suggest that ECT could also impede the "reverse Warburg effect" in TNBC cells by downregulating LDHB.

"Compared to ER^+, TNBC also have increased glycolytic intermediates including glucose-6-phosophate, which is utilized in the PPP to synthesize nucleic acid" (Mittal, Aryal, et al., 2020), which heightens the proliferation and growth of cancer cells (Jóźwiak et al., 2014; Kanaan et al., 2014). EP+Cur treatment also downregulated the PPP, suggesting that this treatment can target glycolysis and its intermediate pathways (PPP), while compromising the "reverse Warburg effect" as well to comprehensively target MDA-MB-231 TNBC cells.

ii. Upregulation of TCA Cycle and OXPHOS Proteins

Upon the downregulation of glycolysis, TNBC cells may utilize alternate compensatory metabolism due to their flexibility to cause resistance to therapies (Echeverria et al., 2019). Considering this, upregulated proteins for EP+Cur treatment in OXPHOS and TCA cycle pathways were also studied. The upregulated proteins for the OXPHOS pathway were: "cytochrome c oxidase subunits 5A (COX5A; ↑3.3×), 5B (COX5B; ↑2.3×) and 6B1 (COX6B1; ↑2.3×), ubiquinol-cytochrome c reductase core proteins 1 (UQCRC1; ↑3.5×), II (UQCRC2; ↑1.7×) and hinge protein (UQCRH; ↑2.6×), subunits of mitochondrial ATP synthase subunits O (ATP5O; ↑1.8×), alpha subunit 1 (ATP5A1; ↑1.5×) and beta polypeptide (ATP5B; ↑2.2×), and Ubiquinone Oxidoreductase Subunit A8 (NDUFA8; ↑2.3×)" (Mittal, Aryal, et al., 2020) (Figure 4.9(b)).

There was a strong interaction among these proteins as revealed by the STRING analysis, which could be attributed to their common function and localization in mitochondria (Figure 4.9(b), right panel). In mitochondria, these proteins localized in various complexes of electron transport chain (ETC), including oxidoreductase complex, cytochrome complex (cytochrome c), and mitochondrial proton-transporting ATP synthase complex. The upregulated OXPHOS proteins of mapped on OXPHOS pathway are also shown in Figure 4.13 ("red stars"). The upregulated proteins are distributed across multiple ETC complexes, such as I, III, IV, and V, suggesting that EP+Cur treated TNBC cells are attempting to activate ETC for ATP generation due to stress response, as glycolysis is blocked.

"While the previous reports have indicated that OXPHOS pathway can rescue the TNBC cells after treatment (Echeverria et al., 2019), here we observed reduction in the clonogenic survival fraction in MDA-MB-231 cells after 9 days of treatment when supplemented with fresh media (Figure 4.2). This indicates that the effect of EP+Cur treatment on MDA-MB-231 cells

were sustained and increase in OXPHOS did not rescue the cells even in nutrient rich conditions" (Mittal, Aryal, et al., 2020).

Elevated OXPHOS activity in MDA-MB-231 cells could also be attributed to the activation of intrinsic apoptotic pathway upon EP+Cur treatment. Our results shown an upregulation of proteins in cytochrome c. The cytochrome c is previously reported to be activated by EP mediated increased intracellular calcium concentration, which triggers apoptosis (Cen & Chen, 2017). In our study, various proteins of calcium signaling pathway were also upregulated by EP+Cur treatment, such as "ATPase plasma membrane Ca^{2+} transporting 1 (ATP2B1; ↑1.6×), ATPase sarcoplasmic/endoplasmic reticulum Ca^{2+} transporting 2 (ATP2A2; ↑3.3×), solute carrier family 25 member 5 (SLC25A5; ↑1.6×), and voltage dependent anion channels 1(VDAC1; ↑3.4×) and 2 (VDAC2; ↑3.6×)" (Mittal, Aryal, et al., 2020). Additionally, the protein processing in endoplasmic reticulum (which serves as calcium storage in cells) was also upregulated in our study (Figure 4.8(a)). "Therefore, apoptosis due to EP+Cur treatment could be influenced by the increase in intracellular calcium concentration due to calcium release from the endoplasmic reticulum and the efflux from extracellular environment, as noted by others (Hanna, Andre, & Mir, 2017)" (Mittal, Aryal, et al., 2020).

Even with suppression in glycolysis and the conversion reaction of lactate to pyruvate, we observed heightened activity of TCA cycle in EP+Cur treatment. This upregulation in TCA cycle could be credited to the upregulation in multiple supplemental pathways (FA degradation, AA metabolism/degradation, tryptophan metabolism), which produce pyruvate and various intermediates, such as acetyle COA and oxaloacetate to supply the TCA cycle. Total eight proteins were upregulated in TCA cycle, "including dihydrolipoamide S-succinyltransferase (DLST; ↑1.9×), fumarate hydratase(FH; ↑2.2×), malate dehydrogenase 2 (MDH2; ↑3×), oxoglutarate dehydrogenase (OGDH; ↑1.8×), pyruvate carboxylase (PC; ↑1.6×), pyruvate dehydrogenases (lipoamide) alpha 1 (PDHA1; ↑1.5×) and beta (PDHB; ↑3×), and succinate-CoA ligase GDP-forming beta subunit (SUCLG2; ↑1.8×)" (Mittal, Aryal, et al., 2020) (Figure 4.9(c)). There was a strong interaction among these proteins, as revealed by STRING interaction analysis (Figure 4.9(c), right panel). These localization of these proteins was found in pyruvate dehydrogenase complex (PDC), oxidoreductase complex, and oxoglutarate dehydrogenase complex.

This upregulation in PDC activity suggests a rerouting of pyruvate metabolism back to the mitochondrion upon EP+Cur treatment. "Inhibition of PDC activity in head and neck cancers and

breast cancers, including TNBC contributes to the Warburg metabolic and malignant phenotype (Gang, Dilda, Hogg, & Blackburn, 2014; McFate et al., 2008)" (Mittal, Aryal, et al., 2020). Moreover, the restoration of PDC activity could reestablish pyruvate metabolism to mitochondria to enhance apoptosis, reduced invasion, and stalled tumor growth.

Collectively the downregulation of glycolysis proteins with TCA cycle and OXPHOS proteins upregulation of suggest a switch in TNBC metabolism from glycolysis to OXPHOS upon EP+Cur treatment. To understand this metabolic switch, we also studied the interaction among proteins of glycolysis and OXPHOS pathways proteins, as shown in Figure 4.9(d). The interaction analysis showed that two distinct clusters are formed by glycolysis (green nodes) and OXPHOS (red nodes) proteins. The five OXPHOS proteins, "COX5A, COX5B, COX6B1, UQCRC1, and UQCRH bind together (blue edges) and jointly react with and/or catalyze ATP5B (black and purple edges)" (Mittal, Aryal, et al., 2020). On the other hand, there is a limited interaction among glycolytic proteins and there appear no binding affinity among them.

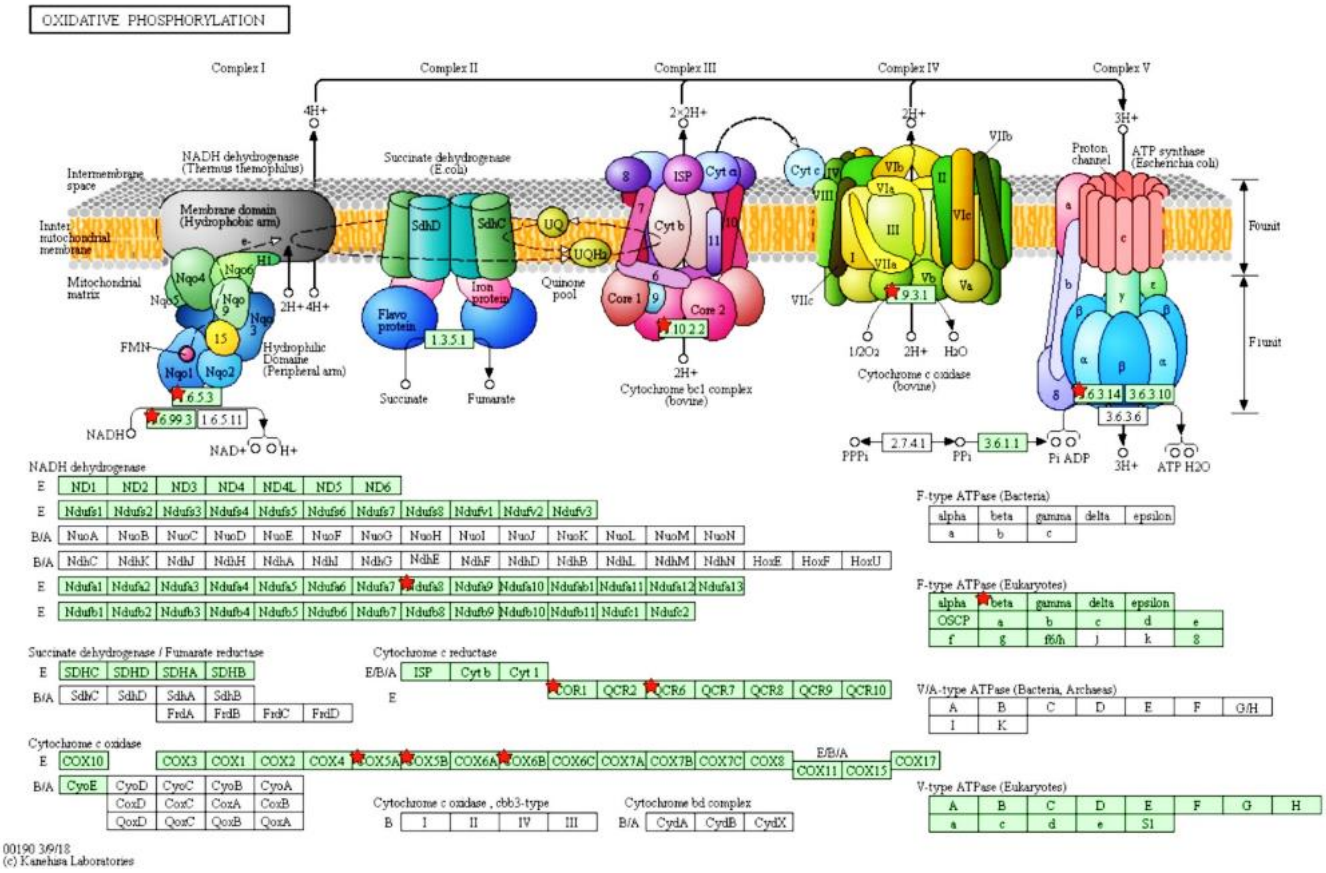

Figure 4.13: Representation of OXPHOS pathway proteins upregulated by EP+curcumin (EP+Cur) from Cur in MDA-MB-231 cells at 12h of treatment. Here Cur concentration of 50µM and EP of 1200V/cm, 100µs, 8 pulses at 1Hz were used. Proteins enriched with GO term "Oxidative phosphorylation" from KEGG database (Kanehisa & Goto, 2000) and were overlapped on the OXPHOS pathway and shown by ★. The visualization is adapted with permission from Kanehisa Laboratories.

E. Downregulation of Focal Adhesion proteins

"Cell proliferation and metastasis require various changes in cell morphology and behavior, the majority of which are initiated at the cell surface as cells exhibit alteration in polarity and adhesion (Schulz et al., 2010). Considering this, we also examined the proteins in the focal adhesion pathway downregulated in the EP+Cur treatment. Figure 4.14 shows 11 downregulated proteins in the focal adhesion pathway and their relative expression levels. Of particular note are the downregulation proteins such as three filamins A (FLNA; ↓1.6×), B (FLNB; ↓1.7×), and C (FLNC; ↓1.9×), alpha-actinin-1 (ACTN1; ↓1.5×) and 4 (ACTN4; ↓1.9×), talin-1 (TLN1; ↓1.8×), and zyxin (ZYX; ↓1.6×), which are commonly upregulated in various aggressive cancers and are

actively involved in cell signaling and cytoskeletal dynamics at the plasma membrane (B. Ma et al., 2016; Ziegler, Moresco, Tu, Yates, & Nardulli, 2014).

The high expression of these three filamins, ACTN4, and TLN1 is previously reported in MDA-MB-231 TNBC cells (Ziegler et al., 2014). The FLNA is positively correlated with lung tumor growth and angiogenesis (Nallapalli et al., 2012) and in other cancers (Yue, Huhn, & Shen, 2013). While the roles of FLNB and FLNC in cancer are not yet clear, they are specifically upregulated in MDA-MB-231 cells compared to other cancer cells (Ziegler et al., 2014). The role of ACTN4 is also previously identified in breast cancer tumorigenesis and is suggested to be an ideal therapeutic target (Hsu & Kao, 2013). The TLN1 is also reported to be upregulated in MDA-MB-231 cells and is identified as one of the key proteins involved in the ovarian cancer cells invasion process using the physical force generated through cytoskeletal remodeling (Ziegler et al., 2014). The ZYX expression is also positively correlated with breast cancer histological stages and metastasis and its depletion is suggested to weaken the cell migration, proliferation and tumorigenesis in a xenograft models (B. Ma et al., 2016). This indicates that Cur + EP can alter the adhesion behavior of MDA-MB-231 cells by compromising key adhesion proteins implicated in cell growth, proliferation, and invasion. This correlates well with a previous observation where EP application significantly altered the MDA-MB-231 cell adhesion (Pehlivanova, Tsoneva, & Tzoneva, 2012)" (Mittal, Aryal, et al., 2020).

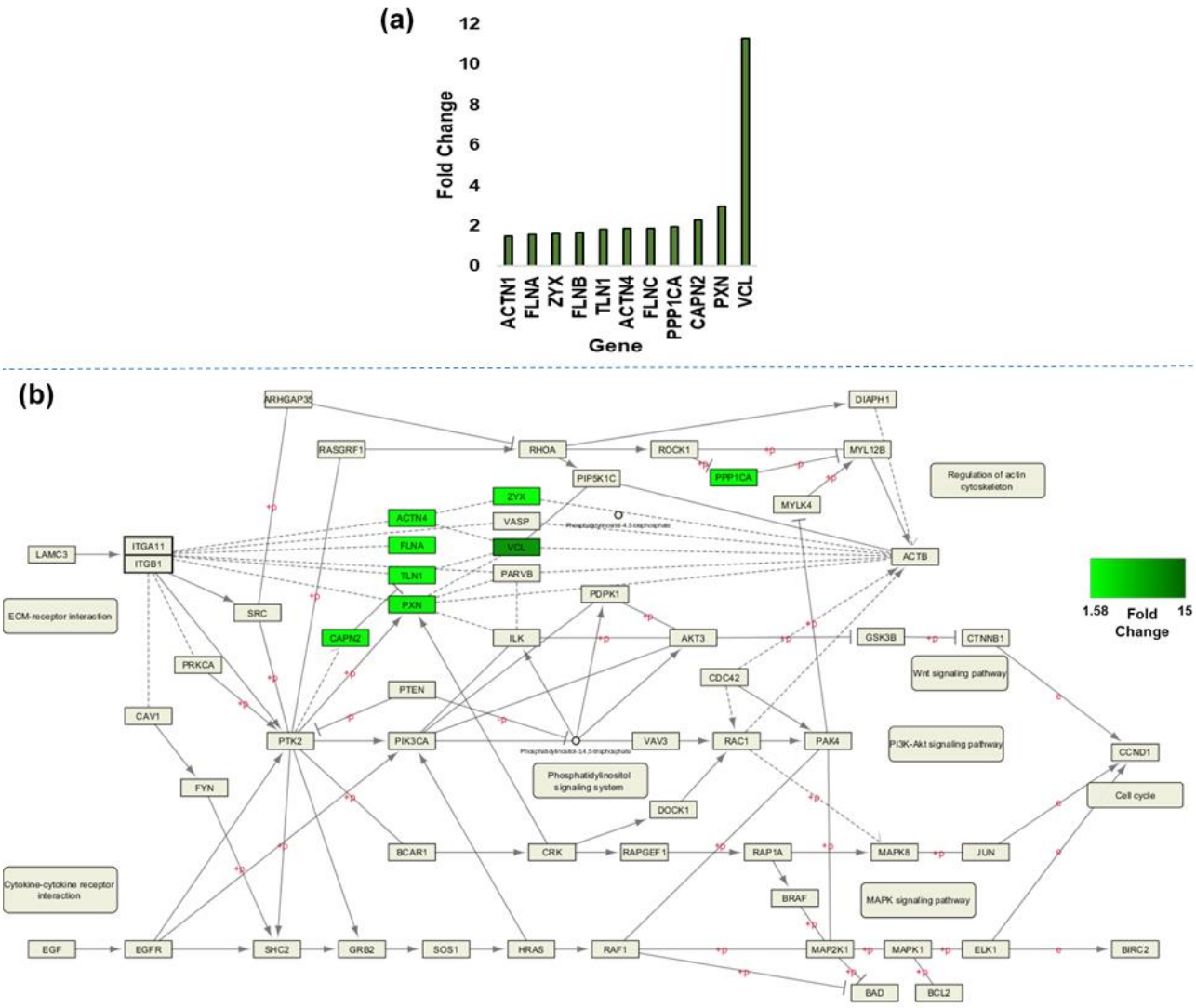

Figure 4.14: Representation of proteins in focal adhesion pathway downregulated by EP+curcumin (EP+Cur) from curcumin (Cur) in MDA-MB-231 cells at 12h of treatment. Here Cur concentration of 50µM and EP of 1200V/cm, 100µs, 8 pulses at 1Hz were used. (a) Relative log2 fold-change in EP+Cur from Cur for the proteins with GO term "Focal adhesion" from KEGG database. (b) Proteins overlapped on focal adhesion pathway. The proteins were mapped to focal adhesion pathway in Cytoscape 3.6.1, where the extent of shading represents fold change.

F. Validation of proteomics results

"Figure 4.15 shows the average luminescence (Lum) as relative light units (RLU), which directly corresponds to H_2O_2 reactive oxygen species (ROS) levels in non-tumorigenic mammary epithelial cells (MCF10A) and MDA-MB-231 cells for different treatments. For MDA-MB-231 cells, the Lum was 9126 for Control, which reduced non-significantly (common letter 'B') to 8797

for Cur, suggesting that Cur alone does not cause a significant change in oxidative stress in TNBC cells at 12h. On the other hand, in MCF10A, the Lum was 3342 for Control, which was significantly (letter 'C') lower by 2.7-fold from MDA-MB-231 Control. This indicates that the baseline oxidative stress in normal mammary epithelial MCF10A cells is significantly lower than the MDA-MB-231 TNBC cells" (Mittal, Aryal, et al., 2020). It is well established that the ROS is constantly higher in cancer cells due to changes in tumor microenvironment, genetic and metabolic profiles (J. Kim, Kim, & Bae, 2016). "Further, in MCF10A cells, the Lum was 3550 for Cur and 3974 for EP+Cur, which were not significantly different from MCF10A Control (share letter 'C'). This suggests that irrespective of the treatment type, normal mammary epithelial MCF10A cells maintain low levels of ROS. However, in MDA-MB-231 cells, the Lum was 21608 for EP+Cur, a 2.4-fold and significant (letter 'A') increase in H_2O_2 levels compared with MDA-MB-231 Ctrl" (Mittal, Aryal, et al., 2020).

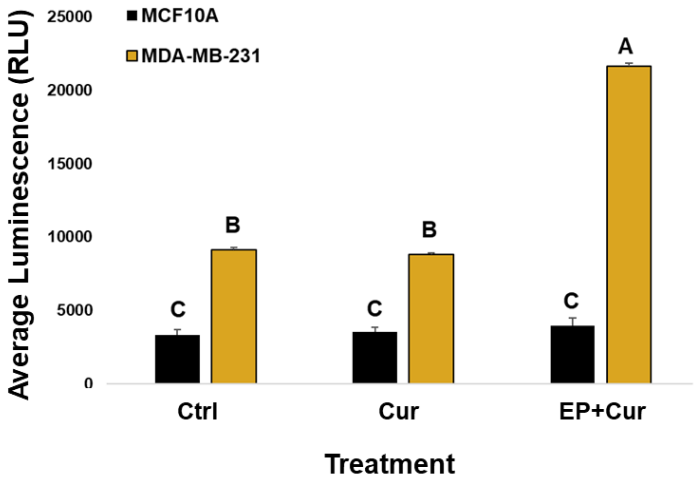

Figure 4.15: The generation of H_2O_2 reactive oxygen species (ROS) in MDA-MB-231 and MCF10A cells at 12h of treatment. Here Cur concentration of 50µM and EP of 1200V/cm, 100µs, 8 pulses at 1Hz were used. Two-way ANOVA analysis was performed to obtain significance. Different letters reveal significant difference - $P<0.05$ from Tukey's test. The results include data from experiments done in triplicate, where error bars represent standard error.

Together these results suggest that curcumin based ECT specifically produces ROS in TNBC cells, leading to excessive oxidative stress to trigger apoptosis, utilizing the crosstalk among metabolism, calcium, and ROS signaling pathways (Gorlach, Bertram, Hudecova, & Krizanova,

2015). The ROS are continuously produced during the cell metabolism and mainly during the OXPHOS in mitochondria (Kumari, Badana, G, G, & Malla, 2018). Upon EP+Cur treatment, the VDAC1 and VDAC2 upregulation could enhance the calcium transport to mitochondria. Such calcium transport could stimulate the OXPHOS to produce ROS, which in turn (ROS) could lead to increased calcium release from endoplasmic reticulum by targeting endoplasmic reticulum-calcium channels to facilitate a positive feedback loop. "This positive feedback loop caused a ROS and calcium load in the cells and opened the mitochondrial permeability transition pore, resulting in the release of pro-apoptotic factors to trigger the apoptosis (Gorlach et al., 2015)" (Mittal, Aryal, et al., 2020).

"Further to validate the glycolytic inhibition observed in the proteomics study, we evaluated the uptake and intracellular levels of key glycolytic metabolites" (Mittal, Aryal, et al., 2020). These results for various metabolites are shown in Figure 4.16 for different treatment conditions after normalization with Ctrl (100%). The Cur treatment significantly reduced the glucose uptake to 49%, compared with Ctrl. An additional reduction in the glucose uptake level to 4% was observed for EP+Cur treatment, significantly different from Ctrl and Cur. These results suggest that while Cur downregulated the glucose uptake in MDA-MB-231 cells, enhanced suppressive effects on glucose uptake were observed for EP+Cur treatment. We also evaluate the intracellular lactate levels for different treatment, as Similar results were also obtained for intracellular lactate levels shown in Figure 4.16(b). The intracellular lactate levels were lowest to 15% for EP+Cur treatment, significantly different from Cur (74%) and Ctrl. The lactate levels were not significantly different for Cur from Ctrl. Similar results were also obtained for intracellular glutamine and glutamate levels shown in Figure 4.16(c-d). The reduction in glutamine (74%) and glutamate (68%) levels upon Cur treatment was not significantly different from Ctrl. On the other hand, EP+Cur treatment resulted in significantly reduced glutamine (6%) and glutamate (11%) levels compared to Ctrl and Cur. Together these results validate our proteomics results that the EP+Cur treatment suppresses glycolysis metabolism.

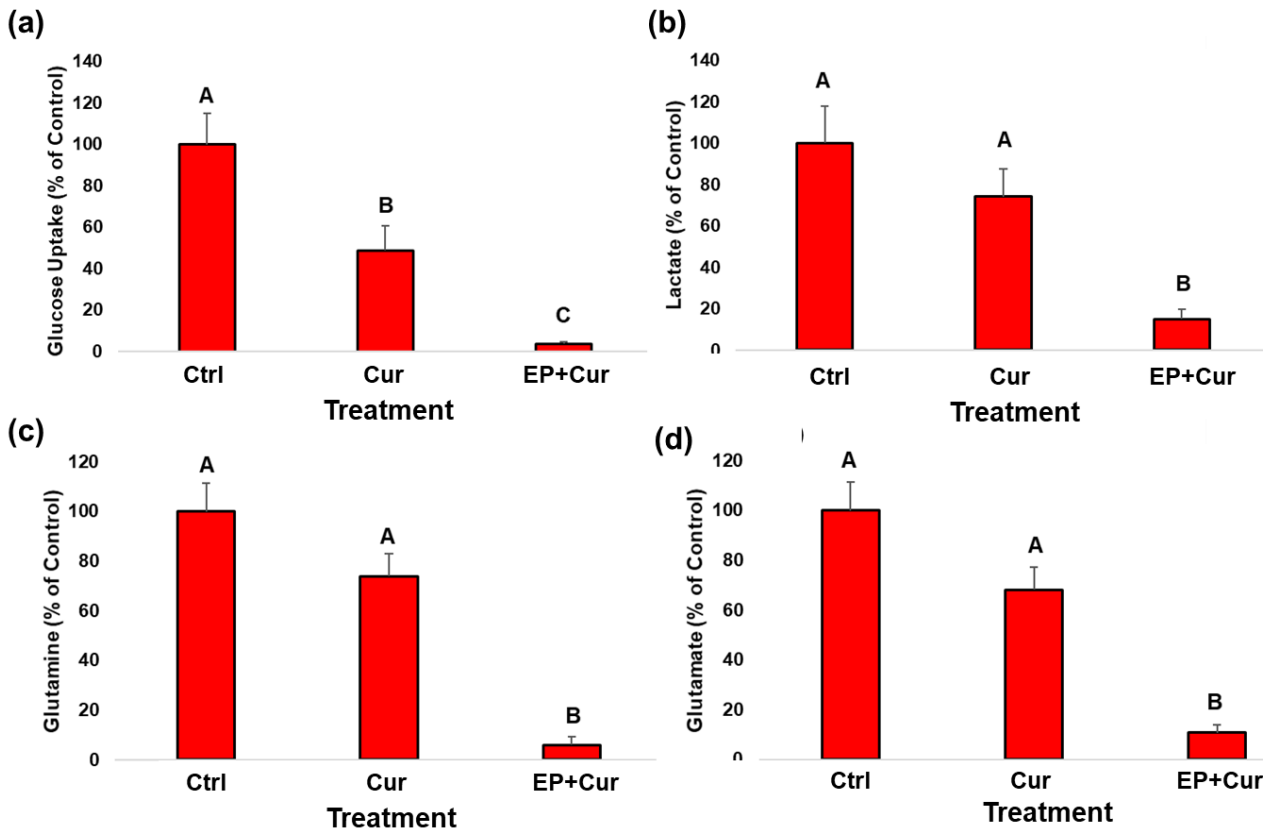

Figure 4.16: Levels of various metabolites at 12h of different treatments in MDA-MB-231 cells. (a) Glucose uptake levels. (b) Intracellular lactate levels. (c) Intracellular glutamine levels. (d) Intracellular glutamate levels. Here curcumin (Cur) concentration of 50µM and EP of 1200V/cm, 100µs, 8 pulses at 1Hz were used. Different letters reveal significant difference - $P<0.05$ from Tukey's test. The results include data from experiments done in triplicate, where error bars represent standard error.

Moreover, we performed immunoblotting to validate the downregulated expression of LDHB for EP+Cur treatment. These results are shown in Figure 4.17 for different treatment conditions, which are reported relative to Ctrl (level 1). The LDHB expression was 1.4 for Cur, which was not significantly different from Ctrl. The LDHB expression reduced to 0.16 for EP+Cur treatment, significantly different from Ctrl and Cur both. This decrease in LDHB levels agrees with our proteomics results, as well as the reduced intracellular levels of lactate for EP+Cur treatment.

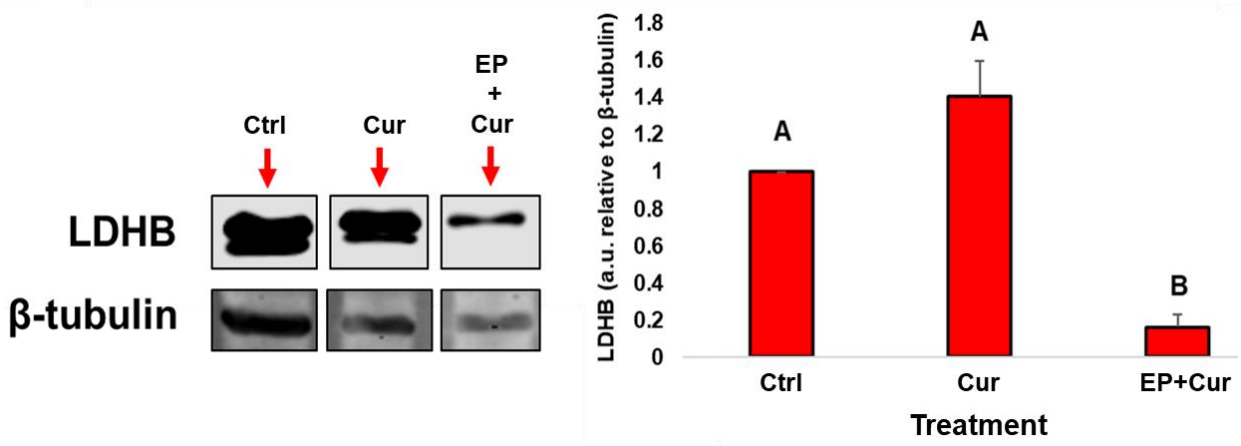

Figure 4.17: LDHB protein expression at 12h of different treatments in MDA-MB-231 cells. The left panel shows typical immunoblots of LDHB and β-tubulin (loading control). The bar graph shows the quantification of LDHB blots with respect to β-tubulin and control (control level=1). Here curcumin (Cur) concentration of 50μM and EP of 1200V/cm, 100μs, 8 pulses at 1Hz were used. The data was subjected to One-way ANOVA for significance. Different letters reveal significant difference - $P<0.05$ from Tukey's test. The results include data from experiments done in triplicate, where error bars represent standard error.

In summary, a label free quantitative proteomics analysis was performed on MDA-MB-231 treated with curcumin and curcumin with EP. The results provide preliminary indications that the EP-based curcumin therapy can exploit the metabolic vulnerabilities of TNBC cells to effectively target them. "EP+Cur comprehensively inhibited glucose metabolism and intermediate metabolite pathways (e.g. PPP) while also impacting the "reverse Warburg effect" to target MDA-MB-231 TNBC cells" (Mittal, Aryal, et al., 2020). This treatment caused a switch in the metabolism with the upregulation of TCA cycle and OXPHOS pathway proteins. This led to excessive generation of ROS to trigger mitochondria mediated apoptosis pathway utilizing the crosstalk among metabolism, calcium and ROS signaling pathways. Figure 4.18 summarizes these results.

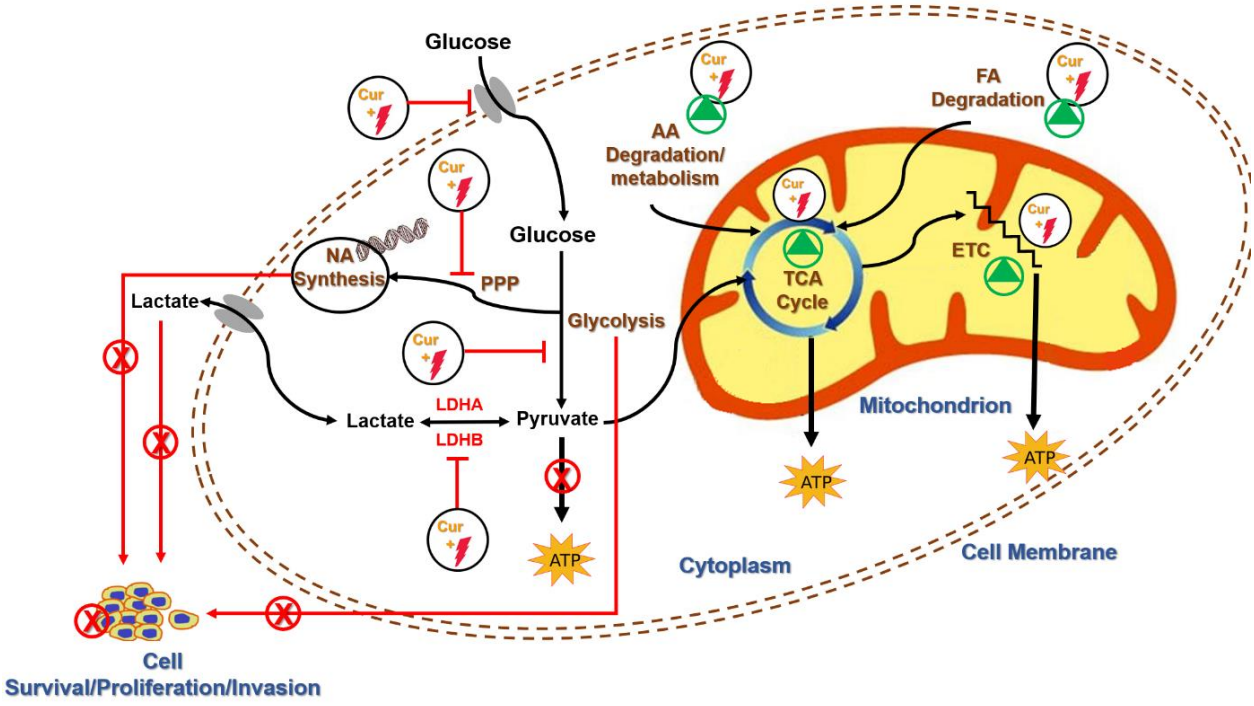

Figure 4.18: Mechanisms of the effects of EP+Cur compared to Cur in MDA-MB-231 cells at 12h of treatment.

4.1.3 Impact of ultra-microsecond (10µs) duration pulses with curcumin on TNBC cells

The research on electroporation is focused more on pulse durations in microsecond, millisecond and nanosecond ranges and there is limited data on the effects observed under the EPs of ultra-microsecond duration (10µs) (Weaver, Smith, Esser, Son, & Gowrishankar, 2012). Considering this, we studied the changes in the MDA-MB-231 cell viability treated with small curcumin dosage (10µM) and high intensity, ultra-microsecond duration electrical pulses.

Figure 4.19(a) shows the cell viability for different treatment conditions, these are: Ctrl, Cur, eight 10µs 2500V/cm pulses+curcumin (EP1+Cur), and eight 10µs 5000V/cm pulses and curcumin (EP2+Cur). "The viability of control was 94% at 0 h, and 93% at 2 h. The viability of curcumin only samples was 88% at 0 h, and 87% at 2 h. The viability was 78% and 75% at 0 h and 2 h respectively for EP1+Cur. For EP2+Cur, the cell viability reduced to 70% and 66% at 0 h and 2 h respectively. This indicates that the increase in the electric field strength from 2500V/cm to 5000V/cm resulted in 8 - 9% reduction in the cell viability. Figure 4.19(b) illustrates the variation in least square (LS) means of the viability, where each line represents a treatment type.

It could be observed that irrespective of the treatment type, only 1 - 3% reduction in the viability was observed at 2 h compared to the viability at 0 h" (Mittal et al., 2017).

A Repeated Measure ANOVA design was used, where the statistical significance was calculated using F-test, followed by multiple comparison using Tukey's test. The F-test results shown in Table 4.4 suggest that only 'Treatment' effect was significant (P<0.05), and the effects of 'Time' and interaction ('Time×Treatment') were not significant. This suggest that not many cells were killed within 2h. Additionally, line slopes for each treatment is close to zero (Figure 4.19(b)), visually confirming the non-significant difference in viabilities at 0h and 2h.

Only the significant effect 'Treatment' was exposed to the Tukey's test to compare the means of various treatment conditions. The Tukey's test results in form of letter report are shown in Figure 4.19(a). Ctrl and Cur samples were not significantly different from each other (same letter 'A'). The viabilities of EP1+Cur and EP2+Cur treatments were significantly different from each other and from Ctrl and Cur as well.

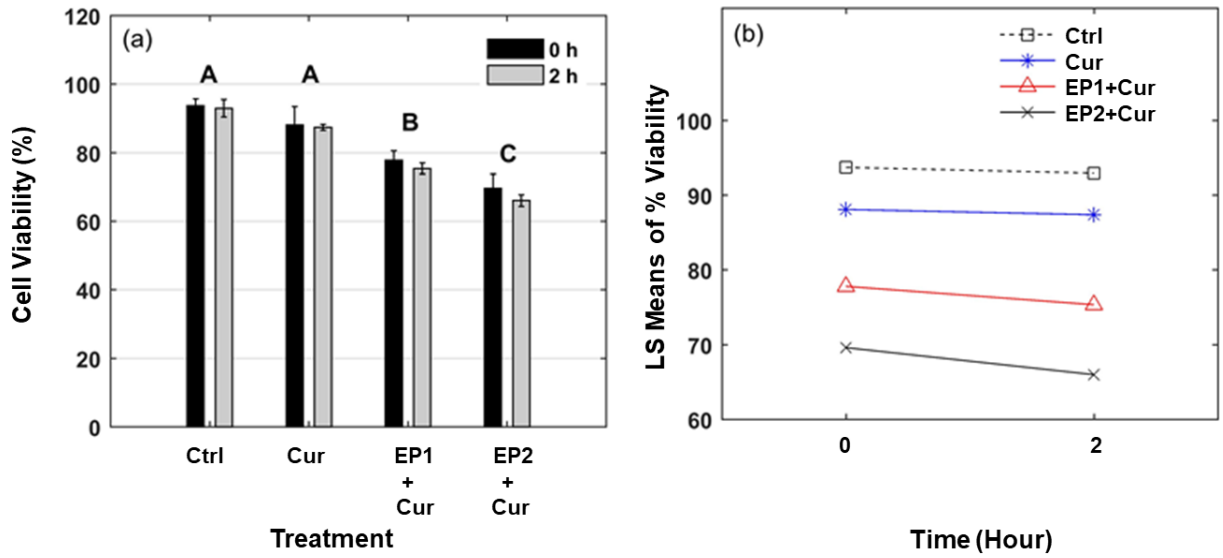

Figure 4.19: (a) MDA-MB-231 cell viability at 0 and 2h for various treatments: control (Ctrl), 10µM curcumin only (Cur), eight 10µs, 2500 V/cm pulses+curcumin (EP1+Cur), and eight 10µs, 5000 V/cm pulses+curcumin (EP2+Cur). (b) LS mean of viability with respect to time. Different letters reveal significant difference - P<0.05 from Tukey's test. The results include data from experiments done in triplicate, where error bars represent standard error.

Table 4.4: F-test results for the repeated measure ANOVA model of MDA-MB-231 cell viability at 0h and 2h for various treatments (* is P<0.05).

Source	DF Numerator	DF Denominator	F Ratio	Prob > F
Treatment	3	8	53.5143	<.0001*
Time	1	8	0.5591	0.476
Treatment×Time	3	8	0.0783	0.97

Figure 4.20 demonstrates the cell viabilities for different treatment conditions, which are normalized with Ctrl viability at 24h (100%). For Cur treatment, the cell viability was 93% at 24h, 101% at 48h, and 59% at 72h. For EP1+Cur treatment, the viability was 39%, 31%, and 22% at 24, 48 and 72h, respectively. EP1+Cur treatment reduced cell viability by 61% at 24h, while there was just 7% reduction for Cur treatment. Increased electrical field strength to 5000V/cm produced a greater cytotoxicity, as the viability was only 15% at 24h, which reduced further to 7% at 48h and 4% at 72h.

A Repeated Measure ANOVA design was used, where the statistical significance was calculated using F-test, followed by multiple comparison using Tukey's test. "Table 4.5 shows the results of F-test conducted on fixed effects, 'Treatment', 'Time', 'Treatment×Time'. It could be observed that all effects are significant (P<0.05). The interaction effect ('Treatment×Time') significance means that the simultaneous influences of 'Treatment' effect and 'Time' effects on cell viability are not additive. Thus, only interaction effect was subjected for Tukey's HSD test to obtain the letter report, and also included in Figure 4.20" (Mittal et al., 2017).

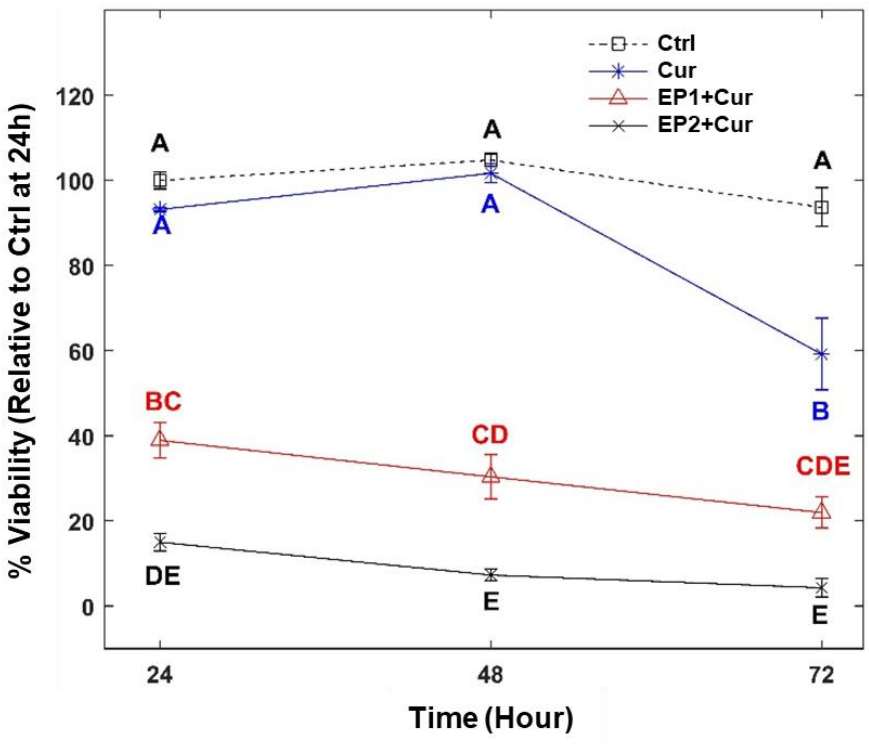

Figure 4.20: MDA-MB-231 cell viability at various time points for different treatments: control (Ctrl), 10µM curcumin only (Cur), eight 10µs, 2500 V/cm pulses+curcumin (EP1+Cur), and eight 10µs, 5000 V/cm pulses+curcumin (EP2+Cur). Different letters reveal significant difference - P<0.05 from Tukey's test. The results include data from experiments done in triplicate, where error bars represent standard error.

Table 4.5: F-test results for the repeated measure ANOVA model of MDA-MB-231 cell viability at 24, 48, and 72h for various treatments (* is P<0.05).

Source	DF Numerator	DF Denominator	F Ratio	Prob > F
Treatment	3	8	276.0768	<.0001*
Time	2	16	32.2382	<.0001*
Treatment*Time	6	16	7.8615	0.0005*

The viabilities of Ctrl sample were not significantly different from each other at 24, 48, and 72h ('A'), which is expected as no treatment was performed on these samples. The Cur sample viabilities at 24h and 48h were not significantly different from each other and from control at 24, 48, and 72h. Only at 72h, Cur treatment showed a significantly reduced viability (letter 'B')

compared to Ctrl. For EP1+Cur, the cell viability was different from Ctrl and Cur viabilities at 24 and 48 h ('A') even at 24h. The viability for EP2+Cur was significantly different from Ctrl, Cur and Ctrl viability at 24h of the treatment.

These results highlight that Cur treatment viability at 24h was only 7% less than that of Ctrl. "Huang et al., showed the changes in proliferation of MDA-MB-231 cells at 24h under 5, 10, 20, 30, 50 and 70μM curcumin (T. Huang et al., 2013) (Figure 4.21(a)). They reported a viability count of 91% with 10μM curcumin at 24h of the treatment, which was not significantly different from the control viability at 24h. This shows a very good correlation with the 93% MDA-MB-231 cell survival we obtained at 24h with 10μM curcumin in our study" (Mittal et al., 2017).

We showed that the viability for Cur treatment did not change significantly at 48h, and a significant reduction of 41% was only observed at 72h. Similar observations were also recorded by Latifah et al., where a low curcumin concentration of 3μg/mL (equivalent to 8.14μM) caused a mere 2% reduction in MDA-MB-231 cell viability at 48h, and a significant reduction to 72%. was observed only at 72h (Latifah et al., 2006). This delayed viability reduction with Cur treatment could be due to the inadequate curcumin cytotoxicity at low dosage (10μM) used in our work. A similar phenomenon at lower curcumin concentrations was also recorded in another study (Jia et al., 2014) (Figure 4.21(b)). In their study using different curcumin concentrations (2, 4, 6, 8, 10, 20, 30, and 40μM), no significant reduction in MDA-MB-231 cell viability was recorded for dosages 10μM or below at 12h and 24h. A significant viability reduction was only recorded for 20, 30, and 40μM concentrations of curcumin.

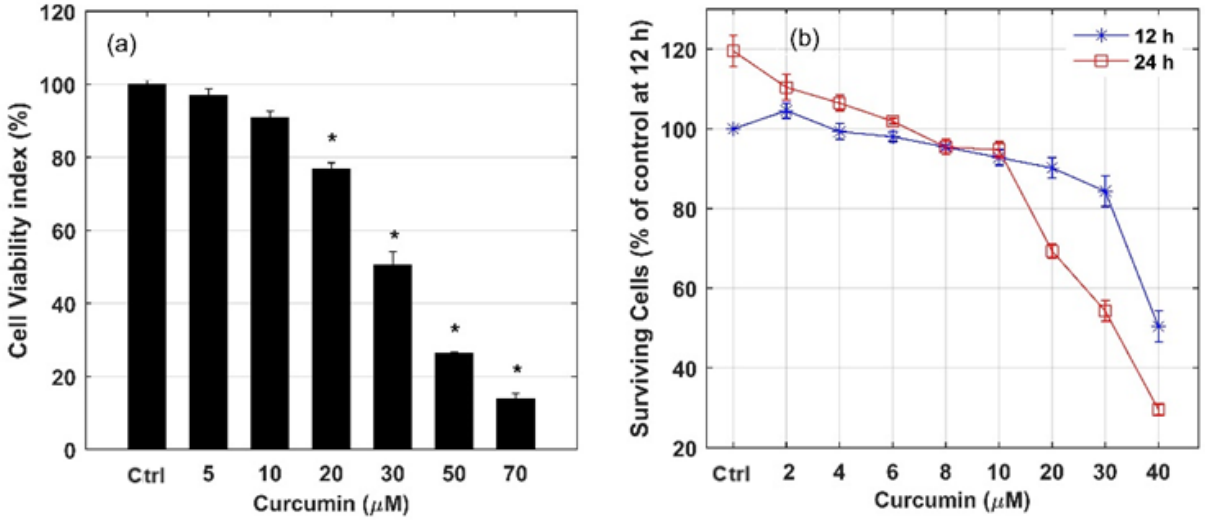

Figure 4.21: The MDA-MB-231 cell viability at different curcumin dosages from literature: (a) (T. Huang et al., 2013). (b) (Jia et al., 2014). Significant difference from Ctrl - *P < 0.05.

"In our study, for 2500V/cm treatment, the loss in cell survival was 61%, 70% and 78% at 24, 48 and 72h. For 5000V/cm, the loss in cell survival ranged from 85% at 24h to 96% at 72h, with respect to 24h control viability. For the samples treated with electrical pulse and curcumin, the changes in cell cytotoxicity were significant only after 24h of the treatment. We obtained a cell survival of 15% at 24h of treatment with 5000V/cm and 10μM curcumin. This is extremely similar to the 14% viability obtained by Huang et al., using 70μM curcumin alone (T. Huang et al., 2013). This indicates that $1/7^{th}$ of the curcumin dose could effectively target aggressive MDA-MB-231 cells, when combined with electrical pulses of 5000V/cm" (Mittal et al., 2017).

4.1.4 The impact of low intensity electrical pulses with curcumin on TNBC cells in adherent condition

Conventionally, eight 100μs duration electrical pulses of 1200V/cm electrical field intensity at 1Hz frequency are used for ECT (Marty et al., 2006; Mir et al., 1999; Sundararajan, 2008). However, recent studies show that even non-invasive, low-intensity electrical pulses (even at 60V/cm) with chemo drugs can effectively target cancer cells without severe inflammatory responses (Hsieh, Lu, Chen, Ma, & Chao, 2017). Considering this, we explored "the effect of

various combinations of non-invasive, low-voltage EPs (200V/cm) with curcumin on the viability, cell cycle and p53 expression profile of MDA-MB-231 cells, a TNBC cell line with high levels of mutant p53" (Mittal, Raman, et al., 2019). Moreover, conventionally *in vitro* ECT is performed on cells in suspension, here we applied non-invasive, low-intensity 200V/cm electrical pulses to plated/adherent MDA-MB-231 cells *in situ*, to better mimic the *in vivo* environment.

"Figure 4.22(a) shows the cell viability under various sample conditions: Ctrl, 50μM Cur, eight 100μs, 200 pulses (EP1), eight 5ms, 200V/cm pulses (EP2), EP1+curcumin (EP1+Cur), and EP2+curcumin (EP2+Cur). All viabilities were normalized with the viability of 24h or 48h Ctrl (100%), respectively. The viability for EP1 was 90% and 89% at 24h and 48h, respectively. The viability for EP2 was 54% at 24h, and 37% at 48h. The viability of the curcumin only sample was 32%, and 21% at 24h and 48h, respectively. The synergy of EPs with curcumin increased cell cytotoxicity. The EP1+Cur treatment reduced viability by 72% at 24h and 88% at 48h from respective control samples. In comparison, curcumin alone induced only a 67% and 79% decrease in the viability from Ctrl samples 24h and 48h, respectively. Increasing the pulse duration to 5ms for EP2+Cur increased the cytotoxic effect, reducing the cell viabilities to 10% and 6% at 24h and 48h, respectively. This indicates a highly nonlinear response, as could be expected in biological effects. A sustained reduction in viability was observed at 48h for all treatments (curcumin only, EP2, EP1+Cur, and EP2+Cur) with the viability decreasing between 5% and 17% from 24h to 48h" (Mittal, Raman, et al., 2019).

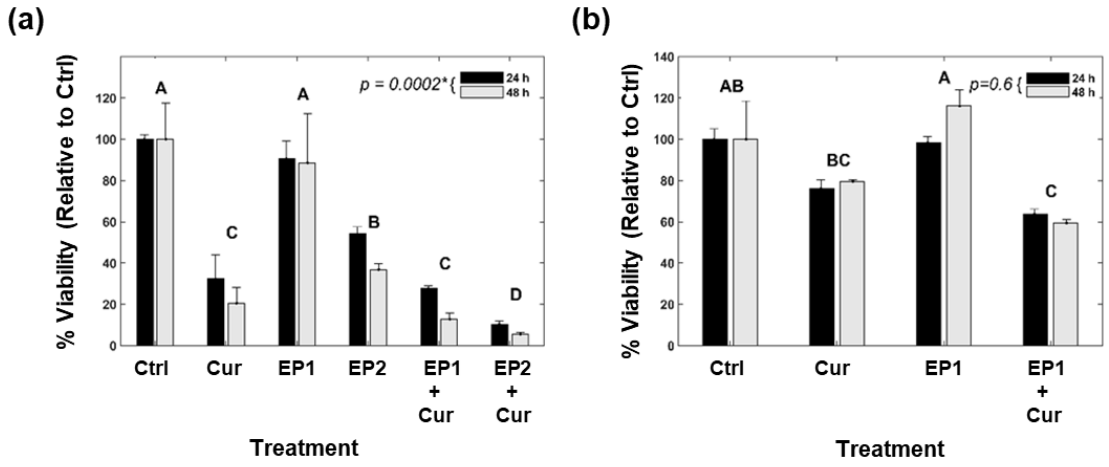

Figure 4.22: Cell viability under different electric pulse conditions for (a) MDA-MB-231 cells. (b) MCF10A cells. Ctrl samples media contained DMSO. Here EP1 and EP2 represent eight 200V/cm EPs at 100µs and 5ms, respectively and Cur represents 50µM of curcumin. The Promega Realtime MT viability assay was used to quantify the viability. Significance was derived using a Repeated Measure ANOVA analysis. Different letters reveal significant difference - P<0.05 from Tukey's test. The results include data from experiments done in triplicate, where error bars represent standard error.

A Repeated Measure ANOVA design was used, where the statistical significance was calculated using F-test, followed by multiple comparison using Tukey's test. "Table 4.6 summarizes the F-test on Fixed effects. The P-values for 'Treatment' and 'Time' were 0.0005 and 0.0002, indicating significance (P<0.05). The significance in 'Time' indicates that viabilities at 48h were significantly different from viabilities at 24h. The P-value for 'Treatment×Time' interaction was 0.0590, indicating that the 'Time' and 'Treatment' were not crossed, but additive" (Mittal, Raman, et al., 2019).

Table 4.6: F-test results for the repeated measure ANOVA model of MDA-MB-231 cell viability at 24h and 48h for various treatments (* is P<0.05).

Source	Mean Square (MS) Numerator	Degree of Freedom (DF) Numerator	F Ratio	Prob > F
Treatment	5.37	5	12.28	0.0005*
Time	1.22	1	30.85	0.0002*
Treatment×Time	0.124	5	3.13	0.0590

"The Tukey's test was conducted on the 'Treatment' effect to determine the significance among the treatment methods. Tukey's test letter report in Figure 4.22(a) indicated that EP1 did not differ significantly from the Ctrl (same letter 'A'). The curcumin only (letter 'C') was significantly different from the Ctrl, EP1 (letter 'A'), and EP2 (letter 'B'). The EP1+Cur (letter 'C') was significantly different from the Ctrl, EP1, and EP2, but not from curcumin only (same letter 'C'). The EP2+Cur (letter 'D') was significantly different from all other samples, indicating the potency of this combination in causing major cell death. This notable increase in cell death compared to the curcumin only sample indicates the enhanced cytotoxicity caused by increased curcumin uptake due to the synergy of electrical pulses and curcumin. Since EP1 and EP2 have the same electric field but much different pulse durations (100μs vs. 5ms), EP2 will induce a much higher membrane potential for a much longer period of time. Thus, EP2 will create more long-lived membrane pores that will either induce more cell death than EP1 without curcumin, or increase curcumin transport into the cell to induce more cell death than EP1 during a combined curcumin and EP treatment. Higher EP2 only viability highlights the synergistic effects produced by EP2+Cur on MDA-MB-231 viability. Viability as low as 6%, obtained with a single application of EP2+Cur indicates that combining the EP with curcumin may target compensatory survival pathways to overcome drug resistance due to heterogeneity. Therefore, one can obtain desirable cell death by appropriately selecting EP parameters for a fixed dosage.

Since *in vivo* ECT treatments will involve both healthy and cancerous cells, we also assessed the viability of a non-cancerous, epithelial cell line, MCF10A, using the same combination of EP and 50μM curcumin. Figure 4.22(b) shows MCF10A viability results and Table 4.7 shows F-test results for Repeated Measure ANOVA. The MCF10A viability was much higher than the MDA-MB-231 viability (Figure 4.22(a)). The ANOVA results indicate that the effect of 'Time' was not significant for MCF10A cell treatment. Therefore, regardless of treatment modality, the viability of MCF10A cells at 48h was not significantly different from the MCF10A viability at 24h (Time effect: $p=0.6$ in Table 4.7). The viability of MCF10A cells for curcumin only treatment was 76% at 24h, and increased to 79% at 48h. These viabilities were not statistically significantly different from the Ctrl viability, indicating that the curcumin treatment does not significantly reduce the viability of MCF10A cells even at 48h (share letter 'B'). The viability of the EP1 sample was 98% and 116% at 24h and 48h, respectively, which was not significantly different from Ctrl (share letter 'A'). The viability for the combination of eight

200V/cm EPs at 100µs with 50µm curcumin (EP1+Cur) was 64% and 59% at 24h and 48h, which was significantly different from the viability of Ctrl and EP1" (Mittal, Raman, et al., 2019).

Table 4.7: F-test results for the repeated measure ANOVA model of MCF10A cell viability at 24h and 48h for various treatments (* is P<0.05).

Source	Mean Square (MS) Numerator	Degree of Freedom (DF) Numerator	F Ratio	Prob > F
Treatment	0.37	3	14.44	0.0014*
Time	0.0045	1	0.298	0.6000
TreatmentxTime	0.016	3	1.07	0.4131

Collectively, the results in Figures 4.22(a) and 4.22(b) indicate that the "impacts observed on the viability of MDA-MB-231 cells were much larger and time sustained compared to the non-cancerous MCF10A mammary epithelial cells. This is due to the different electrical properties of cancer cells compared to normal cells, as discussed by Dr. Haltiwanger in his works (Haltiwanger, n.d.)" (Mittal, Raman, et al., 2019).

Evidence suggests that cancer may be considered an electrical phenomenon, with electrical dysregulation at molecular levels in cancer cells compared to non-cancerous cells (Haltiwanger, n.d.). In general, cancer cells display lower conductivity and membrane capacitance compared to normal cells. For example, whole cell conductivity is 2.81mS/cm in MDA-MB-231 vs. 5.58mS/cm in MCF10A cells and membrane capacitance is 1.81µF/cm^2 in MDA-MB-231 vs. 3.94µF/cm^2 in MCF10A cells. (Qiao, Duan, Chatwin, Sinclair, & Wang, 2010)

The plasma membrane houses various ion channels and transporters, which provide different permeability to different ions, including K^+, Na^+, Ca^{2+}, and Cl^-. Various ion channels (Na^+, K^+, and Cl^-) that possibly lead to the membrane potential are directly involved with the migration of cancer cells. For instance, functional voltage gated sodium channels (VGSCs) is found in various cancers (Brackenbury, 2012), where *in vivo* migration, invasion, and metastasis is augmented by the Na^+ current carried by α subunits. Various research highlight that the siRNA or inhibitor mediated suppression of VGSCs impedes migration and invasion (Fraser et al., 2005; Roger, Besson, & Le Guennec, 2003).

Modifications in the conductance of one or more of these ions can affect the membrane potential, causing depolarization or hyperpolarization. In cancer cells, the intracellular Na^+ concentration is high, and the intracellular concentration of K^+, Ca^{2+}, Mg^{2+}, and Zn^{2+} is low, resulting in more than 5-fold higher Na^+:K^+ ratios in cancer cells compared to normal cells (Nagy, Lustyik, Nagy, Zarándi, & Bertoni-Freddari, 1981), which causes the loss in cell membrane potential (Haltiwanger, n.d.; M. Yang & Brackenbury, 2013).

Cancer cells exhibit lower electrical membrane potential and electrical impedance than the normal cells (Al Ahmad, Al Natour, Mustafa, & Rizvi, 2018). For example, between -10 and -20mV in MDA-MB-231 TNBC cells compared to -80 and -90mV in gilal cells (non-neuronal cells of central nervous system) and between -60 and -70mV in fibroblast and chinese hamster ovary cells (M. Yang & Brackenbury, 2013). Moreover, membrane depolarization directly correlates with the invasiveness of the cancer cells, as revealed by the comparison of membrane potential in different breast cancer cells with varied degree of invasion potential. Among three breast cancer cells (MDA-MB-231, MDA-MB-468, and MCF-7), MDA-MB-231, the most invasive cells of three show highest depolarization with membrane potential of -10 to -20mV compared to MDA-MB-468 with membrane potential of -30mV and MCF-7 with membrane potential of -35 to -40mV (M. Yang & Brackenbury, 2013).

This reduction in membrane potential may launch the normal cells into carcinogenic state. The reduction in membrane potential alters the cellular energy production (metabolism), possibly by impairing the function of electron transport chain in the mitochondria and promoting alternate fermentation pathway (glycolysis) (Haltiwanger, n.d.). The production of lactate through glycolysis results in buildup of lactic acid in ECM to cause acidification. The tumor microenvironment pH is more acidic (6.5-6.9) with extracellular, compared to extracellular pH of normal tissue (7.2-7.5) (M. Chen et al., 2017).

The normal functioning of the electron transport chain is essential for energy production (Hüttemann, Lee, Samavati, Yu, & Doan, 2007; Redza-Dutordoir & Averill-Bates, 2016). The high energy electrons released by the electron carriers NADH and FADH2 traverse through the ETC (Hüttemann et al., 2007). The ETC houses a string of complexes that transport the electron to oxygen by functioning as electron donors and acceptors (Alberts et al., 2002). The transfer of electron between donors and acceptors releases energy. This energy is consumed to propel protons (H^+) into the mitochondrial intermembrane space, which generates a proton gradient and thus a

mitochondria membrane potential (Alberts et al., 2002). This electrochemical gradient forces the protons through ATP synthesis, harnessing the energy as ATP through the proton motive force (PMF) (Alberts et al., 2002). This function of proton pumps for ATP synthesis is suppressed in cancer cells, leading to the dysregulation in the mitochondria potential (Ribas, García-Ruiz, & Fernández-Checa, 2016). Therefore, cancer cells heavily exploit the glycolysis to survive and generate energy, while non-cancerous cells generate energy utilizing oxidation phosphorylation pathway. Moreover, the sustained elevation of sodium and loss of cell membrane potential may act as a mitotic trigger causing cancer cells to go unlimited cell division (mitosis) (Haltiwanger, n.d.). Together these modifications in electrical properties result in distinct electrical profile of cancer cells from the non-cancerous cells and provide a strong motivation that the external electrical pulse application to cancer cells may result into changes at the molecular levels.

"Figure 4.23(a) shows cell cycle patterns that represent the G0/G1, S, and G2 phases of the cell cycle for different treatments. The quantification of the cell population in different phases of the cell cycle is shown in Figure 4.23(b). Cells were synchronized in G0/G1 phase by 24h serum starvation before starting the treatment. The serum starvation treatment (SF control) lined up 78% cells in G0/G1 phase, with 11% of the cells in each of the S, and G2 phases. The DMSO treated samples (Ctrl) showed the progression of the cell cycle as the number of cells in the replication phase (S-phase) and G2 phase increased to 15% and 16% respectively, with 69% of cells in G0/G1 phase. Figure 4.23(a) shows that the distribution of cells for the Ctrl group in the G0/G1, S, and G2 phases was significantly different from the respective phases in the SF control group ($p<0.05$). The EP1 treatment had 73%, 15%, and 12% cells in G0/G1, S, and G2 phases, respectively. The EP2 treatment induced similar behavior with 72%, 17%, and 12% cells in G0/G1, S, and G2 phases, respectively. The distribution of cells in the G0/G1, S, and G2 phases for EP1 and EP2 did not differ significantly from the G0/G1, S, and G2 phase distribution for Ctrl samples. This highlights that the EP application alone does not cause cell cycle arrest" (Mittal, Raman, et al., 2019).

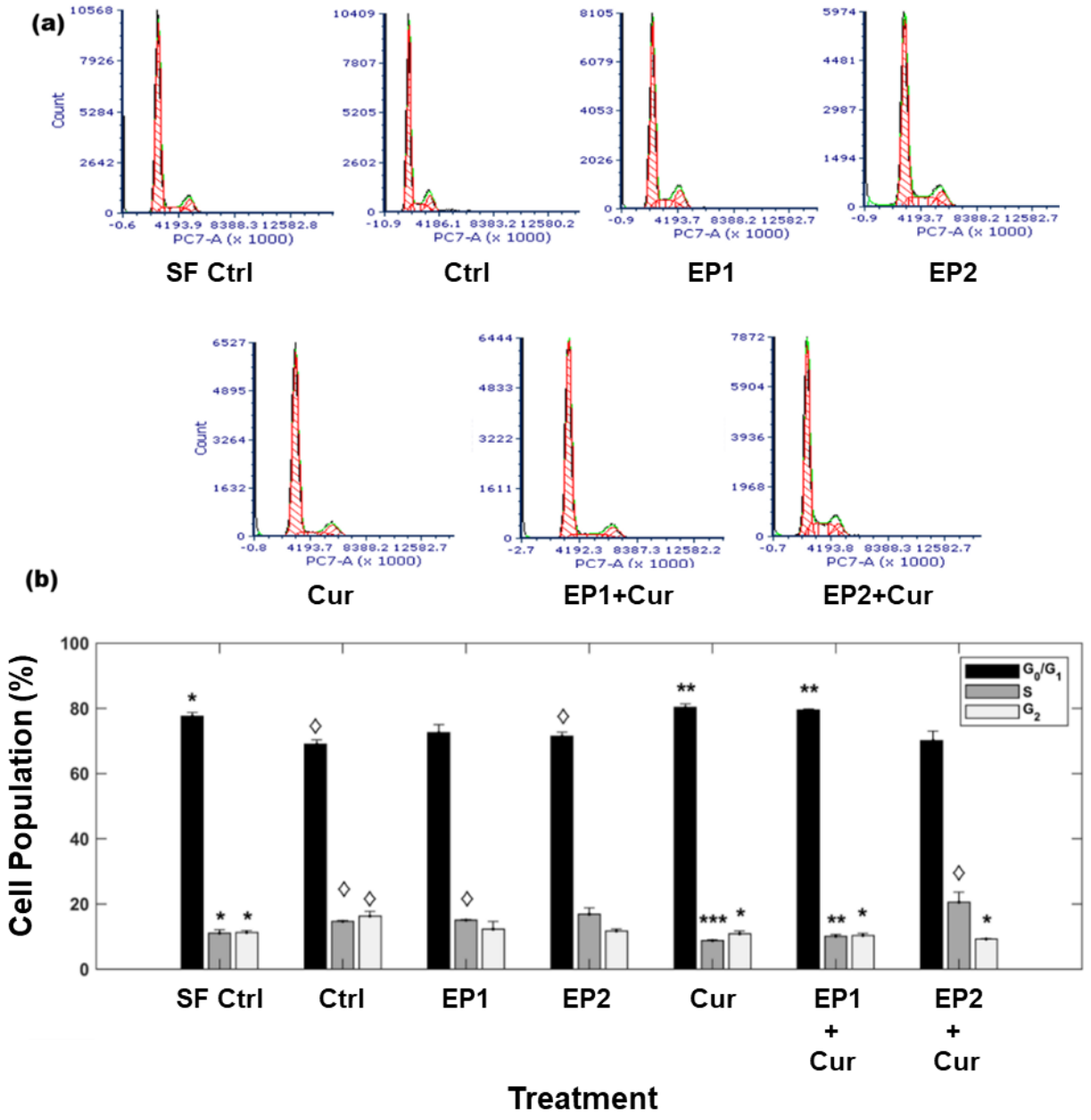

Figure 4.23: Cell cycle profile of MDA-MB-231 at 36h of different treatment conditions. (a) DNA content analysis. (b) Bar graph showing quantification of cells in various cell cycle phases. Here EP1 and EP2 represent the application of eight 200V/cm EPs at 100µs and 5ms, respectively and Cur represents 50µM of curcumin. SF Ctrl samples represents cells collected after 24h of synchronization before starting 36h of treatment. Ctrl samples media contained DMSO. Significant difference from Ctrl - *P<0.05; **P<0.005; ***P<0.0005. Significant difference from SF control -◊P<0.05. The results include data from three experiments done independently, where error bars represent standard error.

"The curcumin only treatment induced significant G0/G1 phase cell cycle arrest with 80% cells in the G0/G1 phase compared to 69% for the Ctrl ($p<0.005$). Moreover, 9% and 11% of the cells were in the S and G2 phases, respectively, which differed significantly from the S ($p<0.0005$) and G2 ($p<0.05$) phases of the Ctrl, indicating a strong shift from S phase in curcumin treatment. The combination of 100µs duration EPs with curcumin in the EP1+Cur treatment arrested 80% of the cells in the G0/G1 phase, significantly different from Ctrl ($p<0.005$). Moreover, EP1+Cur treatment reduced the percentage of cells in the S and G2 phases to 10% each, significantly different from the S ($p<0.005$) and G2 ($p<0.05$) phases in Ctrl. Further, the striking resemblance in the S and G2 phase distributions between EP1+Cur and serum-starved cells (EP1+Cur: 10.1% in S, and 10.4 in G2; SF control: 11.1% in S, and 11.3 in G2) indicates that EP1+Cur halts cell cycle progression in MDA-MB-231 cells.

Interestingly, increasing the pulse duration from 100µs to 5ms for EP2+Cur did not increase the fraction of G0/G1 phase cells. We observed that 70% of the cells were in the G0/G1 phase for the EP2+Cur treatment compared to 69% for the Ctrl, which was not significantly different. However, the fraction of cells in the G2 phase decreased significantly to 9% with an increase in the S phase to 21% compared to 16% and 15% in G2 and S ($p<0.05$) for the Ctrl, respectively. The cell population in the S phase for EP2+Cur differed significantly form the SF control. These observations indicate a strong shift away from the G2 phase for EP2+Cur samples compared to Ctrl ($p<0.05$).

The cell cycle study results highlight that though EP application on its own does not cause cell cycle arrest, different EP parameters at a given curcumin dose can perturb the cell cycle, playing a major role in differential treatment cytotoxicity. While 50µM curcumin caused significant cell cycle arrest in the G0/G1 phase, no significant cell cycle arrest occurred for EP2 only. This highlights mechanistic differences in the cell death caused by these two treatments. Previous studies have also reported G1 arrest with curcumin in MDA-MB-231/Her-2 and other breast cancer cells (H. Li et al., 2012; P. B. Patel, Thakkar, & Patel, 2015; S. H. Sun, Huang, Huang, & Lin, 2012). Similarly, EP1+Cur caused significant cell arrest in the G0/G1 phase, which resembles SF control samples, indicating that pre-synchronized cells did not progress through the cell cycle for EP1+Cur.

Unlike 50µM curcumin and EP1+Cur, the EP2+Cur sample, despite exhibiting the highest cytotoxicity in Figure 4.22(a), had no cell cycle arrest in the G0/G1 phase; however, it did exhibit

a significant reduction in G2 phase population with an increase in S phase population compared to Ctrl, which may suggest that the cells in the S phase were either slowed or arrested and not actively synthesizing DNA compared to Ctrl (A. K. Singh, Sidhu, Deepa, & Maheshwari, 1996). The variations in the cell cycle pattern observed with different EP parameters indicate that one may select appropriate EP parameters to achieve desired cell cycle effects, which could be coupled with drugs targeting a specific phase of cell cycle to synergistically target cancer cells with reduced side effects (e.g. cisplatin and bleomycin, which target DNA synthesis).

Figure 4.24(a) shows the immunoblots of p53 protein for different treatments, and Figure 4.24(b) shows the quantification of p53 expression normalized with β-tubulin and reported relative to the control. The immunoblotting revealed that when MDA-MB-231 cells were exposed to curcumin only treatment for 24h, the expression of p53 protein was significantly downregulated to 0.46, compared to 1 for Ctrl. This correlates very well with other researchers (Chiu & Su, 2009), who assessed 5 to 20μg/mL of curcumin dosage. These authors observed that treatment with 20μg/mL of curcumin (equivalent to 54.29μM) significantly reduced the expression of p53 to ~0.43, compared to 1 for control. We observed similar behavior by combining EP1 with curcumin (EP1+Cur), which significantly downregulated the p53 level to 0.58 from 1 for Ctrl, although p53 level was not significantly different from 50μM curcumin. The reduced p53 level for curcumin only and EP1+Cur treatments compared to the Ctrl correlates very well with our observed reduction in the MDA-MB-231 cell viability and cell cycle control in G0/G1 phase for curcumin only and EP1+Cur. This suggest that the 50μM curcumin and EP1+Cur treatments induce MDA-MB-231 cell death and G0/G1 cell cycle arrest through a p53 dependent mechanism, confirming that targeting mutant p53 in MDA-MB-231 cells can be an effective strategy (Okal et al., 2013; Selivanova & Wiman, 2007; Yi et al., 2013).

Interestingly, we observed a significant 2× increase in the p53 levels for the samples treated with 5ms EPs (EP2) compared to the control. Other studies have reported similar results for low-intensity EP activation of p53 expression (Fukuda et al., 2013; Lepik, Jaks, Kadaja, Värv, & Maimets, 2003). The EP2+Cur treatment also caused a significant 2.3× increase in p53 level compared to the control, while maximizing MDA-MB-231 cytotoxicity. This suggest that the effects induced by longer duration EPs (5ms) may either be p53 level independent or are in response to the reactivation of p53 (Selivanova & Wiman, 2007; Stallings, Gurley, & Rorie, 2013).

Figure 4.25 summarizes the effects of various treatments on cell viability, cell cycle, and p53 expression profile" (Mittal, Raman, et al., 2019).

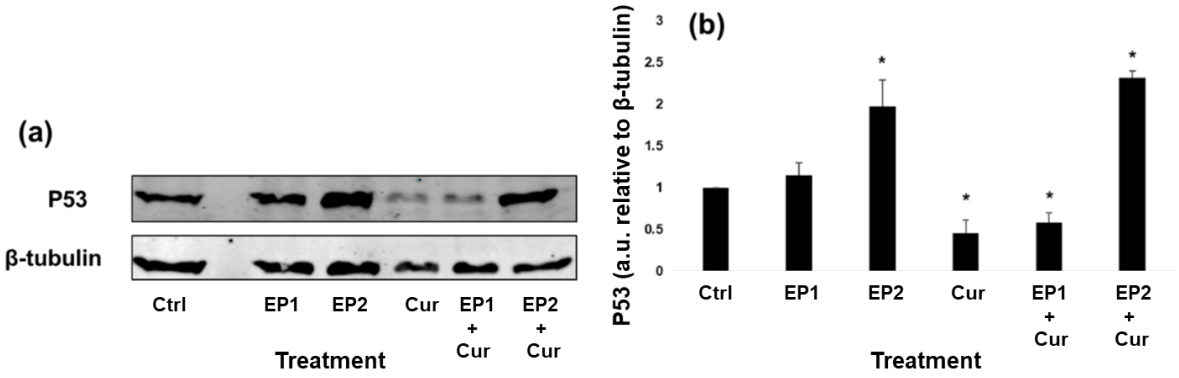

Figure 4.24: The p53 expression levels in the MDA-MB-231 cells for various treatment conditions at 24h. (a) Left panel shows a representative western blot (WB). (b) Right panel shows the quantification of p53 blots. The blots were normalized with β-tubulin and were reported relative to the Ctrl. Ctrl samples media contained DMSO. EP1 and EP2 represent eight 200V/cm EPs at 100µs and 5ms, respectively and Cur represents 50µM of curcumin. Results indicate a significant reduction in p53 expression for Cur and EP1+Cur treatments but a significant increase in P53 for EP2 and EP2+Cur treatments. Significant difference from Ctrl - *P < 0.05. The results include data from experiments done in triplicate, where error bars represent standard error.

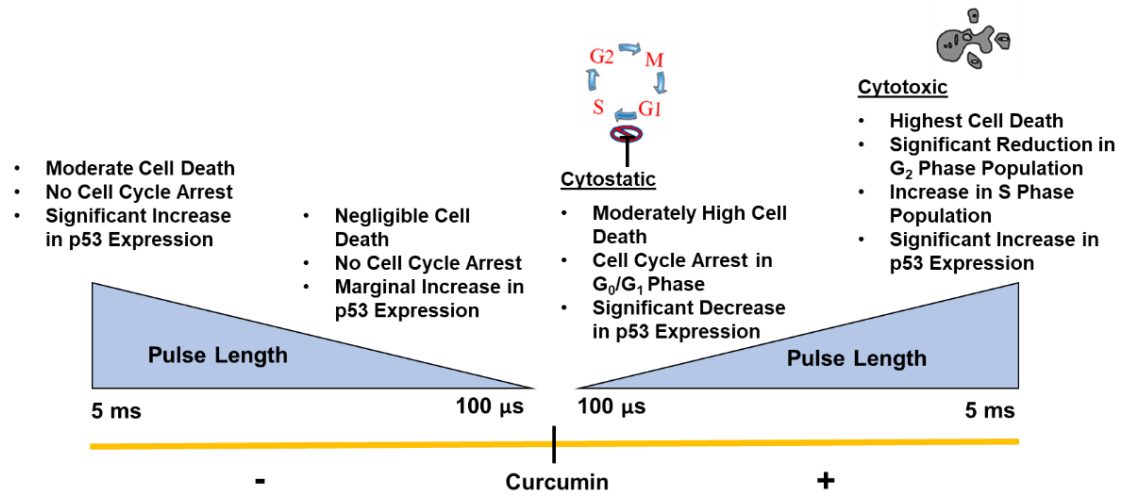

Figure 4.25: Schematic diagram summarizing the effects produced by different treatments on viability, cell cycle, and p53 profiles of MDA-MB-231 cells.

4.2 Turmeric Nanoparticles

4.2.1 Green biosynthesis and characterization of TurNP

Turmeric silver nanoparticles (TurNP) were biosynthesized by mixing dried turmeric tuber aqueous extract with 1mM silver nitrate ($AgNO_3$). Turmeric is richly loaded with proteins and various phytochemicals, including but not limited to flavonoids, phenols, alkaloids, saponin, steroids, tannins, terpenoids, and triterpenes (Oghenejobo & Bethel, 2017; S. Prasad & Aggarwal, 2011). A number of these phytochemicals present in aqueous turmeric extract reduce silver ions (Ag^+) to generate silver nanoparticles, which is evident by color change. Figure 4.26(a) shows the differences in colors of the aqueous turmeric extract and silver nitrate emulsion at days one and three. After three days of incubation in dark, the emulsion color changed from yellow to dark brown, visually confirming the synthesis of TurNP. No color change was observed in 1mM silver nitrate without aqueous turmeric extract. This change in color could be attributed to the surface-plasmon resonance (SPR) (Shameli, Ahmad, Zamanian, et al., 2012).

Figure 4.26(b) shows the characterization of the TurNP using UV-Vis spectroscopy. The absorption spectra of TurNP at day 3 was scanned between 300 to 700nm wavelength range to study the SPR of TurNP. The SPR depends upon the particle size, shape, morphology, composition and dielectric property of the nanoparticles (Kelly, Coronado, Zhao, & Schatz, 2003; Stepanov, 2004). The formation of TurNP was confirmed by observing the peak within the range of SPR for silver nanoparticles (Akther, Priya, Sah, Khan, & Hemalatha, 2019; Alsammarraie et al., 2018; Rasool & Hemalatha, 2017). The peak absorption of TurNP was obtained at 440nm (Figure 4.26(b)), which is within the SPR range of silver nanoparticles (400 to 470nm), confirming the synthesis of TurNP. This correlates well with the a priort study that also observed a prominent peak at 432nm for TurNP (Alsammarraie et al., 2018).

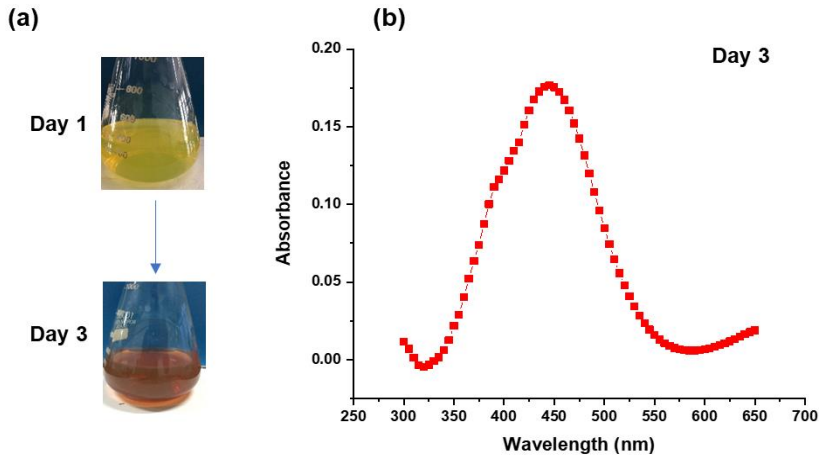

Figure 4.26: (a) Color change in turmeric extract and silver nitrate mixture at day 3 indicating the synthesis of turmeric silver nanoparticles (TurNP). (b) UV-Visible (UV-Vis) absorption spectra of TurNP showing a peak at 440nm to confirm the synthesis of TurNP.

Figure 4.27 shows the EDS characterization. The EDS results show a strong signal for silver ion with all silver peaks confirming the synthesis of TurNP. The optical absorption peak of silver was between the ranges of ~3–4keV, which is typically due to the absorbance of silver nano-crystallites and due to the SPR of silver nanoparticles (Alsammarraie et al., 2018; Kalimuthu, Suresh Babu, Venkataraman, Bilal, & Gurunathan, 2008).

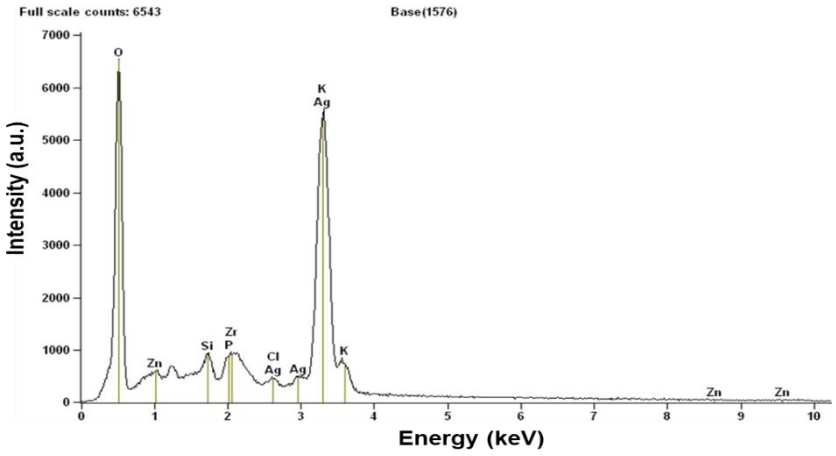

Figure 4.27: Energy-dispersive X-ray spectroscopy (EDS) characterization of turmeric silver nanoparticles (TurNP).

Figure 4.28 shows the results from zeta potential analysis to characterize the stability of the TurNP. The zeta potential provides an estimate of the surface charges on nanoparticles and elucidates the potential physical stability of nanoparticle suspensions (Joseph & Singhvi, 2019). The nanoparticles are least stable at the isoelectric point (zeta potential is zero) (Saeb, Alshammari, Al-Brahim, & Al-Rubeaan, 2014). Regardless of the polarity, higher zeta potential magnitudes indicate a greater stability due to increased electrostatic repulsion forces (Joseph & Singhvi, 2019). Generally, nanoparticles with zeta potential more than ±30mV are considered stable, as they produce sufficient repulsive force to achieve a better physical colloidal stability (Joseph & Singhvi, 2019; Kumar & Dixit, 2017). We observed that the zeta potential for TurNP was -11.9mV, which indicates an incipient instability of TurNP suspension (Figure 4.28) (Kumar & Dixit, 2017).

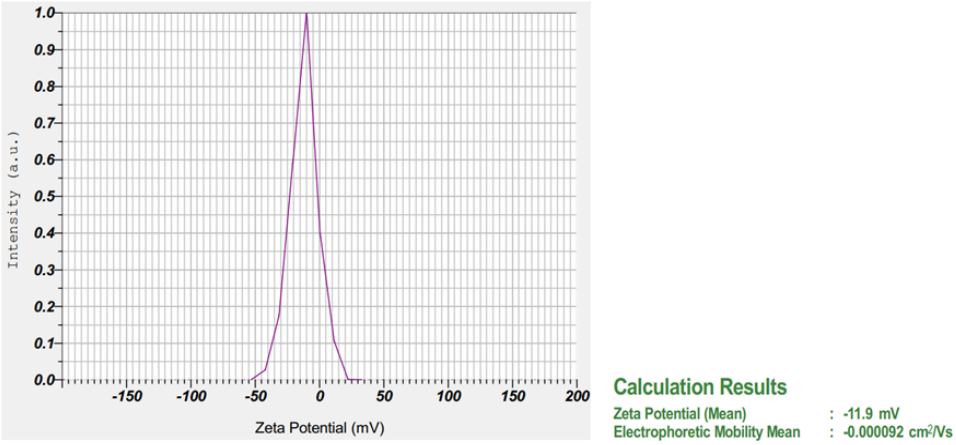

Figure 4.28: Zeta Potential of synthesized turmeric silver nanoparticles (TurNP).

We carried out a Fourier Transform Infrared spectroscopy (FTIR) to study the functional groups responsible for reducing and capping of Ag^{+} to generate TurNP. Figure 4.29 shows the representative FTIR spectrum of TurNP, which correlates well the FTIR spectrum for TurNP in literature (Shameli et al., 2014). Our spectrum shows the peaks at 3365, 2919, 2396, 1612, 1371, 1007, 824, 763, and 486cm^{-1}. Among them, the peak at 3365cm^{-1} can be assigned to hydroxyl (O-H) or amine group (-NH). However, the broadness of the 3365cm^{-1} peak indicates the presence of hydrogen bonding, which suggests a greater likelihood of the hydroxyl group. The peak at 2919cm^{-1} is due to the stretching vibrations of sp^3 hybridized C-H. The peak at 1612cm^{-1} is

assigned to the C=C stretching vibrations and amide I band of proteins (Mude et al., 2009). The 1371cm^{-1} peak is due to the S=O stretching. The peak at 1007cm^{-1} is assigned to stretching vibrations of C–O–C– or C–O groups (Huang et al., 2007; Mude et al., 2009; Shameli, Ahmad, Jaffar Al-Mulla, et al., 2012; Shameli, Ahmad, Zamanian, et al., 2012). The peak at 486cm^{-1} can be due to the silver nanoparticles banding with oxygen from hydroxyl groups of compounds in turmeric (Ag---O), as previously (Shameli, Ahmad, Zamanian, et al., 2012).

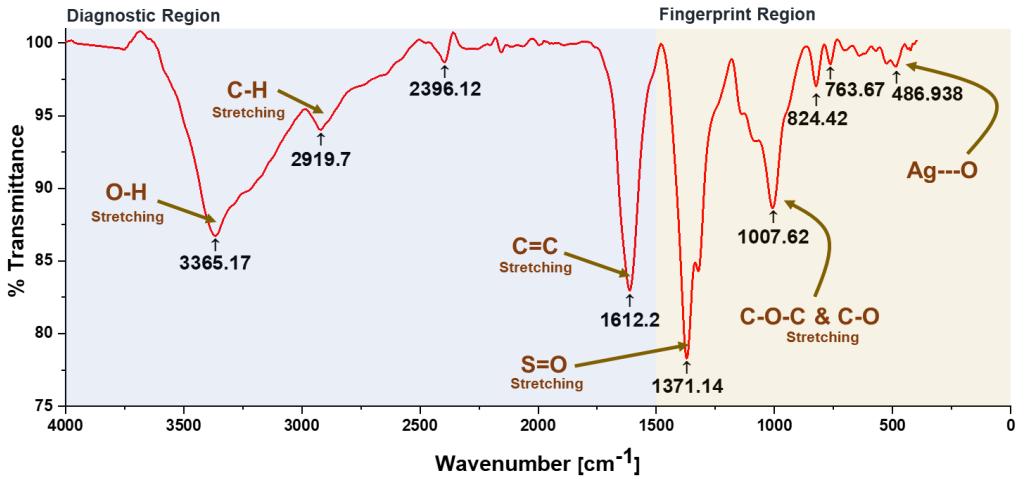

Figure 4.29: Fourier Transform Infrared spectroscopy (FTIR) characterization of turmeric silver nanoparticles (TurNP).

To detect various phytochemicals present in the TurNP, a phytochemical screening assay was performed. The phytochemical screening results shown in Figure 4.30 indicate that out of 12 compounds screened, 6 were present. We identified that the TurNP contains key phytochemicals, such as alkaloid, flavonoid, phenol, saponin, tannin, and terpenoid. Previous studies have shown that the ethanolic extract of turmeric contains all 6 of the phytochemicals we detected in this study (Oghenejobo & Bethel, 2017), while also having anthocyanin, anthraquinones, and steroids, which we did not detect in the TurNP. This indicates that the TurNP comprises various phytochemical found in its parent turmeric (Oghenejobo & Bethel, 2017; S. Prasad & Aggarwal, 2011), retaining the potential of the parent herb.

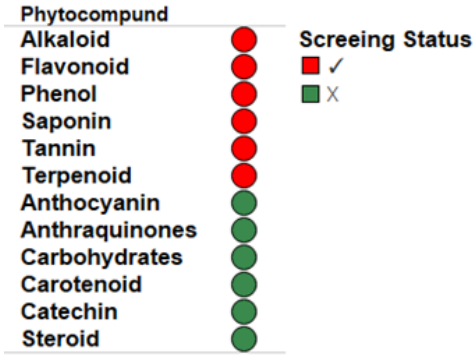

Figure 4.30: The screening status of various phytochemicals in the turmeric silver nanoparticles (TurNP).

The results from FTIR and phytochemical screening studies highlight the mechanism of TurNP biosynthesis. Figure 4.31 shows this mechanism, where phytochemicals, such as alkaloid, flavonoid, phenol, saponin, tannin and terpenoid from aqueous turmeric extract reduce Ag^+ ions to biosynthesize TurNP. During TurNP biosynthesis, the bonds and functional groups, such as O-H, C-H, C=C, S=O, C-O-C, and C-O in these phytochemicals play an important role by working as capping legends.

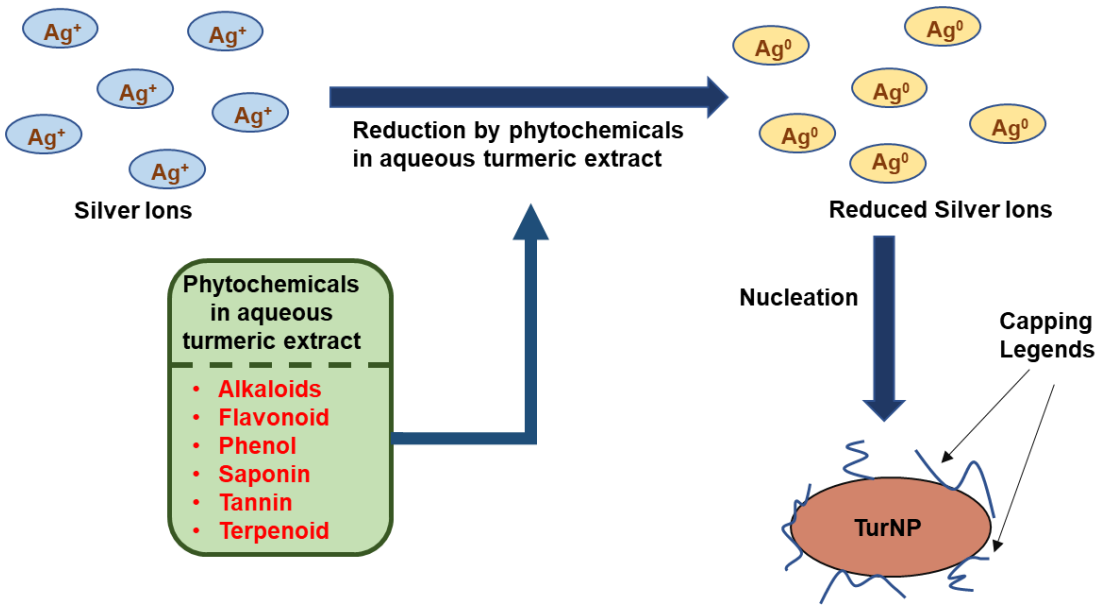

Figure 4.31: The mechanism of turmeric silver nanoparticles (TurNP) formation from aqueous turmeric extract. Idea from (J. Singh et al., 2018).

4.2.2 Antioxidant activity of TurNP

We further studied the radical scavenging ability of TurNP and screened the presence of phytocompounds to characterize their antioxidant potential. Figure 4.32 shows the variation in DPPH radical scavenging capacity for various TurNP concentrations. We observed that the DPPH radical scavenging ability was 59% for 0.1mg/mL, which increased to 77% for 0.5mg/mL. The variation in DPPH radical scavenging ability was linear with the increase in the TurNP concentration, with a high R^2 value of 0.99, demonstrating an excellent fit of the data to the linear model. The increase in the DPPH radical scavenging ability with increase in the TurNP concentration could be due to the higher presence of phenolic substances at the higher concentrations (Loganayaki, Siddhuraju, & Manian, 2013).

Collectively, these results indicate that the TurNP contain various key phytochemicals, which can scavenge free radicals. TurNP can prevent biologically important sites from oxidative damage, which can play an important role in the preventing cancers, cardiovascular diseases, and neurodegenerative diseases (Tacouri, Ramful-Baboolall, & Puchooa, 2013).

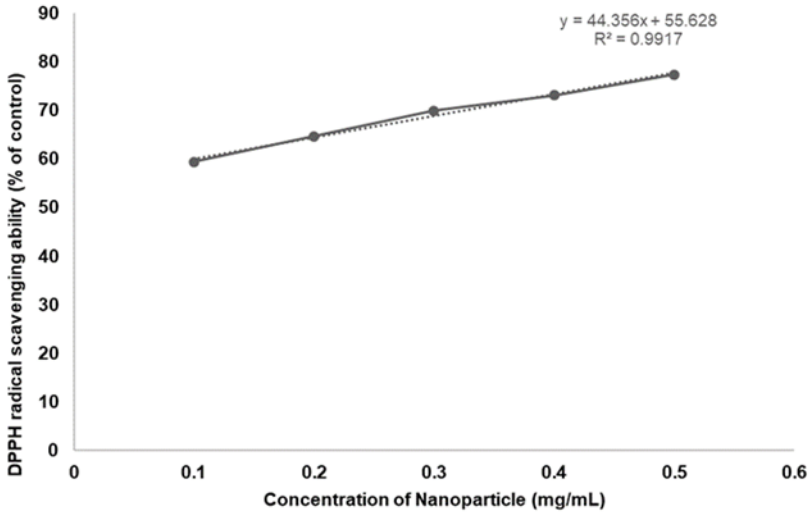

Figure 4.32: Effect of different dosage of turmeric silver nanoparticles (TurNP) on DPPH radical scavenging ability. Results are based on an experiment performed with one replicate.

4.2.3 Anticancer activity of TurNP against triple negative breast cancer

A. Cell viability and parameter optimization studies

i. TurNP dosage curve for MDA-MB-231 TNBC cells

Figure 4.33 shows the MDA-MB-231 cell viability for different TurNP dosages (5, 10, and 25µg/mL) at 12h, 24h, and 36h, which were normalized with the viabilities of Ctrl (100%). For 5µg/mL and 10µg/mL, there was no significant difference in viabilities from Ctrl at all time points, suggesting a limited impact of TurNP at lower dosages. However, at a superior dosage of 25µg/mL, the cell viabilities reduced significantly to 22%, 21% and 28% at 12h, 24h and 36h, respectively. Considering the greater cell death induced by 25µg/mL, a modest TurNP dosage of 15µg/mL was carefully chosen for the ECT studies.

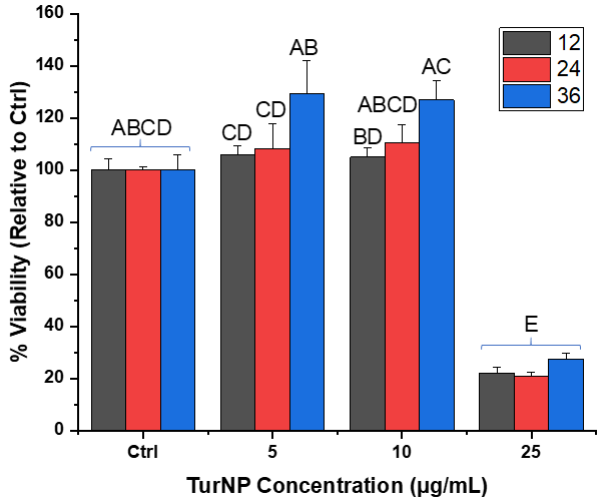

Figure 4.33: Turmeric silver nanoparticles (TurNP) dose curve for MDA-MB-231cells at 12h, 24h, and 36h. Treated MDA-MB-231 cells (20,000) were placed in fresh media with RealTime-Glo MT Cell Viability reagent. The viable cells were quantified by measuring luminescence at different time points (12h, 24h, and 36h). All viabilities were normalized with the viabilities of Ctrl. A Repeated Measure ANOVA analysis was performed to obtain significance. Different letters reveal significant difference - $P<0.05$ from Tukey's test. The results include data from experiments done in triplicate, where error bars represent standard error.

ii. Electrical pulse parameter optimization

Figure 4.34 shows the viabilities of MDA-MB-231 and MCF10A cells for EP treatment with various electrical field strengths to optimize the EP parameters. No MDA-MB-231 cell death was recorded for 600V/cm, and a relational rise in cell death was recorded, with the rise in the electric field strength beyond 600V/cm (Figure 4.34(a)). The 12h viability was 49% at 800V/cm, and 21% at 1000V/cm, which reduced significantly to as low as 9% for the 1200V/cm. These low viabilities were preserved at higher time point of 36h, as there was no significant difference in viabilities for a treatment at different time points.

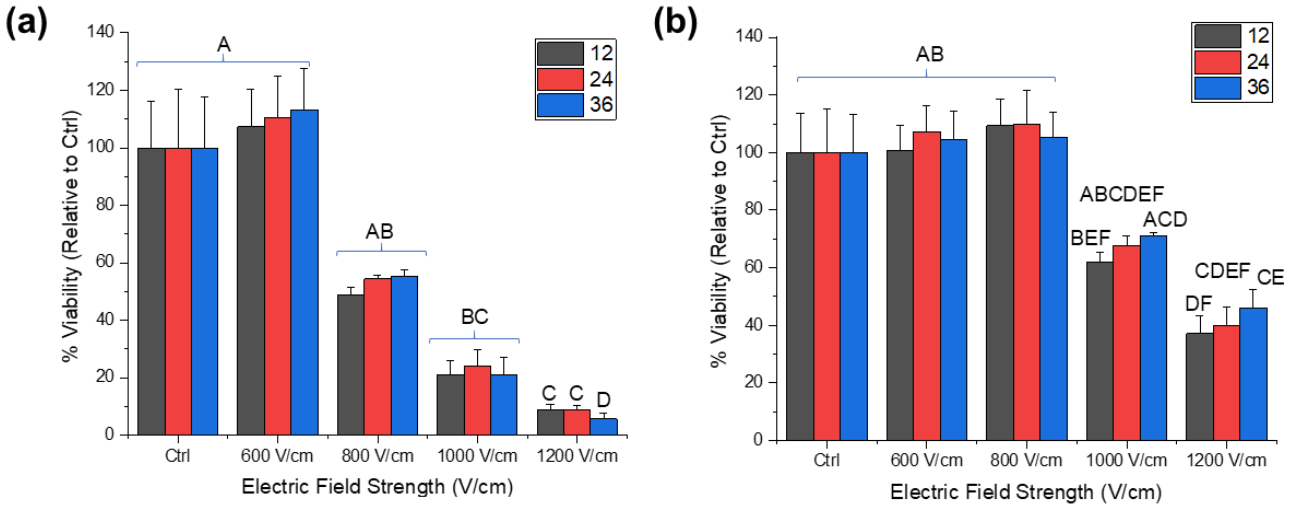

Figure 4.34: Cells viability for EP treatment with various electrical field strengths to optimize the EP parameters in different cells at 12h, 24h, and 36h: (a) MDA-MB-231 cells. (b) MCF10A cells. After treatment, the MDA-MB-231 (20,000) or MCF10A (10,000) cells were placed in fresh media with RealTime-Glo MT Cell Viability reagent. The viable cells were quantified by measuring luminescence at different time points (12h, 24h, and 36h). All viabilities were normalized with the viabilities of Ctrl. A Repeated Measure ANOVA analysis was performed to obtain significance. Different letters reveal significant difference - $P<0.05$ from Tukey's test. The results include data from experiments done in triplicate, where error bars represent standard error.

In comparison, the MCF 10A viabilities were not negatively impacted at the field strength of 600V/cm and 800V/cm, as they were close to 100% at all time points (Figure 4.34(b)). For 1000V/cm, the viability was 62% at 12h, which increased significantly to 71% at 36h from 12h.

The MCF 10A viability decreased significantly to 37% at 12h for 1200V/cm, which increased to 46% at 36h, significantly different from 12h. These results indicate that compared to MDA-MB-231 cells, the effects of EP on the loss in MCF 10A viability were weaker and short lived, as indicated by significant recovery of cell viability at 36h even for the highest field strength in this study.

Considering these results, we selected 800V/cm for the further TurNP ECT studies, as it impacted only MDA-MB-231 cells.

iii. Cell viability studies for TurNP electrochemotherapy

Figure 4.35 shows the MDA-MB-231 and MCF10A cell viabilities for TurNP (15µg/mL), EP (800V/cm), and their combination (EP+ TurNP) at 12h, 24h, and 36h. The viabilities were normalized with the Ctrl viability (100%). The TurNP treatment viability decreased significantly from Ctrl to 64% at 12h, which was 63% and 57% at 36h and 57% 72h, respectively (Figure 4.35(a)). Compared to Ctrl, EP treatment also decreased the viability significantly to 39%, while it was 38% at 36h and 35% at 72h. The viabilities at 24h and 36h for TurNP and EP treatments were significantly different from their 12h viabilities.

For EP+TurNP treatment, the viability dramatically reduced to 9% at 12h, which decreased further to 8% at 24h and 6% at 36h. The 24h and 36h viabilities for EP+TurNP were significantly different from its 12h viability. These results indicate towards the combined and sustained effect of TurNP and EP in EP+TurNP on effective MDA-MB-231 cell death.

In order to demonstrate its non-lethal effects on nearby noncancerous or healthy cells, we also studied the viability of non-tumorigenic mammary epithelial MCF 10A cells ((Figure 4.35(b)). For TurNP treatment MCF 10A viabilities were 78%, 110%, and 92% at 12h, 24h, and 36h, respectively. The MCF 10A viabilities were 97%, 111%, and 106% at 12h, 24h, and 36h, respectively For EP treatment. For EP+TurNP treatment MCF 10A viabilities was 66% at 12h and 89% at 24h, which increased significantly to 100% at 36h, indicating a rapid recovery of MCF 10A cell viability in spite of the initial insult.

These results highlight the specificity of EP+TurNP treatment towards MDA-MB-231 TNBC cells, as the damage to the MCF10A viability was weaker and short lived, and their viability was significantly higher compared to MDA-MB-231 cells.

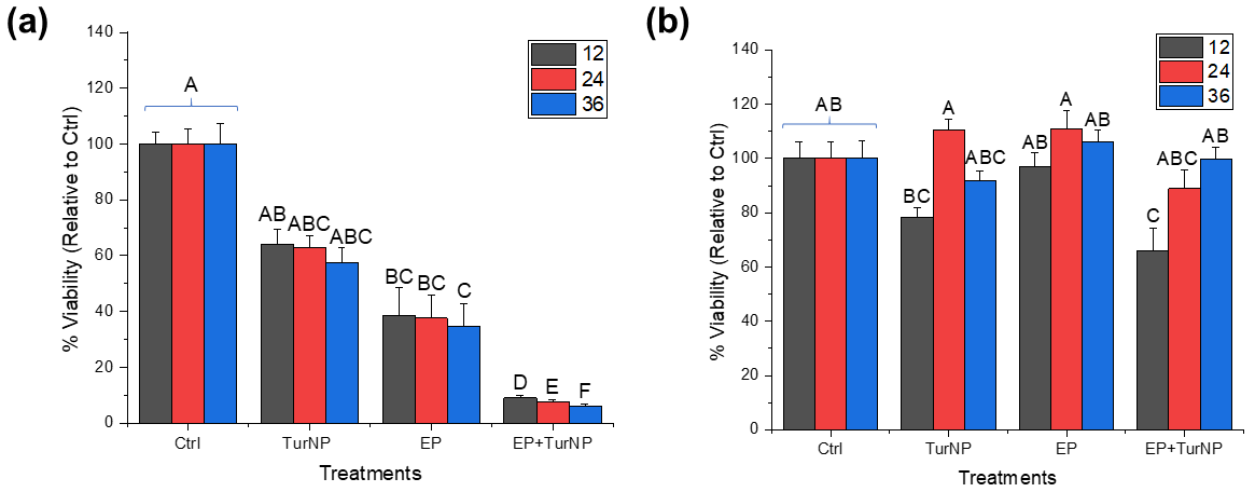

Figure 4.35: Cell viability for turmeric silver nanoparticles (TurNP) at 15µg/mL, EP (800V/cm), and their combination (EP+ TurNP) for different cells at 12h, 24h, and 36h: (a) MDA-MB-231 cells. (b) MCF10A cells. After treatment, the MDA-MB-231 (20,000) or MCF10A (10,000) cells were placed in fresh media with RealTime-Glo MT Cell Viability reagent. The viable cells were quantified by measuring luminescence at different time points (12h, 24h, and 36h). All viabilities were normalized with the viabilities of Ctrl. A Repeated Measure ANOVA analysis was performed to obtain significance. Different letters reveal significant difference - $P<0.05$ from Tukey's test. The results include data from experiments done in triplicate, where error bars represent standard error.

B. Outline of proteomics studies and LC-MS/MS reproducibility

We sought to elucidate the mechanisms of cell death upon EP+TurNP treatment utilizing the quantitative proteomics approach. A label free quantitative proteomics study was performed, as explained in detail in Chapter 3. Proteins with non-zero intensity in at least two of the three biological replicates at 1% false discovery rate and with ≥2 spectral (MS/MS) counts were selected from the raw data for the analysis, leading to a clear detection of 2426 proteins/protein families from 31823 peptides. The relative abundance of a protein in each sample was compared using LFQ values.

The LFQ intensity should be consistent across replicates for the accurate measurement of protein abundance. Considering this, we visualized the log2 LFQ intensities of all replicates for each treatment using a boxplot, as shown in Figure 4.36. These results indicate a consistency in

the LC-MS/MS measurements due to the similarity in the median and interquartile range for triplicates within each treatment.

To further establish the accuracy of the experiments, correlations of LFQ intensities of proteins for replicates across all treatments were quantified, as shown in Figure 4.37. We obtained high coefficient of determination ($R^2 \geq 0.95$), indicating high correlation among replicates within each treatment, while it was lower between replicates from different treatments.

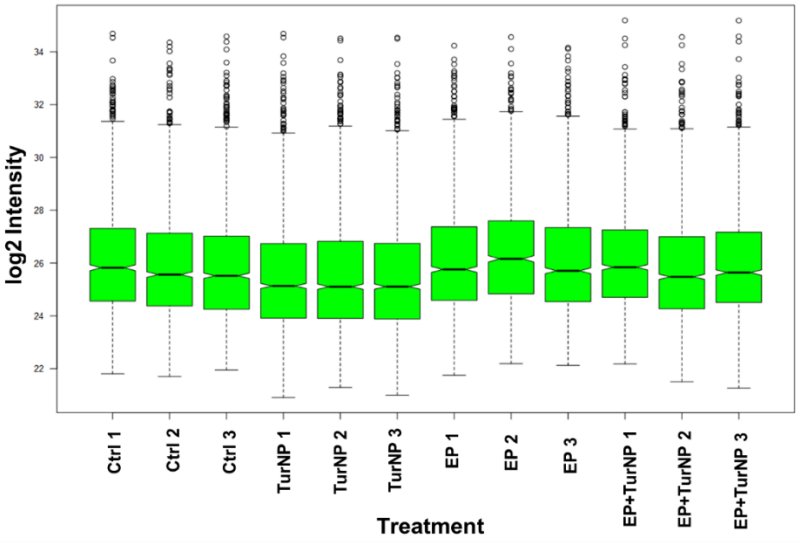

Figure 4.36: Boxplot of LFQ intensity of three biological replicates of each treatment in MDA-MB-231 cells at 12h. Here turmeric silver nanoparticles (TurNP) concentration of 15µg/mL and EP of 800V/cm, 100µs, 8 pulses at 1Hz were used. The LFQ intensities were log2 transformed to generate the boxplot in InfernoRDN tool.

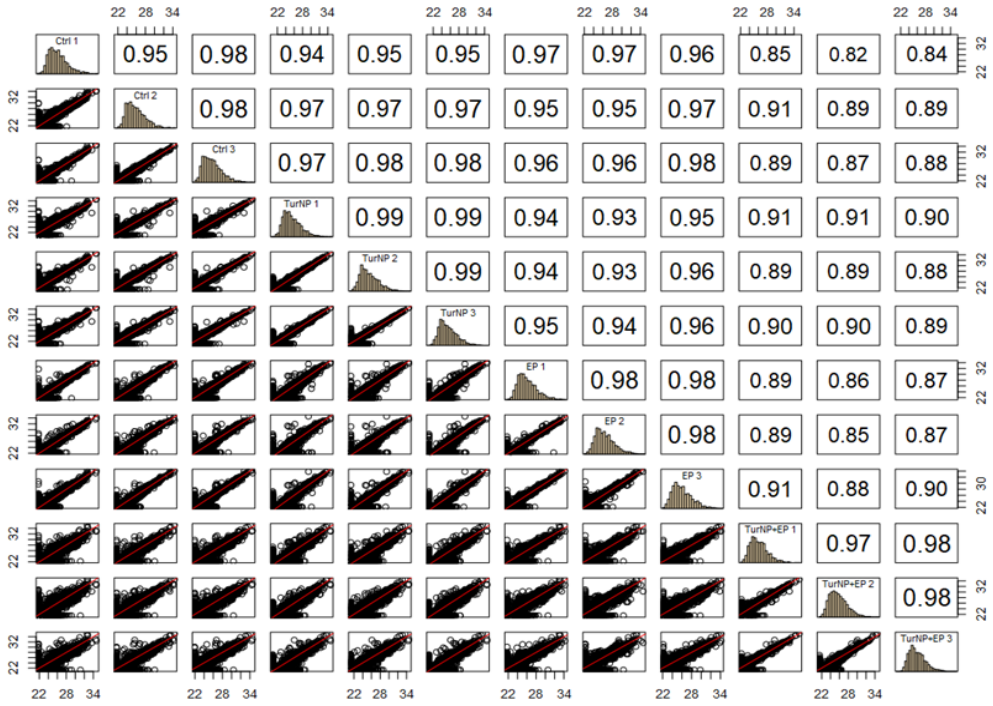

Figure 4.37: Correlation plots of LFQ intensities of proteins for replicates across all treatments in MDA-MB-231 cells at 12h. Here turmeric silver nanoparticles (TurNP) concentration of 15µg/mL and EP of 800V/cm, 100µs, 8 pulses at 1Hz were used. The LFQ intensities were log2 transformed to generate the correlation plots in InfernoRDN tool. The R^2 value is consistently higher for replicates within each treatment.

C. Distribution of proteins in different treatment groups

From total 2426 proteins, the number of proteins in each treatment were classified using LFQ intensity and MS/MS counts (LFQ $\neq 0$ and MS/MS ≥ 2) in ≥ 2 replicates, as shown in Figure 4.38(a) as Venn diagram classification. There were 1698 proteins in Ctrl (69.9% of total 2426), 2200 in TurNP (90.7%), 1485 in EP (61.2%), and 1707 in EP+TurNP (70.4%). Among these, 1196 proteins (49.3%) were common in all four groups. There were 34, 335, 27, and 118 unique proteins in Ctrl, TurNP, EP, and EP+TurNP, respectively. "The highest number of total and unique proteins were found in TurNP. The reduction or loss in both the total and unique number of proteins in the case of EP+TurNP compared to TurNP suggests a substantial impact of EP+TurNP on cellular pathways" (Mittal, Camarillo, et al., 2020).

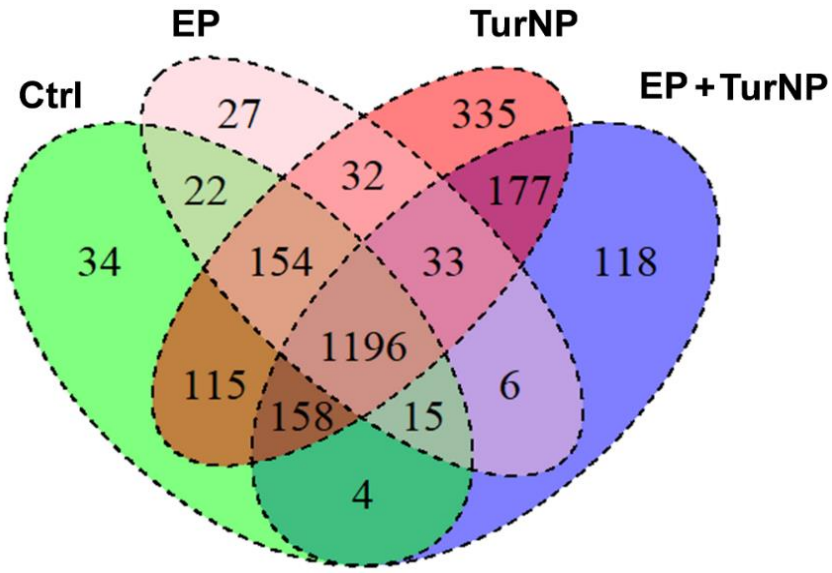

Figure 4.38: Classification of total 2426 proteins in MDA-MB-231 cells at 12h to various treatments. Here turmeric silver nanoparticles (TurNP) concentration of 15µg/mL and EP of 800V/cm, 100µs, 8 pulses at 1Hz were used. A protein was counted in a treatment only when LFQ $\neq 0$ and MS/MS ≥ 2 for ≥ 2 replicates of the treatment.

D. Overview of differentially regulated proteins

The differentially regulated proteins were identified by comparing the LFQ expression values of the proteins commonly and uniquely expressed in various pairwise comparisons ("TurNP vs. Ctrl, EP vs. Ctrl, EP vs. TurNP, EP+TurNP vs Ctrl, EP+TurNP vs. EP, and EP+TurNP vs. TurNP") among four treatment groups. For example, in TurNP vs. Ctrl comparison total 2275 proteins were compared. When the log2 fold-change (Δlog2) for a protein was greater than 0.5 (|Δlog2|>0.5), it was considered to be differently regulated. Figure 4.39 shows these results. The number of upregulated proteins were 269 for TurNP, 44 for EP, 359 for EP+TurNP compared with Ctrl. The number of downregulated proteins were 39 for TurNP, 49 for EP, 380 for EP+TurNP compared with Ctrl. For EP+TurNP, there were 408 upregulated proteins and 564 downregulated proteins compared with TurNP. Compared with EP, EP+TurNP showed 416 upregulated and 346 downregulated proteins. These results suggest that while TurNP and EP treatments regulate proteins, major changes in the proteome are observed upon EP+TurNP treatment.

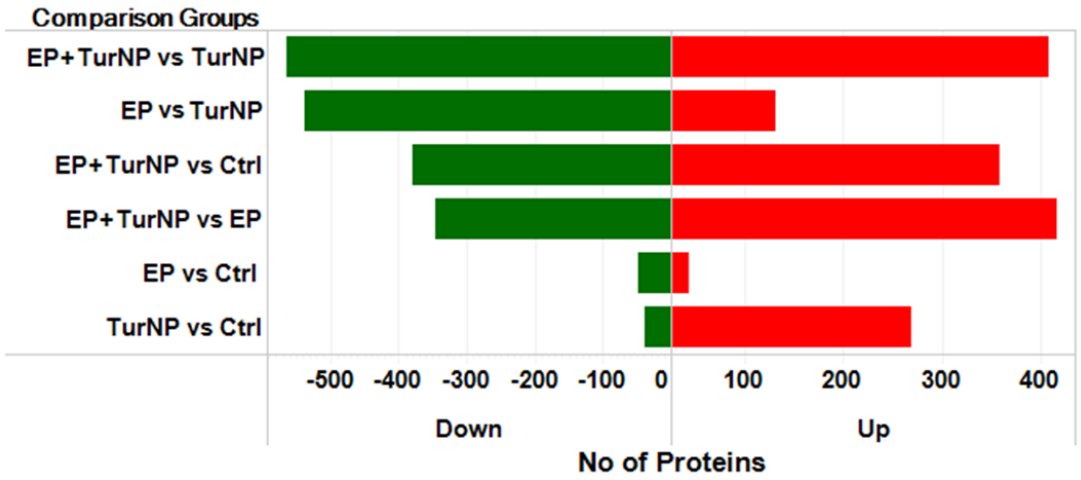

Figure 4.39: The number of significantly up- and downregulated proteins in various pairwise comparisons in MDA-MB-231 cells after 12h of different treatments. Here turmeric silver nanoparticles (TurNP) concentration of 15µg/mL and EP of 800V/cm, 100µs, 8 pulses at 1Hz were used. For a comparison, common and unique proteins in both comparison groups were considered for statistical analysis and to identify significantly up/downregulated proteins (Example- 2275 proteins were utilized for TurNP vs. Ctrl).

A heatmap visualizing the expressions of the differentially regulated proteins and their clustering is shown in Figure 4.40. The heatmap indicates a consistent protein expression pattern, and columns representing triplicates within treatments are clustered together. Between treatments, columns for Ctrl, TurNP, and EP treatments are clustered in proximity to each other, and form a distinct cluster from EP+TurNP, suggesting a major change in proteomics profile for EP+TurNP treatment.

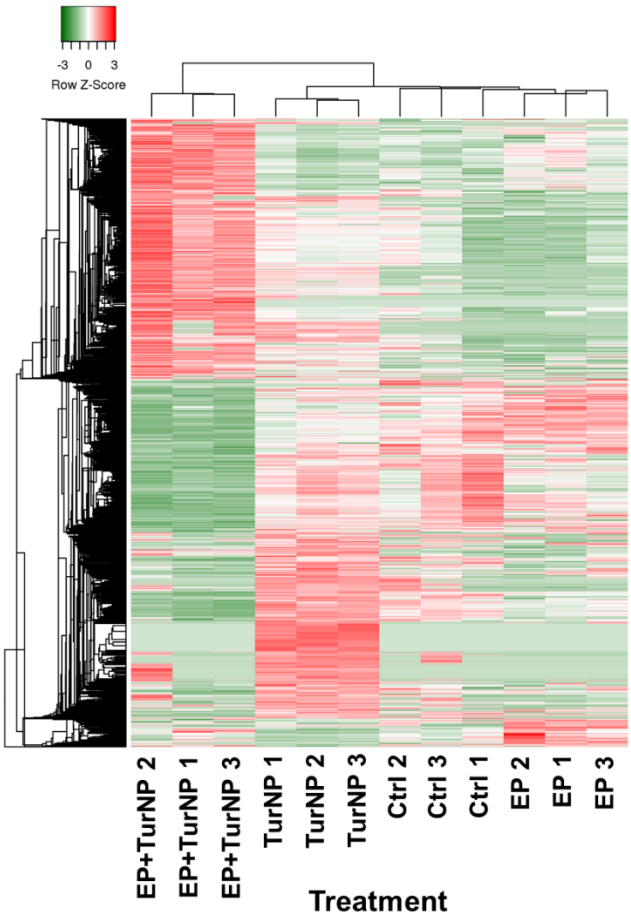

Figure 4.40: A heatmap visualizing the LFQ expressions of the significant differentially expressed proteins and their clustering for various treatments in MDA-MB-231 cells at 12h. Here turmeric silver nanoparticles (TurNP) concentration of 15µg/mL and EP of 800V/cm, 100µs, 8 pulses at 1Hz were used. The Centroid Linkage method and Kendall's Tau distance measurement method were used to cluster proteins in rows and columns. Here red color shows upregulated proteins and green color shows downregulated proteins. This visualization was created using Heatmapper (Babicki et al., 2016).

"Figures 4.41(a-f) show the top 20 significantly upregulated and downregulated proteins and their expression (log2 fold change) levels for 6 pairwise comparisons. The cDNA FLJ60818, a protein highly similar to complement C3 (Uniprot: B4DR57) was the most upregulated protein in TurNP vs. Ctrl with a fold change of 7.77 ($P=2.8\times10^{-7}$)" (Mittal, Camarillo, et al., 2020). The cDNA FLJ60818 was the most upregulated in EP+TurNP vs. Ctrl and EP+TurNP vs. EP with a 9.9-fold change in both ($P=1.3\times10^{-7}$). The cDNA FLJ60818 protein is an uncharacterized protein and resembles complement C3, an immune system protein involved in inflammation development (Nadar & Lip, 2007). "The antithrombin-III (SERPINC1) was the most upregulated in EP vs. Ctrl

with a fold change of 6.18 ($P=6.5\times10^{-06}$), and in EP+TurNP vs. TurNP with a fold change of 6.66 ($P=4.5\times10^{-05}$). The ATP synthase subunit delta, mitochondrial (ATP5D) was the most upregulated protein in EP vs. TurNP with a fold change of 7.38 ($P=6.1\times10^{-7}$)" (Mittal, Camarillo, et al., 2020).

"The 60S ribosomal protein L35 (RPL35) was the most downregulated protein in TurNP vs Ctrl with a fold change of 7.27 ($P=6.7\times10^{-5}$), histone H2A (HIST1H2AB) was the most downregulated protein in EP vs Ctrl with a fold change of 5.75 ($P=8.0\times10^{-4}$), and histone H3.1 (HIST1H3A) was the most downregulated protein with a fold change of 7.86 ($P=1.1\times10^{-2}$) in TurNP vs EP. The thymosin beta-4 (TMSB4X) was the most downregulated protein in EP+TurNP vs Ctrl with a fold change of 10.62 ($P=5.3\times10^{-6}$), in EP+TurNP vs EP with a fold change of 10.34 ($P=1.3\times10^{-6}$), and in EP+TurNP vs TurNP with a fold change of 8.61 ($P=1.9\times10^{-7}$)" (Mittal, Camarillo, et al., 2020).

Figure 4.41: The top-20 upregulated and downregulated proteins in MDA-MB-231 cells at 12h of different treatments with their log2 fold change expression in six pairwise comparisons: (a) TurNP vs. Ctrl, (b) EP vs. Ctrl, (c) EP vs. TurNP, (d) EP+TurNP vs. Ctrl. (e) EP+TurNP vs. EP (f) EP+TurNP vs. TurNP. Here turmeric silver nanoparticles (TurNP) concentration of 15µg/mL and EP of 800V/cm, 100µs, 8 pulses at 1Hz were used. Here Uniprot Accession number (B4DR57) is used for cDNA FLJ60818 as it remains uncharacterized and there exists no gene name.

Figure 4.41 continued

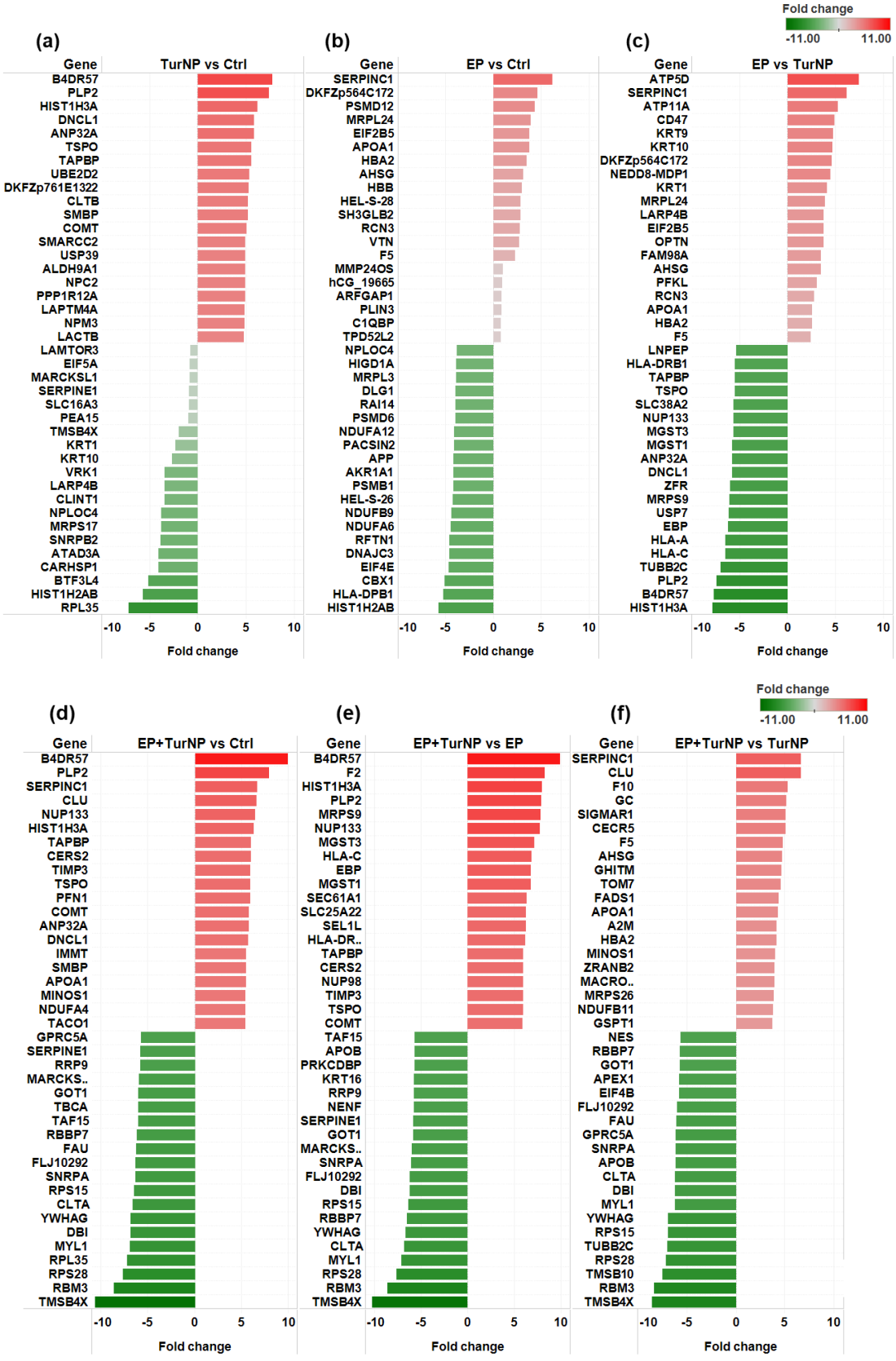

We also studied the cellular localization of the top20 significantly up- and downregulated proteins for EP+TurNP compared to TurNP, and their interaction. These results are shown in Figure 4.42. Out of top 20 upregulated proteins (Figure 4.42(a)), except GSPT1, A2M, and HBA2, 17 were localized in intracellular membrane-bound organelle, mainly in mitochondria and endoplasmic reticulum. Among these 17 proteins, 8 (CECR5, CLU, FADS1, GHITM, MINOS1, MRPS26, NDUFB11, and TOMM7) are mitochondrial, and 8 (AHSG, APOA1, CLU, FADS1, F5, F10, SERPINC1, and SIGMAR1) are part of endoplasmic reticulum. Interestingly, here CLU is shown to be localized both in mitochondria and endoplasmic reticulum. This could be attributed to the fact that the CLU is expressed in multiple isoforms, that show distinct cellular localization (Herring, Moon, Rawal, Chhibber, & Zhao, 2019). Interaction analysis results revealed an interaction among 7 proteins (A2M, AHSG, APOA1, CLU, F5, F10, and SERPINC1), which are mainly localized in endoplasmic reticulum.

On the other hand, among top 20 downregulated proteins (Figure 4.42(b)), except NES and TMSB10, 18 were localized in cytosol, nuclear lumen, intracellular organelle lumen, and ribosome. Majority of these proteins are cytosolic (12 proteins: APOB, CLTA, EIF4B, FAU, GOT1, MYL1, RBBP7, RPS15, RPS28, TMSB4X, TUBB4B, and YWHAG) and from nuclear lumen (10 proteins: APEX1, FAU, GOT1, GPRC5A, MAGOHB, RBBP7, RBM3, RPS15, RPS28, and SNRPA). The overlap in proteins localization in cytosol and nuclear lumen could be attributed to the multiple isoforms of a protein, that show distinct localization. The interaction analysis results revealed an interaction among EIF4B, FAU, RPS15, RPS28, and MAGOHB proteins.

The analysis of the top 20 upregulated and downregulated proteins indicates that compared to TurNP, the EP+TurNP treatment may enhance the activity of proteins in organelles, including mitochondria and endoplasmic reticulum, which actively participate in activating apoptosis, while mainly downregulating proteins of cytosol.

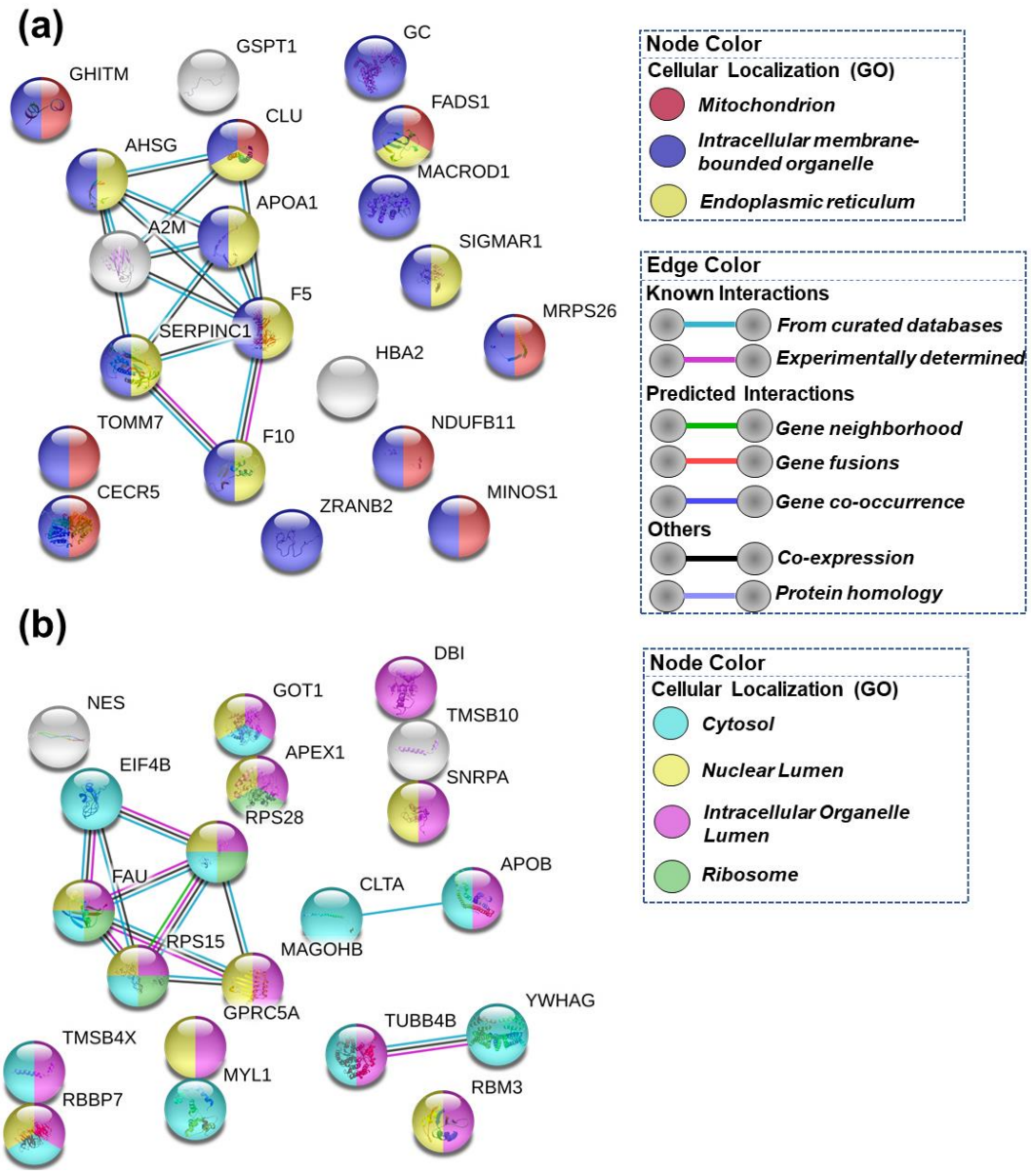

Figure 4.42: String interaction among top-20 significantly up- and downregulated proteins in MDA-MB-231 cells at 12h of treatment for EP+TurNP vs. TurNP comparison group: (a) upregulated, (b) downregulated. Here turmeric silver nanoparticles (TurNP) concentration of 15µg/mL and EP of 800V/cm, 100µs, 8 pulses at 1Hz were used. The top-20 upregulated and downregulated proteins were uploaded to STRING (Szklarczyk et al., 2017) software to study the interaction and functional enrichment using evidence as meaning of network edge. The edge color in figure legend shows active interaction sources used in analysis, where the highest confidence (0.9) setting for minimum required interaction was used. Localization is represented with node color.

E. Functional annotation enrichment analysis of differentially expressed proteins

i. GO enrichment analysis of differentially expressed proteins

"Further, we performed the GO annotation analysis on differentially expressed proteins to identify their cellular component localizations, molecular functions, and biological processes (Figures 4.43(a-c)). No GO enrichment was found for the regulated proteins in TurNP vs. Ctrl, and 3 component, 2 function, and 5 process GO enrichment terms were found for the proteins regulated in EP vs. Ctrl, indicating the low count of regulated proteins in these.

The upregulated proteins were primarily localized in mitochondrion, membrane, mitochondrial inner membrane, integral to membrane, endoplasmic reticulum, endoplasmic reticulum membrane, mitochondrial matrix, and microsome for EP+TurNP compared to TurNP (Figure 4.43(a)). Similar localization profile was also observed for proteins upregulated in EP+TurNP from Ctrl and EP. Majority of downregulated proteins in EP+TurNP vs. TurNP were primarily localized in cytoplasm, cytosol, plasma membrane, and ribonucleoprotein (RNP) complex, as also observed for EP+TurNP vs. Ctrl and EP+TurNP vs. EP. However, only downregulated proteins for EP+TurNP vs. TurNP were localized in cytoskeleton and actin cytoskeleton.

Molecular functional analysis showed higher representation of upregulated proteins related to oxidoreductase activity, catalytic activity, NAD binding, electron carrier activity, NADH dehydrogenase (Ubiquinone) activity, transferase activity, and ATPase activity for EP+TurNP (Figure 4.43(b)). Only the calcium ion binding was upregulated for EP vs. TurNP. The proteins involved in the protein binding, RNA binding, actin binding, structural molecule activity, actin filament binding, and mRNA binding were downregulated for EP+TurNP. The GO term transferase activity, transferring glycosyl groups, which is involved in catalysis of the transfer of a glycosyl group from one compound (donor) to another (acceptor) was downregulated for EP compared to TurNP.

The biological process analysis showed upregulation of proteins related to transport, transmembrane transport, carbon metabolic process, oxidation-reduction process, and respiratory electron transport chain in EP+TurNP compared to Ctrl, TurNP, and EP (Figure 4.43(c)). This correlates well with the breakdown of cell membranes due to electrical pulses. The cellular lipid

metabolic process was only upregulated for EP+TurNP compared to TurNP. The processes, such as, mRNA metabolic process, gene expression, RNA metabolic process, and cellular protein metabolic processes were downregulated for EP+TurNP compared to Ctrl and EP. The mRNA metabolic process and blood coagulation were downregulated for EP+TurNP compared to TurNP, while the translation was only downregulated for EP+TurNP from EP.

Collectively these results suggest that EP application with TurNP may upregulate the membrane proteins to facilitate the increased cellular transport process in MDA-MB-231 cells. Additionally, upregulation in organelle (mitochondrion and ER) proteins and activities, such as oxidoreductase, catalytic, NAD binding, NADH dehydrogenase (Ubiquinone), and electron carrier may activate intrinsic pathways to induce apoptotic cell death" (Mittal, Camarillo, et al., 2020).

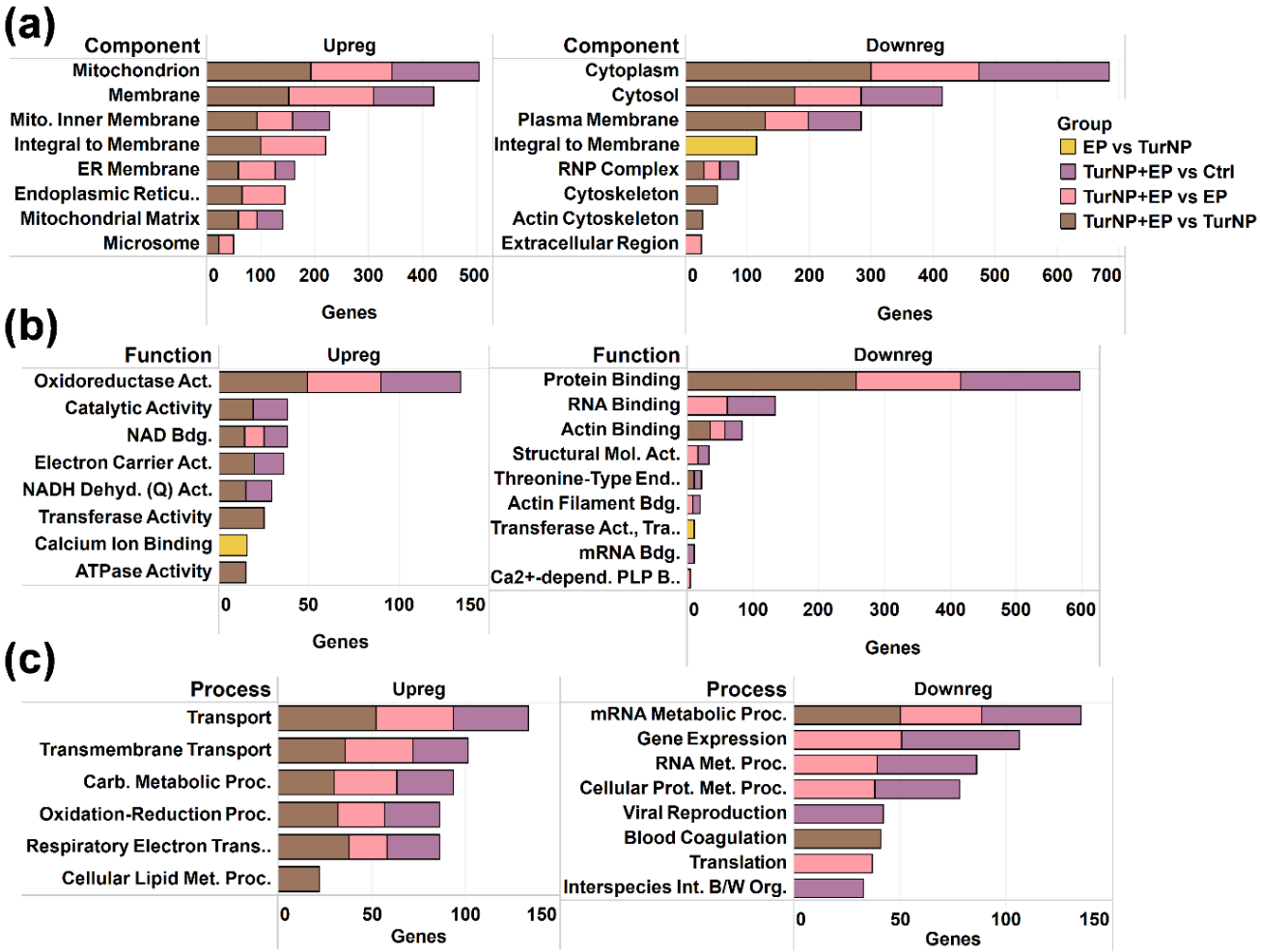

Figure 4.43: Top gene ontology enrichment terms for differently expressed proteins for different comparison groups in MDA-MB-231 cells at 12h of treatments: (a) Cellular component localization (CC), (b) Molecular function (MF), and (c) Biological process (BP). Here turmeric silver nanoparticles (TurNP) concentration of 15µg/mL and EP of 800V/cm, 100µs, 8 pulses at 1Hz were used. Proteins were uploaded to Genecodis (Carmona-Saez et al., 2007) to obtain GO term enrichment. There was no enrichment for differentially expressed proteins for TurNP vs. Ctrl. "Abbreviations: Act-Activity, Bdg-Binding, B/W-Between, Dehyd-Dehydrogenase, ER-Endoplasmic Reticulum, Int-Interaction, Met-metabolic, Org-Organisms, Proc-Process, Prot-Protein, Q-Ubiquinone, RNP-Ribonucleoprotein" (Mittal, Camarillo, et al., 2020).

ii. Pathway enrichment analysis of differentially expressed proteins

"KEGG pathway enrichment for upregulated proteins showed (Figure 4.44(a)) enrichment of OXPHOS, TCA cycle, FA degradation, FA metabolism, amino acid (valine, leucine, isoleucine, and lysin) degradation, glycolysis, peroxisome, pyruvate metabolism, and aromatic amino acid

(tryptophan) metabolism in EP+TurNP compared to Ctrl, TurNP and EP. The OXPHOS was also upregulated for EP from TurNP. The calcium signaling pathway, fatty acid elongation, biosynthesis of unsaturated FA, sulfur metabolism, and sulfur relay system were uniquely upregulated for EP +TurNP from TurNP. Also, ATP-binding cassette (ABC) transporters pathway which activates the transport of various substrates (ions, drugs, protein, peptides, lipids, sugars, and sterols) was uniquely upregulated in EP+TurNP from EP, which included the proteins ATP binding cassette subfamily B member 7(ABCB7, an iron transporter (Dolatshad et al., 2016)), ATP binding cassette subfamily D member 3 (ABCD3), transporter 1, ATP binding cassette subfamily B member(TAP1), transporter 2, ATP binding cassette subfamily B member(TAP2). The lysosome, and aminoacyl-tRNA biosynthesis pathways were upregulated only in TurNP from Ctrl.

The pathways responsible for increased cell proliferation, differentiation, migration, survival, and evasion of cell death and apoptosis were downregulated for EP +TurNP (Figure 4.44(b)). Among these pathways, the regulation of actin cytoskeleton, focal adhesion, PI3K-Akt signaling, adherens junction, Rap1 signaling, MAPK signaling, MicroRNAs in cancer, and hippo signaling pathways were downregulated for EP+TurNP compared to Ctrl, TurNP, and EP. Additionally, Ras signaling, neurotrophin signaling, tight junction, and glycolysis were downregulated in EP+TurNP only from Ctrl, and TurNP. The regulation of actin cytoskeleton, focal adhesion, adherens junction, Rap1 signaling, Ras signaling, neurotrophin signaling, and tight junction pathways were also downregulated for EP from Ctrl, however with less proteins compared to EP+TurNP, highlighting the synergistic effects of TurNP with EP. The T cell receptor signaling pathway was uniquely downregulated in EP compared to Ctrl" (Mittal, Camarillo, et al., 2020).

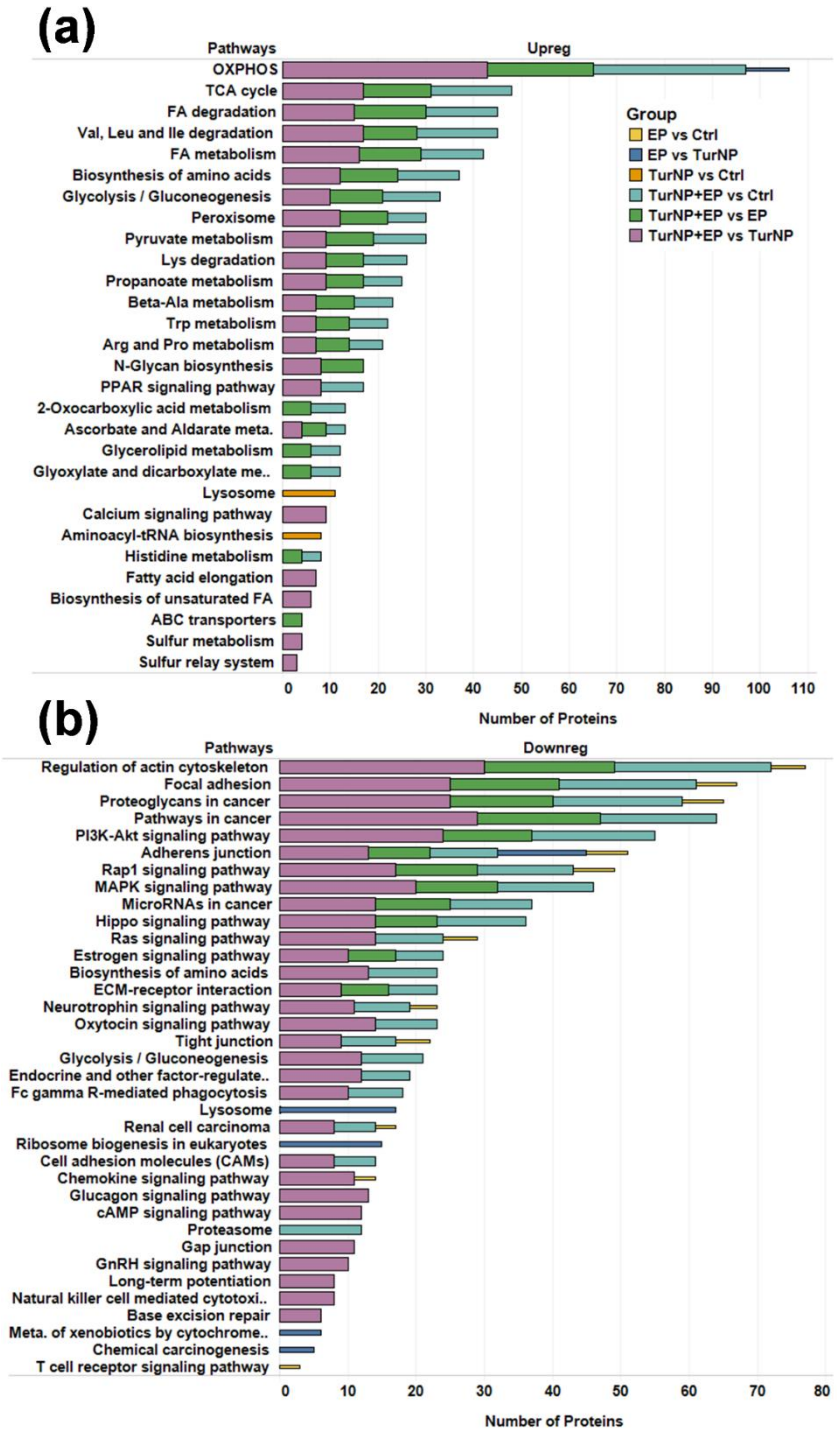

Figure 4.44: Kegg pathways for differently expressed proteins in MDA-MB-231 cells at 12h in various comparisons using DAVID 6.8 (D. W. Huang et al., 2009a, 2009b). (a) Upregulated, and (b) Downregulated. Here turmeric silver nanoparticles (TurNP) concentration of 15µg/mL and EP of 800V/cm, 100µs, 8 pulses at 1Hz were used. "Abbreviations: Ala-Alanine, Asp-Aspartate, Deg-Degradation, FA-Fatty Acid, Ile-Isoleucine, Leu-Leucine, Lys-Lysine, Trp-Tryptophan, Val-Valine" (Mittal, Camarillo, et al., 2020).

F. Impact of EP+TurNP on PI3K-Akt signaling pathway

PI3K is among the most frequently mutated pathways in TNBC (Conway et al., 2019; Pascual & Turner, 2019). The PI3K pathway mutations highlight a major additional subgroup of TNBC, which could be a therapeutic target, as indicated in phase II clinical trials (Pascual & Turner, 2019). "We next examined the downregulated proteins in PI3K-Akt signaling pathway to understand the extent of its inhibition upon EP+TurNP treatment. Table 4.8 shows the list of 25 significantly downregulated PI3K-Akt pathway proteins in at least one comparison, and their fold change (log2)" (Mittal, Camarillo, et al., 2020). A visualization showing downregulated PI3K-Akt proteins for EP+TurNP vs. TurNP mapped on the PI3K-Akt pathway is shown in Figure 4.45, where color shows their relative fold change. The most downregulated protein was GRB2 for EP+TurNP from Ctrl and TurNP. The GRB2 remains a key protein in intracellular signal transduction, which is overexpressed in breast cancers (Giubellino, Burke, & Bottaro, 2008). The GRB2 co-operates with RTKs, including EGFR to activate various oncogenic pathways, such as PI3K-Akt and Ras signaling (as shown in Figure 4.45) (Giubellino et al., 2008). The EGFR was also downregulated significantly. The EGFR is associated with poor TNBC prognosis, as it is commonly overexpressed in these tumors and heightens their aerobic glycolysis (Liao et al., 2019; Lim et al., 2016; Nakai, Hung, & Yamaguchi, 2016). Another oncogenic cell-surface RTK (Torres-Adorno et al., 2019) EPHA2, which is uniquely upregulated in TNBC was also significantly downregulated. EPHA2 inhibition weakens cell proliferation and activates apoptosis (Torres-Adorno et al., 2019). "The G family proteins GNB1 and GNB2 are implicated in cancer proliferation, survival, invasion, metastasis, survival and resistance (Y. Li et al., 2012; Zimmermannova et al., 2017)" (Mittal, Camarillo, et al., 2020).

Table 4.8: The PI3K-Akt pathway proteins which are significantly downregulated for EP+TurNP treatment in one or more comparison groups. Here turmeric silver nanoparticles (TurNP) concentration of 15µg/mL and EP of 800V/cm, 100µs, 8 pulses at 1Hz were used. The significantly regulated proteins are marked with $^{\#}$ (|fold change|≥0.5) and * (P<0.05) in a comparison.

Table 4.8 continued

S.N.	Uniprot Access. No.	Protein Name	Gene Name	EP+TurNP vs Ctrl		EP+TurNP vs EP		EP+TurNP vs TurNP	
				Fold Change	P Value	Fold Change	P Value	Fold Change	P Value
1	P29317	Ephrin type-A receptor 2	EPHA2	-0.66#	6.9×10^{-3}*	-0.48	2.5×10^{-2}*	-1.03#	1.7×10^{-3}*
2	P62879	Guanine nucleotide-binding protein G(I)/G(S)/G(T) subunit beta-2	GNB2	-1.16#	4.5×10^{-4}*	-0.83#	3.3×10^{-3}*	-1.35#	7.6×10^{-4}*
3	P00533	Epidermal growth factor receptor	EGFR	-0.67#	8.4×10^{-3}*	-0.64#	9.0×10^{-3}*	-0.95#	1.4×10^{-3}*
4	P23588	Eukaryotic translation initiation factor 4B	EIF4B	-5.43#	6.0×10^{-6}*	-5.14#	4.6×10^{-8}*	-5.83#	2.4×10^{-8}*
5	P62993	Growth factor receptor-bound protein 2	GRB2	-4.82#	2.6×10^{-7}*	-3.12#	1.2×10^{-1}	-4.72#	2.3×10^{-7}*
6	P17301	Integrin α2	ITGA2	-0.62#	1.3×10^{-2}*	-0.42	2.9×10^{-3}*	-0.97#	6.9×10^{-4}*
7	P26006	Integrin α3	ITGA3	-0.80#	2.5×10^{-3}*	-0.68#	1.1×10^{-3}*	-0.78#	1.6×10^{-3}*
8	P23229	Integrin α6	ITGA6	-0.71#	1.7×10^{-3}*	-0.91#	3.6×10^{-4}*	-0.82#	8.9×10^{-4}*
9	P05556	Integrin β1	ITGB1	-0.85#	1.8×10^{-3}*	-0.67#	1.1×10^{-4}*	-0.91#	2.1×10^{-4}*
10	P16144	Integrin β4	ITGB4	-0.53#	5.7×10^{-5}*	-0.46	6.7×10^{-3}*	-0.66#	4.8×10^{-4}*
11	P01111	GTPase NRas	NRAS	-1.11#	1.3×10^{-3}*	-0.78#	6.2×10^{-3}*	-1.28#	1.7×10^{-3}*
12	P67775	Serine/threonine-protein phosphatase 2A catalytic subunit alpha isoform	PPP2CA	-0.54#	4.1×10^{-3}*	-0.49	2.6×10^{-3}*	-0.53#	4.7×10^{-3}*
13	P07996	Thrombospondin-1	THBS1	-1.19#	2.0×10^{-4}*	-0.68#	6.3×10^{-4}*	-0.79#	3.5×10^{-4}*
14	P31946	14-3-3 protein beta/alpha	YWHAB	-1.78#	1.2×10^{-2}*	-1.51#	1.5×10^{-2}*	-1.71#	8.5×10^{-3}*
15	P62258	14-3-3 protein epsilon	YWHAE	-1.54#	4.3×10^{-4}*	-1.37#	3.2×10^{-3}*	-1.57#	7.4×10^{-4}*
16	P61981	14-3-3 protein gamma	YWHAG	-6.84#	9.1×10^{-6}*	-6.66#	1.4×10^{-5}*	-6.88#	1.6×10^{-7}*
17	P27348	14-3-3 protein theta	YWHAQ	-0.84#	4.3×10^{-2}*	-0.52#	6.8×10^{-2}	-1.07#	1.9×10^{-3}*
18	P63104	14-3-3 protein zeta/delta	YWHAZ	-1.77#	9.2×10^{-3}*	-1.55#	6.1×10^{-3}*	-1.81#	3.0×10^{-3}*
19	P11047	Laminin subunit gamma-1	LAMC1	-0.42#	4.7×10^{-3}*	-0.77#	3.7×10^{-4}*	-0.24	7.7×10^{-3}*
20	P62873	Guanine nucleotide-binding protein G(I)/G(S)/G(T) subunit beta-1	GNB1	0.01	9.5×10^{-1}	0.28	9.1×10^{-2}	-1.07#	3.2×10^{-3}*
21	P23458	Tyrosine-protein kinase JAK1	JAK1	0.00	N/A	0.00	N/A	-3.02#	3.7×10^{-7}*
22	P08648	Integrin α5	ITGA5	-0.28	2.0×10^{-2}*	-0.34	5.7×10^{-2}	-0.53#	2.2×10^{-2}*
23	P06756	Integrin αV	ITGAV	-0.04	6.0×10^{-1}	1.23#	4.0×10^{-1}	-0.64#	1.4×10^{-3}*
24	Q99650	Oncostatin-M-specific receptor subunit beta	OSMR	0.00	N/A	0.00	N/A	-3.17#	1.3×10^{-5}*
25	P54646	5-AMP-activated protein kinase catalytic subunit alpha-2	PRKAA2	0.00	N/A	0.00	N/A	-2.62#	1.1×10^{-5}*

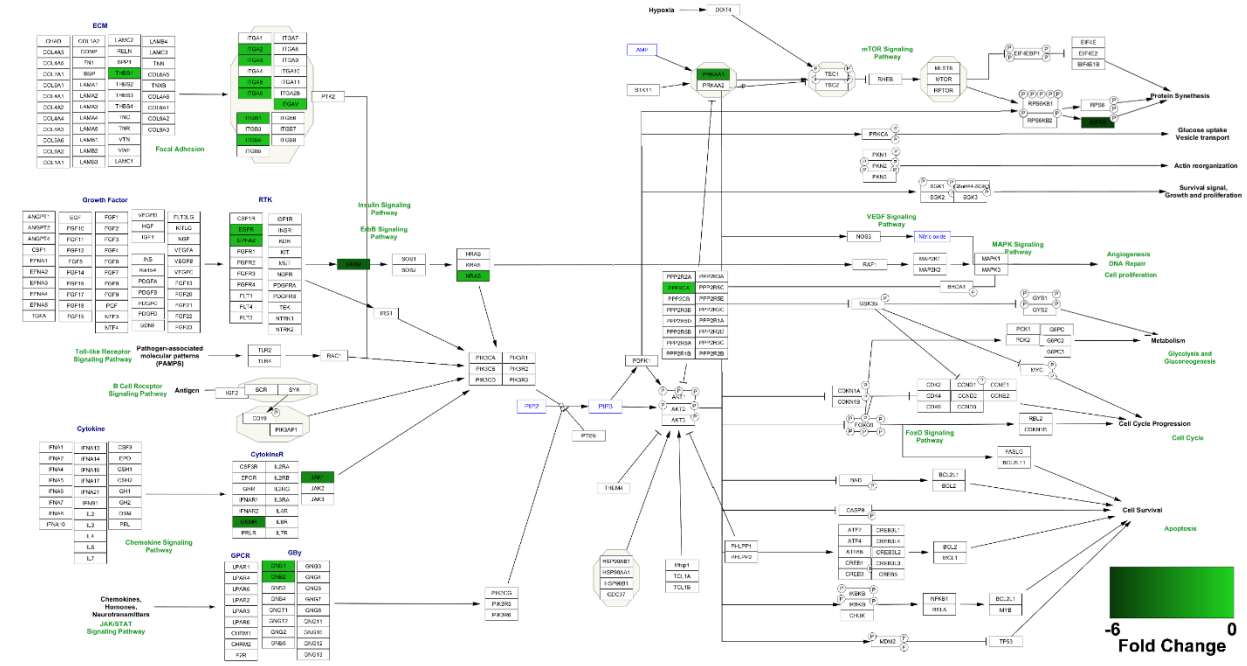

Figure 4.45: The key PI3K-Akt pathway proteins which are significantly downregulated for EP+TurNP from turmeric silver nanoparticles (TurNP) in MDA-MB-231 cells at 12h of treatment. Here TurNP concentration of 15µg/mL and EP of 800V/cm, 100µs, 8 pulses at 1Hz were used. Proteins enriched with GO term "PI3K-Akt Signaling Pathway" in KEGG (Kanehisa & Goto, 2000) analysis were fed to Cytoscape 3.6.1 (Paul Shannon et al., 2003) and mapped to PI3K-Akt Pathway in WikiPathway (Kutmon, Lotia, Evelo, & Pico, 2014), where the extent of shading represents the fold change.

The proteins of 14-3-3 family, such as YWHAB, YWHAE, YWHAG, YWHAQ, and YWHAZ were all downregulated in EP+TurNP. These proteins regulate multiple key signaling pathways, such as cell cycle, autophagy, apoptosis, and glycolysis (Pennington et al., 2018). YWHAZ stimulates chemoresistance and is linked with bad patient outcomes (Pennington et al., 2018). "The YWHAB is reported to be one of the top five highly expressed and connected target proteins (HSP90AB1, CSNK2B, TK1, YWHAB and VIM) in MDA-MB-231 cells, as their knockout in animal models inhibited colony formation, proliferation, migration, anchorage independence and invasion" (Mittal, Aryal, et al., 2020). We have also shown that electrical pulses with curcumin downregulates 14-3-3 family proteins (Mittal, Aryal, et al., 2020).

"Integrin family proteins (integrins α2, α3, α5, α6, αV, β1, and β4) were downregulated for EP+TurNP" (Mittal, Aryal, et al., 2020) (Table 4.8). Integrin family proteins are key transmembrane heterodimers used by cells to bind and respond to extracellular matrix (ECM)

induced intracellular signaling to stimulate cellular growth, survival, and proliferation (Alberts et al., 2007). Integrin expressions are often upregulated in aggressive tumors (Adorno-Cruz & Liu, 2019; Nagata et al., 2013). Twist promoted aerobic glycolysis in breast cancer cells by activating integrin β1/FAK/PI3K–Akt/mTOR pathway (L. Yang et al., 2015). It is reported that elevated expressions of integrins α2, α6, and αV may enhance the malignancy of breast cancer cells (Koistinen & Heino, 2012). We also evaluated the interaction among downregulated integrin family proteins using STRING interaction and clustering analysis (Figure 4.46).

Figure 4.46 also includes other downregulated proteins of PI3K-Akt pathway (blue nodes) and all differentially regulated glycolysis pathway proteins (both up and down - nodes with red color) to evaluate the interaction between two pathways. These results suggest that all proteins of integrin family form a cluster (cluster #1), where integrin β1 interacts with other integrins, such as α2, α3, α5, α6, αV, and β4. The β1 remains the most common beta subunit of integrin, which binds to multiple α subunits (as we also show in Figure 4.46) to significantly impact migration and stemness (Adorno-Cruz & Liu, 2019; Barczyk, Carracedo, & Gullberg, 2010). The α2β1 is highly involved in invasive breast cancer cells and it promotes trans-endothelial migration (Adorno-Cruz & Liu, 2019). Integrin α3β1 can regulate the expression of MMP-2 and MMP-9 to modulate breast cancer cell migration and invasion (Koistinen & Heino, 2012). High integrin α5β1 levels enhance cell invasion in MDA-MB-231 TNBC cells, T24 bladder, and 786-O kidney cancer cells (Mierke, Frey, Fellner, Herrmann, & Fabry, 2011).

"All the integrins together with EGFR, and GRB2 also participate in focal adhesion pathway, as indicated by green color nodes" (Mittal, Aryal, et al., 2020) in Figure 4.46. Integrins also play a role in metabolic reprogramming of cancer cells from OXPHOS to glycolysis (Alday-Parejo, Stupp, & Rüegg, 2019; S. Wang et al., 2016; L. Yang et al., 2015). Other downregulated proteins of PI3K-Akt pathway, such as THBS1 and LAMC1were also clustered together with integrins. LAMC1, a component of ECM, which is implicated in cell adhesion, differentiation, migration and metastasis (Piovan et al., 2012) is also linked with increased Warburg effect in hepatocellular carcinoma, as its downregulation reduced the consumption of glucose, lactate generation with decrease in GLUT1 and LDHA (Ye et al., 2019). THBS1 inhibition prevents in MDA-MB-231 invasion and metastasis (T. N. Wang et al., 1996). "THBS1 is also linked with glycolysis, as highlighted by its interaction with ALDOA in Figure 4.46" (Mittal, Camarillo, et al., 2020), and indicated by reduced THBS1

levels upon LDHA knockdown and reduced lactate concentration in glioma cells (Seliger et al., 2013).

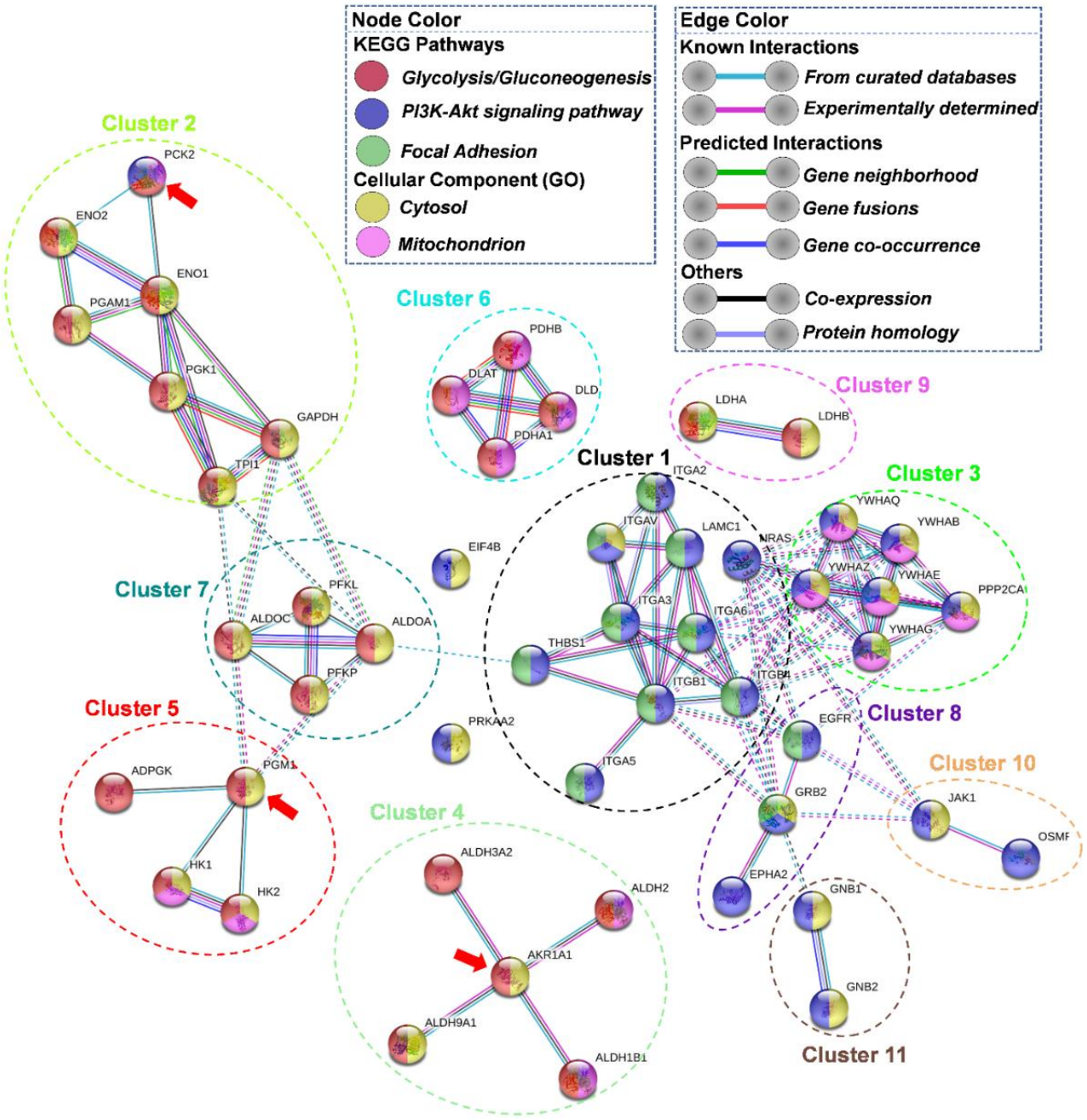

Figure 4.46: String interaction among proteins significantly up- and downregulated in PI3K-Akt signaling and glycolysis pathways in MDA-MB-231 cells at 12h of treatment. Here turmeric silver nanoparticles (TurNP) concentration of 15µg/mL and EP of 800V/cm, 100µs, 8 pulses at 1Hz were used. The proteins were uploaded to STRING (Szklarczyk et al., 2017) software to study the interaction and functional enrichment using evidence as meaning of network edge. The edge color in figure legend shows active interaction sources used in analysis, where the highest confidence (0.9) setting for minimum required interaction was used. The nodes were clustered using MCL clustering using 3 as inflation parameter. Localization is represented with node color displays KEGG (Kanehisa & Goto, 2000) pathways and protein localization. Red arrow show outlier in a up/downregulated glycolytic protein clusters from the other group

G. Metabolic switch in TNBC cells upon EP+TurNP treatment

i. Impact of EP+TurNP on glycolysis pathway

"Figure 4.46 also demonstrates that 26 differentially regulated glycolysis pathway proteins form 6 different clusters (clusters # 2, 4, 5, 6, 7, and 9). Among these proteins, 14 were upregulated, and 12 were downregulated in EP+TurNP for at least one of the three pairwise comparison groups. Table 4.9 lists these proteins and their expressions. The identification and expression of key significantly regulated glycolytic proteins for EP+TurNP compared to TurNP is shown in Figure 4.47" (Mittal, Camarillo, et al., 2020).

a. Downregulated glycolysis pathway proteins

The downregulated glycolysis proteins included aldo-keto reductase family 1 member (A1AKR1A1), ALDOA, ALDOC, ENO1, ENO2, GAPDH, LDHA, LDHB, PGM1, PGK1, PGAM1, TPI1. The AKR1A1 is related with increased radio resistance in laryngeal cancer cells, and its depletion sensitized HCT116 cells expressing p53 to irradiation (J.-S. Kim, Chang, Park, & Hwang, 2012). Aldolase family members (ALDOA, ALDOB, and ALDOC) are the fourth enzyme in the glycolysis (Chang et al., 2018). The ALDOA has a major function in glycolysis, as it maintain the glucose homeostasis (Chang et al., 2018) and its inhibition disrupts the feed-forward glycolytic loop to prevent the cancer cell proliferation (Grandjean et al., 2016). The ALDOC is also involved in fructolysis and is overexpressed in multiple cancers (Chang et al., 2018). Increased PGK1 expression is correlated with higher breast tumor grade in patients and is a prognostic marker of paclitaxel resistance in breast cancer (S. Sun et al., 2015). PGM1 is essential for sustained cancer cell growth (E. Bae et al., 2014). PGAM1 can modulate the cytoskeleton to control breast cancer cell mobility and migration (Gandhi & Das, 2019).

"The ENO1 is highly expressed biomarker of TNBC, and its function is positively related with distinct TNBC metabolism (Miah et al., 2017; Vergara et al., 2013)" (Mittal, Camarillo, et al., 2020). The ENO2, GAPDH, TPI1, and LDHB are overexpressed in TNBC glycolytic subtypes found using a multi-omics (genomics and transcriptomics analysis of TNBC (Gong et al., 2019). The GAPDH may participate in TNBC cell cycle progression (Peng et al., 2017). The expression of TPI1 and LDHB is high in basal-like immune-suppressed subtype of TNBC tumors (Jézéquel et

al., 2019). The LDHA levels correlate with the TNBC malignancy its inhibition prevents brain metastasis (Dong et al., 2017). The LDHA and LDHB catalyze the interconversion of pyruvate to lactate. LDHA is overexpressed in various cancers but LDHB is uniquely overexpressed in basal-like TNBC and works as an "essential gene", as its knockdown causes a significant loss in TNBC cell proliferation and arrests growth in mouse tumors (Dennison et al., 2013; McCleland et al., 2012). "The increased expression of LDHB correlates to significantly poor clinical outcomes (McCleland et al., 2012)" (Mittal, Aryal, et al., 2019). LDHB also plays an important role in "reverse Warburg effect" (Dennison et al., 2013; Markert et al., 1963; McCleland et al., 2012; Porporato et al., 2011; Whitaker-Menezes et al., 2011). Considering the distinct and strong predilection for these key glycolytic enzymes in TNBC, their downregulation upon EP+TurNP treatment makes MDA-MB-231 cells highly susceptible to this treatment.

Table 4.9: The glycolysis pathway proteins which are significantly upregulated and downregulated for EP+TurNP treatment in one or more comparison groups. Here turmeric silver nanoparticles (TurNP) concentration of 15µg/mL and EP of 800V/cm, 100µs, 8 pulses at 1Hz were used. The significantly regulated proteins are marked with # (|fold change|≥0.5) and * (P<0.05) in a comparison.

S.N.	Uniprot Access. No.	Protein Name	Gene Name	EP+TurNP vs Ctrl		EP+TurNP vs EP		EP+TurNP vs TurNP	
				Fold Change	P Value	Fold Change	P Value	Fold Change	P Value
1	Q9BRR6	ADP-dependent glucokinase	ADPGK	4.09#	1.1×10^{-6}*	4.09#	1.1×10^{-6}*	0.28	5.1E-02
2	P30837	Aldehyde dehydrogenase X, mitochondrial	ALDH1B1	0.82#	1×10^{-3}*	0.60#	1.4×10^{-2}*	0.77#	7.3×10^{-4}*
3	P05091	Aldehyde dehydrogenase, mitochondrial	ALDH2	0.89#	3.1×10^{-4}*	0.71#	3.7×10^{-3}*	0.83#	3.7×10^{-3}*
4	P51648	Aldehyde dehydrogenase family 3 member A2	ALDH3A2	4.93#	2.4×10^{-7}*	4.93#	2.4×10^{-7}*	0.97#	9.7×10^{-4}*
5	P49189	4-trimethylaminobutyraldehyde dehydrogenase	ALDH9A1	5.28#	3.5×10^{-7}*	5.28#	3.5×10^{-7}*	0.36	1.3×10^{-2}*
6	Q86YI5	Acetyltransferase component of pyruvate dehydrogenase complex	DLAT	0.87#	2.0×10^{-4}*	0.71#	3.2×10^{-3}*	1.10#	4.9×10^{-5}*
7	P19367	Hexokinase-1	HK1	0.65#	8.7×10^{-2}	0.76#	3.3×10^{-3}*	0.36	2.4×10^{-2}*
8	P52789	Hexokinase-2	HK2	4.87#	6.8×10^{-3}*	5.77#	3.0×10^{-3}*	3.07#	5.7×10^{-3}*
9	Q01813	ATP-dependent 6-phosphofructokinase, platelet type	PFKP	1.17#	5.3×10^{-3}*	1.11#	3.5×10^{-3}*	0.75#	4.4×10^{-3}*
10	P08559	Pyruvate dehydrogenase E1 component subunit alpha, somatic form, mitochondrial	PDHA1	1.16#	1.9×10^{-4}*	1.26#	6.6×10^{-4}*	0.95#	6.3×10^{-3}*
11	P11177	Pyruvate dehydrogenase E1 component subunit beta, mitochondrial	PDHB	0.70#	2.5×10^{-3}*	0.54#	1.5×10^{-2}*	0.76#	1.6×10^{-3}*

Table 4.9 continued

12	P09622	Dihydrolipoyl dehydrogenase, mitochondrial	DLD	0.16	2.1×10^{-1}	0.03	7.5×10^{-1}	$0.69^{\#}$	4.7×10^{-3}*
13	P17858	ATP-dependent 6-phosphofructokinase, liver type	PFKL	$0.86^{\#}$	1.8×10^{-2}*	$0.61^{\#}$	6.1×10^{-2}	$3.69^{\#}$	2.4×10^{-2}*
14	Q16822	Phosphoenolpyruvate carboxykinase [GTP], mitochondrial	PCK2	$0.67^{\#}$	1.5×10^{-3}*	0.49	5.2×10^{-2}	$2.21^{\#}$	2.0×10^{-1}
15	P14550	Aldo-keto reductase family 1 member A1	AKR1A1	$-4.16^{\#}$	7.3×10^{-5}*	0.00	N/A	$-4.52^{\#}$	2.2×10^{-7}*
16	P04075	Fructose-bisphosphate aldolase A	ALDOA	$-1.87^{\#}$	5.3×10^{-3}*	$-1.70^{\#}$	5.4×10^{-4}*	$-1.68^{\#}$	4.9×10^{-4}*
17	**P09972**	**Fructose-bisphosphate aldolase C**	**ALDOC**	**$-1.44^{\#}$**	**3.7×10^{-1}**	**0.00**	**N/A**	**$-4.44^{\#}$**	**6.9×10^{-7}***
18	P06733	Alpha-enolase	ENO1	$-1.68^{\#}$	4.8×10^{-3}*	$-1.08^{\#}$	1.4×10^{-3}*	$-1.67^{\#}$	7.4×10^{-5}*
19	P09104	Gamma-enolase	ENO2	$-5.18^{\#}$	3.7×10^{-5}*	$-3.65^{\#}$	1.2×10^{-1}	$-4.63^{\#}$	4.3×10^{-6}*
20	P04406	Glyceraldehyde-3-phosphate dehydrogenase	GAPDH	$-0.73^{\#}$	5.7×10^{-2}	-0.34	2.2×10^{-2}*	$-0.51^{\#}$	1.0×10^{-3}*
21	P00338	Lactate dehydrogenase A chain	LDHA	$-0.79^{\#}$	8.3×10^{-3}*	-0.15	2.8×10^{-1}	$-1.07^{\#}$	4.6×10^{-4}*
22	P07195	Lactate dehydrogenase B chain	LDHB	$-1.55^{\#}$	1.8×10^{-3}*	$-1.19^{\#}$	2.0×10^{-3}*	$-1.49^{\#}$	2.7×10^{-4}*
23	P36871	Phosphoglucomutase-1	PGM1	$-2.10^{\#}$	7.9×10^{-3}*	$-1.52^{\#}$	9.1×10^{-3}*	$-2.06^{\#}$	3.5×10^{-3}*
24	P00558	Phosphoglycerate kinase 1	PGK1	$-0.91^{\#}$	5.7×10^{-2}	-0.35	3.5×10^{-2}*	$-0.96^{\#}$	1.2×10^{-3}*
25	P18669	Phosphoglycerate mutase 1	PGAM1	$-1.91^{\#}$	1.1×10^{-2}*	$-1.57^{\#}$	1.1×10^{-2}*	$-1.84^{\#}$	6.0×10^{-3}*
26	P60174	Triosephosphate isomerase	TPI1	$-2.17^{\#}$	6.5×10^{-3}*	$-2.05^{\#}$	4.3×10^{-3}*	$-1.87^{\#}$	3.3×10^{-3}*

b. Upregulated glycolysis pathway proteins

Interestingly, we also observed the glycolysis pathway for upregulated proteins in EP+TurNP treatment. The upregulated glycolysis proteins included ADPGK, ALDH1B1, ALDH2, ALDH3A2, ALDH9A1, DLAT, HK1, HK2, PFKP, PDHA1, PDHB, DLD, PFKL, PCK2, as shown in Table 4.9.

Most upregulated proteins were either upstream and/or mitochondrial. These proteins were ADPGK, ALDH1B1, ALDH2, ALDH3A2, ALDH9A1, PFKP, PFKL, HK1, HK2, PCK2, DLAT, DLD, PDHA1, and PDHB. ADPGK is highly expressed both in cancer and normal tissues, and a non-significant change in its level was detected in breast cancers compared to noncancerous tissue of breast (Richter, 2011). Tumor size for over-expressed/knocked out ADPGK in colorectal (HCT116) and lung (H460) carcinoma xenografts were similar to the wild type ADPGK xenografts (Richter, 2011). The ADPGK overexpression/knockout did not affect proliferation or glycolysis but modulated mitochondrial metabolism (Richter, 2011; Richter et al., 2012). The ALDH family members (ALDH1B1, ALDH2, ALDH3A2, ALDH9A1) contribute significantly in the management of oxidative stress within living systems(Surendra Singh et al., 2013). The elevated ALDH levels could be attributed to the stress response due to increased ROS production upon EP+TurNP treatment, which in turn may elevate the expressions of ALDH genes, as reported previously (Luo et al., 2018). The overexpression of PFKP reduces the tumor-initiation and metastatic potential in MDA-MB-231 xenografts by regulating Snail-mediated metabolic reprogramming (N. H. Kim et al., 2017). The HK family enzymes (HK1 and HK2) play a significant role in glycolysis and EGF induces upregulation of HK activity (Lim et al., 2016). However, contrary to this, we observed upregulation in HK enzymes despite EGFR downregulation. The DLAT, DLD, PDHA1, and PDHB are part of PDC, which mediates the transformation of pyruvate into acetyl-CoA (pyruvate metabolism). "Inhibition of PDC activity in head and neck cancers and breast cancers, including TNBC contributes to the Warburg metabolic and malignant phenotype (Gang et al., 2014; McFate et al., 2008)" (Mittal, Aryal, et al., 2020). Moreover, the restoration of PDC activity could reestablish pyruvate metabolism to mitochondria to enhance apoptosis, reduced invasion, and stalled tumor growth. The EP with curcumin also upregulated PDC activity and enhanced apoptosis (Mittal, Aryal, et al., 2020). Along with DLAT, DLD, PDHA1, and PDHB, PCK2 is also involved in the pyruvate metabolism pathway, which was

also enriched for the upregulated proteins in EP+TurNP. The product of pyruvate metabolism is acetyl COA, which replenishes the TCA cycle.

The clustering analysis in Figure 4.46 indicates that most of the upregulated and downregulated proteins form separate clusters. Red arrows highlight occasional outlier in these clusters from the other group. The upregulated proteins form clusters 4, 5, and 6. The downregulated proteins are clustered in 2 and 9. The cluster 7 contains mixed proteins, two from each group (upregulated: PFKL and PFKP; downregulated: ALDOA and ALDOC). The high degree of interaction among the proteins in a cluster highlight their interdependence. The separate clustering of upregulated and downregulated proteins highlights the mutual exclusiveness of the two groups. The mutual exclusiveness of these two groups is also apparent by considering their localization.

The localization analysis in Figure 4.46 indicates that downregulated proteins are localized in cytosol (yellow nodes), and most upregulated proteins are from mitochondrion (pink nodes), again highlighting upregulation in mitochondrion. These observations correlate with the enrichment results for all differentially expressed, indicated in Figures 4.43 and 4.44.

Figure 4.47: The main glycolysis pathway proteins which are significantly downregulated (node color green) and upregulated (node color red) for EP+TurNP from turmeric silver nanoparticles (TurNP) in MDA-MB-231 TNBC cells at 12h of treatment. Here TurNP concentration of 15µg/mL and EP of 800V/cm, 100µs, 8 pulses at 1Hz were used. Proteins enriched with "glycolysis/gluconeogenesis" term in KEGG (Kanehisa & Goto, 2000) were fed to Cytoscape 3.6.1 (Paul Shannon et al., 2003) and mapped to glycolysis Pathway in WikiPathway app (Kutmon et al., 2014), where the extent of shading represents the fold change.

Figure 4.47 continued

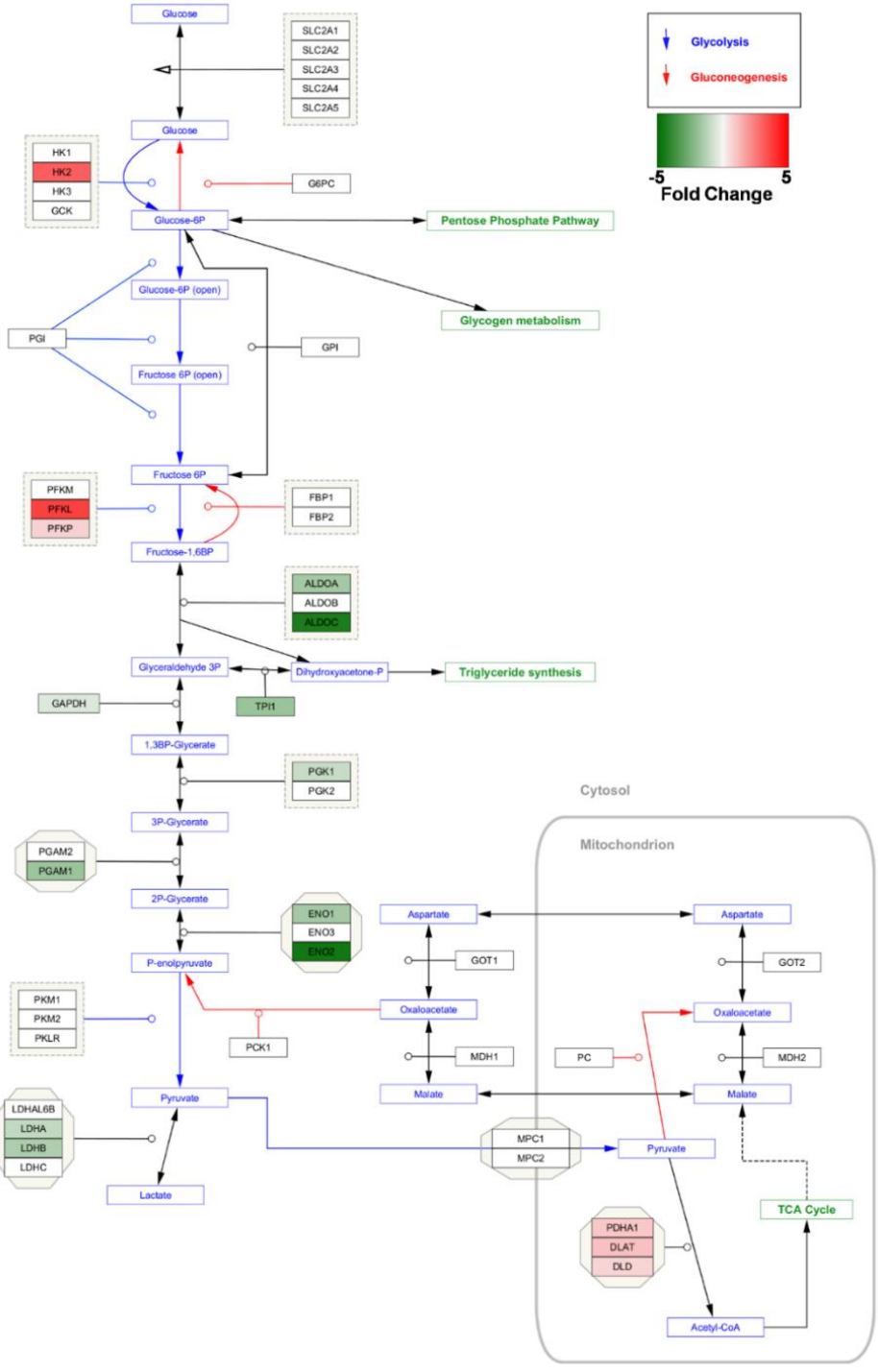

ii. Upregulation of TCA cycle and OXPHOS proteins

There was an upregulation in proteins of TCA cycle and OXPHOS pathways, which highlights a metabolic shift to mitochondria for EP+TurNP treatment, where the MDA-MB-231 cells are dependent upon oxidative substrates for energy generation. Even with suppression in glycolysis and conversion reaction of lactate to pyruvate, we observed increased activity of TCA cycle for EP+TurNP treatment. This upregulation in TCA cycle could be credited to the upregulation in multiple supplemental pathways ("FA degradation/metabolism, AA degradation, peroxisome, pyruvate metabolism, and tryptophan metabolism"), which produce pyruvate and various intermediates, such as acetyle COA and oxaloacetate to supply the TCA cycle.

Elevated OXPHOS activity in MDA-MB-231 cells could also be attributed to the stress response as cells strive to produce energy via different sources since glycolysis is suppressed. This elevated OXPHOS could generate ROS to trigger a mitochondrion mediated intrinsic apoptotic pathway of cell death.

H. Validation of Proteomics Results

i. Correlation between protein and mRNA levels of key glycolysis genes

To validate the proteomics results, we compared the protein levels and mRNA levels of key glycolytic genes LDHB and ENO1, as shown in Figure 4.48, which are normalized with Ctrl (level = 1). A qPCR was performed to quantify mRNA levels after 12h of different treatments. For LDHB, the mRNA expression was 0.7 for TurNP, which decreased to 0.4 for EP and to 0.04 for EP+TurNP (Figure 4.48(a)). In contrast, the LDHB protein expression was 0.9 for TurNP, which decreased to 0.8 for EP and to 0.3 for EP+TurNP.

For ENO1, the lowest mRNA expression was found to be 0.1 for EP+TurNP treatment (Figure 4.48(b)). Similarly, the ENO1 protein expression was minimum at 0.3 for EP+TurNP. "These results demonstrate good correlation between mRNA and protein levels for LDHB and ENO1 and validate that these key glycolytic genes are downregulated at transcription levels upon EP+TurNP treatment" (Mittal, Camarillo, et al., 2020).

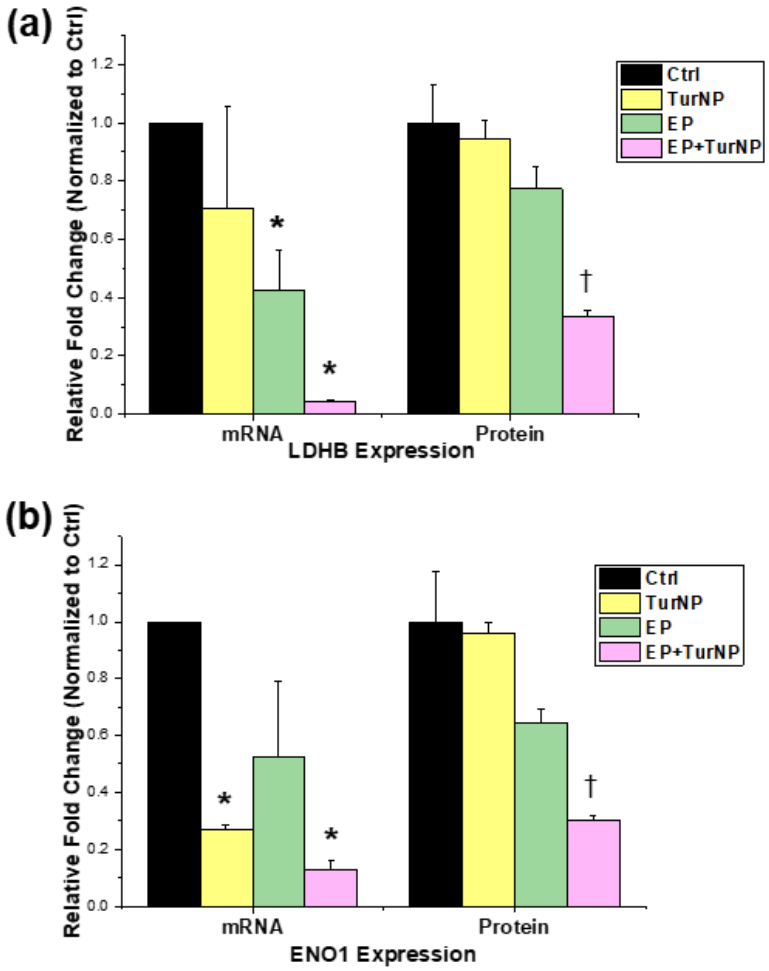

Figure 4.48: The mRNA and protein levels of various genes in MDA-MB-231 cells at 12h of different treatments: (a) LDHB, (b) ENO1. Here turmeric silver nanoparticles (TurNP) concentration of 15µg/mL and EP of 800V/cm, 100µs, 8 pulses at 1Hz were used. The relative mRNA levels were calculated utilizing ΔΔCq approach on qPCR data using 18S ribosomal RNA (18s rRNA) as the internal standard. Here protein levels were extracted from proteomics data. Significant difference ($P < 0.05$) for mRNA (*) and protein (†) expression level was calculated from Ctrl. The results include data from experiments done in triplicate, where error bars represent standard error.

ii. Measurement of ROS levels

Figure 4.49 shows the average Lum to represent H_2O_2 ROS expressions in MDA-MB-231 cells at 12h for different treatments. Compared to Lum of Ctrl at 2199, TurNP and EP treatments caused a significant increase in Lum to 2800 and 3266, respectively. The Lum was highest at 3481 for EP+TurNP treatment, which was 1.6× significantly higher from H_2O_2 levels of Ctrl. These

observations suggest that while TurNP and EP alone can cause significant oxidative stress in MDA-MB-231 cells, their synergy could lead to a further increase in the oxidative stress.

This increased ROS can be attributed to increased OXPHOS activity, which generates "ROS to activate cell death pathways, as we showed for EP application with cisplatin and curcumin in MDA-MB-231 cells (Mittal, Aryal, et al., 2019, 2020). The peroxisome pathway, which involves breaking down the FA for the membrane regeneration can also generate H_2O_2 to trigger apoptosis (Gray, 2001)" (Mittal, Camarillo, et al., 2020). These observations correlate well with our previous results for EP with curcumin and cisplatin.

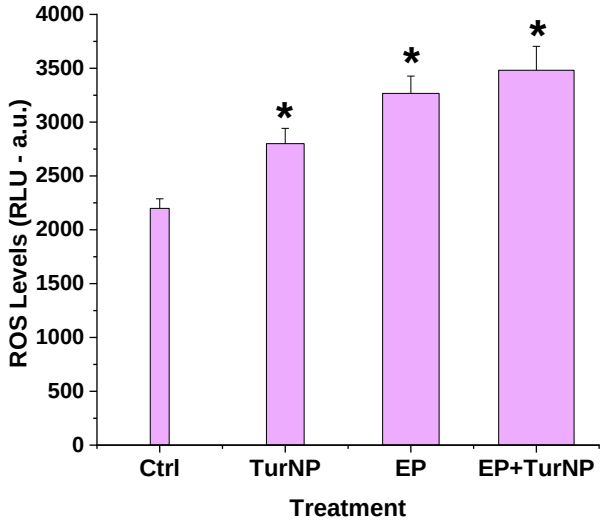

Figure 4.49: The levels of H_2O_2 reactive oxygen species at 12h of different treatments in MDA-MB-231 cells. Here turmeric silver nanoparticles (TurNP) concentration of 15µg/mL and EP of 800V/cm, 100µs, 8 pulses at 1Hz were used. *P < 0.05 indicates significant difference from Ctrl. The results include data from experiments done in triplicate, where error bars represent standard error.

iii. Measurement of the levels of key glycolytic metabolites

To further validate our proteomics findings, we measured the uptake and intracellular levels of main glycolytic metabolites (Figure 4.50(a-d)). The glucose uptake in MDA-MB-231 for various treatments is shown in Figure 4.50(a), which are reported after normalization with Ctrl (100%). The uptake of glucose increased to 157% for TurNP and to 129% for EP, indicating an increased

glucose uptake for these treatments. Interestingly, for EP+TurNP treatment, the glucose uptake was down to 91%, showing an inhibitory effect on glucose uptake, when compared with TurNP and EP. The intracellular lactate levels in Figure 4.50(b) indicate towards greater inhibitory effects of EP+TurNP on the lactate. The lactate levels reduced to 74% for EP+TurNP, while they were 96% for TurNP and 74% for EP. Similar effects were also observed on the intracellular glutamine levels (Figure 4.50(c)), as they reduced to 61% for EP+TurNP, while they were 88% for TurNP and 97% for EP. The glutamate levels in Figure 4.50(d) indicate that EP+TurNP treatment reduced the glutamate levels to 84%, while they increased to 114% for TurNP and 122% for EP. Together these results validate our proteomics results and highlight that EP+TurNP treatment downregulates the uptake and intracellular levels of main glycolytic metabolites to produce inhibitory effects on the glycolysis.

"In summary, our results provide preliminary novel evidences and insights into the anticancer effects of ECT with TurNP against MDA-MB-231 cells. The combined EP+TurNP suppressed key proteins implicated in cancer cell proliferation, differentiation, migration, survival, and evasion of cell death and apoptosis. These proteins were involved in multiple pathways, such as PI3K-Akt signaling and glycolysis and their downregulation altered the metabolic profile of the MDA-MB-231 cells. These results suggest that the suppression of glycolytic metabolism in TNBC could be a potential therapeutic avenue against TNBC" (Mittal, Camarillo, et al., 2020). Figure 4.51 summarizes these results.

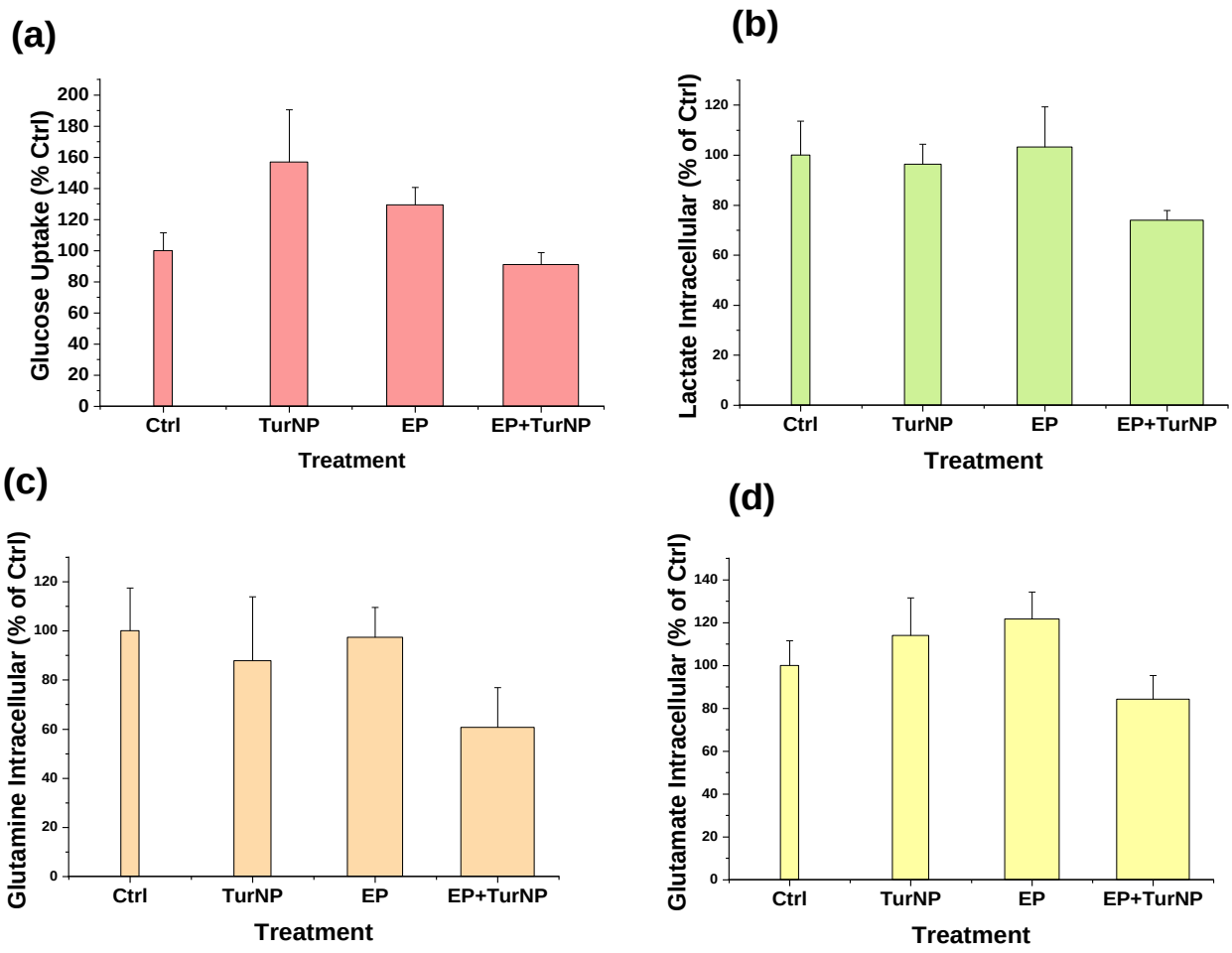

Figure 4.50: The levels of various metabolites at 12h of different treatments in MDA-MB-231 cells. (a) Glucose uptake, (b) Intracellular levels of lactate, (c) Intracellular levels of glutamine, (d) Intracellular levels of glutamate. Here turmeric silver nanoparticles (TurNP) concentration of 15µg/mL and EP of 800V/cm, 100µs, 8 pulses at 1Hz were used. T-test did not indicate any significant difference from Ctrl. The results include data from experiments done in triplicate, where error bars represent standard error.

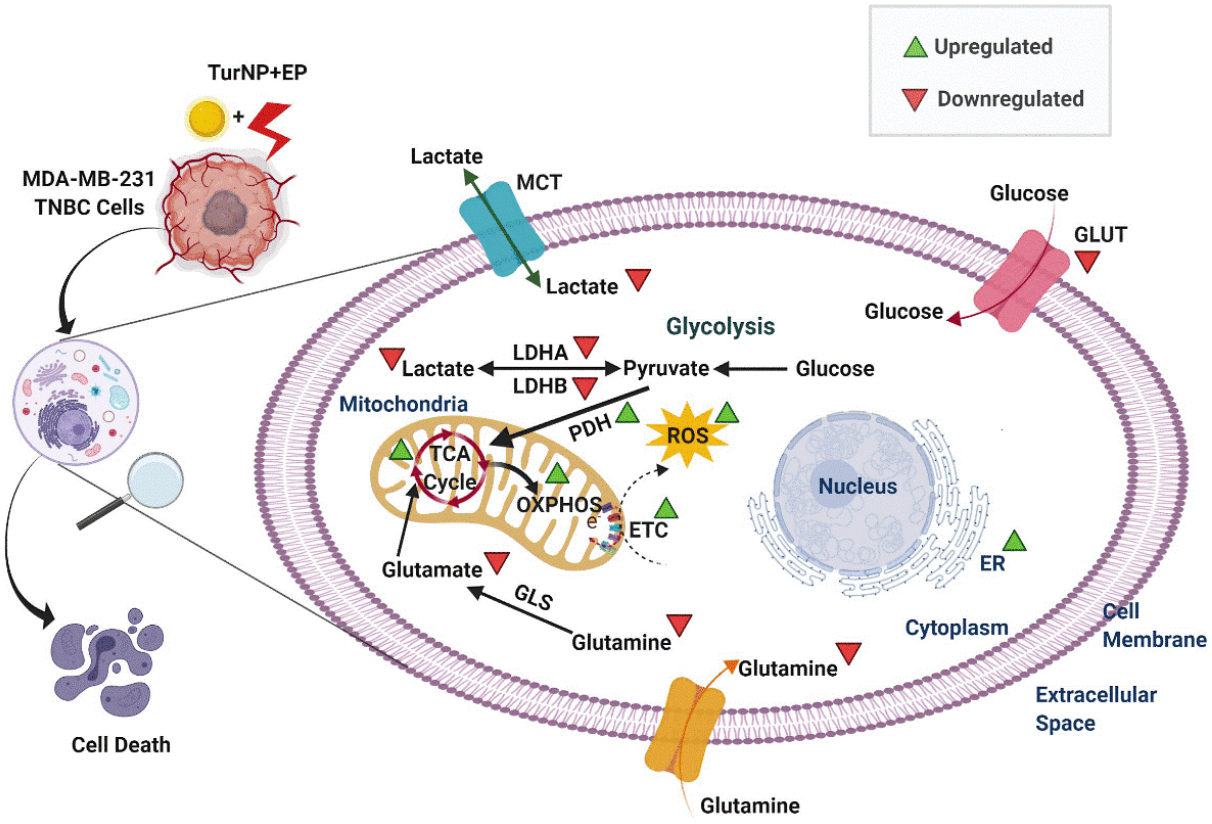

Figure 4.51: A schematic diagram showing an overview of the effects of EP+TurNP treatment in MDA-MB-231 cells. Abbreviations - ETC: Electron Transport Chain; ER: Endoplasmic Reticulum; GLUT: Glucose Transporter; GLS: Glutaminase; LDHA/B: Lactate Dehydrogenase A/B; MCT: Monocarboxylate Transporter; PDH: Pyruvate Dehydrogenase Complex; ROS: Reactive Oxygen Species. The figure was created using BioRender.

4.3 Cisplatin

4.3.1 The impact of conventional microsecond duration electrical pulses with cisplatin on TNBC cells

A. Cell viability studies

The MDA-MB-231 cell viability at 4h for different treatment conditions is shown in Figure 4.52. A flow cytometric assessment of cell viability is shown in Figure 4.52(a). The viability was quantified using two DNA binding dyes and the permeability of cell membrane. The cell viability for cisplatin (CsP) treatment was 96.9%, not significantly different from 96.3% of Ctrl. The viability was 27% for EP and 28.9% for EP+CsP. These viabilities for EP and EP+CsP treatments were significantly different from Ctrl, but not from each other.

Figure 4.52(b) shows the MDA-MB-231 cell viability at 4h and 12h of various treatments, measured using "ATP independent substrate reducing potential". All viabilities were normalized with Ctrl viability at 4h (100%). There were 125% of metabolically active cells at 12h in Ctrl. For CsP treatment, the cell viability was 83% at 4h and 106% at 12h of treatment, not significantly different from Ctrl (Figure 4.52(b)). A decreased viability to 8.8% was observed for EP at 4h, however there was a revival in cell viability to 10.6% at 12h and to 16% at 60h, as shown in Table 4.10. The viability decreased significantly to 4.5% at 4h and 4.2% at 12h for EP+CsP treatment. A further decrease in cell viability to 4% at 60h was observed for EP+CsP, indicating a persistent impact of EP+CsP treatment, in contrast to EP. This indicates the superiority of the combined EP+CsP treatment.

"Since *in vivo* application will involve both healthy and cancerous cells, we assessed the viability of non-tumorigenic mammary epithelial MCF10A cells" (Figure 4.52(c)) (Mittal, Aryal, et al., 2019). The MCF10A cell viability was 75% at 4h and 88% at 12h for EP, and 65% at 4h and 51% at 12h for EP+CsP. These results suggest that the effects of EP+CsP on MDA-MB-231 TNBC cell viability were much higher, time sustained, and specific compared to the MCF10A cells, which maintained higher viability.

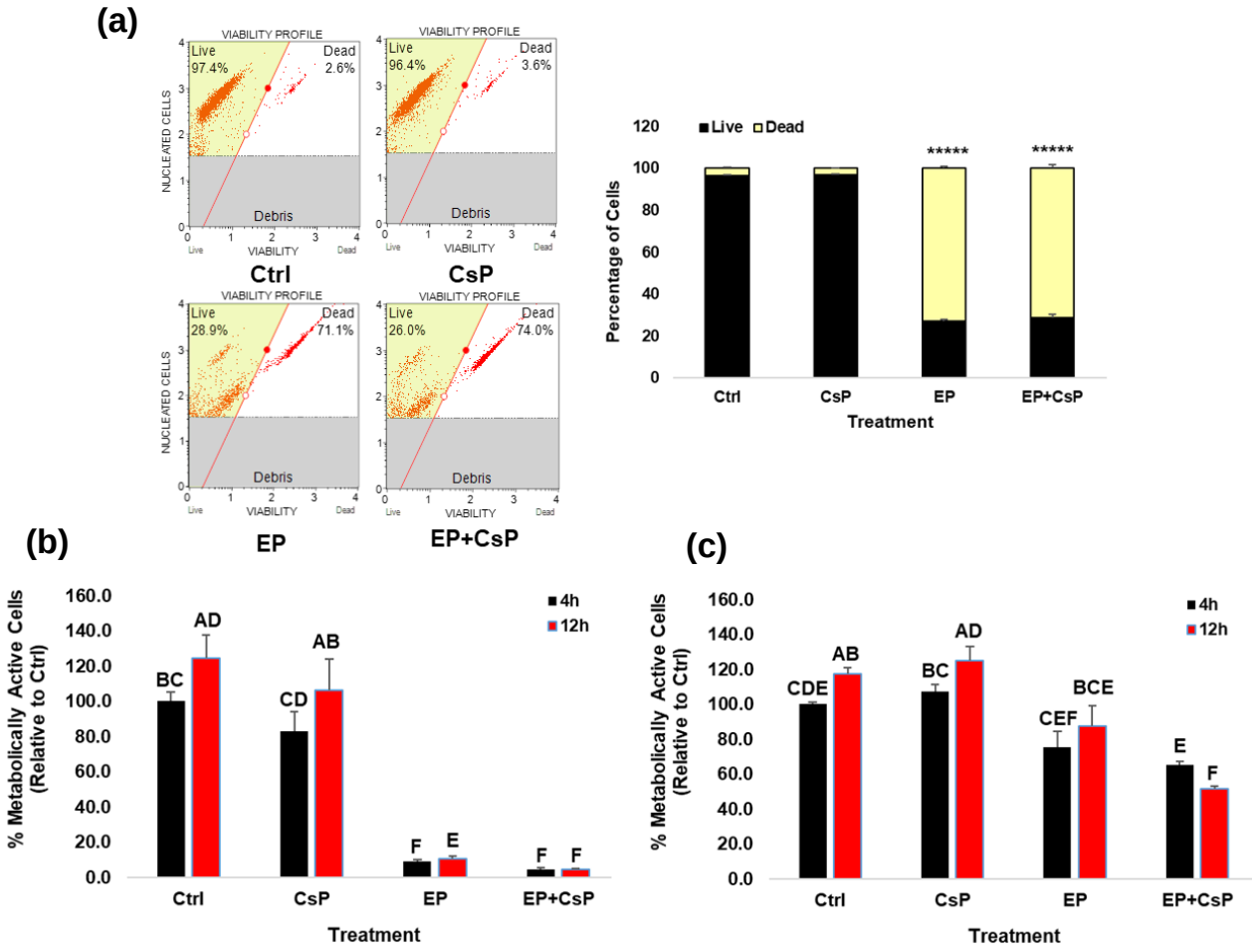

Figure 4.52: (a) The viability of MDA-MB-231 cells viability at 4h of various treatments: Control (Ctrl), Cisplatin (CsP) concentration of 100µM, Electroporation (EP) of 1200V/cm, 100µs, 8 pulses at 1Hz, and EP+Cisplatin (EP+CsP). Cells were maintained with Muse reagent for 5min at room temperature for flowcytometric assessment of cell viability on Muse Cell Analyzer as per the protocol. *****P<0.05 indicates significance from Ctrl. (b-c) The viability of (b) MDA-MB-231 cells and (c) MCF10A cells at 4h and 12h of treatments. Cell viability was measured using Promega MT real time viability kit. Here different letters demonstrate significance (P<0.05) among groups. The results include data from experiments done in triplicate, where error bars represent standard error.

Table 4.10: The viability (mean ± S.E.) of MDA-MB-231 cells up to 60h for various treatments. Here cisplatin (CsP) concentration of 100µM and EP of 1200V/cm, 100µs, 8 pulses at 1Hz were used. The results include data from experiments done in triplicate, where error bars represent standard error.

Treatment	**Time**				
	4h	**12h**	**24h**	**48h**	**60h**
Ctrl	100 ± 5.5	124.7 ± 13	150.8 ± 7.7	189.4 ± 3.8	262.8 ± 9.3
CsP	83.1 ± 11	106.2 ± 17.8	132.6 ± 25	156.1 ± 30.5	241.5 ± 36.4
EP	8.8 ± 1.1	10.6 ± 1.3	11.1 ± 1.5	11.9 ± 1.8	15.9 ± 2.2
EP+CsP	4.5 ± 1	4.2 ± 0.8	3.7 ± 0.7	3.4 ± 0.7	4.0 ± 0.8

B. Overview of proteomic analysis

To understand the mechanism of ECT with cisplatin, utilized the quantitative proteomics approach at 4h of various treatments. A label free quantitative proteomics study was performed, as explained in detail in Chapter 3. Proteins with non-zero intensity in at least two of the three biological replicates with 1% false discovery rate and with ≥2 spectral (MS/MS) counts were selected from the raw data for the analysis, leading to a clear detection of 2867 proteins/protein families from 39622 peptides. The relative abundance of a protein in each sample was compared using LFQ values.

The LFQ intensity should be consistent across replicates for the accurate measurement of protein abundance. Considering this, we visualized the log2 LFQ intensities of all replicates for each treatment using a boxplot (Figure 4.53(a)). These results highlight a consistency in the LC-MS/MS measurements due to the similarity in the median and interquartile range for triplicates within each treatment.

To further establish the accuracy of the experiments, correlations of LFQ intensities of proteins for replicates across all treatments were quantified. We obtained high coefficient of determination ($R^2 \geq 0.99$) for triplicates within Ctrl (Figure 4.53(b)), indicating excellent correlation and quality of our experiments. High R^2 (≥ 0.9) was also obtained for triplicates within other treatments, while it was lower between replicates from different treatments.

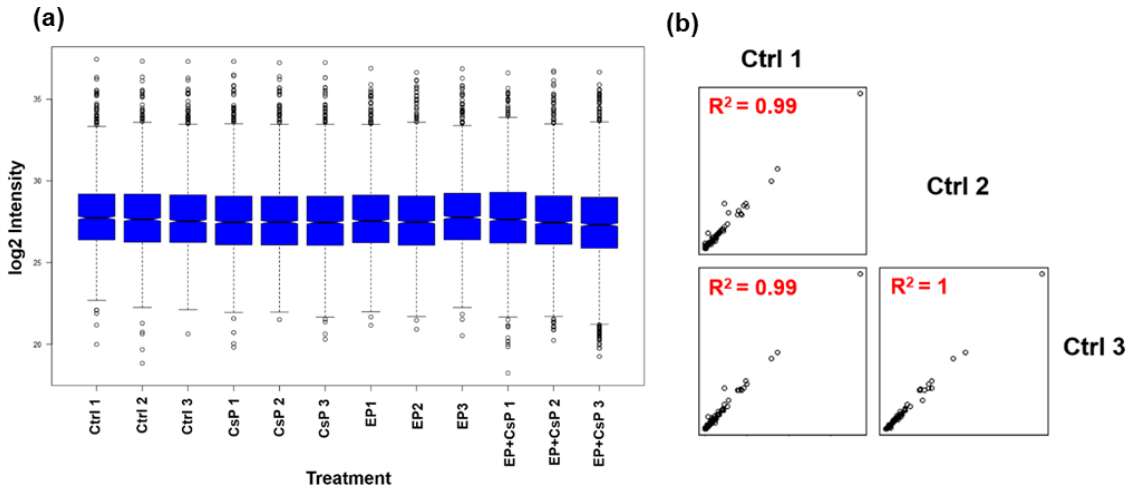

Figure 4.53: Overview of proteomics analysis in MDA-MB-231 cells at 4h of different treatments: (a) Boxplot of LFQ intensities for replicates across all treatments. (b) Correlation plots of LFQ intensities of proteins for replicates across all treatments in MDA-MB-231 cells at 4h. Here cisplatin (CsP) concentration of 100µM and EP of 1200V/cm, 100µs, 8 pulses at 1Hz were used. The R^2 value is consistently higher for replicates within a treatment.

"We used LFQ values and MS/MS counts (LFQ $\neq 0$ and MS/MS ≥ 2 for at least two of the three replicates) to classify the number of common and unique proteins present in each treatment. We identified 2311 proteins in control, 2477 in CsP, 2377 in EP, and 2457 in EP+CsP treated cells, of which 1959 (84.8% of the control) were commonly expressed in all four samples (Figure 4.54). The number of uniquely identified proteins varied from 37 in Ctrl to 115 in CsP, 64 in EP, and 83 in EP+CsP samples. More proteins were identified in CsP than in the EP+CsP (2477 versus 2457) with more unique proteins, suggesting significant impact of ECT on cellular pathways through the increase or through the loss of many protein expressions (i.e., 302 proteins found in CsP were not found in EP+CsP)" (Mittal, Aryal, et al., 2019).

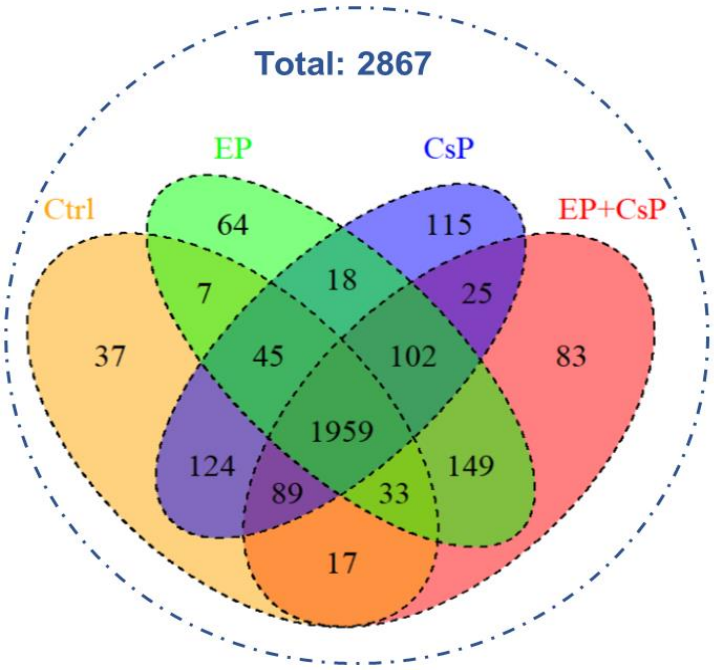

Figure 4.54: Classification of total 2867 proteins in MDA-MB-231 cells at 4h of various treatments. Here cisplatin (CsP) concentration of 100µM and EP of 1200V/cm, 100µs, 8 pulses at 1Hz were used. A protein was counted in a treatment only when it satisfied - LFQ $\neq 0$ and MS/MS ≥ 2 condition in ≥ 2 replicates.

C. Overview of differentially expressed proteins

The differentially expressed proteins were identified by comparing the LFQ expression values of the proteins commonly and uniquely expressed in various pairwise comparisons ("CsP vs. Ctrl; EP vs. Ctrl, EP vs. Csp, EP+CsP vs. Ctrl, EP+CsP vs. EP, EP+CsP vs. CsP") among four treatment groups. When the log2 fold-change (Δlog2) for a protein was greater than 0.5 ($|\Delta\log2|>0.5$), it was considered to be differently regulated.

The number of upregulated proteins were 46 for CsP, 364 for EP, 512 for EP+CsP compared with Ctrl. The number of downregulated proteins were 36 for CsP, 388 for both EP, and EP+CsP compared with Ctrl. For EP+CsP, there were 547 upregulated proteins and 507 downregulated proteins compared with CsP. Compared with EP, EP+CsP showed 13 upregulated and 16 downregulated proteins.

Figure 4.55 shows volcano plots to visualize the statistical significance vs. fold change for proteins in various pairwise comparisons. A heatmap visualizing the expressions of the differentially expressed proteins and their clustering is shown in Figure 4.56. The heatmap

indicates a consistent protein expression pattern, and columns representing triplicates within treatments are clustered together. Between treatments, columns for Ctrl, and CsP treatments are clustered in proximity to each other, and form a distinct cluster from the cluster of EP and EP+TurNP, suggesting a major change in proteomic landscape for EP and EP+TurNP treatment.

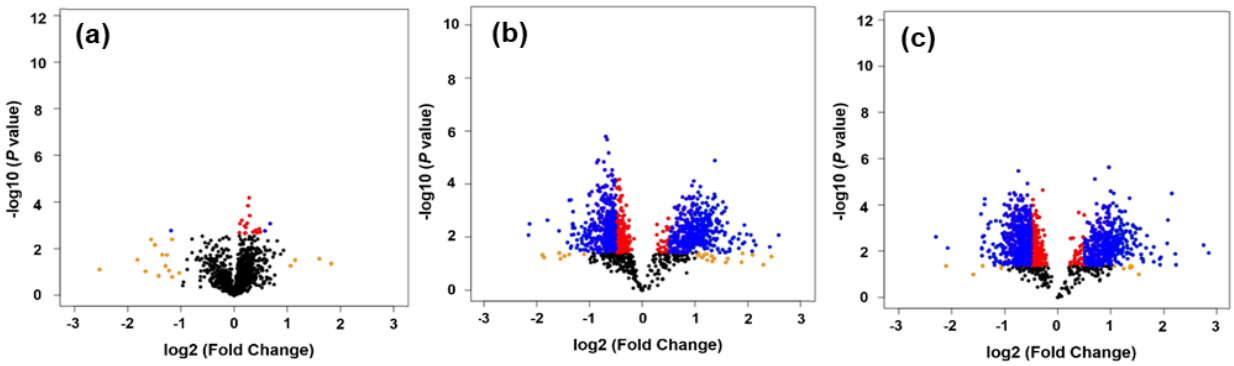

Figure 4.55: Volcano plots to visualize the statistical significance vs. fold change for proteins in MDA-MB-231 cells at 4h in different pairwise comparisons: (a) CsP vs. Ctrl, (b) EP+CsP vs. Ctrl, and (c) EP+CsP vs. CsP. Here cisplatin (CsP) concentration of 100µM and EP of 1200V/cm, 100µs, 8 pulses at 1Hz were used. "Color legend: black- not significantly changed (P>0.05); red- significantly changed but not up/downregulated (P<0.05 and |log2 (fold change)|<0.5); blue- significantly up/downregulated (P<0.05 and |log2 (fold change)|>0.5)".

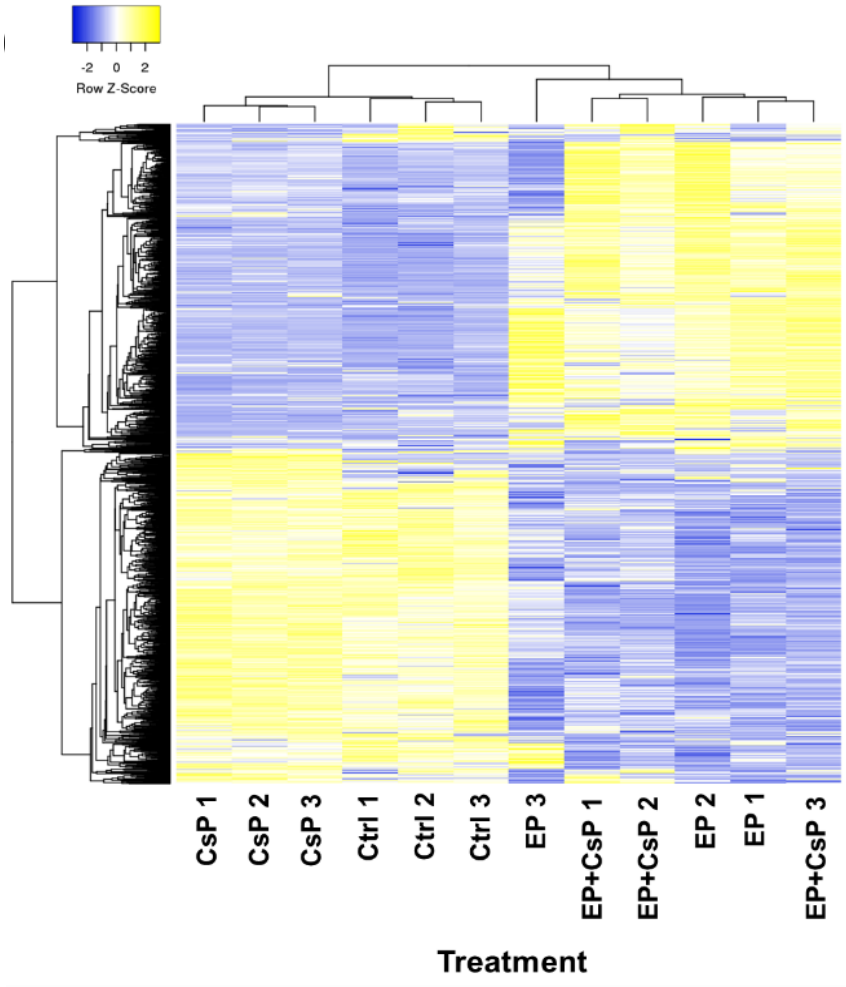

Figure 4.56: A heatmap visualizing the LFQ expressions of the significant differentially expressed proteins and their clustering for various treatments in MDA-MB-231 cells at 4h. Here cisplatin (CsP) concentration of 100µM and EP of 1200V/cm, 100µs, 8 pulses at 1Hz were used. The Average Linkage method and Kendall's Tau distance measurement method were used to cluster proteins in rows and columns. Here yellow color shows upregulated proteins and blue color shows downregulated proteins. This visualization was created using Heatmapper (Babicki et al., 2016).

Figures 4.57(a-f) shows the list of top 20 "upregulated and downregulated proteins and their expression levels (log2 fold change) in different pairwise comparisons" (Mittal, Aryal, et al., 2019). The highly upregulated protein in CsP vs. Ctrl was NipSnap homolog 2 (GBAS) with 8.7-fold change (Figures 4.57(a)). Proteins catenin beta-1 (CTNNB1) and ATP5J2-PTCD1 were the most upregulated in EP vs. Ctrl and EP+CsP vs. Ctrl, with a fold change of 10.4 and 9.7, respectively, (Figures 4.57(b) and (d)).

Titin (TTN) was the highest upregulated protein for EP+CsP from CsP with 9.9-fold change (Figures 4.57(c)). For EP+CsP vs. EP, the most upregulated protein was glutamyl-tRNA (Gln) amidotransferase subunit C, mitochondrial (GATC), with 9.7-fold change (Figures 4.57(f)). The cysteine desulfurase (NFS1) was the most upregulated protein for EP vs. CsP with 9.9-fold change (Figures 4.57(e)).

Among the downregulated proteins, the most downregulated protein was tubulin alpha-1A chain (TUBA1A) for CsP vs. Ctrl with 10.9-fold change (Figures 4.57(a)). The most downregulated protein for EP vs. Ctrl was prefoldin subunit 1 (PFDN1) with 9.1-fold change (Figures 4.57(d)). In EP+CsP vs. Ctrl, diphosphoinositol polyphosphate phosphohydrolase 2 (NUDT4) protein was the most downregulated one with 9.9-fold change (Figures 4.57(b)). Proteins MHC class I antigen (HLA-C) and huntingtin-interacting protein (HYPK) were the most downregulated in EP+CsP vs. EP and EP+CsP vs. CsP, with a fold change of 9.3 and 9.2, respectively (Figures 4.57(c) and (f)). The targeting protein for Xklp2 (TPX2) was the highest downregulated protein for EP vs. CsP with 8.9-fold change (Figures 4.57(e)).

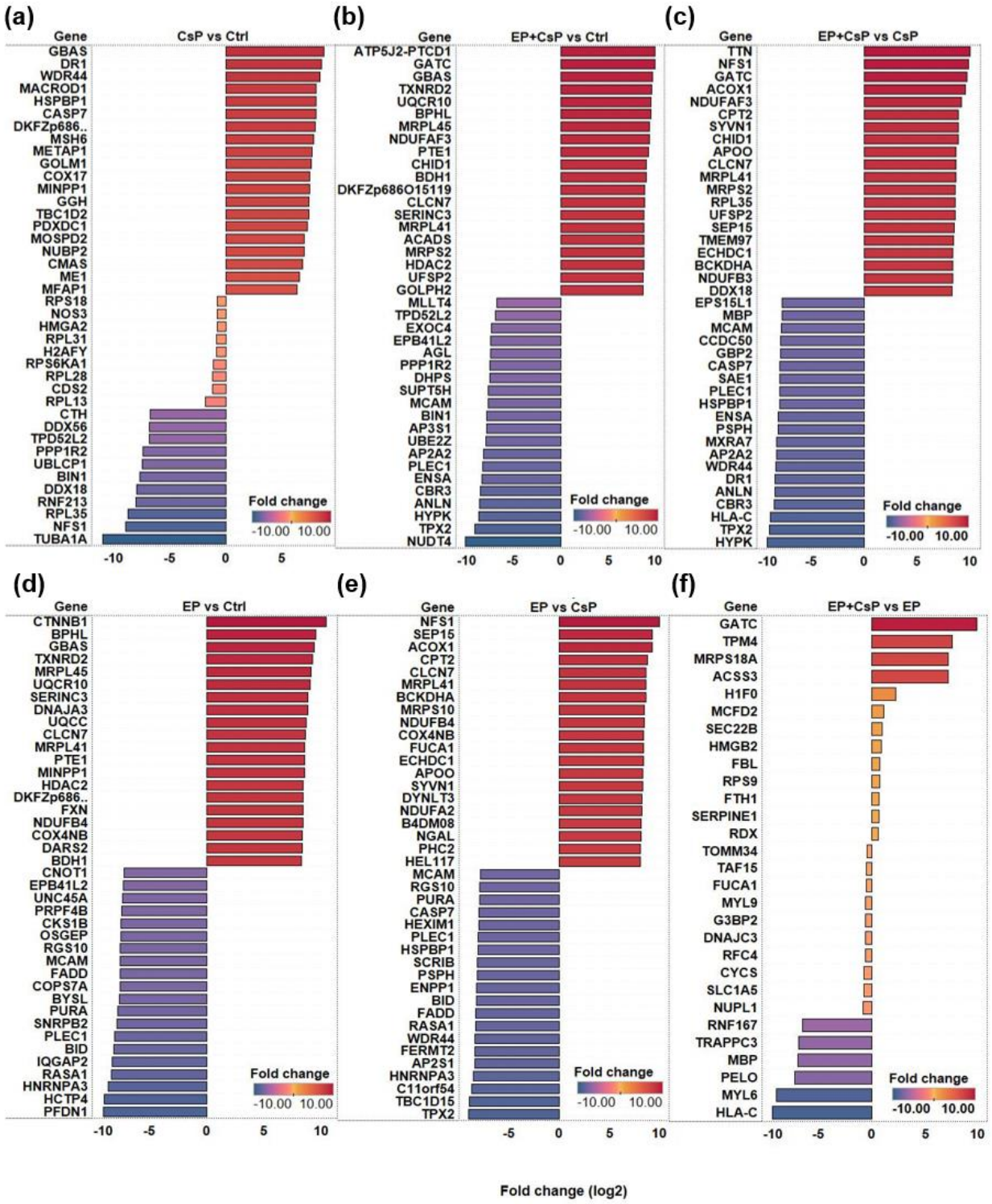

Figure 4.57: The top-20 upregulated and downregulated proteins in MDA-MB-231 cells at 4h of different treatments with their log2 fold change expression for six pairwise comparisons: (a) CsP vs. Ctrl, (b) EP+CsP vs. Ctrl, (c) EP+CsP vs. CsP, (d) EP vs. Ctrl, (e) EP vs. CsP (f) EP+CsP vs. EP. Here cisplatin (CsP) concentration of 100µM and EP of 1200V/cm, 100µs, 8 pulses at 1Hz were used.

We also studied the cellular localization of the top20 up- and downregulated proteins for EP+CsP vs. CsP, and their interaction. These results are shown in Figure 4.58. All top 20 upregulated proteins (Figure 4.58(a)) were localized in intracellular membrane-bound organelle and mainly in mitochondria. String interaction investigation demonstrated a minimal interaction among these proteins. Among top 20 downregulated proteins (Figure 4.58(b)), only 2 proteins were localized in clathrin coat of coated pit and remaining 18 proteins did not show enrichment for any cellular localization. Moreover, the interaction among these downregulated proteins is very limited.

The analysis of top 20 upregulated and downregulated indicates that compared to CsP, the EP+CsP treatment may enhance the activity of proteins in organelles, such as mitochondria, which actively participate in inducing apoptotic cell death.

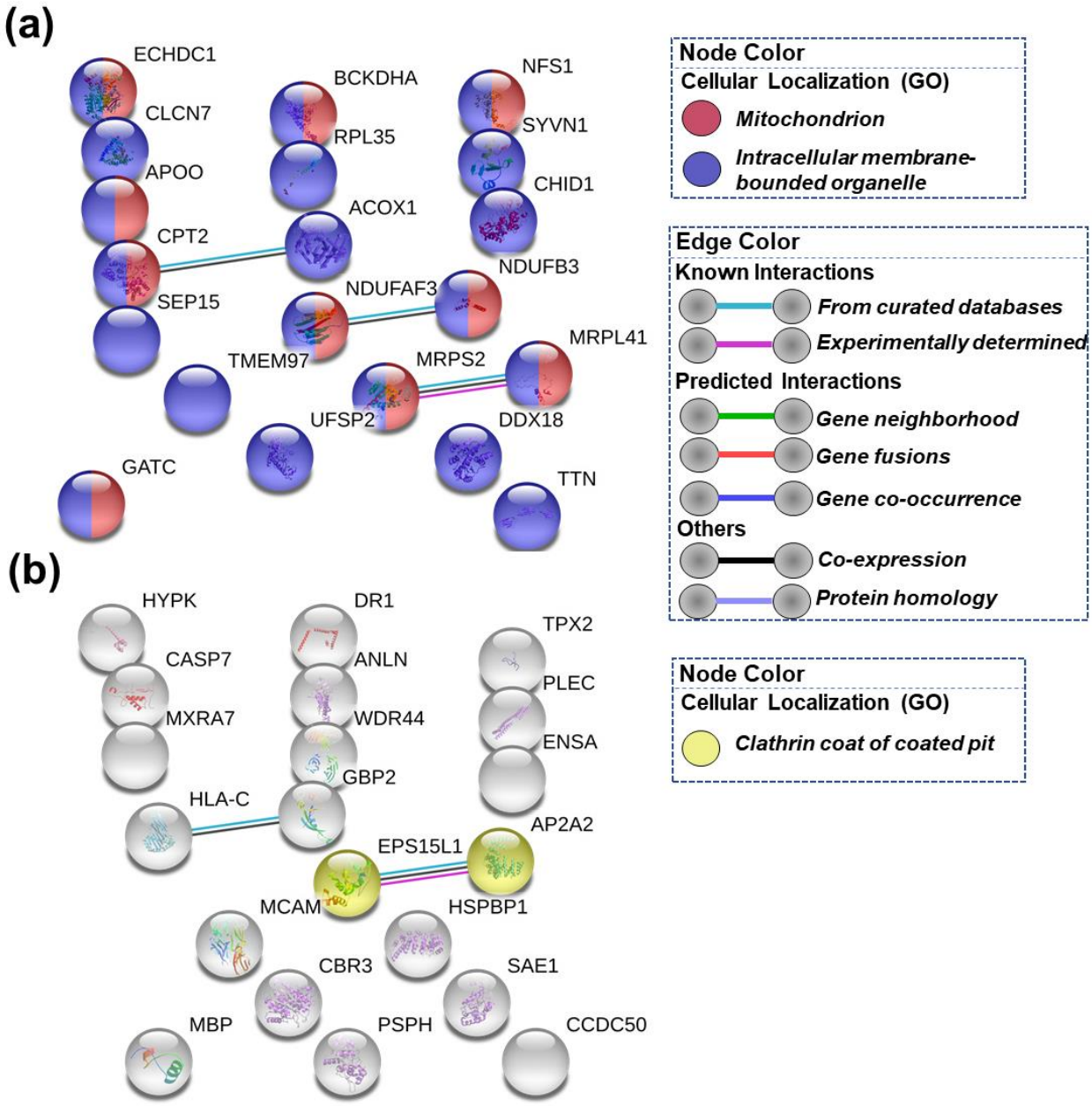

Figure 4.58: String interaction among top-20 significantly upregulated and downregulated proteins in MDA-MB-231 cells at 4h of treatment for EP+CsP vs CsP comparison group: (a) upregulated, (b) downregulated. The top-20 upregulated and downregulated proteins were uploaded to STRING (Szklarczyk et al., 2017) software to study the interaction and functional enrichment using evidence as meaning of network edge. The edge color in figure legend shows active interaction sources used in analysis, where the highest confidence (0.9) setting for minimum required interaction was used. Localization is represented with node color.

D. Functional annotation enrichment analysis of differentially expressed proteins

i. GO enrichment analysis of differentially expressed proteins

"Further, we classified all differentially expressed proteins using GO annotation analysis for cellular component and molecular functions (Figure 4.59(a) and (b)). EP affected a large number of proteins in the extracellular region, as well as in other cellular components, such as protein containing complexes, cell part, organelle (Figure 4.59(a)). For EP+CsP more proteins in membrane, cell part, organelle and macromolecular complexes assembly were upregulated. Molecular function analysis showed higher representation of proteins related to catalytic activity, binding, and structural molecule activity for both EP+CsP and EP (Figure 4.59(b)). However, proteins in molecular function regulator, transcription regulator activity, and molecular transduction activity were uniquely affected for EP, and more proteins related to signal transduction, antioxidant activity, and receptor activity were uniquely affected for EP+CsP. A number of proteins involved in the translational activity were downregulated and more proteins involved in the transport activity were upregulated in the EP+CsP treatment compared to CsP and Ctrl treatments" (Mittal, Aryal, et al., 2019).

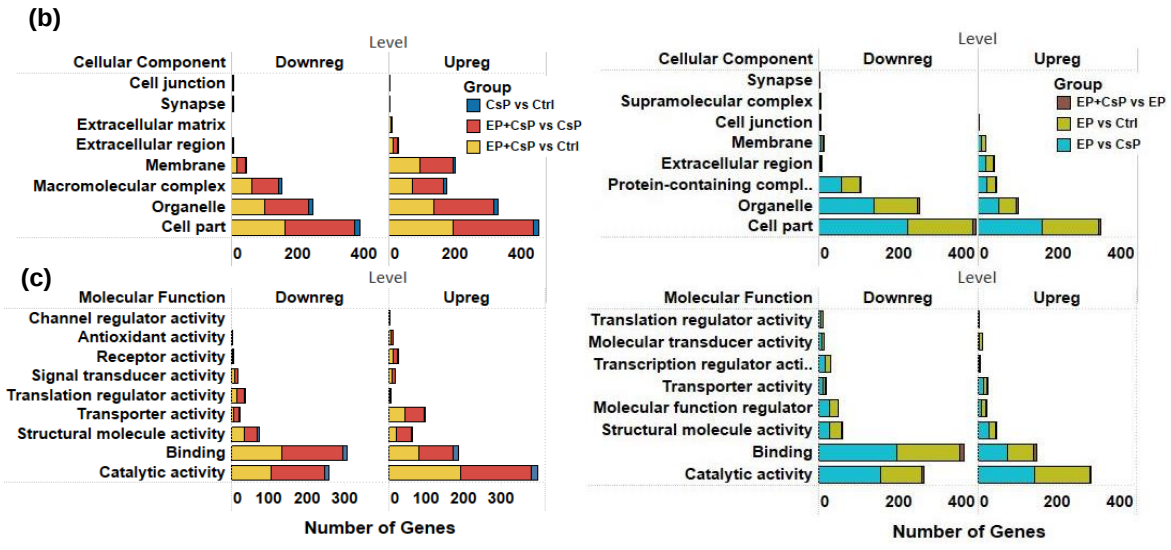

Figure 4.59: The gene ontology enrichment analysis for differentially expressed proteins for different comparison groups in MDA-MB-231 cells at 4h of treatments: (a) Cellular localization and (b) Molecular function. Here cisplatin (CsP) concentration of 100µM and EP of 1200V/cm, 100µs, 8 pulses at 1Hz were used. Proteins were uploaded to PANTHER (Mi et al., 2013) to obtain enrichment.

These observations indicate that EP+CsP treatment affects not only the membrane proteins, but the protein of multiple cellular components, which are involved in diverse molecular functions to produce a cell-wide impact.

ii. Pathway enrichment analysis of differentially expressed proteins

Figure 4.60 shows the results of pathway enrichment analysis for differentially expressed proteins. "The analysis of KEGG pathways for upregulated proteins (Figure 4.60(a)) showed enrichment of OXPHOS, TCA cycle, FA metabolism, aromatic AA (tryptophan) metabolism, calcium and peroxisome proliferator-activated receptor (PPAR) signaling in EP+CsP and EP as compared to the Ctrl or CsP. However, the number of upregulated proteins in these pathways were less for EP compared to EP+CsP, indicating the additional effect of CsP with EP. The lysosome, other glycan degradation, synthesis and degradation of ketone bodies, and ECM-receptor interaction pathways were upregulated in EP, but N-Glycan biosynthesis, FA metabolism, FA elongation, glycerolipid metabolism, biosynthesis of unsaturated FAs, calcium signaling, and ribosome pathways were upregulated only in EP+CsP compared to the Ctrl or CsP. Also, the expression of glutaminase (GLS) increased in EP+CsP and EP treatments compared to the Ctrl and CsP" (Mittal, Aryal, et al., 2019).

Moreover, we observed an upregulation of proteins in PPAR pathway. There was upregulation in long chain fatty acid transport protein 4 (SLC27A4/FATP4) protein for EP+CsP from CsP. The SLC27A4 is involved in the transportation of long-chain fatty acid across the cell membrane, suggesting that in addition to the membrane pore formation for increased transport, EP application may also enhance transport through upregulation of important transport proteins.

"We also observed an upregulation of the calcium signaling pathway proteins only in EP+CsP treated cells from CsP, including the expression of VDAC1, VDAC2, VDAC3 and stromal interaction molecule 1 (STIM1). The VDAC channel proteins facilitate the diffusion of metabolites, ions (including calcium ions) and small hydrophilic molecules across outer mitochondrial membrane and regulate metabolism and mitochondria functions (Shoshan-Barmatz, N. Maldonado, & Krelin, 2017)" (Mittal, Aryal, et al., 2019). The increased calcium concentration due to pro-apoptotic agents elevates the expression of VDAC1 (Shoshan-Barmatz, De, & Meir, 2017). Moreover, STIM1 functions as a calcium sensor and is implicated in the inflow of calcium from extracellular microenvironment (S. Yang, Zhang, & Huang, 2009). Upregulation of these

proteins uniquely for EP+CsP, but not for EP suggests that EP+CsP treatment could cause increase calcium influx into the cells to trigger cell death. Previous report also suggests such increase in intracellular calcium upon EP application (Hanna, Andre, et al., 2017). "Calcium release from endoplasmic reticulum also causes the redistribution of the endoplasmic reticulum calcium sensor STIM (Azimi, Roberts-Thomson, & Monteith, 2014). This links very well with the observed significant upregulation in protein processing in the endoplasmic reticulum pathway, which happens in response to the endoplasmic reticulum stress. It is previously shown that under stimulation, several unfolded and incompletely folded proteins accumulate in the ER lumen to trigger unfolded protein response (UPR), leading to endoplasmic reticulum stress and apoptosis (Luyan Shen et al., 2016)" (Mittal, Aryal, et al., 2019). These results highlight that EP+CsP treatment increases intracellular calcium concentration via increased inflow of calcium and its release from endoplasmic reticulum to cause calcium overload in cells, which produces ROS and triggers apoptosis (Kato & Nishitoh, 2015). Such release of calcium from endoplasmic reticulum and other organelles due to electrical pulse application is shown previously (Hanna, Denzi, Liberti, André, & Mir, 2017).

On the other hand, EP+CsP and EP treatments downregulated the pathways associated with enhanced cancer cell proliferation, migration, differentiation, evasion of cell death and apoptosis (Figure 4.60(b)). These pathways included MAPK, VEGF, and neurotrophin signaling pathways. The EP+CsP treatment uniquely downregulated proteins of hippo signaling, and biosynthesis of AAs pathways compared to Ctrl and CsP. On the contrary, EP treatment uniquely downregulated PPP, base excision repair, Toll-like receptor, T cell receptor, NOD-like receptor, and estrogen signaling pathways compared to Ctrl and CsP.

"The cell cycle pathway was downregulated only in EP+CsP but base excision repair, the pathway involved in the DNA repair throughout the cell cycle was downregulated only in EP. This indicates that presence of CsP is required to impact the cell cycle, and EP alone only slows down the DNA repair process, which is also consistent with the anti-proliferative effect of CsP, which induces cell cycle arrest in cancer cells (Velma, Dasari, & Tchounwou, 2016). An important protein, proliferating cell nuclear antigen (PCNA), which is involved in the repair of DNA damage caused by CsP was significantly downregulated in EP+CsP and EP treatments compared to the CsP (EP+CsP vs CsP - $\downarrow 2\times$, $P = 0.0003$; EP vs CsP - $\downarrow 1.7\times$, $P = 0.0071$) and Ctrl (EP+CsP vs Ctrl - $\downarrow 1.8\times$; $P = 0.0001$; EP vs Ctrl - $\downarrow 1.5\times$, $P = 0.012$). The effect of EP+CsP were larger on PCNA

compared to EP, and may help overcome the CsP resistance, as EP with CsP may increasingly stabilize CsP induced genomic DNA damage (Lingeman, Hickey, & Malkas, 2014). Additionally, downregulated proteins included those in the regulation of actin cytoskeleton, focal adhesion, proteoglycans in cancer, purine metabolism, glycolysis, AA biosynthesis, proteasomes, and ubiquitin mediated proteolysis" (Mittal, Aryal, et al., 2019).

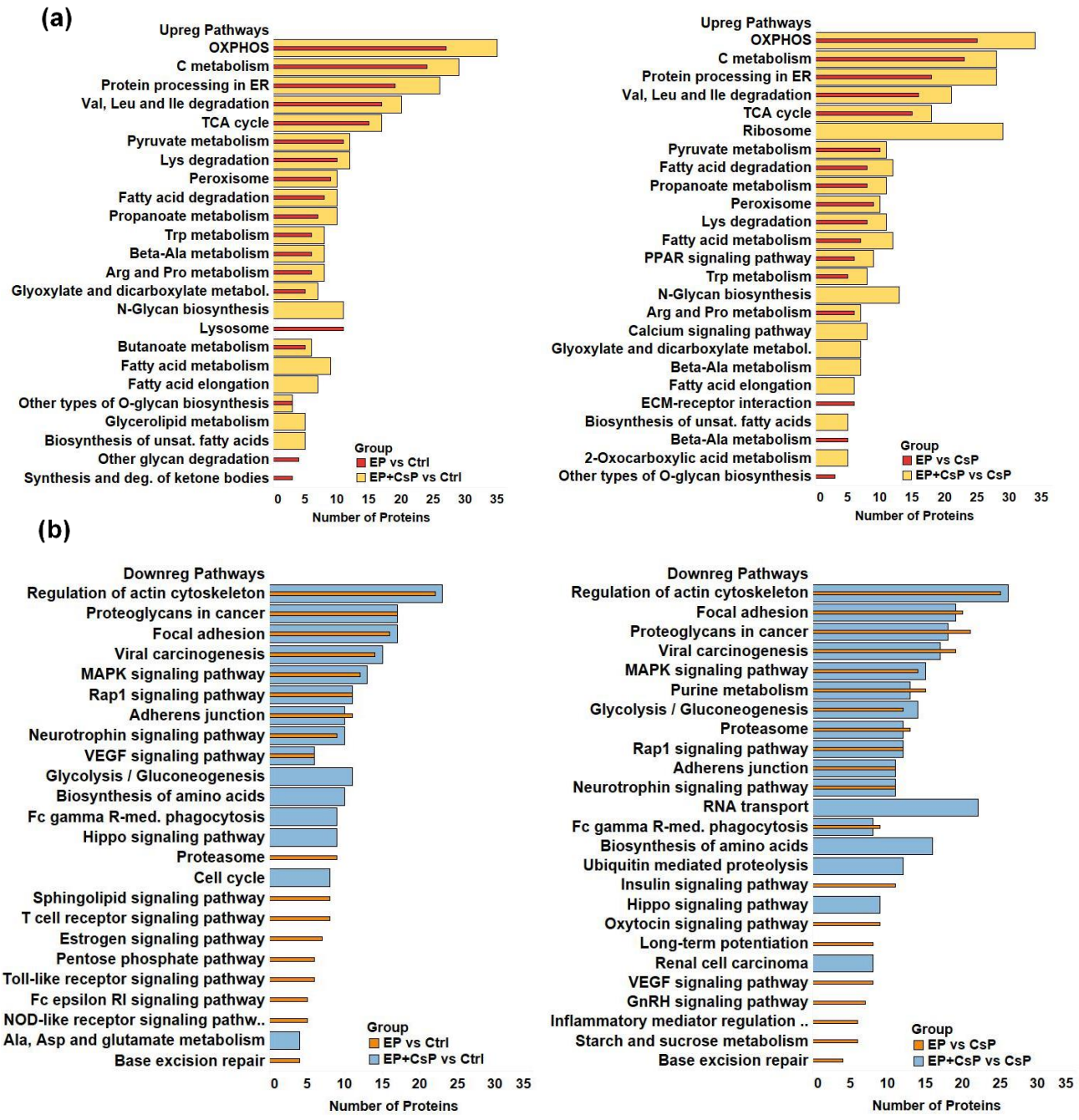

Figure 4.60: KEGG pathways enriched for significantly (a) upregulated and (b) downregulated proteins in MDA-MB-231 cells at 4h of various treatments using DAVID 6.8. Here cisplatin (CsP) concentration of 100µM and EP of 1200V/cm, 100µs, 8 pulses at 1Hz were used. "Abbreviations: Ala-Alanine, Asp-Aspartate, Deg-Degradation, Isoleucine-Ile, Leu-Leucin, Lys-Lysine, Trp-Tryptophan, Val-Valine" (Mittal, Aryal, et al., 2019).

E. Metabolic switch in TNBC cells upon EP+CsP treatment

"The most prominent shift in cellular metabolism was observed for glycolysis, TCA cycle and OXPHOS. We observed downregulation of key glycolysis pathway proteins but upregulation of TCA cycle and OXPHOS. These observations highlight a switch in the metabolism from glycolysis to cellular respiration, with a larger dependency on oxidative energy substrates for energy production for TNBC cells treated with EP+CsP and EP" (Mittal, Aryal, et al., 2019).

i. Downregulation of glycolysis proteins

Among the 28 glycolytic proteins identified in this study, EP+CsP downregulated 11 and 14 of these proteins compared to Ctrl and CsP treatments, respectively. On the other hand, EP downregulated only 12 glycolytic proteins compared to CsP, and no enrichment for glycolysis pathways was found for proteins downregulated in EP compared to Ctrl.

Majority of key glycolysis pathway proteins were downregulated in accord with earlier reports (Dennison et al., 2013; Gong et al., 2019; Grandjean et al., 2016; Markert et al., 1963; McCleland et al., 2012; Miah et al., 2017; Porporato et al., 2011; S. Sun et al., 2015; Vergara et al., 2013; Whitaker-Menezes et al., 2011). "For EP+CsP and EP treatments, the glucose metabolism proteins, notably ALDOA, ENO1, PGK1, LDHA, LDHB were all downregulated, compared to Ctrl and CsP, and acyl-CoA synthetase short-chain family member 2 (ACSS2), compared to CsP. The expression of ACSS2 was reported to be inversely correlated with survival in a cohort of 154 cases of TNBC, indicating that it may be an effective anticancer target (Alderton, 2015). The ENO1 is a potential biomarker of TNBC, and its function in glycolysis is consistent with the distinct TNBC metabolism compared to other breast cancer subtypes (Miah et al., 2017; Vergara et al., 2013)" (Mittal, Aryal, et al., 2019).

The LDHA levels correlate with the TNBC malignancy its inhibition prevents brain metastasis (Dong et al., 2017). LDHA is overexpressed in various cancers but LDHB is uniquely overexpressed in basal-like TNBC and works as an essential gene, as its knockdown causes a significant loss in TNBC cell proliferation and arrests growth in mouse tumors (Dennison et al., 2013; McCleland et al., 2012). "The increased expression of LDHB correlates to significantly poor clinical outcomes (McCleland et al., 2012)" (Mittal, Aryal, et al., 2019). LDHB also plays a critical role in "reverse Warburg effect" (Dennison et al., 2013; Markert et al., 1963; McCleland et al.,

2012; Porporato et al., 2011; Whitaker-Menezes et al., 2011). Considering the distinct and strong predilection for these key glycolytic enzymes in TNBC, their downregulation upon EP+CsP treatment makes MDA-MB-231 TNBC cells highly susceptible to this treatment (Gong et al., 2019; Grandjean et al., 2016; S. Sun et al., 2015). Figure 4.61 visualizes key significantly downregulated proteins mapped to the glycolysis pathways for EP+CsP vs. CsP comparison, where degree of shading represents fold change.

ii. Upregulation of TCA cycle and OXPHOS proteins

Even with suppression in glycolysis and conversion reaction of lactate to pyruvate, we observed increased activity of TCA cycle and OXPHOS. This upregulation in TCA cycle could be supported by the upregulation in multiple supplemental pathways (FA degradation/metabolism/elongation, AA metabolism, glyoxylate and dicarboxylate, PPAR, peroxisome and tryptophan metabolism), which generate pyruvate and various intermediates, such as acetyle COA and oxaloacetate to supply the TCA cycle.

In addition of participating in the FA transport, PPAR pathway supports FA degradation and metabolism, which could stimulate acetyl COA generation to fuel TCA cycle. Similarly, peroxisome pathway participates in breaking down of FA to supply TCA cycle and also to generate cell membrane. This elevation in peroxisome pathway could also be due to the need of membrane regeneration following electroporation. Moreover, peroxisome pathway can produce H_2O_2 ROS to activate apoptosis (Gray, 2001).

These elevated mitochondrial metabolic activities (TCA Cycle and OXPHOS) in MDA-MB-231 cells could also be credited to the stress response as cells strive to produce energy via different sources since glycolysis is suppressed. This elevated OXPHOS could generate ROS to trigger a mitochondrion mediated intrinsic apoptotic pathway of cell death.

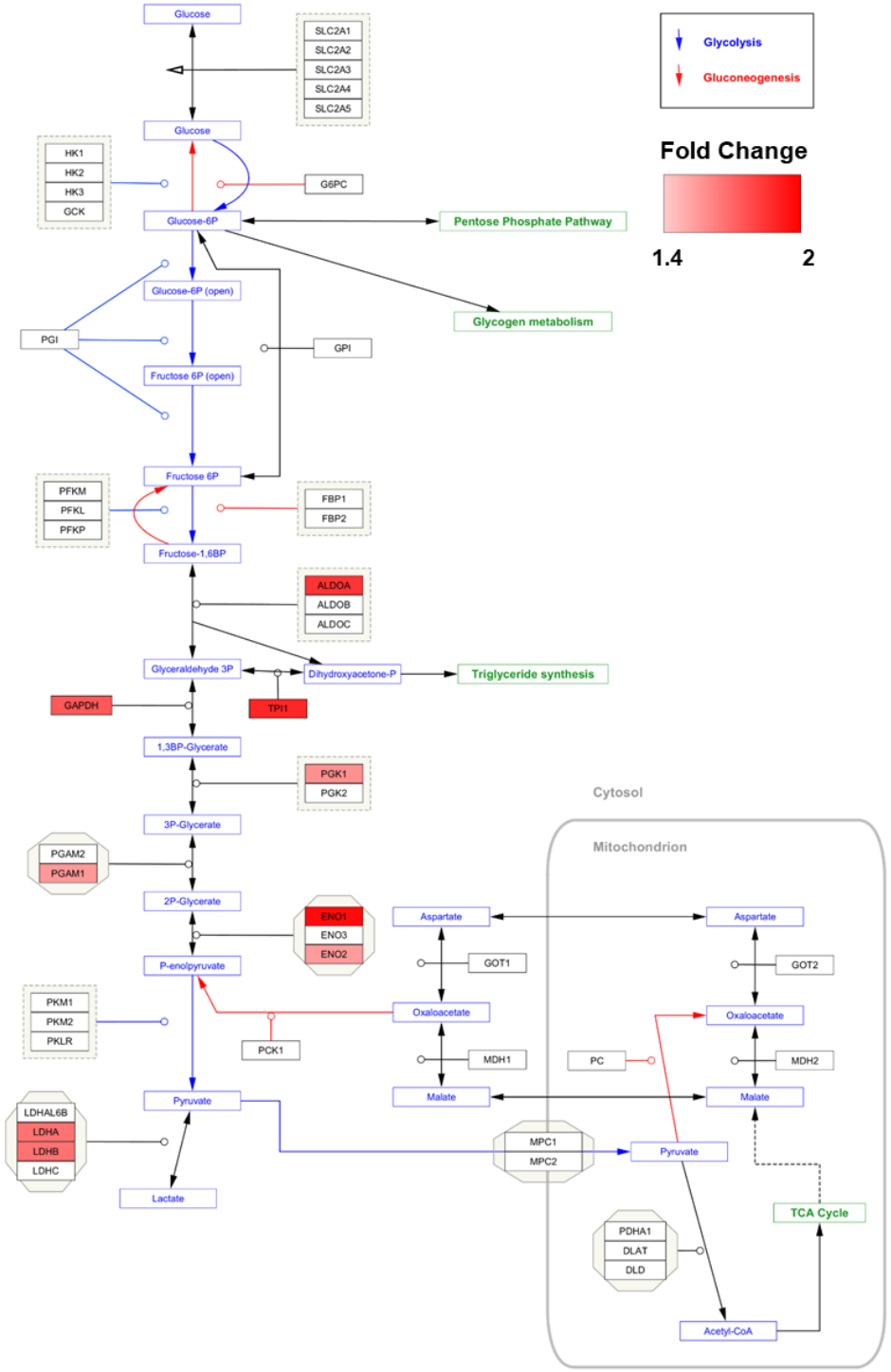

Figure 4.61: The main glycolysis pathway proteins which are significantly downregulated in EP+CsP vs CsP in MDA-MB-231 TNBC cells at 4h of treatment. Here cisplatin (CsP) concentration of 100μM and EP of 1200V/cm, 100μs, 8 pulses at 1Hz were used. Proteins enriched with "glycolysis/gluconeogenesis" term in KEGG (Kanehisa & Goto, 2000) were fed to Cytoscape 3.6.1 (Paul Shannon et al., 2003) and mapped to the glycolysis pathway in WikiPathway app (Kutmon et al., 2014), where the extend of shading represents the fold change.

F. The differences in the effects of EP+CsP and EP in TNBC cells

Table 4.11 shows the expression of 29 proteins significantly regulated in EP+CsP from EP. Among these, "the key proteins were replication factor C subunit 4 (RFC4), Ras GTPase-activating protein-binding protein 2 (G3BP2), radixin (RDX), 40S ribosomal protein S9 (RPS9), 28S ribosomal protein S18a, mitochondrial (MRPS18A). Interestingly, high MS/MS spectral counts were observed for DnaJ homolog subfamily C member 3 (DNAJC3), AA transporter (SLC1A5), cytochrome c (CYCS), rRNA 2-O-methyltransferase fibrillarin (FBL), Ferritin (FTH1), Myosin regulatory light polypeptide 9 (MYL9), Mitochondrial import receptor subunit TOM34 (TOMM34), indicating high abundance of these differentially expressed proteins in EP+CsP compared to EP. A String interaction enrichment analysis (Figures 4.62(a-d)) show uniquely regulated proteins for EP+CsP and EP compared to CsP. There were more upregulated proteins in the mitochondrion for EP+CsP, while EP had more proteins in the endoplasmic reticulum (Figures 4.62(a) and (b)). In case of downregulated unique proteins, EP+CsP affected more cytosolic proteins, while a large number of nucleus proteins were downregulated by EP (Figures 4.62(c) and (d)).

Cancer cells harbor inherent resistance to ROS induced apoptosis (H. Lu, Li, Lu, Qiu, & Fan, 2016), which can significantly compromise the effectiveness of this EP-based therapy. Compared to EP, EP+CsP downregulated SLC1A5, which may sensitize MDA-MB-231 to ROS induced apoptosis (H. Lu et al., 2016), and lead to a sustained effect of EP+CsP, as observed in this study. The RFC4, which promotes DNA double stranded break repair to cause resistance (X. C. Wang et al., 2019), was also downregulated for EP+CsP from EP, indicating that DNA repair could be slower in EP+CsP treated cells. In addition, the expression of G3BP2, which is implicated in the maintenance of breast tumor-initiating cells (TICs) (N. Gupta et al., 2017), was downregulated for EP+CsP, compared to EP. These results specifically highlight the differences in the protein expression profiles for EP+CsP and EP treatments, and suggest that the effects of EP+CsP treatment are more comprehensive, compared to EP" (Mittal, Aryal, et al., 2019).

Table 4.11: The significantly up- and downregulated for EP+CsP from EP. The log2 fold change for these proteins and their spectral counts for triplicates in both treatments are shown. Here cisplatin (CsP) concentration of 100µM and EP of 1200V/cm, 100µs, 8 pulses at 1Hz were used.

S.N.	Uniprot Accession No.	Protein Name	MS/MS EP			MS/MS EP+CsP			Gene Name	Fold change (EP+CsP - EP)	P Value	Regulation
			1	2	3	1	2	3				
1	O43716	Glutamyl-tRNA(Gln) amidotransferase subunit C, mitochondrial	4	3	3	3	5	4	GATC	9.7	1.3×10^{-5}	Up
2	K7ELP0	Tropomyosin alpha-4 chain	0	1	2	3	2	2	TPM4	7.4	1.6×10^{-7}	Up
3	Q5QPA5	28S ribosomal protein S18a, mitochondrial	0	1	0	2	4	1	MRPS18A	7.1	1.9×10^{-5}	Up
4	A0A0B4J1R2	Acyl-CoA synthetase short-chain family member 3, mitochondrial	4	2	0	6	3	6	ACSS3	7.0	5.9×10^{-7}	Up
5	P07305	Histone H1.0	2	2	2	6	5	5	H1F0	2.1	0.02	Up

Table 4.11 continued

6	Q8NI22	Multiple coagulation factor deficiency protein 2	8	5	3	7	5	9	MCFD2	1.1	0.03	Up
7	I1VE18	SEC22 vesicle trafficking protein B	3	2	2	6	3	4	SEC22B	0.9	0.03	Up
8	Q5U071	High mobility group protein B2	3	9	5	7	6	3	HMGB2	0.8	0.02	Up
9	P22087	rRNA 2-O-methyltransferase fibrillarin	10	13	8	18	11	10	FBL	0.7	0.048	Up
10	A0A024R4M0	40S ribosomal protein S9	8	8	6	13	12	14	RPS9	0.7	0.02	Up
11	A0A024R525	Ferritin	7	10	8	25	15	14	FTH1	0.6	0.02	Up
12	P05121	Plasminogen activator inhibitor 1	6	4	3	6	10	4	SERPINE1	0.6	0.04	Up
13	B0YJ88	Radixin	4	4	6	6	4	2	RDX	0.6	0.045	Up
14	A0A090MEW7	HLA class I antigen	2	7	3	2	1	2	HLA-C	-9.3	2.1×10^{-5}	Down
15	G8JLA2	Myosin light polypeptide 6	7	6	6	2	4	4	MYL6	-8.9	8.6×10^{-6}	Down

Table 4.11 continued

16	B3KPC1	Protein pelota homolog	2	2	2	2	1	2	PELO	-7.2	3.6×10^{-6}	Down
17	J3KS94	Myelin basic protein	2	2	1	0	0	0	MBP	-6.9	2.7×10^{-9}	Down
18	O43617	Trafficking protein particle complex subunit 3	5	3	2	1	2	1	TRAPPC3	-6.9	2.03×10^{-8}	Down
19	I3L0L6	E3 ubiquitin-protein ligase RNF167	2	2	3	0	0	1	RNF167	-6.5	1.4×10^{-7}	Down
20	B4E0K0	Nucleoporin p58/p45	5	5	4	5	5	2	NUPL1	-0.9	0.01	Down
21	Q71UA6	Amino acid transporter	12	12	14	14	9	10	SLC1A5	-0.8	0.01	Down
22	C9JFR7	Cytochrome c	12	13	9	7	8	12	CYCS	-0.8	0.02	Down
23	P35249	Replication factor C subunit 4	6	2	2	9	4	1	RFC4	-0.7	0.01	Down
24	A8KA82	DnaJ homolog subfamily C member 3	24	22	22	12	11	20	DNAJC3	-0.7	0.049	Down
25	Q9UN86	Ras GTPase-activating protein-binding protein 2	4	2	7	7	4	5	G3BP2	-0.6	0.03	Down
26	P24844	Myosin regulatory light polypeptide 9	6	11	7	6	5	6	MYL9	-0.6	0.02	Down
27	P04066	Tissue alpha-L-fucosidase	2	2	5	5	2	2	FUCA1	-0.5	0.02	Down
28	Q92804	TATA-binding protein-associated factor 2N	4	8	4	7	6	7	TAF15	-0.5	0.01	Down
29	Q15785	Mitochondrial import receptor subunit TOM34	9	13	5	6	8	7	TOMM34	-0.5	1.2×10^{-5}	Down

Figure 4.62: String interaction among most significantly but uniquely up- and downregulated (|fold change| ≥ 2) proteins for EP+CsP and EP, compared to CsP in MDA-MB-231 cells at 4h of treatment: (a) Uniquely upregulated for EP+CsP vs CsP, (b) Uniquely upregulated for EP vs. CsP, (c) Uniquely downregulated for EP+CsP vs. CsP, (d) Uniquely downregulated in EP vs CsP. Here cisplatin (CsP) concentration of 100µM and EP of 1200V/cm, 100µs, 8 pulses at 1Hz were used. The expression of proteins in EP+CsP and EP were compared to CsP to identify the proteins significantly regulated with at least two-fold (|fold change| ≥ 2) - identified 339 and 348 proteins in EP+CsP and EP, respectively. Among these proteins, proteins common in both EP+CsP and EP were discarded to identify uniquely regulated proteins - identified 154 and 164 unique proteins in EP+CsP and EP, respectively. The unique proteins were fed to STRING (Szklarczyk et al., 2017) to study the interaction and functional enrichment using evidence as meaning of network edge. The edge color in figure legend shows active interaction sources used in analysis, where the medium confidence (0.4) setting for minimum required interaction was used with kmeans clustering (3 clusters). Localization is represented with node color. The query proteins and their first shell interactions are shown by colored nodes. Second shell interaction is shown by white nodes. The unique upregulated proteins for EP+CsP were predominantly mitochondrial. More endoplasmic reticulum proteins were upregulated for EP. Among the uniquely downregulated proteins, more proteins were cytosolic for EP+CsP treatment, while a greater fraction of proteins were from nucleus for EP treatment.

Figure 4.62 continued

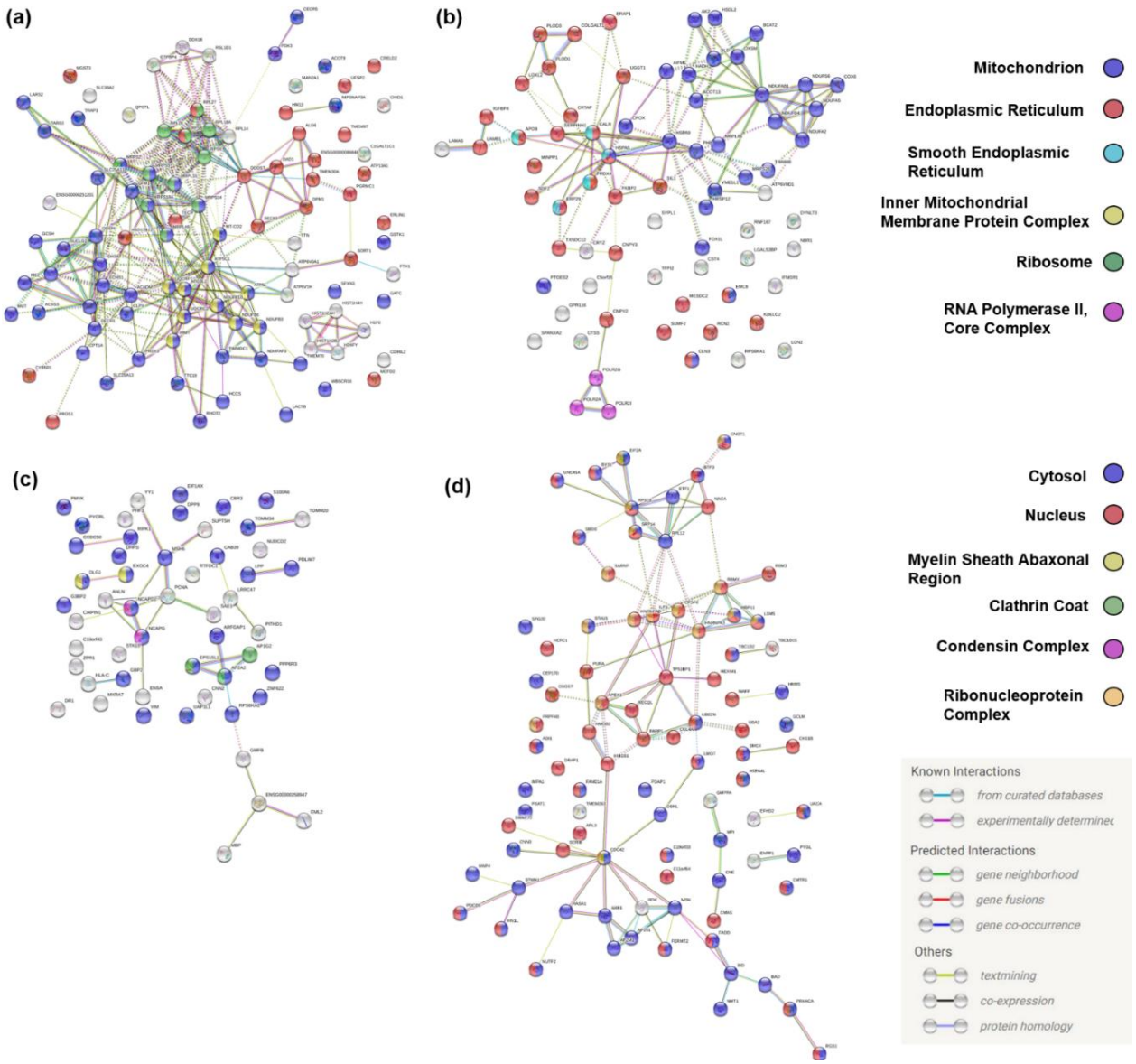

G. Validation of proteomics results

i. Correlation between protein and mRNA levels of key metabolic genes

"To determine whether changes in the protein levels correspond to the changes at the transcript levels, we performed real time quantitative PCR (qPCR) experiments after 4h of treatment for Ctrl, CsP and EP+CsP samples. Figure 4.63 shows mRNA level expressions of ENO1, LDHB, and GLS genes at 4h of the treatments, and the comparison of the protein level changes observed at 4h. The mRNA or protein levels were normalized with mRNA/protein expression levels of the Ctrl (level 1). The mRNA levels of ENO1 and LDHB genes decreased to 0.19 and 0.15 in EP+CsP as compared to the Ctrl, while they were 0.67 and 1.33 for CsP. In comparison, the protein expression of ENO1 and LDHB genes in EP+CsP decreased to 0.56 and 0.61 from the Ctrl, while they were 1.10 and 1.01 for CsP. Though we observed some minor up/down regulation in the mRNA levels of ENO1 and LDHB genes for CsP compared to Ctrl, no statistically significant difference was found, as also observed at the protein level. On the other hand, we observed ~3.5-fold increase in the mRNA level expression of GLS in EP+CsP and CsP, while it also increased by 2.08-fold from Ctrl and 1.8-fold from CsP, at the protein level. Overall, the mRNA level expressions of ENO1, LDHB and GLS correlate well with the protein level expressions. The ENO1 and LDHB mRNAs downregulation in EP+CsP suggest that the key glycolytic enzymes are regulated at the transcription level, which translates to proportional changes observed at the protein level. Increased expression in GLS at the mRNA level and protein level is also consistent with the metabolic shift observed in this study. GLS converts glutamine to glutamate to generate α-ketoglutarate (αKG), which serves as a fuel to the TCA cycle" (Mittal, Aryal, et al., 2019).

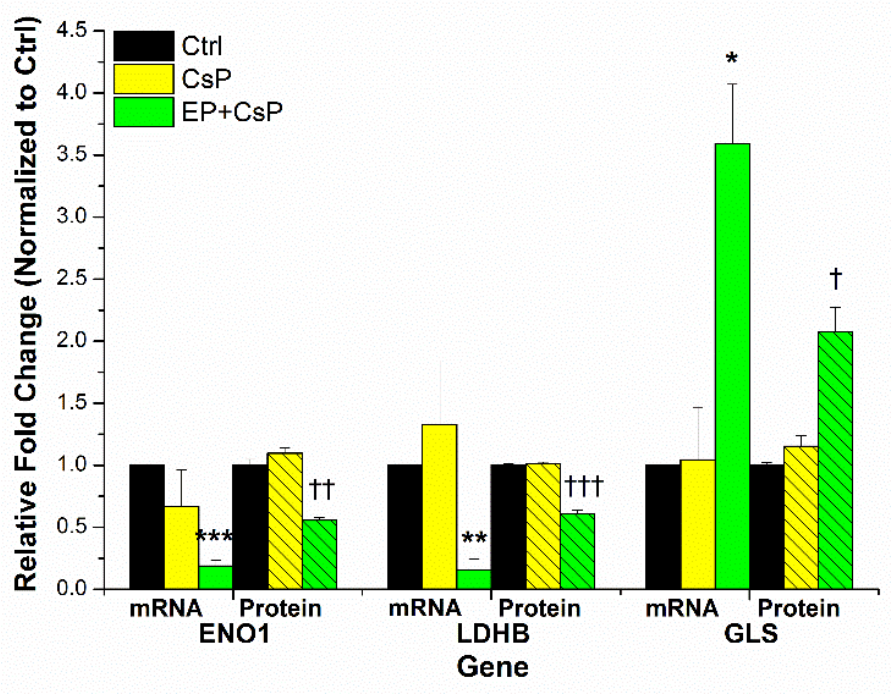

Figure 4.63: (a) The mRNA and protein expression levels of various genes in MDA-MB-231 cells at 4h of different treatments: ENO1, LDHB, and GLS. Here cisplatin (CsP) concentration of 100µM and EP of 1200V/cm, 100µs, 8 pulses at 1Hz were used. The relative mRNA levels were calculated utilizing ΔΔCq approach on qPCR data using glyceraldehyde 3-phosphate dehydrogenase (GAPDH) as the internal standard. Here protein levels were extracted from proteomics data. Significant difference for mRNA (*$P < 0.05$) and protein (†$P < 0.05$) levels was calculated from Ctrl. The results include data from experiments done in triplicate, where error bars represent standard error.

Moreover, we performed immunoblotting to validate the upregulated expression of GLS. These results are shown in Figure 4.64 for different treatment conditions, which are reported relative to Ctrl (level 1). The GLS expression was ~1 for Cur, not significantly different from Ctrl. The GLS expression increased by 6-fold for EP+CsP treatment, significantly different from Ctrl and CsP both. This increase in GLS levels agrees with the increased mRNA and protein levels of GLS.

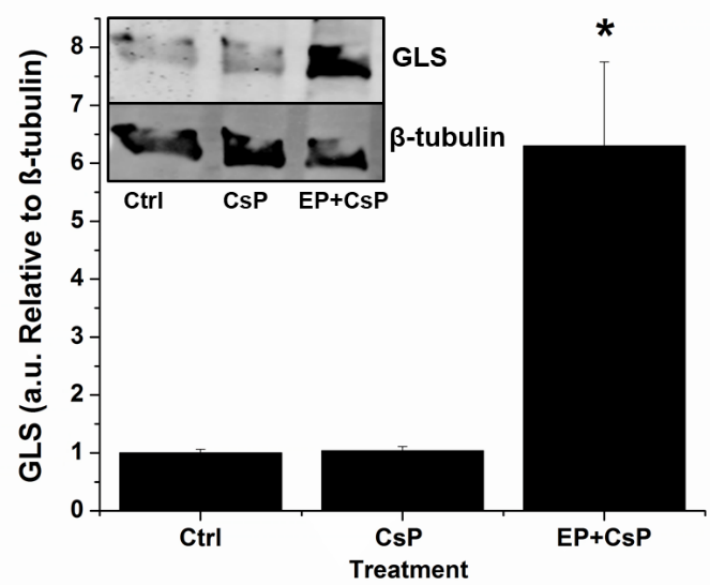

Figure 4.64: GLS protein expression at 4h of different treatments in MDA-MB-231 cells. The inset shows typical immunoblots of GLS and β-tubulin (loading control). The bar graph shows the quantification of GLS blots with respect to β-tubulin and control (control level=1). Here cisplatin (CsP) concentration of 100μM and EP of 1200V/cm, 100μs, 8 pulses at 1Hz were used. Significant difference from Ctrl - *$P < 0.05$. The results include data from experiments done in triplicate, where error bars represent standard error.

ii. Measurement of ROS levels and apoptosis

Figure 4.65 shows the average Lum representing the H_2O_2 ROS expressions in MDA-MB-231 cells at 4h for different treatments. Compared to Lum of Ctrl at 3852, CsP treatment caused a marginal and non-significant increase in Lum to 3873. For EP treatment, the Lum was 4789, a 1.2-fold increase in H_2O_2 levels from Ctrl. The Lum was highest at 5021 for EP+CsP treatment, which was 1.3× significantly higher from H_2O_2 levels of Ctrl. "These results indicate that the treatment with EP+CsP and EP increases ROS production in TNBC cells to cause oxidative stress inducing the cell death" (Mittal, Aryal, et al., 2019). These results correlate well with previous studies, where EP induced ROS generation (Benov, Antonov, & Ribarov, 1994; Gabriel & Teissie, 1994).

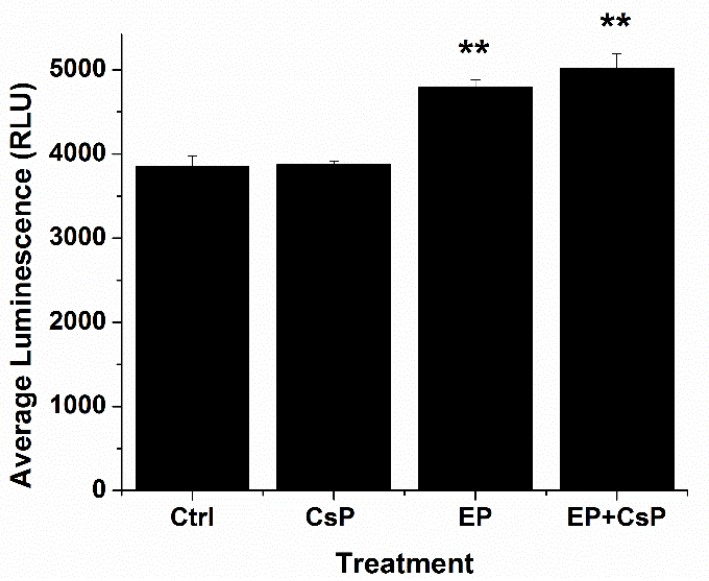

Figure 4.65: The levels of H_2O_2 reactive oxygen species at 4h of different treatments in MDA-MB-231 cells at 4h (N = 5). Here cisplatin (CsP) concentration of 100µM and EP of 1200V/cm, 100µs, 8 pulses at 1Hz were used. $^{**}P<0.005$ indicates significant difference from Ctrl. The results include data from experiments done with five replicates, where error bars represent standard error.

Cell death may follow apoptosis, a programmed cell death pathway, or necrotic pathway of cell death, a toxic and inflammatory process in response of external insult, which results into swelling and rupture of cells (Elmore, 2007). Therefore, we analyzed if the cell death followed the apoptotic and/or necrotic pathway upon EP+CsP treatment, using flowcytometry. The flowcytometric assessment of live, early apoptotic, late apoptotic, and necrotic fraction of cells for various treatments is shown in Figure 4.66. "The EP+CsP treatments reduced the fraction of live cells to 16 and 19% from 86% in Ctrl or CsP. The fraction of cells in the late apoptosis phase increased significantly to 69% from 6% in Ctrl and CsP. There was also an increase of necrotic cell population to 5% from 0.5% in the Ctrl and CsP. We observed that in EP+CsP, a total of 76% of cells were going through apoptosis, compared to only 5% undergoing necrosis. Similar behavior was also observed for the EP treated cells, where the apoptosis was prominent than necrosis with 73% of cells in late apoptosis, compared to 4% in necrosis. This indicates that EP+CsP and EP treatments induce apoptosis in majority of MDA-MB-231 cells, while causing necrosis in minority cell population to cause cell death. Thus, EP with and without CsP increases

the production of ROS to cause oxidative stress and induces the apoptosis" (Mittal, Aryal, et al., 2019).

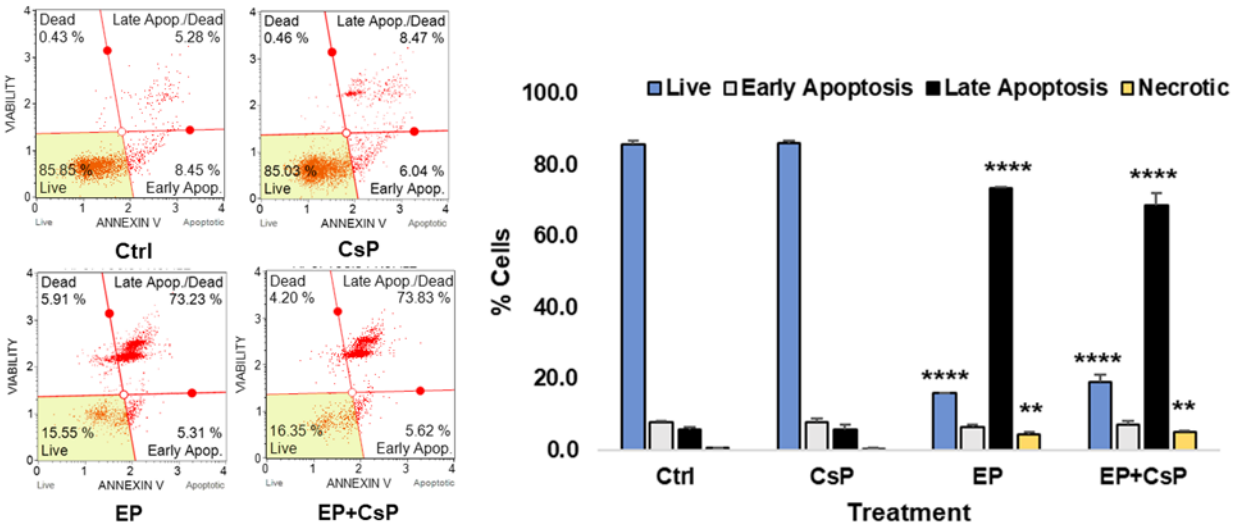

Figure 4.66: Apoptosis profile of MDA-MB-231 cells following 4h of various treatments. Here cisplatin (CsP) concentration of 100µM and EP of 1200V/cm, 100µs, 8 pulses at 1Hz were used. **P<0.005, ****P<0.00005 - indicate significant difference from Ctrl. The results include data from experiments done in triplicate, where error bars represent standard error.

In summary, these results suggest that EP+CsP treatment can modify the MDA-MB-231 cell metabolism by targeting glycolysis and inducing a shift towards TCA cycle and OXPHOS, leading to excessive ROS production to trigger mitochondria mediated apoptosis pathway utilizing the crosstalk among multiple metabolic, calcium, and ROS signaling pathways.

4.4 The impact of selection criterion on the results of proteomics analysis

In our proteomics studies discussed in sections 4.2 and 4.3, proteins with non-zero intensity (LFQ $\neq 0$) in at least two of the three biological replicates with ≥2 spectral (MS/MS) counts were selected from the raw data for the analysis. When we have three replicates for each treatment, a protein could be considered to be expressed in a treatment based on the minimum number of replicates the protein is expressed in (LFQ $\neq$ 0 and MS/MS $\geq$ 2). Therefore, three different selection criteria are possible (A, B, and C), as shown in Figure 4.67. In sections 4.2 and 4.3, we used the selection criterion B - the protein was considered to be expressed in a treatment, if it was expressed in at least two replicates of the three replicates (LFQ $\neq$ 0 and MS/MS $\geq$ 2 for $\geq$ 2 replicates). The selection criterion B was used to classify the proteins in each treatment. These proteins were used to identify differentially regulated proteins in various treatment comparisons. The differentially regulated proteins were then used to study the mechanisms using KEGG pathway and GO function, process, and localization enrichment analyses.

To investigate, if our selection criterion introduced a bias in our analysis and influenced the results, we compared the outcomes from different possible selection criteria (Figure 4.67). For this purpose, we used the TurNP proteomics study data (as discussed in detail in section 4.2.3) and analyzed it for all three different possible selection criteria.

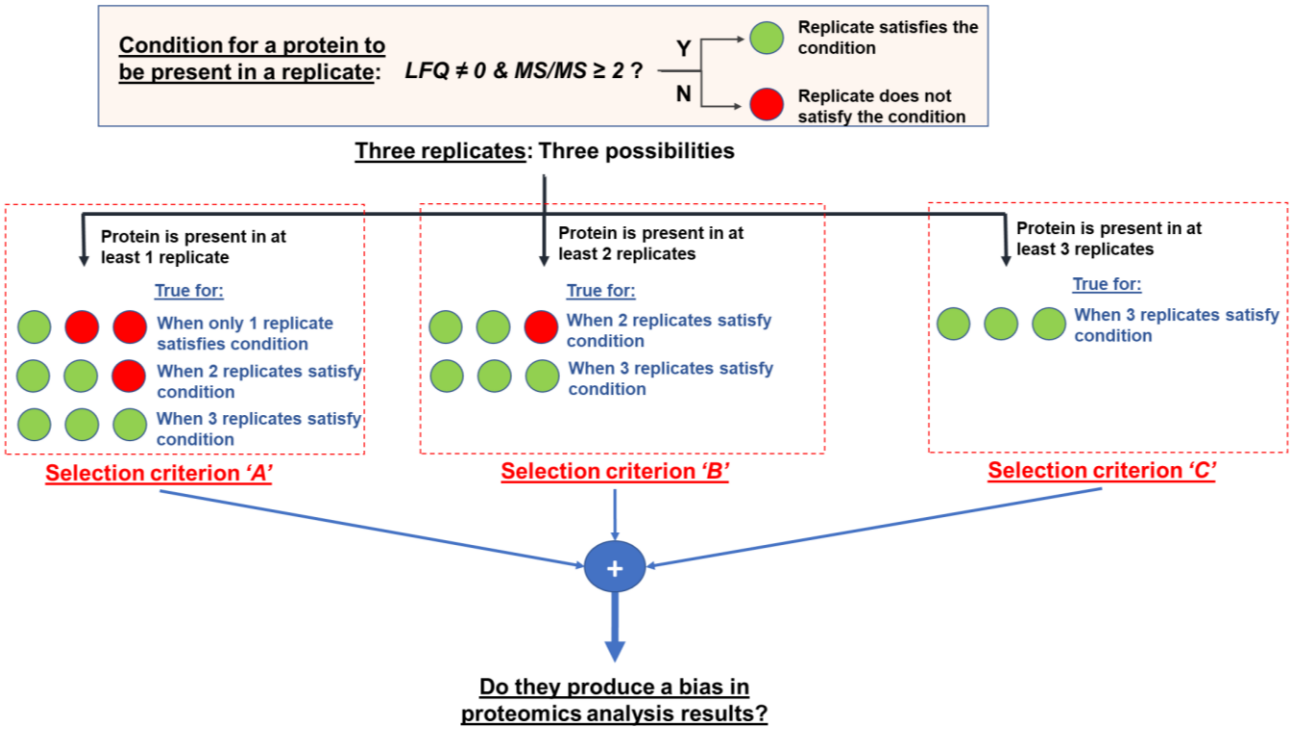

Figure 4.67: Three different selection criteria are possible, based on the minimum number of replicates a protein is expressed: LFQ ≠ 0 and MS/MS ≥ 2.

4.4.1 The impact of selection criteria on the distribution of proteins in different treatments

To study the impact of selection criteria on the number of proteins in various treatment groups, we classified the common and unique proteins for three criteria in each treatment group. These results are shown in Figure 4.68, demonstrating the commonly and uniquely expressed proteins in various treatments. The highest count of 3049 proteins was recorded for the selection criterion A (Figure 4.68(a)), while the lowest number of 2072 proteins were recorded observed for the selection criterion C (Figure 4.68(c)). The protein count was 2426 for the selection criterion B (Figure 4.68(b)). The results indicate that the selection criteria can greatly influence the number of selected proteins form the raw data. These results are expected, as higher number proteins from raw data would qualify the threshold of the liberal selection criterion A, while the lowest number of proteins qualify the threshold of the conservative selection criterion C.

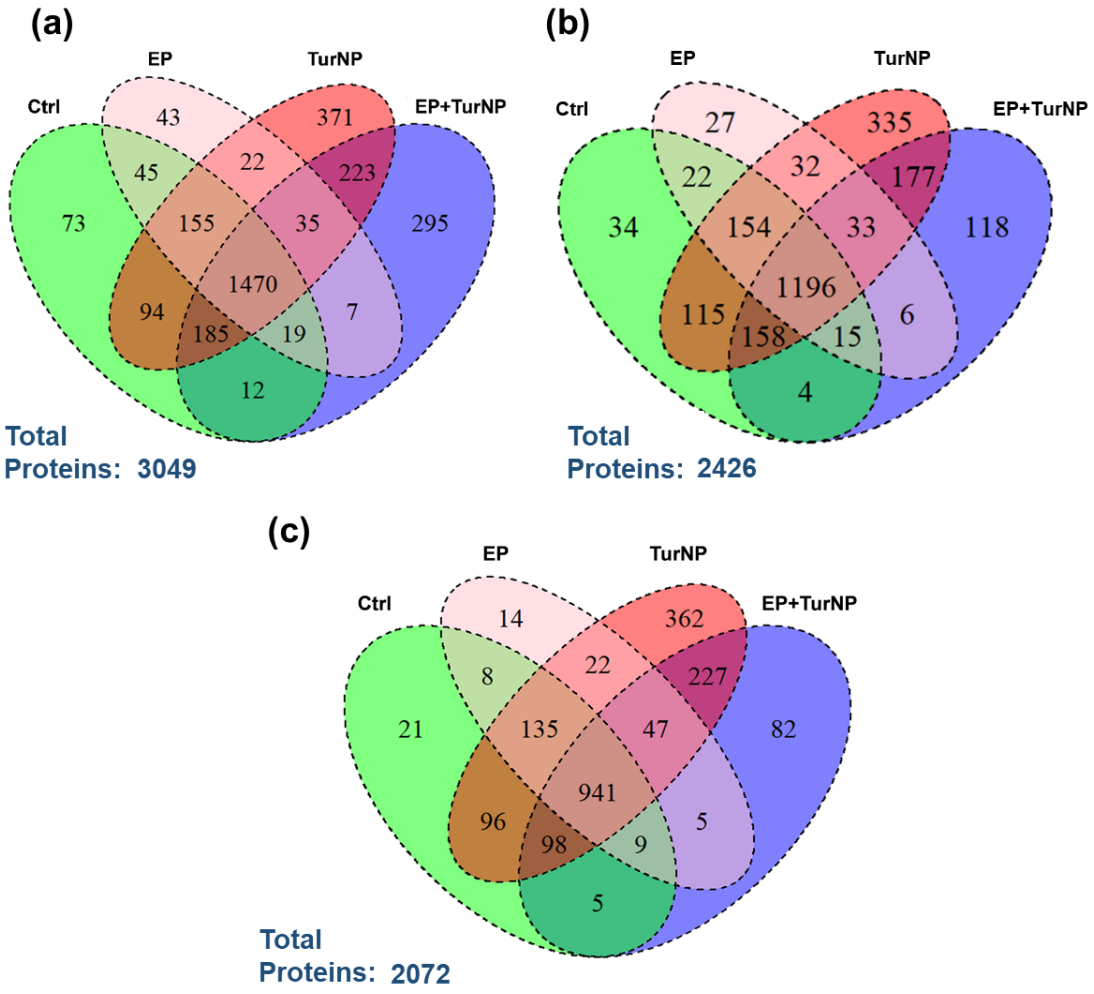

Figure 4.68: Venn diagrams showing the distribution of total proteins across different treatment groups for three different selection criteria. (a) Selection criterion A (protein in at least one replicate), (b) Selection criterion B (protein in at least two replicates), (c) Selection criterion C (protein in at least three replication). Here, turmeric silver nanoparticles (TurNP) concentration of 15µg/mL and EP of 800V/cm, 100µs, 8 pulses at 1Hz were used.

4.4.2 The impact selection criteria on the differentially regulated proteins

We further studied whether, the difference in the protein distribution across different treatments for three selection criteria also impacted the number of differentially regulated proteins. We analyzed the count of differentially regulated proteins in EP+TurNP from TurNP, as shown in Figure 4.69. Compared to TurNP, the number of upregulated proteins in EP+TurNP were 404, 408, and 407 for criteria A, B, and C, respectively. On the contrary, the count of downregulated proteins were 554, 564, and 560 for criteria A, B, and C, respectively. These results revealed that

despite the difference in the total number of proteins for a selection criterion, the number of differentially regulated proteins was similar for all three selection criteria. These findings indicate that the choice of selection criteria does not affect the differentially regulated proteins.

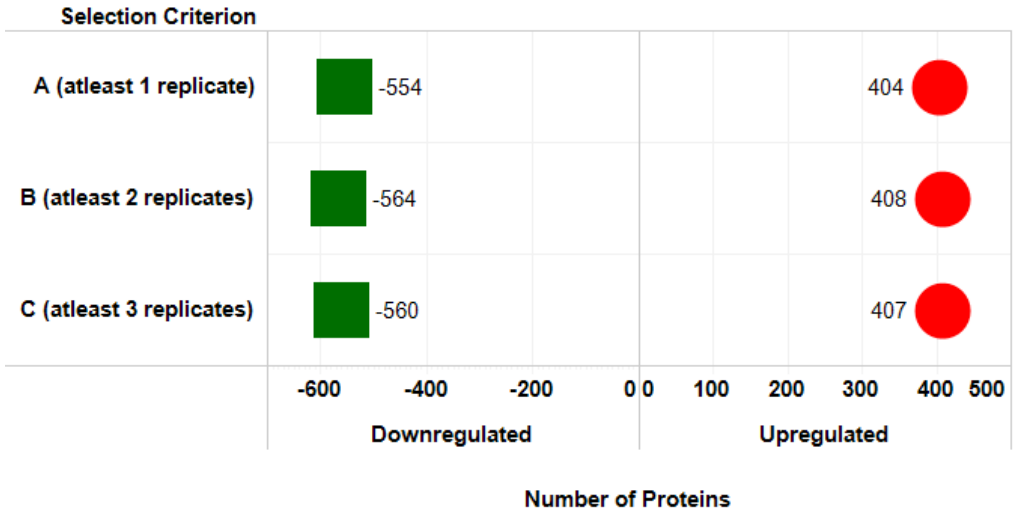

Figure 4.69: Number of significantly upregulated and downregulated proteins for different selection criteria in the EP+TurNP vs TurNP comparison: criterion A (protein in at least one replicate), criterion B (protein in at least two replicates), criterion C (protein in at least three replicates). Here turmeric silver nanoparticles (TurNP) concentration of 15µg/mL and EP of 800V/cm, 100µs, 8 pulses at 1Hz were used. The LFQ values of EP+TurNP were compared to calculate log2 fold-change (Δlog2) and identify significantly regulated proteins ($|\Delta log2| > 0.5$, and $P < 0.05$). In selection criteria A and B, the zero LFQ values were replaced using half of the lowest LFQ values for all proteins in four treatments, which were 445540, 983600, and 1258300 for selection criteria A, B, and C, respectively.

Tables 4.12 and 4.13 show the enriched pathways for significantly up- and downregulated proteins in EP+TurNP compared to TurNP for three selection criteria.

"KEGG pathway enrichment for upregulated proteins (Table 4.12) showed enrichment of OXPHOS, TCA cycle, FA degradation, FA metabolism, amino acid (valine, leucine, isoleucine, and lysin) degradation, glycolysis, peroxisome, pyruvate metabolism, aromatic amino acid (tryptophan) metabolism, etc. in EP+TurNP compared to TurNP" (Mittal, Camarillo, et al., 2020) for all three selection criteria. Overall, the upregulated pathways and their enriched proteins were similar for all three selection criteria, suggesting that the most significantly upregulated proteins were similar.

Table 4.12: Enriched pathways for significantly upregulated proteins in EP+TurNP vs TurNP comparison for three different selection criteria: criterion A (protein in at least one replicate), criterion B (protein in at least two replicates), criterion C (protein in at least three replicates). Here turmeric silver nanoparticles (TurNP) concentration of 15µg/mL and EP of 800V/cm, 100µs, 8 pulses at 1Hz were used. The list of significantly upregulated proteins was uploaded on DAVID 6.8 (D. W. Huang et al., 2009a, 2009b), while using total identified proteins from Venn diagram as background, respectively (i.e. 3049 or 2426 or 2072). Here pathway terms indicated in italic bold are key pathway terms shown in Figure 4.44(a) for selection criterion B.

Selection Criterion A (1 replicate)		**Selection Criterion B (2 replicate)**		**Selection Criterion C (3 replicate)**	
Pathway Terms	**Protein Count**	**Pathway Terms**	**Protein Count**	**Pathway Terms**	**Protein Count**
Metabolic pathways	121	Metabolic pathways	122	Metabolic pathways	122
Huntington's disease	48	Huntington's disease	49	Huntington's disease	49
Parkinson's disease	43	Parkinson's disease	44	Parkinson's disease	44
Oxidative phosphorylation	42	***Oxidative phosphorylation***	43	***Oxidative phosphorylation***	43
Alzheimer's disease	41	Alzheimer's disease	42	Alzheimer's disease	42
Biosynthesis of antibiotics	40	Biosynthesis of antibiotics	40	Biosynthesis of antibiotics	40
Non-alcoholic fatty liver disease (NAFLD)	30	Non-alcoholic fatty liver disease (NAFLD)	31	Non-alcoholic fatty liver disease (NAFLD)	31
Carbon metabolism	27	Carbon metabolism	27	Carbon metabolism	27
TCA cycle	17	***TCA cycle***	17	***TCA cycle***	17
Valine, leucine and isoleucine degradation	17	***Valine, leucine and isoleucine degradation***	17	***Valine, leucine and isoleucine degradation***	17
Fatty acid metabolism	16	***Fatty acid metabolism***	16	***Fatty acid metabolism***	16
Fatty acid degradation	15	***Fatty acid degradation***	15	***Fatty acid degradation***	15
Cardiac muscle contraction	12	Cardiac muscle contraction	12	Cardiac muscle contraction	12
Peroxisome	12	***Peroxisome***	12	***Peroxisome***	12
Biosynthesis of amino acids	12	***Biosynthesis of amino acids***	12	***Biosynthesis of amino acids***	12
Glycolysis / Gluconeogenesis	10	Glycolysis / Gluconeogenesis	10	Glycolysis / Gluconeogenesis	10
Propanoate metabolism	9	***Propanoate metabolism***	9	***Propanoate metabolism***	9
Lysine degradation	9	***Lysine degradation***	9	***Lysine degradation***	9
Calcium signaling pathway	9	***Calcium signaling pathway***	9	***Calcium signaling pathway***	9

Table 4.12 continued

Pyruvate metabolism	9	***Pyruvate metabolism***	9	***Pyruvate metabolism***	9
N-Glycan biosynthesis	8	***N-Glycan biosynthesis***	8	***N-Glycan biosynthesis***	8
PPAR signaling pathway	8	***PPAR signaling pathway***	8	***PPAR signaling pathway***	8
Systemic lupus erythematosus	8	Systemic lupus erythematosus	8	---	
beta-Alanine metabolism	7	***beta-Alanine metabolism***	7	***beta-Alanine metabolism***	7
Tryptophan metabolism	7	***Tryptophan metabolism***	7	***Tryptophan metabolism***	7
Fatty acid elongation	7	***Fatty acid elongation***	7	***Fatty acid elongation***	7
Arginine and proline metabolism	7	***Arginine and proline metabolism***	7	***Arginine and proline metabolism***	7
Biosynthesis of unsaturated fatty acids	6	***Biosynthesis of unsaturated fatty acids***	6	***Biosynthesis of unsaturated fatty acids***	6
Complement and coagulation cascades	6	Complement and coagulation cascades	6	Complement and coagulation cascades	6
Steroid biosynthesis	5	Steroid biosynthesis	5	Steroid biosynthesis	5
2-Oxocarboxylic acid metabolism	5	---		---	
Sulfur metabolism	4	***Sulfur metabolism***	4	***Sulfur metabolism***	4
Ascorbate and aldarate metabolism	4	***Ascorbate and aldarate metabolism***	4	***Ascorbate and aldarate metabolism***	4
Sulfur relay system	3	***Sulfur relay system***	3	---	

On the other hand, the pathway analysis for downregulated proteins (Table 4.13) showed enrichment of the proteins in “regulation of actin cytoskeleton, focal adhesion, PI3K-Akt signaling, adherens junction, Rap1 signaling, MAPK signaling, MicroRNAs in cancer, hippo signaling, Ras signaling, neurotrophin signaling, tight junction, glycolysis, etc.” (Mittal, Camarillo, et al., 2020) in EP+TurNP compared to TurNP for all three selection criteria. Overall, the downregulated pathways and their enriched proteins were similar for all three selection criteria, suggesting that the most significantly downregulated proteins were similar.

Table 4.13: Enriched pathways for significantly downregulated proteins in EP+TurNP vs TurNP comparison for Three different selection criteria: criterion A (protein in at least one replicate), criterion B (protein in at least two replicates), criterion C (protein in at least three replicates). Here turmeric silver nanoparticles (TurNP) concentration of 15µg/mL and EP of 800V/cm, 100µs, 8 pulses at 1Hz were used. The list of significantly downregulated proteins was uploaded on DAVID 6.8 (D. W. Huang et al., 2009a, 2009b), while using total identified proteins from Venn diagram as background, respectively (i.e. 3049 or 2426 or 2072). Here pathway terms indicated in italic bold are key pathway terms shown in Figure 4.44(b) for selection criterion B.

Selection Criterion A (1 replicate)		**Selection Criterion B (2 replicate)**		**Selection Criterion C (3 replicate)**	
Pathway Terms	**Protein Count**	**Pathway Terms**	**Protein Count**	**Pathway Terms**	**Protein Count**
Regulation of actin cytoskeleton	30	***Regulation of actin cytoskeleton***	30	***Regulation of actin cytoskeleton***	30
Pathways in cancer	28	***Pathways in cancer***	29	***Pathways in cancer***	29
Focal adhesion	25	***Focal adhesion***	25	***Focal adhesion***	24
Endocytosis	25	Endocytosis	26	Endocytosis	24
Proteoglycans in cancer	24	***Proteoglycans in cancer***	25	***Proteoglycans in cancer***	25
PI3K-Akt signaling pathway	24	***PI3K-Akt signaling pathway***	24	***PI3K-Akt signaling pathway***	23
MAPK signaling pathway	20	***MAPK signaling pathway***	20	***MAPK signaling pathway***	20
Bacterial invasion of epithelial cells	17	Bacterial invasion of epithelial cells	17	Bacterial invasion of epithelial cells	17
Rap1 signaling pathway	17	***Rap1 signaling pathway***	17	***Rap1 signaling pathway***	17
Hippo signaling pathway	14	***Hippo signaling pathway***	14	***Hippo signaling pathway***	14
Oxytocin signaling pathway	14	***Oxytocin signaling pathway***	14	***Oxytocin signaling pathway***	14
MicroRNAs in cancer	14	***MicroRNAs in cancer***	14	***MicroRNAs in cancer***	15
Dilated cardiomyopathy	13	Dilated cardiomyopathy	13	Dilated cardiomyopathy	13
Glucagon signaling pathway	13	***Glucagon signaling pathway***	13	***Glucagon signaling pathway***	13
Shigellosis	13	Shigellosis	13	Shigellosis	13
Adrenergic signaling in cardiomyocytes	13	Adrenergic signaling in cardiomyocytes	13	Adrenergic signaling in cardiomyocytes	13
Leukocyte transendothelial migration	13	Leukocyte transendothelial migration	14	Leukocyte transendothelial migration	14
Adherens junction	13	***Adherens junction***	13	***Adherens junction***	13

Table 4.13 continued

Oocyte meiosis	13	Oocyte meiosis	13	Oocyte meiosis	13
Biosynthesis of amino acids	13	***Biosynthesis of amino acids***	13	---	
Ras signaling pathway	13	***Ras signaling pathway***	14	***Ras signaling pathway***	14
Proteasome	13	---		---	
Endocrine and other factor-regulated calcium reabsorption	12	***Endocrine and other factor-regulated calcium reabsorption***	12	***Endocrine and other factor-regulated calcium reabsorption***	12
Arrhythmogenic right ventricular cardiomyopathy (ARVC)	12	Arrhythmogenic right ventricular cardiomyopathy (ARVC)	12	Arrhythmogenic right ventricular cardiomyopathy (ARVC)	12
Hypertrophic cardiomyopathy (HCM)	12	Hypertrophic cardiomyopathy (HCM)	12	Hypertrophic cardiomyopathy (HCM)	12
Pathogenic Escherichia coli infection	12	Pathogenic Escherichia coli infection	12	Pathogenic Escherichia coli infection	12
cAMP signaling pathway	12	***cAMP signaling pathway***	12	***cAMP signaling pathway***	12
Insulin signaling pathway	12	Insulin signaling pathway	12	Insulin signaling pathway	12
Glycolysis / Gluconeogenesis	12	***Glycolysis / Gluconeogenesis***	12	***Glycolysis / Gluconeogenesis***	12
Thyroid hormone signaling pathway	11	Thyroid hormone signaling pathway	11	Thyroid hormone signaling pathway	10
Chemokine signaling pathway	11	***Chemokine signaling pathway***	11	***Chemokine signaling pathway***	11
Platelet activation	11	---		Platelet activation	11
Gastric acid secretion	10	Gastric acid secretion	10	Gastric acid secretion	10
Estrogen signaling pathway	10	***Estrogen signaling pathway***	10	***Estrogen signaling pathway***	10
Fc gamma R-mediated phagocytosis	10	***Fc gamma R-mediated phagocytosis***	10	***Fc gamma R-mediated phagocytosis***	10
Neurotrophin signaling pathway	10	***Neurotrophin signaling pathway***	11	***Neurotrophin signaling pathway***	12
Gap junction	10	***Gap junction***	11	***Gap junction***	11
Dopaminergic synapse	10	---		Dopaminergic synapse	10
Salivary secretion	9	Salivary secretion	9	Salivary secretion	9
GnRH signaling pathway	9	***GnRH signaling pathway***	10	***GnRH signaling pathway***	10

Table 4.13 continued

ECM-receptor interaction	9	***ECM-receptor interaction***	9	***ECM-receptor interaction***	9
Long-term potentiation	8	***Long-term potentiation***	8	***Long-term potentiation***	8
Glutamatergic synapse	8	Glutamatergic synapse	8	Glutamatergic synapse	8
Cell adhesion molecules (CAMs)	8	***Cell adhesion molecules (CAMs)***	8	***Cell adhesion molecules (CAMs)***	8
Legionellosis	8	Legionellosis	8	Legionellosis	8
Tight junction	8	***Tight junction***	9	***Tight junction***	9
Pancreatic secretion	8	Pancreatic secretion	8	Pancreatic secretion	8
Bile secretion	7	Bile secretion	7	Bile secretion	7
Renin secretion	7	Renin secretion	7	Renin secretion	7
Insulin secretion	7	Insulin secretion	8	Insulin secretion	8
Circadian entrainment	7	---		Circadian entrainment	7
Base excision repair	6	***Base excision repair***	6	***Base excision repair***	6
Amphetamine addiction	6	Amphetamine addiction	6	---	
Aldosterone-regulated sodium reabsorption	5	---		Aldosterone-regulated sodium reabsorption	5
Protein digestion and absorption	5	Protein digestion and absorption	5	Protein digestion and absorption	5
---		Salmonella infection	11	Salmonella infection	11
---		Axon guidance	10	Axon guidance	10
---		***Natural killer cell mediated cytotoxicity***	8	***Natural killer cell mediated cytotoxicity***	8
---		***Renal cell carcinoma***	8	***Renal cell carcinoma***	8
---		Osteoclast differentiation	6	Osteoclast differentiation	5
---		HTLV-I infection	16	HTLV-I infection	16
---		---		Hepatitis B	9
---		---		Vascular smooth muscle contraction	8
---		---		Serotonergic synapse	7

Table 4.13 continued

---		---		Cholinergic synapse	7
---		---		p53 signaling pathway	6
---		---		Chronic myeloid leukemia	6
---		---		Melanogenesis	6
---		---		T cell receptor signaling pathway	6
---		---		Morphine addiction	5

Together, these analyses indicate that while the choice of selection criteria influences the number of qualified proteins from the raw data for the analysis, the number of differentially regulated proteins and their resulting enrichment analysis remain similar, for the three selection criteria. This could occur because the initial bias introduced by selection criterion in form of different number of proteins washes out as we analyze the data further, eventually leading to comparable results, in the form of similar number of differentially regulated proteins and similar enrichment analysis.

In this scenario, while one may choose any selection criterion, for the proteomics data analysis, moderate selection criterion B, which produced 2426 total proteins (as shown in Figure 4.68) from the raw data for further analysis remains our choice, as it is neither too liberal (like criterion A, which results in highest 3049 total proteins), nor is too conservative (like criterion C, which results in lowest 2072 total proteins).

CHAPTER 5. CONCLUSIONS

In this dissertation, we demonstrated that ECT with curcumin causes an effective MDA-MB-231 TNBC cell death by altering the metabolic profile, with the suppression of key glycolysis proteins. Similar results were also obtained for ECT with TurNP and cisplatin. In summary, ECT with Cur can be effective against TNBCs. ECT with Cur, TurNP, and CsP altered the metabolic profile of MDA-MB-231 TNBC cells, with suppression of key glycolytic proteins and upregulation of oxidative phosphorylation and TCA cycle proteins to generate H_2O_2 and induce cell death. For ECT with Cur and CsP, the majority of cells underwent apoptotic cell death, the preferred pathway, rather than necrosis.

1. Curcumin decreases the viability and colonies of MDA-MB-231 TNBC cells in a dose dependent manner. Increasing concentration beyond 50μM resulted a saturation in the impact of Cur treatment.
2. Compared with Cur, EP (1200V/cm, 100μs, 8 pulses at 1Hz) with Cur (50μM) treatment caused a 2-3.9× significantly lower survival fractions, highlighting a greater cytotoxicity of EP+Cur against MDA-MB-231 cells.
3. The main mechanism of Cur and EP+Cur MDA-MB-231 cell death is apoptosis, the desired pathway, not necrosis.
4. Proteomics analysis for Cur (50μM) and EP+Cur treatments detected 1456 proteins, among them 453 proteins were up- or downregulated, which included kinases, heat shock proteins, transcription factors, structural proteins, and metabolic enzymes.
5. The analysis of top 20 up- and downregulated indicates that the EP+Cur treatment may enhance the activity of proteins in organelles, such as mitochondria and endoplasmic reticulum, which actively participate in inducing apoptotic cell death, while mainly downregulating cytosolic proteins.
6. ECT with curcumin can utilize the metabolic vulnerabilities present in the TNBC cells by targeting glycolysis pathway. Eight key glycolysis proteins (LDHB, LDHA, ENO2, ALDOA, PFKP, PGM1, PGAM1 and PGK1) were downregulated in EP+Cur from Cur. Particularly, the downregulation in LDHB levels was confirmed through immunoblotting, as it is an essential gene for TNBC proliferation and survival, correlates with significantly

poor clinical outcomes. Moreover, EP+Cur downregulated the glucose uptake, and intracellular levels of key glycolytic metabolites, such as lactate, glutamine, and glutamate, which further validate the glycolytic suppression observed in the proteomics study.

7. There was a switch in the metabolism with upregulation of 10 oxidative phosphorylation pathway proteins and 8 TCA cycle proteins in the Cur + EP sample, compared to Cur.
8. ECT with Curcumin increased the H_2O_2 ROS production specifically in MDA-MB-231 TNBC cells, but not in non-cancerous mammary epithelial MCF10A cells. This excessive ROS production could be attributed to the upregulated mitochondrial activity and may cause oxidative stress to induce apoptotic cell death due to the crosstalk among metabolism, calcium and ROS signaling pathways.
9. The application of ultra-microsecond duration (2500V/cm or 5000V/cm, 10µs, 8 pulses at 1Hz) EPs with low dosage of Cur (10µM) significantly reduced the viability of MDA-MB-231 cells to as low as 15% only after 24h of the treatment. In comparison, for the Cur only treatment, a significant reduction in cell viability to just 72% was observed, only at 72h. Furthermore, $1/7^{th}$ of the curcumin dose could target MDA-MB-231 cells, when combined with EPs of 5000V/cm.
10. The application of non-invasive, low-intensity (200V/cm,100µs or 5ms, 8 pulses at 1Hz) EPs with Cur (50µM) to plated/adherent MDA-MB-231 cells showed that the synergy of EP with Cur increased cell death. The cell death was higher with longer duration (5ms) pulses with Cur, compared with microsecond duration (100µs) pulses with Cur. The non-cancerous MCF10A cell viability was much higher than the MDA-MB-231 viability for EP+Cur treatment. The impacts observed on the viability of MDA-MB-231 cells were much larger and time sustained compared to the MCF10A cells.
11. The cell cycle studies revealed that the EP application alone does not cause cell cycle arrest. The Cur alone and microsecond duration pulses with Cur caused significant cell cycle arrest in the G0/G1 phase. However, on the contrary, millisecond duration (5ms) pulses with Cur showed no cell cycle arrest in the G0/G1 phase; however, cells did exhibit a significant reduction in G2 phase population with an increase in S phase population compared to Ctrl, which may suggest that the cells in the S phase were either slowed or arrested and not actively synthesizing DNA compared to Ctrl.
12. Cur alone and EP+Cur with microsecond duration pulses significantly downregulated p53

protein expression. On the other hand, EP+Cur with millisecond duration pulses significantly increased p53 expression. This suggest that the Cur and microsecond duration-based EP+Cur treatments may induce MDA-MB-231 cell death and G0/G1 cell cycle arrest through a p53 dependent mechanism, but the effects induced by millisecond duration-based EP+Cur may either be p53 level independent or are in response to the reactivation of p53.

13. TurNP were synthesized using green biosynthesis technique and were characterized using UV-Vis absorption spectroscopy, energy-dispersive x-ray spectroscopy, Fourier transform infrared spectroscopy, and zeta potential.
14. The phytochemical screening studies indicated that TurNP contains key phytochemicals, such as alkaloid, flavonoid, phenol, saponin, tannin, and terpenoid. The bonds and functional groups, such as O-H, C-H, C=C, S=O, C-O-C, and C-O in these phytochemicals work as capping legends to facilitate the green biosynthesis of TurNP.
15. DPPH radical scavenging activity assay indicated that the TurNP possesses antioxidant activity, which could be attributed to the presence of various key phytochemicals of TurNP.
16. TurNP alone decreases the viability of MDA-MB-231 TNBC cells in a dose dependent manner.
17. Compared to MDA-MB-231 cells, the effects of EP alone on the loss in MCF 10A viability were weaker and short lived, as indicated by significant recovery of cell viability at 36h even for the highest field strength (1200V/cm100µs, 8 pulses at 1Hz) studied.
18. The viability studies indicate the combined and sustained effect of EP (800V/cm, 100µs, 8 pulses at 1Hz) with TurNP (15µg/mL) in EP+TurNP on effective MDA-MB-231 cell death. Our results reveal the combined effect of EP+TurNP treatment in reducing MDA-MB-231 cell viability to as low as 9% at 12 h. EP+TurNP treatment is specific towards MDA-MB-231 TNBC cells, as the damage to the MCF10A viability was weaker and short lived, and they maintained a significantly higher viability, compared to MDA-MB-231 cells.
19. Proteomics results indicate that EP+TurNP treatment significantly influenced expression of a diverse list of proteins, including receptors, transcription factors, structural proteins, kinases, and metabolic enzymes. This include the downregulation of 25 proteins in PI3K-Akt signaling pathway (including GRB2, EGFR, EPHA2, GNB1, GNB2, 14–3–3 family,

and Integrin family proteins).

20. ECT with TurNP can utilize the metabolic vulnerabilities present in the TNBC cells by targeting glycolysis pathway. A total of 12 proteins (LDHB, LDHA, ENO1, ENO2, AKR1A1, ALDOA, ALDOC, PGK1, PGM1, PGAM1, GAPDH, and TPI1) in the glycolytic pathway were downregulated in EP+TurNP. The validation studies demonstrated an excellent correlation between mRNA and protein levels for LDHB and ENO1 and indicated that these key glycolytic genes are downregulated at transcription levels upon EP+TurNP treatment. Moreover, a concomitant reduction in metabolite levels (glucose uptake, and intracellular- lactate, glutamine, and glutamate) was observed for EP+TurNP treatment.
21. EP+TurNP treatment caused a switch in metabolism from glycolysis to oxidative phosphorylation. Compared to TurNP alone, EP+TurNP treatment upregulated 66 endoplasmic reticulum and 193 mitochondrial proteins, enhancing several processes and pathways, including pyruvate metabolism, TCA cycle, and oxidative phosphorylation, which redirected the TNBC metabolism to mitochondria.
22. This switch in the metabolism caused excessive production of H_2O_2 ROS to inflict cell death in MDA-MB-231 cells, demonstrating the potency of this treatment.
23. The EP (1200V/cm, 100µs, 8 pulses at 1Hz) with CsP (100µM) treatment caused an effective and time dependent cell death in MDA-MB-231 TNBC cells. The EP alone also significantly compromised cell viability, and metabolic activity in these cells. However, the cell viability recovered for EP only treatment. With EP+CsP treatment, the effects were long-lasting, and the cells remained metabolically inactive, indicating the superiority of the EP + CsP treatment. The effects of EP+CsP are specific to TNBC cells, as they do not affect the viability of non-tumorigenic mammary epithelial MCF10A cells, as much.
24. Proteomics results indicate that EP+CsP significantly downregulated 14 key glycolysis proteins (including ENO1, LDHA, LDHB, ACSS2, ALDOA, and PGK1), compared to CsP alone. The validation studies demonstrated an excellent correlation between mRNA and protein levels for LDHB and ENO1 and indicated that these key glycolytic genes are downregulated at transcription levels upon EP+TurNP treatment.
25. EP + CsP caused a switch in the metabolism with upregulation of 34 oxidative phosphorylation pathway proteins and 18 TCA cycle proteins compared to CsP alone,

accompanied by the upregulation of proteins linked to several metabolic reactions, which produce TCA cycle intermediates. For validation, the increase in GLS level in the immunoblotting correlates with the mRNA and protein level expressions for EP+CsP.

26. EP + CsP promoted multiple pathways to cause 1.3-fold increase in the H_2O_2 ROS concentration and induced apoptosis in majority of the cells. The proteomics results correlate well with cell viability, western blot, and qPCR data. While some effects were similar for EP, more comprehensive and long-lasting effects were observed for EP+CsP, which demonstrate the potential of EP+CsP against TNBC cells.

CHAPTER 6. RECOMMENDATIONS FOR FUTURE WORK

Future work in the following directions is recommended to further establish the results demonstrated in this dissertation:

1. In this dissertation, in vitro studies were performed to investigate the efficacy and mechanisms of action of ECT with curcumin against TNBCs. Animal studies using TNBC cell xenografts and patient tumor xenografts (PDX) models will be useful to further establish the efficacy of ECT with curcumin in TNBCs.
2. The use of integrative multi-omics studies, including proteomics (at multiple time points), phosphoproteomics, metabolomics, and transcriptomics will provide insights at multiple levels into the molecular mechanisms of the enhanced effects of ECT with curcumin.
    a. In this dissertation, the proteomics studies for ECT with curcumin was conducted at 12h of the treatment. Further proteomics studies at various time points, such as 2h, 24h, 48h, and 72h would reveal early and late cellular responses to the treatment.
    b. Approximately 30% of the proteins encoded by the human genome are phosphorylated, which is an important reversible posttranslational modification and controls nearly every aspect of cells (Cohen, 2002). The phosphorylation regulates protein function, localization, complex formation, and degradation, to mediate multiple pathways, including cell cycle, proliferation, and apoptosis. Therefore, studying the changes in the phosphorylated proteins using phosphoproteomics can be useful to understand the mechanisms of cellular responses to ECT and curcumin treatment.
    c. ECT with curcumin induced major changes in the cellular metabolism. Therefore, metabolomics can be helpful for a comprehensive study of changes in all cellular metabolites upon ECT and curcumin treatment.

d. Transcriptomics studies of all the RNA molecules of cells (i.e. mRNA and other non-coding RNAs) can be used to study the changes in the gene expression upon ECT and curcumin treatment. Additional microarray studies will support these data.

3. LDHB plays a unique role in TNBCs and is an essential gene. Therefore, further studies using EPs for delivering small molecules and genetic materials, such as siRNA and CRISPR/Cas9 to silence LDHB in TNBCs can be conducted. Moreover, studies on individual or co-silencing of other key metabolic genes, including ENO1, ENO2, ALDOA, PGM1, PGAM1 using EP-based siRNA and CRISPR/Cas9 could be useful. These studies could eventually lead to EP-based gene-targeted therapies against TNBCs.
4. Galloflavin, a new LDH inhibitor, which inhibits both LDH isoforms (LDHA and LDHB) can also be effective with ECT against TNBCs. However, no literature exists on using galloflavin with ECT against cancers. Further studies investigating the efficacy of ECT with galloflavin, and their mechanisms of action could advance a novel and targeted ECT-based galloflavin therapy.

REFERENCES

Abdi, H., & Williams, L. J. (2010). Tukey's honestly significant difference (HSD) test. *Encyclopedia of Research Design. Thousand Oaks, CA: Sage*, 1–5.

Abegg, D., Frei, R., Cerato, L., Prasad Hari, D., Wang, C., Waser, J., & Adibekian, A. (2015). Proteome-Wide Profiling of Targets of Cysteine reactive Small Molecules by Using Ethynyl Benziodoxolone Reagents. *Angewandte Chemie International Edition*, *54*(37), 10852–10857. https://doi.org/10.1002/anie.201505641

Adeyinka, A., Nui, Y., Cherlet, T., Snell, L., Watson, P. H., & Murphy, L. C. (2002). Activated mitogen-activated protein kinase expression during human breast tumorigenesis and breast cancer progression. *Clinical Cancer Research : An Official Journal of the American Association for Cancer Research*, *8*(6), 1747–1753.

Adorno-Cruz, V., & Liu, H. (2019, March 1). Regulation and functions of integrin α2 in cell adhesion and disease. *Genes and Diseases*. Chongqing yi ke da xue, di 2 lin chuang xue yuan Bing du xing gan yan yan jiu suo. https://doi.org/10.1016/j.gendis.2018.12.003

Aggarwal, B. B., Sundaram, C., Malani, N., & Ichikawa, H. (2007). CURCUMIN: THE INDIAN SOLID GOLD BT - The Molecular Targets and Therapeutic Uses of Curcumin in Health and Disease. In B. B. Aggarwal, Y.-J. Surh, & S. Shishodia (Eds.) (pp. 1–75). Boston, MA: Springer US. https://doi.org/10.1007/978-0-387-46401-5_1

Aggarwal, B. B., Yuan, W., Li, S., & Gupta, S. C. (2013, September). Curcumin-free turmeric exhibits anti-inflammatory and anticancer activities: Identification of novel components of turmeric. *Molecular Nutrition and Food Research*. https://doi.org/10.1002/mnfr.201200838

Ajitha, B., Kumar Reddy, Y. A., Reddy, P. S., Jeon, H.-J., & Ahn, C. W. (2016). Role of capping agents in controlling silver nanoparticles size, antibacterial activity and potential application as optical hydrogen peroxide sensor. *RSC Advances*, *6*(42), 36171–36179. https://doi.org/10.1039/C6RA03766F

Akram, M., & Siddiqui, S. A. (2012). Breast cancer management: past, present and evolving. *Indian Journal of Cancer*, *49*(3), 277–282. https://doi.org/10.4103/0019-509X.104486

Akther, T., & Hemalatha, S. (2019). Mycosilver Nanoparticles: Synthesis, Characterization and its Efficacy against Plant Pathogenic Fungi. *BioNanoScience*. https://doi.org/10.1007/s12668-019-0607-y

Akther, T., Khan, M. S., & Srinivasan, H. (2018). Novel silver nanoparticles synthesized from anthers of couroupita guianensis Abul. Control growth and biofilm formation in human pathogenic bacteria. *Nano Biomedicine and Engineering*. https://doi.org/10.5101/nbe.v10i3.p250-257

Akther, T., Priya, S., Sah, S. K., Khan, M. S., & Hemalatha, S. (2019). Ta-AgNps are Potential Antimicrobial Resistance Breakers, *9*(2), 376–383. https://doi.org/10.22052/JNS.2019.02.019

Al Ahmad, M., Al Natour, Z., Mustafa, F., & Rizvi, T. A. (2018). Electrical Characterization of Normal and Cancer Cells. *IEEE Access*, *6*, 25979–25986. https://doi.org/10.1109/ACCESS.2018.2830883

Alberts, B., Johnson, A., Lewis, J., Raff, M., Roberts, K., & And Walter, P. (2007). Molecular Biology of the Cell - NCBI Bookshelf. *Amino Acids*. Retrieved from https://www.ncbi.nlm.nih.gov/books/NBK26867/

Alberts, B., Johnson, A., Lewis, J., Raff, M., Roberts, K., & Walter, P. (2002). Electron-Transport Chains and Their Proton Pumps. Retrieved from https://www.ncbi.nlm.nih.gov/books/NBK26904/

Alday-Parejo, B., Stupp, R., & Rüegg, C. (2019, July 1). Are integrins still practicable targets for anti-cancer therapy? *Cancers*. MDPI AG. https://doi.org/10.3390/cancers11070978

Alderton, G. K. (2015). Acetate nourishes stressed tumour cells. *Nature Reviews Cancer*, *15*(2), 67–67. https://doi.org/10.1038/nrc3899

Alimova, I. N., Liu, B., Fan, Z., Edgerton, S. M., Dillon, T., Lind, S. E., & Thor, A. D. (2009). Metformin inhibits breast cancer cell growth, colony formation and induces cell cycle arrest in vitro. *Cell Cycle (Georgetown, Tex.)*, *8*(6), 909–915. https://doi.org/10.4161/cc.8.6.7933

Alsammarraie, F. K., Wang, W., Zhou, P., Mustapha, A., & Lin, M. (2018). Green synthesis of silver nanoparticles using turmeric extracts and investigation of their antibacterial activities. *Colloids and Surfaces B: Biointerfaces*, *171*, 398–405. https://doi.org/10.1016/j.colsurfb.2018.07.059

American Cancer Society. (2018). Breast Cancer Facts & Figures 2017-2018. *Side Effects of Medical Cancer Therapy: Prevention and Treatment: Second Edition*. https://doi.org/10.1007/978-3-319-70253-7_2

Angelo, L. S., Maxwell, D. S., Wu, J. Y., Sun, D., Hawke, D. H., McCutcheon, I. E., … Kurzrock, R. (2013). Binding partners for curcumin in human schwannoma cells: Biologic Implications. *Bioorganic & Medicinal Chemistry*, *21*(4), 932–939. https://doi.org/https://doi.org/10.1016/j.bmc.2012.12.008

Ataollahi, M. R., Sharifi, J., Paknahad, M. R., & Paknahad, A. (2015). Breast cancer and associated factors: a review. *Journal of Medicine and Life*, *8*(Spec Iss 4), 6–11. Retrieved from https://pubmed.ncbi.nlm.nih.gov/28316699

Atkins, H., Hayward, J. L., Klugman, D. J., & Wayte, A. B. (1972). Treatment of early breast cancer: a report after ten years of a clinical trial. *British Medical Journal*, *2*(5811), 423–429. https://doi.org/10.1136/bmj.2.5811.423

Atkins, R. (2008). 21 Century's Grand Engineering Challenges Unveiled. Retrieved February 27, 2019, from http://www8.nationalacademies.org/onpinews/newsitem.aspx?RecordID=02152008

Avanzato, D., Pupo, E., Ducano, N., Isella, C., Bertalot, G., Luise, C., … Lanzetti, L. (2018). High USP6NL Levels in Breast Cancer Sustain Chronic AKT Phosphorylation and GLUT1 Stability Fueling Aerobic Glycolysis. *Cancer Research*, *78*(13), 3432–3444. https://doi.org/10.1158/0008-5472.CAN-17-3018

Azimi, I., Roberts-Thomson, S. J., & Monteith, G. R. (2014). Calcium influx pathways in breast cancer: opportunities for pharmacological intervention. *British Journal of Pharmacology*, *171*(4), 945–960. https://doi.org/10.1111/bph.12486

Babicki, S., Arndt, D., Marcu, A., Liang, Y., Grant, J. R., Maciejewski, A., & Wishart, D. S. (2016). Heatmapper: web-enabled heat mapping for all. *Nucleic Acids Research*, *44*(W1), W147–W153. https://doi.org/10.1093/nar/gkw419

Baclesse, F. (1949). Roentgen therapy as the sole method of treatment of cancer of the breast. *The American Journal of Roentgenology and Radium Therapy*, *62*(3), 311–319; Disc., 349–354.

Bae, E., Kim, H. E., Koh, E., & Kim, K.-S. (2014). Phosphoglucomutase1 is necessary for sustained cell growth under repetitive glucose depletion. *FEBS Letters*, *588*(17), 3074–3080. https://doi.org/10.1016/J.FEBSLET.2014.06.034

Bae, Y. H., Ryu, J. H., Park, H. J., Kim, K. R., Wee, H. J., Lee, O. H., … Bae, S. K. (2013). Mutant p53-Notch1 signaling axis is involved in curcumin-induced apoptosis of breast cancer cells. *Korean Journal of Physiology and Pharmacology*, *17*(4), 291–297. https://doi.org/10.4196/kjpp.2013.17.4.291

Balko, J. M., Cook, R. S., Vaught, D. B., Kuba, M. G., Miller, T. W., Bhola, N. E., … Arteaga, C. L. (2012). Profiling of residual breast cancers after neoadjuvant chemotherapy identifies DUSP4 deficiency as a mechanism of drug resistance. *Nature Medicine*, *18*(7), 1052–1059. https://doi.org/10.1038/nm.2795

Banik, U., Parasuraman, S., Adhikary, A. K., & Othman, N. H. (2017). Curcumin: The spicy modulator of breast carcinogenesis. *Journal of Experimental and Clinical Cancer Research*, *36*(1), 1–16. https://doi.org/10.1186/s13046-017-0566-5

Barczyk, M., Carracedo, S., & Gullberg, D. (2010, January 20). Integrins. *Cell and Tissue Research*. https://doi.org/10.1007/s00441-009-0834-6

Bartlett, D. L. (2011). *Surgical Oncology : Fundamentals, Evidence-Based Approaches and New Technology*. Jaypee Brothers Pvt. Ltd.

Benevento, R., Santoriello, A., Perna, G., & Canonico, S. (2012). Electrochemotherapy of cutaneous metastastes from breast cancer in elderly patients: a preliminary report. *BMC Surgery*, *12 Suppl 1*(Suppl 1), S6. https://doi.org/10.1186/1471-2482-12-S1-S6

Benov, L. C., Antonov, P. A., & Ribarov, S. R. (1994). Oxidative damage of the membrane lipids after electroporation. *General Physiology and Biophysics*, *13*(2), 85–97. Retrieved from http://www.ncbi.nlm.nih.gov/pubmed/7806071

Berners-Price, S. J., & Appleton, T. G. (2000). The Chemistry of Cisplatin in Aqueous Solution BT - Platinum-Based Drugs in Cancer Therapy. In L. R. Kelland & N. P. Farrell (Eds.) (pp. 3–35). Totowa, NJ: Humana Press. https://doi.org/10.1007/978-1-59259-012-4_1

Berstad, P., Coates, R. J., Bernstein, L., Folger, S. G., Malone, K. E., Marchbanks, P. A., … Ursin, G. (2010). A case-control study of body mass index and breast cancer risk in white and African-American women. *Cancer Epidemiology, Biomarkers & Prevention : A Publication of the American Association for Cancer Research, Cosponsored by the American Society of Preventive Oncology*, *19*(6), 1532–1544. https://doi.org/10.1158/1055-9965.EPI-10-0025

Bertucci, F., Finetti, P., Cervera, N., Esterni, B., Hermitte, F., Viens, P., & Birnbaum, D. (2008). How basal are triple-negative breast cancers? *International Journal of Cancer*, *123*(1), 236–240. https://doi.org/10.1002/ijc.23518

Beutler, J. A. (2009). Natural Products as a Foundation for Drug Discovery. *Current Protocols in Pharmacology / Editorial Board, S.J. Enna (Editor-in-Chief) ... [et Al.]*, *46*, 9.11.1-9.11.21. https://doi.org/10.1002/0471141755.ph0911s46

Bigi, L., Galdo, G., Cesinaro, A. M., Vaschieri, C., Marconi, A., Pincelli, C., & Fantini, F. (2016). Electrochemotherapy induces apoptotic death in melanoma metastases: a histologic and immunohistochemical investigation. *Clinical, Cosmetic and Investigational Dermatology*, *9*, 451–459. https://doi.org/10.2147/CCID.S115984

Bonadonna, G., Brusamolino, E., Valagussa, P., Rossi, A., Brugnatelli, L., Brambilla, C., … Veronesi, U. (1976). Combination chemotherapy as an adjuvant treatment in operable breast cancer. *The New England Journal of Medicine*, *294*(8), 405–410. https://doi.org/10.1056/NEJM197602192940801

Bonadonna, G., Monfardini, S., De Lena, M., & Fossati-Bellani, F. (1969). Clinical evaluation of adriamycin, a new antitumour antibiotic. *British Medical Journal*, *3*(5669), 503–506. https://doi.org/10.1136/bmj.3.5669.503

Brackenbury, W. J. (2012). Voltage-gated sodium channels and metastatic disease. *Channels*, *6*(5), 352–361. https://doi.org/10.4161/chan.21910

Bray, F., Ferlay, J., Soerjomataram, I., Siegel, R. L., Torre, L. A., & Jemal, A. (2018). Global cancer statistics 2018: GLOBOCAN estimates of incidence and mortality worldwide for 36 cancers in 185 countries. *CA: A Cancer Journal for Clinicians*, *68*(6), 394–424. https://doi.org/10.3322/caac.21492

Breglio, A. M., Rusheen, A. E., Shide, E. D., Fernandez, K. A., Spielbauer, K. K., McLachlin, K. M., … Cunningham, L. L. (2017). Cisplatin is retained in the cochlea indefinitely following chemotherapy. *Nature Communications*, *8*(1), 1654. https://doi.org/10.1038/s41467-017-01837-1

Brenton, J. D., Carey, L. A., Ahmed, A., & Caldas, C. (2005, October 10). Molecular classification and molecular forecasting of breast cancer: Ready for clinical application? *Journal of Clinical Oncology*. https://doi.org/10.1200/JCO.2005.03.3845

Brouckaert, O., Wildiers, H., Floris, G., & Neven, P. (2012). Update on triple-negative breast cancer: Prognosis and management strategies. *International Journal of Women's Health*, *4*(1), 511–520. https://doi.org/10.2147/IJWH.S18541

Browning, R. J., Reardon, P. J. T., Parhizkar, M., Pedley, R. B., Edirisinghe, M., Knowles, J. C., & Stride, E. (2017). Drug Delivery Strategies for Platinum-Based Chemotherapy. *ACS Nano*, *11*(9), 8560–8578. https://doi.org/10.1021/acsnano.7b04092

Cabula, C., Campana, L. G., Grilz, G., Galuppo, S., Bussone, R., De Meo, L., … Agresti, R. (2015). Electrochemotherapy in the Treatment of Cutaneous Metastases from Breast Cancer: A Multicenter Cohort Analysis. *Annals of Surgical Oncology*, *22*(S3), 442–450. https://doi.org/10.1245/s10434-015-4779-6

Cadigan, K. (2003). Wnt / β-Catenin Signaling | Cell Signaling Technology. Retrieved May 19, 2020, from https://www.cellsignal.com/contents/science-cst-pathways-developmental-biology/wnt-catenin-signaling/pathways-wnt

Cadossi, R., Ronchetti, M., & Cadossi, M. (2014). Locally enhanced chemotherapy by electroporation: clinical experiences and perspective of use of electrochemotherapy. *Future Oncology*, *10*(5), 877–890.

Cailleau, R., Olive, M., & Cruciger, Q. V. (1978). Long-term human breast carcinoma cell lines of metastatic origin: preliminary characterization. *In Vitro*, *14*(11), 911–915. https://doi.org/10.1007/bf02616120

Camarillo, I. G., Xiao, F., Madhivanan, S., Salameh, T., Nichols, M., Reece, L. M., … Sundararajan, R. (2014). 4 - Low and high voltage electrochemotherapy for breast cancer: an in vitro model study BT - Electroporation-Based Therapies for Cancer (pp. 55–102). Woodhead Publishing. https://doi.org/https://doi.org/10.1533/9781908818294.55

Campana, L. G., Edhemovic, I., Soden, D., Perrone, A. M., Scarpa, M., Campanacci, L., … Sersa, G. (2019). Electrochemotherapy – Emerging applications technical advances, new indications, combined approaches, and multi-institutional collaboration. *European Journal of Surgical Oncology*. https://doi.org/10.1016/j.ejso.2018.11.023

Campana, L. G., Falci, C., Basso, M., Sieni, E., & Dughiero, F. (2014). 2 - Clinical electrochemotherapy for chest wall recurrence from breast cancer A2 - Sundararajan, Raji BT - Electroporation-Based Therapies for Cancer (pp. 3–33). Woodhead Publishing. https://doi.org/https://doi.org/10.1533/9781908818294.3

Campana, L. G., Galuppo, S., Valpione, S., Brunello, A., Ghiotto, C., Ongaro, A., & Rossi, C. R. (2014). Bleomycin electrochemotherapy in elderly metastatic breast cancer patients: clinical outcome and management considerations. *Journal of Cancer Research and Clinical Oncology*, *140*(9), 1557–1565. https://doi.org/10.1007/s00432-014-1691-6

Campana, L. G., Marconato, R., Valpione, S., Galuppo, S., Alaibac, M., Rossi, C. R., & Mocellin, S. (2017). Basal cell carcinoma: 10-year experience with electrochemotherapy. *Journal of Translational Medicine*, *15*(1), 122. https://doi.org/10.1186/s12967-017-1225-5

Campana, L. G., Mocellin, S., Basso, M., Puccetti, O., De Salvo, G. L., Chiarion-Sileni, V., … Nitti, D. (2009). Bleomycin-Based Electrochemotherapy: Clinical Outcome from a Single Institution's Experience with 52 Patients. *Annals of Surgical Oncology*, *16*(1), 191–199. https://doi.org/10.1245/s10434-008-0204-8

Campana, L. G., Testori, A., Curatolo, P., Quaglino, P., Mocellin, S., Framarini, M., … Bonadies, A. (2016a). Treatment efficacy with electrochemotherapy: A multi-institutional prospective observational study on 376 patients with superficial tumors. *European Journal of Surgical Oncology*, *42*(12), 1914–1923. https://doi.org/10.1016/j.ejso.2016.06.399

Campana, L. G., Testori, A., Curatolo, P., Quaglino, P., Mocellin, S., Framarini, M., … Bonadies, A. (2016b). Treatment efficacy with electrochemotherapy: A multi-institutional prospective observational study on 376 patients with superficial tumors. *European Journal of Surgical Oncology (EJSO)*, *42*(12), 1914–1923. Retrieved from http://www.ncbi.nlm.nih.gov/pubmed/27424789

Campana, L. G., Valpione, S., Falci, C., Mocellin, S., Basso, M., Corti, L., … Rossi, C. R. (2012). The activity and safety of electrochemotherapy in persistent chest wall recurrence from breast cancer after mastectomy: a phase-II study. *Breast Cancer Research and Treatment*, *134*(3), 1169–1178. https://doi.org/10.1007/s10549-012-2095-4

Carey, L. A., Dees, E. C., Sawyer, L., Gatti, L., Moore, D. T., Collichio, F., … Perou, C. M. (2007). The triple negative paradox: Primary tumor chemosensitivity of breast cancer subtypes. *Clinical Cancer Research*, *13*(8), 2329–2334. https://doi.org/10.1158/1078-0432.CCR-06-1109

Carey, L. A., Perou, C. M., Livasy, C. A., Dressler, L. G., Cowan, D., Conway, K., … Millikan, R. C. (2006). Race, breast cancer subtypes, and survival in the Carolina Breast Cancer Study. *JAMA*, *295*(21), 2492–2502. https://doi.org/10.1001/jama.295.21.2492

Carmona-Saez, P., Chagoyen, M., Tirado, F., Carazo, J. M., & Pascual-Montano, A. (2007). GENECODIS: a web-based tool for finding significant concurrent annotations in gene lists. *Genome Biology*, *8*(1), R3. https://doi.org/10.1186/gb-2007-8-1-r3

Cavallo, J. (2013). Dr. Bernard Fisher's Breast Cancer Research Left a Lasting Legacy of Improved Therapeutic Efficacy and Survival. *The ASCO Post*, 1–6. Retrieved from https://www.ascopost.com/issues/may-15-2013/dr-bernard-fishers-breast-cancer-research-left-a-lasting-legacy-of-improved-therapeutic-efficacy-and-survival/

Čemažar, M., Miklavčič, D., Ščnčar, J., Dolžan, V., Golouh, R., & Serša, G. (1999). Increased platinum accumulation in SA-1 tumour cells after in vivo electrochemotherapy with cisplatin. *British Journal of Cancer*, *79*(9–10), 1386–1391. https://doi.org/10.1038/sj.bjc.6690222

Čemažar, M, Miklavcic, D., Mir, L. M., Belehradek, J., Bonnay, M., Fourcault, D., & Sersa, G. (2001). Electrochemotherapy of tumours resistant to cisplatin: a study in a murine tumour model. *European Journal of Cancer (Oxford, England : 1990)*, *37*(9), 1166–1172. https://doi.org/10.1016/S0959-8049(01)00091-0

Čemažar, Maja, Jarm, T., Miklavčič, D., Lebar, A. M., Ihan, A., Kopitar, N. A., & Serša, G. (1998). Effect of electric-field intensity on electropermeabilization and electrosensitivity of various tumor-cell lines in vitro. *Electromagnetic Biology and Medicine*, *17*(2), 263–272. https://doi.org/10.3109/15368379809022571

Cen, C., & Chen, X. (2017). The Electrode Modality Development in Pulsed Electric Field Treatment Facilitates Biocellular Mechanism Study and Improves Cancer Ablation Efficacy. *Journal of Healthcare Engineering*, *2017*, 1–10. https://doi.org/10.1155/2017/3624613

Chakravarthi, B. V. S. K., & Varambally, S. (2013). Targeting the link between late pregnancy and breast cancer. *ELife*, *2*, e01926–e01926. https://doi.org/10.7554/eLife.01926

Chandrashekar, D. S., Bashel, B., Balasubramanya, S. A. H., Creighton, C. J., Ponce-Rodriguez, I., Chakravarthi, B. V. S. K., & Varambally, S. (2017). UALCAN: A Portal for Facilitating Tumor Subgroup Gene Expression and Survival Analyses. *Neoplasia*, *19*(8), 649–658. https://doi.org/https://doi.org/10.1016/j.neo.2017.05.002

Chang, Y. C., Yang, Y. C., Tien, C. P., Yang, C. J., & Hsiao, M. (2018, August 1). Roles of Aldolase Family Genes in Human Cancers and Diseases. *Trends in Endocrinology and Metabolism*. Elsevier Inc. https://doi.org/10.1016/j.tem.2018.05.003

Chavez, K. J., Garimella, S. V, & Lipkowitz, S. (2011). Triple negative breast cancer cell lines: One tool in the search for better treatment of triple negative breast cancer. *Breast Disease*, *32*, 35–48. https://doi.org/10.3233/BD-2010-0307

Chen, C., Huang, Y.-B., Liu, X.-O., Gao, Y., Dai, H.-J., Song, F.-J., … Chen, K.-X. (2014). Active and passive smoking with breast cancer risk for Chinese females: a systematic review and meta-analysis. *Chinese Journal of Cancer*, *33*(6), 306–316. https://doi.org/10.5732/cjc.013.10248

Chen, J., Lu, L., feng, Y., Wang, H., Dai, L., li, Y., & Zhang, P. (2011). PKD2 mediates multi-drug resistance in breast cancer cells through modulation of P-glycoprotein expression. *Cancer Letters*, *300*(1), 48–56. https://doi.org/10.1016/j.canlet.2010.09.005

Chen, M., Chen, C., Shen, Z., Zhang, X., Chen, Y., Lin, F., … Wu, R. (2017). Extracellular pH is a biomarker enabling detection of breast cancer and liver cancer using CEST MRI. *Oncotarget*, *8*(28), 45759–45767. https://doi.org/10.18632/oncotarget.17404

Chiu, T. L., & Su, C. C. (2009). Curcumin inhibits proliferation and migration by increasing the Bax to Bcl-2 ratio and decreasing NF-kappa Bp65 expression in breast cancer MDA-MB-231 cells. *Int J Mol Med*, *23*.

Christakis, P. (2011). The birth of chemotherapy at Yale. Bicentennial lecture series: Surgery Grand Round. *The Yale Journal of Biology and Medicine*, *84*(2), 169–172. Retrieved from https://pubmed.ncbi.nlm.nih.gov/21698052

Ciucci, A., Gianferretti, P., Piva, R., Guyot, T., Snape, T. J., Roberts, S. M., & Santoro, M. G. (2006). Induction of apoptosis in estrogen receptor-negative breast cancer cells by natural and synthetic cyclopentenones: role of the IkappaB kinase/nuclear factor-kappaB pathway. *Molecular Pharmacology*, *70*(5), 1812–1821. https://doi.org/10.1124/mol.106.025759

Cohen, P. (2002). The origins of protein phosphorylation. *Nature Cell Biology*, *4*(5), E127–E130. https://doi.org/10.1038/ncb0502-e127

Coker-Gurkan, A., Celik, M., Ugur, M., Arisan, E.-D., Obakan-Yerlikaya, P., Durdu, Z. B., & Palavan-Unsal, N. (2018). Curcumin inhibits autocrine growth hormone-mediated invasion and metastasis by targeting NF-kappaB signaling and polyamine metabolism in breast cancer cells. *Amino Acids*, *50*(8), 1045–1069. https://doi.org/10.1007/s00726-018-2581-z

Coleman, M. P., Quaresma, M., Berrino, F., Lutz, J.-M., De Angelis, R., Capocaccia, R., … Young, J. L. (2008). Cancer survival in five continents: a worldwide population-based study (CONCORD). *The Lancet. Oncology*, *9*(8), 730–756. https://doi.org/10.1016/S1470-2045(08)70179-7

Colleoni, M., Cole, B. F., Viale, G., Regan, M. M., Price, K. N., Maiorano, E., … Gusterson, B. A. (2010). Classical cyclophosphamide, methotrexate, and fluorouracil chemotherapy is more effective in triple-negative, node-negative breast cancer: results from two randomized trials of adjuvant chemoendocrine therapy for node-negative breast cancer. *Journal of Clinical Oncology : Official Journal of the American Society of Clinical Oncology*, *28*(18), 2966–2973. https://doi.org/10.1200/JCO.2009.25.9549

Conway, R. E., Iglesias, K., Hired, Z., Rutledge, G., & Kirmani, K. (2019). Abstract 1785: Neprilysin: A potential regulator of PI3K/AKT signaling in triple negative breast cancer cells. In *Molecular and Cellular Biology / Genetics* (pp. 1785–1785). American Association for Cancer Research. https://doi.org/10.1158/1538-7445.AM2019-1785

Cossu-Rocca, P., Orru, S., Muroni, M. R., Sanges, F., Sotgiu, G., Ena, S., … De Miglio, M. R. (2015). Analysis of PIK3CA Mutations and Activation Pathways in Triple Negative Breast Cancer. *PloS One*, *10*(11), e0141763. https://doi.org/10.1371/journal.pone.0141763

Cox, A. D., & Der, C. J. (2010). Ras history: The saga continues. *Small GTPases*, *1*(1), 2–27. https://doi.org/10.4161/sgtp.1.1.12178

Cox, J., & Mann, M. (2008). MaxQuant enables high peptide identification rates, individualized p.p.b.-range mass accuracies and proteome-wide protein quantification. *Nature Biotechnology*, *26*(12), 1367–1372. https://doi.org/10.1038/nbt.1511

Cox, J., Neuhauser, N., Michalski, A., Scheltema, R. A., Olsen, J. V., & Mann, M. (2011). Andromeda: A peptide search engine integrated into the MaxQuant environment. *Journal of Proteome Research*, *10*(4), 1794–1805. https://doi.org/10.1021/pr101065j

Craig, D. W., O'Shaughnessy, J. A., Kiefer, J. A., Aldrich, J., Sinari, S., Moses, T. M., … Carpten, J. D. (2013). Genome and transcriptome sequencing in prospective metastatic triple-negative breast cancer uncovers therapeutic vulnerabilities. *Molecular Cancer Therapeutics*, *12*(1), 104–116. https://doi.org/10.1158/1535-7163.MCT-12-0781

Cruz, E. . (2017). *Cell line profile MDA-MB-231 (ECACC catalogue no. 92020424)*. *European Collection of Authenticated Cell Cultures* (Vol. 2780). Retrieved from https://www.phe-culturecollections.org.uk/products/celllines/generalcell/detail.jsp?refId=85120602&collection=ecacc_gc

Dai, X., Li, T., Bai, Z., Yang, Y., Liu, X., Zhan, J., & Shi, B. (2015). Breast cancer intrinsic subtype classification, clinical use and future trends. *American Journal of Cancer Research*, *5*(10), 2929–2943.

Dasari, S., & Bernard Tchounwou, P. (2014, October 5). Cisplatin in cancer therapy: Molecular mechanisms of action. *European Journal of Pharmacology*. https://doi.org/10.1016/j.ejphar.2014.07.025

Davis, N. M., Sokolosky, M., Stadelman, K., Abrams, S. L., Libra, M., Candido, S., … McCubrey, J. A. (2014). Deregulation of the EGFR/PI3K/PTEN/Akt/mTORC1 pathway in breast cancer: possibilities for therapeutic intervention. *Oncotarget*, *5*(13), 4603–4650. https://doi.org/10.18632/oncotarget.2209

De Giorgi, V., Scarfì, F., Saqer, E., Gori, A., Tomassini, G. M., & Covarelli, P. (2020). The use of cisplatin electrochemotherapy in nonmelanoma skin cancers: A single-center study. *Dermatologic Therapy*, e13547. https://doi.org/10.1111/dth.13547

Dennison, J. B., Molina, J. R., Mitra, S., Gonzalez-Angulo, A. M., Balko, J. M., Kuba, M. G., … Mills, G. B. (2013). Lactate Dehydrogenase B: A Metabolic Marker of Response to Neoadjuvant Chemotherapy in Breast Cancer. *Clinical Cancer Research*, *19*(13), 3703–3713. https://doi.org/10.1158/1078-0432.ccr-13-0623

Dent, R., Trudeau, M., Pritchard, K. I., Hanna, W. M., Kahn, H. K., Sawka, C. A., … Narod, S. A. (2007). Triple-Negative Breast Cancer: Clinical Features and Patterns of Recurrence. *Clinical Cancer Research*, *13*(15), 4429 LP – 4434. Retrieved from http://clincancerres.aacrjournals.org/content/13/15/4429.abstract

DeVita, V. T., Lawrence, T. S., & Rosenberg, S. A. (2015). *DeVita, Hellman, and Rosenberg's cancer: Principles & practice of oncology: Tenth edition*. *DeVita, Hellman, and Rosenberg's Cancer: Principles & Practice of Oncology: Tenth Edition*. Wolters Kluwer Health Adis (ESP).

Dey, N., Barwick, B. G., Moreno, C. S., Ordanic-Kodani, M., Chen, Z., Oprea-Ilies, G., … Leyland-Jones, B. R. (2013). Wnt signaling in triple negative breast cancer is associated with metastasis. *BMC Cancer*, *13*(1), 537. https://doi.org/10.1186/1471-2407-13-537

Dhar, S., Kolishetti, N., Lippard, S. J., & Farokhzad, O. C. (2011). Targeted delivery of a cisplatin prodrug for safer and more effective prostate cancer therapy in vivo. *Proceedings of the National Academy of Sciences of the United States of America*, *108*(5), 1850–1855. https://doi.org/10.1073/pnas.1011379108

Dieterich, M., Stubert, J., Reimer, T., Erickson, N., & Berling, A. (2014). Influence of lifestyle factors on breast cancer risk. *Breast Care (Basel, Switzerland)*, *9*(6), 407–414. https://doi.org/10.1159/000369571

Dietze, E. C., Chavez, T. A., & Seewaldt, V. L. (2018). Obesity and Triple-Negative Breast Cancer: Disparities, Controversies, and Biology. *The American Journal of Pathology*, *188*(2), 280–290. https://doi.org/10.1016/j.ajpath.2017.09.018

Dolatshad, H., Pellagatti, A., Liberante, F. G., Llorian, M., Repapi, E., Steeples, V., … Boultwood, J. (2016). Cryptic splicing events in the iron transporter ABCB7 and other key target genes in SF3B1-mutant myelodysplastic syndromes. *Leukemia*, *30*(12), 2322–2331. https://doi.org/10.1038/leu.2016.149

Dong, T., Liu, Z., Xuan, Q., Wang, Z., Ma, W., & Zhang, Q. (2017). Tumor LDH-A expression and serum LDH status are two metabolic predictors for triple negative breast cancer brain metastasis. *Scientific Reports*, *7*(1), 6069. https://doi.org/10.1038/s41598-017-06378-7

Duncan, J. A., Reeves, J. R., & Cooke, T. G. (1998). BRCA1 and BRCA2 proteins: roles in health and disease. *Molecular Pathology : MP*, *51*(5), 237–247. https://doi.org/10.1136/mp.51.5.237

Echeverria, G. V., Ge, Z., Seth, S., Zhang, X., Jeter-Jones, S., Zhou, X., … Piwnica-Worms, H. (2019). Resistance to neoadjuvant chemotherapy in triple-negative breast cancer mediated by a reversible drug-tolerant state. *Science Translational Medicine*, *11*(488), eaav0936. https://doi.org/10.1126/scitranslmed.aav0936

Edhemovic, I., Gadzijev, E. M., Brecelj, E., Miklavcic, D., Kos, B., Zupanic, A., … Sersa, G. (2011). Electrochemotherapy: A New Technological Approach in Treatment of Metastases in the Liver. *Technology in Cancer Research & Treatment*, *10*(5), 475–485. https://doi.org/10.7785/tcrt.2012.500224

Ekor, M. (2014). The growing use of herbal medicines: Issues relating to adverse reactions and challenges in monitoring safety. *Frontiers in Neurology*, *4 JAN*(January), 1–10. https://doi.org/10.3389/fphar.2013.00177

Elmore, S. (2007). Apoptosis: a review of programmed cell death. *Toxicologic Pathology*, *35*(4), 495–516. https://doi.org/10.1080/01926230701320337

Endoscopic Assisted Electrochemotherapy in Addition to Neoadjuvant Treatment of Locally Advanced Rectal Cancer - Full Text View - ClinicalTrials.gov. (n.d.). Retrieved January 21, 2019, from https://clinicaltrials.gov/ct2/show/NCT03040180

Engebraaten, O., Vollan, H. K. M., & Børresen-Dale, A.-L. (2013). Triple-negative breast cancer and the need for new therapeutic targets. *The American Journal of Pathology*, *183*(4), 1064–1074. https://doi.org/10.1016/j.ajpath.2013.05.033

European Society for Medical Oncology (ESMO). (2018). Breast Cancer: A Guide for Patients. Retrieved May 21, 2020, from https://www.esmo.org/for-patients/patient-guides/breast-cancer

Falk, H., Matthiessen, L. W., Wooler, G., & Gehl, J. (2018). Calcium electroporation for treatment of cutaneous metastases; a randomized double-blinded phase II study, comparing the effect of calcium electroporation with electrochemotherapy. *Acta Oncologica*, *57*(3), 311–319. https://doi.org/10.1080/0284186X.2017.1355109

Fan, H., Liang, Y., Jiang, B., Li, X., Xun, H., Sun, J., … Ma, X. (2016). Curcumin inhibits intracellular fatty acid synthase and induces apoptosis in human breast cancer MDA-MB-231 cells. *Oncology Reports*, *35*(5), 2651–2656. https://doi.org/10.3892/or.2016.4682

Fang, H. Y., Chen, S. B., Guo, D. J., Pan, S. Y., & Yu, Z. L. (2011). Proteomic identification of differentially expressed proteins in curcumin-treated MCF-7 cells. *Phytomedicine : International Journal of Phytotherapy and Phytopharmacology*, *18*(8–9), 697–703. https://doi.org/10.1016/j.phymed.2010.11.012

Farber, S., & Diamond, L. K. (1948). Temporary remissions in acute leukemia in children produced by folic acid antagonist, 4-aminopteroyl-glutamic acid. *The New England Journal of Medicine*, *238*(23), 787–793. https://doi.org/10.1056/NEJM194806032382301

Farris, F. F., Dedrick, R. L., & King, F. G. (1988). Cisplatin pharmacokinetics: applications of a physiological model. *Toxicology Letters*, *43*(1), 117–137. https://doi.org/https://doi.org/10.1016/0378-4274(88)90024-0

Ferlay, J., Ervik, J., Lam, F., Colombet, M., Mery, L., Piñeros, M., … Bray, F. (2018). Global Cancer Observatory: Cancer Today. https://doi.org/L11\n10.1051/0004-6361/201016331

Ferreira, L. C., Arbab, A. S., Jardim-Perassi, B. V., Borin, T. F., Varma, N. R. S., Iskander, A. S. M., … Zuccari, D. A. P. de C. (2015). Effect of Curcumin on Pro-angiogenic Factors in the Xenograft Model of Breast Cancer. *Anti-Cancer Agents in Medicinal Chemistry*, *15*(10), 1285–1296. Retrieved from http://www.ncbi.nlm.nih.gov/pubmed/25991545

Fisher, B., Anderson, S., Bryant, J., Margolese, R. G., Deutsch, M., Fisher, E. R., … Wolmark, N. (2002). Twenty-year follow-up of a randomized trial comparing total mastectomy, lumpectomy, and lumpectomy plus irradiation for the treatment of invasive breast cancer. *The New England Journal of Medicine*, *347*(16), 1233–1241. https://doi.org/10.1056/NEJMoa022152

Fisher, B., Bauer, M., Margolese, R., Poisson, R., Pilch, Y., Redmond, C., … Montague, E. (1985). Five-year results of a randomized clinical trial comparing total mastectomy and segmental mastectomy with or without radiation in the treatment of breast cancer. *The New England Journal of Medicine*, *312*(11), 665–673. https://doi.org/10.1056/NEJM198503143121101

Fisher, B., Brown, A. M., Dimitrov, N. V, Poisson, R., Redmond, C., Margolese, R. G., … Kardinal, C. G. (1990). Two months of doxorubicin-cyclophosphamide with and without interval reinduction therapy compared with 6 months of cyclophosphamide, methotrexate, and fluorouracil in positive-node breast cancer patients with tamoxifen-nonresponsive tumors: results from . *Journal of Clinical Oncology : Official Journal of the American Society of Clinical Oncology*, *8*(9), 1483–1496. https://doi.org/10.1200/JCO.1990.8.9.1483

Fisher, B., Jeong, J.-H., Anderson, S., Bryant, J., Fisher, E. R., & Wolmark, N. (2002). Twenty-five-year follow-up of a randomized trial comparing radical mastectomy, total mastectomy, and total mastectomy followed by irradiation. *The New England Journal of Medicine*, *347*(8), 567–575. https://doi.org/10.1056/NEJMoa020128

Fisher, B., Redmond, C., Fisher, E. R., Bauer, M., Wolmark, N., Wickerham, D. L., … Foster, R. (1985). Ten-year results of a randomized clinical trial comparing radical mastectomy and total mastectomy with or without radiation. *The New England Journal of Medicine*, *312*(11), 674–681. https://doi.org/10.1056/NEJM198503143121102

Fisher, B., Redmond, C., Poisson, R., Margolese, R., Wolmark, N., Wickerham, L., … Pilch, Y. (1989). Eight-year results of a randomized clinical trial comparing total mastectomy and lumpectomy with or without irradiation in the treatment of breast cancer. *The New England Journal of Medicine*, *320*(13), 822–828. https://doi.org/10.1056/NEJM198903303201302

Flegal, K. M., Kruszon-Moran, D., Carroll, M. D., Fryar, C. D., & Ogden, C. L. (2016). Trends in Obesity Among Adults in the United States, 2005 to 2014. *JAMA*, *315*(21), 2284–2291. https://doi.org/10.1001/jama.2016.6458

Fortner, R. T., Sisti, J., Chai, B., Collins, L. C., Rosner, B., Hankinson, S. E., … Eliassen, A. H. (2019). Parity, breastfeeding, and breast cancer risk by hormone receptor status and molecular phenotype: results from the Nurses' Health Studies. *Breast Cancer Research*, *21*(1), 40. https://doi.org/10.1186/s13058-019-1119-y

Frandsen, S. K., & Gehl, J. (2018, January 16). A review on differences in effects on normal and malignant cells and tissues to electroporation-based therapies: A focus on calcium electroporation. *Technology in Cancer Research and Treatment*. SAGE PublicationsSage CA: Los Angeles, CA. https://doi.org/10.1177/1533033818788077

Franken, N. A. P., Rodermond, H. M., Stap, J., Haveman, J., & van Bree, C. (2006). Clonogenic assay of cells in vitro. *Nature Protocols*, *1*(5), 2315–2319. https://doi.org/10.1038/nprot.2006.339

Fraser, S. P., Diss, J. K. J., Chioni, A.-M., Mycielska, M. E., Pan, H., Yamaci, R. F., … Djamgoz, M. B. A. (2005). Voltage-Gated Sodium Channel Expression and Potentiation of Human Breast Cancer Metastasis. *Clinical Cancer Research*, *11*(15), 5381–5389. https://doi.org/10.1158/1078-0432.CCR-05-0327

Freeman, M. D., Gopman, J. M., & Salzberg, C. A. (2018). The evolution of mastectomy surgical technique: from mutilation to medicine. *Gland Surgery*, *7*(3), 308–315. https://doi.org/10.21037/gs.2017.09.07

Fu, D., He, C., Wei, J., Zhang, Z., Luo, Y., Tan, H., & Ren, C. (2018). PGK1 is a Potential Survival Biomarker and Invasion Promoter by Regulating the HIF-1alpha-Mediated Epithelial-Mesenchymal Transition Process in Breast Cancer. *Cellular Physiology and Biochemistry : International Journal of Experimental Cellular Physiology, Biochemistry, and Pharmacology*, *51*(5), 2434–2444. https://doi.org/10.1159/000495900

Fukuda, R., Suico, M. A., Koyama, K., Omachi, K., Kai, Y., Matsuyama, S., … Kai, H. (2013). Mild electrical stimulation at 0.1-ms pulse width induces p53 protein phosphorylation and G2 arrest in human epithelial cells. *Journal of Biological Chemistry*, *288*(22), 16117–16126. https://doi.org/10.1074/jbc.M112.442442

Gabriel, B., & Teissie, J. (1994). Generation of reactive-oxygen species induced by electropermeabilization of Chinese hamster ovary cells and their consequence on cell viability. *European Journal of Biochemistry*, *223*(1), 25–33. https://doi.org/10.1111/j.1432-1033.1994.tb18962.x

Gallardo, M., & Calaf, G. M. (2016). Curcumin inhibits invasive capabilities through epithelial mesenchymal transition in breast cancer cell lines. *International Journal of Oncology*, *49*(3), 1019–1027. https://doi.org/10.3892/ijo.2016.3598

Gandhi, N., & Das, G. (2019). Metabolic Reprogramming in Breast Cancer and Its Therapeutic Implications. *Cells*, *8*(2), 89. https://doi.org/10.3390/cells8020089

Gang, B. P., Dilda, P. J., Hogg, P. J., & Blackburn, A. C. (2014). Targeting of two aspects of metabolism in breast cancer treatment. *Cancer Biology and Therapy*, *15*(11), 1533–1541. https://doi.org/10.4161/15384047.2014.955992

Garrido-Castro, A. C., Lin, N. U., & Polyak, K. (2019). Insights into molecular classifications of triple-negative breast cancer: Improving patient selection for treatment. *Cancer Discovery*. https://doi.org/10.1158/2159-8290.CD-18-1177

Gasljevic, G., Edhemovic, I., Cemazar, M., Brecelj, E., Gadzijev, E. M., Music, M. M., & Sersa, G. (2017). Histopathological findings in colorectal liver metastases after electrochemotherapy. *PLOS ONE*, *12*(7), e0180709. https://doi.org/10.1371/journal.pone.0180709

Gazella, K. A. (2009). Pioneering Biochemist Bharat B. Aggarwal, PhD, of the M.D. Anderson Cancer Center, on Discovering Novel and Effective Cancer Treatments | Natural Medicine Journal. Retrieved April 1, 2019, from https://www.naturalmedicinejournal.com/journal/2009-12/pioneering-biochemist-bharat-b-aggarwal-phd-md-anderson-cancer-center-discovering

Gehl, J. (2005). [Investigational treatment of cancer using electrochemotherapy, electrochemoimmunotherapy and electro-gene transfer]. *Ugeskrift for Laeger*, *167*(34), 3156–3159. Retrieved from http://www.ncbi.nlm.nih.gov/pubmed/16117912

Gehl, J., Sersa, G., Matthiessen, L. W., Muir, T., Soden, D., Occhini, A., … Mir, L. M. (2018, July 3). Updated standard operating procedures for electrochemotherapy of cutaneous tumours and skin metastases. *Acta Oncologica*. Taylor & Francis. https://doi.org/10.1080/0284186X.2018.1454602

Geng, C., Li, J., Ding, F., Wu, G., Yang, Q., Sun, Y., … Tian, X. (2016). Curcumin suppresses 4-hydroxytamoxifen resistance in breast cancer cells by targeting SLUG/Hexokinase 2 pathway. *Biochemical and Biophysical Research Communications*, *473*(1), 147–153. https://doi.org/10.1016/j.bbrc.2016.03.067

Gerratana, L., Fanotto, V., Pelizzari, G., Agostinetto, E., & Puglisi, F. (2016). Do platinum salts fit all triple negative breast cancers? *Cancer Treatment Reviews*, *48*, 34–41. https://doi.org/10.1016/j.ctrv.2016.06.004

Gianfaldoni, S., Gianfaldoni, R., Wollina, U., Lotti, J., Tchernev, G., & Lotti, T. (2017). An Overview on Radiotherapy: From Its History to Its Current Applications in Dermatology. *Open Access Macedonian Journal of Medical Sciences*, *5*(4), 521–525. https://doi.org/10.3889/oamjms.2017.122

Gibson, G. R., Qian, D., Ku, J. K., & Lai, L. L. (2005). Metaplastic breast cancer: clinical features and outcomes. *The American Surgeon*, *71*(9), 725–730.

Gilman, A., & Philips, F. S. (1946). The Biological Actions and Therapeutic Applications of the B-Chloroethyl Amines and Sulfides. *Science (New York, N.Y.)*, *103*(2675), 409–436. https://doi.org/10.1126/science.103.2675.409

Giltnane, J. M., & Balko, J. M. (2014). Rationale for targeting the Ras/MAPK pathway in triple-negative breast cancer. *Discovery Medicine*, *17*(95), 275–283.

Giubellino, A., Burke, T. R., & Bottaro, D. P. (2008, August). Grb2 signaling in cell motility and cancer. *Expert Opinion on Therapeutic Targets*. https://doi.org/10.1517/14728222.12.8.1021

Giuli, M. V, Giuliani, E., Screpanti, I., Bellavia, D., & Checquolo, S. (2019). Notch Signaling Activation as a Hallmark for Triple-Negative Breast Cancer Subtype. *Journal of Oncology*, *2019*, 8707053. https://doi.org/10.1155/2019/8707053

Goel, A. K., Nandy, M., & Sharma, G. (2010). Cisplatin as neoadjuvant chemotherapy in triple negative breast cancer: Exciting early results. *Indian Journal of Medical and Paediatric Oncology : Official Journal of Indian Society of Medical & Paediatric Oncology*, *31*(3), 76–78. https://doi.org/10.4103/0971-5851.73588

Goel, A., Kunnumakkara, A. B., & Aggarwal, B. B. (2008). Curcumin as ``Curecumin'': from kitchen to clinic. *Biochem Pharmacol*, *75*. https://doi.org/10.1016/j.bcp.2007.08.016

Gohr, K., Hamacher, A., Engelke, L. H., & Kassack, M. U. (2017). Inhibition of PI3K/Akt/mTOR overcomes cisplatin resistance in the triple negative breast cancer cell line HCC38. *BMC Cancer*, *17*(1), 711. https://doi.org/10.1186/s12885-017-3695-5

Gong, Y., Ji, P., Xiao, Y., Ma, D., Jin, M.-L., Hu, X., … Shao, Z.-M. (2019). Integrative analysis of metabolic subtypes in triple-negative breast cancer reveals new therapeutic strategies. *Annals of Oncology*, *30*(Supplement_9). https://doi.org/10.1093/annonc/mdz416.002

Goodman, L. S., Wintrobe, M. M., Dameshek, W., Goodman, M. J., Gilman, A., & McLennan, M. T. (1984). Landmark article Sept. 21, 1946: Nitrogen mustard therapy. Use of methyl-bis(beta-chloroethyl)amine hydrochloride and tris(beta-chloroethyl)amine hydrochloride for Hodgkin's disease, lymphosarcoma, leukemia and certain allied and miscellaneous disorders. . *JAMA*, *251*(17), 2255–2261. https://doi.org/10.1001/jama.251.17.2255

Gorlach, A., Bertram, K., Hudecova, S., & Krizanova, O. (2015). Calcium and ROS: A mutual interplay. *Redox Biology*, *6*, 260–271. https://doi.org/10.1016/j.redox.2015.08.010

Grandjean, G., de Jong, P. R., James, B., Koh, M. Y., Lemos, R., Kingston, J., … Powis, G. (2016). Definition of a Novel Feed-Forward Mechanism for Glycolysis-HIF1α Signaling in Hypoxic Tumors Highlights Aldolase A as a Therapeutic Target. *Cancer Research*, *76*(14), 4259–4269. https://doi.org/10.1158/0008-5472.CAN-16-0401

Gray, M. W. (2001). Organelles. *Encyclopedia of Genetics*, 1377–1379. https://doi.org/10.1006/RWGN.2001.0937

Greenup, R., Buchanan, A., Lorizio, W., Rhoads, K., Chan, S., Leedom, T., … Shelley Hwang, E. (2013). Prevalence of BRCA mutations among women with triple-negative breast cancer (TNBC) in a genetic counseling cohort. *Annals of Surgical Oncology*, *20*(10), 3254–3258. https://doi.org/10.1245/s10434-013-3205-1

Grover-McKay, M., Walsh, S. A., Seftor, E. A., Thomas, P. A., & Hendrix, M. J. (1998). Role for glucose transporter 1 protein in human breast cancer. *Pathology Oncology Research : POR*, *4*(2), 115–120. https://doi.org/10.1007/BF02904704

Guarneri, V., Dieci, M. V., & Conte, P. (2013). Relapsed triple-negative breast cancer: challenges and treatment strategies. *Drugs*, *73*(12), 1257–1265. https://doi.org/10.1007/s40265-013-0091-6

Gudmundsdottir, K., & Ashworth, A. (2006). The roles of BRCA1 and BRCA2 and associated proteins in the maintenance of genomic stability. *Oncogene*, *25*(43), 5864–5874. https://doi.org/10.1038/sj.onc.1209874

Guha, M., Srinivasan, S., Raman, P., Jiang, Y., Kaufman, B. A., Taylor, D., … Avadhani, N. G. (2018). Aggressive triple negative breast cancers have unique molecular signature on the basis of mitochondrial genetic and functional defects. *Biochimica et Biophysica Acta (BBA) - Molecular Basis of Disease*, *1864*(4), 1060–1071. https://doi.org/10.1016/J.BBADIS.2018.01.002

Gupta, N., Badeaux, M., Liu, Y., Naxerova, K., Sgroi, D., Munn, L. L., … Garkavtsev, I. (2017). Stress granule-associated protein G3BP2 regulates breast tumor initiation. *Proceedings of the National Academy of Sciences*, *114*(5), 1033–1038. https://doi.org/10.1073/pnas.1525387114

Gupta, S. C., Patchva, S., Koh, W., & Aggarwal, B. B. (2012). Discovery of curcumin, a component of golden spice, and its miraculous biological activities. *Clinical and Experimental Pharmacology & Physiology*, *39*(3), 283–299. https://doi.org/10.1111/j.1440-1681.2011.05648.x

Gutierres, V. O., Campos, M. L., Arcaro, C. A., Assis, R. P., Baldan-Cimatti, H. M., Peccinini, R. G., … Brunetti, I. L. (2015). Curcumin Pharmacokinetic and Pharmacodynamic Evidences in Streptozotocin-Diabetic Rats Support the Antidiabetic Activity to Be via Metabolite(s). *Evidence-Based Complementary and Alternative Medicine*, *2015*, 678218. https://doi.org/10.1155/2015/678218

Haagensen, C. D. (1986). *Diseases of the breast* (3rd ed.). Saunders Co.

Halsted, W. S. (1894). I. The Results of Operations for the Cure of Cancer of the Breast Performed at the Johns Hopkins Hospital from June, 1889, to January, 1894. *Annals of Surgery*, *20*(5), 497–555. https://doi.org/10.1097/00000658-189407000-00075

Halsted, W. S. (1907). I. The Results of Radical Operations for the Cure of Carcinoma of the Breast. *Annals of Surgery*, *46*(1), 1–19. https://doi.org/10.1097/00000658-190707000-00001

Haltiwanger, S. (n.d.). The Electrical Properties of Cancer Cells. Retrieved September 28, 2018, from http://www.royalrife.com/haltiwanger1.pdf

Han, H. S., Diéras, V., Robson, M., Palácová, M., Marcom, P. K., Jager, A., … Puhalla, S. (2018). Veliparib with temozolomide or carboplatin/paclitaxel versus placebo with carboplatin/paclitaxel in patients with BRCA1/2 locally recurrent/metastatic breast cancer: randomized phase II study. *Annals of Oncology : Official Journal of the European Society for Medical Oncology*, *29*(1), 154–161. https://doi.org/10.1093/annonc/mdx505

Hanna, H., Andre, F. M., & Mir, L. M. (2017). Electrical control of calcium oscillations in mesenchymal stem cells using microsecond pulsed electric fields. *Stem Cell Research and Therapy*, *8*(1), 91. https://doi.org/10.1186/s13287-017-0536-z

Hanna, H., Denzi, A., Liberti, M., André, F. M., & Mir, L. M. (2017). Electropermeabilization of Inner and Outer Cell Membranes with Microsecond Pulsed Electric Fields: Quantitative Study with Calcium Ions. *Scientific Reports*, *7*(1), 13079. https://doi.org/10.1038/s41598-017-12960-w

Harris, J. R. (2014). Fifty Years of Progress in Radiation Therapy for Breast Cancer. *American Society of Clinical Oncology Educational Book*, (34), 21–25. https://doi.org/10.14694/EdBook_AM.2014.34.21

Henderson, I. C., Berry, D. A., Demetri, G. D., Cirrincione, C. T., Goldstein, L. J., Martino, S., … Norton, L. (2003). Improved outcomes from adding sequential Paclitaxel but not from escalating Doxorubicin dose in an adjuvant chemotherapy regimen for patients with node-positive primary breast cancer. *Journal of Clinical Oncology : Official Journal of the American Society of Clinical Oncology*, *21*(6), 976–983. https://doi.org/10.1200/JCO.2003.02.063

Herring, S. K., Moon, H.-J., Rawal, P., Chhibber, A., & Zhao, L. (2019). Brain clusterin protein isoforms and mitochondrial localization. *ELife*, *8*, e48255. https://doi.org/10.7554/eLife.48255

Ho, M. Y., & Mackey, J. R. (2014). Presentation and management of docetaxel-related adverse effects in patients with breast cancer. *Cancer Management and Research*, *6*, 253–259. https://doi.org/10.2147/CMAR.S40601

Hoeflich, K. P., O'Brien, C., Boyd, Z., Cavet, G., Guerrero, S., Jung, K., … Lackner, M. R. (2009). In vivo antitumor activity of MEK and phosphatidylinositol 3-kinase inhibitors in basal-like breast cancer models. *Clinical Cancer Research : An Official Journal of the American Association for Cancer Research*, *15*(14), 4649–4664. https://doi.org/10.1158/1078-0432.CCR-09-0317

Holliday, D. L., & Speirs, V. (2011). Choosing the right cell line for breast cancer research. *Breast Cancer Research*, *13*(4), 215. https://doi.org/10.1186/bcr2889

Horie, R., Watanabe, M., Okamura, T., Taira, M., Shoda, M., Motoji, T., … Umezawa, K. (2006). DHMEQ, a new NF-kappaB inhibitor, induces apoptosis and enhances fludarabine effects on chronic lymphocytic leukemia cells. *Leukemia*, *20*(5), 800–806. https://doi.org/10.1038/sj.leu.2404167

Hsieh, C. H., Lu, C. H., Chen, W. T., Ma, B. L., & Chao, C. Y. (2017). Application of non-invasive low strength pulsed electric field to EGCG treatment synergistically enhanced the inhibition effect on PANC-1 cells. *PLoS ONE*, *12*(11), 1–17. https://doi.org/10.1371/journal.pone.0188885

Hsu, K. S., & Kao, H. Y. (2013). Alpha-Actinin 4 and Tumorigenesis of Breast Cancer. In *Vitamins and Hormones* (Vol. 93, pp. 323–351). https://doi.org/10.1016/B978-0-12-416673-8.00005-8

Huang, D. W., Sherman, B. T., & Lempicki, R. A. (2008). Bioinformatics enrichment tools: paths toward the comprehensive functional analysis of large gene lists. *Nucleic Acids Research*, *37*(1), 1–13.

Huang, D. W., Sherman, B. T., & Lempicki, R. A. (2009a). Bioinformatics enrichment tools: paths toward the comprehensive functional analysis of large gene lists. *Nucleic Acids Research*, *37*(1), 1–13. https://doi.org/10.1093/nar/gkn923

Huang, D. W., Sherman, B. T., & Lempicki, R. A. (2009b). Systematic and integrative analysis of large gene lists using DAVID bioinformatics resources. *Nature Protocols*, *4*(1), 44–57. https://doi.org/10.1038/nprot.2008.211

Huang, J., Li, Q., Sun, D., Lu, Y., Su, Y., Yang, X., … Chen, C. (2007). Biosynthesis of silver and gold nanoparticles by novel sundriedCinnamomum camphoraleaf. *Nanotechnology*, *18*(10), 105104. https://doi.org/10.1088/0957-4484/18/10/105104

Huang, T., Chen, Z., & Fang, L. (2013). Curcumin inhibits LPS-induced EMT through downregulation of NF-kappaB-Snail signaling in breast cancer cells. *Oncology Reports*, *29*(1), 117–124. https://doi.org/10.3892/or.2012.2080

Huang, Y., & Zhu, H. (2017). Protein Array-based Approaches for Biomarker Discovery in Cancer. *Genomics, Proteomics & Bioinformatics*, *15*(2), 73–81. https://doi.org/10.1016/j.gpb.2017.03.001

Hugh, J., Hanson, J., Cheang, M. C. U., Nielsen, T. O., Perou, C. M., Dumontet, C., … Vogel, C. (2009). Breast cancer subtypes and response to docetaxel in node-positive breast cancer: use of an immunohistochemical definition in the BCIRG 001 trial. *Journal of Clinical Oncology : Official Journal of the American Society of Clinical Oncology*, *27*(8), 1168–1176. https://doi.org/10.1200/JCO.2008.18.1024

Hussein, Y. R., Bandyopadhyay, S., Semaan, A., Ahmed, Q., Albashiti, B., Jazaerly, T., … Ali-Fehmi, R. (2011). Glut-1 Expression Correlates with Basal-like Breast Cancer. *Translational Oncology*, *4*(6), 321–327. https://doi.org/10.1593/tlo.11256

Hüttemann, M., Lee, I., Samavati, L., Yu, H., & Doan, J. W. (2007). Regulation of mitochondrial oxidative phosphorylation through cell signaling. *Biochimica et Biophysica Acta (BBA) - Molecular Cell Research*, *1773*(12), 1701–1720. https://doi.org/10.1016/J.BBAMCR.2007.10.001

Isakoff, S. J. (2010). Triple Negative Breast Cancer: Role of Specific Chemotherapy Agents. *Cancer J.*, *16*(1), 53–61. https://doi.org/10.1097/PPO.0b013e3181d24ff7.Triple

Isakoff, S. J., Mayer, E. L., He, L., Traina, T. A., Carey, L. A., Krag, K. J., … Ellisen, L. W. (2015). TBCRC009: A multicenter phase II clinical trial of platinum monotherapy with biomarker assessment in metastatic triple-negative breast cancer. *Journal of Clinical Oncology*, *33*(17), 1902–1909. https://doi.org/10.1200/JCO.2014.57.6660

Izuo, M. (2004). Medical history: Seishu Hanaoka and his success in breast cancer surgery under general anesthesia two hundred years ago. *Breast Cancer (Tokyo, Japan)*, *11*(4), 319–324. https://doi.org/10.1007/bf02968037

Jäger, R., Lowery, R. P., Calvanese, A. V, Joy, J. M., Purpura, M., & Wilson, J. M. (2014). Comparative absorption of curcumin formulations. *Nutrition Journal*, *13*, 11. https://doi.org/10.1186/1475-2891-13-11

Jang, S., & Atkins, M. B. (2014). Treatment of BRAF-mutant melanoma: the role of vemurafenib and other therapies. *Clinical Pharmacology and Therapeutics*, *95*(1), 24–31. https://doi.org/10.1038/clpt.2013.197

Jaroszeski, M. J., Dang, V., Pottinger, C., Hickey, J., Gilbert, R., & Heller, R. (2000). Toxicity of anticancer agents mediated by electroporation in vitro. *Anti-Cancer Drugs*, *11*(3), 201–208. Retrieved from http://www.ncbi.nlm.nih.gov/pubmed/10831279

Jézéquel, P., Guette, C., Lasla, H., Gouraud, W., Boissard, A., Guérin-Charbonnel, C., & Campone, M. (2019). iTRAQ-Based Quantitative Proteomic Analysis Strengthens Transcriptomic Subtyping of Triple-Negative Breast Cancer Tumors. *Proteomics*, *19*(21–22), 1800484. https://doi.org/10.1002/pmic.201800484

Jia, T., Zhang, L., Duan, Y., Zhang, M., Wang, G., Zhang, J., & Zhao, Z. (2014). The differential susceptibilities of MCF-7 and MDA-MB-231 cells to the cytotoxic effects of curcumin are associated with the PI3K/Akt-SKP2-Cip/Kips pathway. *Cancer Cell International*, *14*(1), 126. https://doi.org/10.1186/s12935-014-0126-4

Jiang, C., Davalos, R. V., & Bischof, J. C. (2015). A Review of Basic to Clinical Studies of Irreversible Electroporation Therapy. *IEEE Transactions on Biomedical Engineering*, *62*(1), 4–20. https://doi.org/10.1109/TBME.2014.2367543

Jiang, H.-L., Sun, H.-F., Gao, S.-P., Li, L.-D., Huang, S., Hu, X., … Jin, W. (2016). SSBP1 Suppresses TGF -Driven Epithelial-to-Mesenchymal Transition and Metastasis in Triple-Negative Breast Cancer by Regulating Mitochondrial Retrograde Signaling. *Cancer Research*, *76*(4), 952–964. https://doi.org/10.1158/0008-5472.CAN-15-1630

Jing, J., Greshock, J., Holbrook, J. D., Gilmartin, A., Zhang, X., McNeil, E., … Degenhardt, Y. (2012). Comprehensive Predictive Biomarker Analysis for MEK Inhibitor GSK1120212. *Molecular Cancer Therapeutics*, *11*(3), 720 LP – 729. https://doi.org/10.1158/1535-7163.MCT-11-0505

Jones, H. B. (1956). Demographic consideration of the cancer problem. *Transactions of the New York Academy of Sciences*, *18*(4), 298–333. https://doi.org/10.1111/j.2164-0947.1956.tb00453.x

Joseph, E., & Singhvi, G. (2019). Chapter 4 - Multifunctional nanocrystals for cancer therapy: a potential nanocarrier. In A. M. B. T.-N. for D. D. and T. Grumezescu (Ed.) (pp. 91–116). William Andrew Publishing. https://doi.org/https://doi.org/10.1016/B978-0-12-816505-8.00007-2

Joshi, R. P., Hu, Q., Aly, R., Schoenbach, K. H., & Hjalmarson, H. P. (2001). Self-consistent simulations of electroporation dynamics in biological cells subjected to ultrashort electrical pulses. *Physical Review E*, *64*(1), 011913. https://doi.org/10.1103/PhysRevE.64.011913

Jóźwiak, P., Forma, E., Bryś, M., & Krześlak, A. (2014, September 9). O-GlcNAcylation and metabolic reprograming in cancer. *Frontiers in Endocrinology*. Frontiers. https://doi.org/10.3389/fendo.2014.00145

Kalimuthu, K., Suresh Babu, R., Venkataraman, D., Bilal, M., & Gurunathan, S. (2008). Biosynthesis of silver nanocrystals by Bacillus licheniformis. *Colloids and Surfaces B: Biointerfaces*, *65*(1), 150–153. https://doi.org/10.1016/J.COLSURFB.2008.02.018

Kanaan, Y. M., Sampey, B. P., Beyene, D., Esnakula, A. K., Naab, T. J., Ricks-Santi, L. J., … Dewitty, R. L. (2014). Metabolic profile of triple-negative breast cancer in African-American women reveals potential biomarkers of aggressive disease. *Cancer Genomics & Proteomics*, *11*(6), 279–294. Retrieved from http://www.ncbi.nlm.nih.gov/pubmed/25422359

Kanehisa, M., & Goto, S. (2000). KEGG: kyoto encyclopedia of genes and genomes. *Nucleic Acids Research*, *28*(1), 27–30. https://doi.org/10.1093/nar/28.1.27

Kato, H., & Nishitoh, H. (2015). Stress Responses from the Endoplasmic Reticulum in Cancer. *Frontiers in Oncology*, *5*, 93. https://doi.org/10.3389/fonc.2015.00093

Kelly, K. L., Coronado, E., Zhao, L. L., & Schatz, G. C. (2003). The Optical Properties of Metal Nanoparticles: The Influence of Size, Shape, and Dielectric Environment. *The Journal of Physical Chemistry B*, *107*(3), 668–677. https://doi.org/10.1021/jp026731y

Khoshnan, A., Tindell, C., Laux, I., Bae, D., Bennett, B., & Nel, A. E. (2000). The NF-kappa B cascade is important in Bcl-xL expression and for the anti-apoptotic effects of the CD28 receptor in primary human CD4+ lymphocytes. *Journal of Immunology (Baltimore, Md. : 1950)*, *165*(4), 1743–1754. https://doi.org/10.4049/jimmunol.165.4.1743

Khosravi-Shahi, P., Cabezón-Gutiérrez, L., & Custodio-Cabello, S. (2017). Metastatic triple negative breast cancer: Optimizing treatment options, new and emerging targeted therapies. *Asia-Pacific Journal of Clinical Oncology*, (June), 32–39. https://doi.org/10.1111/ajco.12748

Kim, J.-S., Chang, J. W., Park, J. K., & Hwang, S.-G. (2012). Increased aldehyde reductase expression mediates acquired radioresistance of laryngeal cancer cells via modulating p53. *Cancer Biology & Therapy*, *13*(8), 638–646. https://doi.org/10.4161/cbt.20081

Kim, J., Kim, J., & Bae, J.-S. (2016). ROS homeostasis and metabolism: a critical liaison for cancer therapy. *Experimental & Molecular Medicine*, *48*(11), e269. https://doi.org/10.1038/emm.2016.119

Kim, N. H., Cha, Y. H., Lee, J., Lee, S. H., Yang, J. H., Yun, J. S., … Kim, H. S. (2017). Snail reprograms glucose metabolism by repressing phosphofructokinase PFKP allowing cancer cell survival under metabolic stress. *Nature Communications*, *8*. https://doi.org/10.1038/ncomms14374

Kim, S., Kim, D. H., Jung, W.-H., & Koo, J. S. (2013). Metabolic phenotypes in triple-negative breast cancer. *Tumor Biology*, *34*(3), 1699–1712. https://doi.org/10.1007/s13277-013-0707-1

King, F. G., Dedrick, R. L., & Farris, F. F. (1986). Physiological pharmacokinetic modeling ofcis-dichlorodiammineplatinum(II) (DDP) in several species. *Journal of Pharmacokinetics and Biopharmaceutics*, *14*(2), 131–155. https://doi.org/10.1007/BF01065258

Kingston, D. G. I. (2011). Modern Natural Products Drug Discovery and its Relevance to Biodiversity Conservation. *Journal of Natural Products*, *74*(3), 496–511. https://doi.org/10.1021/np100550t

Kis, E. G., Baltás, E., Kinyó, Á., Varga, E., Nagy, N., Gyulai, R., … Oláh, J. (2012). Successful treatment of multiple basaliomas with bleomycinbased electrochemotherapy: A case series of three patients with gorlin-goltz syndrome. *Acta Dermato-Venereologica*, *92*(6), 648–651. https://doi.org/10.2340/00015555-1361

Kis, E. G., Baltás, E., Ócsai, H., Vass, A., Németh, I. B., Varga, E., … Tóth-Molnár, E. (2019). Electrochemotherapy in the treatment of locally advanced or recurrent eyelid-periocular basal cell carcinomas. *Scientific Reports*. https://doi.org/10.1038/s41598-019-41026-2

Koistinen, P., & Heino, J. (2012). Integrins in Cancer Cell Invasion - Madame Curie Bioscience Database - NCBI Books ... Page 1 of 20 Integrins in Cancer Cell Invasion Integrins in Cancer Cell Invasion - Madame Curie Bioscience Database - NCBI Books ... Page 2 of 20, 1–20. Retrieved from https://www.ncbi.nlm.nih.gov/books/NBK6070/

Kontomanolis, E. N., Kalagasidou, S., Pouliliou, S., Anthoulaki, X., Georgiou, N., Papamanolis, V., & Fasoulakis, Z. N. (2018). The Notch Pathway in Breast Cancer Progression. *TheScientificWorldJournal*, *2018*, 2415489. https://doi.org/10.1155/2018/2415489

Kopan, R. (2012). Notch signaling. *Cold Spring Harbor Perspectives in Biology*, *4*(10), a011213. https://doi.org/10.1101/cshperspect.a011213

Kopp, F., Wagner, E., & Roidl, A. (2014). The proto-oncogene KRAS is targeted by miR-200c. *Oncotarget*, *5*(1), 185–195. https://doi.org/10.18632/oncotarget.1427

Kotnik, T., Kramar, P., Pucihar, G., Miklavcic, D., & Tarek, M. (2012). Cell membrane electroporation-Part 1: The phenomenon. *IEEE Electrical Insulation Magazine*, *28*(5), 14–23. https://doi.org/10.1109/MEI.2012.6268438

Kranjc, M., & Miklavčič, D. (2016). Electric Field Distribution and Electroporation Threshold. In *Handbook of Electroporation* (pp. 1–17). Cham: Springer International Publishing. https://doi.org/10.1007/978-3-319-26779-1_4-1

Krishna, B. M., Jana, S., Singhal, J., Horne, D., Awasthi, S., Salgia, R., & Singhal, S. S. (2019). Notch signaling in breast cancer: From pathway analysis to therapy. *Cancer Letters*, *461*, 123–131. https://doi.org/https://doi.org/10.1016/j.canlet.2019.07.012

Krüger, K., Gessner, D. K., Seimetz, M., Banisch, J., Ringseis, R., Eder, K., … Mooren, F. C. (2013). Functional and Muscular Adaptations in an Experimental Model for Isometric Strength Training in Mice. *PLoS ONE*, *8*(11), e79069. https://doi.org/10.1371/journal.pone.0079069

Kujundžić, R. N., Stepanić, V., Milković, L., Gašparović, A. Č., Tomljanović, M., & Trošelj, K. G. (2019). Curcumin and its Potential for Systemic Targeting of Inflamm-Aging and Metabolic Reprogramming in Cancer. *International Journal of Molecular Sciences*, *20*(5), 1180. https://doi.org/10.3390/ijms20051180

Kumar, A., & Dixit, C. K. (2017). 3 - Methods for characterization of nanoparticles. In S. Nimesh, R. Chandra, & N. B. T.-A. in N. for the D. of T. N. A. Gupta (Eds.) (pp. 43–58). Woodhead Publishing. https://doi.org/https://doi.org/10.1016/B978-0-08-100557-6.00003-1

Kumari, S., Badana, A. K., G, M. M., G, S., & Malla, R. (2018). Reactive Oxygen Species: A Key Constituent in Cancer Survival. *Biomarker Insights*, *13*, 1177271918755391–1177271918755391. https://doi.org/10.1177/1177271918755391

Kunnumakkara, A. B., Bordoloi, D., Harsha, C., Banik, K., Gupta, S. C., & Aggarwal, B. B. (2017). Curcumin mediates anticancer effects by modulating multiple cell signaling pathways. *Clinical Science*, *131*(15), 1781–1799. https://doi.org/10.1042/cs20160935

Kunte, C., Letulé, V., Gehl, J., Dahlstroem, K., Curatolo, P., Rotunno, R., … InspECT (the International Network for Sharing Practices on Electrochemotherapy). (2017). Electrochemotherapy in the treatment of metastatic malignant melanoma: a prospective cohort study by InspECT. *British Journal of Dermatology*, *176*(6), 1475–1485. https://doi.org/10.1111/bjd.15340

Kurian, A. W., Fish, K., Shema, S. J., & Clarke, C. A. (2010). Lifetime risks of specific breast cancer subtypes among women in four racial/ethnic groups. *Breast Cancer Research : BCR*, *12*(6), R99. https://doi.org/10.1186/bcr2780

Kutmon, M., Lotia, S., Evelo, C. T., & Pico, A. R. (2014). WikiPathways App for Cytoscape: Making biological pathways amenable to network analysis and visualization. *F1000Research*, *3*, 152. https://doi.org/10.12688/f1000research.4254.2

Kuttan, R., Bhanumathy, P., Nirmala, K., & George, M. C. (1985). Potential anticancer activity of turmeric (Curcuma longa). *Cancer Letters*, *29*(2), 197–202. https://doi.org/10.1016/0304-3835(85)90159-4

Lampe, V., & Milobedzka, J. (1913). Studien über curcumin. *Berichte Der Deutschen Chemischen Gesellschaft*, *46*(2), 2235–2240.

Lampe, V., Milobedzka, J., & Kostaneski, V. (1910). Zur Kenntnis des Curcumins. *Ber Deutsch Chem Ges*, *43*, 2163–2170.

Lanning, N. J., Castle, J. P., Singh, S. J., Leon, A. N., Tovar, E. A., Sanghera, A., … Graveel, C. R. (2017). Metabolic profiling of triple-negative breast cancer cells reveals metabolic vulnerabilities. *Cancer & Metabolism*, *5*(1), 6. https://doi.org/10.1186/s40170-017-0168-x

Larkin, J. O., Collins, C. G., Aarons, S., Tangney, M., Whelan, M., O'Reily, S., … O'Sullivan, G. C. (2007). Electrochemotherapy: Aspects of Preclinical Development and Early Clinical Experience. *Annals of Surgery*, *245*(3), 469–479. https://doi.org/10.1097/01.sla.0000250419.36053.33

Latifah, S., Faujan, H., Sze, L., Raha, A., & Hisyam, A.Li, O. (2006). Curcumin from Turmeric (Curcuma longa) Induced Apoptosis in Human Mammary Carcinoma Cells, *2*(June), 71–79.

Lauritzen, G., Jensen, M. B. F., Boedtkjer, E., Dybboe, R., Aalkjaer, C., Nylandsted, J., & Pedersen, S. F. (2010). NBCn1 and NHE1 expression and activity in DeltaNErbB2 receptor-expressing MCF-7 breast cancer cells: contributions to pHi regulation and chemotherapy resistance. *Experimental Cell Research*, *316*(15), 2538–2553. https://doi.org/10.1016/j.yexcr.2010.06.005

Legin, A. A., Schintlmeister, A., Jakupec, M. A., Galanski, M., Lichtscheidl, I., Wagner, M., & Keppler, B. K. (2014). NanoSIMS combined with fluorescence microscopy as a tool for subcellular imaging of isotopically labeled platinum-based anticancer drugs. *Chemical Science*, *5*(8), 3135–3143. https://doi.org/10.1039/C3SC53426J

Lehmann, B. D., Bauer, J. A., Chen, X., Sanders, M. E., Chakravarthy, A. B., Shyr, Y., & Pietenpol, J. A. (2011). Identification of human triple-negative breast cancer subtypes and preclinical models for selection of targeted therapies. *Journal of Clinical Investigation*, *121*(7), 2750–2767. https://doi.org/10.1172/JCI45014

Lepik, D., Jaks, V., Kadaja, L., Värv, S., & Maimets, T. (2003). Electroporation and carrier DNA cause p53 activation, cell cycle arrest, and apoptosis. *Analytical Biochemistry*, *318*(1), 52–59. https://doi.org/10.1016/S0003-2697(03)00135-0

Li, H., Jin, L., Wu, F., Li, X., You, J., Cao, Z., … Xu, Y. (2012). Effect of curcumin on proliferation , cell cycle , and caspases and MCF-7 cells, *6*(12), 864–870. https://doi.org/10.5897/AJPP11.418

Li, Y., Luo, Y., Wang, X., Shen, S., Yu, H., Yang, J., & Su, Z. (2012). Tumor suppressor gene NGX6 induces changes in protein expression profiles in colon cancer HT-29 cells. *Acta Biochimica et Biophysica Sinica*, *44*(7), 584–590. https://doi.org/10.1093/abbs/gms042

Liao, W. S., Ho, Y., Lin, Y. W., Naveen Raj, E., Liu, K. K., Chen, C., … Chao, J. I. (2019). Targeting EGFR of triple-negative breast cancer enhances the therapeutic efficacy of paclitaxel- and cetuximab-conjugated nanodiamond nanocomposite. *Acta Biomaterialia*, *86*, 395–405. https://doi.org/10.1016/j.actbio.2019.01.025

Lim, S. O., Li, C. W., Xia, W., Lee, H. H., Chang, S. S., Shen, J., … Hung, M. C. (2016). EGFR signaling enhances aerobic glycolysis in triple-negative breast cancer cells to promote tumor growth and immune escape. *Cancer Research*, *76*(5), 1284–1296. https://doi.org/10.1158/0008-5472.CAN-15-2478

Lin, N. U., Vanderplas, A., Hughes, M. E., Theriault, R. L., Edge, S. B., Wong, Y. N., … Weeks, J. C. (2012). Clinicopathologic features, patterns of recurrence, and survival among women with triple-negative breast cancer in the National Comprehensive Cancer Network. *Cancer*, *118*(22), 5463–5472. https://doi.org/10.1002/cncr.27581

Lin, W.-Y., Cooper, C., Camarillo, I., Reece, L. M., Clah, L., Natarajan, A., … Sundararajan, R. (2014). The Effectiveness of Electroporation- based Nanocurcumin and Curcumin Treatments on Human Breast Cancer Cells. In *Proc. ESA Annual Meeting on Electrostatics 2014*. Retrieved from http://www.electrostatics.org/images/ESA_2014_C_Lin_et_al.pdf

Lin, Y., Devin, A., Rodriguez, Y., & Liu, Z. G. (1999). Cleavage of the death domain kinase RIP by caspase-8 prompts TNF-induced apoptosis. *Genes & Development*, *13*(19), 2514–2526. https://doi.org/10.1101/gad.13.19.2514

Lingeman, R. G., Hickey, R. J., & Malkas, L. H. (2014). Expression of a novel peptide derived from PCNA damages DNA and reverses cisplatin resistance. *Cancer Chemotherapy and Pharmacology*, *74*(5), 981–993. https://doi.org/10.1007/s00280-014-2574-x

Liu, H., Zang, C., Fenner, M. H., Possinger, K., & Elstner, E. (2003). PPARgamma ligands and ATRA inhibit the invasion of human breast cancer cells in vitro. *Breast Cancer Research and Treatment*, *79*(1), 63–74. https://doi.org/10.1023/a:1023366117157

Liu, Q., Loo, W. T. Y., Sze, S. C. W., & Tong, Y. (2009). Curcumin inhibits cell proliferation of MDA-MB-231 and BT-483 breast cancer cells mediated by down-regulation of NFκB, cyclinD and MMP-1 transcription. *Phytomedicine*, *16*(10), 916–922. https://doi.org/10.1016/j.phymed.2009.04.008

Loganayaki, N., Siddhuraju, P., & Manian, S. (2013). Antioxidant activity and free radical scavenging capacity of phenolic extracts from Helicteres isora L. and Ceiba pentandra L. *Journal of Food Science and Technology*, *50*(4), 687–695. https://doi.org/10.1007/s13197-011-0389-x

Lu, C.-H., Lin, S.-H., Hsieh, C.-H., Chen, W.-T., & Chao, C.-Y. (2018). Enhanced anticancer effects of low-dose curcumin with non-invasive pulsed electric field on PANC-1 cells. *OncoTargets and Therapy*, *Volume 11*, 4723–4732. https://doi.org/10.2147/OTT.S166264

Lu, H., Li, X., Lu, Y., Qiu, S., & Fan, Z. (2016). ASCT2 (SLC1A5) is an EGFR-associated protein that can be co-targeted by cetuximab to sensitize cancer cells to ROS-induced apoptosis. *Cancer Letters*, *381*(1), 23–30. https://doi.org/10.1016/j.canlet.2016.07.020

Lukong, K. E. (2017). Understanding breast cancer – The long and winding road. *BBA Clinical*, *7*, 64–77. https://doi.org/https://doi.org/10.1016/j.bbacli.2017.01.001

Luo, M., Shang, L., Brooks, M. D., Jiagge, E., Zhu, Y., Buschhaus, J. M., … Wicha, M. S. (2018). Targeting Breast Cancer Stem Cell State Equilibrium through Modulation of Redox Signaling. *Cell Metabolism*, *28*(1), 69-86.e6. https://doi.org/10.1016/j.cmet.2018.06.006

Ma, B., Cheng, H., Gao, R., Mu, C., Chen, L., Wu, S., … Zhu, Y. (2016). Zyxin-Siah2-Lats2 axis mediates cooperation between Hippo and TGF-β signalling pathways. *Nature Communications*, *7*(1), 11123. https://doi.org/10.1038/ncomms11123

Ma, C., Zu, X., Liu, K., Bode, A. M., Dong, Z., Liu, Z., & Kim, D. J. (2019). Knockdown of Pyruvate Kinase M Inhibits Cell Growth and Migration by Reducing NF-kB Activity in Triple-Negative Breast Cancer Cells. *Molecules and Cells*, *42*(9), 628–636. https://doi.org/10.14348/molcells.2019.0038

Ma, H., Ursin, G., Xu, X., Lee, E., Togawa, K., Duan, L., … Bernstein, L. (2017). Reproductive factors and the risk of triple-negative breast cancer in white women and African-American women: a pooled analysis. *Breast Cancer Research : BCR*, *19*(1), 6. https://doi.org/10.1186/s13058-016-0799-9

Ma, H., Wang, Y., Sullivan-Halley, J., Weiss, L., Marchbanks, P. A., Spirtas, R., … Bernstein, L. (2010). Use of four biomarkers to evaluate the risk of breast cancer subtypes in the women's contraceptive and reproductive experiences study. *Cancer Research*, *70*(2), 575–587. https://doi.org/10.1158/0008-5472.CAN-09-3460

Mack, N., Mazzio, E. A., Bauer, D., Flores-Rozas, H., & Soliman, K. F. A. (2017). Stable shRNA Silencing of Lactate Dehydrogenase A (LDHA) in Human MDA-MB-231 Breast Cancer Cells Fails to Alter Lactic Acid Production, Glycolytic Activity, ATP or Survival. *Anticancer Research*, *37*(3), 1205–1212. https://doi.org/10.21873/anticanres.11435

Markelc, B., Sersa, G., & Cemazar, M. (2013). Differential Mechanisms Associated with Vascular Disrupting Action of Electrochemotherapy: Intravital Microscopy on the Level of Single Normal and Tumor Blood Vessels. *PLoS ONE*, *8*(3), e59557. https://doi.org/10.1371/journal.pone.0059557

Markert, C. L., Goodfriend, T. L., Kaplan, N. O., & Kaplan, N. O. (1963). Lactate Dehydrogenase Isozymes: Dissociation and Recombination of Subunits. *Science*, *140*(3573), 1329–1330. https://doi.org/10.1126/science.140.3573.1329

Martin, M., Pienkowski, T., Mackey, J., Pawlicki, M., Guastalla, J.-P., Weaver, C., … Vogel, C. (2005). Adjuvant docetaxel for node-positive breast cancer. *The New England Journal of Medicine*, *352*(22), 2302–2313. https://doi.org/10.1056/NEJMoa043681

Martín, M., Rodríguez-Lescure, A., Ruiz, A., Alba, E., Calvo, L., Ruiz-Borrego, M., … López-Vega, J. M. (2008). Randomized phase 3 trial of fluorouracil, epirubicin, and cyclophosphamide alone or followed by Paclitaxel for early breast cancer. *Journal of the National Cancer Institute*, *100*(11), 805–814. https://doi.org/10.1093/jnci/djn151

Martinho, N., Santos, T. C. B., Florindo, H. F., & Silva, L. C. (2019). Cisplatin-Membrane Interactions and Their Influence on Platinum Complexes Activity and Toxicity. *Frontiers in Physiology*, *9*, 1898. https://doi.org/10.3389/fphys.2018.01898

Marty, M., Sersa, G., Garbay, J. R., Gehl, J., Collins, C. G., Snoj, M., … O'Sullivan, G. C. (2006). Electrochemotherapy – An easy, highly effective and safe treatment of cutaneous and subcutaneous metastases: Results of ESOPE (European Standard Operating Procedures of Electrochemotherapy) study. *European Journal of Cancer Supplements*, *4*(11), 3–13. https://doi.org/10.1016/J.EJCSUP.2006.08.002

Marullo, R., Werner, E., Degtyareva, N., Moore, B., Altavilla, G., Ramalingam, S. S., & Doetsch, P. W. (2013). Cisplatin Induces a Mitochondrial-ROS Response That Contributes to Cytotoxicity Depending on Mitochondrial Redox Status and Bioenergetic Functions. *PLoS ONE*, *8*(11), e81162. https://doi.org/10.1371/JOURNAL.PONE.0081162

Masuda, H., Baggerly, K. A., Wang, Y., Zhang, Y., Gonzalez-Angulo, A. M., Meric-Bernstam, F., … Ueno, N. T. (2013). Differential response to neoadjuvant chemotherapy among 7 triple-negative breast cancer molecular subtypes. *Clinical Cancer Research : An Official Journal of the American Association for Cancer Research*, *19*(19), 5533–5540. https://doi.org/10.1158/1078-0432.CCR-13-0799

Mathe, A., Wong-Brown, M., Morten, B., Forbes, J. F., Braye, S. G., Avery-Kiejda, K. A., & Scott, R. J. (2015). Novel genes associated with lymph node metastasis in triple negative breast cancer. *Scientific Reports*, *5*, 15832. https://doi.org/10.1038/srep15832

Matthiessen, L. W., Chalmers, R. L., Sainsbury, D. C. G., Veeramani, S., Kessell, G., Humphreys, A. C., … Gehl, J. (2011). Management of cutaneous metastases using electrochemotherapy. *Acta Oncologica (Stockholm, Sweden)*, *50*(5), 621–629. https://doi.org/10.3109/0284186X.2011.573626

Matthiessen, L. W., Johannesen, H. H., Hendel, H. W., Moss, T., Kamby, C., & Gehl, J. (2012). Electrochemotherapy for large cutaneous recurrence of breast cancer: A phase II clinical trial. *Acta Oncologica*, *51*(6), 713–721. https://doi.org/10.3109/0284186X.2012.685524

Matthiessen, L. W., Keshtgar, M., Curatolo, P., Kunte, C., Grischke, E.-M., Odili, J., … Gehl, J. (2018). Electrochemotherapy for Breast Cancer-Results From the INSPECT Database. *Clinical Breast Cancer*, *18*(5), e909–e917. https://doi.org/10.1016/j.clbc.2018.03.007

Mavaddat, N., Barrowdale, D., Andrulis, I. L., Domchek, S. M., Eccles, D., Nevanlinna, H., … Antoniou, A. C. (2012). Pathology of breast and ovarian cancers among BRCA1 and BRCA2 mutation carriers: results from the Consortium of Investigators of Modifiers of BRCA1/2 (CIMBA). *Cancer Epidemiology, Biomarkers & Prevention : A Publication of the American Association for Cancer Research, Cosponsored by the American Society of Preventive Oncology*, *21*(1), 134–147. https://doi.org/10.1158/1055-9965.EPI-11-0775

Mayer, M. P., & Bukau, B. (2005). Hsp70 chaperones: cellular functions and molecular mechanism. *Cellular and Molecular Life Sciences : CMLS*, *62*(6), 670–684. https://doi.org/10.1007/s00018-004-4464-6

McAndrew, N., & DeMichele, A. (2018). Neoadjuvant Chemotherapy Considerations in Triple-Negative Breast Cancer. *The Journal of Targeted Therapies in Cancer*, *7*(1), 52–69. Retrieved from https://pubmed.ncbi.nlm.nih.gov/29577076

McCleland, M. L., Adler, A. S., Shang, Y., Hunsaker, T., Truong, T., Peterson, D., … Firestein, R. (2012). An Integrated Genomic Screen Identifies LDHB as an Essential Gene for Triple-Negative Breast Cancer. *Cancer Research*, *72*(22), 5812–5823. https://doi.org/10.1158/0008-5472.can-12-1098

McFate, T., Mohyeldin, A., Lu, H., Thakar, J., Henriques, J., Halim, N. D., … Verma, A. (2008). Pyruvate dehydrogenase complex activity controls metabolic and malignant phenotype in cancer cells. *Journal of Biological Chemistry*, *283*(33), 22700–22708. https://doi.org/10.1074/jbc.M801765200

Mckinnon, N. E. (1954). CONTROL OF CANCER MORTALITY. *The Lancet*, *263*(6805), 251–255. https://doi.org/https://doi.org/10.1016/S0140-6736(54)90892-2

McManus, M. M., Weiss, K. R., & Hughes, D. P. M. (2014). Understanding the Role of Notch in Osteosarcoma BT - Current Advances in Osteosarcoma. In M. D. Kleinerman Eugenie S. (Ed.) (pp. 67–92). Cham: Springer International Publishing. https://doi.org/10.1007/978-3-319-04843-7_4

McWhirter, R. (1948). The value of simple mastectomy and radiotherapy in the treatment of cancer of the breast. *The British Journal of Radiology*, *21*(252), 599–610. https://doi.org/10.1259/0007-1285-21-252-599

Mi, H., Muruganujan, A., Casagrande, J. T., & Thomas, P. D. (2013). Large-scale gene function analysis with the PANTHER classification system. *Nature Protocols*, *8*(8), 1551–1566. https://doi.org/10.1038/nprot.2013.092

Miah, S., Banks, C. A. S., Adams, M. K., Florens, L., Lukong, K. E., & Washburn, M. P. (2017). Advancement of mass spectrometry-based proteomics technologies to explore triple negative breast cancer. *Molecular BioSystems*, *13*(1), 42–55. https://doi.org/10.1039/C6MB00639F

Micheau, O, Lens, S., Gaide, O., Alevizopoulos, K., & Tschopp, J. (2001). NF-kappaB signals induce the expression of c-FLIP. *Molecular and Cellular Biology*, *21*(16), 5299–5305. https://doi.org/10.1128/MCB.21.16.5299-5305.2001

Micheau, Olivier, & Tschopp, J. (2003). Induction of TNF receptor I-mediated apoptosis via two sequential signaling complexes. *Cell*, *114*(2), 181–190. https://doi.org/10.1016/s0092-8674(03)00521-x

Michel, O., Kulbacka, J., Saczko, J., Mączyńska, J., Błasiak, P., Rossowska, J., & Rzechonek, A. (2018). Electroporation with Cisplatin against Metastatic Pancreatic Cancer: *In Vitro* Study on Human Primary Cell Culture. *BioMed Research International*, *2018*, 1–12. https://doi.org/10.1155/2018/7364539

Mierke, C. T., Frey, B., Fellner, M., Herrmann, M., & Fabry, B. (2011). Integrin α5β1 facilitates cancer cell invasion through enhanced contractile forces. *Journal of Cell Science*, *124*(3), 369–383. https://doi.org/10.1242/jcs.071985

Miklavčič, D., Pucihar, G., Pavlovec, M., Ribarič, S., Mali, M., Maček-Lebar, A., … Serša, G. (2005). The effect of high frequency electric pulses on muscle contractions and antitumor efficiency in vivo for a potential use in clinical electrochemotherapy. *Bioelectrochemistry*, *65*(2), 121–128. https://doi.org/https://doi.org/10.1016/j.bioelechem.2004.07.004

Millikan, R. C., Newman, B., Tse, C.-K., Moorman, P. G., Conway, K., Dressler, L. G., … Perou, C. M. (2008). Epidemiology of basal-like breast cancer. *Breast Cancer Research and Treatment*, *109*(1), 123–139. https://doi.org/10.1007/s10549-007-9632-6

Mir, L. M., Bureau, M. F., Gehl, J., Rangara, R., Rouy, D., Caillaud, J.-M., … Scherman, D. (1999). High-efficiency gene transfer into skeletal muscle mediated by electric pulses. *Proceedings of the National Academy of Sciences*, *96*(8), 4262–4267. https://doi.org/10.1073/pnas.96.8.4262

Mir, & Orlowski. (1999). Mechanisms of electrochemotherapy. *Advanced Drug Delivery Reviews*, *35*(1), 107–118. Retrieved from http://www.ncbi.nlm.nih.gov/pubmed/10837692

Mirzoeva, O. K., Das, D., Heiser, L. M., Bhattacharya, S., Siwak, D., Gendelman, R., … Korn, W. M. (2009). Basal subtype and MAPK/ERK kinase (MEK)-phosphoinositide 3-kinase feedback signaling determine susceptibility of breast cancer cells to MEK inhibition. *Cancer Research*, *69*(2), 565–572. https://doi.org/10.1158/0008-5472.CAN-08-3389

Mittal, L., Aryal, U. K., Camarillo, I. G., Ferreira, R. M., & Sundararajan, R. (2019). Quantitative proteomic analysis of enhanced cellular effects of electrochemotherapy with Cisplatin in triple-negative breast cancer cells. *Scientific Reports*, *9*(1), 13916. https://doi.org/10.1038/s41598-019-50048-9

Mittal, L., Aryal, U. K., Camarillo, I. G., Raman, V., & Sundararajan, R. (2020). Effective electrochemotherapy with curcumin in MDA-MB-231-human, triple negative breast cancer cells: A global proteomics study. *Bioelectrochemistry*, *131*, 107350. https://doi.org/10.1016/j.bioelechem.2019.107350

Mittal, L., Camarillo, I. G., Aryal, U. K., & Sundararajan, R. (2019). Global Proteomic Analysis of Breast Cancer Cell Plasma Membrane Electroporation. In *2019 IEEE Conference on Electrical Insulation and Dielectric Phenomena (CEIDP)* (pp. 725–728). https://doi.org/10.1109/CEIDP47102.2019.9009762

Mittal, L., Camarillo, I. G., Varadarajan, G. S., Srinivasan, H., Aryal, U. K., & Sundararajan, R. (2020). High-throughput, Label-Free Quantitative Proteomic Studies of the Anticancer Effects of Electrical Pulses with Turmeric Silver Nanoparticles: an in vitro Model Study. *Scientific Reports*, *10*(1), 7258. https://doi.org/10.1038/s41598-020-64128-8

Mittal, L., Raman, V., Camarillo, I. G., Garner, A. L., & Sundararajan, R. (2019). Viability and cell cycle studies of metastatic triple negative breast cancer cells using low voltage electrical pulses and herbal curcumin. *Biomedical Physics and Engineering Express*, *5*(2), 025040. https://doi.org/10.1088/2057-1976/aaf2c3

Mittal, L., Raman, V., Camarillo, I. G., & Sundararajan, R. (2017). Ultra-microsecond pulsed curcumin for effective treatment of triple negative breast cancers. *Biochemical and Biophysical Research Communications*, *491*(4), 1015–1020. https://doi.org/https://doi.org/10.1016/j.bbrc.2017.08.002

Mittal, L., S., R., M., S. A., T., J. S., Akther, T., S., P., … S., H. (2020). Turmeric-silver-nanoparticles for effective treatment of breast cancer and to break CTX-M-15 mediated antibiotic resistance in Escherichia coli. *Inorganic and Nano-Metal Chemistry*, 1–8. https://doi.org/10.1080/24701556.2020.1812644

Montero, J. C., Esparis-Ogando, A., Re-Louhau, M. F., Seoane, S., Abad, M., Calero, R., … Pandiella, A. (2014). Active kinase profiling, genetic and pharmacological data define mTOR as an important common target in triple-negative breast cancer. *Oncogene*, *33*(2), 148–156. https://doi.org/10.1038/onc.2012.572

Montgomery, D. C. (2012). *Design and Analysis of Experiments, 8th Edition*. John Wiley & Sons, Incorporated. Retrieved from https://books.google.com/books?id=XQAcAAAAQBAJ

Mude, N., Ingle, A., Gade, A., & Rai, M. (2009). Synthesis of Silver Nanoparticles Using Callus Extract of Carica papaya — A First Report. *Journal of Plant Biochemistry and Biotechnology*, *18*(1), 83–86. https://doi.org/10.1007/BF03263300

Mukherjee, S. (2010). *The emperor of all maladies : a biography of cancer*. Scribner.

Murugan, K., Shanmugasamy, S., Al-Sohaibani, S., Vignesh, N., Palanikannan, K., Vimala, A., & Kumar, G. R. (2015). TaxKB: a knowledge base for new taxane-related drug discovery. *BioData Mining*, *8*, 19. https://doi.org/10.1186/s13040-015-0053-5

Nadar, S. K., & Lip, G. Y. H. (2007, April). New insights into complement C3 and inflammation in hypertension. *Journal of Human Hypertension*. https://doi.org/10.1038/sj.jhh.1002160

Nagamatsu, I., Onishi, H., Matsushita, S., Kubo, M., Kai, M., Imaizumi, A., … Katano, M. (2014). NOTCH4 Is a Potential Therapeutic Target for Triple-negative Breast Cancer. *Anticancer Research*, *34*(1), 69–80. Retrieved from http://ar.iiarjournals.org/content/34/1/69.abstract

Nagata, M., Noman, A. A., Suzuki, K., Kurita, H., Ohnishi, M., Ohyama, T., … Takagi, R. (2013). ITGA3 and ITGB4 expression biomarkers estimate the risks of locoregional and hematogenous dissemination of oral squamous cell carcinoma. *BMC Cancer*, *13*. https://doi.org/10.1186/1471-2407-13-410

Nagy, I. Z., Lustyik, G., Nagy, V. Z., Zarándi, B., & Bertoni-Freddari, C. (1981). Intracellular Na+:K+ ratios in human cancer cells as revealed by energy dispersive x-ray microanalysis. *The Journal of Cell Biology*, *90*(3), 769–777. https://doi.org/10.1083/jcb.90.3.769

Nair, A., Amalraj, A., Jacob, J., Kunnumakkara, A. B., & Gopi, S. (2019, January 1). Non-curcuminoids from turmeric and their potential in cancer therapy and anticancer drug delivery formulations. *Biomolecules*. MDPI AG. https://doi.org/10.3390/biom9010013

Nakai, K., Hung, M. C., & Yamaguchi, H. (2016). A perspective on anti-EGFR therapies targeting triple-negative breast cancer. *American Journal of Cancer Research*. E-Century Publishing Corporation.

Nallapalli, R. K., Ibrahim, M. X., Zhou, A. X., Bandaru, S., Sunkara, S. N., Redfors, B., … Akyürek, L. M. (2012). Targeting filamin A reduces K-RAS-induced lung adenocarcinomas and endothelial response to tumor growth in mice. *Molecular Cancer*, *11*(1), 50. https://doi.org/10.1186/1476-4598-11-50

National Cancer Institute. (n.d.). NCI Dictionary of Cancer Terms. Retrieved May 2, 2020, from https://www.cancer.gov/publications/dictionaries/cancer-terms

National Center for Biotechnology Information. PubChem Database. (2004a). Cisplatin. Retrieved April 5, 2020, from https://pubchem.ncbi.nlm.nih.gov/compound/cis-Platin

National Center for Biotechnology Information. PubChem Database. (2004b). Curcumin. Retrieved April 5, 2020, from https://pubchem.ncbi.nlm.nih.gov/compound/Curcumin

Nayak, S., Goveas, L. C., & Vaman Rao, C. (2017). Biosynthesis of Silver Nanoparticles Using Turmeric Extract and Evaluation of Its Anti-Bacterial Activity and Catalytic Reduction of Methylene Blue. In *Materials, Energy and Environment Engineering*. https://doi.org/10.1007/978-981-10-2675-1_31

Neu, J. C., & Krassowska, W. (1999). Asymptotic model of electroporation. *Physical Review E*, *59*(3), 3471–3482. https://doi.org/10.1103/PhysRevE.59.3471

Newington, J. T., Rappon, T., Albers, S., Wong, D. Y., Rylett, R. J., & Cumming, R. C. (2012). Overexpression of pyruvate dehydrogenase kinase 1 and lactate dehydrogenase A in nerve cells confers resistance to amyloid β and other toxins by decreasing mitochondrial respiration and reactive oxygen species production. *Journal of Biological Chemistry*, *287*(44), 37245–37258. https://doi.org/10.1074/jbc.M112.366195

Newman, D. and C. (2012). Natural Products as Sources of New Drugs over the 30 Years. *Journal of Natural Products*, *75*(3), 311–335. https://doi.org/10.1021/np200906s.Natural

Nyante, S. J., Gierach, G. L., Dallal, C. M., Freedman, N. D., Park, Y., Danforth, K. N., … Brinton, L. A. (2014). Cigarette smoking and postmenopausal breast cancer risk in a prospective cohort. *British Journal of Cancer*, *110*(9), 2339–2347. https://doi.org/10.1038/bjc.2014.132

Oghenejobo, M., & Bethel, O. U. (2017). Antibacterial evaluation, phytochemical screening and ascorbic acid assay of turmeric (Curcuma longa). https://doi.org/10.15406/mojbb.2017.04.00063

Oh, S., Kim, H., Nam, K., & Shin, I. (2017). Glut1 promotes cell proliferation, migration and invasion by regulating epidermal growth factor receptor and integrin signaling in triple-negative breast cancer cells. *BMB Reports*, *50*(3), 132–137. https://doi.org/10.5483/bmbrep.2017.50.3.189

Okal, A., Mossalam, M., Matissek, K. J., Dixon, A. S., Moos, P. J., & Lim, C. S. (2013). A Chimeric p53 evades mutant p53 transdominant inhibition in cancer cells. *Molecular Pharmaceutics*, *10*(10), 3922–3933. https://doi.org/10.1021/mp400379c

Okano, M., Kumamoto, K., Saito, M., Onozawa, H., Saito, K., Abe, N., … Takenoshita, S. (2015). Upregulated Annexin A1 promotes cellular invasion in triple-negative breast cancer. *Oncology Reports*, *33*(3), 1064–1070. https://doi.org/10.3892/or.2015.3720

Ooms, L. M., Binge, L. C., Davies, E. M., Rahman, P., Conway, J. R. W., Gurung, R., … Mitchell, C. A. (2015). The Inositol Polyphosphate 5-Phosphatase PIPP Regulates AKT1-Dependent Breast Cancer Growth and Metastasis. *Cancer Cell*, *28*(2), 155–169. https://doi.org/10.1016/j.ccell.2015.07.003

Oppenheimer, A. (1937). TURMERIC (CURCUMIN) IN BILIARY DISEASES. *The Lancet*. https://doi.org/10.1016/S0140-6736(00)98193-5

Overview | Electrochemotherapy for primary basal cell carcinoma and primary squamous cell carcinoma | Guidance | NICE. (2014). Retrieved June 2, 2019, from https://www.nice.org.uk/guidance/IPG478

Pai, S. G., Carneiro, B. A., Mota, J. M., Costa, R., Leite, C. A., Barroso-Sousa, R., … Giles, F. J. (2017). Wnt/beta-catenin pathway: modulating anticancer immune response. *Journal of Hematology & Oncology*, *10*(1), 101. https://doi.org/10.1186/s13045-017-0471-6

Palange, A. L., Mascolo, D. Di, Singh, J., Franceschi, M. S. De, Carallo, C., Gnasso, A., & Decuzzi, P. (2012). Modulating the vascular behavior of metastatic breast cancer cells by curcumin treatment. *Frontiers in Oncology*, *2*, 161. https://doi.org/10.3389/fonc.2012.00161

Palzkill, T. (2002). *Proteomics*. Boston: Kluwer Academic Publishers. https://doi.org/10.1007/b112610

Pandya, S., & Moore, R. G. (2011). Breast Development and Anatomy. *Clinical Obstetrics and Gynecology*, *54*(1). Retrieved from https://journals.lww.com/clinicalobgyn/Fulltext/2011/03000/Breast_Development_and_Anatomy.14.aspx

Paplomata, E., & O'Regan, R. (2014). The PI3K/AKT/mTOR pathway in breast cancer: targets, trials and biomarkers. *Therapeutic Advances in Medical Oncology*, *6*(4), 154–166. https://doi.org/10.1177/1758834014530023

Park, S.-J., Yoon, B.-H., Kim, S.-K., & Kim, S.-Y. (2019). GENT2: an updated gene expression database for normal and tumor tissues. *BMC Medical Genomics*, *12*(Suppl 5), 101. https://doi.org/10.1186/s12920-019-0514-7

Pascual, J., & Turner, N. C. (2019). Targeting the PI3-kinase pathway in triple-negative breast cancer. *Annals of Oncology*. https://doi.org/10.1093/annonc/mdz133

Patel, N. M., Nozaki, S., Shortle, N. H., Bhat-Nakshatri, P., Newton, T. R., Rice, S., … Nakshatri, H. (2000). Paclitaxel sensitivity of breast cancer cells with constitutively active NF-kappaB is enhanced by IkappaBalpha super-repressor and parthenolide. *Oncogene*, *19*(36), 4159–4169. https://doi.org/10.1038/sj.onc.1203768

Patel, P. B., Thakkar, V. R., & Patel, J. S. (2015). Cellular Effect of Curcumin and Citral Combination on Breast Cancer Cells: Induction of Apoptosis and Cell Cycle Arrest. *Journal of Breast Cancer*, *18*(3), 225. https://doi.org/10.4048/jbc.2015.18.3.225

Patil, T. N., & Srinivasan, M. (1971). Hypocholesteremic effect of curcumin in induced hypercholesteremic rats. *Indian Journal of Experimental Biology*, *9*(2), 167–169. Retrieved from http://europepmc.org/abstract/MED/5092727

Patterson, S. D., & Aebersold, R. H. (2003). Proteomics: The first decade and beyond. *Nature Genetics*, *33*(3S), 311–323. https://doi.org/10.1038/ng1106

Pavlides, S., Whitaker-Menezes, D., Castello-Cros, R., Flomenberg, N., Witkiewicz, A. K., Frank, P. G., … Lisanti, M. P. (2009). The reverse Warburg effect: aerobic glycolysis in cancer associated fibroblasts and the tumor stroma. *Cell Cycle (Georgetown, Tex.)*, *8*(23), 3984–4001. https://doi.org/10.4161/cc.8.23.10238

Pehlivanova, V. N., Tsoneva, I. H., & Tzoneva, R. D. (2012). Multiple effects of electroporation on the adhesive behaviour of breast cancer cells and fibroblasts. *Cancer Cell International*, *12*(1), 9. https://doi.org/10.1186/1475-2867-12-9

Pelicano, H., Zhang, W., Liu, J., Hammoudi, N., Dai, J., Xu, R.-H., … Huang, P. (2014). Mitochondrial dysfunction in some triple-negative breast cancer cell lines: role of mTOR pathway and therapeutic potential. *Breast Cancer Research : BCR*, *16*(5), 434. https://doi.org/10.1186/s13058-014-0434-6

Peng, C., Ma, W., Xia, W., & Zheng, W. (2017). Integrated analysis of differentially expressed genes and pathways in triple-negative breast cancer. *Molecular Medicine Reports*, *15*(3), 1087–1094. https://doi.org/10.3892/mmr.2017.6101

Pennington, K., Chan, T., Torres, M., & Andersen, J. (2018, October 18). The dynamic and stress-adaptive signaling hub of 14-3-3: emerging mechanisms of regulation and context-dependent protein–protein interactions. *Oncogene*. Nature Publishing Group. https://doi.org/10.1038/s41388-018-0348-3

Perou, C. M. (2010). Molecular stratification of triple-negative breast cancers. *The Oncologist, 15 Suppl 5*, 39–48. https://doi.org/10.1634/theoncologist.2010-S5-39

Perou, C. M., Sørlie, T., Eisen, M. B., van de Rijn, M., Jeffrey, S. S., Rees, C. A., … Botstein, D. (2000). Molecular portraits of human breast tumours. *Nature*, *406*(6797), 747–752. https://doi.org/10.1038/35021093

Pignanelli, C., Ma, D., Noel, M., Ropat, J., Mansour, F., Pupulin, S., … Pandey, S. (2017). Selective Targeting of Cancer Cells by Oxidative Vulnerabilities with Novel Curcumin Analogs. *Scientific Reports*, (January), 1–25. https://doi.org/10.1038/s41598-017-01230-4

Pileczki, V., Braicu, C., Gherman, C. D., & Berindan-Neagoe, I. (2012). TNF-α gene knockout in triple negative breast cancer cell line induces apoptosis. *International Journal of Molecular Sciences*, *14*(1), 411–420. https://doi.org/10.3390/ijms14010411

Pimple, B. P., & Badole, S. L. (2014). Chapter 67 - Polyphenols: A Remedy for Skin Wrinkles. In R. R. Watson, V. R. Preedy, & S. B. T.-P. in H. H. and D. Zibadi (Eds.) (pp. 861–869). San Diego: Academic Press. https://doi.org/https://doi.org/10.1016/B978-0-12-398456-2.00067-0

Piovan, C., Palmieri, D., Di Leva, G., Braccioli, L., Casalini, P., Nuovo, G., … Croce, C. M. (2012). Oncosuppressive role of p53-induced miR-205 in triple negative breast cancer. *Molecular Oncology*, *6*(4), 458–472. https://doi.org/10.1016/j.molonc.2012.03.003

Poggio, F., Bruzzone, M., Ceppi, M., Pondé, N. F., La Valle, G., Del Mastro, L., … Lambertini, M. (2018). Platinum-based neoadjuvant chemotherapy in triple-negative breast cancer: A systematic review and meta-analysis. *Annals of Oncology*, *29*(7), 1497–1508. https://doi.org/10.1093/annonc/mdy127

Pogoda, K., Niwińska, A., Murawska, M., & Pieńkowski, T. (2013). Analysis of pattern, time and risk factors influencing recurrence in triple-negative breast cancer patients. *Medical Oncology (Northwood, London, England)*, *30*(1), 388. https://doi.org/10.1007/s12032-012-0388-4

Poma, P., Labbozzetta, M., D'Alessandro, N., & Notarbartolo, M. (2017). NF-kappaB Is a Potential Molecular Drug Target in Triple-Negative Breast Cancers. *Omics : A Journal of Integrative Biology*, *21*(4), 225–231. https://doi.org/10.1089/omi.2017.0020

Poole, C. J., Earl, H. M., Hiller, L., Dunn, J. A., Bathers, S., Grieve, R. J., … Brunt, A. M. (2006). Epirubicin and cyclophosphamide, methotrexate, and fluorouracil as adjuvant therapy for early breast cancer. *New England Journal of Medicine*, *355*(18), 1851–1862.

Porporato, P. E., Dhup, S., Dadhich, R. K., Copetti, T., & Sonveaux, P. (2011). Anticancer Targets in the Glycolytic Metabolism of Tumors: A Comprehensive Review. *Frontiers in Pharmacology*, *2*, 49. https://doi.org/10.3389/fphar.2011.00049

Porta, C., Paglino, C., & Mosca, A. (2014). Targeting PI3K/Akt/mTOR Signaling in Cancer. *Frontiers in Oncology*, *4*, 64. https://doi.org/10.3389/fonc.2014.00064

Prasad, C. P., Rath, G., Mathur, S., Bhatnagar, D., & Ralhan, R. (2009). Potent growth suppressive activity of curcumin in human breast cancer cells: Modulation of Wnt/β-catenin signaling. *Chemico-Biological Interactions*, *181*(2), 263–271. https://doi.org/10.1016/j.cbi.2009.06.012

Prasad, S., & Aggarwal, B. B. (2011). Turmeric, the golden spice: From traditional medicine to modern medicine. In *Herbal Medicine: Biomolecular and Clinical Aspects: Second Edition*.

Prescott, J., Ma, H., Bernstein, L., & Ursin, G. (2007). Cigarette Smoking Is Not Associated with Breast Cancer Risk in Young Women. *Cancer Epidemiology Biomarkers &Amp; Prevention*, *16*(3), 620 LP – 622. https://doi.org/10.1158/1055-9965.EPI-06-0873

Probst, U., Fuhrmann, I., Beyer, L., & Wiggermann, P. (2018). Electrochemotherapy as a New Modality in Interventional Oncology: A Review. *Technology in Cancer Research & Treatment*, *17*, 1533033818785329. https://doi.org/10.1177/1533033818785329

Pubmed.gov. (2020). curcumin - Search Results - PubMed. Retrieved June 9, 2020, from https://pubmed.ncbi.nlm.nih.gov/?term=curcumin

Qiao, G., Duan, W., Chatwin, C., Sinclair, A., & Wang, W. (2010). Electrical properties of breast cancer cells from impedance measurement of cell suspensions. *Journal of Physics: Conference Series*, *224*, 12081. https://doi.org/10.1088/1742-6596/224/1/012081

Qu, J., Sun, W., Zhong, J., Lv, H., Zhu, M., Xu, J., … Huang, M. (2017). Phosphoglycerate mutase 1 regulates dNTP pool and promotes homologous recombination repair in cancer cells. *The Journal of Cell Biology*, *216*(2), 409–424. https://doi.org/10.1083/jcb.201607008

Rakha, E. A., & Chan, S. (2011). Metastatic triple-negative breast cancer. *Clinical Oncology (Royal College of Radiologists (Great Britain))*, *23*(9), 587–600. https://doi.org/10.1016/j.clon.2011.03.013

Raman, V. (2019). *Inhibition of Metabolism and Induction of Apoptosis in Triple Negative Breast Cancer Cells By Lippia Origanoides Plant Extracts*. Purdue University Graduate School. https://doi.org/10.25394/PGS.7868354.V1

Raman, V., Aryal, U. K., Hedrick, V., Ferreira, R. M., Fuentes Lorenzo, J. L., Stashenko, E. E., … Camarillo, I. G. (2018). Proteomic Analysis Reveals That an Extract of the Plant Lippia origanoides Suppresses Mitochondrial Metabolism in Triple-Negative Breast Cancer Cells. *Journal of Proteome Research*, *17*, 3370–3383. research-article. https://doi.org/10.1021/acs.jproteome.8b00255

Rasmussen, H. H., Orntoft, T. F., Wolf, H., & Celis, J. E. (1996). Towards a Comprehensive Database of Proteins From the Urine of Patients With Bladder Cancer. *The Journal of Urology*, *155*(6), 2113–2119. https://doi.org/10.1016/S0022-5347(01)66119-6

Rasool, U., & Hemalatha, S. (2017). Marine endophytic actinomycetes assisted synthesis of copper nanoparticles (CuNPs): Characterization and antibacterial efficacy against human pathogens. *Materials Letters*, *194*, 176–180. https://doi.org/10.1016/J.MATLET.2017.02.055

Raudenska, M., Balvan, J., Fojtu, M., Gumulec, J., & Masarik, M. (2019). Unexpected therapeutic effects of cisplatin. *Metallomics*, *11*(7), 1182–1199. https://doi.org/10.1039/C9MT00049F

Ravindranath, V., & Chandrasekhara, N. (1980). Absorption and tissue distribution of curcumin in rats. *Toxicology*, *16*(3), 259–265. https://doi.org/10.1016/0300-483x(80)90122-5

Ray, C., & Baum, M. (1985). *Psychological Aspects of Early Breast Cancer*. Springer New York.

Rayner, D. M., & Cutts, S. M. (2014). Anthracyclines. In *Side Effects of Drugs Annual* (Vol. 36, pp. 683–694). Elsevier B.V. https://doi.org/10.1016/B978-0-444-63407-8.00045-9

Rebersek, M., Cufer, T., Cemazar, M., Kranjc, S., & Sersa, G. (2004). Electrochemotherapy with cisplatin of cutaneous tumor lesions in breast cancer. *Anti-Cancer Drugs*, *15*(6), 593–597. https://doi.org/10.1097/01.cad.0000132234.30674.df

Reda, A., Refaat, A., Abd-Rabou, A. A., Mahmoud, A. M., Adel, M., Sabet, S., & Ali, S. S. (2019). Role of mitochondria in rescuing glycolytically inhibited subpopulation of triple negative but not hormone-responsive breast cancer cells. *Scientific Reports*, *9*(1), 13748. https://doi.org/10.1038/s41598-019-50141-z

Redza-Dutordoir, M., & Averill-Bates, D. A. (2016). Activation of apoptosis signalling pathways by reactive oxygen species. *Biochimica et Biophysica Acta - Molecular Cell Research*, *1863*(12), 2977–2992. https://doi.org/10.1016/j.bbamcr.2016.09.012

Reedijk, M., Odorcic, S., Chang, L., Zhang, H., Miller, N., McCready, D. R., … Egan, S. E. (2005). High-level Coexpression of JAG1 and NOTCH1 Is Observed in Human Breast Cancer and Is Associated with Poor Overall Survival. *Cancer Research*, *65*(18), 8530 LP – 8537. https://doi.org/10.1158/0008-5472.CAN-05-1069

Reiter, A. (2010). *Even Doctors Cry: Love, Death, Scandal and a Terribly Flawed Medical System*. Langdon st Pr.

Rems, L. (2017). Lipid pores: Molecular and continuum models. In *Handbook of Electroporation* (Vol. 1, pp. 3–23). https://doi.org/10.1007/978-3-319-32886-7_76

Ribas, V., García-Ruiz, C., & Fernández-Checa, J. C. (2016). Mitochondria, cholesterol and cancer cell metabolism. *Clinical and Translational Medicine*, *5*(1), 22. https://doi.org/10.1186/s40169-016-0106-5

Richter, S. (2011). *Role of Adp-Dependent Glucokinase in Cancer Biology*. The University of Auckland. Retrieved from https://researchspace.auckland.ac.nz/handle/2292/13195

Richter, S., Richter, J. P., Mehta, S. Y., Gribble, A. M., Sutherland-Smith, A. J., Stowell, K. M., … Wilson, W. R. (2012). Expression and role in glycolysis of human ADP-dependent glucokinase. *Molecular and Cellular Biochemistry*, *364*(1–2), 131–145. https://doi.org/10.1007/s11010-011-1212-8

Roger, S., Besson, P., & Le Guennec, J.-Y. (2003). Involvement of a novel fast inward sodium current in the invasion capacity of a breast cancer cell line. *Biochimica et Biophysica Acta*, *1616*(2), 107–111. Retrieved from http://www.ncbi.nlm.nih.gov/pubmed/14561467

Rols, M. P., Bachaud, J. M., Giraud, P., Chevreau, C., Roché, H., & Teissié, J. (2000). Electrochemotherapy of cutaneous metastases in malignant melanoma. *Melanoma Research*, *10*(5), 468–474. https://doi.org/10.1097/00008390-200010000-00009

Rols, M. P., Tamzali, Y., & Teissié, J. (2002). Electrochemotherapy of horses. A preliminary clinical report. *Bioelectrochemistry (Amsterdam, Netherlands)*, *55*(1–2), 101–105. Retrieved from http://www.ncbi.nlm.nih.gov/pubmed/11786351

Rose, D. P., & Vona-Davis, L. (2009). Influence of obesity on breast cancer receptor status and prognosis. *Expert Review of Anticancer Therapy*, *9*(8), 1091–1101. https://doi.org/10.1586/era.09.71

Rosner, D., Bedwani, R. N., Vana, J., Baker, H. W., & Murphy, G. P. (1980). Noninvasive breast carcinoma: results of a national survey by the American College of Surgeons. *Annals of Surgery*, *192*(2), 139–147. https://doi.org/10.1097/00000658-198008000-00001

Russnes, H. G., Lingjærde, O. C., Børresen-Dale, A.-L., & Caldas, C. (2017). Breast Cancer Molecular Stratification: From Intrinsic Subtypes to Integrative Clusters. *The American Journal of Pathology*, *187*(10), 2152–2162. https://doi.org/https://doi.org/10.1016/j.ajpath.2017.04.022

Sabol, R. A., Bowles, A. C., Côté, A., Wise, R., O'Donnell, B., Matossian, M. D., … Bunnell, B. A. (2019). Leptin produced by obesity-altered adipose stem cells promotes metastasis but not tumorigenesis of triple-negative breast cancer in orthotopic xenograft and patient-derived xenograft models. *Breast Cancer Research*, *21*(1), 67. https://doi.org/10.1186/s13058-019-1153-9

Sabova, L., Kretova, M., & Luciakova, K. (2013). New insights into the role of NF1 in cancer. *Neoplasma*, *60*(3), 233–239. https://doi.org/10.4149/neo_2013_031

Saeb, A. T. M., Alshammari, A. S., Al-Brahim, H., & Al-Rubeaan, K. A. (2014). Production of Silver Nanoparticles with Strong and Stable Antimicrobial Activity against Highly Pathogenic and Multidrug Resistant Bacteria. *The Scientific World Journal*, *2014*, 704708. https://doi.org/10.1155/2014/704708

Sánchez-Tilló, E., de Barrios, O., Siles, L., Cuatrecasas, M., Castells, A., & Postigo, A. (2011). β-catenin/TCF4 complex induces the epithelial-to-mesenchymal transition (EMT)-activator ZEB1 to regulate tumor invasiveness. *Proceedings of the National Academy of Sciences of the United States of America*, *108*(48), 19204–19209. https://doi.org/10.1073/pnas.1108977108

Sarrio, D., Rodriguez-Pinilla, S. M., Hardisson, D., Cano, A., Moreno-Bueno, G., & Palacios, J. (2008). Epithelial-mesenchymal transition in breast cancer relates to the basal-like phenotype. *Cancer Research*, *68*(4), 989–997. https://doi.org/10.1158/0008-5472.CAN-07-2017

Schäfer, R., Tchernitsa, O. I., & Sers, C. (2006). Global Effects of Ras Signaling on the Genetic Program in Mammalian Cells BT - RAS Family GTPases. In C. Der (Ed.) (pp. 169–198). Dordrecht: Springer Netherlands. https://doi.org/10.1007/1-4020-4708-8_8

Schmadeka, R., Harmon, B. E., & Singh, M. (2014). Triple-Negative Breast Carcinoma: Current and Emerging Concepts. *American Journal of Clinical Pathology*, *141*(4), 462–477. https://doi.org/10.1309/AJCPQN8GZ8SILKGN

Schraufstatter, E., & Bernt, H. (1949). Antibacterial Action of Curcumin and Related Compounds. *Nature*, *164*(4167), 456–457. https://doi.org/10.1038/164456a0

Schulz, W. A., Ingenwerth, M., Djuidje, C. E., Hader, C., Rahnenführer, J., & Engers, R. (2010). Changes in cortical cytoskeletal and extracellular matrix gene expression in prostate cancer are related to oncogenic ERG deregulation. *BMC Cancer*, *10*(1), 505. https://doi.org/10.1186/1471-2407-10-505

Seliger, C., Leukel, P., Moeckel, S., Jachnik, B., Lottaz, C., Kreutz, M., … Hau, P. (2013). Lactate-modulated induction of THBS-1 activates Transforming growth factor (TGF)-beta2 and migration of glioma cells in vitro. *PLoS ONE*, *8*(11), e78935. https://doi.org/10.1371/journal.pone.0078935

Selivanova, G., & Wiman, K. G. (2007). Reactivation of mutant p53: molecular mechanisms and therapeutic potential. *Oncogene*, *26*(15), 2243–2254. https://doi.org/10.1038/sj.onc.1210295

Serša, G., Čemažar, M., & Miklavcic, D. (1995). Antitumor effectiveness of electrochemotherapy with cis-diamminedichloroplatinum(II) in mice. *Undefined*. Retrieved from https://www.semanticscholar.org/paper/Antitumor-effectiveness-of-electrochemotherapy-with-Serša-Čemažar/607c912ba79624d41e7aab81c9583ffbf213115d

Sersa, G, Cemazar, M., & Miklavcic, D. (1995). Antitumor effectiveness of electrochemotherapy with cis-diamminedichloroplatinum(II) in mice. *Cancer Research*, *55*(15), 3450–3455. Retrieved from http://www.ncbi.nlm.nih.gov/pubmed/7614485

Sersa, G, Stabuc, B., Cemazar, M., Jancar, B., Miklavcic, D., & Rudolf, Z. (1998). Electrochemotherapy with cisplatin: potentiation of local cisplatin antitumour effectiveness by application of electric pulses in cancer patients. *European Journal of Cancer (Oxford, England : 1990)*, *34*(8), 1213–1218. https://doi.org/10.1016/s0959-8049(98)00025-2

Sersa, G, Stabuc, B., Cemazar, M., Miklavcic, D., & Rudolf, Z. (2000a). Electrochemotherapy with cisplatin: clinical experience in malignant melanoma patients. *Clinical Cancer Research : An Official Journal of the American Association for Cancer Research*, *6*(3), 863–867. Retrieved from http://www.ncbi.nlm.nih.gov/pubmed/10741708

Sersa, G, Stabuc, B., Cemazar, M., Miklavcic, D., & Rudolf, Z. (2000b). Electrochemotherapy with cisplatin: the systemic antitumour effectiveness of cisplatin can be potentiated locally by the application of electric pulses in the treatment of malignant melanoma skin metastases. *Melanoma Research*, *10*(4), 381–385. https://doi.org/10.1097/00008390-200008000-00010

Sersa, Gregor, Bosnjak, M., Cemazar, M., & Heller, R. (2016). Preclinical Studies on Electrochemotherapy, 1–15. https://doi.org/10.1007/978-3-319-26779-1_45-1

Sersa, Gregor, Cemazar, M., & Rudolf, Z. (2003). *Electrochemotherapy: advantages and drawbacks in treatment of cancer patients Review Article*. *Cancer Therapy* (Vol. 1). Retrieved from https://pdfs.semanticscholar.org/ef4a/d524d99c6c2b9fd5a3b7fecd3c3c99660df7.pdf

Sersa, Gregor, Cufer, T., Paulin, S. M., Cemazar, M., & Snoj, M. (2012). Electrochemotherapy of chest wall breast cancer recurrence. *Cancer Treatment Reviews*, *38*(5), 379–386. https://doi.org/10.1016/j.ctrv.2011.07.006

Shah, M. Y., & Calin, G. A. (2011). MicroRNAs miR-221 and miR-222: a new level of regulation in aggressive breast cancer. *Genome Medicine*, *3*(8), 56. https://doi.org/10.1186/gm272

Shameli, K., Ahmad, M. Bin, Jaffar Al-Mulla, E. A., Ibrahim, N. A., Shabanzadeh, P., Rustaiyan, A., … Zidan, M. (2012). Green biosynthesis of silver nanoparticles using callicarpa maingayi stem bark extraction. *Molecules*. https://doi.org/10.3390/molecules17078506

Shameli, K., Ahmad, M. Bin, Jazayeri, S. D., Shabanzadeh, P., Sangpour, P., Jahangirian, H., & Gharayebi, Y. (2012). Investigation of antibacterial properties silver nanoparticles prepared via green method. *Chemistry Central Journal*, *6*(1), 73. https://doi.org/10.1186/1752-153X-6-73

Shameli, K., Ahmad, M. Bin, Shabanzadeh, P., Jaffar Al-Mulla, E. A., Zamanian, A., Abdollahi, Y., … Haroun, R. Z. (2014). Effect of Curcuma longa tuber powder extract on size of silver nanoparticles prepared by green method. *Research on Chemical Intermediates*, *40*(3), 1313–1325. https://doi.org/10.1007/s11164-013-1040-4

Shameli, K., Ahmad, M. Bin, Zamanian, A., Sangpour, P., Shabanzadeh, P., Abdollahi, Y., & Zargar, M. (2012). Green biosynthesis of silver nanoparticles using Curcuma longa tuber powder. *International Journal of Nanomedicine*, *7*, 5603–5610. https://doi.org/10.2147/IJN.S36786

Shanmugam, M. K., Rane, G., Kanchi, M. M., Arfuso, F., Chinnathambi, A., Zayed, M. E., … Sethi, G. (2015). *The multifaceted role of curcumin in cancer prevention and treatment*. *Molecules* (Vol. 20). https://doi.org/10.3390/molecules20022728

Shannon, P., Markiel, A., Ozier, O., Baliga, N. S., Wang, J. T., Ramage, D., … Ideker, T. (2003). Cytoscape: A Software Environment for Integrated Models of Biomolecular Interaction Networks. *Genome Research*, *13*(11), 2498–2504. https://doi.org/10.1101/gr.1239303

Shannon, Paul, Markiel, A., Ozier, O., Baliga, N. S., Wang, J. T., Ramage, D., … Ideker, T. (2003). Cytoscape: a software environment for integrated models of biomolecular interaction networks. *Genome Research*, *13*(11), 2498–2504.

Shapira, N. (2017). The potential contribution of dietary factors to breast cancer prevention. *European Journal of Cancer Prevention : The Official Journal of the European Cancer Prevention Organisation (ECP)*, *26*(5), 385–395. https://doi.org/10.1097/CEJ.0000000000000406

Sharma, G. N., Dave, R., Sanadya, J., Sharma, P., & Sharma, K. K. (2010). Various types and management of breast cancer: an overview. *Journal of Advanced Pharmaceutical Technology & Research*, *1*(2), 109–126. Retrieved from https://pubmed.ncbi.nlm.nih.gov/22247839

Sharma, O. P. (1976). Antioxidant activity of curcumin and related compounds. *Biochemical Pharmacology*, *25*(15), 1811–1812. https://doi.org/10.1016/0006-2952(76)90421-4

Sharma, R. A., Steward, W. P., & Gescher, A. J. (2007). Pharmacokinetics and pharmacodynamics of curcumin. *Advances in Experimental Medicine and Biology*, *595*, 453–470. https://doi.org/10.1007/978-0-387-46401-5_20

Shen, Liangliang, O'Shea, J. M., Kaadige, M. R., Cunha, S., Wilde, B. R., Cohen, A. L., … Ayer, D. E. (2015). Metabolic reprogramming in triple-negative breast cancer through Myc suppression of TXNIP. *Proceedings of the National Academy of Sciences of the United States of America*, *112*(17), 5425–5430. https://doi.org/10.1073/pnas.1501555112

Shen, Luyan, Wen, N., Xia, M., Zhang, Y. U., Liu, W., Xu, Y. E., & Sun, L. (2016). Calcium efflux from the endoplasmic reticulum regulates cisplatin-induced apoptosis in human cervical cancer HeLa cells. *Oncology Letters*, *11*(4), 2411–2419. https://doi.org/10.3892/ol.2016.4278

Shi, P., Liu, W., Tala, Wang, H., Li, F., Zhang, H., … Chen, C. (2017). Metformin suppresses triple-negative breast cancer stem cells by targeting KLF5 for degradation. *Cell Discovery*, *3*(1), 17010. https://doi.org/10.1038/celldisc.2017.10

Shoshan-Barmatz, V., De, S., & Meir, A. (2017). The Mitochondrial Voltage-Dependent Anion Channel 1, Ca2+ Transport, Apoptosis, and Their Regulation. *Frontiers in Oncology*, *7*, 60. https://doi.org/10.3389/fonc.2017.00060

Shoshan-Barmatz, V., N. Maldonado, E., & Krelin, Y. (2017). VDAC1 at the crossroads of cell metabolism, apoptosis and cell stress. *Cell Stress*, *1*(1), 11–36. https://doi.org/10.15698/cst2017.10.104

Siddik, Z. H. (2003). Cisplatin: mode of cytotoxic action and molecular basis of resistance. *Oncogene*, *22*(47), 7265–7279. https://doi.org/10.1038/sj.onc.1206933

Siddiqui, F. A., Prakasam, G., Chattopadhyay, S., Rehman, A. U., Padder, R. A., Ansari, M. A., … Iqbal, M. A. (2018). Curcumin decreases Warburg effect in cancer cells by down-regulating pyruvate kinase M2 via mTOR-HIF1α inhibition. *Scientific Reports*, *8*(1), 8323. https://doi.org/10.1038/s41598-018-25524-3

Siegel, R. L., Miller, K. D., & Jemal, A. (2019). Cancer statistics, 2019. *CA: A Cancer Journal for Clinicians*, *69*(1), 7–34. https://doi.org/10.3322/caac.21551

Sigurethsson, H. H., Olesen, C. W., Dybboe, R., Lauritzen, G., & Pedersen, S. F. (2015). Constitutively active ErbB2 regulates cisplatin-induced cell death in breast cancer cells via pro- and antiapoptotic mechanisms. *Molecular Cancer Research : MCR*, *13*(1), 63–77. https://doi.org/10.1158/1541-7786.MCR-14-0011

Singh, A. K., Sidhu, G. S., Deepa, T., & Maheshwari, R. K. (1996). Curcumin inhibits the proliferation and cell cycle progression of human umbilical vein endothelial cell. *Cancer Letters*, *107*(1), 109–115.

Singh, J., Dutta, T., Kim, K.-H., Rawat, M., Samddar, P., & Kumar, P. (2018). 'Green' synthesis of metals and their oxide nanoparticles: applications for environmental remediation. *Journal of Nanobiotechnology*, *16*(1), 84. https://doi.org/10.1186/s12951-018-0408-4

Singh, S., & Aggarwal, B. B. (1995). Activation of transcription factor NF-κB is suppressed by curcumin (diferulolylmethane). *Journal of Biological Chemistry*. https://doi.org/10.1074/jbc.270.42.24995

Singh, Surendra, Brocker, C., Koppaka, V., Chen, Y., Jackson, B. C., Matsumoto, A., … Vasiliou, V. (2013, March). Aldehyde dehydrogenases in cellular responses to oxidative/ electrophilicstress. *Free Radical Biology and Medicine*. https://doi.org/10.1016/j.freeradbiomed.2012.11.010

Sivaraman, V. S., Wang, H., Nuovo, G. J., & Malbon, C. C. (1997). Hyperexpression of mitogen-activated protein kinase in human breast cancer. *The Journal of Clinical Investigation*, *99*(7), 1478–1483. https://doi.org/10.1172/JCI119309

Skol, A. D., Sasaki, M. M., & Onel, K. (2016). The genetics of breast cancer risk in the post-genome era: thoughts on study design to move past BRCA and towards clinical relevance. *Breast Cancer Research : BCR*, *18*(1), 99. https://doi.org/10.1186/s13058-016-0759-4

Smith, L., Welham, K. J., Watson, M. B., Drew, P. J., Lind, M. J., & Cawkwell, L. (2007). The Proteomic Analysis of Cisplatin Resistance in Breast Cancer Cells. *Oncology Research Featuring Preclinical and Clinical Cancer Therapeutics*, *16*(11), 497–506. https://doi.org/10.3727/096504007783438358

Sørlie, T., Perou, C. M., Tibshirani, R., Aas, T., Geisler, S., Johnsen, H., … Børresen-Dale, A.-L. (2001). Gene expression patterns of breast carcinomas distinguish tumor subclasses with clinical implications. *Proceedings of the National Academy of Sciences*, *98*(19), 10869 LP – 10874. https://doi.org/10.1073/pnas.191367098

Sørlie, T., Tibshirani, R., Parker, J., Hastie, T., Marron, J. S., Nobel, A., … Botstein, D. (2003). Repeated observation of breast tumor subtypes in independent gene expression data sets. *Proceedings of the National Academy of Sciences*, *100*(14), 8418 LP – 8423. https://doi.org/10.1073/pnas.0932692100

Soule, H. D., Maloney, T. M., Wolman, S. R., Brenz, R., Russo, J., Pauley, R. J., … McGrath, C. M. (1990). Isolation and Characterization of a Spontaneously Immortalized Human Breast Epithelial Cell Line, MCF-10. *Cancer Research*, *50*(18), 6075–6086.

Srimal, R. C., & Dhawan, B. N. (1973). Pharmacology of diferuloyl methane (curcumin), a non-steroidal anti-inflammatory agent. *The Journal of Pharmacy and Pharmacology*, *25*(6), 447–452. https://doi.org/10.1111/j.2042-7158.1973.tb09131.x

Srinivasan, K. R. (1953). A CHROMATOGRAPHIC STUDY OF THE CURCUMINOIDS IN CURCUMA LONGA, L. *Journal of Pharmacy and Pharmacology*, *5*(1), 448–457. https://doi.org/10.1111/j.2042-7158.1953.tb14007.x

Srinivasan, M. (1972). Effect of curcumin on blood sugar as seen in a diabetic subject. *Indian Journal of Medical Sciences*, *26*(4), 269–270.

Staff, N. P., Grisold, A., Grisold, W., & Windebank, A. J. (2017). Chemotherapy-induced peripheral neuropathy: A current review. *Annals of Neurology*, *81*(6), 772–781. https://doi.org/10.1002/ana.24951

Stallings, V. L., Gurley, K. M., & Rorie, C. J. (2013). Triple Negative Breast Cancer Cell Lines with TP53 Mutations are Able to Undergo Cell Death. *International Journal of Science and Research (IJSR) ISSN (Online Index Copernicus Value Impact Factor*, *14*(9), 2319–7064. Retrieved from https://www.ijsr.net/archive/v4i9/SUB158256.pdf

Stark, A., Kleer, C. G., Martin, I., Awuah, B., Nsiah-Asare, A., Takyi, V., … Newman, L. (2010). African ancestry and higher prevalence of triple-negative breast cancer: findings from an international study. *Cancer*, *116*(21), 4926–4932. https://doi.org/10.1002/cncr.25276

Stepanov, A. L. (2004). Optical properties of metal nanoparticles synthesized in a polymer by ion implantation: A review. *Technical Physics*, *49*(2), 143–153. https://doi.org/10.1134/1.1648948

Suba, Z. (2013). Circulatory estrogen level protects against breast cancer in obese women. *Recent Patents on Anti-Cancer Drug Discovery*, *8*(2), 154–167. https://doi.org/10.2174/1574892811308020004

Suba, Z. (2014). Triple-negative breast cancer risk in women is defined by the defect of estrogen signaling: preventive and therapeutic implications. *OncoTargets and Therapy*, *7*, 147–164. https://doi.org/10.2147/OTT.S52600

Sun, S. H., Huang, H. C., Huang, C., & Lin, J. K. (2012). Cycle arrest and apoptosis in MDA-MB-231/Her2 cells induced by curcumin. *European Journal of Pharmacology*, *690*(1–3), 22–30. https://doi.org/10.1016/j.ejphar.2012.05.036

Sun, S., Liang, X., Zhang, X., Liu, T., Shi, Q., Song, Y., … Pang, D. (2015). Phosphoglycerate kinase-1 is a predictor of poor survival and a novel prognostic biomarker of chemoresistance to paclitaxel treatment in breast cancer. *British Journal of Cancer*, *112*(8), 1332–1339. https://doi.org/10.1038/bjc.2015.114

Sun, X.-D., Liu, X.-E., & Huang, D.-S. (2012). Curcumin induces apoptosis of triple-negative breast cancer cells by inhibition of EGFR expression. *Molecular Medicine Reports*, *6*(6), 1267–1270.

Sun, X., Wang, M., Wang, M., Yu, X., Guo, J., Sun, T., … Xu, Y. (2020). Metabolic Reprogramming in Triple-Negative Breast Cancer . *Frontiers in Oncology* . Retrieved from https://www.frontiersin.org/article/10.3389/fonc.2020.00428

Sundararajan, R. (2008). Nanoelectroporation: A First Look BT - Electroporation Protocols: Preclinical and Clinical Gene Medicine. In S. Li (Ed.) (pp. 109–128). Totowa, NJ: Humana Press. https://doi.org/10.1007/978-1-59745-194-9_7

Surakasula, A., Nagarjunapu, G. C., & Raghavaiah, K. V. (2014). A comparative study of pre- and post-menopausal breast cancer: Risk factors, presentation, characteristics and management. *Journal of Research in Pharmacy Practice*, *3*(1), 12–18. https://doi.org/10.4103/2279-042X.132704

Szklarczyk, D., Morris, J. H., Cook, H., Kuhn, M., Wyder, S., Simonovic, M., … von Mering, C. (2017). The STRING database in 2017: quality-controlled protein–protein association networks, made broadly accessible. *Nucleic Acids Research*, *45*(D1), D362–D368. https://doi.org/10.1093/nar/gkw937

Tacouri, D. D., Ramful-Baboolall, D., & Puchooa, D. (2013). In vitro bioactivity and phytochemical screening of selected spices used in Mauritian foods. *Asian Pacific Journal of Tropical Disease*, *3*(4), 253–261. https://doi.org/10.1016/S2222-1808(13)60066-3

The American Cancer Society medical and editorial content team. (2019a). Breast-conserving Surgery (Lumpectomy) | BCS Breast Surgery. Retrieved May 2, 2020, from https://www.cancer.org/cancer/breast-cancer/treatment/surgery-for-breast-cancer/breast-conserving-surgery-lumpectomy.html

The American Cancer Society medical and editorial content team. (2019b). Mastectomy | Mastectomies for Breast Cancer. Retrieved May 2, 2020, from https://www.cancer.org/cancer/breast-cancer/treatment/surgery-for-breast-cancer/mastectomy.html

The Global Library of Women's Medicine. (n.d.). cisplatin (cis-platinum). Retrieved July 2, 2020, from https://www.glowm.com/resources/glowm/cd/pages/drugs/c063.html

Tian, M., Zhong, Y., Zhou, F., Xie, C., Zhou, Y., & Liao, Z. (2015). Platinum-based therapy for triple-negative breast cancer treatment: A meta-analysis. *Molecular and Clinical Oncology*, *3*(3), 720–724. https://doi.org/10.3892/mco.2015.518

Tilli, T. M., Carels, N., Tuszynski, J. A., & Pasdar, M. (2016). Validation of a network-based strategy for the optimization of combinatorial target selection in breast cancer therapy: siRNA knockdown of network targets in MDA-MB-231 cells as an in vitro model for inhibition of tumor development. *Oncotarget*, *7*(39), 63189–63203. https://doi.org/10.18632/oncotarget.11055

Toden, S., & Goel, A. (2017). The Holy Grail of Curcumin and its Efficacy in Various Diseases: Is Bioavailability Truly a Big Concern? *Journal of Restorative Medicine*. https://doi.org/10.14200/jrm.2017.6.0101

Torres-Adorno, A. M., Vitrac, H., Qi, Y., Tan, L., Levental, K. R., Fan, Y. Y., … Ueno, N. T. (2019). Eicosapentaenoic acid in combination with EPHA2 inhibition shows efficacy in preclinical models of triple-negative breast cancer by disrupting cellular cholesterol efflux. *Oncogene*, *38*(12), 2135–2150. https://doi.org/10.1038/s41388-018-0569-5

Trivers, K. F., Lund, M. J., Porter, P. L., Liff, J. M., Flagg, E. W., Coates, R. J., & Eley, J. W. (2009). The epidemiology of triple-negative breast cancer, including race. *Cancer Causes & Control : CCC*, *20*(7), 1071–1082. https://doi.org/10.1007/s10552-009-9331-1

Tsimberidou, A.-M., Braiteh, F., Stewart, D. J., & Kurzrock, R. (2009). Ultimate fate of oncology drugs approved by the us food and drug administration without a randomized Trial. *Journal of Clinical Oncology : Official Journal of the American Society of Clinical Oncology*, *27*(36), 6243–6250. https://doi.org/10.1200/JCO.2009.23.6018

Tung, N., Lin, N. U., Kidd, J., Allen, B. A., Singh, N., Wenstrup, R. J., … Garber, J. E. (2016). Frequency of Germline Mutations in 25 Cancer Susceptibility Genes in a Sequential Series of Patients With Breast Cancer. *Journal of Clinical Oncology : Official Journal of the American Society of Clinical Oncology*, *34*(13), 1460–1468. https://doi.org/10.1200/JCO.2015.65.0747

Uniprot.org. (n.d.). What are proteomes? Retrieved September 6, 2018, from https://www.uniprot.org/help/proteome

Urbańska, K., & Orzechowski, A. (2019). Unappreciated Role of LDHA and LDHB to Control Apoptosis and Autophagy in Tumor Cells. *International Journal of Molecular Sciences*, *20*(9), 2085. https://doi.org/10.3390/ijms20092085

Urien, S., & Lokiec, F. (2004). Population pharmacokinetics of total and unbound plasma cisplatin in adult patients. *British Journal of Clinical Pharmacology*, *57*(6), 756–763. https://doi.org/10.1111/j.1365-2125.2004.02082.x

Urru, S. A. M., Gallus, S., Bosetti, C., Moi, T., Medda, R., Sollai, E., … Orrù, S. (2018). Clinical and pathological factors influencing survival in a large cohort of triple-negative breast cancer patients. *BMC Cancer*, *18*(1), 56. https://doi.org/10.1186/s12885-017-3969-y

Uscanga-Perales, G. I., Santuario-Facio, S. K., & Ortiz-López, R. (2016). Triple negative breast cancer: Deciphering the biology and heterogeneity. *Medicina Universitaria*, *18*(71), 105–114. https://doi.org/https://doi.org/10.1016/j.rmu.2016.05.007

Vabulas, R. M., Raychaudhuri, S., Hayer-Hartl, M., & Hartl, F. U. (2010). Protein folding in the cytoplasm and the heat shock response. *Cold Spring Harbor Perspectives in Biology*, *2*(12), a004390–a004390. https://doi.org/10.1101/cshperspect.a004390

Valvona, C. J., Fillmore, H. L., Nunn, P. B., & Pilkington, G. J. (2016). The Regulation and Function of Lactate Dehydrogenase A: Therapeutic Potential in Brain Tumor. *Brain Pathology*, *26*(1), 3–17. https://doi.org/10.1111/bpa.12299

Varghese, E., Samuel, S., Abotaleb, M., Cheema, S., Mamtani, R., & Büsselberg, D. (2018). The "Yin and Yang" of Natural Compounds in Anticancer Therapy of Triple-Negative Breast Cancers. *Cancers*, *10*(10), 346. https://doi.org/10.3390/cancers10100346

Vaughan, R. A., Garcia-Smith, R., Dorsey, J., Griffith, J. K., Bisoffi, M., & Trujillo, K. A. (2013). Tumor necrosis factor alpha induces Warburg-like metabolism and is reversed by anti-inflammatory curcumin in breast epithelial cells. *International Journal of Cancer*, *133*(10), 2504–2510. https://doi.org/10.1002/ijc.28264

Velma, V., Dasari, S. R., & Tchounwou, P. B. (2016). Low Doses of Cisplatin Induce Gene Alterations, Cell Cycle Arrest, and Apoptosis in Human Promyelocytic Leukemia Cells. *Biomarker Insights*, *11*, 113–121. https://doi.org/10.4137/BMI.S39445

Vergara, D., Simeone, P., del Boccio, P., Toto, C., Pieragostino, D., Tinelli, A., … Maffia, M. (2013). Comparative proteome profiling of breast tumor cell lines by gel electrophoresis and mass spectrometry reveals an epithelial mesenchymal transition associated protein signature. *Mol. BioSyst.*, *9*(6), 1127–1138. https://doi.org/10.1039/C2MB25401H

Verrill, M. (2009). Chemotherapy for early-stage breast cancer: a brief history. *British Journal of Cancer*, *101 Suppl*, S2-5. https://doi.org/10.1038/sj.bjc.6605268

Vogel, A., & Pelletier, J. (1815). Examen chimique de la racine de Curcuma. *J Pharm*, *1*, 289–300.

Vona-Davis, L., Rose, D. P., Hazard, H., Howard-McNatt, M., Adkins, F., Partin, J., & Hobbs, G. (2008). Triple-negative breast cancer and obesity in a rural Appalachian population. *Cancer Epidemiology, Biomarkers & Prevention : A Publication of the American Association for Cancer Research, Cosponsored by the American Society of Preventive Oncology*, *17*(12), 3319–3324. https://doi.org/10.1158/1055-9965.EPI-08-0544

Wahdan-Alaswad, R. S., Edgerton, S. M., Salem, H. S., & Thor, A. D. (2018). Metformin Targets Glucose Metabolism in Triple Negative Breast Cancer. *Journal of Oncology Translational Research*, *4*(1), 129. https://doi.org/10.4172/2476-2261.1000129

Wahdan-Alaswad, R. S., Fan, Z., Edgerton, S. M., Liu, B., Deng, X.-S. S., Arnadottir, S. S., … Thor, A. D. (2013). Glucose promotes breast cancer aggression and reduces metformin efficacy. *Cell Cycle*, *12*(24), 3759–3769. https://doi.org/10.4161/cc.26641

Wang, Jigang, Zhang, J., Zhang, C.-J., Wong, Y. K., Lim, T. K., Hua, Z.-C., … Lin, Q. (2016). In situ Proteomic Profiling of Curcumin Targets in HCT116 Colon Cancer Cell Line. *Scientific Reports*, *6*(1), 22146. https://doi.org/10.1038/srep22146

Wang, Jun, Zhang, P., Zhong, J., Tan, M., Ge, J., Tao, L., … Tong, X. (2016). The platelet isoform of phosphofructokinase contributes to metabolic reprogramming and maintains cell proliferation in clear cell renal cell carcinoma. *Oncotarget*, *7*(19), 27142–27157. https://doi.org/10.18632/oncotarget.8382

Wang, K., Fan, H., Chen, Q., Ma, G., Zhu, M., Zhang, X., … Yu, J. (2015). Curcumin inhibits aerobic glycolysis and induces mitochondrial-mediated apoptosis through hexokinase II in human colorectal cancer cells in vitro. *Anti-Cancer Drugs*, *26*(1), 15–24. https://doi.org/10.1097/CAD.0000000000000132

Wang, S., Xie, J., Li, J., Liu, F., Wu, X., & Wang, Z. (2016). Cisplatin suppresses the growth and proliferation of breast and cervical cancer cell lines by inhibiting integrin β5-mediated glycolysis. *American Journal of Cancer Research*, *6*(5), 1108–1117.

Wang, T. N., Qian, X. H., Granick, M. S., Solomon, M. P., Rothman, V. L., Berger, D. H., & Tuszynski, G. P. (1996). Thrombospondin-1 (TSP-1) promotes the invasive properties of human breast cancer. In *Journal of Surgical Research* (Vol. 63, pp. 39–43). Academic Press Inc. https://doi.org/10.1006/jsre.1996.0219

Wang, W., Nag, S. A., & Zhang, R. (2015). Targeting the NFκB signaling pathways for breast cancer prevention and therapy. *Current Medicinal Chemistry*, *22*(2), 264–289. https://doi.org/10.2174/0929867321666141106124315

Wang, X. C., Yue, X., Zhang, R. X., Liu, T. Y., Pan, Z. Z., Yang, M. J., … Liu, R. Y. (2019). Genome-wide RNAi screening identifies RFC4 as a factor that mediates radioresistance in colorectal cancer by facilitating nonhomologous end joining repair. *Clinical Cancer Research*, *25*(14), 4567–4579. https://doi.org/10.1158/1078-0432.CCR-18-3735

Wani, M. C., Taylor, H. L., Wall, M. E., Coggon, P., & McPhail, A. T. (1971). Plant antitumor agents. VI. The isolation and structure of taxol, a novel antileukemic and antitumor agent from Taxus brevifolia. *Journal of the American Chemical Society*, *93*(9), 2325–2327. https://doi.org/10.1021/ja00738a045

Weaver, J. C., Smith, K. C., Esser, A. T., Son, R. S., & Gowrishankar, T. R. (2012). A brief overview of electroporation pulse strength–duration space: A region where additional intracellular effects are expected. *Bioelectrochemistry*, *87*, 236–243. https://doi.org/10.1016/j.bioelechem.2012.02.007

Weinberg, R. A. (Robert A. (2014). The biology of cancer. Retrieved from https://books.google.com/books?hl=en&lr=&id=MzMmAgAAQBAJ&oi=fnd&pg=PR4&dq=info:93JxZw3164UJ:scholar.google.com&ots=A1QjZ8165c&sig=1YP9XR8i5hpQJTzIDEewX-gQNwE#v=onepage&q&f=false

Werner, C., Doenst, T., & Schwarzer, M. (2016). Chapter 4 - Metabolic Pathways and Cycles. In M. Schwarzer & T. B. T.-T. S. G. to C. M. Doenst (Eds.) (pp. 39–55). Boston: Academic Press. https://doi.org/https://doi.org/10.1016/B978-0-12-802394-5.00004-2

Whelan, M. C., Larkin, J. O., Collins, C. G., Cashman, J., Breathnach, O., Soden, D. M., & O'Sullivan, G. C. (2006). Effective treatment of an extensive recurrent breast cancer which was refractory to multimodal therapy by multiple applications of electrochemotherapy. *European Journal of Cancer Supplements*, *4*(11), 32–34. https://doi.org/https://doi.org/10.1016/j.ejcsup.2006.07.006

Whitaker-Menezes, D., Martinez-Outschoorn, U. E., Lin, Z., Ertel, A., Flomenberg, N., Witkiewicz, A. K., … Lisanti, M. P. (2011). Evidence for a stromal-epithelial "lactate shuttle" in human tumors. *Cell Cycle*, *10*(11), 1772–1783. https://doi.org/10.4161/cc.10.11.15659

Wilson, R. E., Donegan, W. L., Mettlin, C., Natarajan, N., Smart, C. R., & Murphy, G. P. (1984). The 1982 national survey of carcinoma of the breast in the United States by the American College of Surgeons. *Surgery, Gynecology & Obstetrics*, *159*(4), 309–318.

Wirth, T., & Baltimore, D. (1988). Nuclear factor NF-kappa B can interact functionally with its cognate binding site to provide lymphoid-specific promoter function. *The EMBO Journal*, *7*(10), 3109–3113. Retrieved from https://pubmed.ncbi.nlm.nih.gov/3141147

Witkiewicz, M. W. A. U.-D. M. A. U.-M. L. A. U.-J. K.-G. A. U.-A. B. A. U.-W. (2016). Initial experiences of the use of electrochemotherapy in the treatment of skin metastases. *Initial Experiences of the Use of Electrochemotherapy in the Treatment of Skin Metastases*. https://doi.org/10.5603/NJO.2016.0022

Wong, E., Chaudhry, S., & Rossi, M. (2016). Breast cancer | McMaster Pathophysiology Review. *McMaster University*. Retrieved from http://www.pathophys.org/breast-cancer/

World Health Organization. (n.d.). Breast cancer: prevention and control. Retrieved May 23, 2020, from https://www.who.int/cancer/detection/breastcancer/en/index2.html%0Ahttps://www.who.int/cancer/detection/breastcancer/en/%0Ahttp://www.who.int/cancer/detection/breastcancer/en/

Xu, J., Prosperi, J. R., Choudhury, N., Olopade, O. I., & Goss, K. H. (2015). β-Catenin is required for the tumorigenic behavior of triple-negative breast cancer cells. *PloS One*, *10*(2), e0117097–e0117097. https://doi.org/10.1371/journal.pone.0117097

Yan, S.-H. (2013). An early history of human breast cancer: West meets East. *Chinese Journal of Cancer*, *32*(9), 475–477. https://doi.org/10.5732/cjc.013.10097

Yang, L., Hou, Y., Yuan, J., Tang, S., Zhang, H., Zhu, Q., … Liu, M. (2015). Twist promotes reprogramming of glucose metabolism in breast cancer cells through PI3K/AKT and p53 signaling pathways. *Oncotarget*, *6*(28), 25755–25769. https://doi.org/10.18632/oncotarget.4697

Yang, M., & Brackenbury, W. J. (2013). Membrane potential and cancer progression. *Frontiers in Physiology*, *4*, 185. https://doi.org/10.3389/fphys.2013.00185

Yang, S., Zhang, J. J., & Huang, X.-Y. (2009). Orai1 and STIM1 Are Critical for Breast Tumor Cell Migration and Metastasis. *Cancer Cell*, *15*(2), 124–134. https://doi.org/10.1016/j.ccr.2008.12.019

Yao, H., He, G., Yan, S., Chen, C., Song, L., Rosol, T. J., & Deng, X. (2017). Triple-negative breast cancer: is there a treatment on the horizon? *Oncotarget*, *8*(1), 1913–1924. https://doi.org/10.18632/oncotarget.12284

Ye, G. X., Qin, Y., Wang, S., Pan, D. B., Xu, S. Q., Wu, C. J., … Shen, H. J. (2019). Lamc1 promotes the Warburg effect in hepatocellular carcinoma cells by regulating PKM2 expression through AKT pathway. *Cancer Biology and Therapy*, *20*(5), 711–719. https://doi.org/10.1080/15384047.2018.1564558

Yee, L. D., Mortimer, J. E., Natarajan, R., Dietze, E. C., & Seewaldt, V. L. (2020). Metabolic Health, Insulin, and Breast Cancer: Why Oncologists Should Care About Insulin. *Frontiers in Endocrinology*, *11*, 58. https://doi.org/10.3389/fendo.2020.00058

Yi, Y. W., Kang, H. J., Kim, H. J., Kong, Y., Brown, M. M., & Bae, I. (2013). Targeting Mutant p53 by a SIRT1 Activator YK-3-237 Inhibits the Proliferation of Triple-Negative Breast Cancer Cells. *Oncotarget*, *4*(7), 984–994. https://doi.org/10.18632/oncotarget.1070

Yu, W., Chen, Y., Dubrulle, J., Stossi, F., Putluri, V., Sreekumar, A., … Sandulache, V. C. (2018). Cisplatin generates oxidative stress which is accompanied by rapid shifts in central carbon metabolism. *Scientific Reports*, *8*(1), 4306. https://doi.org/10.1038/s41598-018-22640-y

Yue, J., Huhn, S., & Shen, Z. (2013, February 6). Complex roles of filamin-A mediated cytoskeleton network in cancer progression. *Cell and Bioscience*. BioMed Central. https://doi.org/10.1186/2045-3701-3-7

Ždralević, M., Brand, A., Di Ianni, L., Dettmer, K., Reinders, J., Singer, K., … Kreutz, M. (2018). Double genetic disruption of lactate dehydrogenases A and B is required to ablate the "Warburg effect" restricting tumor growth to oxidative metabolism. *The Journal of Biological Chemistry*, *293*(41), 15947–15961. https://doi.org/10.1074/jbc.RA118.004180

Zeng, G., Apte, U., Cieply, B., Singh, S., & Monga, S. P. S. (2007). siRNA-mediated beta-catenin knockdown in human hepatoma cells results in decreased growth and survival. *Neoplasia (New York, N.Y.)*, *9*(11), 951–959. https://doi.org/10.1593/neo.07469

Zhang, D., Jin, N., Sun, W., Li, X., Liu, B., Xie, Z., … Geng, M. (2017). Phosphoglycerate mutase 1 promotes cancer cell migration independent of its metabolic activity. *Oncogene*, *36*(20), 2900–2909. https://doi.org/10.1038/onc.2016.446

Zhang, F.-J., Zhang, H.-S., Liu, Y., & Huang, Y.-H. (2015). Curcumin inhibits Ec109 cell growth via an AMPK-mediated metabolic switch. *Life Sciences*, *134*, 49–55. https://doi.org/10.1016/j.lfs.2015.05.016

Zhou, Y., Chen, J., Li, Q., Huang, W., Lan, H., & Jiang, H. (2015). Association Between Breastfeeding and Breast Cancer Risk: Evidence from a Meta-analysis. *Breastfeeding Medicine*, *10*(3), 175–182. https://doi.org/10.1089/bfm.2014.0141

Ziegler, Y. S., Moresco, J. J., Tu, P. G., Yates, J. R., & Nardulli, A. M. (2014). Plasma membrane proteomics of human breast cancer cell lines identifies potential targets for breast cancer diagnosis and treatment. *PLoS ONE*, *9*(7), e102341. https://doi.org/10.1371/journal.pone.0102341

Zielinski, D. C., Filipp, F. V., Bordbar, A., Jensen, K., Smith, J. W., Herrgard, M. J., … Palsson, B. O. (2015). Pharmacogenomic and clinical data link non-pharmacokinetic metabolic dysregulation to drug side effect pathogenesis. *Nature Communications*, *6*, 1–15. https://doi.org/10.1038/ncomms8101

Zimmermann, U., Pilwat, G., & Riemann, F. (1974). Dielectric breakdown of cell membranes. *Biophysical Journal*, *14*(11), 881–899. https://doi.org/10.1016/S0006-3495(74)85956-4

Zimmermannova, O., Doktorova, E., Stuchly, J., Kanderova, V., Kuzilkova, D., Strnad, H., … Zaliova, M. (2017). An activating mutation of GNB1 is associated with resistance to tyrosine kinase inhibitors in ETV6-ABL1-positive leukemia. *Oncogene*, *36*(43), 5985–5994. https://doi.org/10.1038/onc.2017.210

LIST OF PUBLICATIONS

Journal Publications

Mittal, L., Camarillo, I. G., Varadarajan, G. S., Srinivasan, H., Aryal, U. K., and Sundararajan, R. (2020). High-throughput, Label-Free Quantitative proteomics studies of the anticancer effects of electrical pulses with turmeric silver nanoparticles: an in vitro model study. ***Scientific Reports***, 10(1), 7258. https://doi.org/10.1038/s41598-020-64128-8.

Mittal, L., Aryal, U. K., Camarillo, I. G., Raman, Vishak, and Sundararajan, R. (2020). Effective electrochemotherapy with curcumin in MDA-MB-231 human, triple negative breast cancer cells: a global proteomics study. ***Bioelectrochemistry***, 131, 107350. https://doi.org/10.1016/J.BIOELECHEM.2019.107350.

Mittal, L., S., R., M., S. A., T., J. S., Akther, T., S., P., … Sundararajan, R., and Srinivasan, H., (2020). Turmeric-silver-nanoparticles for effective treatment of breast cancer and to break CTX-M-15 mediated antibiotic resistance in Escherichia coli. ***Inorganic and Nano-Metal Chemistry***, 1–8. https://doi.org/10.1080/24701556.2020.1812644.

Mittal, L., Aryal, U. K., Camarillo, I. G., Ferreira, R. M., and Sundararajan, R. (2019). Quantitative proteomic analysis of enhanced cellular effects of electrochemotherapy with cisplatin in triple-negative breast cancer cells. ***Scientific Reports***, 9(1), 13916. https://doi.org/10.1038/s41598-019-50048-9.

Mittal, L., Raman, V., Camarillo, I. G., Garner, A. L., and Sundararajan, R. (2019). Viability and cell cycle studies of metastatic triple negative breast cancer cells using low voltage electrical pulses and herbal curcumin. ***Biomedical Physics & Engineering Express***, 5(2), 25040. https://doi.org/10.1088/2057-1976/aaf2c3.

Mittal, L., Raman, V., Camarillo, I. G., and Sundararajan, R. (2017). Ultra-microsecond pulsed curcumin for effective treatment of triple negative breast Cancers. ***Biochemical and Biophysical Research Communications***, 491(4), 1015-1020. https://doi.org/10.1016/j.bbrc.2017.08.002.

Mittal, L., Raman, V., Camarillo, I. G., and Sundararajan, R. (2017). Electrical pulse-mediated Veliparib for the treatment of triple negative breast cancer: An in vitro model study. ***International Journal on Current Research and Academic Review***, 5(3), 53-64. https://doi.org/10.20546/ijcrar.2017.503.009.

Journal Manuscripts in Review

Bazzolo B., **Mittal, L.**, Sieni, E., Piovan, A., Filippini, R., Conconi, M. T., and Sundararajan, R. (2020). The electrical pulse application enhances intra-cellular localization and potentiates cytotoxicity of curcumin in breast cancer cells. Submitted for publication in *Bioelectrochemistry*.

Sundararajan, R., **Mittal, L.**, Camarillo, I. G., and (2020). Electrochemotherapy modulates mammary tumor growth in rats on a western diet supplemented with curcumin. Under revision for publication in *Biomedicines*.

International Conference Proceedings

Mittal, L., Aryal, U. K., Camarillo, I. G., and Sundararajan, R., (2019). Global proteomic analysis of breast cancer cell plasma membrane electroporation. ***IEEE Conference on Electrical Insulation and Dielectric Phenomena (CEIDP)***, Richland, USA. https://doi.org/10.1109/CEIDP47102.2019.9009762.

Mittal, L., Camarillo, I. G., Hemalatha, S., Aryal, U. K., Musleh, A. A., GowriSree, V., Sieni, E., Sgarbossa, P., Natarajan, A., and Sundararajan, R. (2019). Turmeric silver nanoparticles with electrical pulses against triple negative breast cancer cells: An insight into the mechanism via quantitative proteomic analysis. ***Annual Meeting of the Electrostatics Society of America, Rochester***, USA.

Sundararajan, R., **Mittal, L.**, Sieni, E., Parupudi, T., Raman, V., and, Camarillo, I. G. (2018). Turmeric herbal chemotherapy for metastatic triple negative breast cancer. ***Electrostatics Joint Conference***, Boston, USA.

Mittal, L., Raman, V., Camarillo, I. G., Garner, A. L., Fairbanks A.J., Dunn G. A., and Sundararajan, R. (2017). Synergy of micro and nanosecond electrical pulses with chemotherapeutics on human cancer cell viability. ***IEEE Conference on Electrical Insulation and Dielectric Phenomena (CEIDP)***, Fort Worth, Texas, USA, 596-599. https://doi.org/10.1109/CEIDP.2017.8257574.

AWARDS AND HONORS

09/2019 ***ISEBTT Travel Grant***, Doreen J. Putrah Cancer Research Foundation - To attend 2019 3rd World Congress on Electroporation, Toulouse, France

06/2019 ***First Place, Student Paper Competition***, 2019 Annual Meeting of the Electrostatics Society of America, Rochester, NY, USA

06/2019 ***Dean's Graduate Student Travel Grant***, Purdue Polytechnic Institute, Purdue University - To attend 2019 Annual Meeting of the Electrostatics Society of America, Rochester, NY, USA

05/2019 ***Purdue Interdisciplinary Audience Choice Award***, 2019 Office of Interdisciplinary Graduate Programs (OIGP) Spring Reception, Purdue University

04/2019 ***2019 Bilsland Dissertation Fellowship***, The Graduate School, Purdue University

10/2018 ***2018 IEEE Dielectrics and Electrical Insulation Society (DEIS) Fellowship*** for research proposal *"**Proteomic Analysis of Breast Cancer Cell Plasma Membrane Electroporation using Ultra-Microsecond and Other Pulses**"*

05/2018 ***2018 Indo-US Science and Technology Forum (IUSSTF) Research Internships in Science & Engineering (RISE) Award***

05/2018 ***Best Poster Award***, 2018 14th Annual Purdue Polytechnic Faculty Convocation

05/2018 ***Honorable Mention: Most Outstanding Interdisciplinary Project Award***, 2018 OIGP Spring Reception, Purdue University

09/2017 ***PGSG Travel Grant***, Purdue University - To attend 2019 2nd World Congress on Electroporation, Norfolk, VA, USA

APPENDIX A.

A.1. MATLAB code to classify proteins for Venndiagram for curcumin proteomics study

```
clear all;
close all;

data=readtable('C:\randomepath\filename.xlsx');   %% Input Proteomics data file path and filename (excel format) and store in 'Data'
rawint12=table2array(data(:,14)); %% Pulling the LFQ value of Curcumin sample and storing in an array (14th column in excel sheet)
EPrawint12=table2array(data(:,15)); %% Pulling the LFQ value of EP+Curcumin sample and storing in an array (15th column in excel sheet)

count12=table2array(data(:,16)); %% Pulling the MS/MS value of Curcumin sample and storing in an array  (16th column in excel sheet)
EPcount12=table2array(data(:,17)); %% Pulling the MS/MS value of EP+Curcumin sample and storing in an array )17th column in excel sheet)
j=1;
A=0;B=0; C=0;
AA=1;BB=1; CC=1;

for i=1:2020           %% Run the For loop for the length of the data. Here in input data there were 2020 rows (This changes based on the data).

%%%%%%%%%%%%%%%%%%%%%%%%%%%%%%%%%%%%%%%%%%%%%%%%%%%%%%%%%%%%%%%%%%%%%%%%%%%%%%%%%%%%%%%%%%%%%%%%%%%%%%

    %% for the proteins present in only Curcumin only sample
      if rawint12(i,1)~=0 && EPrawint12(i,1)==0           %% Condition: LFQ value is non-zero for Curcumin sample but zero for EP+Curcumin
         if count12(i,1)> 1                         %% Condition: MS/MS is 2 or more for non-zero Curcumin sample
            A=A+1;                               %% Increasing the counter if both the conditions satisfy
            disp(i+1);                           %% Just displays the iteration count
            Unique_Sample1(AA,:)=data(i,:);              %% Stores the whole row for the iteration (only if it satisfies the condition) from 'data' into a sub-data variable.
            AA=AA+1;                              %% increases the index to be able to store next row in Unique_Sample1 variable for next iteration
         end
      end

%%%%%%%%%%%%%%%%%%%%%%%%%%%%%%%%%%%%%%%%%%%%%%%%%%%%%%%%%%%%%%%%%%%%%%%%%%%%%%%%%%%%%%%%%%%%%%%%%%%%%%

       %% for the proteins present in EP+Curcumin only
      if rawint12(i,1)==0 && EPrawint12(i,1)~=0         %% LFQ value is non-zero for EP+Curcumin sample but zero for Curcumin
         if EPcount12(i,1)>1                        %% Condition: MS/MS is 2 or more for non-zero EP+Curcumin sample
            B=B+1;                               %% Increasing the counter if both the conditions satisfy
            disp(i+1);                           %% Just displays the iteration count
            Unique_Sample2(BB,:)=data(i,:);              %% Stores the whole row for the iteration (only if it satisfies the condition) from 'data' into a sub-data variable.
            BB=BB+1;                              %% increases the index to be able to store next row in Unique_Sample2 variable for next iteration
         end
      end
   %%%%%%%%%%%%%%%%%%%%%%%%%%%%%%%%%%%%%%%%%%%%%%%%%%%%%%%%%%%%%%%%%%%%%%%%%%%%%%%%%%%%%%%%%%%%%%%%%%%%%%%%%%

      %% for the proteins present in Curcumin and EP+Curcumin
      if rawint12(i,1)~=0 && EPrawint12(i,1)~=0        %% LFQ value is non-zero for both in Curcumin and EP+Curcumin samples
```

```
        if count12(i,1)>1 && EPcount12(i,1)>1        %% Condition: MS/MS is 2 or more for both in Curcumin and EP+Curcumin samples
            C=C+1;                                   %% Increasing the counter if both the conditions satisfy
               disp(i+1);                            %% Just displays the iteration count
             Unique_Sample3(CC,:)=data(i,:);         %% Stores the whole row for the iteration (only if it satisfies the condition) from 'data' into a sub-data variable.
            CC=CC+1;                                 %% increases the index to be able to store next row in Unique_Sample3 variable for next iteration
          end
       end


    %%%  Output  %%%%%%%%%%%%%%%%%%%%%%%%%%%%%%%%%%

    disp(A);                                         %% Displays the number of proteins in only Curcumin only sample
    disp(B);                                         %% Displays the number of proteins in only EP+Curcumin only sample
    disp(C);                                         %% Displays the number of proteins common for Curcumin and EP+Curcumin samples
    Sum=A+B+C;
    disp(Sum)                                        %% Displays the sum of all the common and unique proteins
end
%% Saving the unique and common proteins in separate output data files
if(A~=0)
   writetable(Unique_Sample1, C:\randomepath\Cur+EP Unique.xlsx'); %% Saves the file for unique proteins in only Curcumin only sample  – Provide the output path by replacing 'C:\randomepath'
end
if(B~=0)
   writetable(Unique_Sample2,' C:\randomepath\Tur+EP  Unique.xlsx'); %% Saves the file for unique proteins in only EP+Curcumin only sample – Provide the output path

end
if(C~=0)
   writetable(Unique_Sample3,' C:\randomepath\Common.xlsx');       %% Saves the file for common proteins in Curcumin and EP+Curcumin samples – Provide the output path
end
```

A.2. MATLAB code used to classify proteins for Venndiagram for different selection criterion

A.2.1. Selection criterion A (protein in at least 1 replicate)

```
clc;clear all;close all;

data=  readtable('\\client\f$\Dropbox\Research\Experiments\Proteomics\2019_TurNP  Prot\Analysis  4  Thesis\Input data\proteinGroups Labeld_Only TurNP data.xlsx'); %% Input Proteomics data file path and filename (excel format) and store in 'Data'


%% pulling LFQ data from input file.


LFQ1_1=table2array(data(:,7)); %% Pulling the LFQ value of Treatment 1, replicate 1 and storing in an array (7th column in excel sheet)
LFQ1_2=table2array(data(:,8)); %% LFQ- Treatment 1, Replicate 2
LFQ1_3=table2array(data(:,9)); %% LFQ- Treatment 1, Replicate 3

LFQ2_1=table2array(data(:,10)); %% LFQ- Treatment 2, Replicate 1
LFQ2_2=table2array(data(:,11)); %% LFQ- Treatment 2, Replicate 2
```

```
LFQ2_3=table2array(data(:,12)); %% LFQ- Treatment 2, Replicate 3


LFQ3_1=table2array(data(:,13)); %% LFQ- Treatment 3, Replicate 1
LFQ3_2=table2array(data(:,14)); %% LFQ- Treatment 3, Replicate 2
LFQ3_3=table2array(data(:,15)); %% LFQ- Treatment 3, Replicate 3

LFQ4_1=table2array(data(:,16)); %% LFQ- Treatment 4, Replicate 1
LFQ4_2=table2array(data(:,17)); %% LFQ- Treatment 4, Replicate 2
LFQ4_3=table2array(data(:,18)); %% LFQ- Treatment 4, Replicate 3

MS1_1=table2array(data(:,19));  %% Pulling the MS/MS value of Treatment 1, replicate 1 and storing in an array
MS1_2=table2array(data(:,20));  %% MS/MS- Treatment 1, Replicate 2
MS1_3=table2array(data(:,21));  %% MS/MS- Treatment 1, Replicate 3

MS2_1=table2array(data(:,22));  %% MS/MS- Treatment 2, Replicate 1
MS2_2=table2array(data(:,23));  %% MS/MS- Treatment 2, Replicate 2
MS2_3=table2array(data(:,24));  %% MS/MS- Treatment 2, Replicate 3

MS3_1=table2array(data(:,25));  %% MS/MS- Treatment 3, Replicate 1
MS3_2=table2array(data(:,26));  %% MS/MS- Treatment 3, Replicate 2
MS3_3=table2array(data(:,27));  %% MS/MS- Treatment 3, Replicate 3

MS4_1=table2array(data(:,28));  %% MS/MS- Treatment 4, Replicate 1
MS4_2=table2array(data(:,29));  %% MS/MS- Treatment 4, Replicate 2
MS4_3=table2array(data(:,30));  %% MS/MS- Treatment 4, Replicate 3


j=1;
A=0;B=0; C=0; D=0; E=0; F=0; G=0; H=0; I=0; K=0; L=0; M=0; N=0; O=0; P=0;
AAA=1;BBB=1; CCC=1; DDD=1; EEE=1; FFF=1; GGG=1; HHH=1; III=1; KKK=1; LLL=1; MMM=1; NNN=1; OOO=1;
PPP=1;

Trt1(1:3810,1)=0;         %% initialize arrays of the data length (3810 rows in our input here) with zero
Trt2(1:3810,1)=0;
Trt3(1:3810,1)=0;
Trt4(1:3810,1)=0;
for i=1:length(LFQ1_1)



    if LFQ1_1(i,1)~=0 && MS1_1(i,1)>1    %% Condition for Treatment1, replicate 1: LFQ is non-zero and MS/MS is 2 or more
       Trt1(i,1)=1;
    end
    if LFQ1_2(i,1)~=0 && MS1_2(i,1)>1     %% Condition for Treatment1, replicate 2
       Trt1(i,1)=Trt1(i,1)+1;
    end
    if LFQ1_3(i,1)~=0 && MS1_3(i,1)>1     %% Condition for Treatment1, replicate 3
       Trt1(i,1)=Trt1(i,1)+1;
    end


    if LFQ2_1(i,1)~=0 && MS2_1(i,1)>1    %% Condition for Treatment2, replicate 1: LFQ is non-zero and MS/MS is 2 or more
       Trt2(i,1)=1;
    end
    if LFQ2_2(i,1)~=0 && MS2_2(i,1)>1     %% Condition for Treatment2, replicate 2
       Trt2(i,1)=Trt2(i,1)+1;
    end
    if LFQ2_3(i,1)~=0 && MS2_3(i,1)>1     %% Condition for Treatment2, replicate 2
       Trt2(i,1)=Trt2(i,1)+1;
    end
```

```
    if LFQ3_1(i,1)~=0 && MS3_1(i,1)>1    %% Condition for Treatment3, replicate 1: LFQ is non-zero and MS/MS is 2 or more
       Trt3(i,1)=1;
    end
    if LFQ3_2(i,1)~=0 && MS3_2(i,1)>1    %% Condition for Treatment3, replicate 2
       Trt3(i,1)=Trt3(i,1)+1;
    end
    if LFQ3_3(i,1)~=0 && MS3_3(i,1)>1    %% Condition for Treatment2, replicate 3
       Trt3(i,1)=Trt3(i,1)+1;
    end

    if LFQ4_1(i,1)~=0 && MS4_1(i,1)>1    %% Condition for Treatment4, replicate 1: LFQ is non-zero and MS/MS is 2 or more
       Trt4(i,1)=1;
    end
    if LFQ4_2(i,1)~=0 && MS4_2(i,1)>1    %% Condition for Treatment4, replicate 2
       Trt4(i,1)=Trt4(i,1)+1;
    end
    if LFQ4_3(i,1)~=0 && MS4_3(i,1)>1    %% Condition for Treatment4, replicate 3
       Trt4(i,1)=Trt4(i,1)+1;
    end

    %%% unique in Tratment1 (LFQ != 0 and MS/MS >1 (2 or more) for at least one of the three replicates)
    if Trt1(i,1)>0 && Trt2(i,1)<1 && Trt3(i,1)<1 && Trt4(i,1)<1
       A=A+1;
       disp(i+1);
       AA(AAA,:)= data(i,:);
       AAA=AAA+1;

    end


%%% unique in Treatment2 only
    if Trt1(i,1)<1 && Trt2(i,1)>0 && Trt3(i,1)<1 && Trt4(i,1)<1
       B=B+1;
       disp(i+1);
       BB(BBB,:)= data(i,:);
       BBB=BBB+1;

    end

%%% unique in Treatment3 only
    if Trt1(i,1)<1 && Trt2(i,1)<1 && Trt3(i,1)>0 && Trt4(i,1)<1
       C=C+1;
       disp(i+1);
       CC(CCC,:)= data(i,:);
       CCC=CCC+1;

    end

%%% unique in Treatment4 only
    if Trt1(i,1)<1 && Trt2(i,1)<1 && Trt3(i,1)<1 && Trt4(i,1)>0
       D=D+1;
       disp(i+1);
       DD(DDD,:)= data(i,:);
       DDD=DDD+1;

    end



  %%% common in Treatment1 and Treatment2
    if Trt1(i,1)>0 && Trt2(i,1)>0 && Trt3(i,1)<1 && Trt4(i,1)<1
```

```
      E=E+1;
      disp(i+1);
EE(EEE,:)= data(i,:);
 EEE=EEE+1;

  end

%%% common in Treatment1 and Treatment3
  if Trt1(i,1)>0 && Trt2(i,1)<1 && Trt3(i,1)>0 && Trt4(i,1)<1
      F=F+1;
      disp(i+1);
      FF(FFF,:)= data(i,:);
      FFF=FFF+1;

  end

  %%% common in Treatment1 and Tratment4
  if Trt1(i,1)>0 && Trt2(i,1)<1 && Trt3(i,1)<1 && Trt4(i,1)>0
      G=G+1;
      disp(i+1);
      GG(GGG,:)= data(i,:);
      GGG=GGG+1;
 end

  %%% common in Treatment2 and Treatment3
  if Trt1(i,1)<1 && Trt2(i,1)>0 && Trt3(i,1)>0 && Trt4(i,1)<1
       H=H+1;
       disp(i+1);
       HH(HHH,:)= data(i,:);
       HHH=HHH+1;
end



  %%% common in Treatment2 and Treatment4
  if Trt1(i,1)<1 && Trt2(i,1)>0 && Trt3(i,1)<1 && Trt4(i,1)>0
      I=I+1;
      disp(i+1);
      II(III,:)= data(i,:);
      III=III+1;

  end
  %%% common in Treatment3 and Treatment4
  if Trt1(i,1)<1 && Trt2(i,1)<1 && Trt3(i,1)>0 && Trt4(i,1)>0
      K=K+1;
      disp(i+1);
      KK(KKK,:)= data(i,:);
      KKK=KKK+1;

  end
  %%% common in Treatment1, Treatment2 and Treatment3
  if Trt1(i,1)>0 && Trt2(i,1)>0 && Trt3(i,1)>0 && Trt4(i,1)<1
      L=L+1;
      disp(i+1);
      LL(LLL,:)= data(i,:);
      LLL=LLL+1;
  end


  %%% common in Treatment1, Treatment2, and Treatment4
  if Trt1(i,1)>0 && Trt2(i,1)>0 && Trt3(i,1)<1 && Trt4(i,1)>0
      M=M+1;
```

```
        disp(i+1);
        MM(MMM,:)= data(i,:);
        MMM=MMM+1;
    end

    %%% common in Treatment2, Treatment3, and Treatment4
    if Trt1(i,1)<1 && Trt2(i,1)>0 && Trt3(i,1)>0 && Trt4(i,1)>0
        N=N+1;
        disp(i+1);
        NN(NNN,:)= data(i,:);
        NNN=NNN+1;
    end

    %%% common in Treatment1, Treatment3, and Treatment4
    if Trt1(i,1)>0 && Trt2(i,1)<1 && Trt3(i,1)>0 && Trt4(i,1)>0
        P=P+1;
        disp(i+1);
        PP(PPP,:)= data(i,:);
        PPP=PPP+1;
    end

    %%% common in all 4: Treatment1, Treatment2, Treatment3, and Treatment4
    if Trt1(i,1)>0 && Trt2(i,1)>0 && Trt3(i,1)>0 && Trt4(i,1)>0
        O=O+1;
        disp(i+1);
        OO(OOO,:)= data(i,:);
        OOO=OOO+1;
    end

  %%% Results  %%%%%%%%%%%%%%%%%%%%%%%%%%%%%%%%%%%%%%%%%%%%%%%%%%%%%%%%%%%%

      Sum=A+B+C+D+E+F+G+H+I+K+L+M+N+O+P;
end
results=[A;B;C;D;E;F;G;H;I;K;L;M;N;P;O;Sum];    %% Stores the number of proteins in unique and common in a variable 'results'
disp(results)                                   %% Displays the number of proteins in unique and common in a variable 'results'


%% Saving the unique and common proteins in separate output data files
%% Abbreviations in output file names- S1: Treatment1; S2: Treatment2; S3: Treatment3; S4: Treatment 4.
%% Note: Replace 'Insert_Your_output_folder_Path' below with a path of the folder, where you want the output files to be saved

if (A)>0
writetable(AA,'Insert_Your_output_folder_Path\unique prots in S1.xlsx');
end
if (B)>0
writetable(BB,'Insert_Your_output_folder_Path\unique prots in S2.xlsx');
end
if (C)>0
writetable(CC,'Insert_Your_output_folder_Path\unique prots in S3.xlsx');
end
if (D)>0
writetable(DD,'Insert_Your_output_folder_Path\unique prots in S4.xlsx');
end
if (E)>0
writetable(EE,'Insert_Your_output_folder_Path\common prots S1_n_S2.xlsx');
end
if (F)>0
writetable(FF,'Insert_Your_output_folder_Path\common prots S1_n_S3.xlsx');
end
if (G)>0
writetable(GG,'Insert_Your_output_folder_Path\common prots S1_n_S4.xlsx');
end
```

```
if (H)>0
writetable(HH,'Insert_Your_output_folder_Path\common prots S2_n_S3.xlsx');
end
if (I)>0
writetable(II,'Insert_Your_output_folder_Path\common prot_S2_n_S4.xlsx');
end
if (K)>0
writetable(KK,'Insert_Your_output_folder_Path\common prots S3_n_S4.xlsx');
end
if (L)>0
writetable(LL,'Insert_Your_output_folder_Path\common prots S1_n_S2_n_S3.xlsx');
end
if (M)>0
writetable(MM,'Insert_Your_output_folder_Path\common prots S1_n_S2_n_S4.xlsx');
end
if (N)>0
writetable(NN,'Insert_Your_output_folder_Path\common prots S2_n_S3_n_S4.xlsx');
end
if (O)>0
writetable(OO,'Insert_Your_output_folder_Path\common prots S1_n_S2_n_S3_n_S4.xlsx');
end
if (P)>0
writetable(PP,'Insert_Your_output_folder_Path\common prots S1_n_S3_n_S4.xlsx');
end
```

A.2.2. Selection criterion B (protein in at least 2 replicates)

This MATLAB code was used for turmeric silver nanoparticles and cisplatin proteomics studies.

```
clc;clear all;close all;

data= readtable('F:\Dropbox\Research\Experiments\Proteomics\2019_TurNP Prot\Analysis\Raw source data finally used\proteinGroups Labeld_Only TurNP data.xlsx');  %% Input Proteomics data file path and filename (excel format) and store in 'Data'

%% pulling LFQ data not iBAQ.

LFQ1_1=table2array(data(:,7)); %% Pulling the LFQ value of Treatment 1, replicate 1 and storing in an array (7th column in excel sheet)
LFQ1_2=table2array(data(:,8)); %% LFQ- Treatment 1, Replicate 2
LFQ1_3=table2array(data(:,9)); %% LFQ- Treatment 1, Replicate 32

LFQ2_1=table2array(data(:,10)); %% LFQ- Treatment 2, Replicate 1
LFQ2_2=table2array(data(:,11)); %% LFQ- Treatment 2, Replicate 2
LFQ2_3=table2array(data(:,12)); %% LFQ- Treatment 2, Replicate 3


LFQ3_1=table2array(data(:,13)); %% LFQ- Treatment 3, Replicate 1
LFQ3_2=table2array(data(:,14)); %% LFQ- Treatment 3, Replicate 2
LFQ3_3=table2array(data(:,15)); %% LFQ- Treatment 3, Replicate 3

LFQ4_1=table2array(data(:,16)); %% LFQ- Treatment 4, Replicate 1
LFQ4_2=table2array(data(:,17)); %% LFQ- Treatment 4, Replicate 2
LFQ4_3=table2array(data(:,18)); %% LFQ- Treatment 4, Replicate 4

MS1_1=table2array(data(:,19)); %% Pulling the MS/MS value of Treatment 1, replicate 1 and storing in an array
MS1_2=table2array(data(:,20)); %% MS/MS- Treatment 1, Replicate 2
MS1_3=table2array(data(:,21)); %% MS/MS- Treatment 1, Replicate 3
```

```
MS2_1=table2array(data(:,22)); %% MS/MS- Treatment 2, Replicate 1
MS2_2=table2array(data(:,23)); %% MS/MS- Treatment 1, Replicate 2
MS2_3=table2array(data(:,24)); %% MS/MS- Treatment 2, Replicate 3

MS3_1=table2array(data(:,25)); %% MS/MS- Treatment 3, Replicate 1
MS3_2=table2array(data(:,26)); %% MS/MS- Treatment 3, Replicate 2
MS3_3=table2array(data(:,27)); %% MS/MS- Treatment 3, Replicate 3

MS4_1=table2array(data(:,28)); %% MS/MS- Treatment 4, Replicate 2
MS4_2=table2array(data(:,29)); %% MS/MS- Treatment 4, Replicate 2
MS4_3=table2array(data(:,30)); %% MS/MS- Treatment 4, Replicate 3


j=1;
A=0;B=0; C=0; D=0; E=0; F=0; G=0; H=0; I=0; K=0; L=0; M=0; N=0; O=0; P=0;
AAA=1;BBB=1; CCC=1; DDD=1; EEE=1; FFF=1; GGG=1; HHH=1; III=1; KKK=1; LLL=1; MMM=1; NNN=1; OOO=1;
PPP=1;


Trt1(1:3810,1)=0;  %% initialize arrays of the data length (3810 rows in our input here) with zero
Trt2(1:3810,1)=0;
Trt3(1:3810,1)=0;
Trt4(1:3810,1)=0;
for i=1:length(LFQ1_1)

    if LFQ1_1(i,1)~=0 && MS1_1(i,1)>1   %% Condition for Treatment1, replicate 1: LFQ is non-zero and MS/MS is 2 or more
       Trt1(i,1)=1;
    end
    if LFQ1_2(i,1)~=0 && MS1_2(i,1)>1   %% Condition for Treatment1, replicate 2
       Trt1(i,1)=Trt1(i,1)+1;
    end
    if LFQ1_3(i,1)~=0 && MS1_3(i,1)>1   %% Condition for Treatment1, replicate 2
       Trt1(i,1)=Trt1(i,1)+1;
    end


    if LFQ2_1(i,1)~=0 && MS2_1(i,1)>1   %% Condition for Treatment2, replicate 1: LFQ is non-zero and MS/MS is 2 or more
       Trt2(i,1)=1;
    end
    if LFQ2_2(i,1)~=0 && MS2_2(i,1)>1   %% Condition for Treatment2, replicate 2
       Trt2(i,1)=Trt2(i,1)+1;
    end
    if LFQ2_3(i,1)~=0 && MS2_3(i,1)>1   %% Condition for Treatment2, replicate 3
       Trt2(i,1)=Trt2(i,1)+1;
    end


    if LFQ3_1(i,1)~=0 && MS3_1(i,1)>1   %% Condition for Treatment3, replicate 1: LFQ is non-zero and MS/MS is 2 or more
       Trt3(i,1)=1;
    end
    if LFQ3_2(i,1)~=0 && MS3_2(i,1)>1   %% Condition for Treatment3, replicate 2
       Trt3(i,1)=Trt3(i,1)+1;
    end
    if LFQ3_3(i,1)~=0 && MS3_3(i,1)>1   %% Condition for Treatment3, replicate 3
       Trt3(i,1)=Trt3(i,1)+1;
    end

    if LFQ4_1(i,1)~=0 && MS4_1(i,1)>1   %% Condition for Treatment4, replicate 1: LFQ is non-zero and MS/MS is 2 or more
       Trt4(i,1)=1;
    end
    if LFQ4_2(i,1)~=0 && MS4_2(i,1)>1   %% Condition for Treatment4, replicate 2
```

```
        Trt4(i,1)=Trt4(i,1)+1;
    end
    if LFQ4_3(i,1)~=0 && MS4_3(i,1)>1   %% Condition for Treatment4, replicate 3
        Trt4(i,1)=Trt4(i,1)+1;
    end

 %%% unique in Tratment1 (LFQ != 0 and MS/MS >1 (2 or more) for at least one of the three replicates)
    if Trt1(i,1)>1 && Trt2(i,1)<2 && Trt3(i,1)<2 && Trt4(i,1)<2
        A=A+1;
        disp(i+1);
        AA(AAA,:)= data(i,:);
        AAA=AAA+1;

    end

 %%% unique in Treatment2 only
    if Trt1(i,1)<2 && Trt2(i,1)>1 && Trt3(i,1)<2 && Trt4(i,1)<2
        B=B+1;
        disp(i+1);
        BB(BBB,:)= data(i,:);
        BBB=BBB+1;

    end

%%% unique in Treatment3 only
    if Trt1(i,1)<2 && Trt2(i,1)<2 && Trt3(i,1)>1 && Trt4(i,1)<2
        C=C+1;
        disp(i+1);
        CC(CCC,:)= data(i,:);
        CCC=CCC+1;

    end

%%% unique in Treatment4 only
    if Trt1(i,1)<2 && Trt2(i,1)<2 && Trt3(i,1)<2 && Trt4(i,1)>1
        D=D+1;
        disp(i+1);
        DD(DDD,:)= data(i,:);
        DDD=DDD+1;

    end

%%% common in Treatment1 and Treatment2
    if Trt1(i,1)>1 && Trt2(i,1)>1 && Trt3(i,1)<2 && Trt4(i,1)<2
        E=E+1;
        disp(i+1);
        EE(EEE,:)= data(i,:);
        EEE=EEE+1;

    end
 %%% common in Treatment1 and Treatment3
    if Trt1(i,1)>1 && Trt2(i,1)<2 && Trt3(i,1)>1 && Trt4(i,1)<2
        F=F+1;
        disp(i+1);
  FF(FFF,:)= data(i,:);
   FFF=FFF+1;

    end
 %%% common in Treatment1 and Tratment4
    if Trt1(i,1)>1 && Trt2(i,1)<2 && Trt3(i,1)<2 && Trt4(i,1)>1
        G=G+1;
        disp(i+1);
```

```
        GG(GGG,:)= data(i,:);
        GGG=GGG+1;

    end
%%% common in Treatment2 and Treatment3
    if Trt1(i,1)<2 && Trt2(i,1)>1 && Trt3(i,1)>1 && Trt4(i,1)<2
        H=H+1;
        disp(i+1);
        HH(HHH,:)= data(i,:);
        HHH=HHH+1;

    end

%%% common in Treatment2 and Treatment4
    if Trt1(i,1)<2 && Trt2(i,1)>1 && Trt3(i,1)<2 && Trt4(i,1)>1
        I=I+1;
        disp(i+1);
        II(III,:)= data(i,:);
         III=III+1;

    end
%%% common in Treatment3 and Treatment4
    if Trt1(i,1)<2 && Trt2(i,1)<2 && Trt3(i,1)>1 && Trt4(i,1)>1
        K=K+1;
        disp(i+1);
        KK(KKK,:)= data(i,:);
        KKK=KKK+1;

    end
%%% common in Treatment1, Treatment2 and Treatment3
    if Trt1(i,1)>1 && Trt2(i,1)>1 && Trt3(i,1)>1 && Trt4(i,1)<2
        L=L+1;
        disp(i+1);
        LL(LLL,:)= data(i,:);
        LLL=LLL+1;

    end
%%% common in Treatment1, Treatment2, and Treatment4
    if Trt1(i,1)>1 && Trt2(i,1)>1 && Trt3(i,1)<2 && Trt4(i,1)>1
        M=M+1;
        disp(i+1);
        MM(MMM,:)= data(i,:);
        MMM=MMM+1;
    end

%%% common in Treatment2, Treatment3, and Treatment4
    if Trt1(i,1)<2 && Trt2(i,1)>1 && Trt3(i,1)>1 && Trt4(i,1)>1
        N=N+1;
        disp(i+1);
        NN(NNN,:)= data(i,:);
        NNN=NNN+1;
    end

%%% common in Treatment1, Treatment3, and Treatment4
    if Trt1(i,1)>1 && Trt2(i,1)<2 && Trt3(i,1)>1 && Trt4(i,1)>1
        P=P+1;
        disp(i+1);
        PP(PPP,:)= data(i,:);
        PPP=PPP+1;
    end
 %%%%%%%%%%%%%%%%%%%%%%%%%%%%%%%%%%%%%%%%%%%%%%%%%%
```

```
    %%% common in all 4: Treatment1, Treatment2, Treatment3, and Treatment4
        if Trt1(i,1)>1 && Trt2(i,1)>1 && Trt3(i,1)>1 && Trt4(i,1)>1
            O=O+1;
            disp(i+1);
            OO(OOO,:)= data(i,:);
            OOO=OOO+1;
        end

    %%% Results  %%%%%%%%%%%%%%%%%%%%%%%%%%%%%%%%%%%%%%%%%%%%%

       Sum=A+B+C+D+E+F+G+H+I+K+L+M+N+O+P;
end
results=[A;B;C;D;E;F;G;H;I;K;L;M;N;P;O;Sum];    %% Stores the number of proteins in unique and common in a variable 'results'
disp(results)                                   %% Displays the number of proteins in unique and common in a variable 'results'

%% Saving the unique and common proteins in separate output data files
%% Abbreviations in output file names- S1: Treatment1; S2: Treatment2; S3: Treatment3; S4: Treatment 4.
%% Note: Replace 'Insert_Your_output_folder_Path' below with a path of the folder, where you want the output files to be saved

if (A)>0
writetable(AA,'Insert_Your_output_folder_Path\unique prots in S1.xlsx');
end
if (B)>0
writetable(BB,'Insert_Your_output_folder_Path\unique prots in S2.xlsx');
end
if (C)>0
writetable(CC,'Insert_Your_output_folder_Path\unique prots in S3.xlsx');
end
if (D)>0
writetable(DD,'Insert_Your_output_folder_Path\unique prots in S4.xlsx');
end
if (E)>0
writetable(EE,'Insert_Your_output_folder_Path\common prots S1_n_S2.xlsx');
end
if (F)>0
writetable(FF,'Insert_Your_output_folder_Path\common prots S1_n_S3.xlsx');
end
if (G)>0
writetable(GG,'Insert_Your_output_folder_Path\common prots S1_n_S4.xlsx');
end
if (H)>0
writetable(HH,'Insert_Your_output_folder_Path\common prots S2_n_S3.xlsx');
end
if (I)>0
writetable(II,'Insert_Your_output_folder_Path\common prot_S2_n_S4.xlsx');
end
if (K)>0
writetable(KK,'Insert_Your_output_folder_Path\common prots S3_n_S4.xlsx');
end
if (L)>0
writetable(LL,'Insert_Your_output_folder_Path\common prots S1_n_S2_n_S3.xlsx');
end
if (M)>0
writetable(MM,'Insert_Your_output_folder_Path\common prots S1_n_S2_n_S4.xlsx');
end
if (N)>0
writetable(NN,'Insert_Your_output_folder_Path\common prots S2_n_S3_n_S4.xlsx');
end
if (O)>0
writetable(OO,'Insert_Your_output_folder_Path\common prots S1_n_S2_n_S3_n_S4.xlsx');
end
if (P)>0
```

```
writetable(PP,'Insert_Your_output_folder_Path\common prots S1_n_S3_n_S4.xlsx');
end
```

A.2.3. Selection criterion C (protein in at least 3 replicates)

```
clc;clear all;close all;

data= readtable('\\client\f$\Dropbox\Research\Experiments\Proteomics\2019_TurNP Prot\Analysis 4 Thesis\Input data\proteinGroups Labeld_Only TurNP data.xlsx');

%% pulling LFQ data from input file.

LFQ1_1=table2array(data(:,7)); %% Pulling the LFQ value of Treatment 1, replicate 1 and storing in an array (7th column in excel sheet)
LFQ1_2=table2array(data(:,8)); %% LFQ- Treatment 1, Replicate 2
LFQ1_3=table2array(data(:,9)); %% LFQ- Treatment 1, Replicate 3

LFQ2_1=table2array(data(:,10)); %% LFQ- Treatment 2, Replicate 1
LFQ2_2=table2array(data(:,11)); %% LFQ- Treatment 2, Replicate 2
LFQ2_3=table2array(data(:,12)); %% LFQ- Treatment 2, Replicate 3


LFQ3_1=table2array(data(:,13)); %% LFQ- Treatment 3, Replicate 1
LFQ3_2=table2array(data(:,14)); %% LFQ- Treatment 3, Replicate 2
LFQ3_3=table2array(data(:,15)); %% LFQ- Treatment 3, Replicate 3

LFQ4_1=table2array(data(:,16)); %% LFQ- Treatment 4, Replicate 1
LFQ4_2=table2array(data(:,17)); %% LFQ- Treatment 4, Replicate 2
LFQ4_3=table2array(data(:,18)); %% LFQ- Treatment 4, Replicate 3

MS1_1=table2array(data(:,19)); %% Pulling the MS/MS value of Treatment 1, replicate 1 and storing in an array
MS1_2=table2array(data(:,20)); %% MS/MS- Treatment 1, Replicate 2
MS1_3=table2array(data(:,21)); %% MS/MS- Treatment 1, Replicate 3

MS2_1=table2array(data(:,22)); %% MS/MS- Treatment 2, Replicate 1
MS2_2=table2array(data(:,23)); %% MS/MS- Treatment 2, Replicate 2
MS2_3=table2array(data(:,24)); %% MS/MS- Treatment 2, Replicate 3

MS3_1=table2array(data(:,25)); %% MS/MS- Treatment 3, Replicate 1
MS3_2=table2array(data(:,26)); %% MS/MS- Treatment 3, Replicate 2
MS3_3=table2array(data(:,27)); %% MS/MS- Treatment 3, Replicate 3

MS4_1=table2array(data(:,28)); %% MS/MS- Treatment 4, Replicate 1
MS4_2=table2array(data(:,29)); %% MS/MS- Treatment 4, Replicate 2
MS4_3=table2array(data(:,30)); %% MS/MS- Treatment 4, Replicate 3


j=1;
A=0;B=0; C=0; D=0; E=0; F=0; G=0; H=0; I=0; K=0; L=0; M=0; N=0; O=0; P=0;
AAA=1;BBB=1; CCC=1; DDD=1; EEE=1; FFF=1; GGG=1; HHH=1; III=1; KKK=1; LLL=1; MMM=1; NNN=1; OOO=1; PPP=1;


Trt1(1:3810,1)=0;          %% initialize arrays of the data length (3810 rows in our input here) with zero
Trt2(1:3810,1)=0;
Trt3(1:3810,1)=0;
Trt4(1:3810,1)=0;
for i=1:length(LFQ1_1)
```

```
if LFQ1_1(i,1)~=0 && MS1_1(i,1)>1 %% Condition for Treatment1, replicate 1: LFQ is non-zero and MS/MS is 2 or more
   Trt1(i,1)=1;
end
if LFQ1_2(i,1)~=0 && MS1_2(i,1)>1 %% Condition for Treatment1, replicate 2
   Trt1(i,1)=Trt1(i,1)+1;
end
if LFQ1_3(i,1)~=0 && MS1_3(i,1)>1 %% Condition for Treatment1, replicate 3
   Trt1(i,1)=Trt1(i,1)+1;
end


if LFQ2_1(i,1)~=0 && MS2_1(i,1)>1 % Condition for Treatment2, replicate 1: LFQ is non-zero and MS/MS is 2 or more
   Trt2(i,1)=1;
end
if LFQ2_2(i,1)~=0 && MS2_2(i,1)>1 %% Condition for Treatment2, replicate 2
   Trt2(i,1)=Trt2(i,1)+1;
end
if LFQ2_3(i,1)~=0 && MS2_3(i,1)>1 %% Condition for Treatment2, replicate 3
   Trt2(i,1)=Trt2(i,1)+1;
end


if LFQ3_1(i,1)~=0 && MS3_1(i,1)>1 % Condition for Treatment3, replicate 1: LFQ is non-zero and MS/MS is 2 or more
   Trt3(i,1)=1;
end
if LFQ3_2(i,1)~=0 && MS3_2(i,1)>1 %% Condition for Treatment3, replicate 2
   Trt3(i,1)=Trt3(i,1)+1;
end
if LFQ3_3(i,1)~=0 && MS3_3(i,1)>1 %% Condition for Treatment3, replicate 3
   Trt3(i,1)=Trt3(i,1)+1;
end

if LFQ4_1(i,1)~=0 && MS4_1(i,1)>1 %% Condition for Treatment4, replicate 1: LFQ is non-zero and MS/MS is 2 or more
   Trt4(i,1)=1;
end
if LFQ4_2(i,1)~=0 && MS4_2(i,1)>1 %% Condition for Treatment4, replicate 2
   Trt4(i,1)=Trt4(i,1)+1;
end
if LFQ4_3(i,1)~=0 && MS4_3(i,1)>1 %% Condition for Treatment4, replicate 3
   Trt4(i,1)=Trt4(i,1)+1;
end

 %%% unique in Tratment1 (LFQ != 0 and MS/MS >1 (2 or more) for at least three replicates)
if Trt1(i,1)>2 && Trt2(i,1)<3 && Trt3(i,1)<3 && Trt4(i,1)<3
   A=A+1;
   disp(i+1);
   AA(AAA,:)= data(i,:);
   AAA=AAA+1;

end


 %%% unique in Treatment2 only
if Trt1(i,1)<3 && Trt2(i,1)>2 && Trt3(i,1)<3 && Trt4(i,1)<3
   B=B+1;
   disp(i+1);
   BB(BBB,:)= data(i,:);
   BBB=BBB+1;
```

```
  end

  %%% unique in Treatment3 only
  if Trt1(i,1)<3 && Trt2(i,1)<3 && Trt3(i,1)>2 && Trt4(i,1)<3
     C=C+1;
     disp(i+1);
     CC(CCC,:)= data(i,:);
     CCC=CCC+1;

   end

%%% unique in Treatment4 only
  if Trt1(i,1)<3 && Trt2(i,1)<3 && Trt3(i,1)<3 && Trt4(i,1)>2
     D=D+1;
     disp(i+1);
     DD(DDD,:)= data(i,:);
     DDD=DDD+1;

  end


%%% common in Treatment1 and Treatment2
  if Trt1(i,1)>2 && Trt2(i,1)>2 && Trt3(i,1)<3 && Trt4(i,1)<3
     E=E+1;
     disp(i+1);
     EE(EEE,:)= data(i,:);
     EEE=EEE+1;

  end

%%% common in Treatment1 and Treatment3
  if Trt1(i,1)>2 && Trt2(i,1)<3 && Trt3(i,1)>2 && Trt4(i,1)<3
     F=F+1;
     disp(i+1);
     FF(FFF,:)= data(i,:);
     FFF=FFF+1;
    if i==2571
    disp("it is ENO2 from Ctrl and CsP");
    end
  end

  %%% common in Treatment1 and Tratment4
  if Trt1(i,1)>2 && Trt2(i,1)<3 && Trt3(i,1)<3 && Trt4(i,1)>2
     G=G+1;
     disp(i+1);
     GG(GGG,:)= data(i,:);
     GGG=GGG+1;
 end

  %%% common in Treatment2 and Treatment3
  if Trt1(i,1)<3 && Trt2(i,1)>2 && Trt3(i,1)>2 && Trt4(i,1)<3
       H=H+1;
     disp(i+1);
     HH(HHH,:)= data(i,:);
     HHH=HHH+1;
end


  %%% common in Treatment2 and Treatment4
  if Trt1(i,1)<3 && Trt2(i,1)>2 && Trt3(i,1)<3 && Trt4(i,1)>2
     I=I+1;
     disp(i+1);
```

```
        II(III,:)= data(i,:);
        III=III+1;

    end
    %%% common in Treatment3 and Treatment4
    if Trt1(i,1)<3 && Trt2(i,1)<3 && Trt3(i,1)>2 && Trt4(i,1)>2
        K=K+1;
        disp(i+1);
        KK(KKK,:)= data(i,:);
        KKK=KKK+1;

    end
    %%% common in Treatment1, Treatment2 and Treatment3
    if Trt1(i,1)>2 && Trt2(i,1)>2 && Trt3(i,1)>2 && Trt4(i,1)<3
        L=L+1;
        disp(i+1);
        LL(LLL,:)= data(i,:);
        LLL=LLL+1;
    end


    %%% common in Treatment1, Treatment2, and Treatment4
    if Trt1(i,1)>2 && Trt2(i,1)>2 && Trt3(i,1)<3 && Trt4(i,1)>2
        M=M+1;
        disp(i+1);
        MM(MMM,:)= data(i,:);
        MMM=MMM+1;
    end

    %%% common in Treatment2, Treatment3, and Treatment4
    if Trt1(i,1)<3 && Trt2(i,1)>2 && Trt3(i,1)>2 && Trt4(i,1)>2
        N=N+1;
        disp(i+1);
        NN(NNN,:)= data(i,:);
        NNN=NNN+1;
    end

    %%% common in Treatment1, Treatment3, and Treatment4
    if Trt1(i,1)>2 && Trt2(i,1)<3 && Trt3(i,1)>2 && Trt4(i,1)>2
        P=P+1;
        disp(i+1);
        PP(PPP,:)= data(i,:);
        PPP=PPP+1;
    end

    %%% common in all 4: Treatment1, Treatment2, Treatment3, and Treatment4
    if Trt1(i,1)>2 && Trt2(i,1)>2 && Trt3(i,1)>2 && Trt4(i,1)>2
        O=O+1;
        disp(i+1);
        OO(OOO,:)= data(i,:);
        OOO=OOO+1;
    end

 %%%%%%%%%%%%%%%%%%%%%%%%%%%%%%%%%%%%%%%%%%%%%%%%%%%%%%%%

   Sum=A+B+C+D+E+F+G+H+I+K+L+M+N+O+P;
end

results=[A;B;C;D;E;F;G;H;I;K;L;M;N;P;O;Sum];     %% Stores the number of proteins in unique and common in a array 'results'
disp(results)                            %% Displays the number of proteins in unique and common in the array 'results'

%% Saving the unique and common proteins in separate output data files
```

```
%% Abbreviations in output file names- S1: Treatment1; S2: Treatment2; S3: Treatment3; S4: Treatment 4.
%% Note: Replace 'Insert_Your_output_folder_Path' below with a path of the folder, where you want the output files to be saved


if (A)>0
writetable(AA,'Insert_Your_output_folder_Path\unique prots in S1.xlsx');
end
if (B)>0
writetable(BB,'Insert_Your_output_folder_Path\unique prots in S2.xlsx');
end
if (C)>0
writetable(CC,'Insert_Your_output_folder_Path\unique prots in S3.xlsx');
end
if (D)>0
writetable(DD,'Insert_Your_output_folder_Path\unique prots in S4.xlsx');
end
if (E)>0
writetable(EE,'Insert_Your_output_folder_Path\common prots S1_n_S2.xlsx');
end
if (F)>0
writetable(FF,'Insert_Your_output_folder_Path\common prots S1_n_S3.xlsx');
end
if (G)>0
writetable(GG,'Insert_Your_output_folder_Path\common prots S1_n_S4.xlsx');
end
if (H)>0
writetable(HH,'Insert_Your_output_folder_Path\common prots S2_n_S3.xlsx');
end
if (I)>0
writetable(II,'Insert_Your_output_folder_Path\common prot_S2_n_S4.xlsx');
end
if (K)>0
writetable(KK,'Insert_Your_output_folder_Path\common prots S3_n_S4.xlsx');
end
if (L)>0
writetable(LL,'Insert_Your_output_folder_Path\common prots S1_n_S2_n_S3.xlsx');
end
if (M)>0
writetable(MM,'Insert_Your_output_folder_Path\common prots S1_n_S2_n_S4.xlsx');
end
if (N)>0
writetable(NN,'Insert_Your_output_folder_Path\common prots S2_n_S3_n_S4.xlsx');
end
if (O)>0
writetable(OO,'Insert_Your_output_folder_Path\common prots S1_n_S2_n_S3_n_S4.xlsx');
end
if (P)>0
writetable(PP,'Insert_Your_output_folder_Path\common prots S1_n_S3_n_S4.xlsx');
end
```